frontiers | Research Topics

Molecular and multi-omic approaches in understanding cancer biology and anticancer therapies: Current perspectives and new challenges.

Edited by
Basel A. Abdel-Wahab, Yosra A. Helmy and Essa M. Saied

Published in
Frontiers in Pharmacology
Frontiers in Oncology

ISSN 1664-8714
ISBN 978-2-8325-2861-7
DOI 10.3389/978-2-8325-2861-7

About Frontiers

Frontiers is more than just an open access publisher of scholarly articles: it is a pioneering approach to the world of academia, radically improving the way scholarly research is managed. The grand vision of Frontiers is a world where all people have an equal opportunity to seek, share and generate knowledge. Frontiers provides immediate and permanent online open access to all its publications, but this alone is not enough to realize our grand goals.

Frontiers journal series

The Frontiers journal series is a multi-tier and interdisciplinary set of open-access, online journals, promising a paradigm shift from the current review, selection and dissemination processes in academic publishing. All Frontiers journals are driven by researchers for researchers; therefore, they constitute a service to the scholarly community. At the same time, the *Frontiers journal series* operates on a revolutionary invention, the tiered publishing system, initially addressing specific communities of scholars, and gradually climbing up to broader public understanding, thus serving the interests of the lay society, too.

Dedication to quality

Each Frontiers article is a landmark of the highest quality, thanks to genuinely collaborative interactions between authors and review editors, who include some of the world's best academicians. Research must be certified by peers before entering a stream of knowledge that may eventually reach the public - and shape society; therefore, Frontiers only applies the most rigorous and unbiased reviews. Frontiers revolutionizes research publishing by freely delivering the most outstanding research, evaluated with no bias from both the academic and social point of view. By applying the most advanced information technologies, Frontiers is catapulting scholarly publishing into a new generation.

What are Frontiers Research Topics?

Frontiers Research Topics are very popular trademarks of the *Frontiers journals series*: they are collections of at least ten articles, all centered on a particular subject. With their unique mix of varied contributions from Original Research to Review Articles, Frontiers Research Topics unify the most influential researchers, the latest key findings and historical advances in a hot research area.

Find out more on how to host your own Frontiers Research Topic or contribute to one as an author by contacting the Frontiers editorial office: frontiersin.org/about/contact

Molecular and multi-omic approaches in understanding cancer biology and anticancer therapies: Current perspectives and new challenges.

Topic editors

Basel A. Abdel-Wahab — Assiut University, Egypt

Yosra A. Helmy — University of Kentucky, United States

Essa M. Saied — Humboldt University of Berlin, Germany

Citation

Abdel-Wahab, B. A., Helmy, Y. A., Saied, E. M., eds. (2023). *Molecular and multi-omic approaches in understanding cancer biology and anticancer therapies: Current perspectives and new challenges*. Lausanne: Frontiers Media SA. doi: 10.3389/978-2-8325-2861-7

Table of contents

frontiers | Frontiers in Pharmacology

TYPE Editorial
PUBLISHED 15 June 2023
DOI 10.3389/fphar.2023.1236158

OPEN ACCESS

EDITED AND REVIEWED BY
Olivier Feron,
Université catholique de Louvain,
Belgium

*CORRESPONDENCE
Basel A. Abdel-Wahab,
basel_post@msn.com

RECEIVED 07 June 2023
ACCEPTED 12 June 2023
PUBLISHED 15 June 2023

CITATION
Abdel-Wahab BA, Helmy YA and Saied EM (2023), Editorial: Molecular and multi-omic approaches in understanding cancer biology and anticancer therapies: current perspectives and new challenges. *Front. Pharmacol.* 14:1236158. doi: 10.3389/fphar.2023.1236158

Editorial: Molecular and multi-omic approaches in understanding cancer biology and anticancer therapies: current perspectives and new challenges

Basel A. Abdel-Wahab[1]*, Yosra A. Helmy[2] and Essa M. Saied[3]

[1]Department of Medical Pharmacology, Faculty of Medicine, Assiut University, Assiut, Egypt, [2]Department of Veterinary Science, College of Agriculture, Food, and Environment, University of Kentucky, Lexington, KY, United States, [3]Institute for Chemistry, Humboldt Universität zu Berlin, Berlin, Germany

KEYWORDS

multiomics, colon cancer, prostate cancer, ovarian cancer, breast cancer, lung cancer

Editorial on the Research Topic
Molecular and multi-omic approaches in understanding cancer biology and anticancer therapies: current perspectives and new challenges

1 The aim and scope of this Research Topic

A holistic understanding of cancer biology and pathophysiological features is crucial. Multi-omics approaches integrate multiple datasets to understand cancer molecular and clinical features. This data-driven study reveals the complexity of cells and their environment, improving survival prediction and therapeutic outcomes. This specific Research Topic is to encourage talented researchers working in the field of multi-omics and cancer to publish their work with Frontiers in Pharmacology. The Research Topic features 11 articles, including 10 original and one review articles, in a multidisciplinary collaboration among multiomic-bioinformatic, *invitro*, and clinical studies. These articles cover several cancer types, including pancreatic, ovarian, cervical, colorectal and lung cancer.

2 Overview of contributors

Necroptosis is a new target for cancer immunotherapy, enhancing tumor immunogenicity. Fang et al. through a comprehensive analytical study determined necroptosis subtypes and investigate the roles of necroptosis in pancreatic cancer therapy. Immunological cell infiltrations, immunological checkpoints, HLA molecules, and the cancer-immunity cycle were used to assess the immunogenic properties. Authors identified five subtypes of necroptosis in pancreatic cancer, with diverse prognosis, immunogenicity, and chemosensitivity. Future research should evaluate its relevance in combined therapeutic regimens and chemotherapy choices.

Ovarian cancer (OC) treatment still needs more molecular biomarkers for accurate prognostic and therapeutic decision-making. Assidi investigated the expression patterns of N-cadherin (N-CAD), which has been demonstrated to be overexpressed in numerous advanced carcinomas and determined their links with the clinicopathological characteristics of OC patients and assessed its prognostic value. N-CAD overexpression in OC is associated with a poor prognosis, as evidenced by increased recurrence and mortality rates, in addition to its molecular role to distant metastasis Assidi.

Cervical cancer, is the fourth most common cancer globally. In contrast to conventional interventions, Kori et al. focused on inflammatory proteins that classify cervical cancer patients by considering individual differences between cancer patients. Also, authors repurposed anti-inflammatory drugs using gene signature reversal and molecular docking. They suggested 5 novel drugs (aldosterone, BMS-345541, etodolac, hydrocortisone, and prednisone) for the treatment of both HPV subtypes, as well as 4 novel anti-inflammatory drugs (AS-601245, betamethasone, narciclasin, and methylprednisolone) for the treatment of HPV-16.

Endometriosis is a chronic, estrogen-dependent, inflammatory disease with an unknown etiology. characterized by the outward development of endometrial tissue. Integrated bioinformatics analysis was implemented by Wang Z. et al. to disclose the underlying molecular mechanisms of this disease. reveals the underlying molecular mechanisms of this disease. They identified four endometriosis-specific genes, predicting 51 potential drugs and revealing immunological function associations. Endometriosis has been classified into three subtypes with distinct mechanisms and immune characteristics. This study identified the characteristic genes and new molecular subtypes of endometriosis, thereby contributing to its early diagnosis and treatment.

Lung adenocarcinoma (LUAD) is the most prevalent histological subtype of lung cancer, and regulatory cell death is an attractive target for cancer therapy. Recent research suggests that cuproptosis being a promising target for cancer therapy. Nonetheless, the function of cuproptosis-related genes (CRGs) in the LUAD process remains unknown. Wang S. et al. found that DLD, LIAS, PDHB, DLAT, and LIPA1 were central genes in 10 differentially expressed CRGs enriched in mitochondrial respiration-dependent cell death, providing insights for treatment and immunotherapy drugs targeting cuproptosis.

A member of the transcriptional enhancer factor (TEF) family of transcription factors, TEA domain transcription factor 4 (TEAD4) is linked to the development and progression of several malignancies, including lung adenocarcinoma (LUAD). Nonetheless, the role of this gene in the progression of LUAD unclear. Gong et al. via gene analysis found that TEAD4 was substantially correlated with LUAD patients' poor prognosis. Moreover, there was a robust correlation between high TEAD4 expression and immunotherapeutic resistance. This study revealed that TEAD4 is a predictor of prognosis related to immune regulation and a novel therapeutic target for LUAD.

A very diverse malignant carcinoma is gastric cancer (GC). Lin et al. used exosome-based classification to help tailor treatment for gastric cancer (GC). They created an exosome-based gene signature and assessed immunological characteristics, immune checkpoint inhibitor responses, and genetic changes utilizing computational techniques. There were two clusters of exosome-relevant phenotypes (A and B), and phenotype B had a worse prognosis and an inflammatory tumor microenvironment (TME) than phenotype A. The exosome-based gene signature predicted GC prognosis and genomic changes. This research provides a conceptual framework to better understand the functions of exosomes in immune escape mechanisms and GC genomic changes.

Ferroptosis, an iron-dependent necrosis in cancer, is associated with poor prognosis, inflammatory tumor microenvironment, and susceptibility to chemotherapeutic drugs. A systematic analysis by Xiao et al. identified subtypes and highlights the potential for tailored care. The PCA computational approach was used to create the ferroptosis index. It was found that there were strong correlations between clinicopathological features and FPI. High FPI was also associated with a poor prognosis, an inflammatory tumor microenvironment (TME), and high susceptibility to chemotherapeutic drugs.

A growing body of research has shown the biological significance of oxidative stress in the tumorigenicity and progression of colorectal cancer (CRC). In their study, Cao et al. developed an oxidative stress-related signature to predict clinical outcomes and therapeutic responses in colorectal cancer patients. The signature was associated with defined genes as ACOX1, CPT2, and UCN, and showed potential for survival prediction. This could improve prognosis and adjuvant therapy decisions. Cao et al. work created an oxidative stress-related signature that can potentially improve prognosis prediction and adjuvant therapy decisions.

Prostate cancer (PRAD) is a deadly disease with drug resistance and poor prognosis. Li et al. studied somatic mutations, somatic copy-number changes (SCNAs), DNA methylation, and mRNA expression in multi-omics profiling for G protein-coupled receptors (GPCRs) in the primary PRAD patients, identifying four potential medicines and novel biomarkers for treatment. These findings from the multi-omics analysis of GPCRs offer fresh perspectives on the underlying mechanisms of primary PRAD and the potential of GPCRs in the creation of PRAD-specific treatment approaches.

Tumor resistance to therapy remains a significant barrier, primarily due to intratumoral heterogeneity. Single cell profiling tools can identify clones with similar characteristics, potentially improving long-term therapeutic response in brain tumors. Murdaugh and Anastas in their review investigated the potential for single cell multi-omic analyses to reveal mechanisms of glioma resistance to therapy and discussed opportunities to apply these methods to enhance long-term therapeutic response in pediatric high-grade glioma with few treatment options.

3 Conclusion

In conclusion, this Research Topic has provided original research and updated reviews of early-stage researchers related

to multi-omics research in cancer etiology, and therapy. Our knowledge of the pathophysiology of many types of cancers and new treatment options are both furthered by these investigations. The evidence collected from this Research Topic is also expected to be translated into more precise and practical clinical approaches to predict and treat relevant human disorders in the future.

Author contributions

All authors listed have made a substantial, direct, and intellectual contribution to the work and approved it for publication.

Conflict of interest

The authors declare that the research was conducted in the absence of any commercial or financial relationships that could be construed as a potential conflict of interest.

Publisher's note

frontiers | Frontiers in Oncology

ORIGINAL RESEARCH
published: 28 April 2022
doi: 10.3389/fonc.2022.870820

High N-Cadherin Protein Expression in Ovarian Cancer Predicts Poor Survival and Triggers Cell Invasion

Mourad Assidi [1,2*]

[1] Center of Excellence in Genomic Medicine Research, King Abdulaziz University, Jeddah, Saudi Arabia, [2] Medical Laboratory Department, Faculty of Applied Medical Sciences, King Abdulaziz University, Jeddah, Saudi Arabia

Ovarian cancer (OC) is among the most lethal cancer among all gynaecological malignancies. Since most OC patients are diagnosed only at advanced stages mainly because of their imperceptible/nonspecific symptoms, survival rates are low. Therefore, more molecular biomarkers are needed to achieve more effective molecular stratification for better prognostic and theranostic outcomes. The cadherin family, particularly N-cadherin (N-CAD; also known as CDH2), is critical for cell-cell adhesion and epithelial-mesenchymal transition (EMT) of cancer. N-CAD protein has also been shown to be overexpressed in many advanced carcinomas. The aim of this study was to investigate the expression patterns of N-CAD protein, determine their correlations with the clinicopathological features of OC patients, and evaluate its prognostic value and involvement in EMT and metastasis. Protein expression of N-CAD was studied in 117 formalin-fixed and paraffin-embedded (FFPE) blocks from patients diagnosed with OC using Tissue Microarray and immunohistochemistry techniques. The N-CAD protein was overexpressed in 58% of our OC cohort. Furthermore, its cytoplasmic overexpression was significantly correlated with tumor grade (p= 0.05), tumor subtype (p= 0.05), tumor necrosis (p= 0.01), and age at menarche (p= 0.002). Interestingly, Kaplan-Meier analysis showed a significant correlation of disease-free survival (DFS) with OC patients with cytoplasmic N-CAD overexpression (p< 0.03, log rank). Patients with high N-CAD expression have approximately twice the recurrence rate at 5-year follow-up. The results of this study demonstrate a poor prognostic role of N-CAD overexpression in OC, which is reflected in higher recurrence and death rates of OC and its molecular contribution to EMT and distant metastasis. Therefore, OC patients with overexpressed N-CAD need to be monitored more frequently and closely. Further studies with larger patient cohorts are needed to validate these findings, demystify the role of N-CAD in OC pathophysiology, and further investigate its role as a potential therapeutic target.

Keywords: N-Cadherin, ovarian cancer, immunohistochemistry, prognosis, EMT, tissue microarray, survival

OPEN ACCESS

Edited by:
Essa M. Saied, Humboldt University of Berlin, Germany

Reviewed by:
Andrew Lindsay, University College Cork, Ireland
Evangeli S. Lampri, University of Ioannina, Greece
Cristiana Simionescu, University of Medicine and Pharmacy of Craiova, Romania

***Correspondence:**
Mourad Assidi
mourad.assidi@gmail.com

Specialty section:
This article was submitted to Pharmacology of Anti-Cancer Drugs, a section of the journal Frontiers in Oncology

Received: *07 February 2022*
Accepted: *04 April 2022*
Published: *28 April 2022*

Citation:
Assidi M (2022) High N-Cadherin Protein Expression in Ovarian Cancer Predicts Poor Survival and Triggers Cell Invasion. Front. Oncol. 12:870820. doi: 10.3389/fonc.2022.870820

INTRODUCTION

Ovarian cancer (OC) is the 7th most common cancer in women and the 3rd deadliest gynaecological cancer worldwide (1). In Saudi Arabia, OC affects more than 3% of Saudi women (2–4). This higher mortality rate of OC worldwide seems to be related to the fact that this malignant disease is asymptomatic, especially at early stages (5). In addition, most OC symptoms are nonspecific, misleading and may be confused with other gastrointestinal, urologic, or other diseases (6). Pelvic or abdominal pain and abdominal distension, increased urinary frequency, and some eating disorders such as early satiety are the common OC symptoms in the early stages, while women with advanced stages have a pelvic mass that extends beyond the adnexa (7). OC is classified according to the cellular origin of the malignancy, i.e., epithelial, stromal, or germinal cells. Of note, the vast majority (90%) of OC is of epithelial origin (8). Standard treatment options for OC depend on the type and stage of OC and include surgery along with platinum-based chemotherapy such as carboplatin and paclitaxel, either adjuvant, neoadjuvant, or sometimes both (9). Although 80% of patients diagnosed at an early stage respond to first-line chemotherapy, efficient early diagnosis of OC is still unattainable.

Since most OC patients are not diagnosed until the stage of metastasis, treatment options are not effective enough and are more diverted towards to alleviating symptoms rather than curing the disease. In fact, the 5-year survival rate for OC patients diagnosed with advanced stage disease is about 30% compared to 93% for early stage counterparts (10). Additionally, most OC patients relapse after completion of first-line treatment and require retreatment, mainly with chemotherapy (11). Despite, standard therapies are widely used in the treatment of OC, the prognosis and survival of OC are still poor. In addition, current management and treatment options are challenged by OC heterogeneity, in which a cluster of multiple cells with different genetic and epigenetic features occurs in the same ovarian malignant mass. Furthermore, individuals at the same stage of OC and treated with the same treatment plan have different outcomes. Taken together, these findings highlight the current challenges in optimizing/personalizing current therapeutic strategies for better outcomes (12, 13) and underscore the urgent need for additional effective biomarkers for earlier detection, better prognosis, and more accurate stratification of patients to achieve better individualized treatment options and survival outcomes.

Carbohydrate antigen 125 (CA125) is the first biomarker discovered for the detection of OC. Its level in serum is elevated in most epithelial OC (14). However, the sensitivity of CA125 in OC early stages remains too low, and its level correlates with other diseases such as endometriosis, pregnancy, ovarian cysts, and inflammatory peritoneal diseases. To improve the specificity of OC detection, other biomarkers such as Human Epididymis Protein 4 (HE4) have been developed. HE4 is more sensitive than CA125 and is found in approximately 100% of serous and endometroid subtypes, but its concentration can be influenced by many factors such as body mass index (BMI) (15), smoking (16), and lower HE4 concentration in patients using oral contraceptives (17). Although the combination of CA125 and HE4 has been shown to provide better diagnostic efficacy for risk prediction of OC (18), they are still not accurate and effective enough. More molecular biomarkers are needed to achieve better prognostic, therapeutic and prediction results. Cadherins are important transmembrane glycoproteins that are critical for cell-cell adhesion, especially in epithelial tissues. They were first described as single-pass transmembrane glycoproteins involved in cell–cell adhesion, and are now considered important players in cell polarity and tissue morphology (19). They are also thought to play a direct role in carcinogenesis and metastasis in many cancers (20, 21). In some cases of epithelial carcinoma, epithelial cells lose cell-cell adhesion and polarity and develop migratory and invasive behavior. This process, termed epithelial-mesenchymal transition (EMT), is critical for the development of metastases in cancer progression. A fundamental event in EMT is the "cadherin switch", defined as loss of E-cadherin expression and increased expression of N-cadherin during cancer progression (22, 23). N-cadherin, also known as CDH2, is a cell-adhesion molecule mapped to 18q11.2 (24). It is a 135 KDa protein that belongs to the family of transmembrane molecules and mediates calcium- dependent intercellular adhesion. It consists of five extracellular cadherin repeats. The cytoplasmic domain of N-cadherin is anchored to the intercellular actin cytoskeleton by interaction with the β-, α-, and γ-catenin complex. *CDH2* is expressed in various tissues, including the nervous system, brain, cardiac and skeletal muscles, blood vessels, and hematopoietic function (25, 26). N-cadherin is mainly expressed in the nervous system and promotes intercellular adhesion of neuronal cells, while its expression is low in normal tissues (25–29). However, it has been reported that overexpressed N-cadherin is associated with cell migration, angiogenesis, aggressiveness, and metastasis in many cancers such as breast, lung, bladder, prostate, and hepatocellular carcinomas (25–29). Moreover, the level of soluble N-cadherin in the serum of cancer patients is much higher than that in healthy individuals. As a result, N-cadherin has been suggested as a potential therapeutic target for tumour invasion and metastasis (30). In OC, the role of N-cadherin expression is unclear and there are few studies that have investigated N-cadherin expression in OC (31), especially in the Arabian peninsula. With this background, this study aimed to evaluate N-CAD protein expression patterns as a potential pro-metastatic molecular biomarker that could help improve OC prognosis and management. The associations between N-CAD protein expression patterns with patients' clinicopathological parameters and its prognostic value in OC were investigated.

PATIENTS AND METHODS

Patients

Formalin-fixed, paraffin-embedded (FFPE) tissues from patients diagnosed with OC and treated mainly at the departments of pathology and gynaecology at King Abdulaziz University Hospital (KAUH) between 1995 and 2014 were used for this

study after obtaining informed consent. This retrospective study includes 117 primary OC patients classified based on histopathological features, mainly according to Tumor Node Metastasis (TNM) classification system. Patients' medical records were used to collect all pathological and clinical data after IRB approval from KAUH (IRB number: KAUH-189-14).

Tissue Microarray and Automated Immunostaining

Our group had previously transferred the OC FFPE tissue samples into a tissue microarray (TMA) format. Haematoxylin and Eosin (H&E) from each block (donor block) were used to determine tumor regions. Subsequently, all H&E stained slides from all blocks were reviewed by a pathologist to select the tumour areas to be punched/cored. The details of TMA construction mapping, and validation have been described elsewhere (32, 33).

Immunohistochemistry (IHC) was performed on ovarian cancer TMA slides using an automated staining system (Benchmark XT, Ventana Medical System, Inc. Tucson, Arizona, USA), except for antibodies, which they were applied manually. Reagents were removed from the refrigerator to reach room temperature before starting the run. The slides were labelled with a barcode. The concentrated N-CAD rabbit polyclonal antibody (catalog # ab66025, Abcam, dilution: 1:20) was used. The detailed protocol of the IHC procedure was performed as described elsewhere (32, 34). Briefly, the automated Ventana began the run by deparaffinizing the paraffin-embedded tissue sections with EZ Prep™. They were then pre-treated with Cell Conditioning buffer (CC1) to induce/activate the epitopes of the antigens (antigen retrieval). Then, 50µl of the optimized antibody was applied manually for 30 minutes at room temperature. This was followed by washing steps using the UltraView Universal DAB Detection Kit (Lot. No. E00534) which, contains: Copper, 1.1% hydrogen peroxide solutions, DAB substrate, SA-HRP contains a conjugated streptavidin horseradish peroxidase solution and inhibitor. For counterstaining, staining was completed with hematoxylin II for 8 min. and post-counterstaining by bluing reagent for 4 min.

After completion of the run, the slides were removed from the instrument and rinsed with a mild detergent followed by tap water to remove LCS and buffer residue. Then the slides were immersed in different concentrations of alcohol buffer (70, 95 and 100%) and then cleaned in xylene, for 3 minutes, twice for each solution. Finally, a drop of mounting medium was added to the slide and covered with a glass coverslip. The stained slides were manually scored to check the expression of the biomarkers under the light microscope using the staining patterns.

Scoring and Evaluation of Biomarkers Expression

Evaluation of protein expression of all OC was assessed using a regular Nikon light microscope at ×40 magnification blind to the clinicopathological parameters of the patients. The staining was classified into four groups: 1) negative 2) weak 3) moderate and 4) high expression. The intensity of staining and the percentage of positively stained cells were used to calculate the staining index score according to the following formula

$$I = 0xf0 + 1xf1 + 2xf2 + 3xf3$$

Where (I) is the staining index score and (f0 to f3) are the proportions of cells that have a given staining intensity (from 0 to +3) (33, 35). This I score is useful for the selection of the best IHC expression cut-off/discriminator during statistical analysis.

Statistical Analysis

Statistical analyses were performed using the SPSS® software package (version 22). The frequency tables were analyzed using the chi-square test to assess the significance of the correlation between the categorical variables (age, stage, grade, BMI, lymph node status, recurrence, …).

Univariate survival analysis was performed using the Kaplan-Meier method. Tests with $p < 0.05$ were considered statistically significant.

RESULTS

Expression Pattern of N-Cadherin Protein Profiles in Ovarian Cancer

Expression of N-cadherin protein was observed in both membrane and cytoplasm, but mainly in cytoplasm. The frequencies of expression patterns of cytoplasmic N-cadherin protein receptors in 117 OC samples evaluated by the IHC technique were: no expression (0, 3%), weak expression (+1, 39%), moderate expression (+2, 44%) and strong expression patterns (+3, 14%), respectively (**Figure 1**).

Correlation Of Cytoplasmic N-Cadherin Protein Expression With Clinicopathological Features

Our data showed that cytoplasmic N-cadherin expression was not associated with age, lymph node involvement, and tumor stage. However, significant correlations were found with tumor grade, tumor subtype, tumor necrosis, and age at menarche. In poorly differentiated tumors, expression of N-Cad was low compared to well/intermediately differentiated tumors (p= 0.05). Among histological subtypes, serous tumors showed low N-CAD expression compared to mucinous/other subtypes that showed high expression of N-CAD profile (p= 0.05). On the other hand, OC tissues with tumor necrosis showed high N-cad expression compared to their counterparts (p= 0.01). Interestingly, OC patients with early onset of menarche had tumors with high N-cad expression (p= 0.002) (**Table 1**).

Correlation Of Cytoplasmic N-Cadherin Protein Expression With Survival Outcome

Throughout the follow-up period, univariate survival analyses with a cut-off point for N-cad expression (low (0, 1+) vs. high expression (2+,3+)) as a discriminator showed the best prognosis. Thus, at 5 years, disease recurrence occurred in 42% of patients whose OC tissues had low N-cad expression

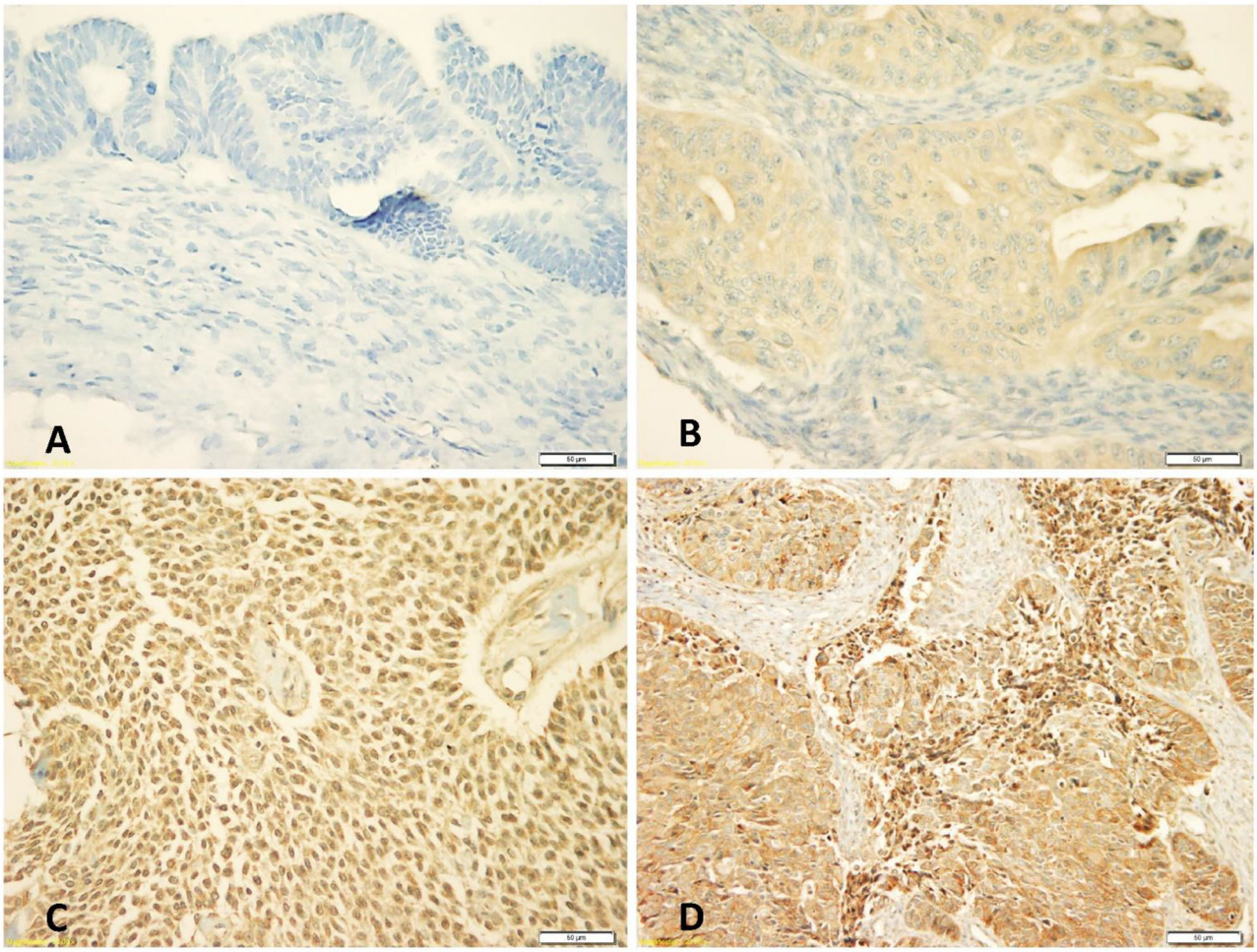

FIGURE 1 | Immunohistochemical staining patterns of cytoplasmic N-cadherin protein expression at 40x magnification: **(A)** Negative cytoplasmic expression, **(B)** Weak cytoplasmic expression, **(C)** Moderate cytoplasmic expression, **(D)** Strong cytoplasmic expression.

compared with approximately 78% of patients whose OC tissues had high N-cad protein expression ($p < 0.03$, log rank, **Figure 2**). On the other hand, the same trend was observed with less significance in patients who died from the disease. Using the same cut-off point described above, approximately 22% of patients whose OC tissues had low N-cad expression died compared to approximately 60% of patients who had high N-CAD expression in their OC tissues (p=0.1, log rank, **Figure 3**). The Kaplan-Meier survival curves clearly show that shorter survival was associated with high N-cad protein expression, while patients with low N-cad expression had a lower recurrence rate and thus longer survival.

DISCUSSIONS

In 2021, more than 21,000 new cases were diagnosed with OC worldwide, and about 13,770 patients have died from this deadly disease (36). Several factors are believed to contribute to this increasing incidence and higher mortality rates. Apart from the difficulty of detecting the disease at early stages, the OC treatment options are not very effective at advanced stages, mainly because of the heterogeneity and complexity of this malignant disease. The higher complexity of OC is the result of various intertwined genetic and epigenetic factors that lead to aberrant gene expression and inconsistent treatment outcomes (37). In conjunction with clinicopathological factors such as age, grade, stage, and lymph node invasion, OMICs tools have provided an unprecedented understanding of the molecular complexity and disease progression of the diseases. In particular for OC, many genes have been reported as mutated, including *BRCA1, BRCA2, BRIP1, RAD51C, RAD51D, MSH2, MLH1, PMS2*, and *MSH6*. These and other candidate genes have been associated with a higher risk of OC (38, 39). Despite numerous efforts to identify reliable OC biomarkers, early detection strategies still rely mainly on CA125 and HE4, which have not been shown to be specific and sensitive enough (40, 41). Therefore, additional efforts are needed to develop new

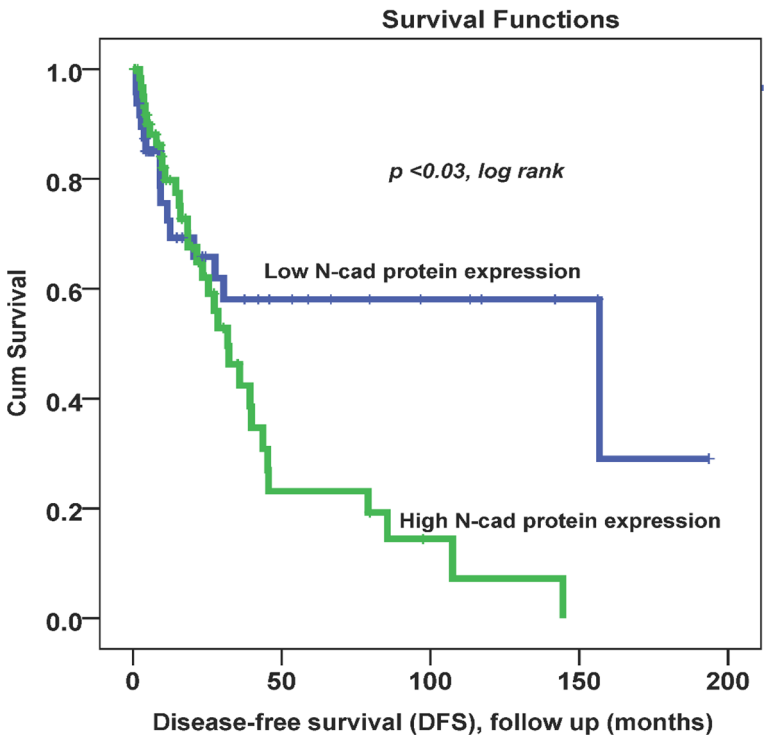

FIGURE 2 | Cytoplasmic N-cadherin expression patterns in OC cohort using the cut-off (low (0, 1+) vs. high (2+, 3+)) as a determinant of disease-free survival (DFS) in univariate (Kaplan-Meier) analysis ($p < 0.03$, log-rank).

theranostic tools that can alleviate the suffering of OC patients and improve the treatment of the disease. Currently, the focus is on identifying more effective and clinically useful prognostic markers at the genomic and proteomic levels to detect OC at an early, curable stage and potentially support therapeutic decision making. In this regard, N-CAD has been reported to be expressed in several cancer types and has been associated with several clinicopathological parameters as well as survival outcomes. However, the clinical and prognostic significance of N-CAD in OC has not been well studied, especially in the Arabic Peninsula. Therefore, we conducted this study to investigate the N-CAD expression patterns and evaluate its prognostic value in our cohort of OC patients.

Our study showed that the protein N-CAD was expressed mainly in the cytoplasm of 58% of our patients' tumor cells, with a recorded expression also in the cell membrane. Similarly, Quattrocchi et al. reported that 99% (158 cases) of their OC cohort expressed N-CAD protein in the cytoplasm (42). However, other studies reported membranous N-CAD expression in 32% of their cohort (43). These discrepancies could be due to cohort size, ethnicity, proportion of histological subtypes, and the complicated molecular heterogeneity of OC within each subtype (44).

The results of this study showed also that the expression of N-CAD protein was significantly associated with some clinicopathological characteristics including histological subtype, grade, tumor necrosis and age of menarche ($p< 0.05$) (**Table 1**). These findings are consistent with many studies that reported significant correlations of N-CAD expression in OC with histologic subtypes (45, 46) and grade (45). On the other hand, they found a significant association between N-CAD protein expression and tumor stage, which is not confirmed by our results. Furthermore, and in agreement with our results, other studies on OC reported no significant correlation between the expression of N-CAD and other clinicopathological parameters such as tumor stage, patient's age, BMI, and tumor size (43, 47). Our results showed that 57% of our patients' cohort were below 50 years (**Table 1**). There is a noticeable early onset of OC in the Saudi population compared to the United Kingdom for example where, according to Cancer Research UK, 53% of OC cases were diagnosed at 65 and over. Possible reasons associated to genomic, environmental and lifestyle factors deserve to be investigated to explain this early onset phenomenon.

In Kaplan-Meier survival analysis, N-CAD protein expression was significantly associated with DFS (p=0.03). In fact, patients with higher N-CAD expression have approximately twice the recurrence rate at 5-year follow-up time (42% vs. 78% recurrence at 60 months; $p < 0.03$, log rank, **Figure 2**). A similar trend was also observed with lower significance for DSS, in which patients with higher N-CAD expression who died more rapidly from the disease compared with their counterparts with low N-CAD

TABLE 1 | Correlation between cytoplasmic N-cadherin protein expression patterns and clinicopathological features of OC.

Patients features	Number of cases (%)	Cytoplasmic N-cadherin Protein Expression patterns: N (%)		*p*-value
		Low Expression (0, 1+)	High Expression (2+, 3+)	
Age				
< 50	67 (57%)	26 (39%)	41 (61%)	0.62
> 50	49 (42%)	24 (49%)	25 (51%)	
Missing	1 (1%)			
Tumor size				
1-5 cm	25 (21%)	12(48%)	13 (52%)	0.90
6-10 cm	30 (26%)	13 (43%)	17 (57%)	
>10 cm	57 (49%)	23 (41%)	34 (59%)	
Missing	5 (4%)			
Histological subtype				
Serous	50 (43%)	26 (52%)	24 (48%)	0.05
Mucinous	28 (24%)	9 (32%)	19 (68%)	
Other types	35 (30%)	12 (34%)	23 (66%)	
Missing	4 (3%)			
Tumor grade				
low grade (WD)	15 (13%)	7 (47%)	8 (53%)	0.05
Intermediate	19 (16%)	5 (26%)	14 (74%)	
High grade (PD)	63 (54%)	33 (52%)	30 (48%)	
Missing	20 (17%)			
Lympho-vascular invasion				
Negative	54 (46%)	23 (43%)	31 (57%)	0.35
Positive	39 (33%)	18 (46%)	21 (54%)	
Missing	24 (21%)			
Tumor necrosis				
Negative	57 (49%)	18 (31%)	39 (69%)	0.01
Positive	45 (38%)	25 (56%)	20 (44%)	
Missing	15 (13%)			
BMI				
< 23	8 (7%)	1 (13%)	7 (87%)	0.43
23-26	28 (24%)	10 (36%)	18 (64%)	
> 26	52 (44%)	25 (48%)	27 (52%)	
Missing	29 (25%)			
Age of menarche				
< 13	19 (16%)	1 (5%)	18 (95%)	0.002
> 13	67 (57%)	36 (54%)	31 (46%)	
Missing	31 (27%)			
Tumor stage				
Low stage (I,II)	41 (35%)	19 (46%)	22 (54%)	0.77
High stage (III,IV)	66 (56%)	28 (43%)	38 (57%)	
Missing	10 (9%)			
Recurrence status				
None	51 (44%)	21 (41%)	30 (59%)	0.71
Yes	36 (31%)	14 (39%)	22 (61%)	
Missing	30 (25%)			

Red p-values are statistically significant.

expression (**Figure 3**). In general, the Kaplan-Meier survival curves clearly show that shorter survival and higher recurrence rates were associated with overexpression of the N-CAD protein. These results are consistent with those of Quattrocchi *et al.*, who reported that all patients in their cohort with N-CAD overexpression relapsed by the first year of follow-up time. In the same study, patients with higher E-CAD expression survived shorter than their counterparts with lower N-CAD expression (42). Two important meta-analysis studies using all published data and freely available sources about N-Cadherin showed similar survival outcomes as our results. In fact, they confirmed that N-CAD overexpression is a negative prognosticator of OC (48, 49). When we assessed the freely available KM plotter analysis of TCGA database (https://kmplot.com/analysis/), it appears that this platform did not cover the N-Cadherin protein expression (CDH2) in OC. However, the mRNA data showed that *CDH2* gene expression is a good prognosticator of OC (50) (http://kmplot.com/analysis/index.

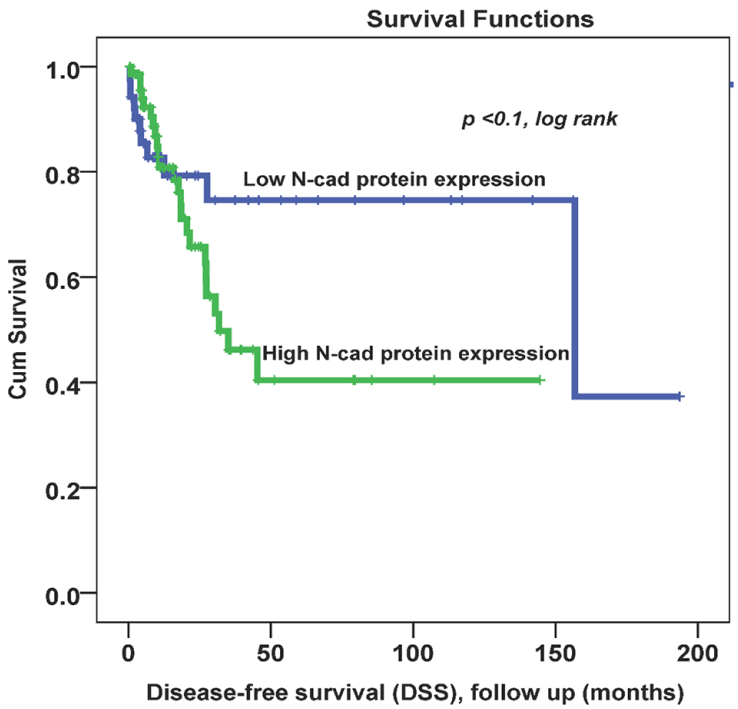

FIGURE 3 | Cytoplasmic N-cadherin expression patterns in OC cohort using the cut-off (low (0, 1+) vs. high (2+, 3+)) as a determinant of disease -specific survival (DSS) in univariate (Kaplan-Meier) analysis ($p < 0.1$, log-rank).

php?p=service). For the protein Atlas database (https://www.proteinatlas.org), the CDH2 protein was not a significant prognosticator in OC possibly due to the heterogeneity of the cohort (51) (https://www.proteinatlas.org/ENSG00000170558-CDH2/pathology).

The survival data indicated that poor disease progression associated with high N-CAD protein expression appears to be either a marker of OC aggressiveness or actively involved in the pathophysiology of disease progression, recurrence, and metastasis. Similar studies in other cancers (breast, lung, bladder, prostate, …) confirmed that overexpression of N-CAD protein was associated with poor treatment outcomes, cell migration, angiogenesis, disease aggressiveness, and metastasis (25–29). Thus, overexpression of N-cadherin in colorectal cancer was significantly associated with poor disease-specific survival and disease-free survival, as well as with many clinicopathological characteristics such as tumor size, lymph node, stage, and grade (52). Similarly, high expression of N-cadherin in bladder cancer was shown to be associated with grade, tumor stage, and poorer recurrence- free survival (53).

Taken together, these results seem to be related to the role of N-CAD in the mesenchymal phenotype, which promotes cell mobility and invasion (31, 54). In fact, several reports have shown that when epithelial tumor cells switch from expressing E-CAD to expressing N-CAD (cadherin switch phenomenon), they acquire the ability to activate Fibroblast Growth Factor Receptor (FGFR) pathways. Our results together with our previous study about E-Cad expression in the same cohort confirmed the cadherin switch (32). In fact, while the E-CAD expression was decreasing at the advanced stages (starting from the EMT and marked by cancer invasion and migration), the N-CAD expression was increasing; and both markers were prognosticators of poor survival outcomes (32). In fact, once N-CAD is overexpressed, it has been shown to affect tumor cell polarity and behavior through its direct interaction with the FGFR, which regulates cancer cell motility and invasion (55, 56). Also, N-CAD was reported to interact with other receptors on tumor cells to promote motility and migration such as Platelet Derived Growth Factor Receptor (PDGFR). This mechanism occurs when the NHERF protein binds the N-CAD with the ß-catenin to the PDGFR to form a complex that drives tumor cells to migrate and motility (56) (**Figure 4**). These molecular mechanisms of N- CAD protein overexpression, summarized in **Figure 4**, played a key role in the phenotypic changes of tumor cells that were actively involved in migration to distant metastases. This pro-metastatic role of N-CAD was also confirmed *in vitro* with epithelial cells engineered to overexpress N-CAD. These cells have been shown to alter their morphology and behavior, adopting a motile phenotype similar to that observed in cells undergoing EMT (57, 58). This pro-metastatic phenotype depends also on the expression of other interacting proteins in addition to N- CAD, as mentioned previously and summarized in **Figure 4** (58, 59).

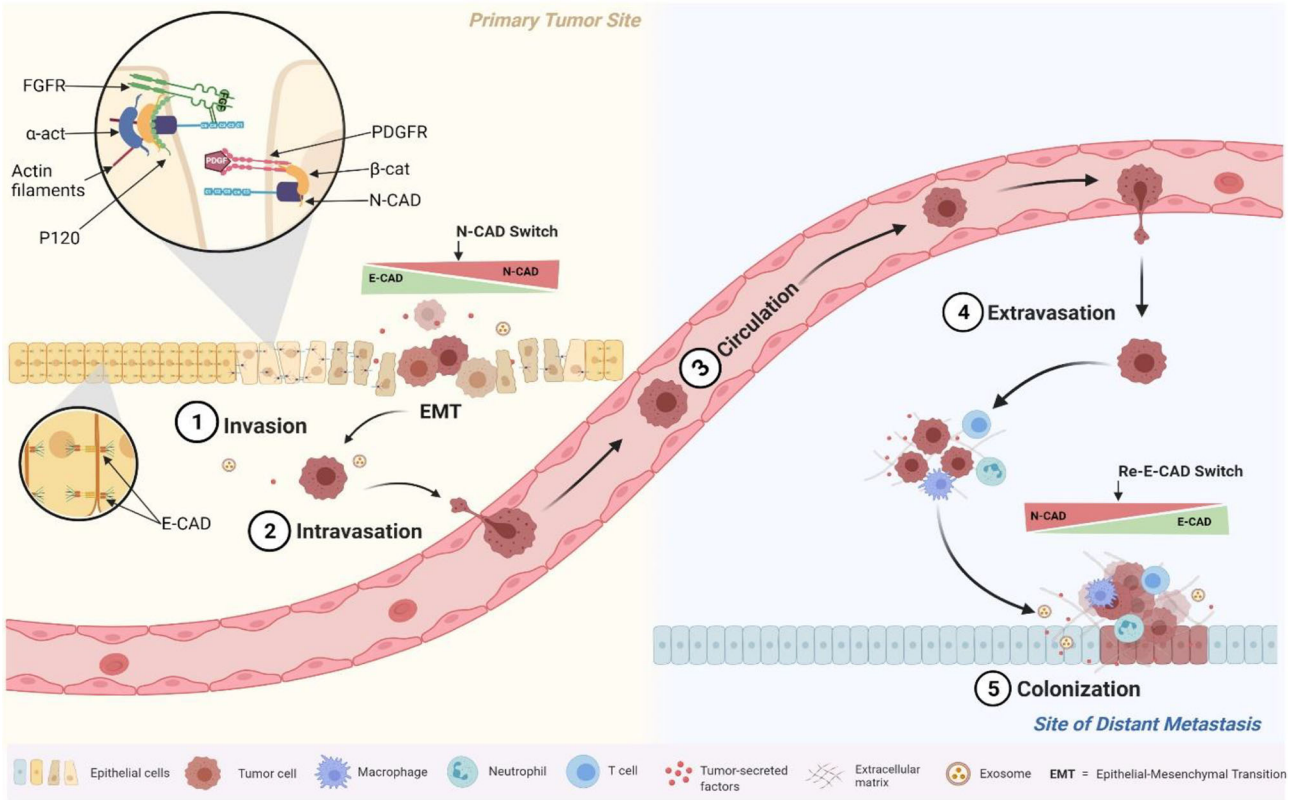

FIGURE 4 | Schematic illustration of the molecular and cellular events triggered by the N-cadherin switch at EMT. Overexpressed N-cadherin binds and stabilizes FGFR on the cell surface to initiate cell signalling cascades, and to PDGFR to increase cell motility through interactions with ß-catenin.

This study demonstrated a prognostic role of N-CAD in OC, the first to be reported in the Arabic Peninsula. OC patients overexpressing the N-CAD protein had a poor prognosis, as evidenced by higher rates of both OC recurrence and death, as well as its molecular contribution in EMT and distant metastasis; and thus required more frequent and closer follow-up. Further studies with larger patient cohorts are needed to validate these findings, investigate further the role of N-CAD in OC pathophysiology, and explore its role as a potential therapeutic target.

DATA AVAILABILITY STATEMENT

The original contributions presented in the study are included in the article/supplementary material. Further inquiries can be directed to the corresponding author.

ETHICS STATEMENT

The study was approved by the Institutional Ethical Review Board of King Abdulaziz University Hospital, Jeddah, Saudi Arabia (Ref. number: KAUH-189-14). The patients/ participants provided their written informed consent to participate in this study.

AUTHOR CONTRIBUTIONS

The author confirms being the sole contributor of this work and has approved it for publication.

FUNDING

This work was funded by the Deanship of Scientific Research (DSR), King Abdulaziz University, Jeddah, under grant No. (D-545-117-1443). The author, therefore, gratefully acknowledges the DSR technical and financial support.

ACKNOWLEDGMENTS

The author is grateful to Prof. Abdelbaset Buhmeida, MD., PhD. for validating the IHC scoring, and for F. Yahya and Dr. P. N. Pushparaj for exporting **Figure 4** using Biorender.com.

REFERENCES

1. Momenimovahed Z, Tiznobaik A, Taheri S, Salehiniya H. Ovarian Cancer in the World: Epidemiology and Risk Factors. *Int J women Health* (2019) 11:287–99. doi: 10.2147/IJWH.S197604
2. Ferlay J, Ervik M, Lam F, Colombet M, Mery L, Piñeros M, et al. *Saudi Arabia Fact Sheets. Lyon, France: International Agency for Research on Cancer (IARC).* (2018).
3. Al-Zahrani AS, Al-Mutlaq HM, Radwi AN, Bazarbashi SM. *Cancer Incidence Report Saudi Arabia 2013 Riyadh, Saudi Arabia: National Health Information Center.* (2016).
4. Althubiti MA, Nour Eldein MM. Trends in the Incidence and Mortality of Cancer in Saudi Arabia. *Saudi Med J* (2018) 39(12):1259–62. doi: 10.15537/smj.2018.12.23348
5. Shabir S, Gill PK. Global Scenario on Ovarian Cancer – Its Dynamics, Relative Survival, Treatment, and Epidemiology. *Adesh Univ J Med Sci Res* (2020) 2:17–25. doi: 10.25259/aujmsr_16_2019
6. Olson SH, Mignone L, Nakraseive C, Caputo TA, Barakat RR, Harlap S. Symptoms of Ovarian Cancer. *Obstet Gynecol* (2001) 98(2):212–7. doi: 10.1016/s0029-7844(01)014570
7. Goff B. Symptoms Associated With Ovarian Cancer. *Clin Obstet Gynecol* (2012) 55(1):36–42. doi: 10.1097/GRF.0b013e3182480523
8. Holschneider CH, Berek JS. Ovarian Cancer: Epidemiology, Biology, and Prognostic Factors. *Semin Surg Oncol* (2000) 19(1):3–10. doi: 10.1002/1098-2388(200007/08)19:1<3
9. Colombo N, Sessa C, du Bois A, Ledermann J, McCluggage WG, McNeish I, et al. Esmo-Esgo Consensus Conference Recommendations on Ovarian Cancer: Pathology and Molecular Biology, Early and Advanced Stages, Borderline Tumours and Recurrent Disease†. *Ann Oncol* (2019) 30(5):672–705. doi: 10.1093/annonc/mdz062
10. Siegel RL, Miller KD, Jemal A. Cancer Statistics, 2020. *CA Cancer J Clin* (2020) 70(1):7–30. doi: 10.3322/caac.21590
11. Pujade-Lauraine E, Wagner U, Aavall-Lundqvist E, Gebski V, Heywood M, Vasey PA, et al. Pegylated Liposomal Doxorubicin and Carboplatin Compared With Paclitaxel and Carboplatin for Patients With Platinum-Sensitive Ovarian Cancer in Late Relapse. *J Clin Oncol* (2010) 28(20):3323–9. doi: 10.1200/jco.2009.25.7519
12. Minlikeeva AN, Freudenheim JL, Cannioto RA, Eng KH, Szender JB, Mayor P, et al. History of Thyroid Disease and Survival of Ovarian Cancer Patients: Results From the Ovarian Cancer Association Consortium, a Brief Report. *Br J Cancer* (2017) 117(7):1063–9. doi: 10.1038/bjc.2017.267
13. Testa U, Petrucci E, Pasquini L, Castelli G, Pelosi E. Ovarian Cancers: Genetic Abnormalities, Tumor Heterogeneity and Progression, Clonal Evolution and Cancer Stem Cells. *Medicines* (2018) 5(1):16. doi: 10.3390/medicines5010016
14. Cannistra SA. Cancer of the Ovary. *N Engl J Med* (2004) 351(24):2519–29. doi: 10.1056/NEJMra041842
15. Bolstad N, Øijordsbakken M, Nustad K, Bjerner J. Human Epididymis Protein 4 Reference Limits and Natural Variation in a Nordic Reference Population. *Tumour Biol* (2012) 33(1):141–8. doi: 10.1007/s13277-011-0256-4
16. Fortner RT, Vitonis AF, Schock H, Hüsing A, Johnson T, Fichorova RN, et al. Correlates of Circulating Ovarian Cancer Early Detection Markers and Their Contribution to Discrimination of Early Detection Models: Results From the Epic Cohort. *J Ovarian Res* (2017) 10(1):20–. doi: 10.1186/s13048-017-0315-6
17. Ferraro S, Schiumarini D, Panteghini M. Human Epididymis Protein 4: Factors of Variation. *Clinic Chim Acta* (2015) 438:171–7. doi: 10.1016/j.cca.2014.08.020
18. Dochez V, Caillon H, Vaucel E, Dimet J, Winer N, Ducarme G. Biomarkers and Algorithms for Diagnosis of Ovarian Cancer: Ca125, He4, Rmi and Roma, a Review. *J Ovarian Res* (2019) 12(1):28. doi: 10.1186/s13048-019-0503-7
19. Hajra KM, Fearon ER. Cadherin and Catenin Alterations in Human Cancer. *Gene Chromosomes Cancer* (2002) 34(3):255–68. doi: 10.1002/gcc.10083
20. Colás-Algora N, Millán J. How Many Cadherins Do Human Endothelial Cells Express? *Cell Mol Life Sci* (2019) 76(7):1299–317. doi: 10.1007/s00018-018-2991-9
21. Oda H, Takeichi M. Evolution: Structural and Functional Diversity of Cadherin at the Adherens Junction. *J Cell Biol* (2011) 193(7):1137–46. doi: 10.1083/jcb.201008173
22. Kalluri R, Weinberg RA. The Basics of Epithelial-Mesenchymal Transition. *J Clin Invest* (2009) 119(6):1420–8. doi: 10.1172/jci39104
23. Hazan RB, Qiao R, Keren R, Badano I, Suyama K. Cadherin Switch in Tumor Progression. *Ann N Y Acad Sci* (2004) 1014:155–63. doi: 10.1196/annals.1294.016
24. Velázquez-Fernández D, Laurell C, Geli J, Höög A, Odeberg J, Kjellman M, et al. Expression Profiling of Adrenocortical Neoplasms Suggests a Molecular Signature of Malignancy. *Surgery* (2005) 138(6):1087–94. doi: 10.1016/j.surg.2005.09.031
25. Drivalos A, Chrisofos M, Efstathiou E, Kapranou A, Kollaitis G, Koutlis G, et al. Expression of A5-Integrin, A7-Integrin, E-Cadherin, and N-Cadherin in Localized Prostate Cancer. *Urology Oncol* (2016) 34(4):165. doi: 10.1016/j.urolonc.2015.10.016
26. Saadatmand S, de Kruijf EM, Sajet A, Dekker-Ensink NG, van Nes JGH, Putter H, et al. Expression of Cell Adhesion Molecules and Prognosis in Breast Cancer. *Br J Surg* (2012) 100(2):252–60. doi: 10.1002/bjs.8980
27. Seo DD, Lee HC, Kim HJ, Min HJ, Kim KM, Lim YS, et al. Neural Cadherin Overexpression Is a Predictive Marker for Early Postoperative Recurrence in Hepatocellular Carcinoma Patients. *J Gastroenterol Hepatol* (2008) 23 (7Pt1):1112–8. doi: 10.1111/j.1440-1746.2007.05182.x
28. Muramaki M, Miyake H, Terakawa T, Kusuda Y, Fujisawa M. Expression Profile of E-Cadherin and N-Cadherin in Urothelial Carcinoma of the Upper Urinary Tract Is Associated With Disease Recurrence in Patients Undergoing Nephroureterectomy. *Urology* (2011) 78(6):1443.e7–.e12. doi: 10.1016/j.urology.2011.07.1388
29. Hui L, Zhang S, Dong X, Tian D, Cui Z, Qiu X. Prognostic Significance of Twist and N-Cadherin Expression in Nsclc. *PloS One* (2013) 8(4):e62171. doi: 10.1371/journal.pone.0062171
30. Cao Z-Q, Wang Z, Leng P. Aberrant N-Cadherin Expression in Cancer. *Biomed Pharmacoth* (2019) 118:109320. doi: 10.1016/j.biopha.2019.109320
31. Hudson LG, Zeineldin R, Stack MS. Phenotypic Plasticity of Neoplastic Ovarian Epithelium: Unique Cadherin Profiles in Tumor Progression. *Clin Exp Meta* (2008) 25(6):643–55. doi: 10.1007/s10585-008-9171-5
32. Assidi M, Jafri MA, Abu-Elmagd M, NP P, Saddick S, Messaoudi S, et al. Prognostic Value of E-Cadherin and Its Tumor Suppressor Role in Saudi Women With Advanced Epithelial Ovarian Cancer. *Libya J Med* (2021) 16 (1):1994741. doi: 10.1080/19932820.2021.1994741
33. Assidi M, Yahya FM, Al-Zahrani MH, Elkhatib R, Zari A, Elaimi A, et al. Leptin Protein Expression and Promoter Methylation in Ovarian Cancer: A Strong Prognostic Value With Theranostic Promises. *Int J Mol Sci* (2021) 22 (23):12872. doi: 10.3390/ijms222312872
34. Assidi M, Gomaa W, Jafri M, Hanbazazh M, Al-Ahwal M, Pushparaj P, et al. Prognostic Value of Osteopontin (Spp1) in Colorectal Carcinoma Requires a Personalized Molecular Approach. *Tumour Biol* (2019) 41 (9):1010428319863627. doi: 10.1177/1010428319863627
35. Buhmeida A, Dallol A, Merdad A, Al-Maghrabi J, Gari MA, Abu-Elmagd MM, et al. High Fibroblast Growth Factor 19 (Fgf19) Expression Predicts Worse Prognosis in Invasive Ductal Carcinoma of Breast. *Tumour Biol* (2014) 35(3):2817–24. doi: 10.1007/s13277-013-1374-y
36. Siegel RL, Miller KD, Fuchs HE, Jemal A. Cancer Statistics, 2021. *CA: Cancer J Clin* (2021) 71(1):7–33. doi: 10.3322/caac.21654
37. Bast RC Jr, Hennessy B, Mills GB. The Biology of Ovarian Cancer: New Opportunities for Translation. *Nat Rev* (2009) 9(6):415–28. doi: 10.1038/nrc2644
38. Suszynska M, Ratajska M, Kozlowski P. Brip1, Rad51c, and Rad51d Mutations Are Associated With High Susceptibility to Ovarian Cancer: Mutation Prevalence and Precise Risk Estimates Based on a Pooled Analysis of ~30,000 Cases. *J Ovarian Res* (2020) 13(1):50. doi: 10.1186/s13048-020-00654-3
39. Norquist BM, Harrell MI, Brady MF, Walsh T, Lee MK, Gulsuner S, et al. Inherited Mutations in Women With Ovarian Carcinoma. *JAMA Oncol* (2016) 2(4):482–90. doi: 10.1001/jamaoncol.2015.5495
40. Yurkovetsky ZR, Linkov FY, Malehorn DE, Lokshin AE. Multiple Biomarker Panels for Early Detection of Ovarian Cancer. *Future Oncol* (2006) 2(6):733–41. doi: 10.2217/14796694.2.6.733
41. Bandiera E, Zanotti L, Fabricio AS, Bucca E, Squarcina E, Romani C, et al. Cancer Antigen 125, Human Epididymis 4, Kallikrein 6, Osteopontin and Soluble Mesothelin-Related Peptide Immunocomplexed With

Immunoglobulin M in Epithelial Ovarian Cancer Diagnosis. *Clin Chem Lab Med* (2013) 51(9):1815–24. doi: 10.1515/cclm-2013-0151
42. Quattrocchi L, Green AR, Martin S, Durrant L, Deen S. The Cadherin Switch in Ovarian High-Grade Serous Carcinoma Is Associated With Disease Progression. *Virchow Arch* (2011) 459(1):21–9. doi: 10.1007/s00428-011-1082-1
43. Dochiț CM, Stepan AE, Mărgăritescu C, Florescu MM, Simionescu CE. Immunoexpression of E-, P-And N-Cadherins in Ovarian Serous Malignant Tumors. *Roman J Morpholog Embryolog* (2019) 60(4):1215–9.
44. Peralta Soler A, Knudsen KA, Tecson-Miguel A, McBrearty FX, Han AC, Salazar H. Expression of E-Cadherin and N-Cadherin in Surface Epithelial-Stromal Tumors of the Ovary Distinguishes Mucinous From Serous and Endometrioid Tumors. *Hum Pathol* (1997) 28(6):734–9. doi: 10.1016/s0046-8177(97)90184-2
45. Marques FR, Fonsechi-Carvasan GA, De Angelo Andrade LAL, Böttcher-Luiz F. Immunohistochemical Patterns for A and B-Catenin, E- and N-Cadherin Expression in Ovarian Epithelial Tumors. *Gynecol Oncol* (2004) 94(1):16–24. doi: 10.1016/j.ygyno.2004.03.037
46. Patel IS, Madan P, Getsios S, Bertrand MA, MacCalman CD. Cadherin Switching in Ovarian Cancer Progression. *Int J Cancer* (2003) 106(2):172–7. doi: 10.1002/ijc.11086
47. Adham SA, Al Harrasi I, Al Haddabi I, Al Rashdi A, Al Sinawi S, Al Maniri A, et al. Immunohistological Insight Into the Correlation Between Neuropilin-1 and Epithelial-Mesenchymal Transition Markers in Epithelial Ovarian Cancer. *J Histochem Cytochem* (2014) 62(9):619–31. doi: 10.1369/0022155414538821
48. Luo Y, Yu T, Zhang Q, Fu Q, Hu Y, Xiang M, et al. Upregulated N-Cadherin Expression Is Associated With Poor Prognosis in Epithelial-Derived Solid Tumours: A Meta-Analysis. *Eur J Clin Invest* (2018) 48(4):e12903. doi: 10.1111/eci.12903
49. Mrozik KM, Blaschuk OW, Cheong CM, Zannettino ACW, Vandyke K. N-Cadherin in Cancer Metastasis, Its Emerging Role in Haematological Malignancies and Potential as a Therapeutic Target in Cancer. *BMC Cancer* (2018) 18(1):939. doi: 10.1186/s12885-018-4845-0
50. Gyorffy B, Lánczky A, Szállási Z. Implementing an Online Tool for Genome-Wide Validation of Survival-Associated Biomarkers in Ovarian-Cancer Using Microarray Data From 1287 Patients. *Endoc-Relate Cancer* (2012) 19(2):197–208. doi: 10.1530/erc-11-0329
51. Uhlén M, Fagerberg L, Hallström BM, Lindskog C, Oksvold P, Mardinoglu A, et al. Tissue-Based Map of the Human Proteome. *Science* (2015) 347 (6220):1260419. doi: 10.1126/science.1260419
52. Yan X, Yan L, Liu S, Shan Z, Tian Y, Jin Z. N-Cadherin, a Novel Prognostic Biomarker, Drives Malignant Progression of Colorectal Cancer. *Mol Med Rep* (2015) 12(2):2999–3006. doi: 10.3892/mmr.2015.3687
53. Abufaraj M, Shariat SF, Haitel A, Moschini M, Foerster B, Chłosta P, et al. Prognostic Role of N-Cadherin Expression in Patients With Non–Muscle-Invasive Bladder Cancer. *Urolog Oncol* (2017) 35(5):264–71. doi: 10.1016/j.urolonc.2017.01.012
54. Hazan RB, Phillips GR, Qiao RF, Norton L, Aaronson SA. Exogenous Expression of N-Cadherin in Breast Cancer Cells Induces Cell Migration, Invasion, and Metastasis. *J Cell Biol* (2000) 148(4):779–90. doi: 10.1083/jcb.148.4.779
55. Wheelock MJ, Johnson KR. Cadherin-Mediated Cellular Signaling. *Curr Opin Cell Biol* (2003) 15(5):509–14. doi: 10.1016/S0955-0674(03)00101-7
56. Williams E-J, Williams G, Howell FV, Skaper SD, Walsh FS, Doherty P. Identification of an N-Cadherin Motif That Can Interact With the Fibroblast Growth Factor Receptor and Is Required for Axonal Growth. *J Biol Chem* (2001) 276(47):43879–86. doi: 10.1074/jbc.M105876200
57. Tran NL, Nagle RB, Cress AE, Heimark RL. N-Cadherin Expression in Human Prostate Carcinoma Cell Lines: An Epithelial-Mesenchymal Transformation Mediating Adhesion With Stromal Cells. *Am J Pathol* (1999) 155(3):787–98. doi: 10.1016/S0002-9440(10)65177-2
58. Dongre A, Weinberg RA. New Insights Into the Mechanisms of Epithelial-Mesenchymal Transition and Implications for Cancer. *Nat Rev Mol Cell Biol* (2019) 20(2):69–84. doi: 10.1038/s41580-018-0080-4
59. Fedor-Chaiken M, Meigs TE, Kaplan DD, Brackenbury R. Two Regions of Cadherin Cytoplasmic Domains Are Involved in Suppressing Motility of a Mammary Carcinoma Cell Line. *J Biol Chem* (2003) 278(52):52371–8. doi: 10.1074/jbc.M310576200

Conflict of Interest: The author declares that the research was conducted in the absence of any commercial or financial relationships that could be construed as a potential conflict of interest.

Publisher's Note: All claims expressed in this article are solely those of the authors and do not necessarily represent those of their affiliated organizations, or those of the publisher, the editors and the reviewers. Any product that may be evaluated in this article, or claim that may be made by its manufacturer, is not guaranteed or endorsed by the publisher.

frontiers | Frontiers in Pharmacology

ORIGINAL RESEARCH
published: 04 May 2022
doi: 10.3389/fphar.2022.874780

A Four-Gene Prognostic Signature Based on the TEAD4 Differential Expression Predicts Overall Survival and Immune Microenvironment Estimation in Lung Adenocarcinoma

Xiaoxia Gong[1], *Ning Li*[2], *Chen Sun*[3], *Zhaoshui Li*[4] *and Hao Xie*[1]*

[1]School of Life Science and Technology, MOE Key Laboratory of Developmental Genes and Human Diseases, Southeast University, Nanjing, China, [2]Cardiovascular Department, Qingdao Hiser Hospital Affiliated to Qingdao University, Qingdao, China, [3]Hematology Department, Qingdao Hiser Hospital Affiliated to Qingdao University, Qingdao, China, [4]Qingdao Medical College, Qingdao University, Qingdao, China

OPEN ACCESS

Edited by:
Essa M. Saied,
Humboldt University of Berlin, Germany

Reviewed by:
Ratnakar Tiwari,
Northwestern University, United States
Sonam Mittal,
Medical College of Wisconsin, United States

***Correspondence:**
Hao Xie
hxie@seu.edu.cn

Specialty section:
This article was submitted to Pharmacology of Anti-Cancer Drugs, a section of the journal Frontiers in Pharmacology

Received: 13 February 2022
Accepted: 08 April 2022
Published: 04 May 2022

Citation:
Gong X, Li N, Sun C, Li Z and Xie H (2022) A Four-Gene Prognostic Signature Based on the TEAD4 Differential Expression Predicts Overall Survival and Immune Microenvironment Estimation in Lung Adenocarcinoma. Front. Pharmacol. 13:874780. doi: 10.3389/fphar.2022.874780

Background: TEA domain transcription factor 4 (TEAD4) is a member of the transcriptional enhancer factor (TEF) family of transcription factors, which is studied to be linked to the tumorigenesis and progression of various forms of cancers, including lung adenocarcinoma (LUAD). However, the specific function of this gene in the progression of LUAD remains to be explored.

Method: A total of 19 genes related to the Hippo pathway were analyzed to identify the significant genes involved in LUAD progression. The TCGA-LUAD data (n = 585) from public databases were mined, and the differentially expressed genes (DEGs) in patients with the differential level of *TEAD4* were identified. The univariate Cox regression, zero LASSO regression coefficients, and multivariate Cox regression were performed to identify the independent prognostic signatures. The immune microenvironment estimation in the two subgroups, including immune cell infiltration, HLA family genes, and immune checkpoint genes, was assessed. The Gene Set Enrichment Analysis (GSEA) and GO were conducted to analyze the functional enrichment of DEGs between the two risk groups. The potential drugs for the high-risk subtypes were forecasted *via* the mode of action (moa) module of the connectivity map (CMap) database.

Results: *TEAD4* was found to be significantly correlated with poor prognosis in LUAD-patients. A total of 102 DEGs in *TEAD4*-high vs. *TEAD4*-low groups were identified. Among these DEGs, four genes (*CPS1*, *ANLN*, *RHOV*, and *KRT6A*) were identified as the independent prognostic signature to conduct the Cox risk model. The immune microenvironment estimation indicated a strong relationship between the high *TEAD4* expression and immunotherapeutic resistance. The GSEA and GO showed that pathways, including cell cycle regulation, were enriched in the high-risk group, while immune response-related and metabolism biological processes were enriched in the low-risk group. Several small molecular perturbagens targeting *CFTR* or *PLA2G1B*, by the mode of action (moa) modules of the glucocorticoid receptor agonist, cyclooxygenase inhibitor, and

NFkB pathway inhibitor, were predicted to be suited for the high-risk subtypes based on the high *TEAD4* expression.

Conclusion: The current study revealed *TEAD4* is an immune regulation–related predictor of prognosis and a novel therapeutic target for LUAD.

Keywords: lung adenocarcinoma, TEAD4, prognostic signature, immune microenvironment estimation, biomarker

INTRODUCTION

Lung cancer is one of the main causes of cancer-related death and is responsible for approximately 1.8 million deaths each year (Bray et al., 2018; Hoy et al., 2019). Approximately, 85% of these patients had non–small cell lung cancer (NSCLC), and the rest had small cell lung cancer (SCLC) (Sher et al., 2008; Byers and Rudin, 2015; Denisenko et al., 2018). Lung adenocarcinoma (LUAD) is the most common type of non–small cell lung cancer (NSCLC) and comprises approximately 40% of all lung cancer cases (Denisenko et al., 2018). Despite the improvement in current technology and techniques, the overall survival of LUAD has not been significantly improved, and only a fraction of patients benefited from therapies (Yamanashi et al., 2017; Schenk et al., 2021). Therefore, it is urgent to identify and explore more efficient therapeutic targets to further improve its prognosis.

The Hippo signaling pathway is evolutionarily conserved across higher order vertebrates, and by modulating target genes, it regulates multiple bioprocesses, including cell proliferation, survival, differentiation, and fate determination, as well as organ size and tissue homeostasis (Mohajan et al., 2021). Many of these roles are mediated by the transcriptional effectors Yes-associated protein (YAP) and its paralog transcriptional coactivator with the PDZ-binding motif (TAZ), which direct gene expression by control of a family of sequence-specific transcription factors called TEA DNA-binding proteins (TEAD1–4) that mediate proliferation and pro-survival genes (Dey et al., 2020; Masliantsev et al., 2021; Mohajan et al., 2021). Aberration of the Hippo pathway and YAP/TAZ-TEAD activity was recently shown to be linked to carcinogenesis in lung cancer (Huang et al., 2017; Liu et al., 2017; Gu et al., 2020). Overexpression of YAP/TAZ is associated with the development, progression, and poor prognosis of the disease (Mohajan et al., 2021). Therefore, the Hippo pathway is a novel tumor molecular biomarker and potential therapeutic target for LUAD. As one main component of the Hippo pathway, TEAD4 is a transcriptional enhancer–associated domain (TEAD) family protein (Pobbati and Hong, 2013) that plays biological roles by binding with DNA elements *via* its specific DNA-binding domains or through interaction with transcription coactivators (i.e., YAP/TAZ) by transactivation domains (Zhou et al., 2017; Gu et al., 2020). More recently, *TEAD4* has been demonstrated in tumorigenesis and cancer progression, including cancers of the breast (He et al., 2019; Wu Y et al., 2021), prostate (Chen CL et al., 2021), gastric (Shuai et al., 2020), bladder (Wu et al., 2019; Wang J et al., 2021), thyroid (Zhang et al., 2022), and lungs (Zhou et al., 2017; Gu et al., 2020; Hu et al., 2021; Yan et al., 2022). Previous studies have reported that *TEAD4* is upregulated in LUAD and is closely related to disease prognosis (Hu et al., 2021). However, the specific molecular mechanism of *TEAD4* regulation on the prognosis of LUAD is not understood.

The aim of the present study was to determine whether *TEAD4* could serve as a potential predictor of the prognosis of LUAD. We analyzed TCGA-LUAD samples with high and low *TEAD4* expressions, constructed a four-gene prognostic signature based on the *TEAD4* differential expression, and determined that *TEAD4* was an immune regulation-related predictor of prognosis for LUAD.

MATERIALS AND METHODS

Data Acquisition

Gene expression sequencing data (HTSEQ-Counts and HTSEQ-FPKM) and the corresponding annotation of LUAD (n = 585) were acquired from the Genomic Data Commons (GDC) Portal (https://portal.gdc.cancer.gov/) of The Cancer Genome Atlas (TCGA) database (Tomczak et al., 2015). Excluding the data from the same patient, a total of 568 LUAD samples, including 58 normal (n_{normal} = 58) and 510 LUAD patients (n_{LUAD} = 510), were retained for the following differentially expressed gene (DEG) analysis. For the DEGs in *TEAD4*-high vs. *TEAD4*-low groups, the 510 samples of patients were divided into two subtypes according to the median TPM of *TEAD4*.

The clinical survival data (n = 738) and the phenotype data (n = 877) of TCGA-LUAD–matched patients were acquired from the GDC of the TCGA database. A total of 497 samples (n = 497), which contains both RNA-seq and survival data, were brought into the Cox model. For the nomogram analysis, a total of 383 samples (n = 383) were retained.

Gene Expression Omnibus (GEO) LUAD datasets were acquired and cleared up by the GEOquery R package. The validation sets of the Cox model were performed using GSE13213 (Tomida et al., 2009), GSE30219 (Rousseaux et al., 2013), and GSE31210 (Okayama et al., 2012), which contains 621 samples of LUAD.

Identification of DEGs and the Enrichment Analysis

The DEGs with the threshold of fold change:2 and p-value < 0.05 were identified using HTSEQ-FPKM of TCGA-LUAD by the Deseq 2 R package (Love et al., 2014) and visualized by the ggplot2 R package. Gene Ontology (GO) (Ashburner et al., 2000)

and Kyoto Encyclopedia of Genes and Genomes (KEGG) (Ogata et al., 1999) pathway enrichment analysis were conducted by clusterProfiler R package (Yu et al., 2012) and visualized by the ggplot2 R package. The Gene Set Enrichment Analysis (GSEA) (Subramanian et al., 2005) was performed by the WebGestalt online database (http://www.webgestalt.org/).

Establishment and Validation of Prognostic Signature

Based on the TCGA-LUAD dataset (n = 497), univariate Cox regression, LASSO regression, and multivariate Cox regression analyses were used to screen the prognostic genes and establish the prognostic model. The survival R package was used to calculate the association between the expression of each DEG and overall survival (OS), and genes with p-value < 0.05 were retained for the following LASSO regression analysis. Glmnet and survival R package were used for the LASSO regression analysis to screen the significant variables in univariate Cox regression analysis. In order to obtain more accurate independent prognostic factors (prognostic characteristic genes), multivariate Cox regression analysis was used for the final screening. The risk score was calculated as follows: risk score = (exp-gene1*coef-gene1) + (exp-gene2*coef-gene2) + (exp-gene n*coef-gene n). Patients were divided into high- and low-risk groups based on the median of the risk score.

Time-dependent receiver operating characteristic (ROC) curves were used to assess survival predictions, and the Time ROCR package was used to calculate the area under the ROC curve (AUC) value to measure prognosis and predict accuracy. Survcomp R package was used for the C-index analysis. For the nomogram analysis, phenotype data (n = 382) were used and the clinical indexes, including age, gender, race, TNM staging, and stage, were brought into the COX regression analysis. For the external model construction, the risk score of the four independent prognostic signatures was calculated by the survival R package.

TME Estimate Analysis

Stromal score, immune score, ESTIMATE score, and tumor purity score were calculated based on the mRNA expression (HTSEQ-Counts) by an estimate R package (Yoshihara et al., 2013). The significant static analysis was performed by the Wilcoxon rank-sum test.

The gene expression matrix data (HTSEQ-FPKM) were uploaded to CIBERSORT (Newman et al., 2015), and the immune cell infiltration matrix was obtained. ggplot2 R package was used to visualize the distribution of infiltration of 22 types of immune cells in each sample. The significant static analysis was performed by the Wilcoxon rank-sum test.

Correlation Analysis of the Multigene

The correlation analysis of multiple genes was performed by Spearman's correlation analysis and displayed by pheatmap R package.

Chemotherapeutics Forecast

The chemotherapeutics forecast was performed using the mode of action (moa) module of the connectivity map (CMap, https://clue.io/command).

Statistical Analysis

The statistical analysis was calculated *via* the Wilcoxon rank-sum test and unpaired t-text. All statistical tests were bilateral. All statistical tests and visualization were performed in R software (version 4.0.2).

RESULTS

High *TEAD4* Expression Is Associated With Poor Prognosis in LUAD

We selected 19 Hippo pathway-related genes (Wang et al., 2018) (**Supplementary Table S1**) and detected their expression levels in LUAD. The results showed that among these 19 genes, 11 (*TAOK2*, *TAOK3*, *WWC1*, *SAV1*, *STK4*, *MOB1B*, *LATS1*, *LATS2*, *TAP1*, *TEAD1*, and *TEAD4*) were downregulated in LUAD, while four (*STK3*, *TAZ*, *TEAD2*, and *TEAD3*) were upregulated in LUAD compared to adjacent normal samples (**Figure 1A**, **Supplementary Table S2**). To further evaluate the potential role of these genes in LUAD, the correlation between prognosis and these genes was analyzed, which showed that the expression of *TAOK2* was significantly associated with a superior prognosis (**Figures 1B, C**), while the expressions of *STK3*, *LATS2*, and *TEAD4* were associated with a poor outcome in LUAD (**Figures 1B, D–F**, **Supplementary Table S3**). These results suggest that the Hippo pathway plays an important role in the tumorigenesis and development of LUAD.

Univariate and multivariate regression analyses were performed for the four (*TAOK2*, *STK3*, *LATS2*, and *TEAD4*) prognosis-related genes, indicating that *STK3* (HR (HR.95L, HR.95H) =1.37 (0.96, 1.95), p = 0.077, **Supplementary Table S4**) and *TEAD4* (HR (HR.95L, HR.95H) =1.44 (1.17, 1.77), p = 0.0004, **Supplementary Table S4**) were independent prognostic signatures. Notably, *TEAD4* was found to have a prognostic value. Therefore, we focused on the analysis of *TEAD4*.

Identification of DEGs Associated With *TEAD4* Differential Expression

To explain the molecular mechanism of *TEAD4* in LUAD, the patients were divided into subgroups, *TEAD4*-high expression (*TEAD4*-high, n = 255) and *TEAD4*-low expression (*TEAD4*-low, n = 255), based on the median value, and the differentially expressed genes (DEGs) between the two subgroups were analyzed. A total of 102 DEGs (51 genes were up-regulated and 51 genes were downregulated) were identified in the *TEAD4*-high vs. *TEAD4*-low groups (**Figures 2A,B**, **Supplementary Figure S1**, **Supplementary Table S5**). The subsequent Kyoto Encyclopedia of Genes and Genomes (KEGG) and Gene Ontology (GO) results showed that upregulated genes in the *TEAD4*-high group belonged to pathways of the cell cycle, etc. (**Figure 2C**), and categories

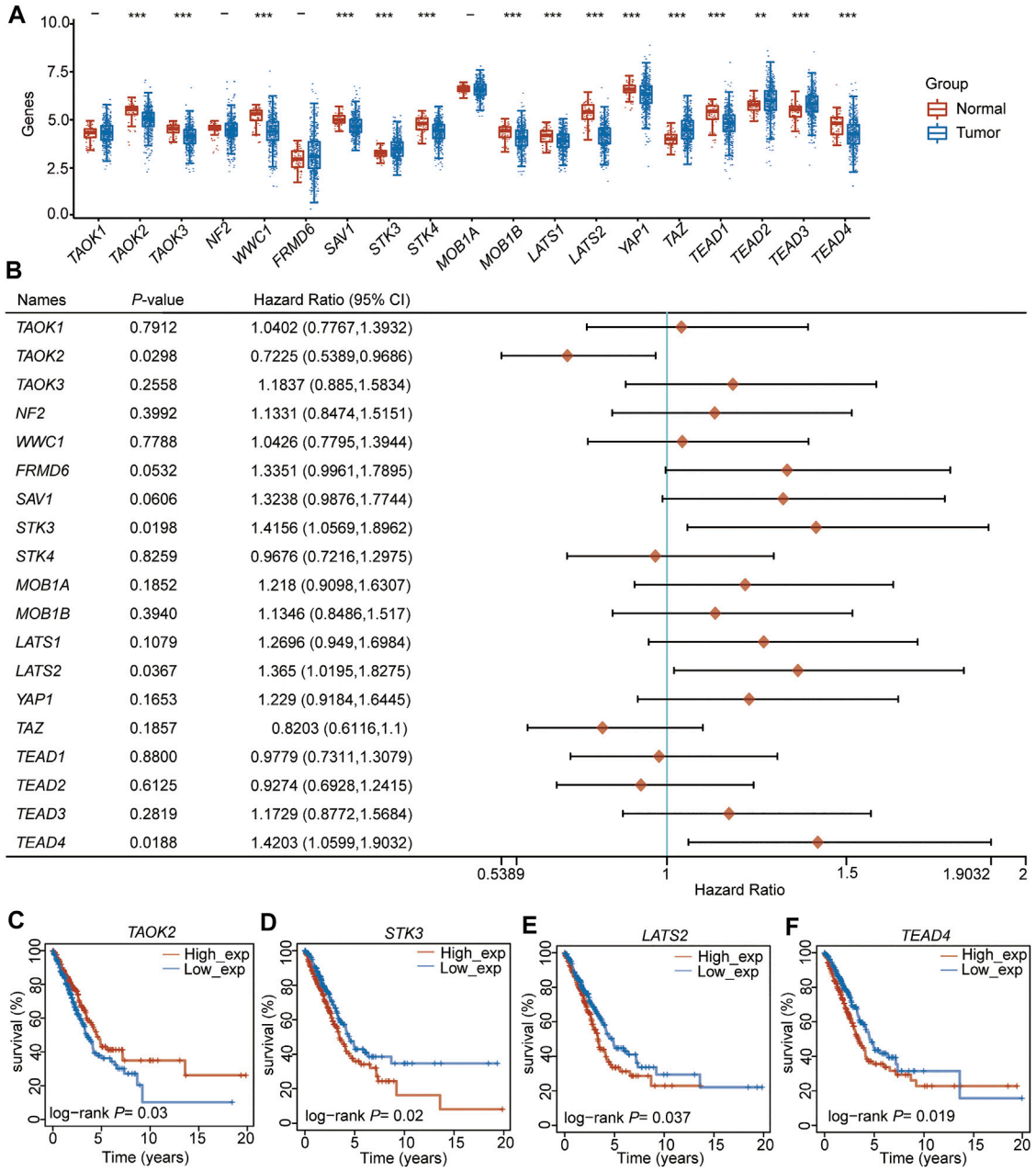

FIGURE 1 | TEAD4 is downregulated in LUAD and associated with a poor prognosis. **(A)** Expression level (TPM) of the Hippo pathway-related genes in LUAD compared to adjacent normal samples. **(B)** Forest showing the prognosis of the Hippo pathway–related genes in LUAD. **(C–F)** Relationship between *TAOK2* **(C)**, *STK3* **(D)**, *LATS2* **(E)**, and *TEAD4* **(F)** expressions and OS in LUAD.

related to organelle fission, nuclear division, and chromosome segregation, etc. (**Figure 2D**). The downregulated genes in the *TEAD4*-high group belonged to pathways of pertussis, cytokine–cytokine receptor interaction, phagosome, etc. (**Figure 2E**), and were involved in bioprocesses of the humoral immune response, respiratory gaseous exchange by the respiratory system, and metabolic process, etc. (**Figure 2F**). These results demonstrate that the differential expression of this gene may lead to changes in the gene expression, which causes the dysregulation of cellular bioprocesses, including the cell division, immune response, and metabolic process.

Establishment of a Prognostic Signature Based on the High *TEAD4* Expression in TCGA-LUAD

Among the 102 DEGs, 83 were found to be differentially expressed in LUAD tissues (n = 510) compared to adjacent

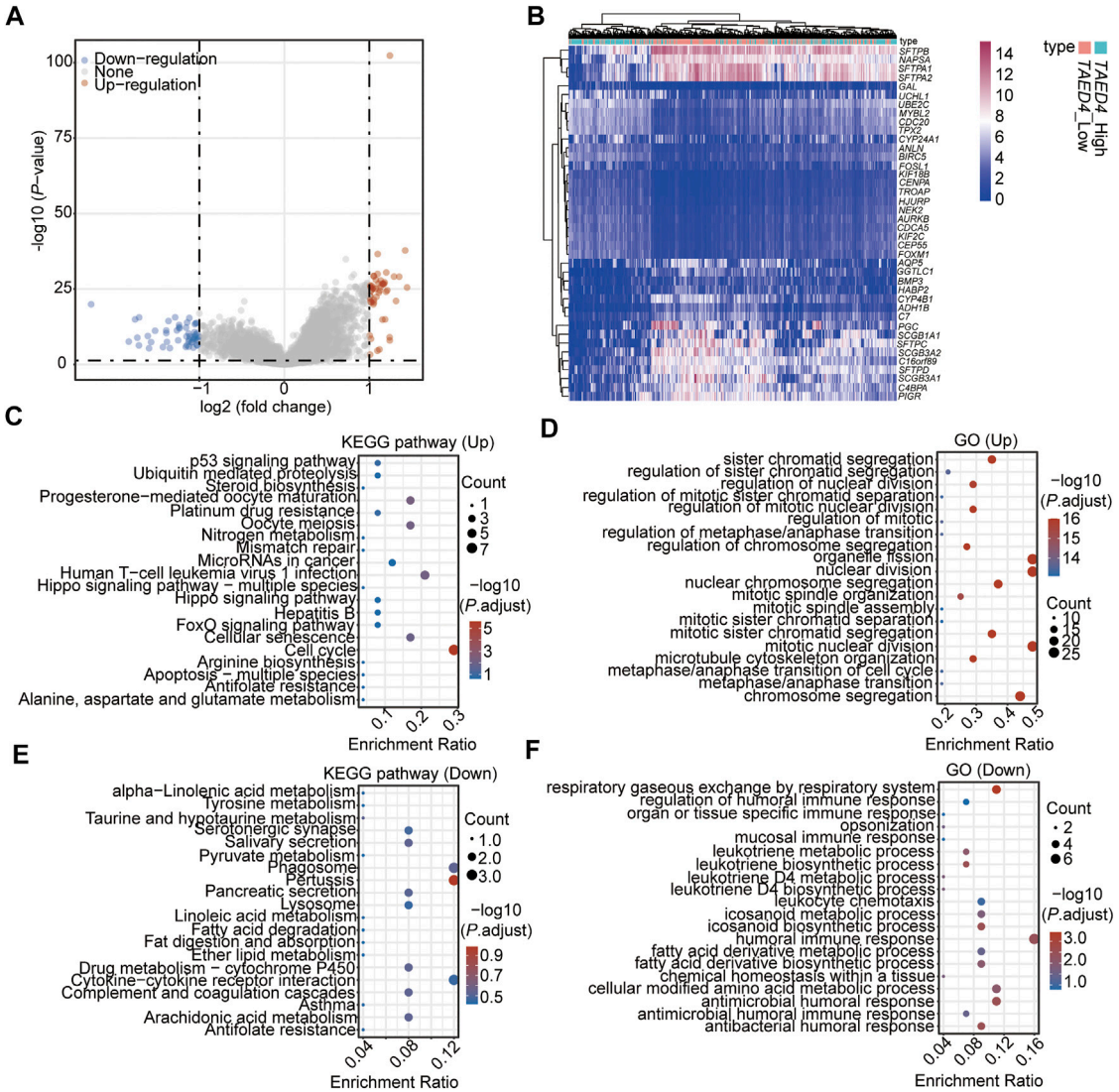

FIGURE 2 | Identification of DEGs associated with the TEAD4 differential expression. **(A)** Volcano plot showing the DEGs in *TEAD4*-high vs. *TEAD4*-low groups. **(B)** Heatmap showing the top 20 up- and top 20 downregulated genes in *TEAD4*-high vs. *TEAD4*-low groups. **(C)** KEGG analysis of upregulated genes in the *TEAD4*-high group. **(D)** Enriched GO terms of upregulated genes in the *TEAD4*-high group. **(E)** KEGG analysis of downregulated genes in the *TEAD4*-high group. **(F)** Enriched GO terms of downregulated genes in the *TEAD4*-high group.

normal tissues (n = 58) (**Supplementary Table S6**). These 83 DEGs were used to perform the univariate Cox regression analysis, and 74 genes ($p < 0.05$, **Supplementary Table S7**) were identified as prognostic genes. After suffering from zero LASSO regression coefficients, eight genes were identified to perform the multivariate Cox regression analysis (**Figures 3A, B**, **Supplementary Table S8**). Finally, four genes, carbamoyl phosphate synthetase 1 (*CPS1*), anillin actin-binding protein (*ANLN*), ras homolog family member V (*RHOV*), and keratin 6A (*KRT6A*), were identified as independent prognostic factors (**Figure 3C**, **Supplementary Table S9**). Based on the median of the risk score calculated by the expressions of these four genes, the 497 patients (patients without information on overall survival were excluded, $n_{497} = n_{510}$-n_{13}) were divided into two subtypes of high-risk and low-risk (**Figure 3C**, **Supplementary Table S10**). The high-risk subtype had significantly higher mortality rates than the low-risk group (**Figure 3C**). In addition, the expressions of the four independent prognostic signatures were higher in the high-risk group than in the low-risk subtype (**Figure 3C**), and the expression of each gene was positively correlated with the others (**Figure 3D**). Meanwhile, we found that these four signatures were positively correlated with the *TEAD4* expression (**Figure 3D**). These genes, which were all upregulated in LUAD, were highly expressed in the *TEAD4*-high subgroup (**Figure 3E**). The four genes and *TEAD4* were all significantly and positively associated with the risk score (**Figures 3F–J**). In addition, *TEAD4*, *ANLN*, *RHOV*, and *KRT6A* were all associated with the poor prognosis in LUAD (**Figures 3K–M**), indicating

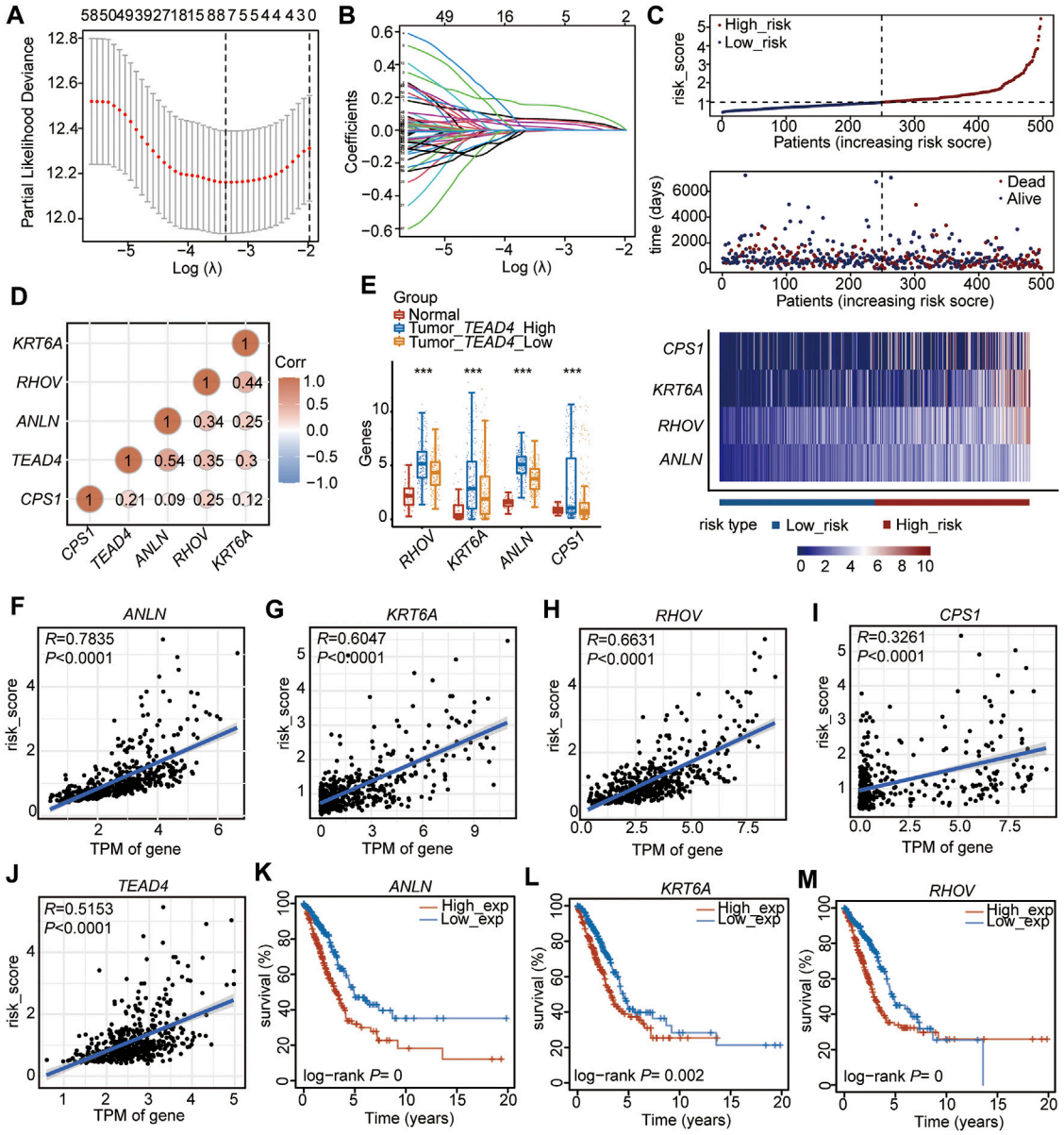

FIGURE 3 | Establishment of the prognostic signature based on the high TEAD4 expression in TCGA-LUAD. **(A)** Stepwise Cox proportional risk regression model to screen the prognostic genes. **(B)** LASSO coefficient spectrum of prognostic gene screening. **(C)** Risk score distribution, survival status of patients, and heatmap of prognostic gene distribution in the training cohort. **(D)** Correlation analysis of prognostic genes and *TEAD4* in LUAD. The circle size represents significance. **(E)** TPM of the four prognostic genes in LUAD samples with *TEAD4*-high expressions, LUAD samples with *TEAD4*-low expressions, and the corresponding adjacent normal samples. The statistical significance was calculated *via* the Wilcoxon rank-sum test, ***$p < 0.001$. **(F–J)** Correlation analysis between the prognostic genes and risk score. **(K–M)** Relationship between *ANLN* **(K)**, *KRT6A* **(L)**, and *RHOV* **(M)** expressions and OS in LUAD.

that these prognostic genes are of great significance for the evaluation of the LUAD outcome.

Internal Validation of the Prognostic Signature

We then evaluated the constructed risk model, and the overall survival (OS) analysis showed that the high-risk subtype had a poor prognosis (p =2.74e-07) (**Figure 4A**). The ROC curve was used to predict the prognosis at 1, 3, and 5 years, which showed that the prediction efficiency of the model was feasible (1-year AUC = 0.73; 3-year AUC = 0.713; 5-year AUC = 0.628) (**Figure 4B**). The concordance index (C-index) analysis also showed a consistent result (C-index = 0.6733, p = 2.704004e-15). Thereafter, the nomogram was constructed, and the clinical indices (**Table 1**, n = 382, age, gender, race, NTM staging) were incorporated into the nomogram to predict the OS of patients. The clinical indices of

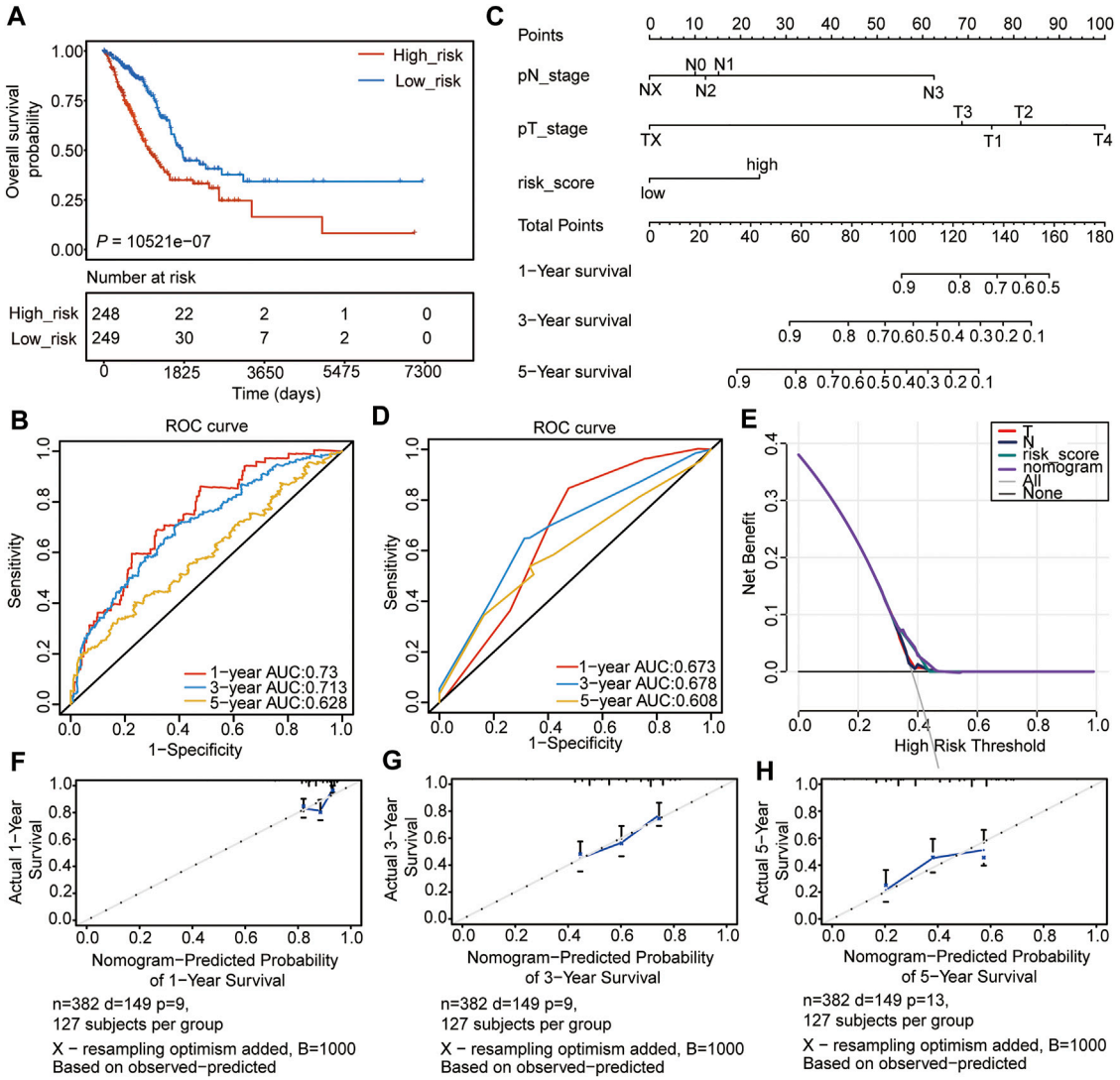

FIGURE 4 | Internal validation of the prognostic signature. **(A)** OS of high- and low-risk groups. **(B)** ROC analyses of the model for 1-, 3-, and 5-years. **(C)** Nomogram to predict the prognosis of patients with LUAD. **(D)** ROC analyses of the nomogram model for 1-, 3-, and 5-years. **(E)** DCA result of the nomogram model. **(F–H)** The calibration analysis of the nomogram predicted the probability of 1-year survival **(F)**, 3-years survival **(G)**, and 1-year survival **(H)**.

pT_satging and pN_satging were retained for further analysis after Cox regression analysis (**Figure 4C**). The ROC curve and C-index were used to predict the nomogram model, which showed a feasible result (1-year AUC = 0.673; 3-year AUC = 0.678; 5-year AUC = 0.608, C-index = 0.6763, p = 4.9488e-11) (**Figure 4D**). Moreover, the results of decision curve analysis (DCA) and calibration analysis of the nomogram predicted probability and also suggested the accuracy of the Cox model (**Figures 4E–H**).

Validation of the Cox Risk Model With Internal and External Sets

To verify the accuracy of the four prognostic genes in predicting the outcome of LUAD, we selected 250 samples randomly from the 497 samples and re-reconstructed the Cox risk model using the four prognostic genes. We recalculated the risk score and divided the 250 samples into high- (n = 125) and low-risk (n = 125) subgroups, according to the median of the risk score (**Figure 5A**, **Supplementary Table S11**). Consistent with the previous results, the high-risk subtype had a higher mortality rate and higher expression levels of the four genes (**Figure 5A**). In addition, the high-risk subtype had a poor outcome compared to the low-risk subtype (p = 4.063e-04, **Figure 5B**). The ROC curve and C-index results also showed a feasible result (1-year AUC = 0.776; 3-year AUC = 0.711; 5-year AUC = 0.639, C-index = 0.6914, p = 1.719663e-11) (**Figure 5C**). Moreover, the clinical indices of pT_satging, pN_satging, and stage were retained for further analysis after Cox regression analysis (n = 243, **Supplementary Table S12**),

TABLE 1 | Clinical index of LUAD patients used in the Cox model.

Characteristic	Level	Overall	High-risk	Low-risk
n (dead/alive)		382 (149/233)	194 (92/102)	188 (57/131)
Age, n (%)	≥65	213 (55.76%)	103 (53.09%)	110 (58.51%)
	<65	169 (44.24%)	91 (46.91%)	78 (41.49%)
Gender, n (%)	Male	170 (44.50%)	89 (45.87%)	81 (43.08%)
	Female	212 (55.50%)	105 (54.13%)	107 (56.92%)
N stage, n (%)	N0	249 (65.18%)	124 (63.91%)	125 (66.48%)
	N1	65 (17.01%)	35 (18.04%)	30 (15.96%)
	N2	56 (14.65%)	31 (15.97%)	25 (13.29%)
	N3	1 (0.26%)	1 (0.51%)	0 (0)
	NX	11 (2.90%)	3 (1.57%)	8 (4.27%)
M stage, n (%)	M0	241 (63.08%)	122 (62.88%)	119 (63.29%)
	M1	21 (5.49%)	10 (5.15%)	11 (5.85%)
	MX	120 (31.43%)	62 (31.97%)	58 (30.84%)
T stage, n (%)	T1	132 (34.55%)	65 (33.50%)	67 (35.63%)
	T2	196 (51.30%)	96 (49.48%)	100 (53.19%)
	T3	40 (10.47%)	24 (12.37%)	16 (8.51%)
	T4	13 (3.40%)	8 (4.12%)	5 (2.67%)
	TX	1 (0.28%)	1 (0.53%)	0 (0%)
Pathologic stage, n (%)	Stage I	209 (54.71%)	96 (49.48%)	113 (60.10%)
	Stage II	87 (22.77%)	55 (28.35%)	32 (17.02%)
	Stage III	59 (15.44%)	31 (15.97%)	28 (14.89%)
	Stage IV	21 (5.49%)	10 (5.15%)	11 (5.85%)
	N/A	6 (1.59%)	2 (1.05%)	4 (2.14)

and the corresponding ROC curve and C-index showed considerable results (1-year AUC = 0.701; 3-year AUC = 0.67; 5-year AUC = 0.631, C-index = 0.6932, p = 2.873223e-09) (**Figure 5D**). The DCA and calibration were also performed, and the results showed the high accuracy of the Cox model (**Figures 5E–H**).

To further validate the Cox model, GEO data sets, including GSE13213 (n = 117), GSE31210 (n = 226), and GSE30219 (n = 278), were acquired to construct the Cox model using the four-gene prognostic signature. In each validation set, patients were stratified into high- and low-risk groups, according to the median of the risk score (**Table 2**, **Supplementary Table S13**). The Kaplan–Meier survival analyses showed that patients in the high-risk subtype had significantly worse prognoses in all three validation sets (**Supplementary Figures S2A–C**). The ROC curve results showed that the AUCs of 1, 3, and 5 years in validation set 1 ranged from 0.71 to 0.95 (**Supplementary Figure S2D**), the AUCs of 1, 3, and 5 years in validation set 2 ranged from 0.722 to 0.925 (**Supplementary Figure S2E**), and the AUCs of 1, 3, and 5 years in validation set 3 ranged from 0.679 to 0.749 (**Supplementary Figure S2F**), which indicated the high accuracy of the model for evaluating prognosis. These demonstrate that the four-gene independent prognostic signature could be a promising factor for LUAD to predict the progression of tumor cells.

Tumor Microenvironment Estimation of the Cox Model

Subsequently, the tumor microenvironment (TME) in the two risk subtypes was analyzed, including the stromal score, immune score, ESTIMATE score, and tumor purity. The results showed that the high-risk subtype was featured with a lower stromal score, immune score, and ESTIMATE score (**Figures 6A–C**), as well as a higher tumor purity (**Figure 6D**). The subsequent relationship between the TME score and OS was analyzed and showed that high immune and ESTIMATE scores were associated with a good outcome in patients with LUAD (**Figures 6F,G**), while increased tumor purity was correlated with a poor prognosis (**Figure 6H**). The stromal score had no significant correlation with the prognosis in LUAD (**Figure 6E**).

Infiltrating Proportion of Immune Cells in the Two Risk-Groups

Immune cell infiltration was then analyzed, and the proportion of immune cell infiltration in the TME was first calculated by the CIBERSORT algorithm (**Supplementary Table S14**). The landscape of immune cells in the LUAD-TME showed great heterogeneity (**Figure 7A**). Among these, macrophages and T cells were the main groups (**Figure 7A**). Notably, the high-risk group had a lower proportion of plasma cells, resting memory CD4 T cells, monocytes, resting dendritic cells, and resting mast cells (**Figure 7B**). Meanwhile, the proportions of CD8 T cells, activated memory CD4 T cells, resting NK cells, M0 macrophages, M1 macrophages, activated dendritic cells, activated mast cells, and neutrophils were higher in the high-risk group (**Figure 7B**). These results suggest that the two risk groups had a distinct TME, which may alter the oncotherapeutic effect.

HLA Family Gene Analysis of the Cox Model

HLA family genes are the most complex and polymorphic genes which contain the most concentrated genes related to

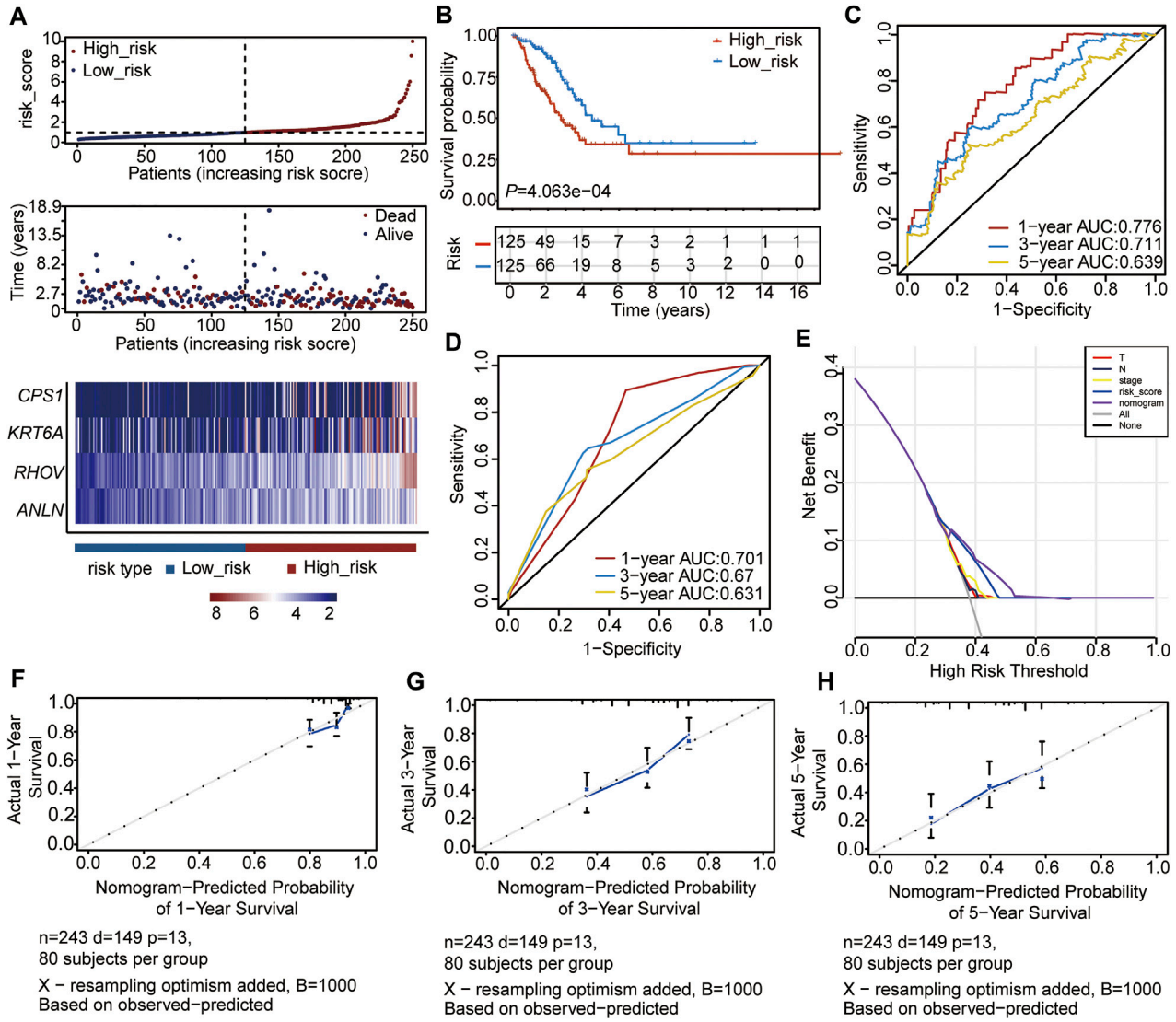

FIGURE 5 | Validation of the Cox model with internal data. **(A)** Risk score distribution, survival status of patients, and heatmap of prognostic gene distribution in the validation set. **(B)** OS of high- and low-risk groups. **(C)** ROC curve of the Cox model for 1, 3, and 5 years. **(D)** ROC curve of the nomogram model for 1, 3, and 5 years. **(E)** DCA result of the nomogram model **(F–H)** Calibration analysis of the nomogram predicted the probability of 1-year survival **(F)**, 3-year survival **(G)**, and 5-year survival **(H)**.

TABLE 2 | Information of GEO data sets used in the validation of the Cox model.

Validation Set	GEO accession	Platform	Overall (1/0)	High-risk (1/0)	Low-risk (1/0)
Set 1	GSE13213	GPL6480	117 (49/68)	58 (33/25)	59 (16/43)
Set 2	GSE31210	GPL570	226 (35/191)	113 (29/84)	113 (6/107)
Set 3	GSE30219	GPL570	278 (188/90)	139 (111/28)	139 (77/62)

immune regulation that are involved in multiple diseases. We analyzed major histocompatibility complex, class I (MHC-I) and major histocompatibility complex, class II (MHC-II) expression between the two risks groups, and the two common HLA genes (**Supplementary Table S1**). The results showed that five of six MHC-I genes (*HLA-A*, *HLA-B*, *HLA-C*, *HLA-E*, and *HLA-F*) and all MHC-II genes were significantly under-expressed in the high-risk group (**Figure 8A**), indicating a feasible poor antitumor immune response in the high-risk group.

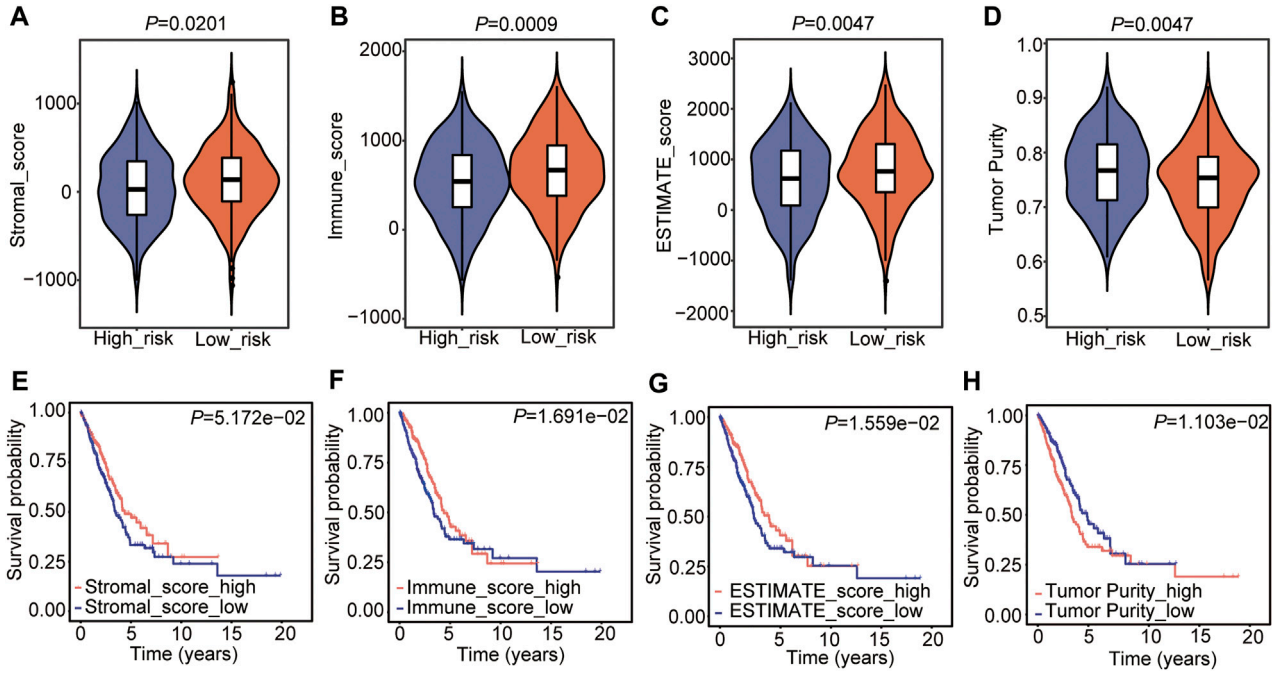

FIGURE 6 | Tumor microenvironment estimation of the Cox model. **(A–D)** Comparison of the stromal score **(A)**, immune score **(B)**, estimate score **(C)**, and tumor purity **(D)** in the two risk groups. The statistical significance was calculated *via* the Wilcoxon rank-sum test. **(E–H)** The relationship between stromal score **(E)**, immune score **(F)**, estimate score **(G)**, and tumor purity **(H)** and OS in LUAD.

Immune Checkpoint Gene Analysis in the Two Risk Subtypes

We then detected immune checkpoint genes, including *CD274* (*PD-L1*), *PDCD1* (*PD-1*), *LAG3* (CD223), *HAVCR2*, *CTLA4*, *PDCD1LG2*, *SIGLEC15*, and *TIGIT*, in the two risk subtypes (**Supplementary Table S1**). The results showed that the expression levels of *CD274* (*PD-L1*) and *LAG3* (CD223) were higher in the high-risk group than in the low-risk group (**Figures 9A,B**). Other genes were not different between the two groups (**Figures 9C–H**). These results suggested that a high *TEAD4* expression may predict immune checkpoint activity and reduce the immune checkpoint block (ICB) efficacy, thus promoting tumor cell survival and metastasis.

Identification and Enrichment Analysis of DEGs Between the Two Risk Subtypes

To analyze the molecular bioprocess of the four prognostic biomarkers, DEGs in the high- vs. low-risk group were further analyzed. The volcano plot showed that with the threshold of fold change = 1.5 and $p < 0.05$, a total of 106 genes (45 genes were higher and 61 genes were lower in the high-risk group) were differentially expressed between the two groups (**Figure 10A**, **Supplementary Table S15**). The subsequent GO analysis showed that these DEGs were cell division regulation-related genes (**Figure 10B**). The Gene Set Enrichment Analysis (GSEA) result showed that genes enriched in the high-risk group were cell cycle regulation-regulated genes (**Figures 10C–G**), and genes enriched in the low-risk group were immune response- and metabolism-related genes (**Figure 10C**). These results were consistent with the DEGs based on the high *TEAD4* expression, suggesting that the high *TEAD4* expression affects the cell cycle, immune response, and metabolism regulation. Through this regulatory mechanism, the proliferation and invasion capacity of cancer cells were improved. Hence, *TEAD4* is a valuable biomarker for the prognostic prediction of patients with LUAD.

The Small-Molecule Perturbagen Chemotherapeutics Forecast for High-Risk Patients

According to the DEGs in the two risk subtypes, the adjuvant chemotherapeutics for high-risk patients were predicted *via* the mode of action (moa) module of the CMap database. The results showed that several small-molecule perturbagens (e.g., diflorasone, aloisine, apigenin, and mepacrine), targeting the CF transmembrane conductance regulator (*CFTR*), phospholipase A2 group IB (*PLA2G1B*), cell division cycle 25A (*CDC25A*), chitinase acidic (*CHIA*), TTK protein kinase (*TTK*), and forkhead box M1 (*FOXM1*), were the potential chemotherapeutics for the patients with a higher risk score. We also found that these potential chemotherapeutics may function by the moa of the CDK inhibitor, CFTR channel agonist, cytochrome p450 inhibitor, glucocorticoid receptor agonist, a cyclooxygenase inhibitor, and NFkB pathway inhibitor (**Figure 11**).

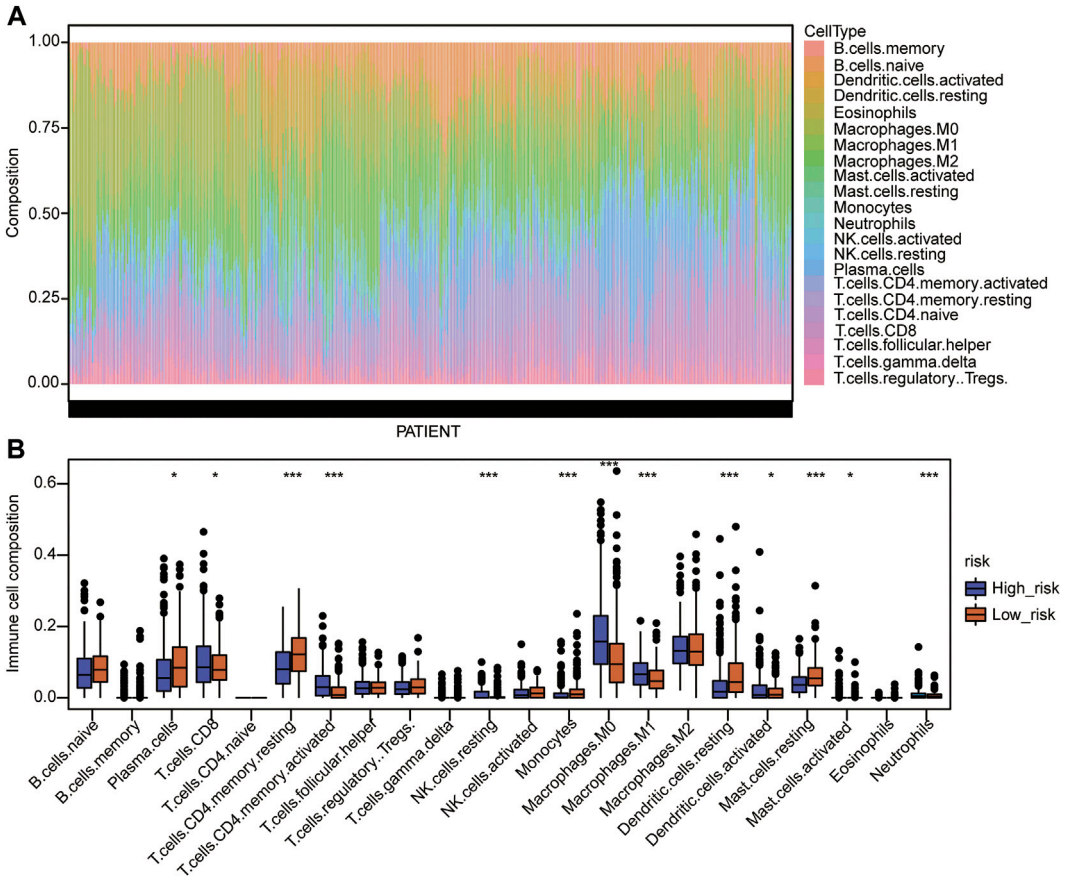

FIGURE 7 | Immune cell infiltration analysis of the Cox model. **(A)** Landscape of immune cell infiltration in the TME of TCGA-LUAD. **(B)** Comparison of immune cell infiltration in the TME of the two risk groups. The statistical significance was calculated *via* the Wilcoxon rank-sum test, $^{*}p < 0.05$, $^{**}p < 0.01$, and $^{***}p < 0.001$.

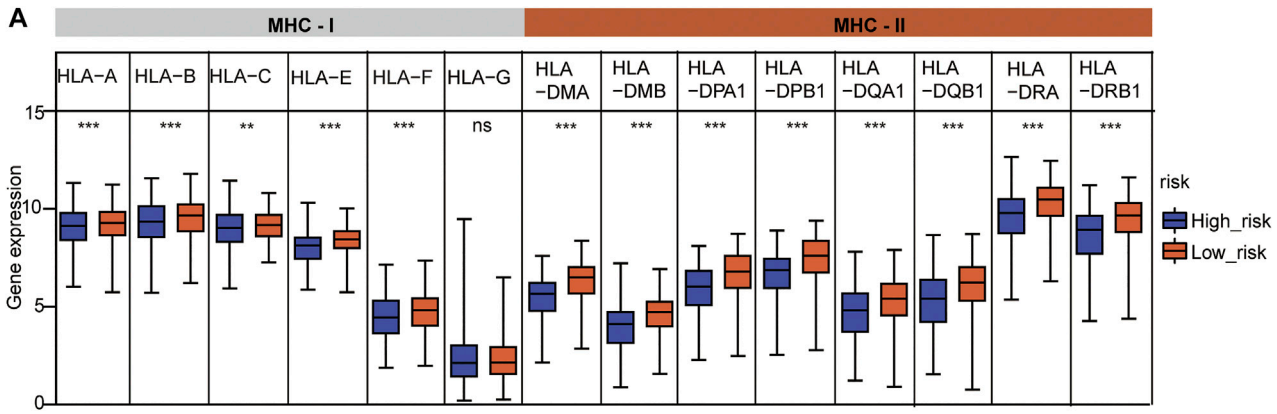

FIGURE 8 | HLA gene expression analysis between the two risk subtypes. **(A)** HLA family expression analysis in the two risk groups. The statistical significance was calculated *via* *t*-test, $^{**}p < 0.01$ and $^{***}p < 0.001$.

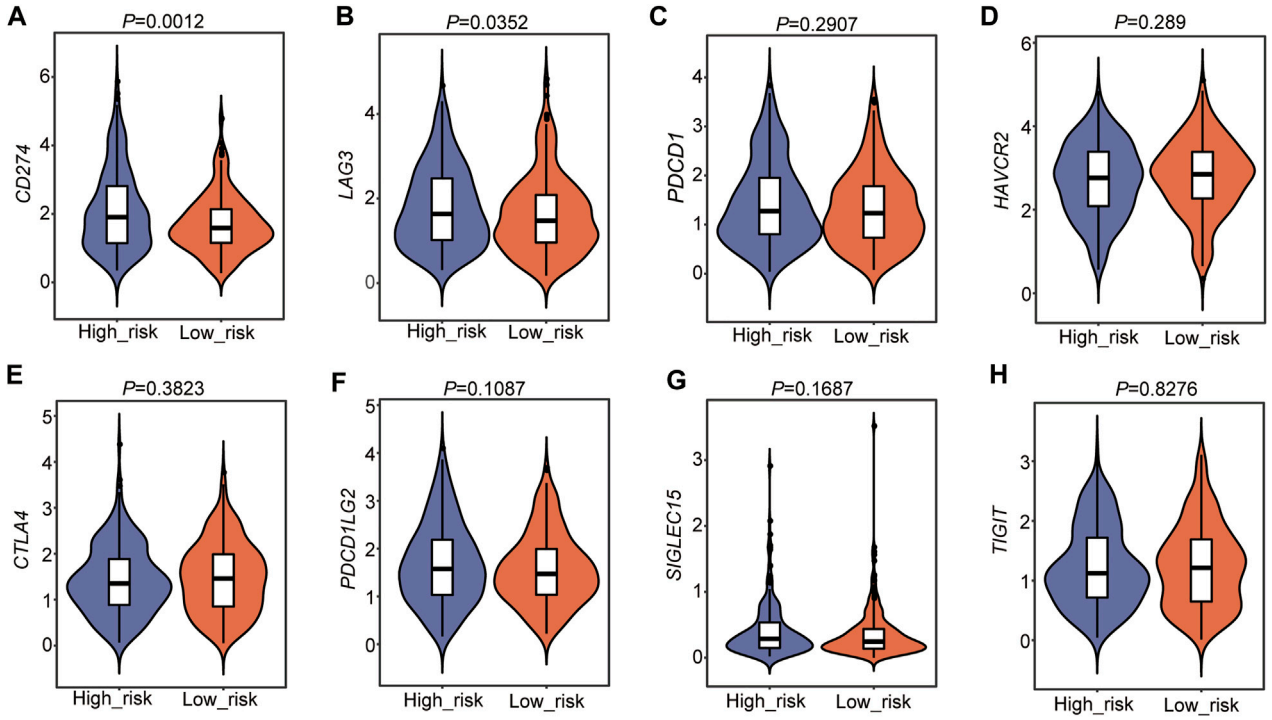

FIGURE 9 | Immune checkpoint gene analysis in the two risk subtypes. **(A–H)** Immune checkpoint gene analysis in the two risk groups. The statistical significance was calculated *via* the Wilcoxon rank-sum test.

DISCUSSION

LUAD, one of the most frequently diagnosed cancers, is a heterogeneous disease that is commonly triggered by the alteration of key genes including oncogenes and tumor suppressors (de Sousa and Carvalho, 2018; Gavralidis and Gainor, 2020). A better understanding of the risk genes of LUAD and their specific molecular mechanism will facilitate the prevention and management of LUAD. With the rapid development of molecular biological technology and public databases, increasing numbers of biomarkers associated with the prognosis and diagnosis of LUAD have been acknowledged in recent years. However, few factors are of real clinical value.

This current study reveals an immune regulation-related biomarker, *TEAD4*, for the prognosis prediction and diagnosis of LUAD. *TEAD4* is widely studied as a Hippo signaling pathway-related transcription enhancer factor domain family gene, that interacts with YAP/TAZ to act as a transcription factor (Wu Y et al., 2021). This study first showed that the high *TEAD4* expression is associated with the prognosis in LUAD patients. Subsequent analysis determined that *TEAD4* was an independent prognostic signature in LUAD. In addition, the DEGs related to the *TEAD4* differential expression were involved in pathways of the cell cycle, immune response, and metabolism regulation. Increasing evidence suggests that the dysregulation of the immune response has been widely reported to be linked to antitumor immune escape and associated with poor outcomes in cancers (Gerada and Ryan, 2020). Dysfunction of metabolites and their regulators is emerging as a key factor affecting both cancer progression and therapeutic responses (O'Sullivan et al., 2019; Wu Q et al., 2021; Xia et al., 2021). These results all indicate that LUAD patients with different *TEAD4* levels may have distinguishing antitumor abilities and further outcomes. TEAD4 has been reported to be a protumor factor in LUAD, including its functions in promoting cancer cell proliferation, migration, and therapy resistance (Zhang et al., 2018; Gu et al., 2020; Hu et al., 2021; Yan et al., 2022). Our conclusions are consistent with these reports. However, the molecular mechanism of this gene in LUAD has not been systematically studied in previous reports. This study conducted a systematic analysis of a large number of samples that, combined with the clinical risk factors for LUAD, revealed more possible mechanisms of its pro-metastatic effects in LUAD and explained more potential reasons for the poor prognosis caused by its high expression at the macro level. This provides possible research directions for further studies on the anticancer function of this gene, such as metabolic regulation and the relationship between macrophage infiltration and *TEAD4* disorder. Our result that *TEAD4* is downregulated in LUAD seems to conflict with the prognostic result in our study, but it can be explained by the following possibility. First, during tumorigenesis, a large number of genes are changed at the expression level. The general trend is that oncogenes are

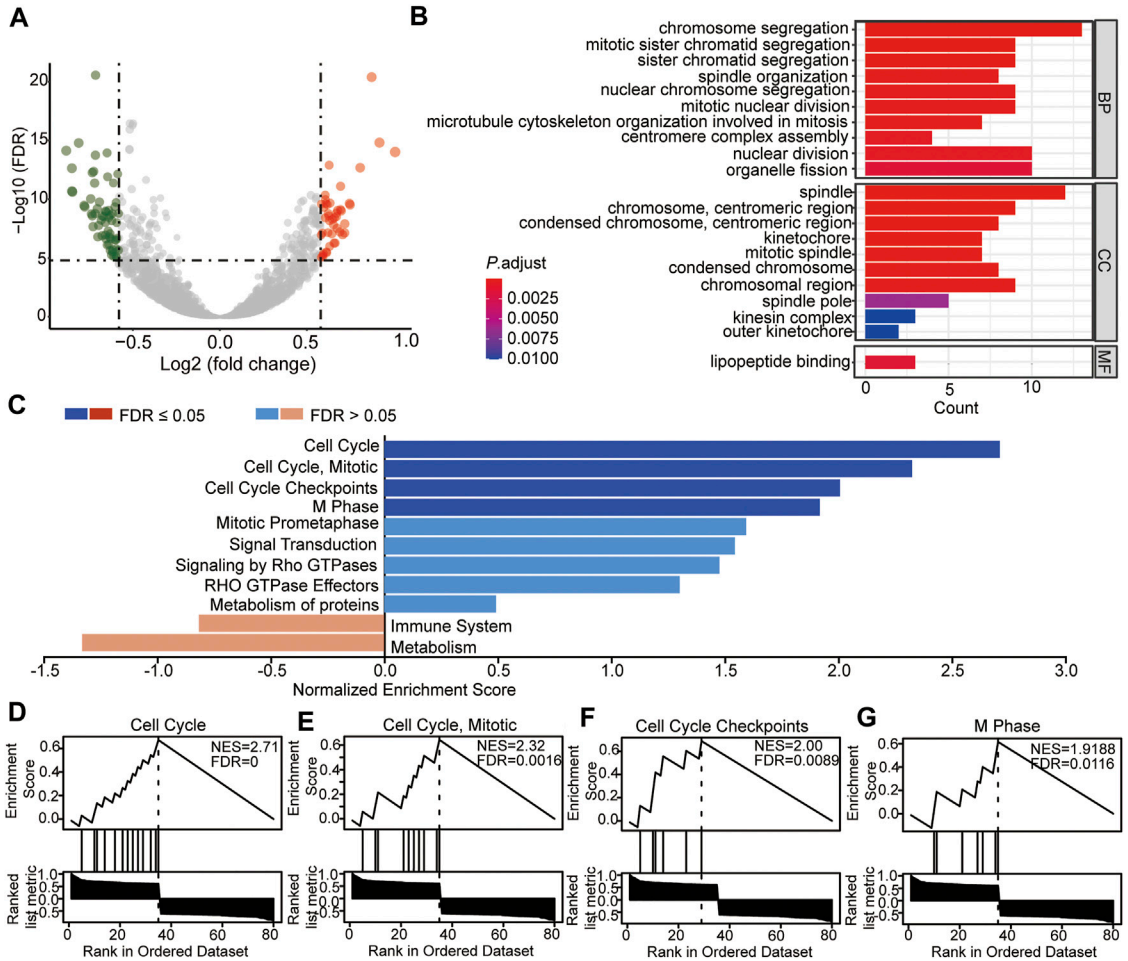

FIGURE 10 | Identification and enrichment analysis of DEGs between the two risk-subtypes. **(A)** Volcano plot showing the DEGs in high-risk vs. low-risk groups. **(B)** Enriched GO terms of DEGs in the high-risk group. **(C)** GSEA analysis of DEGs in the high-risk group **(D–G)** GSEA enrichment with the threshold of FDR<0.05 of DEGs in the high-risk group. NES: normalized enrichment score.

activated by upregulation, while tumor suppressors are disrupted in the function (Lee and Muller, 2010). These factors all predispose the development of tumor cells. However, tumor cells live in a complex microenvironment composed of a variety of cells, including immune cells, cancer-associated fibroblasts, cancer stem cells, the extracellular matrix, and blood vessels (Arneth, 2019). Tumor growth is jointly regulated by these multiple cells and their secreted factors, and some protumor genes were not upregulated to limit their unlimited growth. Moreover, there is considerable gene expression heterogeneity in tumors among different populations. The results of RNA sequencing represent the overall expression of genes in all cancer patients but not the specific expression of genes in individuals. In summary, the regulatory role of *TEAD4* in LUAD still needs to be further explored, which is of great significance for finding novel potential therapeutic targets for LUAD.

Among the 102 DEGs in *TEAD4*-high expression subtypes, four genes including *CPS1*, *ANLN*, *RHOV*, and *KRT6A*, were identified to be independent prognostic signatures after univariate Cox regression, LASSO regression, and multivariate Cox regression. The four genes were all positively correlated with the *TEAD4* expression in LUAD, indicating that they were *TEAD4*-related signatures. The enhanced expression of this four-gene signature represents the populations of high risk. However, this was caused by the high *TEAD4* expression. In other words, the high expression of *TEAD4* led to a poor outcome partly by improving the four-gene signature expression. This study highlighted the relationship between the overall survival and immune microenvironment estimation of patients and the elevated expression of these genes and indicated that the high expression of TEAD4 predicted the poor outcome and the potential immunotherapeutic resistance by improving the four-gene signature expression. In addition, similar to *TEAD4*, three of these genes (*ANLN*, *KRT6A*, and *RHOV*) were associated with poor outcomes in LUAD, which were all recognized as oncogenic genes. For instance, *ANLN* is a well-

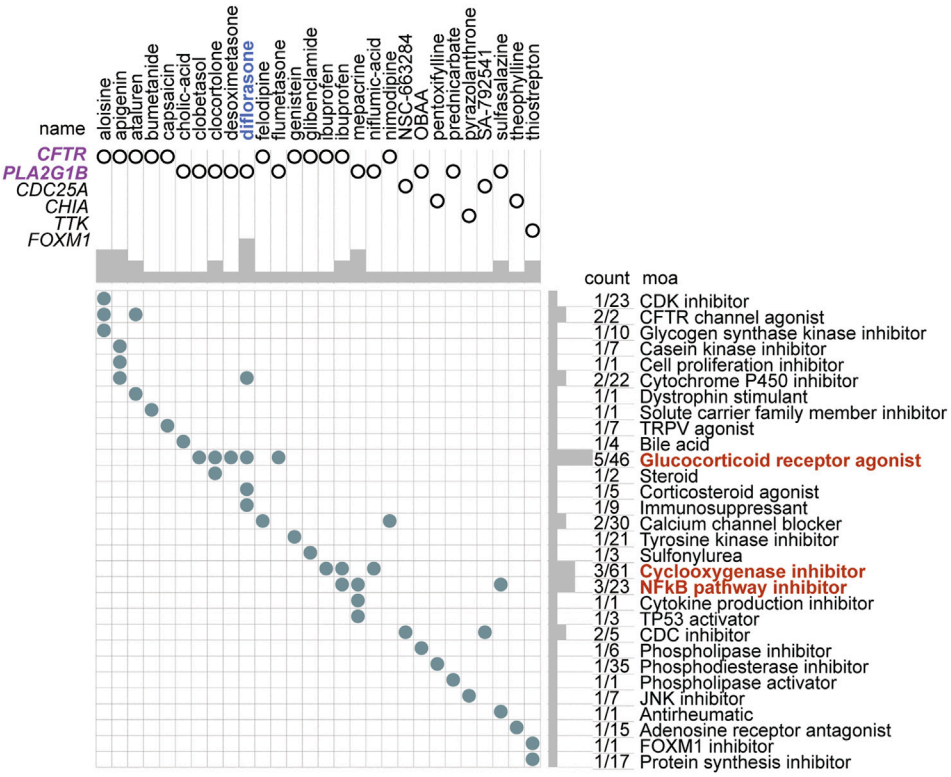

FIGURE 11 | Small-molecule perturbagen chemotherapeutics forecast for high-risk patients based on the DEGs. The chemotherapeutics forecast for the high-risk patients is based on the DEGs.

known oncogene that promotes carcinogenesis and therapeutic resistance in multiple types of cancers, such as LUAD (Long et al., 2018; Xu et al., 2019; Deng et al., 2021), oral cancer (Wang B et al., 2021), colorectal cancer (Liu et al., 2022), breast cancer (Wang et al., 2020; Maryam and Chin, 2021), pancreatic cancer (Wang et al., 2019), and head and neck squamous cell carcinoma (Guo et al., 2021). *RHOV* has been widely studied to promote LUAD cell growth, metastasis, and therapeutic resistance (Chen H et al., 2021; Zhang et al., 2021). In addition, *KRT6A* has been shown to participate in tumor proliferation, invasion, EMT, and cancer stem cell transformation in lung cancer (Yang et al., 2020; Zhou J et al., 2021; Che et al., 2021). *CPS1* has been reported to be an oncogene that is upregulated and has prognostic significance in LUAD (Wu et al., 2020). Our study here found that *CPS1*, *ANLN*, *RHOV*, and *KRT6A* were *TEAD4*-related independent prognostic signatures in LUAD. This finding indicates that the four genes were regulated by *TEAD4* or the Hippo pathway, which provides an innovative theoretical basis for further research on the regulatory mechanism of these genes. It also provides more possibilities for studying the anticancer mechanism of these genes. Additionally, our study is the first to combine these four oncogenic genes and divide the LUAD sample into two risk subgroups according to the risk score, calculated by the combination of the expressions of the four genes and the survival of patients. Compared with previous studies on the four genes, the present study focuses more on the analysis of the common prognostic value of the four genes in combination with clinical risk factors. These four genes were innovatively identified as independent risk factors for LUAD to predict prognosis in conjunction with other clinical risk factors and provide a new theoretical basis for the choice of individual treatment for patients. Finally, through systematic analysis of data from different databases, the consistent results confirm the prognostic value of the four-gene signature and further highlight the non-negligible role of these genes in human cancer.

The TME estimation of the two risk subtypes suggests that the high-risk group has higher stromal, immune, and ESTIMATE scores, as well as a lower score of tumor purity. The proportions of plasma cells, resting memory CD4 T cells, monocytes, resting dendritic cells, and resting mast cells were lower in the high-risk group, while the proportions of CD8 T cells, activated memory CD4 T cells, resting NK cells, M0 macrophages, M1 macrophages, activated dendritic cells, activated mast cells, and neutrophils were higher. Tumor-associated macrophages (TAMs) are among the most abundant immune cells in the TME and act to enhance tumor progression and metastasis (Mantovani et al., 2017; Cassetta and Pollard, 2018; Lopez-Yrigoyen et al., 2021). High infiltration of TAMs is associated

with poor prognosis in several types of cancer, such as breast cancer, ovarian cancer, bladder cancer, and NSCLC (Yin et al., 2017; Zhao et al., 2017; Kowal et al., 2019; Lopez-Yrigoyen et al., 2021). The microenvironmental stimuli and signals that encounter each specific tissue always induce macrophage polarization. According to the specific inducers, two major macrophage subpopulations, classically activated or inflammatory (M1) and alternatively activated or anti-inflammatory (M2) macrophages, have been identified (M0 macrophages are naïve macrophages without polarization) (Miao et al., 2017; Huang et al., 2019; Kang et al., 2020). Functionally, M1 macrophages have robust antimicrobial and antitumoral activity, by removing pathogens during infection (Shapouri-Moghaddam et al., 2018), while M2 macrophages participate in angiogenesis, immunoregulation, tumor formation, and progression (Shapouri-Moghaddam et al., 2018). The different levels of infiltration of immune cells directly determine the different prognoses of patients.

As another indicator of immune escape, MHC-I and MHC-II molecules were found to be lower in the high-risk subtype than in the low-risk group. Degrading MHC-I is always a cause of immune evasion, a major obstacle for cancer therapy, which has been implicated in resistance to immune checkpoint blockade (ICB) therapy (McGranahan et al., 2017; Rodig et al., 2018; Burr et al., 2019; Yamamoto et al., 2020a; Yamamoto et al., 2020b; Zhou Y et al., 2021; Dhatchinamoorthy et al., 2021). During the process of immune evasion, MHC-I downregulation is one major mechanism to avoid antitumor immunity by reducing recognition by cytotoxic $CD8^+$ T cells, often correlating with poor prognosis (Cornel et al., 2020). In addition to MHC-I and MHC-II, an antigen-presenting complex traditionally associated with professional antigen-presenting cells (APCs) is critical in antitumor immunity (Axelrod et al., 2019). Tumor-specific MHC-II is reported to be associated with superior prognosis, allowing recognition of tumor cells by the immune system, thus playing a role in immunotherapy and improving the response to ICB therapy (Mortara et al., 2006; Forero et al., 2016; Johnson et al., 2016). The downregulated MHC-I and MHC-II molecules in the high-risk subtypes indicate the potential strong immune escape and ICB therapy resistance of the patients in this group.

Moreover, immune checkpoint genes were also detected, and the results showed that *CD274* (*PD-L1*) and *LAG3* (CD223) were highly expressed in the high-risk subtype. PD-L1 (Programmed death-ligand 1) is expressed on several types of tumor cells, mediating the tumor-induced immune suppression (immune checkpoint) by binding with the receptor PD-1 (programmed cell death protein 1), which is highly expressed in activated T cells, B cells, dendritic cells, and natural killer cells (Dermani et al., 2019). The binding of PD-L1 to PD-1 on T cells results in the inhibition of cancer cells by destruction by T cells, thus promoting immune escape (Gou et al., 2020). Therefore, PD-L1 or PD-1 monoclonal antibodies have been used for cancer treatment (Bagchi et al., 2021; Carlino et al., 2021; Doroshow et al., 2021). A higher level of PD-L1 predicts a worse outcome in patients. In addition, *LAG3* (lymphocyte activation gene 3, CD223) is another kind of inhibitory receptor (IRs) that has been reported to play a negative regulatory role in cancer immunology by interacting with its ligands (Wang M et al., 2021). *LAG3* expression is also shown to be positively associated with *CD274* (*PD-L1*) (Wang M et al., 2021). TEAD4 is known as a transcription factor associated with resistance to different therapeutic approaches (Jiao et al., 2017; Yu et al., 2021; Yan et al., 2022). Unfortunately, these studies were not confirmed in patients with LUAD. Our study systematically analyzed the TME in patients with LUAD and demonstrated that a high expression of *TEAD4* is associated with a poor anti-tumor immune response, with evidence of a lower immune score and HLA family components and higher levels of immune checkpoint genes in the high-risk subgroups based on the high *TEAD4* expression. This not only reinforces previous research but also provides new insights into the mechanisms of this gene involved in therapy resistance. Finally, DEGs between the two risk groups were identified, and the subsequent GO and GSEA showed that cell division and cell cycle regulation-related genes were enriched in the high-risk group, while immune response- and metabolism-related genes were enriched in the low-risk group. This is consistent with *TEAD4*-high expression-related DEGs, as well as the TME result in the Cox model, further confirming the conclusion in this study.

According to these DEGs, the forecasted adjuvant small-molecule drugs for the high-risk subtype are perturbations targeting *CFTR*, *PLA2G1B*, *CDC25A*, *CHIA*, *TTK*, and *OXM1* by the moa of the CDK inhibitor, CFTR channel agonist, cytochrome p450 inhibitor, glucocorticoid receptor agonist, cyclooxygenase inhibitor, or NFkB pathway inhibitor. Targeting these pathways may be an efficient therapeutic strategy for patients with high levels of *TEAD4*. A total of 28 potential small-molecule drugs were predicted based on the specific differentially expressed genes in these populations. This not only provided a novel solution to the low survival of patients with LUAD but also laid a theoretical foundation for further drug research and development.

However, there are several limitations to the present study that should be stated. First, despite the fact that bioinformatic technology is powerful in efficiently understanding biological functions, the underlying mechanisms of these genes in LUAD still need further cellular explorations. Moreover, clinical tissues and paired adjacent normal tissues should be collected to further detect the protein expression level of TEAD4, as well as the related cell cycle and immune response genes in LUAD. Second, as this is a retrospective study, missing data and selection biases were inevitable, and the statistical power might be low. Therefore, further studies with a large sample size are warranted to increase the statistical power. Finally, due to lack of data about immunotherapies, the relationship between the *TEAD4* expression and ICB therapy response cannot be investigated. More clinical and demographic characteristics of LUAD patients need to be included in further studies.

In summary, our results suggest that *TEAD4* is a novel molecular biomarker for diagnosis and prognosis, predicting overall survival and immune microenvironment estimation in

LUAD. However, large prospective studies are warranted, and further experimental validation should be performed to prove the prognostic value of this gene in LUAD.

DATA AVAILABILITY STATEMENT

Publicly available datasets were analyzed in this study. These data can be found at: https://xenabrowser.net/datapages/?cohort=GDC%20TCGA%20Lung%20Adenocarcinoma%20(LUAD)&removeHub=https%3A%2F%2Fxena.treehouse.gi.ucsc.edu%3A443.

AUTHOR CONTRIBUTIONS

Conceptualization, XG; data curation, XG and HX; formal analysis, XG; funding acquisition, HX; investigation, NL and ZL; methodology, NL and CS; project administration, HX; supervision, HX; validation, HX; visualization, XG; writing—original draft, XG; writing—review and editing, HX.

FUNDING

This work was supported by grants from the Natural Science Foundation of China (31301146 to HX), the Natural Science Foundation of Jiangsu Province (BK20130605 to HX), and the Fundamental Research Funds for the Central Universities to HX (2242020K40214).

SUPPLEMENTARY MATERIAL

The Supplementary Material for this article can be found online at: https://www.frontiersin.org/articles/10.3389/fphar.2022.874780/full#supplementary-material

Supplementary Figure S1 | Heatmap of DEGs in *TEAD4*-high vs. *TEAD4*-low groups.

Supplementary Figure S2 | Validation of the Cox model with GEO data. **(A–C)** Overall survival of high- and low-risk groups, respectively, in GEO validation set#1 **(A)**, validation set#2 **(B)**, and validation set#3 **(C)**. **(D–F)** ROC analyses of the model for 1, 3, and 5 years, respectively, in GEO validation set#1 **(D)**, validation set#2 **(E)**, and validation set#3 **(F)**.

REFERENCES

Arneth, B. (2019). Tumor Microenvironment. *Medicina (Kaunas)* 56 (1), 15. doi:10.3390/medicina56010015

Ashburner, M., Ball, C. A., Blake, J. A., Botstein, D., Butler, H., Cherry, J. M., et al. (2000). Gene Ontology: Tool for the Unification of Biology. The Gene Ontology Consortium. *Nat. Genet.* 25 (1), 25–29. doi:10.1038/75556

Axelrod, M. L., Cook, R. S., Johnson, D. B., and Balko, J. M. (2019). Biological Consequences of MHC-II Expression by Tumor Cells in Cancer. *Clin. Cancer Res.* 25 (8), 2392–2402. doi:10.1158/1078-0432.CCR-18-3200

Bagchi, S., Yuan, R., and Engleman, E. G. (2021). Immune Checkpoint Inhibitors for the Treatment of Cancer: Clinical Impact and Mechanisms of Response and Resistance. *Annu. Rev. Pathol.* 16, 223–249. doi:10.1146/annurev-pathol-042020-042741

Bray, F., Ferlay, J., Soerjomataram, I., Siegel, R. L., Torre, L. A., and Jemal, A. (2018). Global Cancer Statistics 2018: GLOBOCAN Estimates of Incidence and Mortality Worldwide for 36 Cancers in 185 Countries. *CA Cancer J. Clin.* 68 (6), 394–424. doi:10.3322/caac.21492

Burr, M. L., Sparbier, C. E., Chan, K. L., Chan, Y. C., Kersbergen, A., Lam, E. Y. N., et al. (2019). An Evolutionarily Conserved Function of Polycomb Silences the MHC Class I Antigen Presentation Pathway and Enables Immune Evasion in Cancer. *Cancer Cell* 36 (4), 385. doi:10.1016/j.ccell.2019.08.008

Byers, L. A., and Rudin, C. M. (2015). Small Cell Lung Cancer: where Do We Go from Here? *Cancer* 121 (5), 664–672. doi:10.1002/cncr.29098

Carlino, M. S., Larkin, J., and Long, G. V. (2021). Immune Checkpoint Inhibitors in Melanoma. *Lancet* 398 (10304), 1002–1014. doi:10.1016/S0140-6736(21)01206-X

Cassetta, L., and Pollard, J. W. (2018). Targeting Macrophages: Therapeutic Approaches in Cancer. *Nat. Rev. Drug Discov.* 17 (12), 887–904. doi:10.1038/nrd.2018.169

Che, D., Wang, M., Sun, J., Li, B., Xu, T., Lu, Y., et al. (2021). KRT6A Promotes Lung Cancer Cell Growth and Invasion through MYC-Regulated Pentose Phosphate Pathway. *Front. Cel Dev. Biol.* 9, 694071. doi:10.3389/fcell.2021.694071

Chen CL, C. L., Hsu, S. C., Chung, T. Y., Chu, C. Y., Wang, H. J., Hsiao, P. W., et al. (2021). Arginine Is an Epigenetic Regulator Targeting TEAD4 to Modulate OXPHOS in Prostate Cancer Cells. *Nat. Commun.* 12 (1), 2398. doi:10.1038/s41467-021-22652-9

Chen H, H., Xia, R., Jiang, L., Zhou, Y., Xu, H., Peng, W., et al. (2021). Overexpression of RhoV Promotes the Progression and EGFR-TKI Resistance of Lung Adenocarcinoma. *Front. Oncol.* 11, 619013. doi:10.3389/fonc.2021.619013

Cornel, A. M., Mimpen, I. L., and Nierkens, S. (2020). MHC Class I Downregulation in Cancer: Underlying Mechanisms and Potential Targets for Cancer Immunotherapy. *Cancers (Basel)* 12 (7), 1760. doi:10.3390/cancers12071760

de Sousa, V. M. L., and Carvalho, L. (2018). Heterogeneity in Lung Cancer. *Pathobiology* 85 (1-2), 96–107. doi:10.1159/000487440

Deng, F., Xu, Z., Zhou, J., Zhang, R., and Gong, X. (2021). ANLN Regulated by miR-30a-5p Mediates Malignant Progression of Lung Adenocarcinoma. *Comput. Math. Methods Med.* 2021, 9549287. doi:10.1155/2021/9549287

Denisenko, T. V., Budkevich, I. N., and Zhivotovsky, B. (2018). Cell Death-Based Treatment of Lung Adenocarcinoma. *Cell Death Dis.* 9 (2), 117. doi:10.1038/s41419-017-0063-y

Dermani, F. K., Samadi, P., Rahmani, G., Kohlan, A. K., and Najafi, R. (2019). PD-1/PD-L1 Immune Checkpoint: Potential Target for Cancer Therapy. *J. Cel Physiol.* 234 (2), 1313–1325. doi:10.1002/jcp.27172

Dey, A., Varelas, X., and Guan, K. L. (2020). Targeting the Hippo Pathway in Cancer, Fibrosis, Wound Healing and Regenerative Medicine. *Nat. Rev. Drug Discov.* 19 (7), 480–494. doi:10.1038/s41573-020-0070-z

Dhatchinamoorthy, K., Colbert, J. D., and Rock, K. L. (2021). Cancer Immune Evasion through Loss of MHC Class I Antigen Presentation. *Front. Immunol.* 12, 636568. doi:10.3389/fimmu.2021.636568

Doroshow, D. B., Bhalla, S., Beasley, M. B., Sholl, L. M., Kerr, K. M., Gnjatic, S., et al. (2021). PD-L1 as a Biomarker of Response to Immune-Checkpoint Inhibitors. *Nat. Rev. Clin. Oncol.* 18 (6), 345–362. doi:10.1038/s41571-021-00473-5

Forero, A., Li, Y., Chen, D., Grizzle, W. E., Updike, K. L., Merz, N. D., et al. (2016). Expression of the MHC Class II Pathway in Triple-Negative Breast Cancer Tumor Cells Is Associated with a Good Prognosis and Infiltrating Lymphocytes. *Cancer Immunol. Res.* 4 (5), 390–399. doi:10.1158/2326-6066.CIR-15-0243

Gavralidis, A., and Gainor, J. F. (2020). Immunotherapy in EGFR-Mutant and ALK-Positive Lung Cancer: Implications for Oncogene-Driven Lung Cancer. *Cancer J.* 26 (6), 517–524. doi:10.1097/PPO.0000000000000491

Gerada, C., and Ryan, K. M. (2020). Autophagy, the Innate Immune Response and Cancer. *Mol. Oncol.* 14 (9), 1913–1929. doi:10.1002/1878-0261.12774

Gou, Q., Dong, C., Xu, H., Khan, B., Jin, J., Liu, Q., et al. (2020). PD-L1 Degradation Pathway and Immunotherapy for Cancer. *Cel Death Dis.* 11 (11), 955. doi:10.1038/s41419-020-03140-2

Gu, C., Huang, Z., Chen, X., Liu, C., Rocco, G., Zhao, S., et al. (2020). TEAD4 Promotes Tumor Development in Patients with Lung Adenocarcinoma via ERK Signaling Pathway. *Biochim. Biophys. Acta Mol. Basis Dis.* 1866 (12), 165921. doi:10.1016/j.bbadis.2020.165921

Guo, E., Mao, X., Wang, X., Guo, L., An, C., Zhang, C., et al. (2021). Alternatively Spliced ANLN Isoforms Synergistically Contribute to the Progression of Head and Neck Squamous Cell Carcinoma. *Cel Death Dis.* 12 (8), 764. doi:10.1038/s41419-021-04063-2

He, L., Yuan, L., Sun, Y., Wang, P., Zhang, H., Feng, X., et al. (2019). Glucocorticoid Receptor Signaling Activates TEAD4 to Promote Breast Cancer Progression. *Cancer Res.* 79 (17), 4399–4411. doi:10.1158/0008-5472.CAN-19-0012

Hoy, H., Lynch, T., and Beck, M. (2019). Surgical Treatment of Lung Cancer. *Crit. Care Nurs. Clin. North. Am.* 31 (3), 303–313. doi:10.1016/j.cnc.2019.05.002

Hu, Y., Mu, H., and Deng, Z. (2021). The Transcription Factor TEAD4 Enhances Lung Adenocarcinoma Progression through Enhancing PKM2 Mediated Glycolysis. *Cell Biol. Int.* 45 (10), 2063–2073. doi:10.1002/cbin.11654

Huang, H., Zhang, W., Pan, Y., Gao, Y., Deng, L., Li, F., et al. (2017). YAP Suppresses Lung Squamous Cell Carcinoma Progression via Deregulation of the DNp63-GPX2 Axis and ROS Accumulation. *Cancer Res.* 77 (21), 5769–5781. doi:10.1158/0008-5472.CAN-17-0449

Huang, Y., Du, K. L., Guo, P. Y., Zhao, R. M., Wang, B., Zhao, X. L., et al. (2019). IL-16 Regulates Macrophage Polarization as a Target Gene of Mir-145-3p. *Mol. Immunol.* 107, 1–9. doi:10.1016/j.molimm.2018.12.027

Jiao, S., Li, C., Hao, Q., Miao, H., Zhang, L., Li, L., et al. (2017). VGLL4 Targets a TCF4-TEAD4 Complex to Coregulate Wnt and Hippo Signalling in Colorectal Cancer. *Nat. Commun.* 8, 14058. doi:10.1038/ncomms14058

Johnson, D. B., Estrada, M. V., Salgado, R., Sanchez, V., Doxie, D. B., Opalenik, S. R., et al. (2016). Melanoma-specific MHC-II Expression Represents a Tumour-Autonomous Phenotype and Predicts Response to Anti-PD-1/PD-L1 Therapy. *Nat. Commun.* 7, 10582. doi:10.1038/ncomms10582

Kang, M., Huang, C. C., Lu, Y., Shirazi, S., Gajendrareddy, P., Ravindran, S., et al. (2020). Bone Regeneration Is Mediated by Macrophage Extracellular Vesicles. *Bone* 141, 115627. doi:10.1016/j.bone.2020.115627

Kowal, J., Kornete, M., and Joyce, J. A. (2019). Re-education of Macrophages as a Therapeutic Strategy in Cancer. *Immunotherapy* 11 (8), 677–689. doi:10.2217/imt-2018-0156

Lee, E. Y., and Muller, W. J. (2010). Oncogenes and Tumor Suppressor Genes. *Cold Spring Harb. Perspect. Biol.* 2 (10), a003236. doi:10.1101/cshperspect.a003236

Liu, Y., Xing, Y., and Cai, L. (2017). Role of Hippo Signaling Pathway in Lung Cancer. *Zhongguo Fei Ai Za Zhi* 20 (9), 629–634. doi:10.3779/j.issn.1009-3419.2017.09.07

Liu, Y., Cao, P., Cao, F., Wang, S., He, Y., Xu, Y., et al. (2022). ANLN, Regulated by SP2, Promotes Colorectal Carcinoma Cell Proliferation via PI3K/AKT and MAPK Signaling Pathway. *J. Invest. Surg.* 35 (2), 268–277. doi:10.1080/08941939.2020.1850939

Long, X., Zhou, W., Wang, Y., and Liu, S. (2018). Prognostic Significance of ANLN in Lung Adenocarcinoma. *Oncol. Lett.* 16 (2), 1835–1840. doi:10.3892/ol.2018.8858

Lopez-Yrigoyen, M., Cassetta, L., and Pollard, J. W. (2021). Macrophage Targeting in Cancer. *Ann. N. Y Acad. Sci.* 1499 (1), 18–41. doi:10.1111/nyas.14377

Love, M. I., Huber, W., and Anders, S. (2014). Moderated Estimation of Fold Change and Dispersion for RNA-Seq Data with DESeq2. *Genome Biol.* 15 (12), 550. doi:10.1186/s13059-014-0550-8

Mantovani, A., Marchesi, F., Malesci, A., Laghi, L., and Allavena, P. (2017). Tumour-associated Macrophages as Treatment Targets in Oncology. *Nat. Rev. Clin. Oncol.* 14 (7), 399–416. doi:10.1038/nrclinonc.2016.217

Maryam, A., and Chin, Y. R. (2021). ANLN Enhances Triple-Negative Breast Cancer Stemness through TWIST1 and BMP2 and Promotes its Spheroid Growth. *Front. Mol. Biosci.* 8, 700973. doi:10.3389/fmolb.2021.700973

Masliantsev, K., Karayan-Tapon, L., and Guichet, P. O. (2021). Hippo Signaling Pathway in Gliomas. *Cells* 10 (1), 184. doi:10.3390/cells10010184

McGranahan, N., Rosenthal, R., Hiley, C. T., Rowan, A. J., Watkins, T. B. K., Wilson, G. A., et al. (2017). Allele-Specific HLA Loss and Immune Escape in Lung Cancer Evolution. *Cell* 171 (6), 1259. doi:10.1016/j.cell.2017.10.001

Miao, X., Leng, X., and Zhang, Q. (2017). The Current State of Nanoparticle-Induced Macrophage Polarization and Reprogramming Research. *Int. J. Mol. Sci.* 18 (2), 336. doi:10.3390/ijms18020336

Mohajan, S., Jaiswal, P. K., Vatanmakarian, M., Yousefi, H., Sankaralingam, S., Alahari, S. K., et al. (2021). Hippo Pathway: Regulation, Deregulation and Potential Therapeutic Targets in Cancer. *Cancer Lett.* 507, 112–123. doi:10.1016/j.canlet.2021.03.006

Mortara, L., Castellani, P., Meazza, R., Tosi, G., De Lerma Barbaro, A., Procopio, F. A., et al. (2006). CIITA-induced MHC Class II Expression in Mammary Adenocarcinoma Leads to a Th1 Polarization of the Tumor Microenvironment, Tumor Rejection, and Specific Antitumor Memory. *Clin. Cancer Res.* 12 (11 Pt 1), 3435–3443. doi:10.1158/1078-0432.CCR-06-0165

Newman, A. M., Liu, C. L., Green, M. R., Gentles, A. J., Feng, W., Xu, Y., et al. (2015). Robust Enumeration of Cell Subsets from Tissue Expression Profiles. *Nat. Methods* 12 (5), 453–457. doi:10.1038/nmeth.3337

Ogata, H., Goto, S., Sato, K., Fujibuchi, W., Bono, H., and Kanehisa, M. (1999). KEGG: Kyoto Encyclopedia of Genes and Genomes. *Nucleic Acids Res.* 27 (1), 29–34. doi:10.1093/nar/27.1.29

Okayama, H., Kohno, T., Ishii, Y., Shimada, Y., Shiraishi, K., Iwakawa, R., et al. (2012). Identification of Genes Upregulated in ALK-Positive and EGFR/KRAS/ALK-negative Lung Adenocarcinomas. *Cancer Res.* 72 (1), 100–111. doi:10.1158/0008-5472.CAN-11-1403

O'Sullivan, D., Sanin, D. E., Pearce, E. J., and Pearce, E. L. (2019). Metabolic Interventions in the Immune Response to Cancer. *Nat. Rev. Immunol.* 19 (5), 324–335. doi:10.1038/s41577-019-0140-9

Pobbati, A. V., and Hong, W. (2013). Emerging Roles of TEAD Transcription Factors and its Coactivators in Cancers. *Cancer Biol. Ther.* 14 (5), 390–398. doi:10.4161/cbt.23788

Rodig, S. J., Gusenleitner, D., Jackson, D. G., Gjini, E., Giobbie-Hurder, A., Jin, C., et al. (2018). MHC Proteins Confer Differential Sensitivity to CTLA-4 and PD-1 Blockade in Untreated Metastatic Melanoma. *Sci. Transl. Med.* 10 (450), eaar3342. doi:10.1126/scitranslmed.aar3342

Rousseaux, S., Debernardi, A., Jacquiau, B., Vitte, A. L., Vesin, A., Nagy-Mignotte, H., et al. (2013). Ectopic Activation of Germline and Placental Genes Identifies Aggressive Metastasis-Prone Lung Cancers. *Sci. Transl. Med.* 5 (186), 186ra66. doi:10.1126/scitranslmed.3005723

Schenk, E. L., Patil, T., Pacheco, J., and Bunn, P. A. (2021). 2020 Innovation Based Optimism for Lung Cancer Outcomes. *Oncologist* 26 (3), e454–e472. doi:10.1002/onco.13590

Shapouri-Moghaddam, A., Mohammadian, S., Vazini, H., Taghadosi, M., Esmaeili, S. A., Mardani, F., et al. (2018). Macrophage Plasticity, Polarization, and Function in Health and Disease. *J. Cel Physiol.* 233 (9), 6425–6440. doi:10.1002/jcp.26429

Sher, T., Dy, G. K., and Adjei, A. A. (2008). Small Cell Lung Cancer. *Mayo Clin. Proc.* 83 (3), 355–367. doi:10.4065/83.3.355

Shuai, Y., Ma, Z., Liu, W., Yu, T., Yan, C., Jiang, H., et al. (2020). TEAD4 Modulated LncRNA MNX1-AS1 Contributes to Gastric Cancer Progression Partly through Suppressing BTG2 and Activating BCL2. *Mol. Cancer* 19 (1), 6. doi:10.1186/s12943-019-1104-1

Subramanian, A., Tamayo, P., Mootha, V. K., Mukherjee, S., Ebert, B. L., Gillette, M. A., et al. (2005). Gene Set Enrichment Analysis: a Knowledge-Based Approach for Interpreting Genome-wide Expression Profiles. *Proc. Natl. Acad. Sci. U S A.* 102 (43), 15545–15550. doi:10.1073/pnas.0506580102

Tomczak, K., Czerwińska, P., and Wiznerowicz, M. (2015). The Cancer Genome Atlas (TCGA): an Immeasurable Source of Knowledge. *Contemp. Oncol. (Pozn)* 19 (1A), A68–A77. doi:10.5114/wo.2014.47136

Tomida, S., Takeuchi, T., Shimada, Y., Arima, C., Matsuo, K., Mitsudomi, T., et al. (2009). Relapse-related Molecular Signature in Lung Adenocarcinomas Identifies Patients with Dismal Prognosis. *J. Clin. Oncol.* 27 (17), 2793–2799. doi:10.1200/JCO.2008.19.7053

Wang, Y., Xu, X., Maglic, D., Dill, M. T., Mojumdar, K., Ng, P. K., et al. (2018). Comprehensive Molecular Characterization of the Hippo Signaling Pathway in Cancer. *Cell Rep.* 25 (5), 1304. doi:10.1016/j.celrep.2018.10.001

Wang, A., Dai, H., Gong, Y., Zhang, C., Shu, J., Luo, Y., et al. (2019). ANLN-induced EZH2 Upregulation Promotes Pancreatic Cancer Progression by Mediating miR-218-5p/LASP1 Signaling axis. *J. Exp. Clin. Cancer Res.* 38 (1), 347. doi:10.1186/s13046-019-1340-7

Wang, F., Xiang, Z., Huang, T., Zhang, M., and Zhou, W. B. (2020). ANLN Directly Interacts with RhoA to Promote Doxorubicin Resistance in Breast Cancer Cells. *Cancer Manag. Res.* 12, 9725–9734. doi:10.2147/CMAR.S261828

Wang J, J., Shen, C., Zhang, J., Zhang, Y., Liang, Z., Niu, H., et al. (2021). TEAD4 Is an Immune Regulating-Related Prognostic Biomarker for Bladder Cancer and Possesses Generalization Value in Pan-Cancer. *DNA Cel Biol.* 40 (6), 798–810. doi:10.1089/dna.2021.0164

Wang B, B., Zhang, X. L., Li, C. X., Liu, N. N., Hu, M., and Gong, Z. C. (2021). ANLN Promotes Carcinogenesis in Oral Cancer by Regulating the PI3K/mTOR Signaling Pathway. *Head Face Med.* 17 (1), 18. doi:10.1186/s13005-021-00269-z

Wang M, M., Du, Q., Jin, J., Wei, Y., Lu, Y., and Li, Q. (2021). LAG3 and its Emerging Role in Cancer Immunotherapy. *Clin. Transl. Med.* 11 (3), e365. doi:10.1002/ctm2.365

Wu, Y., Zheng, Q., Li, Y., Wang, G., Gao, S., Zhang, X., et al. (2019). Metformin Targets a YAP1-TEAD4 Complex via AMPKα to Regulate CCNE1/2 in Bladder Cancer Cells. *J. Exp. Clin. Cancer Res.* 38 (1), 376. doi:10.1186/s13046-019-1346-1

Wu, G., Zhao, Z., Yan, Y., Zhou, Y., Wei, J., Chen, X., et al. (2020). CPS1 Expression and its Prognostic Significance in Lung Adenocarcinoma. *Ann. Transl. Med.* 8 (6), 341. doi:10.21037/atm.2020.02.146

Wu Y, Y., Li, M., Lin, J., and Hu, C. (2021). Hippo/TEAD4 Signaling Pathway as a Potential Target for the Treatment of Breast Cancer. *Oncol. Lett.* 21 (4), 313. doi:10.3892/ol.2021.12574

Wu Q, Q., Yu, X., Li, J., Sun, S., and Tu, Y. (2021). Metabolic Regulation in the Immune Response to Cancer. *Cancer Commun. (Lond)* 41 (8), 661–694. doi:10.1002/cac2.12182

Xia, L., Oyang, L., Lin, J., Tan, S., Han, Y., Wu, N., et al. (2021). The Cancer Metabolic Reprogramming and Immune Response. *Mol. Cancer* 20 (1), 28. doi:10.1186/s12943-021-01316-8

Xu, J., Zheng, H., Yuan, S., Zhou, B., Zhao, W., Pan, Y., et al. (2019). Overexpression of ANLN in Lung Adenocarcinoma Is Associated with Metastasis. *Thorac. Cancer* 10 (8), 1702–1709. doi:10.1111/1759-7714.13135

Yamamoto, K., Venida, A., Yano, J., Biancur, D. E., Kakiuchi, M., Gupta, S., et al. (2020). Autophagy Promotes Immune Evasion of Pancreatic Cancer by Degrading MHC-I. *Nature* 581 (7806), 100–105. doi:10.1038/s41586-020-2229-5

Yamamoto, K., Venida, A., Perera, R. M., and Kimmelman, A. C. (2020). Selective Autophagy of MHC-I Promotes Immune Evasion of Pancreatic Cancer. *Autophagy* 16 (8), 1524–1525. doi:10.1080/15548627.2020.1769973

Yamanashi, K., Okumura, N., Takahashi, A., Nakashima, T., and Matsuoka, T. (2017). Surgical and Survival Outcomes of Lung Cancer Patients with Intratumoral Lung Abscesses. *J. Cardiothorac. Surg.* 12 (1), 44. doi:10.1186/s13019-017-0607-3

Yan, W., Chung, C. Y., Xie, T., Ozeck, M., Nichols, T. C., Frey, J., et al. (2022). Intrinsic and Acquired Drug Resistance to LSD1 Inhibitors in Small Cell Lung Cancer Occurs through a TEAD4-Driven Transcriptional State. *Mol. Oncol.* 16 (6), 1309–1328. doi:10.1002/1878-0261.13124

Yang, B., Zhang, W., Zhang, M., Wang, X., Peng, S., and Zhang, R. (2020). KRT6A Promotes EMT and Cancer Stem Cell Transformation in Lung Adenocarcinoma. *Technol. Cancer Res. Treat.* 19, 1533033820921248. doi:10.1177/1533033820921248

Yin, S., Huang, J., Li, Z., Zhang, J., Luo, J., Lu, C., et al. (2017). The Prognostic and Clinicopathological Significance of Tumor-Associated Macrophages in Patients with Gastric Cancer: A Meta-Analysis. *PLoS One* 12 (1), e0170042. doi:10.1371/journal.pone.0170042

Yoshihara, K., Shahmoradgoli, M., Martínez, E., Vegesna, R., Kim, H., Torres-Garcia, W., et al. (2013). Inferring Tumour Purity and Stromal and Immune Cell Admixture from Expression Data. *Nat. Commun.* 4, 2612. doi:10.1038/ncomms3612

Yu, G., Wang, L. G., Han, Y., and He, Q. Y. (2012). clusterProfiler: an R Package for Comparing Biological Themes Among Gene Clusters. *OMICS* 16 (5), 284–287. doi:10.1089/omi.2011.0118

Yu, M., Peng, Z., Qin, M., Liu, Y., Wang, J., Zhang, C., et al. (2021). Interferon-γ Induces Tumor Resistance to Anti-PD-1 Immunotherapy by Promoting YAP Phase Separation. *Mol. Cel* 81 (6), 1216–e9. doi:10.1016/j.molcel.2021.01.010

Zhang, Q., Fan, H., Zou, Q., Liu, H., Wan, B., Zhu, S., et al. (2018). TEAD4 Exerts Pro-metastatic Effects and Is Negatively Regulated by miR6839-3p in Lung Adenocarcinoma Progression. *J. Cel Mol. Med.* 22 (7), 3560–3571. doi:10.1111/jcmm.13634

Zhang, D., Jiang, Q., Ge, X., Shi, Y., Ye, T., Mi, Y., et al. (2021). RHOV Promotes Lung Adenocarcinoma Cell Growth and Metastasis through JNK/c-Jun Pathway. *Int. J. Biol. Sci.* 17 (10), 2622–2632. doi:10.7150/ijbs.59939

Zhang, B., Wang, Q., Ji, Y., Zhang, X., Xue, L., Shi, Q., et al. (2022). TEAD4 Overexpression Suppresses Thyroid Cancer Progression and Metastasis *In Vitro* by Modulating Wnt Signaling. *J. Biosci.* 47, 3. doi:10.1007/s12038-021-00238-3

Zhao, X., Qu, J., Sun, Y., Wang, J., Liu, X., Wang, F., et al. (2017). Prognostic Significance of Tumor-Associated Macrophages in Breast Cancer: A Meta-Analysis of the Literature. *Oncotarget* 8 (18), 30576–30586. doi:10.18632/oncotarget.15736

Zhou, Y., Huang, T., Zhang, J., Wong, C. C., Zhang, B., Dong, Y., et al. (2017). TEAD1/4 Exerts Oncogenic Role and Is Negatively Regulated by miR-4269 in Gastric Tumorigenesis. *Oncogene* 36 (47), 6518–6530. doi:10.1038/onc.2017.257

Zhou J, J., Jiang, G., Xu, E., Zhou, J., Liu, L., and Yang, Q. (2021). Identification of SRXN1 and KRT6A as Key Genes in Smoking-Related Non-small-cell Lung Cancer through Bioinformatics and Functional Analyses. *Front. Oncol.* 11, 810301. doi:10.3389/fonc.2021.810301

Zhou Y, Y., Bastian, I. N., Long, M. D., Dow, M., Li, W., Liu, T., et al. (2021). Activation of NF-kappaB and P300/CBP Potentiates Cancer Chemoimmunotherapy through Induction of MHC-I Antigen Presentation. *Proc. Natl. Acad. Sci. U S A.* 118 (8), e2025840118. doi:10.1073/pnas.2025840118

Conflict of Interest: The authors declare that the research was conducted in the absence of any commercial or financial relationships that could be construed as a potential conflict of interest.

frontiers | Frontiers in Pharmacology

ORIGINAL RESEARCH
published: 18 May 2022
doi: 10.3389/fphar.2022.862502

Comprehensive Analysis of Necroptosis in Pancreatic Cancer for Appealing its Implications in Prognosis, Immunotherapy, and Chemotherapy Responses

Kun Fang[1,2], *De-Sheng Tang*[1,2], *Chang-Sheng Yan*[1,2], *Jiamin Ma*[1,2], *Long Cheng*[1,2], *Yilong Li*[1,2] *and Gang Wang*[1,2]*

[1]*Department of Pancreatic and Biliary Surgery, First Affiliated Hospital of Harbin Medical University, Harbin, China,* [2]*Key Laboratory of Hepatosplenic Surgery, First Affiliated Hospital of Harbin Medical University, Harbin, China*

Objective: Necroptosis represents a new target for cancer immunotherapy and is considered a form of cell death that overcomes apoptosis resistance and enhances tumor immunogenicity. Herein, we aimed to determine necroptosis subtypes and investigate the roles of necroptosis in pancreatic cancer therapy.

Methods: Based on the expression of prognostic necroptosis genes in pancreatic cancer samples from TCGA and ICGC cohorts, a consensus clustering approach was implemented for robustly identifying necroptosis subtypes. Immunogenic features were evaluated according to immune cell infiltrations, immune checkpoints, HLA molecules, and cancer–immunity cycle. The sensitivity to chemotherapy agents was estimated using the pRRophetic package. A necroptosis-relevant risk model was developed with a multivariate Cox regression analysis.

Results: Five necroptosis subtypes were determined for pancreatic cancer (C1~C5) with diverse prognosis, immunogenic features, and chemosensitivity. In particular, C4 and C5 presented favorable prognosis and weakened immunogenicity; C2 had high immunogenicity; C1 had undesirable prognosis and high genetic mutations. C5 was the most sensitive to known chemotherapy agents (cisplatin, gemcitabine, docetaxel, and paclitaxel), while C4 displayed resistance to aforementioned agents. The necroptosis-relevant risk model could accurately predict prognosis, immunogenicity, and chemosensitivity.

OPEN ACCESS

Edited by:
Yosra A. Helmy,
University of Kentucky, United States

Reviewed by:
Yichun Wang,
Nanjing Medical University, China
Ben Liu,
Tianjin Medical University Cancer Institute and Hospital, China

****Correspondence:***
Gang Wang
wgilu79@163.com

Specialty section:
This article was submitted to Pharmacology of Anti-Cancer Drugs, a section of the journal Frontiers in Pharmacology

Received: *26 January 2022*
Accepted: *19 April 2022*
Published: *18 May 2022*

Citation:
Fang K, Tang D-S, Yan C-S, Ma J, Cheng L, Li Y and Wang G (2022) Comprehensive Analysis of Necroptosis in Pancreatic Cancer for Appealing its Implications in Prognosis, Immunotherapy, and Chemotherapy Responses. Front. Pharmacol. 13:862502. doi: 10.3389/fphar.2022.862502

Abbreviations: CDF, cumulative distribution function; CNV, copy number variation; EMT, epithelial–mesenchymal transition; GDSC, Genomics of Drug Sensitivity in Cancer; GO, Gene Ontology; GSVA, gene set variation analysis; HLA, human leukocyte antigen; HR, hazards ratio; ICGC, International Cancer Genome Consortium; IC50, half-maximal inhibitory concentration; KEGG, Kyoto Encyclopedia of Genes and Genomes; limma, linear models for microarray data; MAF, mutation annotation format; MLKL, mixed lineage kinase domain-like; PACA-AU, Pancreatic Cancer-Australia; PACA-CA, Pancreatic Cancer-Canada; pan-F-TBRS, pan-fibroblast TGFβ response; PCA, principal component analysis; ROC, receiver operator characteristic; RIPK1, receptor-interacting protein kinase 1; SNV, single-nucleotide variant; ssGSEA, single-sample gene set enrichment analysis; TCGA, The Cancer Genome Atlas; TRIM28, tripartite motif protein 28.

Conclusion: Our findings provided a conceptual framework for comprehending necroptosis in pancreatic cancer biology. Future work is required for evaluating its relevance in the design of combined therapeutic regimens and guiding the best choice for immuno- and chemotherapy.

Keywords: necroptosis, pancreatic cancer, prognosis, immunogenicity, immunotherapy, chemosensitivity

INTRODUCTION

Pancreatic cancer is one of the most lethal human cancers with an undesirable five-year survival rate < 10% (Yu et al., 2021). In 2018, there were 458,918 newly diagnosed pancreatic cancer cases and 432,242 death cases worldwide (Rawla et al., 2019). Surgical resection is currently the only therapeutic option with curative potential (Zhu et al., 2019a). Nevertheless, when diagnosed, about 80–85% patients have developed an unresectable or metastatic state (Tao et al., 2021). Even for the minority of patients who have the opportunity to receive surgical resection, only 20% can survive for 5 years (Zhu et al., 2020). Adjuvant chemotherapy with FOLFIRINOX (fluorouracil, irinotecan, leucovorin, and oxaliplatin) as a standard treatment option can prolong patients' long-term outcomes, with a median overall survival of 54.4 months (Park W. et al., 2021). Nevertheless, intrinsic and acquired resistance to chemotherapy is still a thorny issue in pancreatic cancer therapy (Zhu et al., 2019b). At present, a few clinical trials are ongoing to evaluate the efficacy of immunotherapy in pancreatic cancer (O'Hara et al., 2021; Pang et al., 2021; Zhu et al., 2021). Regrettably, none of these trials fail to show satisfying outcomes (Schizas et al., 2020). Hence, it is urgently required to design novel therapeutic regimens specifically targeting pancreatic cancer biology.

Necroptosis is a form of regulated necrotic cell death mainly mediated by receptor-interacting protein kinase 1 (RIPK1), RIPK3, and mixed lineage kinase domain-like (MLKL) protein (Gong et al., 2019). Necroptosis has become a new target for cancer immunotherapy because it is considered a form of cell death overcoming apoptosis resistance that enhances tumor immunogenicity, which is particularly important for the treatment of immune-desert tumors (Tang et al., 2020b). For instance, RIPK3 activation-triggered de-inhibition of tripartite motif protein 28 (TRIM28) in tumor cells results in increased immunostimulatory cytokine production within the tumor microenvironment and thus contributes to robust cytotoxic antitumor immunity (Park H. H. et al., 2021). Previous studies have uncovered the significance of necroptosis in pancreatic cancer. For instance, necroptosis facilitates pancreatic cancer cell migration and invasion through releasing CXCL5 (Ando et al., 2020). The aurora kinase inhibitor CCT137690 triggers necroptosis in pancreatic cancer cells through RIPK1, RIPK3, and MLKL and thus suppresses tumor growth (Xie et al., 2017). Necroptosis-induced CXCL1 and Mincle signaling facilitate macrophage-mediated adaptive immune inhibition and thus enhance pancreatic cancer progression (Seifert et al., 2016). In-depth understanding of necroptosis is crucial for immune surveillance and treatment management.

In our study, we clustered five robust necroptosis subtypes of pancreatic cancer, following the consensus clustering approach based on prognostic necroptosis genes. The five necroptosis subtypes displayed diverse prognosis, immunogenic features, genomic mutations, and chemosensitivity, providing a reference for combined therapeutic regimens and guiding the best choice of patients for immuno- and chemotherapy. Moreover, we developed a necroptosis-relevant risk model for reflecting necroptosis subtypes in clinical practice.

MATERIALS AND METHODS

Collection and Integration of Transcriptomic Data on Pancreatic Cancer

This study retrospectively collected transcriptomic data on pancreatic cancer from public databases after removing normal tissue specimens and specimens without clinical follow-up data, including the Cancer Genome Atlas (TCGA; https://www.cancer.gov/tcga; n = 177) as well as Pancreatic Cancer-Australia (PACA-AU; n = 91) and Pancreatic Cancer-Canada (PACA-CA; n = 234) from the International Cancer Genome Consortium (ICGC; https://www.icgc-argo.org) (Zhang et al., 2019). Due to samples from different platforms, the batch effects were removed utilizing the ComBat function of the sva package (version 3.42.0) (Leek et al., 2012). A principal component analysis (PCA) was conducted to evaluate the data before and after the removal of the batch effects. The follow-up data and clinicopathological characteristics were also collected. Moreover, single-nucleotide variant (SNV) and copy number variation (CNV) data on pancreatic cancer were retrieved from TCGA project. After reviewing the previously published literature, we collected 159 necroptosis genes, as listed in **Supplementary Table S1**. The GSE21501 cohort containing expression profiling and follow-up information of 101 pancreatic cancer patients was downloaded from the Gene Expression Omnibus (GEO) repository (https://www.ncbi.nlm.nih.gov/gds/), which was used as the external validation cohort (Stratford et al., 2010; Stratford et al., 2017). **Supplementary Figure S1** depicted the workflow of our study.

Consensus Clustering Analysis

Univariate Cox regression models were conducted between necroptosis genes and pancreatic cancer survival, and genes with $p < 0.05$ were determined for a consensus clustering analysis. A consensus clustering approach offers quantitative and visual stability evidence to estimate the number of unsupervised classes within a specified data set. The ConsensusClusterPlus package (version 1.58.0) adopts the

consensus clustering approach, comprising consensus matrix, empirical cumulative distribution function (CDF), and delta area plots (Wilkerson and Hayes, 2010). Through implementing the consensus clustering analysis, necroptosis subtypes were clustered based on the expression values of prognostic necroptosis genes across pancreatic cancer specimens. The number of clusters k was set as 2–9, and 80% of the samples were sampled using a re-sampling method. After multiple sampling, stable and reliable unsupervised classes were found in line with the following parameters: re-samplings = 50, proportion of items to sample = 0.8, proportion of features to sample = 1, and distance = "pearson". PCA was conducted to visualize the difference in expression levels of prognostic necroptosis genes among diverse necroptosis subtypes.

Gene Set Variation Analysis

GSVA, a non-parametric and unsupervised gene set enrichment approach, can estimate the enrichment score of specific pathways or signatures in accordance with transcriptomic profiles (Hänzelmann et al., 2013). The 50 hallmarks of gene sets were retrieved from the Molecular Signatures Database (Liberzon et al., 2015). The activity of each hallmark pathway was quantified using the single-sample gene set enrichment analysis (ssGSEA) function.

Estimation of Tumor Immunogenicity

The relative infiltrations of immune cell populations were estimated with the ssGSEA function derived from the GSVA package (Hänzelmann et al., 2013) on the basis of the expression values of 782 meta-genes (Charoentong et al., 2017) in pancreatic cancer specimens. The mRNA expressions of known immune checkpoints and human leukocyte antigen (HLA) molecules were quantified in each pancreatic cancer specimen.

Cancer–Immunity Cycle

Chen and Mellman proposed a cancer–immunity cycle to evaluate antitumor immune responses, containing seven steps: 1) release of cancer antigens, 2) cancer antigen presentation, 3) priming and activation, 4) trafficking of T cells to tumors, 5) infiltration of T cells into tumors, 6) recognition of cancer cells by T cells, and 7) killing of cancer cells (Karasaki et al., 2017). The levels of each step within the cancer–immunity cycle were quantified using the ssGSEA approach.

Quantification of Known Biological Processes

The gene sets of known biological processes were retrieved from Mariathasan et al. (2018), containing epithelial–mesenchymal transition (EMT1-3), immune checkpoint, antigen processing machinery, CD8 T effector, angiogenesis, pan-fibroblast TGFβ response (pan-F-TBRS), DNA damage repair, FGFR3-related genes, KEGG-discovered histones, Fanconi anemia, cell cycle, cell cycle regulators, DNA replication, nucleotide excision repair, homologous recombination, mismatch repair, and WNT target. The enrichment score of aforementioned biological processes was quantified using the ssGSEA approach.

Chemosensitivity Analysis

The therapeutic responses to known chemotherapy agents (cisplatin, gemcitabine, docetaxel, and paclitaxel) were estimated using the pRRophetic package (Geeleher et al., 2014). Through construction of the ridge regression model on the basis of the Genomics of Drug Sensitivity in Cancer (GDSC) pharmacogenomics database (www.cancerRxgene.org) (Yang et al., 2013) and transcriptomic data, the half-maximal inhibitory concentration (IC50) of each chemotherapeutic agent was calculated across pancreatic cancer specimens.

Analysis of SNV and CNV Data

Utilizing the maftools package (version 2.10.0) (Mayakonda et al., 2018), SNV data were analyzed and visualized on the basis of the mutation annotation format (MAF) of pancreatic cancer. GISTIC2.0 (Mermel et al., 2011) was implemented to analyze copy number amplification and deletion.

Identification of Necroptosis-Relevant Genes

A differential expression analysis was implemented between any two necroptosis subtypes utilizing linear models for the microarray data (limma; version 3.50.0) package (Ritchie et al., 2015). Genes with adjusted p-value<0.05 were screened, and necroptosis-relevant genes were determined following the intersection of differentially expressed genes.

Functional Enrichment Analyses

Utilizing the clusterProfiler package (version 4.2.0) (Yu et al., 2012), a functional enrichment analysis of necroptosis-relevant genes was carried out, comprising Gene Ontology (GO) and Kyoto Encyclopedia of Genes and Genomes (KEGG) pathway enrichment analyses.

Generation of a Necroptosis-Relevant Risk Model

Prognostic necroptosis–relevant genes with $p < 0.05$ were determined through univariate Cox regression models, which were ranked by using the randomForestSRC package (version 2.14.0), following number of replication = 100, number of step = 5, Monte Carlo iteration number = 100, and genes with relative importance ˃ 0.4. Thereafter, a necroptosis-relevant risk model was generated on the basis of the expression of the most important genes and regression coefficients from a multivariate Cox regression model. Following calculation of the necroptosis-relevant risk score of each pancreatic cancer patient, high- and low-risk groups were separated in accordance with the median value of risk score. Receiver operator characteristic (ROC) curves at 1-, 3-, and 5-year survival were conducted to evaluate the predictive reliability of the necroptosis-relevant risk model in pancreatic cancer survival. Using the GEPIA web tool (http://gepia.cancer-pku.cn/), the expression of genes in the necroptosis-relevant risk model was examined in pancreatic cancer (n = 179) and normal tissues (n = 171).

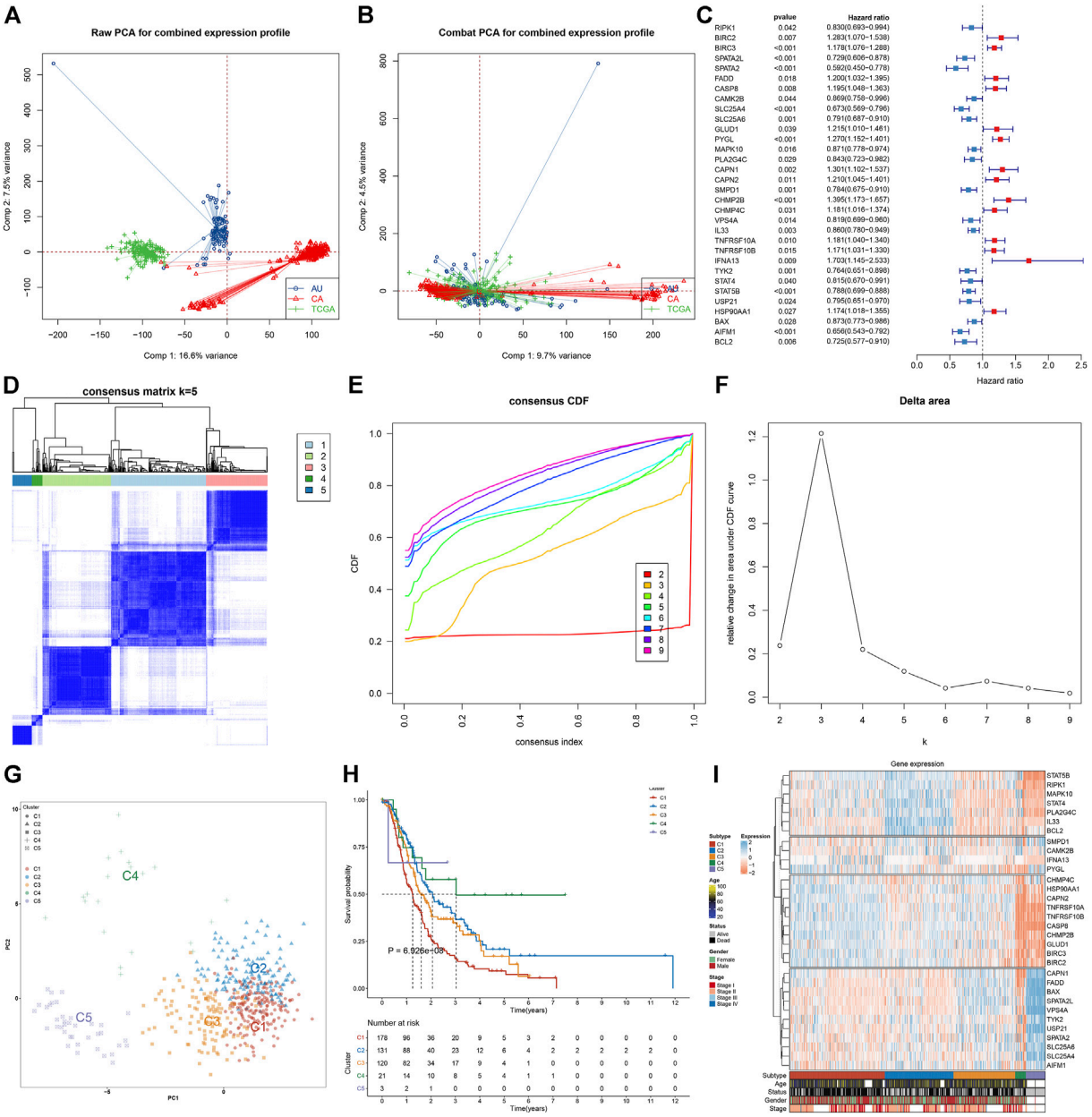

FIGURE 1 | Characterization of five necroptosis subtypes with diverse survival outcomes for pancreatic cancer in the integrated TCGA, PACA-AU, and PACA-CA cohorts. **(A,B)** PCA plots show the data before and after the removal of the batch effects. **(C)** Forest plots visualize the hazard ratios and p-values of prognostic necroptosis genes for pancreatic cancer patients utilizing univariate Cox regression models. Red, risk factor; blue, protective factor. **(D)** Based on the expression values of prognostic necroptosis genes, the consensus matrix is shown when $k = 5$. The rows and columns of the matrix represent samples. The values of the consensus matrix range from 0 (cannot be clustered) to 1 (always clustered) in white to dark blue. **(E)** Consensus CDF plot when k = 2–9. **(F)** Delta area plot when $k = 2–9$. The delta area score (y-axis) indicates the relative change in cluster stability. **(G)** PCA plots visualize the difference among five necroptosis subtypes, following the expression values of prognostic necroptosis genes across pancreatic cancer specimens. **(H)** Survival analysis of five necroptosis subtypes. **(I)** Heatmap visualizes the expression of prognostic necroptosis genes in diverse necroptosis subtypes.

Construction of a Prognostic Nomogram

In the nomogram, the line length indicates the degree of influence of a specific variable and diverse values of this variable on outcomes. After univariate and multivariate Cox regression models, a nomogram was generated on the basis of independent prognostic factors through the rms package (version 6.2-0), showing the intuitive and effective results of the risk model. Calibration curves were utilized to validate the predictive accuracy of the nomogram-predicted survival probabilities for 1-, 3-, and 5-year survival.

Statistical Analysis

R software (version 3.6.1) was implemented for data processing. Univariate and multivariate Cox regression analyses were conducted, and the hazards ratio (HR) and p-value were calculated to evaluate the correlations of variables with pancreatic cancer survival. Kaplan–Meier curves and log-rank test were depicted for the survival difference between groups. The difference between two groups was compared with student's t-test or Wilcoxon test, while comparison between three groups was presented through the Kruskal–Wallis test. A correlation analysis was carried out *via* Pearson's or Spearman's test. The C-index was calculated for estimating the prediction performance through the survival package. $p < 0.05$ indicated statistical significance.

RESULTS

Characterization of Five Necroptosis Subtypes With Diverse Survival Outcomes for Pancreatic Cancer

We retrospectively collected transcriptomic data on pancreatic cancer from TCGA, PACA-AU, and PACA-CA cohorts. The batch effects of integrated data were eliminated for subsequent analyses, which were visualized through PCA (**Figures 1A,B**). Among 159 necroptosis genes, 18 genes (*SPATA2*, *AIFM1*, *SLC25A4*, *BCL2*, *SPATA2L*, *TYK2*, *SMPD1*, *STAT5B*, *SLC25A6*, *USP21*, *STAT4*, *VPS4A*, *RIPK1*, *PLA2G4C*, *IL33*, *CAMK2B*, *MAPK10*, and *BAX*) were protective factors of pancreatic cancer prognosis, while 14 genes (*TNFRSF10B*, *HSP90AA1*, *BIRC3*, *TNFRSF10A*, *CHMP4C*, *CASP8*, *FADD*, *CAPN2*, *GLUD1*, *PYGL*, *BIRC2*, *CAPN1*, *CHMP2B*, and *IFNA13*) were risk factors of prognosis, as depicted in **Figure 1C**. These prognostic necroptosis genes were utilized for the consensus clustering analysis. When $k = 5$, pancreatic cancer samples were clearly separated into five clusters (**Figure 1D**). **Figure 1E** depicted the CDF when k takes different values, and we found that when k = 5, CDF reached the approximate maximum, indicative of cluster stability. **Figure 1F** showed the relative change in CDF of k compared to k-1. When $k = 6$, CDF only slightly decreased, so 5 was the appropriate value of k. Ultimately, five necroptosis subtypes were identified for pancreatic cancer, namely, C1 ($n = 187$), C2 ($n = 135$), C3 ($n = 121$), C4 ($n = 21$), and C5 ($n = 38$). PCA also confirmed the reliability of necroptosis subtypes (**Figure 1G**). The survival analysis demonstrated the remarkable survival difference among necroptosis subtypes (**Figure 1H**). The C1 subtype had the worst survival outcomes, followed by C3, C2, C4, and C5. **Figure 1I** depicted the prominent expression difference of prognostic necroptosis genes among diverse subtypes. The accuracy and reliability of necroptosis subtypes were confirmed in the TCGA cohort (**Supplementary Figures S2A-F**).

Necroptosis Subtypes With Diverse Immunogenic Features

Further analysis was conducted to uncover the mechanisms underlying five necroptosis subtypes. In **Figure 2A**, tumorigenic pathways (hedgehog signaling, KRAS, angiogenesis, glycolysis, etc.) were remarkably activated in C1 and C2 subtypes, contributing to an undesirable prognosis. C4 and C5 subtypes presented the relatively high infiltrations of immune cells, while C2 was characterized by low infiltrations of immune cells (**Figure 2B**). Most immune checkpoints were markedly downregulated in C4 and C5 subtypes, while their upregulations were found in C2 (**Figure 2C**). Tumors can evade T-cell responses through losing the major histocompatibility complex (MHC)/HLA class I and II molecules (Godfrey et al., 2018). In **Figure 2D**, we observed the loss of HLA class I and II molecules in C4 and C5. Differently, C2 displayed the prominent activation of HLA molecules, followed by relatively modest expression in C1 and C3. C4 and C5 subtypes presented the relatively low levels of almost all steps within the cancer–immunity cycle in comparison to other subtypes; meanwhile, the C2 subtype had the highest activation of each step (**Figure 2E**). Similarly, CD8 T effector and antigen processing machinery, immune checkpoint, and stromal activation (EMT1-3) were relatively downregulated in C4 and C5 (**Figure 2F**); C2 had relatively high levels of immune and stromal activation pathways; and C1–3 presented the enhanced cell cycle progression (cell cycle, cell cycle regulators, DNA replication, etc.). Overall, five necroptosis subtypes had diverse immunogenic features.

Necroptosis Subtypes With Different Chemosensitivity and Tumor Mutation Features

We compared the sensitivity to known chemotherapy agents (cisplatin, gemcitabine, docetaxel, and paclitaxel) in five necroptosis subtypes. As depicted in **Figure 3A**, C4 had the highest IC50 values of cisplatin, gemcitabine, docetaxel, and paclitaxel, while C5 presented the lowest IC50 values of aforementioned chemotherapy agents, indicating that C4 presented the highest probability of chemotherapy resistance while C5 was the most sensitive to these chemotherapy agents. We also investigated that C1 and C3 had relatively higher tumor mutation burden (TMB) than other subtypes (**Figure 3B**). KRAS (53%) and TP53 (53%) were the most frequent mutant genes. The widespread copy number amplification (**Figure 3C**) and deletion (**Figure 3D**) occurred in pancreatic cancer specimens. Among five necroptosis subtypes, C2 and C4 had the relatively decreased fractions of genome altered (FGAs), as depicted in **Figure 3E**. Moreover, we noted the relatively lowered copy number amplification and deletion in C2 and C4 in comparison to other subtypes (**Figure 3F**). Aforementioned data uncovered the difference in tumor mutations among necroptosis subtypes.

Generation of a Necroptosis-Relevant Risk Model for Pancreatic Cancer Prognosis

Through the intersection of DEGs (adjusted $p < 0.05$) between any two subtypes, we determined 591 necroptosis-relevant genes (**Supplementary Table S2**). Their biological significance was further analyzed through GO and KEGG enrichment analyses. In **Figure 4A**, necroptosis-relevant genes were remarkably linked

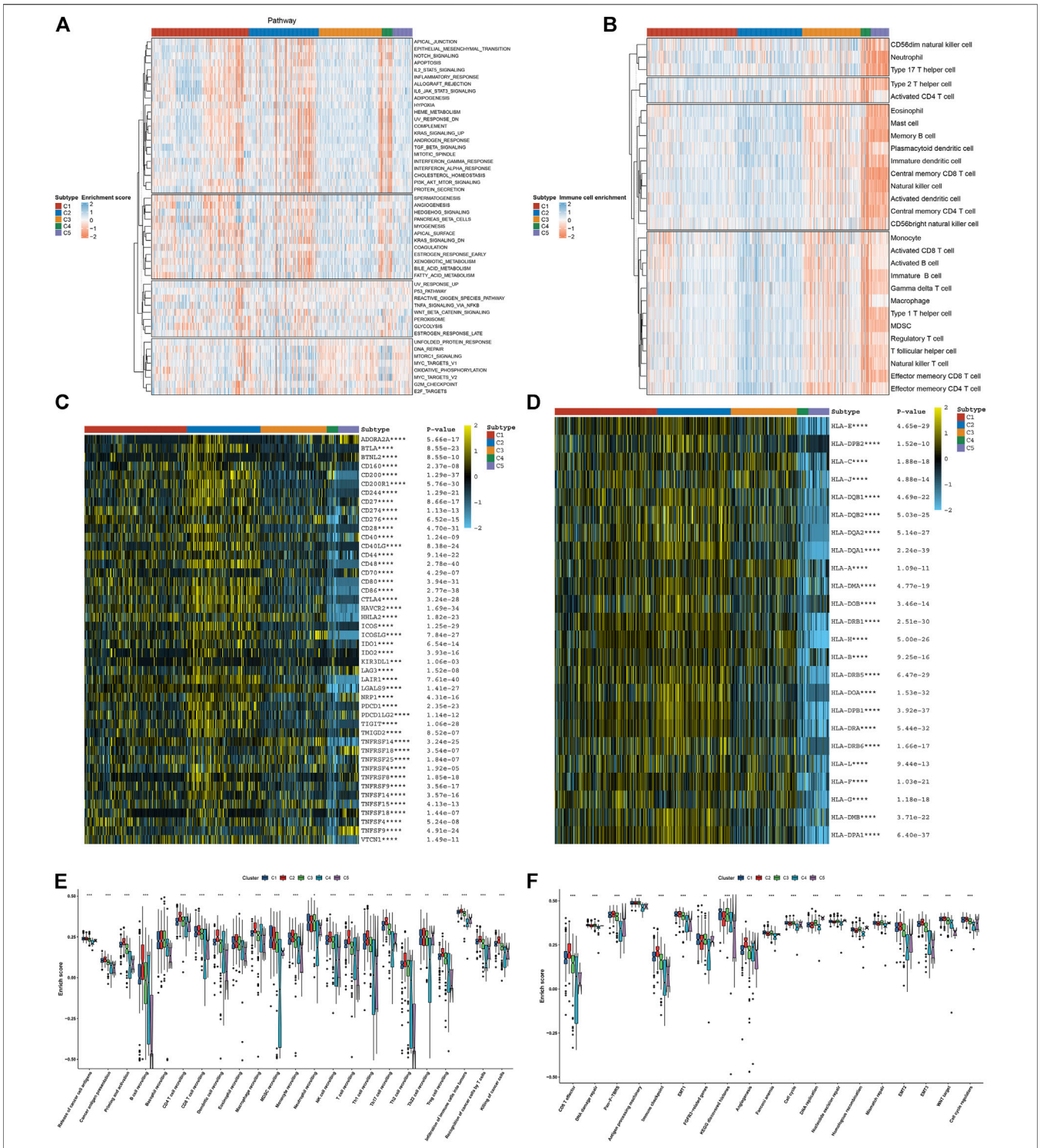

FIGURE 2 | Five necroptosis subtypes with diverse immunogenic features. **(A)** Quantification of the activation levels of known hallmarks of cancer pathways in five necroptosis subtypes. **(B)** Estimation of the infiltration levels of immune cell populations in diverse necroptosis subtypes. **(C,D)** Visualization of the mRNA expression of **(C)** immune checkpoints and **(D)** HLA molecules across necroptosis subtypes. **(E)** Comparison of the enrichment scores of all steps within the cancer–immunity cycle among five necroptosis subtypes. **(F)** Comparison of the enrichment scores of known biological processes in five necroptosis subtypes. *$p < 0.05$; **$p < 0.01$; ***$p < 0.001$; and ****$p < 0.0001$.

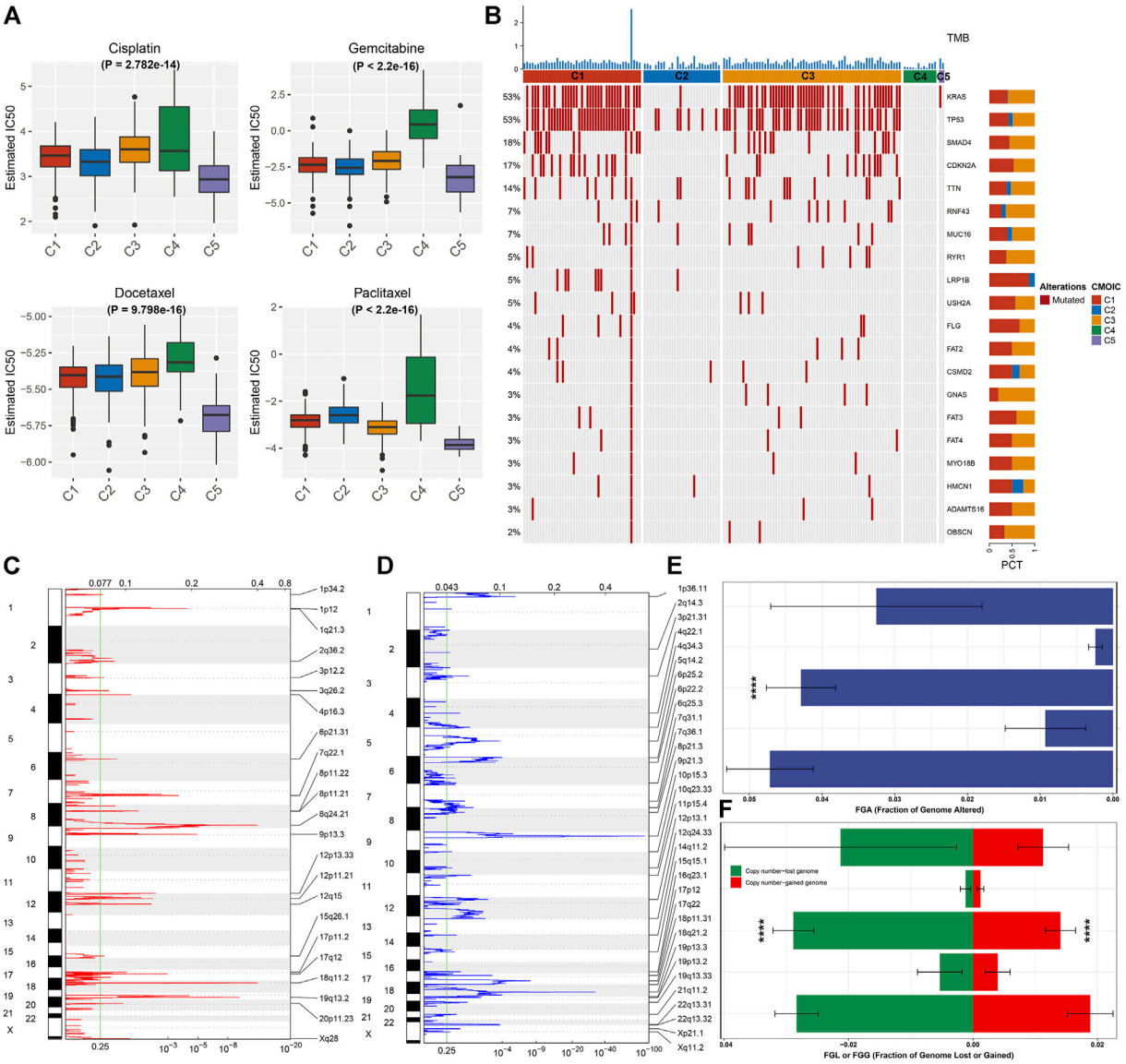

FIGURE 3 | Necroptosis subtypes with different chemosensitivity and tumor mutation features. **(A)** Comparison of the IC50 values of chemotherapy agents (cisplatin, gemcitabine, docetaxel, and paclitaxel) among five necroptosis subtypes. **(B)** Waterfall diagram depicts the first 20 mutated genes and TMB (upper of the panel) across necroptosis subtypes. **(C,D)** Chromosome arms with significant amplification and deletion (q-value <0.25). The focal peak of amplification and deletion is separately visualized. Red indicates copy number amplification, while blue represents copy number deletion. **(E)** Comparison of the fraction of genome altered (FGA) among necroptosis subtypes. **(F)** Comparison of the copy number amplification (red) and deletion (green) in five necroptosis subtypes. ****$p < 0.0001$.

with regulation of protein localization to the membrane. Moreover, they had prominent associations with tumorigenic pathways (p53 signaling pathway and cell senescence) and immune pathways (Th17 cell differentiation, PD-L1 expression, PD-1 checkpoint pathway in cancer, Th1 and Th2 cell differentiation, etc.), indicative of the critical roles of necroptosis-relevant genes in pancreatic cancer progression (**Figure 4B**). Among all necroptosis-relevant genes, 207 displayed significant correlations to pancreatic cancer prognosis (**Supplementary Table S3**). Using the random forest approach, we determined the most important genes with the relative importance > 0.4 (**Figures 4C,D**). A multivariate Cox regression model was constructed in line with the following formula: risk score = 0.119399555 * MYEOV expression + (−0.258345687) * HDAC4 expression + 0.26238863 * TLDC1 expression + (−0.395042137) * PITPNA +0.175544976 * FNDC3B expression + 0.338675676 * HMGXB4 expression + (−0.150557275) * BAX expression. Following the calculation of the risk score, all patients were separated into high- and low-risk groups (**Figure 4E**). The high-risk group had more dead patients relative to the low-risk group (**Figure 4F**). The survival analysis demonstrated the survival advantage of low-risk patients

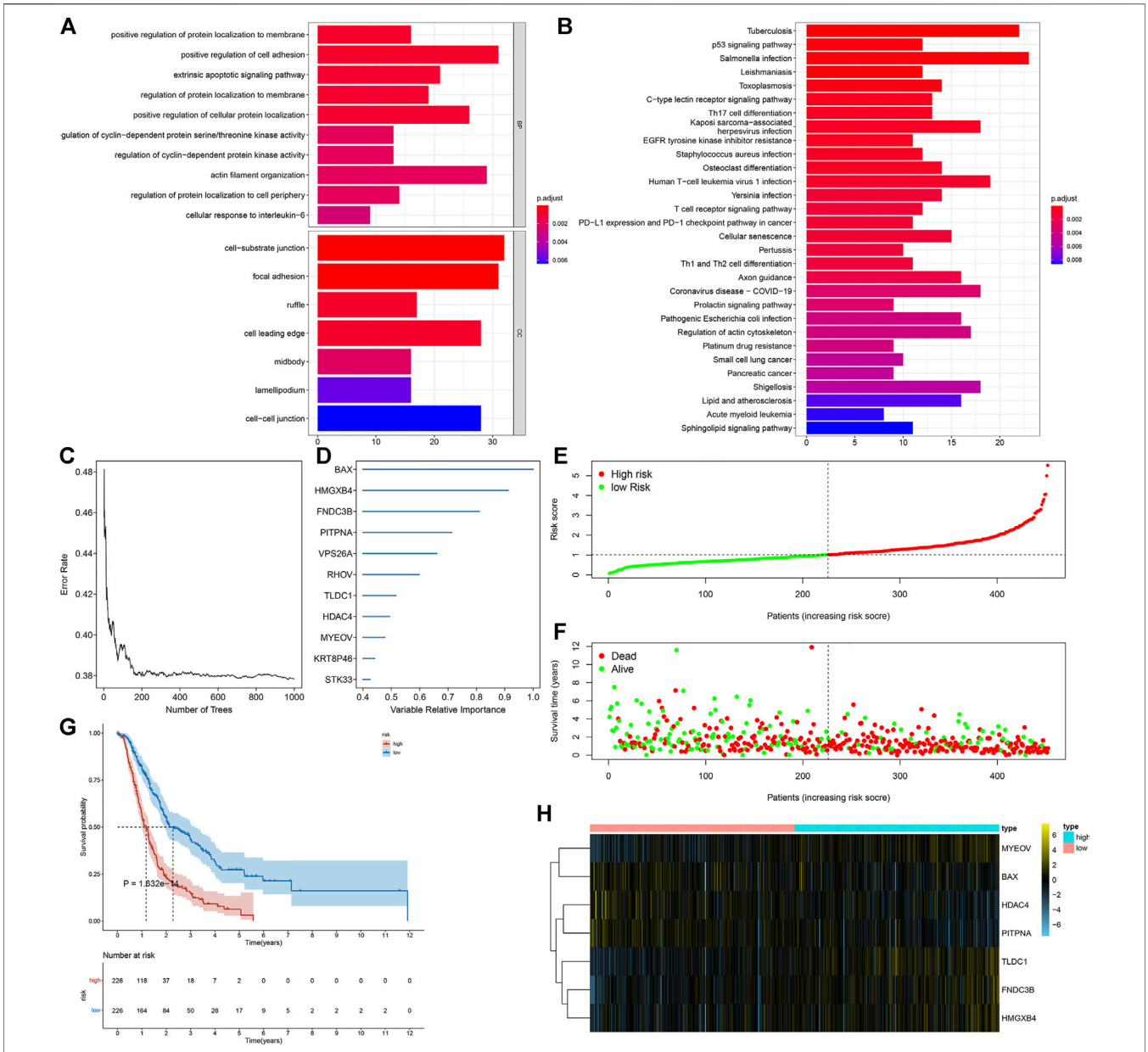

FIGURE 4 | Generation of a necroptosis-relevant risk model for pancreatic cancer prognosis. **(A,B)** GO and KEGG enrichment results of necroptosis-relevant genes. **(C,D)** Most important necroptosis-relevant genes ordered by the relative importance through the random forest approach. **(E,F)** Distribution of the risk score and survival status in high- and low-risk groups. **(G)** Survival analysis of high- and low-risk groups. **(H)** Heatmap depicts the expression of genes in the necroptosis-relevant risk model between two groups.

(**Figure 4G**). The difference in expression of aforementioned genes between groups is visualized in **Figure 4H**.

Necroptosis-Relevant Risk Model as a Reliable and Independent Prognostic Indicator of Pancreatic Cancer

Uni- and multivariate Cox regression analyses uncovered that age- and necroptosis-relevant risk models were both independently associated with pancreatic cancer survival (**Figures 5A,B**). AUCs at 1-, 3-, and 5-year survival were separately 0.714, 0.724, and 0.757, indicative of the reliability of the necroptosis-relevant risk model in predicting survival outcomes (**Figure 5C**). To facilitate the clinical application of the necroptosis-relevant risk model, we generated a nomogram following integration of age (**Figure 5D**). Calibration curves demonstrated the predictive accuracy of this nomogram in pancreatic cancer survival (**Figures 5E–G**). In addition, we also performed a stratified analysis and demonstrated that the risk model can serve as an

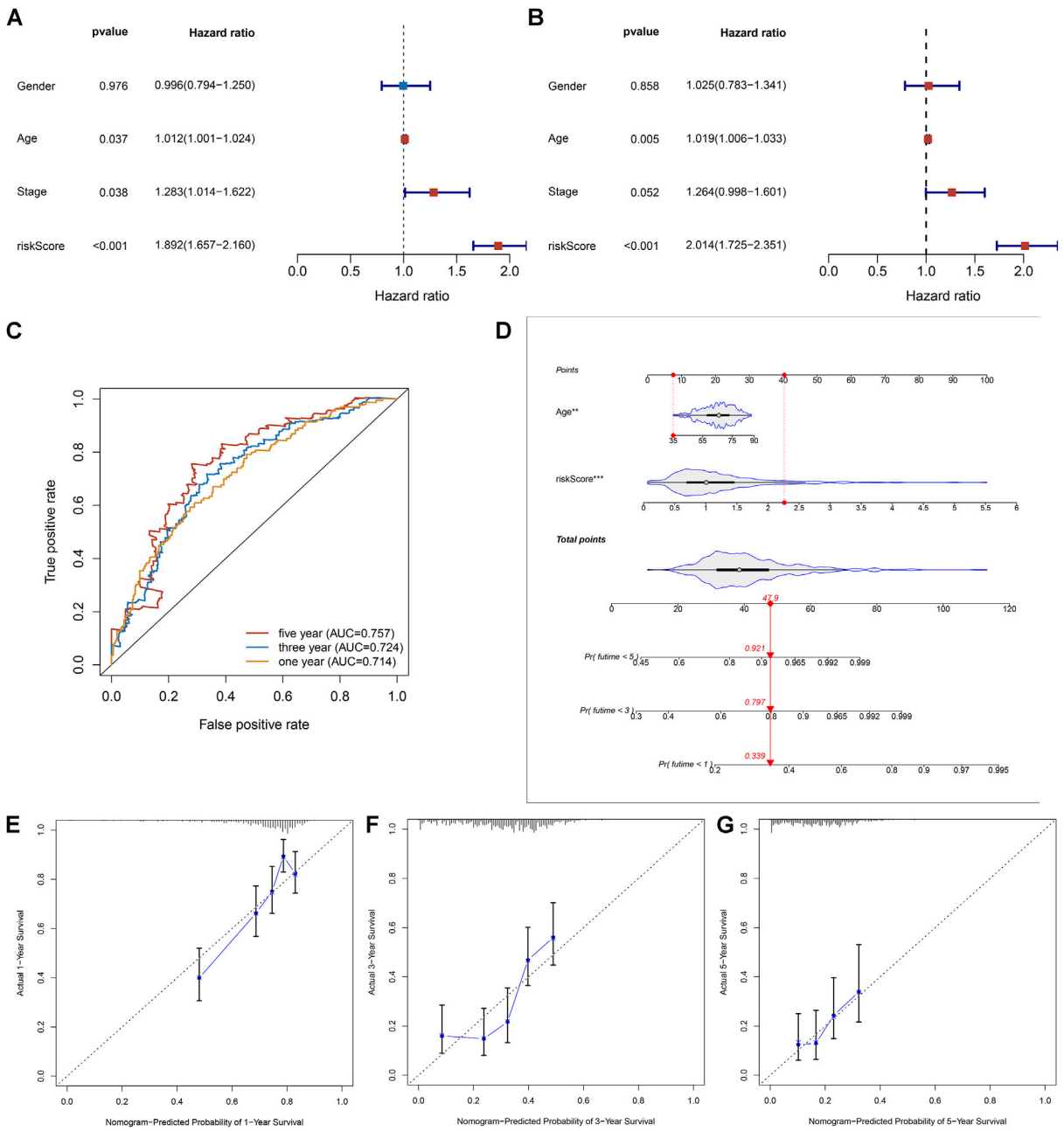

FIGURE 5 | Necroptosis-relevant risk model as a reliable and independent prognostic indicator of pancreatic cancer. **(A,B)** Forest plots show the correlations of the necroptosis-relevant risk score, age, and stage with pancreatic cancer prognosis through **(A)** uni- and **(B)** multivariate Cox regression models. **(C)** ROC curves at 1-, 3-, and 5-year survival for the necroptosis-relevant risk score. **(D)** Generation of an age- and risk score–based prognostic nomogram. **(E–G)** Calibration curves depict the deviations between nomogram-predicted probabilities of 1-, 3-, and 5-year survival and actual survival outcomes.

independent prognostic factor without consideration of the impact of age (**Supplementary Figures S3A,B**).

Externally Verifying the Necroptosis-Relevant Risk Model

The robustness of the necroptosis-relevant risk model was verified in the GSE21501 cohort. In accordance with the same formula, we computed the necroptosis-relevant risk score of each pancreatic cancer patient in the external cohort (**Figure 6A**). As expected, high-risk patients had poorer survival outcomes than low-risk patients (**Figure 6B**). AUCs at 1- and 3-year survival were separately 0.69 and 0.71 (**Figure 6C**), demonstrating the excellent performance in predicting prognosis. Compared with the existing prognostic models constructed by Chen et al. (2021), Xiao et al. (2022), and Zhang et al. (2022), the necroptosis-relevant risk model had a higher C-index (**Figure 6D**), indicating the advantage of this model in predicting prognosis. We also examined the expression of genes in

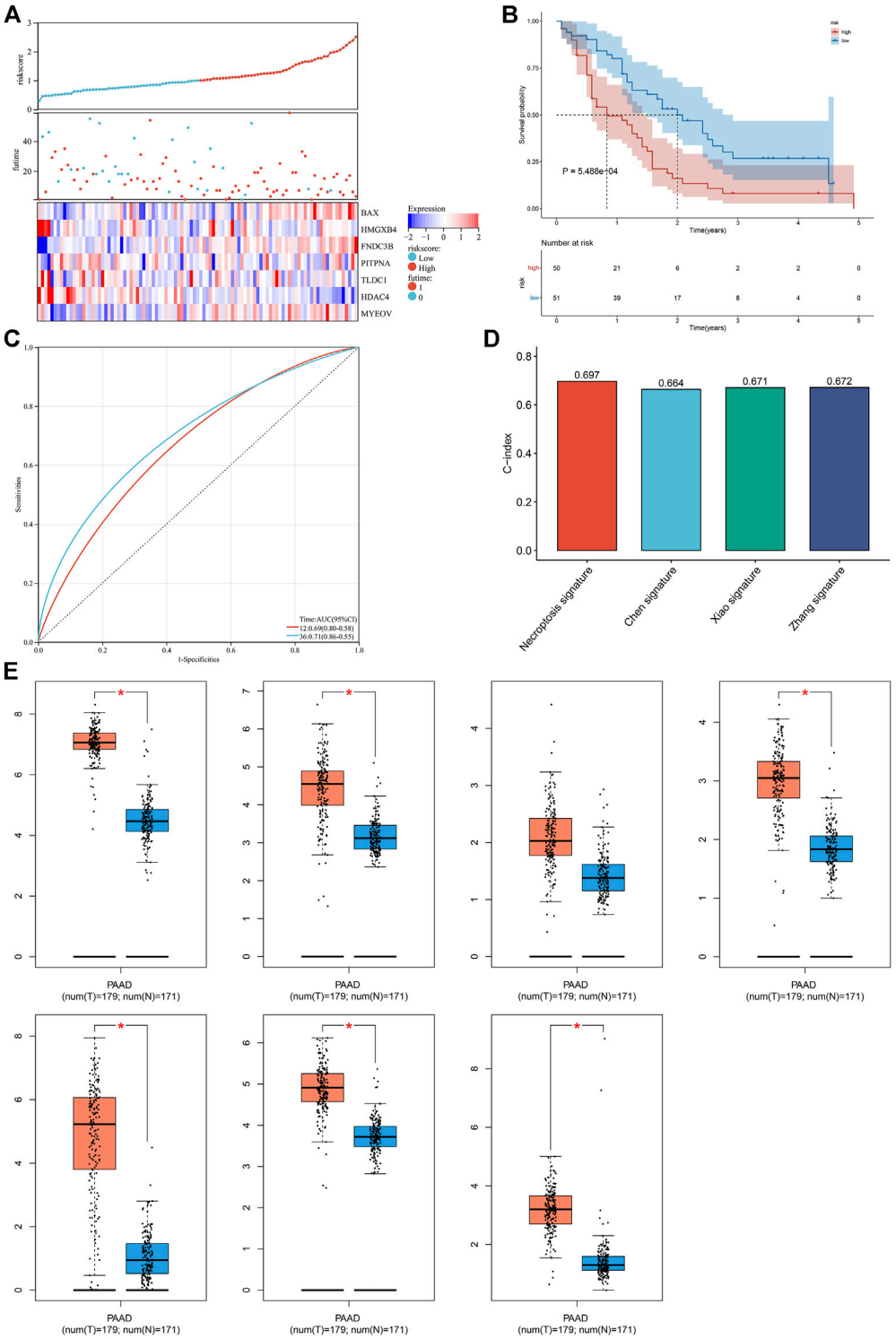

FIGURE 6 | External verification of the necroptosis-relevant risk model. **(A)** Distribution of the necroptosis-relevant risk score, survival status, and expression of necroptosis-relevant genes in the GSE21501 cohort. **(B,C)** Survival analysis and ROC curves in the GSE21501 cohort. **(D)** Comparison of the C-index of the necroptosis-relevant risk score with known prognostic signatures. **(E)** Box plots of the expression of necroptosis-relevant genes using the GEPIA web tool. *$p < 0.05$.

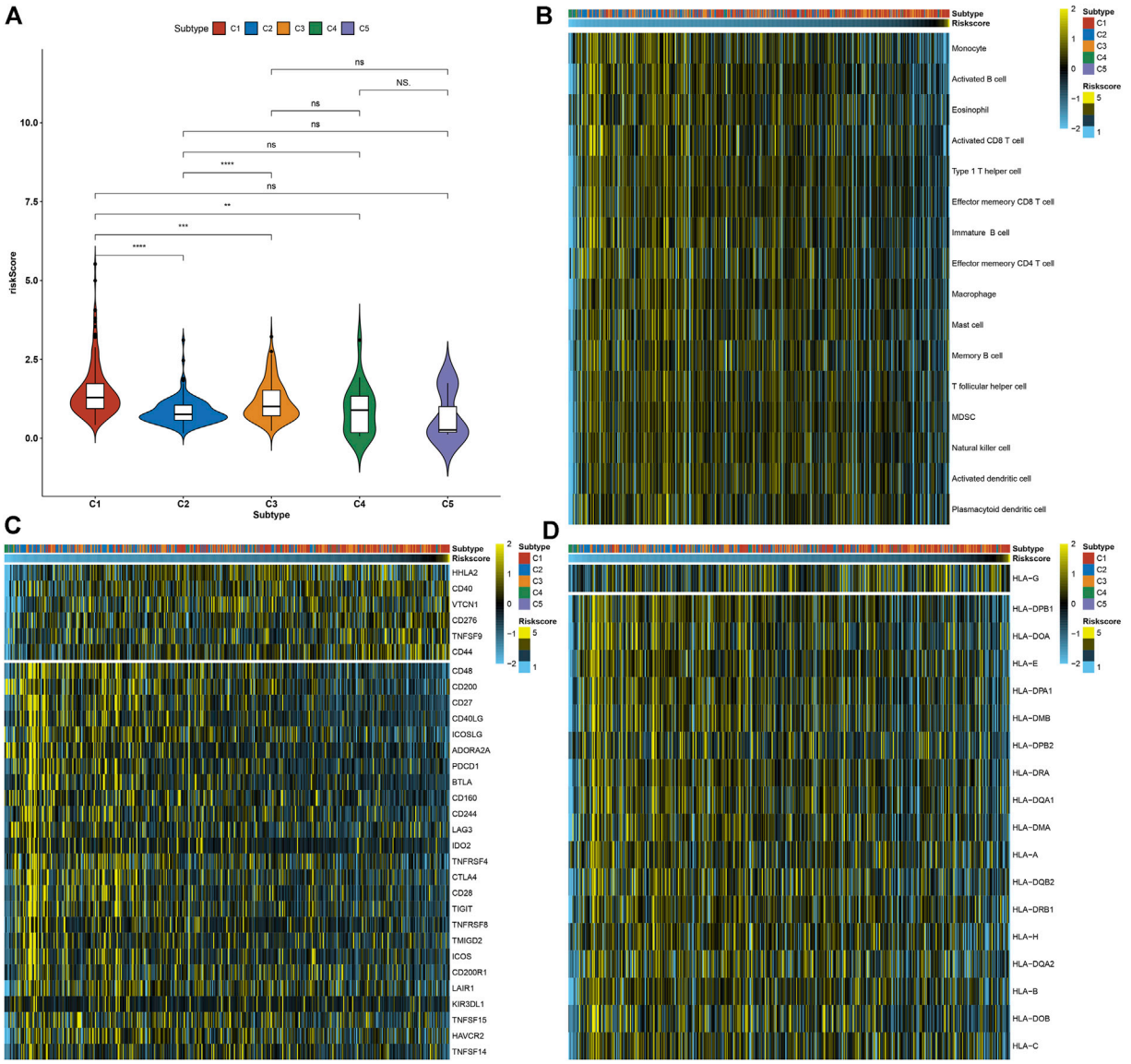

FIGURE 7 | Necroptosis-relevant risk model links with tumor immunogenicity for pancreatic cancer. **(A)** Distribution of the necroptosis-relevant risk score in five necroptosis subtypes. Ns: not significant; $^{**}p < 0.01$; $^{***}p < 0.001$; and $^{****}p < 0.0001$. **(B)** Visualization of the infiltrations of immune cell populations in pancreatic cancer specimens ordered by the necroptosis-relevant risk score. **(C,D)** Quantification of the mRNA expression of **(C)** immune checkpoints and **(D)** HLA molecules in pancreatic cancer specimens ordered by the necroptosis-relevant risk score.

the necroptosis-relevant risk model using the GEPIA web tool. BAX, FNDC3B, HDAC4, HMGXB4, MYEOV, and TLDC1 displayed upregulated expressions in pancreatic cancer than normal tissues (**Figure 6E**).

Necroptosis-Relevant Risk Model Correlates With Tumor Immunogenicity for Pancreatic Cancer

Compared with other necroptosis subtypes, C1 presented a relatively higher necroptosis-relevant risk score, followed by C3 (**Figure 7A**), indicating the heterogeneity in the risk score among diverse necroptosis subtypes. Further analysis was conducted to evaluate the correlations of necroptosis-relevant risk score with tumor immunogenicity. In **Figure 7B**, as the necroptosis-relevant risk score increased, the infiltrations of immune cells gradually decreased, indicative of the negative correlations of the necroptosis-relevant risk score with immune cell infiltrations. Moreover, we noted that the necroptosis-relevant risk score was negatively linked with the expression of immune checkpoints and HLA molecules (**Figures 7C,D**). The aforementioned data indicated the role of the necroptosis-relevant risk model in tumor immunogenicity of pancreatic cancer.

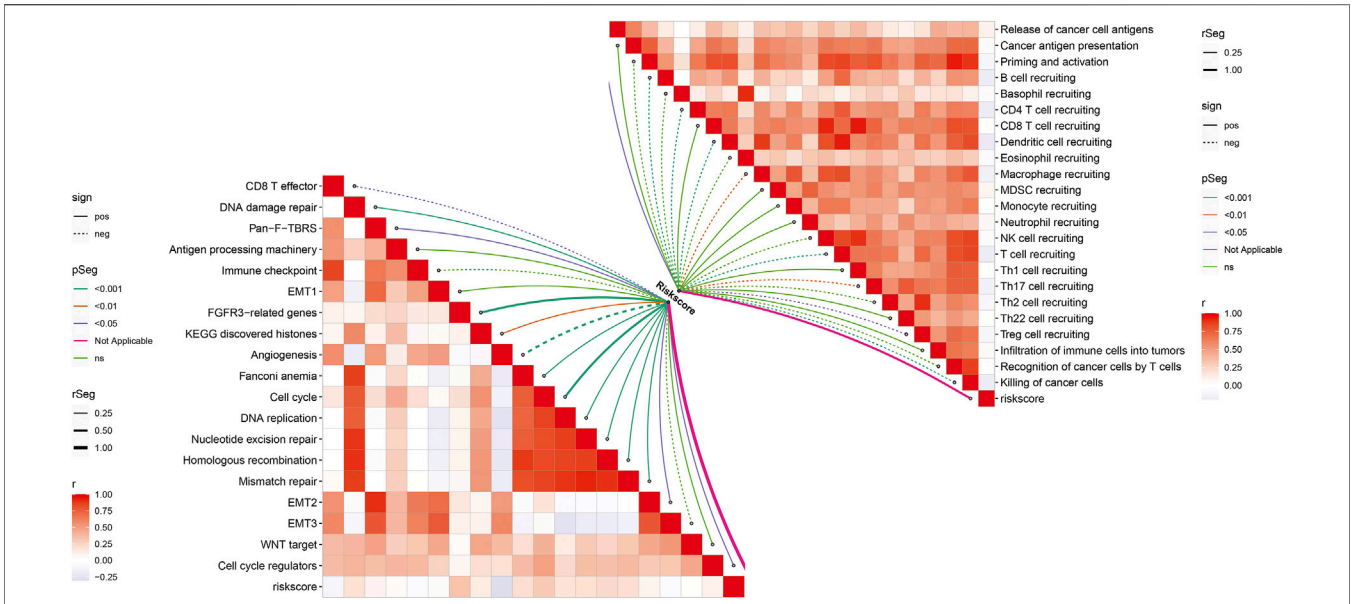

FIGURE 8 | Necroptosis-relevant risk model links with the cancer–immunity cycle and known biological processes in pancreatic cancer. Spearman's correlation analysis was conducted between the necroptosis-relevant risk score and all steps within the cancer–immunity cycle and known biological processes.

Necroptosis-Relevant Risk Model Links With the Cancer Immunity Cycle and Known Biological Processes

In **Figure 8**, we noted that the necroptosis-relevant risk score presented a significantly positive correlation to the release of cancer cell antigens but displayed significantly negative correlations to recruiting of B cells, CD4 T cells, dendritic cell, macrophages, T cells, Th17 cells, Treg cells, and killing of cancer cells, indicative of the remarkable interactions of the necroptosis-relevant risk score with the cancer–immunity cycle. Moreover, necroptosis-relevant risk score was negatively linked with CD8 T effector, and angiogenesis but was positively associated with pan-F-TBRS, FGFR3-related genes, EMT2, KEGG discovered histones, Fanconi anemia, cell cycle, cell cycle regulators, DNA replication, DNA damage repair, nucleotide excision repair, homologous recombination, and mismatch repair, indicative of the mechanisms underlying the necroptosis-relevant risk score.

Necroptosis-Relevant Risk Model Correlates With Chemosensitivity of Pancreatic Cancer

Further analysis was conducted to evaluate the correlations between the necroptosis-relevant risk score and chemosensitivity of pancreatic cancer. No remarkable differences of the IC50 values of cisplatin and gemcitabine were noticed between high- and low-risk groups (**Figures 9A,B**). But the high-risk group presented the prominently reduced IC50 values of docetaxel and paclitaxel relative to the low-risk group (**Figures 9C,D**). This indicated that high-risk patients were more likely to be sensitive to docetaxel and paclitaxel.

DISCUSSION

Since there are currently no specific molecular biomarkers for detecting necroptosis, identifying necroptosis usually requires combined detection approaches (Niu et al., 2022). Under transmission electron microscopy, necrotic morphology is identified. Detecting necroptosis by biomarkers mainly focuses on the pivotal molecular events involving necroptosis. Nevertheless, the exact roles of necroptosis in pancreatic cancer remain to be adequately clarified. Herein, we proposed five necroptosis-based molecular subtypes and a necroptosis-relevant risk model for pancreatic cancer through integrated analysis of necroptosis genes, which expanded the understanding of necroptosis in pancreatic cancer biology.

Consensus clustering analysis is beneficial to provide patients with more accurate therapy, referring to a situation where diverse clusters are acquired for a specific dataset and desired for aggregating the clustering results to obtain an in-depth clustering solution (Li et al., 2020). On the basis of the expression values of prognostic necroptosis genes, five necroptosis subtypes were determined for pancreatic cancer, with diverse survival outcomes. C1 subtype had the worst survival outcomes, followed by C3, C2, C4 and C5. Tumorigenic pathways (hedgehog signaling, KRAS, angiogenesis, glycolysis, etc.) were remarkably activated in C1 and C2 subtypes, contributing to unfavorable survival outcomes. The five subtypes presented diverse expression patterns of

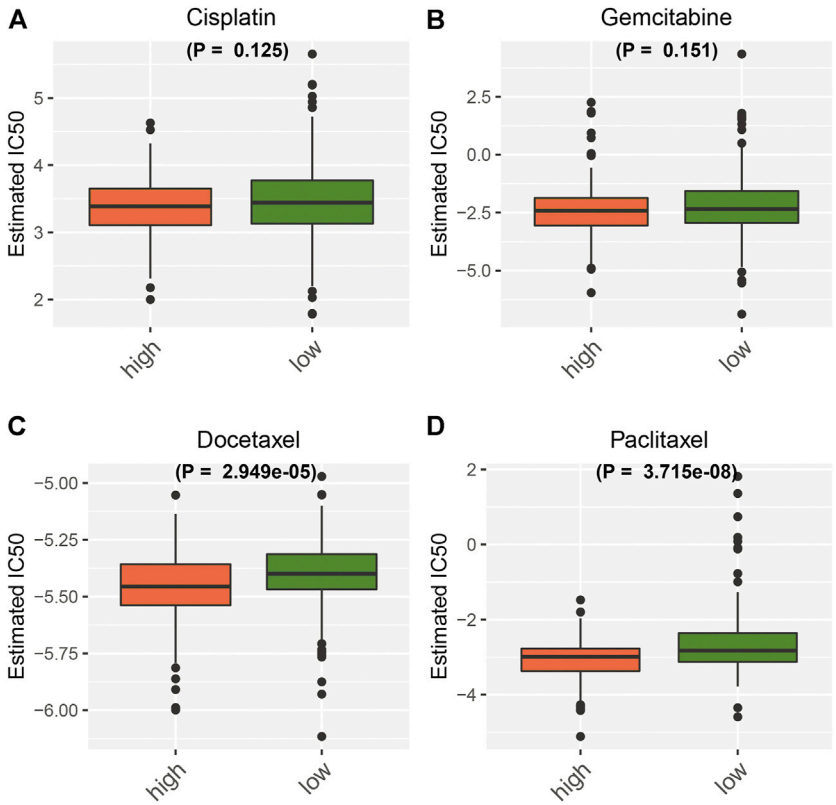

FIGURE 9 | Necroptosis-relevant risk model correlates with the chemosensitivity of pancreatic cancer. Box plots show the IC50 values of **(A)** cisplatin, **(B)** gemcitabine, **(C)** docetaxel, and **(D)** paclitaxel in high- and low-risk groups.

necroptosis genes. Elucidating the exact regulatory mechanisms of necroptosis can facilitate the development of new therapeutic strategies to overcome apoptosis resistance in pancreatic cancer. Tumors express various MHC molecules, which can be targets for specific cytotoxic T lymphocytes, resulting in them to be immunogenic. Most immune checkpoints and HLA molecules were markedly downregulated in C4 and C5 subtypes while their upregulations were found in the C2 subtype. This indicated that tumors in C4 and C5 with robust T-cell immunosurveillance presented disable antigen presentation to evade immunorecognition. The cancer–immunity cycle contains seven stepwise steps for obtaining an efficient control of tumor growth through the immune system, which is initiated *via* the release of neo-antigens produced by genomic instability (Huntington et al., 2020). Cancer-associated antigens are captured by dendritic cells, and after dendritic cells migrate to lymph nodes, they trigger and activate tumor-specific cytolytic $CD8^+$ T cells. These effector cells migrate and penetrate the tumor stroma, where they are able to recognize and kill tumor cells. The cytotoxic response mediated by T cells releases new tumor antigens and promotes the cancer immune cycle. In comparison to other subtypes, C4 and C5 had the relatively rate-limiting steps within the cancer immune cycle. Hence, five subtypes possessed diverse immunogenic features and were predictive of immunotherapeutic responses.

Accumulated evidence suggests the links of necroptosis with chemotherapy resistance (Gong et al., 2019). Cisplatin is a crucial agent for treatment of pancreatic cancer patients with BRCA1/2 or PALB2 mutation (Kong et al., 2020). Apoptosis resistance represents a primary obstacle resulting in chemotherapy failure. Bypassing the apoptotic pathway to induce cancer cell death is a promising therapeutic option to overcome this issue (Gong et al., 2019). Necroptosis is an alternative mode of programmed cell death to overcome apoptosis resistance. Experimental evidence shows that cisplatin induces necroptosis with tumor necrosis factor α (TNFα)-dependent and independent pathways (Xu et al., 2017). Moreover, multitargeted kinase inhibitor KW-2449 alleviates cisplatin-induced nephrotoxicity through targeting RIPK1-independent necroptosis (Rui et al., 2021). Combination therapy of CD95L and gemcitabine facilitates RIP1-independent necroptosis in pancreatic cancer cells (Pietkiewicz et al., 2015). Necroptosis can alleviate docetaxel resistance in prostate cancer (Markowitsch et al., 2021) and breast cancer (Mann et al., 2020). Five necroptosis-based molecular subtypes presented diverse sensitivity to chemotherapeutic agents (cisplatin, gemcitabine, docetaxel, and paclitaxel). Among them, the C4 subtype presented the highest probability of chemotherapy resistance while C5 subtype was most sensitive to these chemotherapy agents,

indicating that patients with the C5 subtype were most likely to benefit from chemotherapy. Moreover, the necroptosis-relevant risk score can predict the sensitivity to docetaxel and paclitaxel in pancreatic cancer.

A necroptosis-relevant risk model was developed for predicting pancreatic cancer survival and responses to immuno- and chemotherapy, comprising MYEOV, HDAC4, TLDC1, PITPNA, FNDC3B, HMGXB4, and BAX. External validation confirmed that this model was capable of accurately predicting pancreatic cancer patients' survival outcomes. The genes in the necroptosis-relevant risk model were upregulated in pancreatic cancer in comparison to normal tissues. Previous research has uncovered the significance of aforementioned genes in pancreatic cancer progression. For instance, MYEOV upregulation is linked with undesirable survival outcome of pancreatic cancer (Tang et al., 2020a), which elevates the HES1 expression and triggers pancreatic cancer progression through enhancing SOX9 trans-activity (Liang et al., 2020). HDAC4 correlates with the proliferative capacity and metastases of pancreatic cancer (Cohen et al., 2013). TLDC1 can facilitate proliferation and migration of pancreatic cancer cells (Yuan et al., 2021).

Several limitations should be pointed out in this study. First of all, clinical information retrieved from TCGA and ICGC projects is not complete, especially the therapy, which may assist in comprehending whether necroptosis genes are biomarkers of therapeutic responses. Second, the mechanisms how necroptosis modulate the precise process of pancreatic cancer are indistinct. Third, the necroptosis-relevant risk model is required to verify in large-scale and multicenter clinical cohorts. Despite these limitations, this study does offer a comprehensive overview of necroptosis gene profiling in pancreatic cancer, and aforementioned limitations will be solved if there are sufficient data in our further research.

CONCLUSION

Collectively, we characterized five robust necroptosis subtypes for pancreatic cancer with diverse prognosis, immunogenic features, genomic mutations, and chemosensitivity. Furthermore, we established a necroptosis-relevant risk model for reflecting necroptosis in clinical practice. Our findings offered a reference for combined therapeutic regimens and might guide the optimal selection of patients for immuno- and chemotherapy.

DATA AVAILABILITY STATEMENT

The original contributions presented in the study are included in the article/**Supplementary Material**, further inquiries can be directed to the corresponding author.

AUTHOR CONTRIBUTIONS

Conception and design: GW and KF. Collection and assembly of data: D-ST, C-SY, JM, and LC. Data analysis and interpretation: KF, D-ST, C-SY, JM, and YL. Manuscript writing: KF, D-ST, and C-SY. Manuscript revision: GW. Final approval of the manuscript: all authors.

FUNDING

This work is funded by the Ningxia Hui Autonomous Region Key Research and Development Project (2021BEG03083), National Nature Scientific Foundation of China (82070657). Applied technology research and development project of Heilongjiang Province (GA20C019). Outstanding youth funds of the first affiliated hospital of Harbin Medical University (HYD2020JQ0006). Research projects of Chinese Research Hospital Association (Y2019FH-DTCC-SB1).

SUPPLEMENTARY MATERIAL

The Supplementary Material for this article can be found online at: https://www.frontiersin.org/articles/10.3389/fphar.2022.862502/full#supplementary-material

REFERENCE

Ando, Y., Ohuchida, K., Otsubo, Y., Kibe, S., Takesue, S., Abe, T., et al. (2020). Necroptosis in Pancreatic Cancer Promotes Cancer Cell Migration and Invasion by Release of CXCL5. *PLoS One* 15 (1), e0228015. doi:10.1371/journal.pone.0228015

Charoentong, P., Finotello, F., Angelova, M., Mayer, C., Efremova, M., Rieder, D., et al. (2017). Pan-cancer Immunogenomic Analyses Reveal Genotype-Immunophenotype Relationships and Predictors of Response to Checkpoint Blockade. *Cell Rep.* 18 (1), 248–262. doi:10.1016/j.celrep.2016.12.019

Chen, H., Zu, F., Zeng, T., Chen, Z., Wei, J., Liu, P., et al. (2021). Prognostic Value and Correlation with Tumor Immune Infiltration of a Novel Metabolism-Related Gene Signature in Pancreatic Cancer. *Front. Oncol.* 11, 757791. doi:10.3389/fonc.2021.757791

Cohen, A. L., Piccolo, S. R., Cheng, L., Soldi, R., Han, B., Johnson, W. E., et al. (2013). Genomic Pathway Analysis Reveals that EZH2 and HDAC4 Represent Mutually Exclusive Epigenetic Pathways across Human Cancers. *BMC Med. Genomics* 6, 35. doi:10.1186/1755-8794-6-35

Geeleher, P., Cox, N., and Huang, R. S. (2014). pRRophetic: An R Package for Prediction of Clinical Chemotherapeutic Response from Tumor Gene Expression Levels. *PLoS One* 9 (9), e107468. doi:10.1371/journal.pone.0107468

Godfrey, D. I., Le Nours, J., Andrews, D. M., Uldrich, A. P., and Rossjohn, J. (2018). Unconventional T Cell Targets for Cancer Immunotherapy. *Immunity* 48 (3), 453–473. doi:10.1016/j.immuni.2018.03.009

Gong, Y., Fan, Z., Luo, G., Yang, C., Huang, Q., Fan, K., et al. (2019). The Role of Necroptosis in Cancer Biology and Therapy. *Mol. Cancer* 18 (1), 100. doi:10.1186/s12943-019-1029-8

Hänzelmann, S., Castelo, R., and Guinney, J. (2013). GSVA: Gene Set Variation Analysis for Microarray and RNA-Seq Data. *BMC Bioinforma.* 14, 7. doi:10.1186/1471-2105-14-7

Huntington, N. D., Cursons, J., and Rautela, J. (2020). The Cancer-Natural Killer Cell Immunity Cycle. *Nat. Rev. Cancer* 20 (8), 437–454. doi:10.1038/s41568-020-0272-z

Karasaki, T., Nagayama, K., Kuwano, H., Nitadori, J. I., Sato, M., Anraku, M., et al. (2017). An Immunogram for the Cancer-Immunity Cycle: Towards Personalized Immunotherapy of Lung Cancer. *J. Thorac. Oncol.* 12 (5), 791–803. doi:10.1016/j.jtho.2017.01.005

Kong, F., Liu, X., Zhou, Y., Hou, X., He, J., Li, Q., et al. (2020). Downregulation of METTL14 Increases Apoptosis and Autophagy Induced by Cisplatin in Pancreatic Cancer Cells. *Int. J. Biochem. Cell Biol.* 122, 105731. doi:10.1016/j.biocel.2020.105731

Leek, J. T., Johnson, W. E., Parker, H. S., Jaffe, A. E., and Storey, J. D. (2012). The Sva Package for Removing Batch Effects and Other Unwanted Variation in High-Throughput Experiments. *Bioinformatics* 28 (6), 882–883. doi:10.1093/bioinformatics/bts034

Li, J., Xie, L., Xie, Y., and Wang, F. (2020). Bregmannian Consensus Clustering for Cancer Subtypes Analysis. *Comput. Methods Programs Biomed.* 189, 105337. doi:10.1016/j.cmpb.2020.105337

Liang, E., Lu, Y., Shi, Y., Zhou, Q., and Zhi, F. (2020). MYEOV Increases HES1 Expression and Promotes Pancreatic Cancer Progression by Enhancing SOX9 Transactivity. *Oncogene* 39 (41), 6437–6450. doi:10.1038/s41388-020-01443-4

Liberzon, A., Birger, C., Thorvaldsdóttir, H., Ghandi, M., Mesirov, J. P., and Tamayo, P. (2015). The Molecular Signatures Database (MSigDB) Hallmark Gene Set Collection. *Cell Syst.* 1 (6), 417–425. doi:10.1016/j.cels.2015.12.004

Mann, J., Yang, N., Montpetit, R., Kirschenman, R., Lemieux, H., and Goping, I. S. (2020). BAD Sensitizes Breast Cancer Cells to Docetaxel with Increased Mitotic Arrest and Necroptosis. *Sci. Rep.* 10 (1), 355. doi:10.1038/s41598-019-57282-1

Mariathasan, S., Turley, S. J., Nickles, D., Castiglioni, A., Yuen, K., Wang, Y., et al. (2018). TGFβ Attenuates Tumour Response to PD-L1 Blockade by Contributing to Exclusion of T Cells. *Nature* 554 (7693), 544–548. doi:10.1038/nature25501

Markowitsch, S. D., Juetter, K. M., Schupp, P., Hauschulte, K., Vakhrusheva, O., Slade, K. S., et al. (2021). Shikonin Reduces Growth of Docetaxel-Resistant Prostate Cancer Cells Mainly through Necroptosis. *Cancers (Basel)* 13 (4), 882. doi:10.3390/cancers13040882

Mayakonda, A., Lin, D. C., Assenov, Y., Plass, C., and Koeffler, H. P. (2018). Maftools: Efficient and Comprehensive Analysis of Somatic Variants in Cancer. *Genome Res.* 28 (11), 1747–1756. doi:10.1101/gr.239244.118

Mermel, C. H., Schumacher, S. E., Hill, B., Meyerson, M. L., Beroukhim, R., and Getz, G. (2011). GISTIC2.0 Facilitates Sensitive and Confident Localization of the Targets of Focal Somatic Copy-Number Alteration in Human Cancers. *Genome Biol.* 12 (4), R41. doi:10.1186/gb-2011-12-4-r41

Niu, X., Chen, L., Li, Y., Hu, Z., and He, F. (2022). Ferroptosis, Necroptosis, and Pyroptosis in the Tumor Microenvironment: Perspectives for Immunotherapy of SCLC. *Semin Cancer Biol.* S1044-579X(22)00065-7. doi:10.1016/j.semcancer.2022.03.009

O'Hara, M. H., O'Reilly, E. M., Varadhachary, G., Wolff, R. A., Wainberg, Z. A., Ko, A. H., et al. (2021). CD40 Agonistic Monoclonal Antibody APX005M (Sotigalimab) and Chemotherapy, with or without Nivolumab, for the Treatment of Metastatic Pancreatic Adenocarcinoma: an Open-Label, Multicentre, Phase 1b Study. *Lancet Oncol.* 22 (1), 118–131. doi:10.1016/s1470-2045(20)30532-5

Pang, N., Shi, J., Qin, L., Chen, A., Tang, Y., Yang, H., et al. (2021). IL-7 and CCL19-Secreting CAR-T Cell Therapy for Tumors with Positive Glypican-3 or Mesothelin. *J. Hematol. Oncol.* 14 (1), 118. doi:10.1186/s13045-021-01128-9

Park, H. H., Kim, H. R., Park, S. Y., Hwang, S. M., Hong, S. M., Park, S., et al. (2021a). RIPK3 Activation Induces TRIM28 Derepression in Cancer Cells and Enhances the Anti-tumor Microenvironment. *Mol. Cancer* 20 (1), 107. doi:10.1186/s12943-021-01399-3

Park, W., Chawla, A., and O'Reilly, E. M. (2021b). Pancreatic Cancer: A Review. *JAMA* 326 (9), 851–862. doi:10.1001/jama.2021.13027

Pietkiewicz, S., Eils, R., Krammer, P. H., Giese, N., and Lavrik, I. N. (2015). Combinatorial Treatment of CD95L and Gemcitabine in Pancreatic Cancer Cells Induces Apoptotic and RIP1-Mediated Necroptotic Cell Death Network. *Exp. Cell Res.* 339 (1), 1–9. doi:10.1016/j.yexcr.2015.10.005

Rawla, P., Sunkara, T., and Gaduputi, V. (2019). Epidemiology of Pancreatic Cancer: Global Trends, Etiology and Risk Factors. *World J. Oncol.* 10 (1), 10–27. doi:10.14740/wjon1166

Ritchie, M. E., Phipson, B., Wu, D., Hu, Y., Law, C. W., Shi, W., et al. (2015). Limma Powers Differential Expression Analyses for RNA-Sequencing and Microarray Studies. *Nucleic Acids Res.* 43 (7), e47. doi:10.1093/nar/gkv007

Rui, C., Shi, S. N., Ren, W., Qin, X., Zhuang, C., Chen, X., et al. (2021). The Multitargeted Kinase Inhibitor KW-2449 Ameliorates Cisplatin-Induced Nephrotoxicity by Targeting RIPK1-Mediated Necroptosis. *Biochem. Pharmacol.* 188, 114542. doi:10.1016/j.bcp.2021.114542

Schizas, D., Charalampakis, N., Kole, C., Economopoulou, P., Koustas, E., Gkotsis, E., et al. (2020). Immunotherapy for Pancreatic Cancer: A 2020 Update. *Cancer Treat. Rev.* 86, 102016. doi:10.1016/j.ctrv.2020.102016

Seifert, L., Werba, G., Tiwari, S., Giao Ly, N. N., Alothman, S., Alqunaibit, D., et al. (2016). The Necrosome Promotes Pancreatic Oncogenesis *via* CXCL1 and Mincle-Induced Immune Suppression. *Nature* 532 (7598), 245–249. doi:10.1038/nature17403

Stratford, J. K., Bentrem, D. J., Anderson, J. M., Fan, C., Volmar, K. A., Marron, J. S., et al. (2010). A Six-Gene Signature Predicts Survival of Patients with Localized Pancreatic Ductal Adenocarcinoma. *PLoS Med.* 7 (7), e1000307. doi:10.1371/journal.pmed.1000307

Stratford, J. K., Yan, F., Hill, R. A., Major, M. B., Graves, L. M., Der, C. J., et al. (2017). Genetic and Pharmacological Inhibition of TTK Impairs Pancreatic Cancer Cell Line Growth by Inducing Lethal Chromosomal Instability. *PLoS One* 12 (4), e0174863. doi:10.1371/journal.pone.0174863

Tang, R., Ji, J., Ding, J., Huang, J., Gong, B., Zhang, X., et al. (2020a). Overexpression of MYEOV Predicting Poor Prognosis in Patients with Pancreatic Ductal Adenocarcinoma. *Cell Cycle* 19 (13), 1602–1610. doi:10.1080/15384101.2020.1757243

Tang, R., Xu, J., Zhang, B., Liu, J., Liang, C., Hua, J., et al. (2020b). Ferroptosis, Necroptosis, and Pyroptosis in Anticancer Immunity. *J. Hematol. Oncol.* 13 (1), 110. doi:10.1186/s13045-020-00946-7

Tao, J., Yang, G., Zhou, W., Qiu, J., Chen, G., Luo, W., et al. (2021). Targeting Hypoxic Tumor Microenvironment in Pancreatic Cancer. *J. Hematol. Oncol.* 14 (1), 14. doi:10.1186/s13045-020-01030-w

Wilkerson, M. D., and Hayes, D. N. (2010). ConsensusClusterPlus: A Class Discovery Tool with Confidence Assessments and Item Tracking. *Bioinformatics* 26 (12), 1572–1573. doi:10.1093/bioinformatics/btq170

Xiao, M., Liang, X., Yan, Z., Chen, J., Zhu, Y., Xie, Y., et al. (2022). A DNA-Methylation-Driven Genes Based Prognostic Signature Reveals Immune Microenvironment in Pancreatic Cancer. *Front. Immunol.* 13, 803962. doi:10.3389/fimmu.2022.803962

Xie, Y., Zhu, S., Zhong, M., Yang, M., Sun, X., Liu, J., et al. (2017). Inhibition of Aurora Kinase A Induces Necroptosis in Pancreatic Carcinoma. *Gastroenterology* 153 (5), 1429. doi:10.1053/j.gastro.2017.07.036

Xu, Y., Ma, H. B., Fang, Y. L., Zhang, Z. R., Shao, J., Hong, M., et al. (2017). Cisplatin-induced Necroptosis in TNFα Dependent and Independent Pathways. *Cell Signal.* 31, 112–123. doi:10.1016/j.cellsig.2017.01.004

Yang, W., Soares, J., Greninger, P., Edelman, E. J., Lightfoot, H., Forbes, S., et al. (2013). Genomics of Drug Sensitivity in Cancer (GDSC): A Resource for Therapeutic Biomarker Discovery in Cancer Cells. *Nucleic Acids Res.* 41 (Database issue), D955–D961. doi:10.1093/nar/gks1111

Yu, G., Wang, L. G., Han, Y., and He, Q. Y. (2012). clusterProfiler: An R Package for Comparing Biological Themes Among Gene Clusters. *Omics* 16 (5), 284–287. doi:10.1089/omi.2011.0118

Yu, S., Zhang, C., and Xie, K. P. (2021). Therapeutic Resistance of Pancreatic Cancer: Roadmap to its Reversal. *Biochim. Biophys. Acta Rev. Cancer* 1875 (1), 188461. doi:10.1016/j.bbcan.2020.188461

Yuan, P., Tang, C., Chen, B., Lei, P., Song, J., Xin, G., et al. (2021). miR-32-5p Suppresses the Proliferation and Migration of Pancreatic Adenocarcinoma Cells by Targeting TLDC1. *Mol. Med. Rep.* 24 (5), 752. doi:10.3892/mmr.2021.12392

Zhang, J., Bajari, R., Andric, D., Gerthoffert, F., Lepsa, A., Nahal-Bose, H., et al. (2019). The International Cancer Genome Consortium Data Portal. *Nat. Biotechnol.* 37 (4), 367–369. doi:10.1038/s41587-019-0055-9

Zhang, J., Liu, Z., Zhang, Z., Tang, R., Zeng, Y., and Chen, P. (2022). Identification of a Glycolysis-Related Gene Signature for Predicting Pancreatic Cancer Survival. *J. Gastrointest. Oncol.* 13 (1), 380–399. doi:10.21037/jgo-22-17

Zhu, X., Niu, X., and Ge, C. (2019a). Inhibition of LINC00994 Represses Malignant Behaviors of Pancreatic Cancer Cells: Interacting with miR-765-3p/RUNX2 axis. *Cancer Biol. Ther.* 20 (6), 799–811. doi:10.1080/15384047.2018.1564566

Zhu, X., Niu, X., Li, T., Liu, C., Chen, L., and Tan, G. (2019b). Identification of Research Trends Concerning Application of Stent Implantation in the Treatment of Pancreatic Diseases by Quantitative and Biclustering Analysis: a Bibliometric Analysis. *PeerJ* 7, e7674. doi:10.7717/peerj.7674

Zhu, X., Kong, Q., Niu, X., Chen, L., and Ge, C. (2020). Mapping Intellectual Structure and Research Performance for the Nanoparticles in Pancreatic Cancer Field. *Int. J. Nanomedicine* 15, 5503–5516. doi:10.2147/ijn.S253599

Zhu, X., Cao, Y., Liu, W., Ju, X., Zhao, X., Jiang, L., et al. (2021). Stereotactic Body Radiotherapy Plus Pembrolizumab and Trametinib versus Stereotactic Body Radiotherapy Plus Gemcitabine for Locally Recurrent Pancreatic Cancer after Surgical Resection: An Open-Label, Randomised, Controlled, Phase 2 Trial. *Lancet Oncol.* 22 (8), 1093–1102. doi:10.1016/s1470-2045(21)00286-2

Conflict of Interest: The authors declare that the research was conducted in the absence of any commercial or financial relationships that could be construed as a potential conflict of interest.

Publisher's Note: All claims expressed in this article are solely those of the authors and do not necessarily represent those of their affiliated organizations, or those of the publisher, the editors, and the reviewers. Any product that may be evaluated in this article, or claim that may be made by its manufacturer, is not guaranteed or endorsed by the publisher.

frontiers | Frontiers in Pharmacology

ORIGINAL RESEARCH
published: 03 June 2022
doi: 10.3389/fphar.2022.884090

A Novel Exosome-Relevant Molecular Classification Uncovers Distinct Immune Escape Mechanisms and Genomic Alterations in Gastric Cancer

Yubiao Lin[1†], Kaida Huang[1†], Zhezhen Cai[2†], Yide Chen[1†], Lihua Feng[1], Yingqin Gao[1], Wenhui Zheng[1], Xin Fan[1], Guoqin Qiu[3], Jianmin Zhuang[2]* and Shuitu Feng[1]**

[1]Department of Oncology, Xiamen Haicang Hospital, Xiamen, China, [2]Department of General Surgery, Xiamen Haicang Hospital, Xiamen, China, [3]Chenggong Hospital Affiliated to Xiamen University, Xiamen, China

OPEN ACCESS

Edited by:
Essa M. Saied,
Humboldt University of Berlin, Germany

Reviewed by:
Sonam Mittal,
Medical College of Wisconsin, United States
Hamed Barabadi,
Shahid Beheshti University of Medical Sciences, Iran

***Correspondence:**
Guoqin Qiu
qiuguoqin@163.com
Jianmin Zhuang
zhjmck@163.com
Shuitu Feng
fengshuitu@163.com

[†]These authors have contributed equally to this work and share first authorship

Specialty section:
This article was submitted to Pharmacology of Anti-Cancer Drugs, a section of the journal Frontiers in Pharmacology

Received: 25 February 2022
Accepted: 29 April 2022
Published: 03 June 2022

Citation:
Lin Y, Huang K, Cai Z, Chen Y, Feng L, Gao Y, Zheng W, Fan X, Qiu G, Zhuang J and Feng S (2022) A Novel Exosome-Relevant Molecular Classification Uncovers Distinct Immune Escape Mechanisms and Genomic Alterations in Gastric Cancer. Front. Pharmacol. 13:884090. doi: 10.3389/fphar.2022.884090

Objective: Gastric cancer (GC) is a highly heterogeneous malignant carcinoma. This study aimed to conduct an exosome-based classification for assisting personalized therapy for GC.

Methods: Based on the expression profiling of prognostic exosome-related genes, GC patients in The Cancer Genome Atlas (TCGA) cohort were classified using the unsupervised consensus clustering approach, and the reproducibility of this classification was confirmed in the GSE84437 cohort. An exosome-based gene signature was developed *via* Least Absolute Shrinkage and Selection Operator (LASSO) regression analysis. Immunological features, responses to immune checkpoint inhibitors, and genetic alterations were evaluated *via* computational methods.

Results: Two exosome-relevant phenotypes (A and B) were clustered, and this classification was independent of immune subtypes and TCGA subtypes. Exosome-relevant phenotype B had a poorer prognosis and an inflamed tumor microenvironment (TME) relative to phenotype A. Patients with phenotype B presented higher responses to the anti-CTLA4 inhibitor. Moreover, phenotype B occurred at a higher frequency of genetic mutation than phenotype A. The exosome-based gene signature (GPX3, RGS2, MATN3, SLC7A2, and SNCG) could independently and accurately predict GC prognosis, which was linked to stromal activation and immunosuppression.

Conclusion: Our findings offer a conceptual frame to further comprehend the roles of exosomes in immune escape mechanisms and genomic alterations of GC. More work is required to evaluate the reference value of exosome-relevant phenotypes for designing immunotherapeutic regimens.

Abbreviations: GC, gastric cancer; OS, overall survival; ICIs, immune checkpoint inhibitors; TME, tumor microenvironment; ECM, extracellular matrix; CNV, copy number variation; CDF, cumulative distribution function; PCA, principal component analysis; GSVA, Gene Set Variation Analysis; MSigDB, Molecular Signatures Database; ssGSEA, single-sample Gene Set Enrichment Analysis; Pan-F-TBRS, pan-fibroblast TGFb response signature; TIDE, Tumor Immune Dysfunction and Exclusion; CTLs, cytotoxic T lymphocytes; SubMap, Subclass Mapping; GDSC, Genomics of Drug Sensitivity in Cancer; IC_{50}, half-maximal inhibitory concentration; GO, Gene Ontology; KEGG, Kyoto Encyclopedia of Genes and Genomes; GSEA, Gene Set Enrichment Analysis; LASSO, Least Absolute Shrinkage and Selection Operator; ROC, receiver operating characteristic; DFS, disease-free survival; DSS, disease-specific survival; PFS, progression-free survival; CTRP, Cancer Therapeutics Response Portal; qRT-PCR, quantitative real-time polymerase chain reaction.

Keywords: gastric cancer, exosomes, immunotherapy, tumor microenvironment, immune escape

INTRODUCTION

Gastric cancer (GC) is one of the most common malignant carcinomas diagnosed globally, seriously jeopardizing human health (Bray et al., 2018). Despite the remarkable progress of therapies, the 5-year overall survival (OS) of advanced patients is merely 20% (Chen Y. et al., 2021). Cisplatin, paclitaxel, 5-fluorouracil, and doxorubicin remain the main chemotherapeutic agents against GC. Nevertheless, chemotherapeutic resistance is a common cause of recurrence and metastases of GC (Lin et al., 2020). Immunotherapy represented by immune checkpoint inhibitors (ICIs) against PD-1/L1 and CTLA-4 presents the durable therapeutic effects for the minority of GC patients; undesirably, most patients cannot respond to it (Shitara et al., 2018; Shitara et al., 2020; Janjigian et al., 2021). Thus, a more effective systemic treatment is urgently required.

Exosomes, a subgroup of extracellular vesicles with 30–150 nm, are secreted by nearly all cell types, which transmit cellular molecular components [protein, DNA, lipid, messenger RNA (mRNA), and non-coding RNA, etc.], thereby promoting cell-to-cell communication (Tang et al., 2021). Tumor progression is regarded as a multistep process, and accumulated evidence has suggested that the tumor microenvironment (TME) in which tumor cells grow and survive also exerts an important role in tumor progression (Zeng et al., 2019). Tumor cells elicit diverse alterations in biological behaviors *via* directly or indirectly interacting with the TME components (Jiang et al., 2019). Exosomes mediate the communications between the TME and tumor cells. For instance, tumor-associated macrophage-released exosomes facilitate the migration of GC cells through transferring apolipoprotein E (Zheng et al., 2018). Exosomal miR-451 released by GC cells enhances T-helper 17 cell differentiation (Liu F. et al., 2018). Recurrence and metastases are the main obstacles to favorable survival outcomes of GC (Chen D. et al., 2021). Tumor cells break away from the primary cancer nest and enter the circulatory system *via* blood vessels or lymph vessels, thereby facilitating tumor metastases (Cai et al., 2020). For avoiding the blockage of the extracellular matrix (ECM) and promoting the remodeling of the tumor-friendly TME, tumor cells release biologically active factors to elicit the communications of tumor cells with stromal subsets, thereby creating a favorable condition for cancer metastases (Sathe et al., 2020). Exosomes exert a crucial role in this process *via* carrying DNA, lipid, or ncRNA (Zhang et al., 2021). For instance, lymph node metastasis-GC cells educate mesenchymal stem cells through exosomal Wnt5a-triggered activation of the YAP pathway (Wang et al., 2021). In addition, exosomes released by tumor cells can hinder the activation of the immune system and the development of immune cells, thereby blocking the immune defense mechanism of tumor cells and eliciting the immune escape mechanism. Moreover, experimental evidence has demonstrated that exosomes participate in the chemotherapeutic resistance of GC (Lin et al., 2020). For instance, exosomes carrying miR-500a-3p trigger cisplatin resistance and stemness through the negative modulation of FBXW7 in GC (Lin et al., 2020). Tumor-associated macrophage-derived exosomal CRNDE attributes to cisplatin resistance in GC (Xin et al., 2021). The molecular subtype classification of GC provides an opportunity for personalized therapy. Thus, it is of significance to comprehensively recognize the exosome-relevant molecular classification in GC. This study conducted two exosome-relevant phenotypes with distinct immune escape mechanisms and genomic alterations in GC.

MATERIALS AND METHODS

Data Acquisition

This study collected three gene expression profile cohorts for GC: TCGA-STAD (n = 350) from TCGA (https://portal.gdc.cancer.gov/), GSE84437 (n = 433) (Yoon et al., 2020), and GSE15459 (n = 192) (Muratani et al., 2014) from the GEO repository (https://www.ncbi.nlm.nih.gov/gds/). RNA-seq data (FPKM value) of TCGA-STAD cohort were downloaded from the Genomic Data Commons (https://portal.gdc.cancer.gov/) using the TCGAbiolinks package (Colaprico et al., 2016). FPKM value was transformed to TPM value. For the GSE84437 cohort on the Illumina platform, the normalized matrix files were directly downloaded. For the GSE15459 on the Affymetrix platform, the raw "CEL" files were downloaded, which were normalized utilizing a robust multi-array averaging approach. For TCGA-STAD cohort, somatic mutation and copy number variation (CNV) profiles were also retrieved. Through reviewing the published literature, we collected 121 exosome-related genes, as listed in **Supplementary Table S1**.

Unsupervised Consensus Clustering Analysis

The ConsensusClusterPlus package was applied for consistent clustering and determining exosome-relevant phenotypes on the basis of expression profiling of prognostic exosome-related genes derived from univariate Cox regression analysis (p-value < 0.05) (Wilkerson and Hayes, 2010). Through the Euclidean squared distance metric and the K-means clustering approach, GC specimens were classified as k clusters from k = 2 to 9. Approximately 80% of the specimens were chosen at each iteration. Following 100 iterations, the classification results were acquired, which were visualized into the heatmaps of the consensus matrix. The optimal number of clusters was identified in accordance with a cumulative distribution function (CDF) plot and an item tracking plot. The accuracy of this classification was verified through principal-component analysis (PCA). The classification was externally verified in the GSE84437 cohort.

Gene Set Variation Analysis

The GSVA package was used for exploring the potential biological functions and progress variations of each phenotype

(Hänzelmann et al., 2013). The Hallmark gene sets were derived from the Molecular Signatures Database (Liberzon et al., 2015).

Evaluation of Immunological Status

The relative abundance of each immune cell component within the TME was quantified *via* applying the single-sample Gene Set Enrichment Analysis (ssGSEA) approach. The marker gene sets of 28 immune cell types were acquired from Bindea et al. (2013). The immunomodulators that comprised MHCs, receptors, chemokines, and immune-stimulators and immune-inhibitors were curated from the study of Charoentong et al. (2017). Moreover, known immune checkpoints were retrieved from Auslander et al. (2018). Mariathasan et al. established the gene sets of immune ($CD8^+$ T effector, antigen processing machinery) and stromal [pan-fibroblast TGFb response signature (Pan-F-TBRS), epithelial-mesenchymal transition (EMT), and angiogenesis] pathways. Their levels were quantified with the ssGSEA.

Evaluation of Responses to Immune Checkpoint Inhibitors

The Tumor Immune Dysfunction and Exclusion (TIDE) algorithm was applied for predicting the responses to ICIs (Jiang et al., 2018). This computational method was implemented on the basis of two tumor immune escape mechanisms: inducing T-cell dysfunction in tumors with increased infiltration of cytotoxic T lymphocytes (CTLs) and preventing T-cell infiltration in tumors with reduced infiltration of CTLs. The Subclass Mapping (SubMap) approach was applied for evaluating the expression similarity between the groups and the distinct responses to ICIs (Hoshida et al., 2007). Based on the GSEA approach, the degree of commonality between the groups was deduced. Adjusted *p*-value <0.05 indicated significant similarity between the groups.

Drug Sensitivity Analysis

Using the pRRophetic package (Geeleher et al., 2014), a ridge regression model was built on the basis of the Genomics of Drug Sensitivity in Cancer (GDSC) cell line expression profiles (Yang et al., 2013). The half-maximal inhibitory concentration (IC_{50}) values of compounds were estimated across GC specimens.

Mutational Analysis

Through the maftools package (Mayakonda et al., 2018), somatic variants were analyzed and the overall mutation status was compared between the two phenotypes. Moreover, the top 20 mutated genes were visualized. Through the GISTIC2.0 approach, the recurrently amplified and deleted regions were defined (Mermel et al., 2011).

Differential Expression Analysis

Through the limma package (Ritchie et al., 2015), the significantly altered genes between the phenotypes were identified according to the following threshold: |log2fold change| > 1 and adjusted *p*-value < 0.05. The *p*-value from Benjamini–Hochberg correction was adjusted for multiple comparisons by a false discovery rate.

Enrichment Analysis

Gene Ontology (GO) enrichment and Kyoto Encyclopedia of Genes and Genomes (KEGG) pathway analysis were conducted *via* the clusterprofiler package (Yu et al., 2012). With the criteria of adjusted *p*-value < 0.05, significant GO terms and KEGG pathways were screened. The Gene Set Enrichment Analysis (GSEA) was also carried out (Subramanian et al., 2005). The gene set "c2.cp.kegg.v6.2.symbols.gmt" was chosen as the reference.

Prognostic Signature Construction

The Least Absolute Shrinkage and Selection Operator (LASSO) is a penalized regression analysis that can screen variables from high dimensional data to build risk signatures. Herein, the LASSO analysis was conducted in TCGA cohort to determine the most valuable genes in GC prognosis. The optimal value of the tuning parameter (λ) was identified after a ten-fold cross-verification utilizing the minimum and 1- standard error (SE) criteria. The prognostic signature was built by multivariate Cox regression analysis. On the basis of the signature, the risk score was constructed in line with the following formula: risk score = $\sum coef\,ficient\,of\;gene\,i * expression\,of\;gene\,i$. GC patients were equally classified into high- and low-risk groups in accordance with the median value of the risk score. The prediction accuracy of the signature was evaluated *via* time-independent receiver operating characteristic (ROC) curves. Moreover, the prognostic value of the signature was externally verified in the GSE15459 cohort.

Nomogram Establishment

Univariate Cox regression analysis on the clinical features and prognostic signature was conducted in TCGA cohort. The significant prognostic factors with *p*-value < 0.05 were incorporated into the multivariate Cox regression analysis. Through the rms package, the nomogram was built by incorporating factors with prediction significance (*p*-value < 0.05) from the multivariate analysis. Time-dependent ROC curves were drawn for determining the prediction accuracy of the nomogram. A calibration plot was used for assessing the agreement between the predicted and actual outcomes.

Patients and Specimens

In total, fresh-frozen 20 paired GC and para-carcinoma tissues were acquired with signed informed consent from Xiamen Haicang Hospital. All patients did not receive any treatment before surgery. All procedures involving human specimens gained the approval of the Ethics Committee of Xiamen Haicang Hospital (KY-2020014).

Quantitative Real-Time Polymerase Chain Reaction

Total RNA extraction from tissues was implemented with a Trizol kit in line with the manufacturer's instructions. Afterward, the extracted RNA was reverse transcribed into cDNA. qRT-PCR was conducted with a LightCycler 480 system (Roche, Germany). The sequences of primers used for qRT-PCR were as follows: GPX3,

TABLE 1 | Prognostic exosome-related genes in GC *via* the univariate analysis.

Exosome-related gene	Hazard ratio	Lower 95% CI	Upper 95% CI	*p*-value
CP	1.345545	1.058641	1.710204	0.015279
CYP11A1	1.473560	1.030760	2.106583	0.033494
RHO	4.395776	1.357214	14.23714	0.013536
ABCB5	2.313005	1.434912	3.728447	0.000577
ADCYAP1	1.511357	1.126606	2.027505	0.005865
MRPL4	0.198812	0.054168	0.729698	0.014893
ADRA1B	1.736174	1.261456	2.389539	0.000711
CD82	0.386935	0.161835	0.925132	0.032766
POSTN	2.154474	1.158856	4.005467	0.015268
HTR7	1.798705	1.116122	2.898735	0.015901
CYP19A1	1.993157	1.347986	2.947118	0.000547
DUSP1	3.428910	1.520732	7.731423	0.002973
ABCC9	1.411726	1.050760	1.896693	0.022103
HRNR	4.134901	1.015019	16.84442	0.047618
DOK7	0.668056	0.501564	0.889813	0.005812

5′-GCCGGGGACAAGAGAAGT-3′ (forward) and 5′-GAG GACGTATTTGCCAGCAT-3′ (reverse); RGS2, 5′-AAGATT GGAAGACCCGTTTGAG-3′ (forward) and 5′-GCAAGACCA TATTTGCTGGCT-3′ (reverse); MATN3, 5′-TCTCCCGGA TAATCGACACTC-3′ (forward) and 5′-CAAGGGTGTGAT TCGACCCA-3′ (reverse); SLC7A2, 5′-GACCTTTGCCCGATG TCTGAT-3′ (forward) and 5′-AGCAGCGGCATAATTTGG TGT-3′ (reverse); SNCG, 5′-TGAGCAGCGTCAACACTGTG-3′ (forward) and 5′-GAGGTGACCGCGATGTTCTC-3′ (reverse); and GAPDH, 5′-CTGGGCTACACTGAGCACC-3′ (forward) and 5′-AAGTGGTCGTTGAGGGCAATG-3′ (reverse). The relative mRNA expression was calculated with the $2^{-\Delta\Delta Ct}$ method.

Statistical Analysis

All data processing was implemented using R 3.6.1 software. The Kaplan–Meier analysis of OS, disease-free survival (DFS), disease-specific survival (DSS), and progression-free survival (PFS) was conducted and compared with log-rank tests. Student's t-test and Wilcoxon test were performed to conduct the comparisons of the two groups. Pearson and Spearman correlation tests were applied to evaluate the associations between variables. Through the Gene Set Cancer Analysis web-based analysis platform (Liu CJ. et al., 2018), the frequency of the CNV and somatic mutation of genes was analyzed across pan-cancer. Moreover, the Spearman correlation of drug sensitivity and gene expression was analyzed on the basis of the Cancer Therapeutics Response Portal (CTRP) and the GDSC databases. All statistical *p*-values were two-sided, with p-value < 0.05 as statistically significant.

RESULTS

Construction of Two Exosome-Relevant Phenotypes in Gastric Cancer

This study collected 121 exosome-related genes from the published literature. Among them, 15 exosome-related genes were significantly linked to OS outcomes of GC patients (**Table 1**). On the basis of expression profiling of prognostic exosome-related genes, we conducted a consensus clustering analysis in TCGA cohort, in which GC patients were initially classified into different k (k = 2–9) clusters. In accordance with the consensus matrix, CDF, and tracking plot, the optimal cluster was achieved when k = 2 (**Figures 1A–D**). The two clusters of GC specimens were separated from one another in accordance with PCA (**Figure 1E**). Therefore, GC specimens were classified into two exosome-relevant phenotypes, namely, exosome-relevant phenotype A (n = 154) and phenotype B (n = 196). Exosome-relevant phenotype A presented a remarkable advantage of OS, DFS, DSS, and PFS outcomes relative to phenotype B (**Figures 1F–I**). To guarantee the reproducibility and robustness of exosome-relevant phenotypes derived from TCGA cohort, this classification was validated in the GSE84437 cohort. The two phenotypes displayed high consistency with TCGA cohort (**Supplementary Figures S1A–F**).

Distinct Immunological Status in Exosome-Related Phenotypes

This study further investigated the specific biological mechanisms and immunological status of each phenotype in TCGA cohort. The heterogeneity in the activation of hallmark pathways was observed in two exosome-related phenotypes. As shown in **Figure 2A**, most hallmark pathways were activated in exosome-related phenotype B relative to phenotype A, such as inflammatory or immune activation pathways (interferon-gamma response, allograft rejection, IL6-JAK-STAT3 signaling, inflammatory response, IL2-STAT5 signaling, complement, etc.), stromal activation pathways (EMT, angiogenesis, etc.), and tumorigenic pathways (hedgehog signaling, hypoxia, Notch signaling, TGF-beta signaling, etc.). Moreover, exosome-related phenotype B displayed remarkably higher immune cell infiltration within the TME relative to phenotype A (**Figure 2B**). In **Figures 2C,D**, most immunomodulatory molecules (chemokines, immuno-inhibitors, immuno-stimulators, MHC, and receptors) displayed a prominently higher expression in exosome-related phenotype B than phenotype A. We also noted that immune checkpoints were

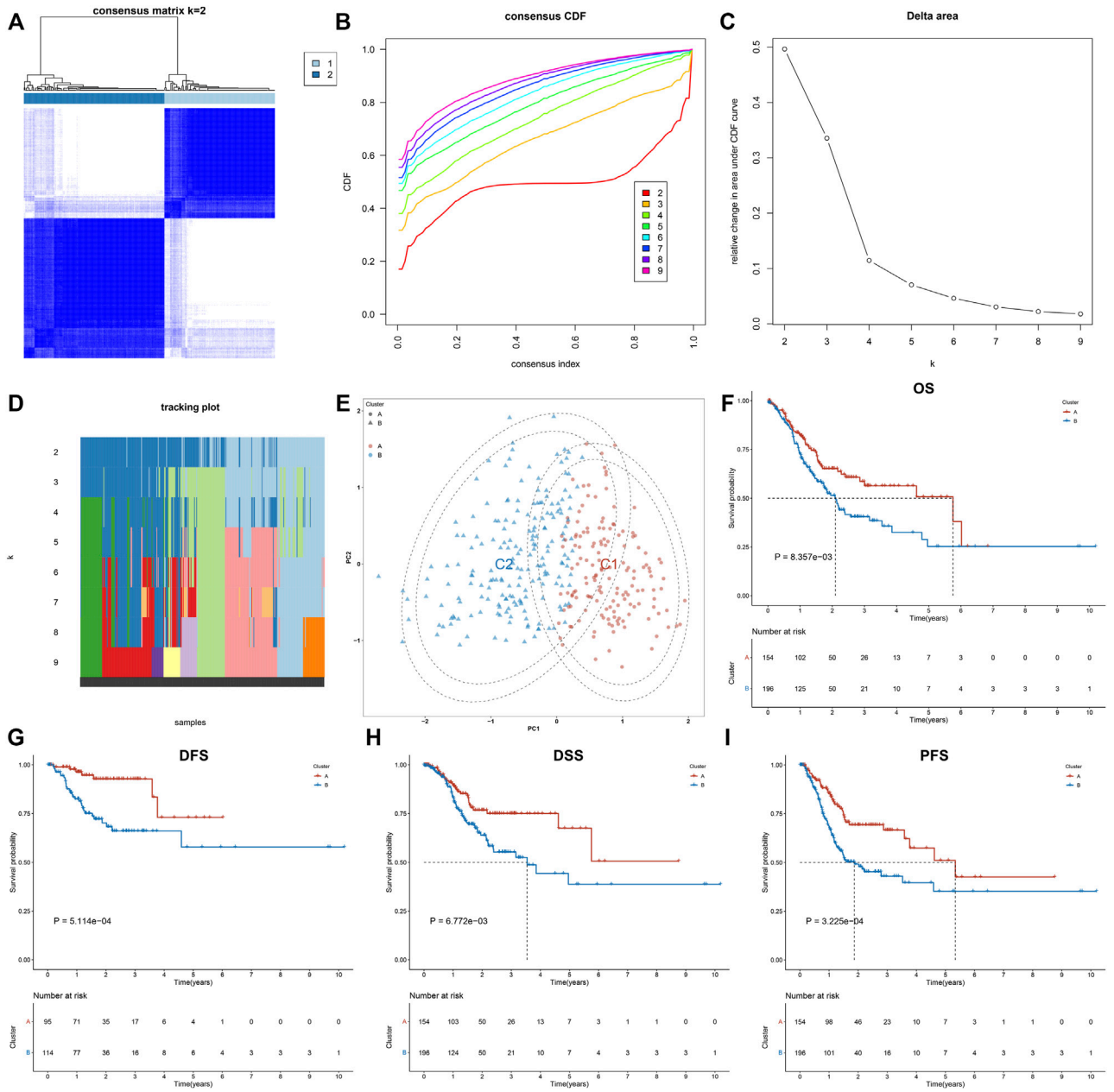

FIGURE 1 | Construction of two exosome-relevant phenotypes with distinct clinical outcomes in GC. **(A)** Consensus score matrix of GC specimens when k = 2. **(B)** CDF of the consensus matrix for each k (indicated by colors). **(C)** Relative alterations in the area under CDF curves. **(D)** Tracking plot for each k. **(E)** PCA plot by expression profiling of 15 prognostic exosome-related genes. Each point indicates each specimen, with unique colors representing exosome-relevant phenotypes. **(F–I)** Kaplan–Meier analysis of **(F)** OS, **(G)** DFS, **(H)** DSS, and **(I)** PFS in two exosome-relevant phenotypes.

markedly upregulated in exosome-related phenotype B relative to phenotype A (**Figure 2E**). Our ssGSEA results also confirmed the activation of $CD8^+$ T effector, pan-F-TBRS, EMT1-3, and angiogenesis in phenotype B. Overall, exosome-related phenotype B presented an inflamed TME in comparison to phenotype A (**Figure 2F**). This study applied the submap approach to compare the similarity of the expression profiling between exosome-related phenotypes and 47 melanoma patients who received ICIs. Our results showed that GC patients in exosome-related phenotype B presented higher responses to anti-CTLA4 therapy (**Figure 3A**).

Interplay Between Exosome-Related Phenotypes and Immunological and Molecular Subtypes of Gastric Cancer

We observed the interactions between exosome-related phenotypes and immunological subtypes. In **Figure 3B**,

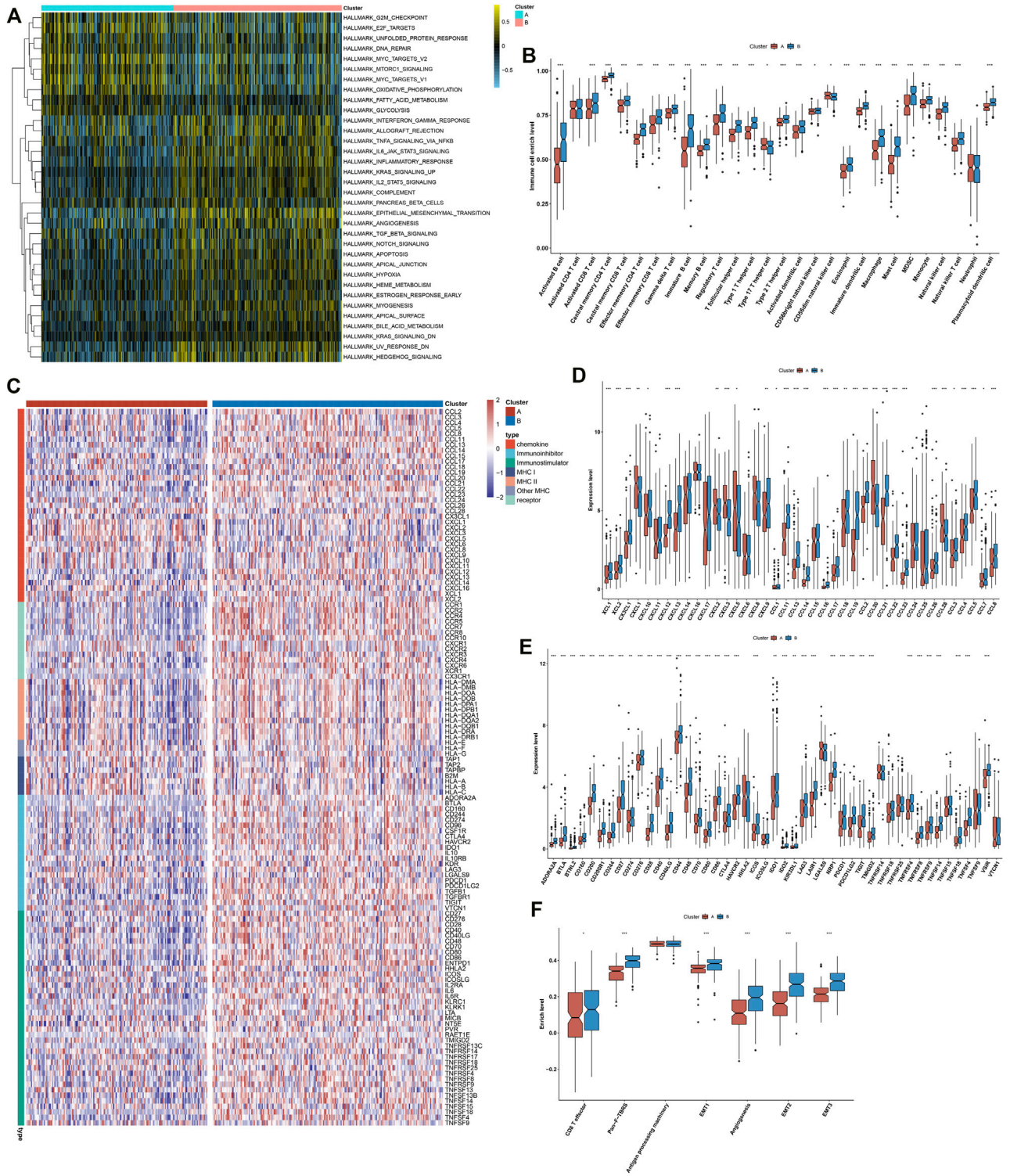

FIGURE 2 | Distinct immunological status in exosome-related phenotypes. **(A)** Visualization of the levels of hallmark pathways in exosome-related phenotypes A and B. **(B)** Differences in the infiltration levels of 28 immune cell types between the phenotypes. **(C)** Visualization of the expression of immunomodulatory molecules (chemokines, immuno-inhibitors, immuno-stimulators, MHC, and receptors) in the two phenotypes. **(D,E)** Differences in the expression of **(D)** chemokines and **(E)** immune checkpoints between phenotypes. **(F)** Comparisons of the levels of immune and stromal pathways between phenotypes. **p*-value < 0.05; ***p*-value < 0.01; and ****p*-value < 0.001.

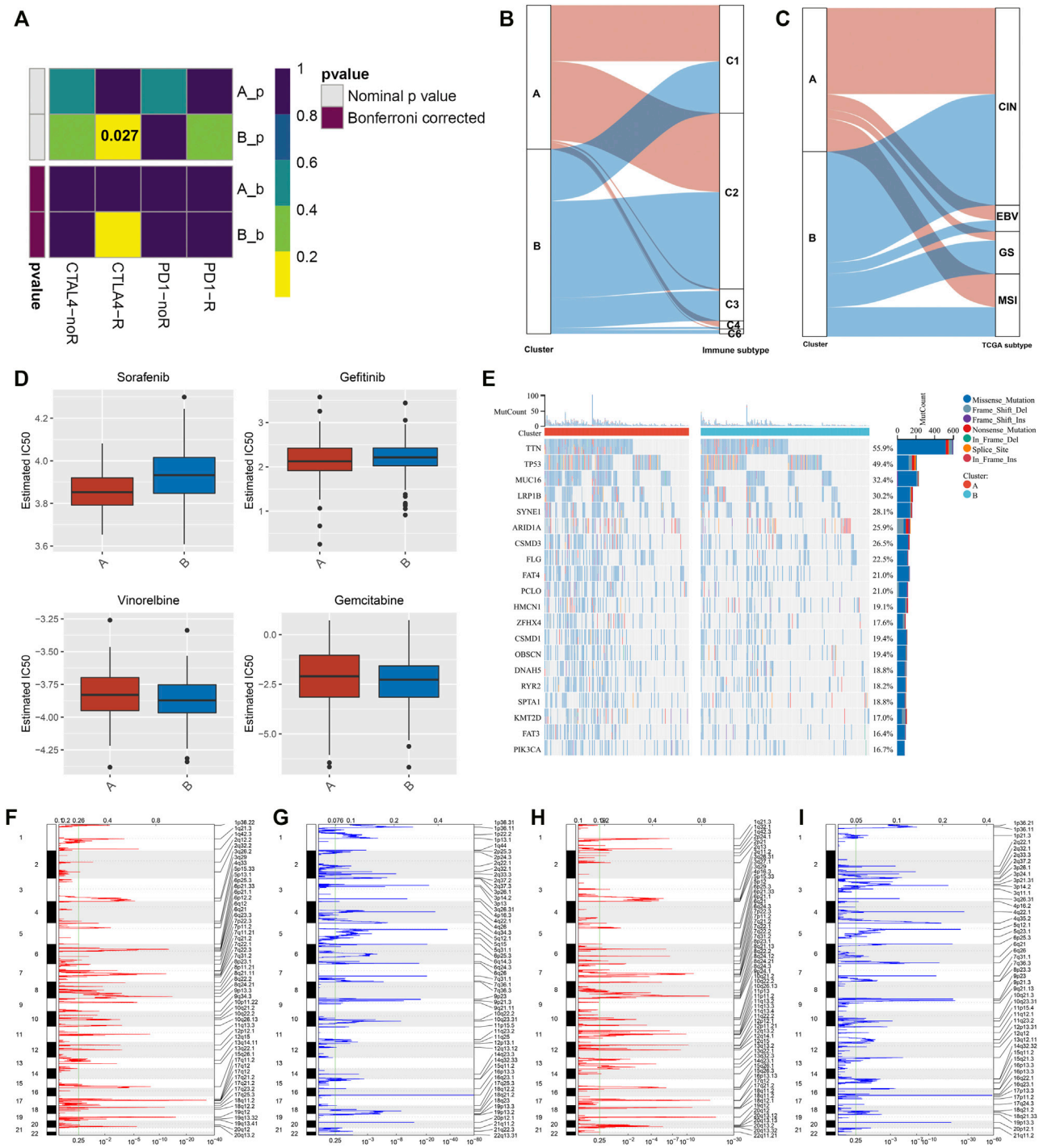

FIGURE 3 | Responses to ICIs, interplay with immunological and molecular subtypes, drug sensitivity, and genomic alterations in exosome-related phenotypes. **(A)** Submap analysis of the similarity of the expression profiling between GC patients in TCGA cohort and 47 previous melanoma subjects who received ICIs. **(B)** Alluvial diagram depicting the interactions between the two exosome-related phenotypes and immunological subtypes. **(C)** Alluvial diagram depicting the interactions between two exosome-related phenotypes and molecular subtypes of GC. **(D)** Differences in estimated IC_{50} values of sorafenib, gefitinib, vinorelbine, and gemcitabine between the exosome-related phenotypes. **(E)** Mutational frequency of the top 20 genes in two exosome-related phenotypes. Gene symbols are ranked in accordance with the frequency of gene mutation. Each column indicates each specimen and the upper panel indicates TMB. **(F–I)** Somatic copy number alterations in exosome-related phenotype **(F,G)** A and **(H,I)** phenotype B. On the x-axis, focal amplification or deletion is separately represented by red or blue bars. The position of chromosomes is shown along the y-axis. The green line indicates the significance threshold of $q < 0.25$.

exosome-related phenotypes spanned five of the six immunological subtypes, including C1-wound healing, C2-interferon (IFN)-γ dominant, C3-inflammatory, C4-lymphocyte depleted, and C6-transforming growth factor-β (TGF-β) dominant subtypes. The relatively equal distribution of exosome-related phenotypes was found in C1 and C2 subtypes. Further observation found that C3 and C6 subtypes were particularly dominant in exosome-related phenotype B, while C4 was enriched in exosome-related phenotype A. Thereafter, we evaluated the interactions between exosome-related phenotypes and molecular subtypes. It was found that exosome-related phenotypes spanned chromosomal instability (CIN), Epstein–Barr virus (EBV), genomic stability (GS), and microsatellite instability (MSI) (**Figure 3C**). However, there was no substantial heterogeneity in the distribution of exosome-related phenotypes. Further investigation showed that the GS subtype was remarkably dominant in exosome-related phenotype B. Overall, exosome-related phenotypes were linked to immunological and molecular subtypes of GC.

Drug Sensitivity in Exosome-Related Phenotypes

Further analysis was conducted to evaluate the differences in sensitivity to sorafenib, gefitinib, vinorelbine, and gemcitabine between exosome-related phenotypes. As shown in **Figure 3D**, there were remarkably lower IC_{50} values of sorafenib and gefitinib in exosome-related phenotype A relative to phenotype B, indicating that GC patients in exosome-related phenotype A were more likely to respond to sorafenib and gefitinib. We also noted that exosome-related phenotype B had significantly lower IC_{50} values of vinorelbine and gemcitabine in comparison to exosome-related phenotype A, indicating that patients in exosome-related phenotype B presented higher sensitivity to vinorelbine and gemcitabine.

Landscape of Genomic Alterations in Exosome-Related Phenotypes

Somatic mutations in the two exosome-related phenotypes were investigated. There were substantial differences in gene mutations between the phenotypes (**Figure 3E**). TTN (55.9%), TP53 (49.4%), MUC16 (32.4%), and LRP1B (30.2%) were the most frequently mutated genes. Higher TMB was investigated in exosome-related phenotype A relative to phenotype B. Thereafter, an analysis of CNV was presented in two phenotypes. No substantial difference in copy number-amplification was investigated between the phenotypes, but exosome-related phenotype A displayed a higher frequency of copy number-deletion relative to phenotype B (**Figures 3F–I**).

Screening Significantly Altered Genes Between Exosome-Related Phenotypes

For finding the genes most correlated to exosome-related phenotypes, we conducted differential expression analysis between two phenotypes. Under the threshold of |log2fold change| > 1 and adjusted *p*-value < 0.05, 773 significantly altered genes were determined (**Figure 4A**; **Supplementary Table S2**). Further observation showed that these significantly altered genes were linked to cell migration, immune or inflammatory response, protein activation (**Figure 4B**), and extracellular components (**Figure 4C**). Moreover, the significantly altered genes were correlated to molecular functions of signaling receptor binding, structural molecule activity, antigen binding, extracellular matrix structural constituent, etc. (**Figure 4D**). It was also found that the significantly altered genes were enriched in tumorigenic pathways such as cell adhesion molecules, focal adhesion, ECM-receptor interaction, and PI3K-Akt and TGF-beta signaling pathways (**Figure 4E**). For validating the reliability of the KEGG pathway analysis, we conducted the GSEA based on the significantly altered genes. As shown in **Figure 4F**, the significantly altered genes displayed positive interactions with the B-cell receptor signaling pathway, ECM-receptor interaction, focal adhesion, leukocyte trans-endothelial migration, and Th1 and Th2 cell differentiation, whereas they were negatively linked to base excision repair, DNA replication, homologous recombination, mismatch repair, and nucleotide excision repair (**Figure 4G**). Thus, the aforementioned significantly altered genes might exert important roles in GC.

Construction of the Exosome-Based Gene Signature

The univariate analysis showed that 266 significantly altered genes were significantly linked with GC prognosis (**Supplementary Table S3**). The LASSO analysis was conducted based on the prognostic significantly altered genes. Through the minimum and 1-SE criteria, five genes (GPX3, RGS2, MATN3, SLC7A2, and SNCG) were chosen to establish the exosome-based gene signature in TCGA cohort (**Figures 5A,B**). The risk score of each patient was calculated, and all patients were stratified into high- and low-risk groups following the median value (**Figure 5C**). The high-risk group had more cases with dead status and reduced expression of the aforementioned five genes. For evaluating the prognostic implication of this model, the difference in the OS between the groups was estimated. As shown in **Figure 5D**, high-risk patients presented a significantly reduced OS than their counterparts in TCGA cohort. Time-independent ROC curves demonstrated that the signature was accurately predictive of GC patients' OS (**Figure 5E**). Moreover, the associations between the signature and OS were evaluated *via* uni- and multivariate analysis. As shown in **Figure 5F**, the signature, age, and stage were independent risk factors of OS. For examining the robustness of the signature, the prediction performance was tested in the GSE15459 cohort. With the same formula, GC patients were stratified into high- and low-risk groups (**Supplementary Figure S2A**). Consistent with the outcomes of TCGA cohort, high-risk patients presented a significantly poorer OS than their counterparts (**Supplementary Figure S2B**), with a high prediction accuracy (**Supplementary Figure S2C**). For providing clinicians with a quantitative approach for predicting GC patients' outcomes, the nomogram was built by incorporating the aforementioned independent risk factors

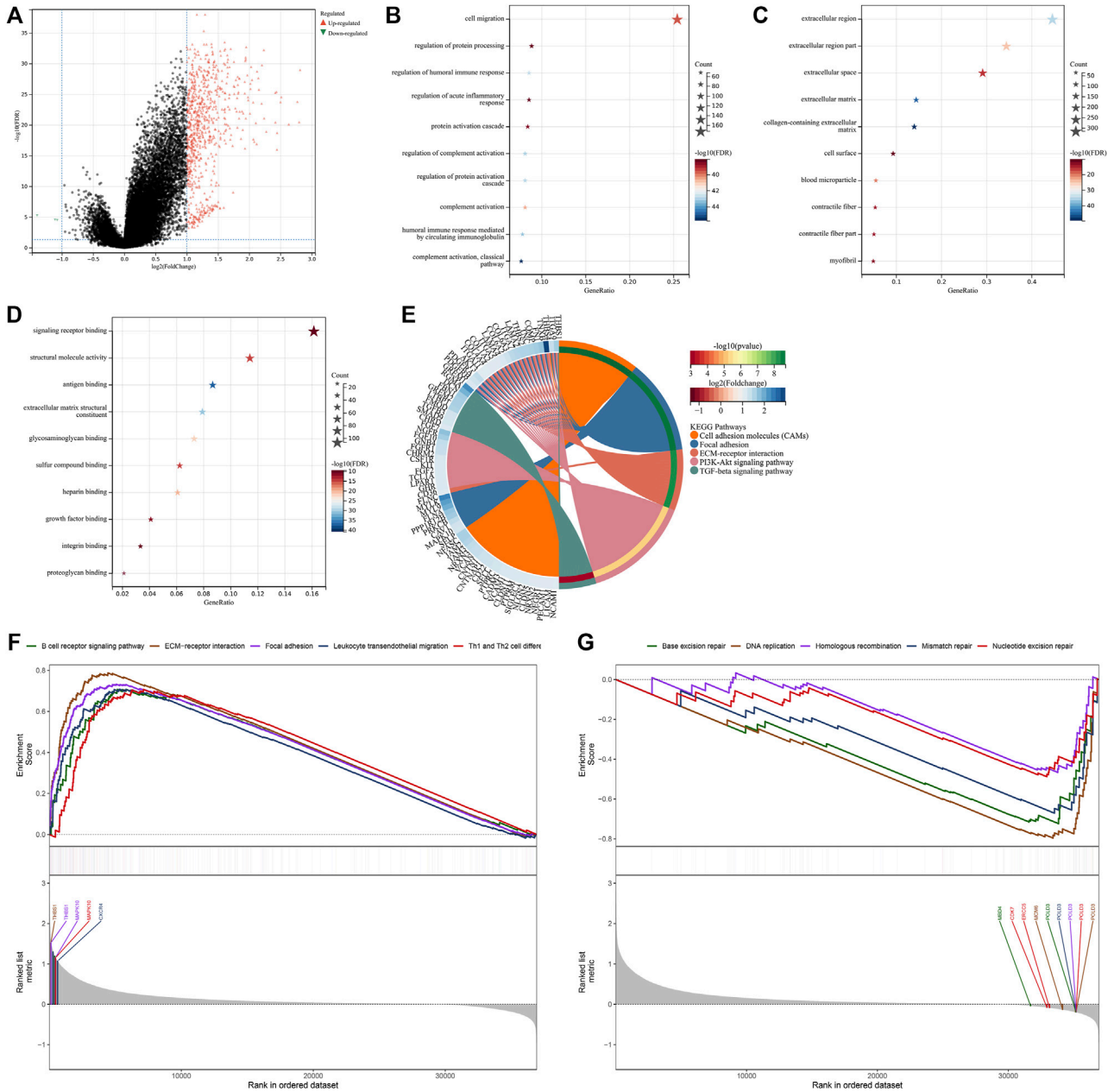

FIGURE 4 | Screening significantly altered genes between the exosome-related phenotypes and analysis of their biological implications. **(A)** Volcano plot for up- and downregulated genes in exosome-related phenotype A when compared with phenotype B. **(B–D)** Visualization of the top ten **(B)** biological processes, **(C)** cellular components, and **(D)** molecular functions, respectively. **(E)** Visualization of the top five KEGG pathways enriched by significantly altered genes. **(F)** GSEA for the signaling pathways positively correlated to significantly altered genes. **(G)** GSEA for the signaling pathways negatively associated with significantly altered genes.

(**Figure 5G**). On the basis of the nomogram, a score was calculated for an individual patient for predicting the 1-, 3-, and 5-year OS. Further observation showed that the exosome-based gene signature contributed to the most risk points in comparison to age and histological staging. Time-independent ROC curves demonstrated that the nomogram presented high accuracy in predicting OS (**Figure 5H**). The calibration plot showed that the nomogram-predicted OS fit well with the actual outcomes (**Figure 5I**). Thus, the exosome-based gene signature could optimize risk stratification and accurately predict GC patients' OS.

Exosome-Based Gene Signature is Linked to Stromal Activation and Immunosuppression

Further investigation showed that the exosome-based gene signature presented positive interactions with stromal activation pathways,

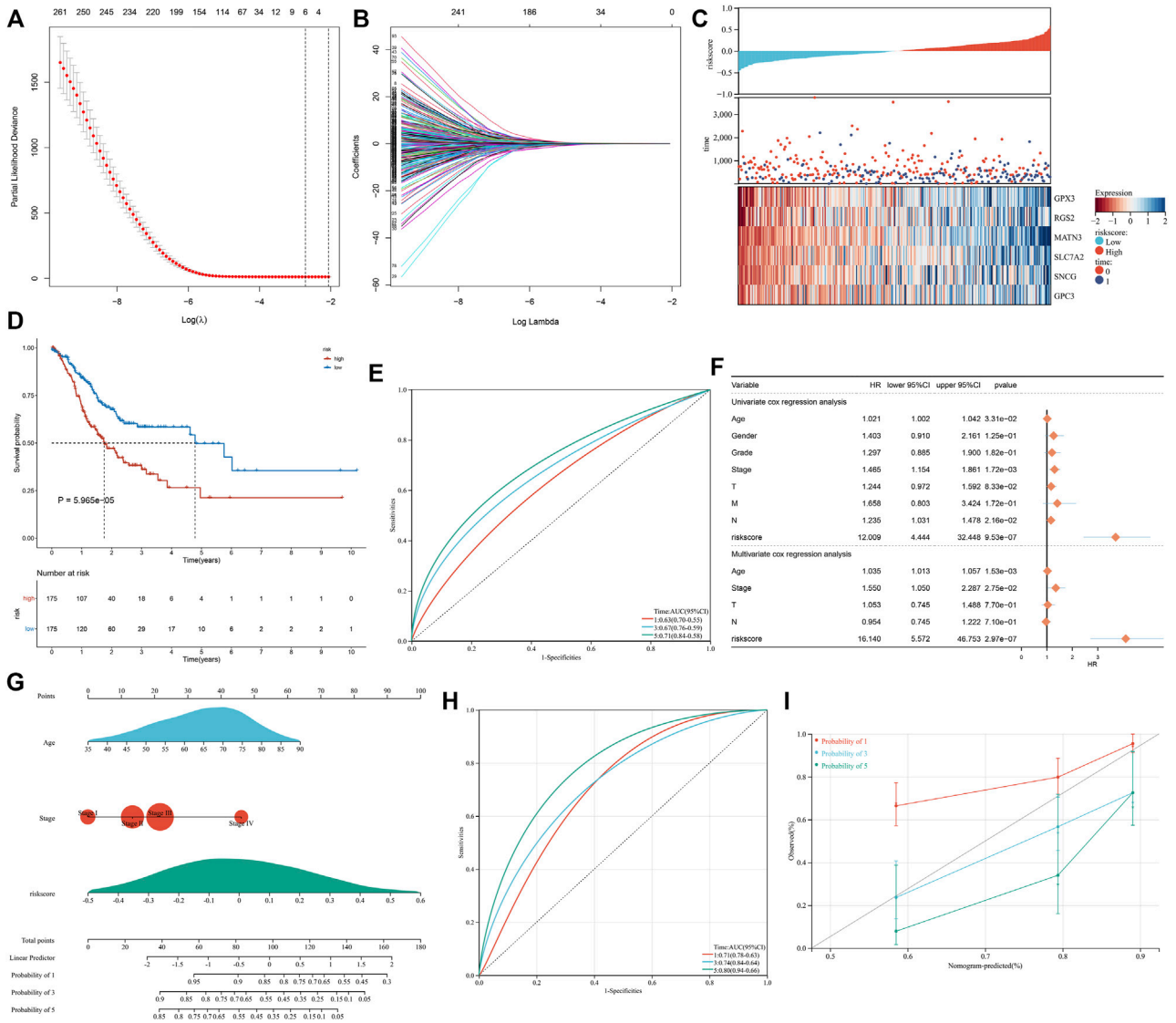

FIGURE 5 | Construction of the exosome-based gene signature for GC in TCGA cohort. **(A)** Partial likelihood deviance in the LASSO regression model *via* the ten-fold cross verification. The vertical dotted lines represent the optimal values utilizing the minimum and 1-SE criteria. **(B)** LASSO coefficient profiling. **(C)** Overview of the risk score distribution (upper), survival status (middle), and expression of genes that made up the signature (lower). **(D)** Kaplan–Meier curves of OS in TCGA cohort, divided into high- and low-risk groups. **(E)** Time-independent ROC curves showing the prediction accuracy of this signature. **(F)** Forest plot showing the associations of risk score and clinical features with OS according to uni- and multivariate Cox regression models. **(G)** Construction of the nomogram that incorporated the risk score, age, and histological staging. **(H)** Time-independent ROC curves showing the prediction accuracy of the nomogram. **(I)** Calibration plot showing the agreement between the nomogram-predicted and actual 1-, 3-, and 5-year outcomes. The x-axis represents the nomogram-predicted OS, and the y-axis represents the actual OS. The ideal performance of the nomogram is shown by the dashed line along the 45°line.

such as focal adhesions, ECM receptor interaction, TGF-beta, and WNT and mTOR signaling pathways (**Figure 6A**). Moreover, this signature was negatively linked to proteasome, base excision repair, and DNA replication (**Figure 6B**). As shown in **Figure 6C**, the exosome-based gene signature was positively correlated to EMT1-3, angiogenesis, and pan-F-TBRS, consistent with the GSEA results. It was also found that this signature displayed a negative association with antigen processing machinery. Immunosuppressive myeloid cells such as MDSC, tumor-associated macrophages, and regulatory T cells displayed significantly higher infiltration in the high-risk group relative to the low-risk group (**Figure 6D**). Overall, the exosome-based gene signature was linked to stromal activation and immunosuppression in GC.

Landscape of Genetic alterations, Drug Sensitivity, and Immune Cell Infiltration in the Exosome-Based Gene Signature

There were widespread amplifications and deletions of five genes (GPX3, RGS2, MATN3, SLC7A2, and SNCG) across

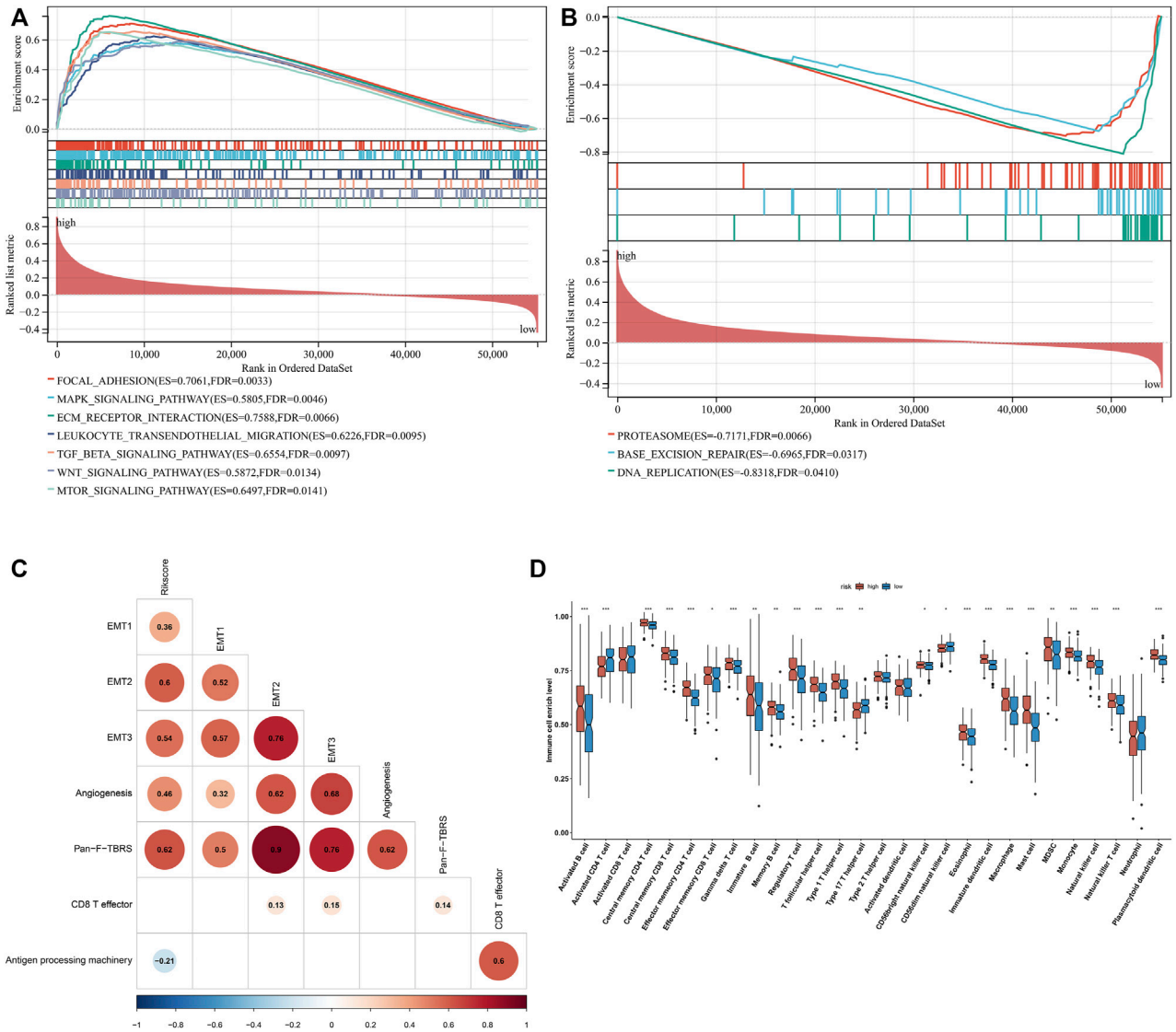

FIGURE 6 | Exosome-based gene signature is linked to stromal activation and immunosuppression in GC. **(A)** GSEA showing the signaling pathways positively linked to the exosome-based gene signature. **(B)** GSEA showing the signaling pathways negatively associated with the signature. **(C)** Associations of the signature with stromal and immune activation pathways that were quantified by the ssGSEA approach. **(D)** Comparisons of the relative abundance levels of 28 immune cell types in the high-risk group relative to the low-risk group. **p*-value < 0.05; ***p*-value < 0.01; and ****p*-value < 0.001.

pan-cancer (**Figure 7A**). Most cancer types had a relatively high mutation frequency of the aforementioned genes (**Figure 7B**). On the basis of the GDSC and CTRP projects, all of them were remarkably linked to the sensitivity to THZ-2-49, Bosutinib, CGP-082996, XMD8-85, Z-LLNle-CHO, Temsirolimus, AZD6482, BEZ235, Dasatinib, CHIR-99021, EHT 1864 (**Figure 7C**), BRD9647, pluripotin, compound 23 citrate, avicin D, lovastatin, prochlorperazine, NVP-ADW742, dasatinib, and austocystin D (**Figure 7D**). Moreover, they presented prominent correlations to the infiltrations of immune cells (activated B cell, activated CD4 T cell, activated CD8 T cell, activated dendritic cell, CD56bright natural killer cell, CD56dim natural killer cell, central memory CD4 T cell, central memory CD8 T cell, effector memory CD4 T cell, effector memory CD8 T cell, eosinophil, gamma delta T cell, immature B cell, macrophage, mast cell, MDSC, memory B cell, monocyte, natural killer cell, natural killer T cell, neutrophil, plasmacytoid dendritic cell, regulatory T cell, T follicular helper cell, type 1 helper cell, type 17 helper cell, and type 2 helper cell) within the TME of GC (**Figure 7E**). The aforementioned data indicated the implications of GPX3, RGS2, MATN3, SLC7A2, and SNCG in GC.

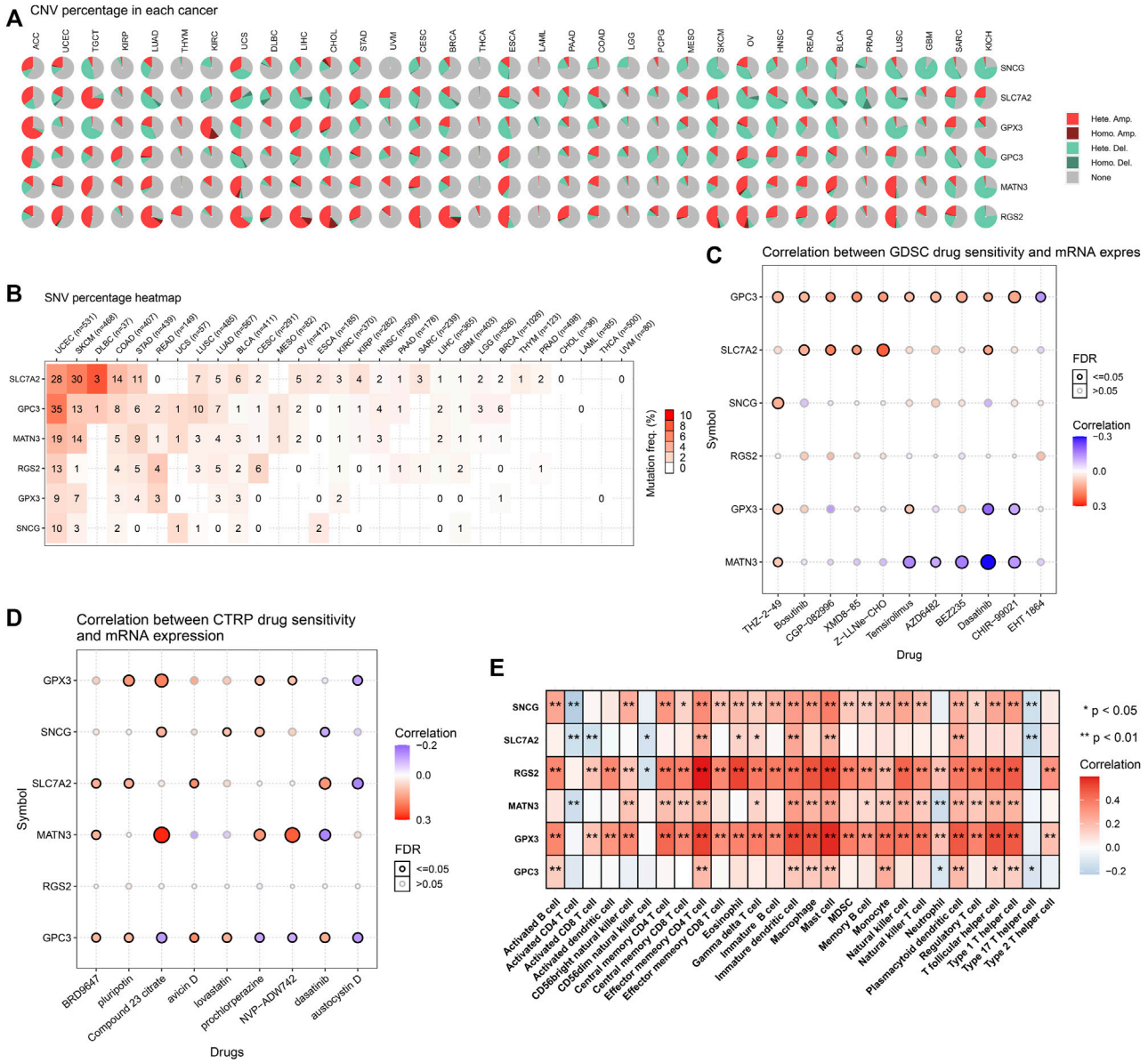

FIGURE 7 | Landscape of genetic alterations, drug sensitivity, and immune cell infiltration in the exosome-based gene signature. **(A)** Percentage of CNVs of each gene in the exosome-based gene signature across pan-cancer. **(B)** Mutation frequencies of each gene in the signature across pan-cancer. **(C)** Associations of mRNA expression of each gene with sensitivity to small molecular compounds in accordance with the GDSC database. **(D)** Associations of mRNA expression of each gene with sensitivity to small molecular compounds in accordance with the CTRP database. **(E)** Associations of mRNA expression of each gene with immune cell infiltration in the TME.

Experimental Verification of Altered Genes From Exosome-Based Phenotypes

To validate altered genes from the exosome-based phenotypes, we collected 20 paired GC and para-carcinoma tissues. Our qRT-PCR results confirmed that GPX3 and RGS2 were significantly downregulated in GC than in para-carcinoma tissues (**Figures 8A,B**). In addition, MATN3, SLC7A2, and SNCG were significantly upregulated in GC compared with para-carcinoma tissues (**Figures 8C–E**).

DISCUSSION

GC is a highly heterogeneous malignant carcinoma and the classification of GC based on molecular subtypes is essential to personalized therapy (Lin et al., 2020). A few subtype systems have been conducted, such as ACRG and TCGA subtypes (Serra et al., 2019). Nevertheless, the exosome-based classification of GC is not well defined. Herein, we conducted the exosome-based classification on the basis of the expression profiling of 15 prognostic exosome-related genes. The reproducibility of this

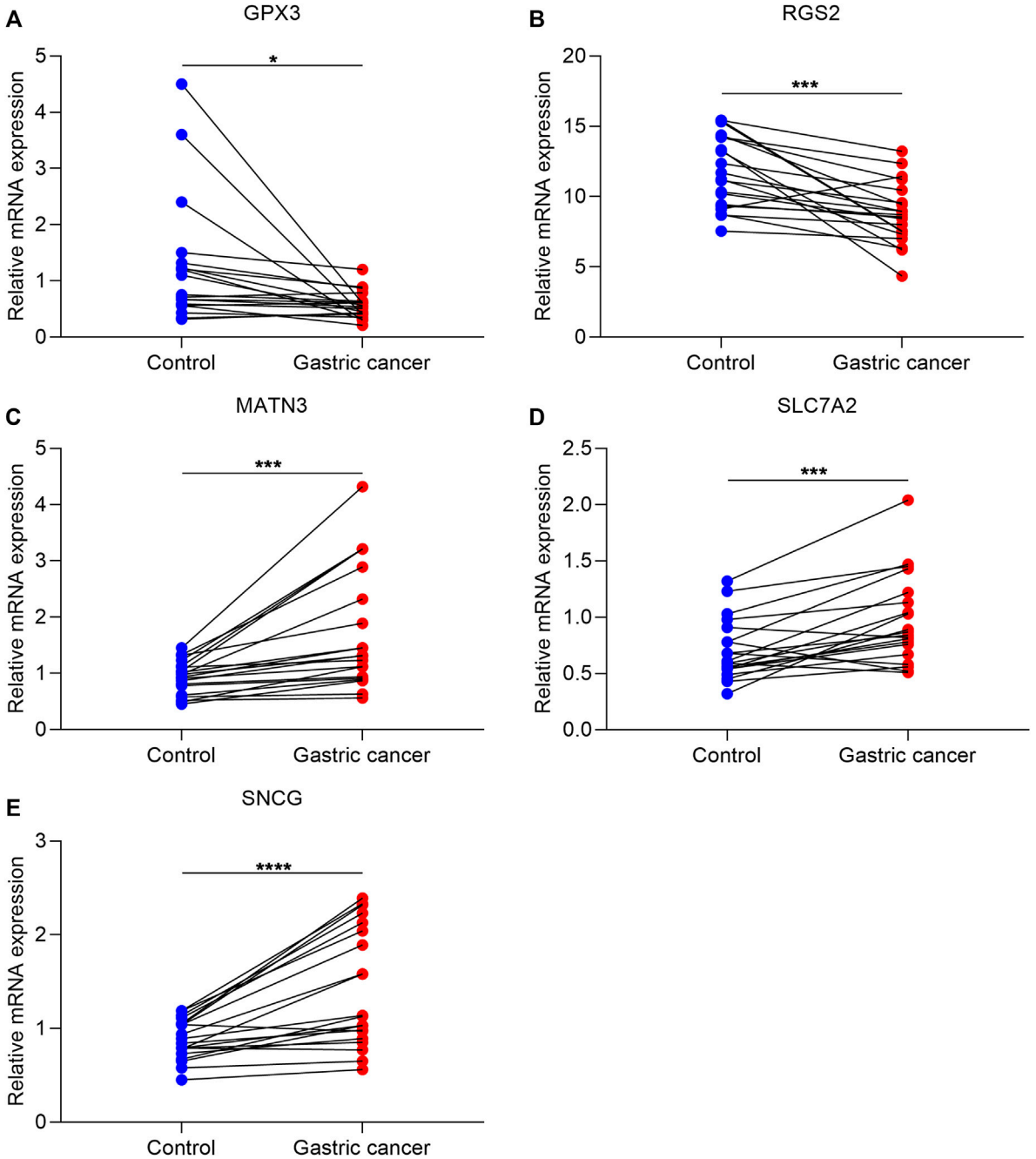

FIGURE 8 | Experimental verification of altered genes from exosome-based phenotypes. **(A–E)** qRT-PCR for validating the mRNA expression of GPX3, RGS2, MATN3, SLC7A2, and SNCG in 20 paired GC and para-carcinoma tissues. ∗*p*-value<0.05; ∗∗∗*p*-value<0.001; and ∗∗∗∗*p*-value<0.0001.

classification was confirmed in the independent cohort. The exosome-relevant phenotypes we proposed were independent of existing classifications (immune subtypes and TCGA subtypes), indicating that this classification deserves in-depth analysis.

Exosome-related phenotype B had poorer OS, DSS, DFS, and PFS relative to phenotype A. Further analysis uncovered that phenotype B displayed the activation of tumorigenic pathways (hedgehog signaling, hypoxia, Notch signaling, TGF-beta signaling, etc.), contributing to an undesirable prognosis. Immunotherapy presents durable antitumor activity against GC therapy. Nevertheless, this therapy still faces many challenges (Shitara et al., 2018; Shitara et al., 2020; Janjigian et al., 2021). It has been realized that TME is of complexity and diversity concerning immunological status (Liu et al., 2020). Thus, the prediction of the responses to ICIs on the basis of

the TME cell infiltrations represents an important procedure to enhance the efficacy of current ICIs and to exploit new immunotherapeutic regimens (Zhang et al., 2020). The immune evasion mechanisms exert crucial roles in immunotherapy (Kong et al., 2020). Exosome-related phenotype B displayed the activation of inflammatory or immune activation pathways (interferon-gamma response, allograft rejection, IL6-JAK-STAT3 signaling, inflammatory response, IL2-STAT5 signaling, complement, $CD8^+$ T effector, etc.) and stromal activation pathways (EMT, angiogenesis, etc.). Moreover, exosome-related phenotype B displayed remarkably higher immune cell infiltration within the TME and higher expression of immunomodulatory molecules (chemokines, immuno-inhibitors, immuno-stimulators, MHC, and receptors) and immune checkpoints relative to phenotype A. Thus, exosome-related phenotype B had an inflamed TME. A clinical trial showed the low responses of GC patients to tremelimumab, an anti-CTLA4 inhibitor (Kelly et al., 2020). It was predicted that GC patients with exosome-related phenotype B displayed higher responses to anti-CTLA4 therapy. This also demonstrated that the exosome-related phenotype might be an underlying indicator for predicting the response to ICIs.

Higher somatic mutation and copy number-deletion occurred in exosome-related phenotype B. Despite ICIs being a key discovery in GC treatment, chemotherapy remains an important regimen for postoperative treatment (Qiu et al., 2020). Exosome-related phenotype A had higher sensitivity to sorafenib and gefitinib, while exosome-related phenotype B had higher sensitivity to vinorelbine and gemcitabine. Experimental evidence has demonstrated that exosomes derived from tumor cells can mediate the resistance to sorafenib (Qu et al., 2016), gefitinib (Kang et al., 2018), and gemcitabine (Mikamori et al., 2017). Thus, this classification might predict sensitivity to sorafenib, gefitinib, vinorelbine, and gemcitabine.

We established the exosome-based gene signature (comprising GPX3, RGS2, MATN3, SLC7A2, and SNCG) that was an independent prognostic indicator of GC. Moreover, the nomogram was built by incorporating this exosome-based gene signature and age and histological staging, which provided clinicians with a quantitative approach for predicting GC patients' outcomes. The signature was linked to stromal activation and immunosuppression of GC. A few limitations should be pointed out in our study. First, our analysis was only focused on exosome-related genes in GC tissues. Second, the possibility of selection bias in this retrospective study cannot be ruled out. Third, GC is a highly heterogeneous malignancy. Two exosome-based phenotypes to predict the responses to ICIs might be inadequate.

CONCLUSION

Collectively, we constructed two exosome-relevant phenotypes in GC based on exosome-related genes, characterized by distinct survival outcomes, immunological status, and drug sensitivity. In addition, we determined and experimentally verified five altered genes (GPX3, RGS2, MATN3, SLC7A2, and SNCG) from exosome-based phenotypes. Based on the aforementioned genes, we established the exosome-based gene signature that could accurately predict patients' prognosis and was linked to stromal activation and immunosuppression. Altogether, our findings demonstrated the molecular mechanisms underlying exosomes in GC, which could assist us in comprehending the immune infiltration and immune evasion mechanisms in GC. The exosome-based phenotype could be used for stratifying GC patients and identifying patients who might respond to ICIs or chemotherapy.

DATA AVAILABILITY STATEMENT

The datasets presented in this study can be found in online repositories. The names of the repository/repositories and accession number(s) can be found in the article/ **Supplementary Material**.

ETHICS STATEMENT

The studies involving human participants were reviewed and approved by Xiamen Haicang Hospital (KY-2020014). The patients/participants provided their written informed consent to participate in this study.

AUTHOR CONTRIBUTIONS

SF, JZ, and GQ conceived and designed the study. YL, KH, ZC, and YC conducted most of the experiments and data analysis, and wrote the manuscript. LF, YG, WZ, and XF participated in collecting data and helped to draft the manuscript. All authors reviewed and approved the final version of the manuscript.

FUNDING

This research was supported by the Science and Technology Planning Project of Haicang District Bureau of Industry and Information Technology of Xiamen City (350205z20212001, 350205z20212003); the Science and Technology Program of Xiamen City (3502Z20184049, 3502Z20194055); the Science and Technology Program of Xiamen City-Medical and Health Guidance Project (3502Z20209252, 3502Z20209164); the Science and Technology Program of Haicang District of Xiamen City-Social Development and Soft Science (350205Z20202006); and the Horizontal Project of Office of Science and Technology, Xiamen University (XDHT2019206A).

SUPPLEMENTARY MATERIAL

The Supplementary Material for this article can be found online at: https://www.frontiersin.org/articles/10.3389/fphar.2022.884090/full#supplementary-material

Supplementary Figure S1 | External validation of two exosome-relevant phenotypes in the GSE84437 cohort. **(A)** Consensus score matrix of GC specimens when k = 2. **(B)** CDF of consensus matrix for each k (indicated by colors). **(C)** Relative alterations in the area under CDF curves. **(D)** Tracking plot for each k. **(E)** PCA plot by expression profiling of 15 prognostic exosome-related genes. Each point indicates each specimen, with unique colors representing exosome-relevant phenotypes. **(F)** Kaplan–Meier analysis of OS in two exosome-relevant phenotypes.

Supplementary Figure S2 | External verification of the prognostic implication of the exosome-based gene signature for GC in the GSE15459 cohort. **(A)** Overview of risk score distribution (upper), survival status (middle), and expression of genes that made up the signature (lower). **(B)** Kaplan–Meier curves of OS in the GSE15459 cohort, separated into high- and low-risk groups. **(C)** Time-independent ROC curves showing the prediction accuracy of the model.

Supplementary Table S1 | List of exosome-related genes.

Supplementary Table S2 | List of significantly altered genes between exosome-related phenotypes.

Supplementary Table S3 | List of significantly altered genes that were significantly linked with GC prognosis.

REFERENCES

Auslander, N., Zhang, G., Lee, J. S., Frederick, D. T., Miao, B., Moll, T., et al. (2018). Robust Prediction of Response to Immune Checkpoint Blockade Therapy in Metastatic Melanoma. *Nat. Med.* 24 (10), 1545–1549. doi:10.1038/s41591-018-0157-9

Bindea, G., Mlecnik, B., Tosolini, M., Kirilovsky, A., Waldner, M., Obenauf, A. C., et al. (2013). Spatiotemporal Dynamics of Intratumoral Immune Cells Reveal the Immune Landscape in Human Cancer. *Immunity* 39 (4), 782–795. doi:10.1016/j.immuni.2013.10.003

Bray, F., Ferlay, J., Soerjomataram, I., Siegel, R. L., Torre, L. A., and Jemal, A. (2018). Global Cancer Statistics 2018: GLOBOCAN Estimates of Incidence and Mortality Worldwide for 36 Cancers in 185 Countries. *CA Cancer J. Clin.* 68 (6), 394–424. doi:10.3322/caac.21492

Cai, W. Y., Dong, Z. N., Fu, X. T., Lin, L. Y., Wang, L., Ye, G. D., et al. (2020). Identification of a Tumor Microenvironment-Relevant Gene Set-Based Prognostic Signature and Related Therapy Targets in Gastric Cancer. *Theranostics* 10 (19), 8633–8647. doi:10.7150/thno.47938

Charoentong, P., Finotello, F., Angelova, M., Mayer, C., Efremova, M., Rieder, D., et al. (2017). Pan-cancer Immunogenomic Analyses Reveal Genotype-Immunophenotype Relationships and Predictors of Response to Checkpoint Blockade. *Cell Rep.* 18 (1), 248–262. doi:10.1016/j.celrep.2016.12.019

Chen, D., Liu, Z., Liu, W., Fu, M., Jiang, W., Xu, S., et al. (2021a). Predicting Postoperative Peritoneal Metastasis in Gastric Cancer with Serosal Invasion Using a Collagen Nomogram. *Nat. Commun.* 12 (1), 179. doi:10.1038/s41467-020-20429-0

Chen, Y., Sun, Z., Chen, W., Liu, C., Chai, R., Ding, J., et al. (2021b). The Immune Subtypes and Landscape of Gastric Cancer and to Predict Based on the Whole-Slide Images Using Deep Learning. *Front. Immunol.* 12, 685992. doi:10.3389/fimmu.2021.685992

Colaprico, A., Silva, T. C., Olsen, C., Garofano, L., Cava, C., Garolini, D., et al. (2016). TCGAbiolinks: an R/Bioconductor Package for Integrative Analysis of TCGA Data. *Nucleic Acids Res.* 44 (8), e71. doi:10.1093/nar/gkv1507

Geeleher, P., Cox, N., and Huang, R. S. (2014). pRRophetic: an R Package for Prediction of Clinical Chemotherapeutic Response from Tumor Gene Expression Levels. *PLoS One* 9 (9), e107468. doi:10.1371/journal.pone.0107468

Hänzelmann, S., Castelo, R., and Guinney, J. (2013). GSVA: Gene Set Variation Analysis for Microarray and RNA-Seq Data. *BMC Bioinforma.* 14, 7. doi:10.1186/1471-2105-14-7

Hoshida, Y., Brunet, J. P., Tamayo, P., Golub, T. R., and Mesirov, J. P. (2007). Subclass Mapping: Identifying Common Subtypes in Independent Disease Data Sets. *PLoS One* 2 (11), e1195. doi:10.1371/journal.pone.0001195

Janjigian, Y. Y., Shitara, K., Moehler, M., Garrido, M., Salman, P., Shen, L., et al. (2021). First-line Nivolumab Plus Chemotherapy versus Chemotherapy Alone for Advanced Gastric, Gastro-Oesophageal Junction, and Oesophageal Adenocarcinoma (CheckMate 649): a Randomised, Open-Label, Phase 3 Trial. *Lancet* 398 (10294), 27–40. doi:10.1016/s0140-6736(21)00797-2

Jiang, P., Gu, S., Pan, D., Fu, J., Sahu, A., Hu, X., et al. (2018). Signatures of T Cell Dysfunction and Exclusion Predict Cancer Immunotherapy Response. *Nat. Med.* 24 (10), 1550–1558. doi:10.1038/s41591-018-0136-1

Jiang, Y., Xie, J., Huang, W., Chen, H., Xi, S., Han, Z., et al. (2019). Tumor Immune Microenvironment and Chemosensitivity Signature for Predicting Response to Chemotherapy in Gastric Cancer. *Cancer Immunol. Res.* 7 (12), 2065–2073. doi:10.1158/2326-6066.Cir-19-0311

Kang, M., Ren, M., Li, Y., Fu, Y., Deng, M., and Li, C. (2018). Exosome-mediated Transfer of lncRNA PART1 Induces Gefitinib Resistance in Esophageal Squamous Cell Carcinoma via Functioning as a Competing Endogenous RNA. *J. Exp. Clin. Cancer Res.* 37 (1), 171. doi:10.1186/s13046-018-0845-9

Kelly, R. J., Lee, J., Bang, Y. J., Almhanna, K., Blum-Murphy, M., Catenacci, D. V. T., et al. (2020). Safety and Efficacy of Durvalumab and Tremelimumab Alone or in Combination in Patients with Advanced Gastric and Gastroesophageal Junction Adenocarcinoma. *Clin. Cancer Res.* 26 (4), 846–854. doi:10.1158/1078-0432.Ccr-19-2443

Kong, X., Fu, M., Niu, X., and Jiang, H. (2020). Comprehensive Analysis of the Expression, Relationship to Immune Infiltration and Prognosis of TIM-1 in Cancer. *Front. Oncol.* 10, 1086. doi:10.3389/fonc.2020.01086

Liberzon, A., Birger, C., Thorvaldsdóttir, H., Ghandi, M., Mesirov, J. P., and Tamayo, P. (2015). The Molecular Signatures Database (MSigDB) Hallmark Gene Set Collection. *Cell Syst.* 1 (6), 417–425. doi:10.1016/j.cels.2015.12.004

Lin, H., Zhang, L., Zhang, C., and Liu, P. (2020). Exosomal MiR-500a-3p Promotes Cisplatin Resistance and Stemness via Negatively Regulating FBXW7 in Gastric Cancer. *J. Cell Mol. Med.* 24 (16), 8930–8941. doi:10.1111/jcmm.15524

Liu, C. J., Hu, F. F., Xia, M. X., Han, L., Zhang, Q., and Guo, A. Y. (2018a). GSCALite: a Web Server for Gene Set Cancer Analysis. *Bioinformatics* 34 (21), 3771–3772. doi:10.1093/bioinformatics/bty411

Liu, F., Bu, Z., Zhao, F., and Xiao, D. (2018b). Increased T-Helper 17 Cell Differentiation Mediated by Exosome-Mediated microRNA-451 Redistribution in Gastric Cancer Infiltrated T Cells. *Cancer Sci.* 109 (1), 65–73. doi:10.1111/cas.13429

Liu, X., Niu, X., and Qiu, Z. (2020). A Five-Gene Signature Based on Stromal/Immune Scores in the Tumor Microenvironment and its Clinical Implications for Liver Cancer. *DNA Cell Biol.* 39 (9), 1621–1638. doi:10.1089/dna.2020.5512

Mayakonda, A., Lin, D. C., Assenov, Y., Plass, C., and Koeffler, H. P. (2018). Maftools: Efficient and Comprehensive Analysis of Somatic Variants in Cancer. *Genome Res.* 28 (11), 1747–1756. doi:10.1101/gr.239244.118

Mermel, C. H., Schumacher, S. E., Hill, B., Meyerson, M. L., Beroukhim, R., and Getz, G. (2011). GISTIC2.0 Facilitates Sensitive and Confident Localization of the Targets of Focal Somatic Copy-Number Alteration in Human Cancers. *Genome Biol.* 12 (4), R41. doi:10.1186/gb-2011-12-4-r41

Mikamori, M., Yamada, D., Eguchi, H., Hasegawa, S., Kishimoto, T., Tomimaru, Y., et al. (2017). MicroRNA-155 Controls Exosome Synthesis and Promotes Gemcitabine Resistance in Pancreatic Ductal Adenocarcinoma. *Sci. Rep.* 7, 42339. doi:10.1038/srep42339

Muratani, M., Deng, N., Ooi, W. F., Lin, S. J., Xing, M., Xu, C., et al. (2014). Nanoscale Chromatin Profiling of Gastric Adenocarcinoma Reveals Cancer-Associated Cryptic Promoters and Somatically Acquired Regulatory Elements. *Nat. Commun.* 5, 4361. doi:10.1038/ncomms5361

Qiu, X. T., Song, Y. C., Liu, J., Wang, Z. M., Niu, X., and He, J. (2020). Identification of an Immune-Related Gene-Based Signature to Predict Prognosis of Patients with Gastric Cancer. *World J. Gastrointest. Oncol.* 12 (8), 857–876. doi:10.4251/wjgo.v12.i8.857

Qu, Z., Wu, J., Wu, J., Luo, D., Jiang, C., and Ding, Y. (2016). Exosomes Derived from HCC Cells Induce Sorafenib Resistance in Hepatocellular Carcinoma Both *In Vivo* and *In Vitro*. *J. Exp. Clin. Cancer Res.* 35 (1), 159. doi:10.1186/s13046-016-0430-z

Ritchie, M. E., Phipson, B., Wu, D., Hu, Y., Law, C. W., Shi, W., et al. (2015). Limma Powers Differential Expression Analyses for RNA-Sequencing and Microarray Studies. *Nucleic Acids Res.* 43 (7), e47. doi:10.1093/nar/gkv007

Sathe, A., Grimes, S. M., Lau, B. T., Chen, J., Suarez, C., Huang, R. J., et al. (2020). Single-Cell Genomic Characterization Reveals the Cellular Reprogramming of the Gastric Tumor Microenvironment. *Clin. Cancer Res.* 26 (11), 2640–2653. doi:10.1158/1078-0432.Ccr-19-3231

Serra, O., Galán, M., Ginesta, M. M., Calvo, M., Sala, N., and Salazar, R. (2019). Comparison and Applicability of Molecular Classifications for Gastric Cancer. *Cancer Treat. Rev.* 77, 29–34. doi:10.1016/j.ctrv.2019.05.005

Shitara, K., Özgüroğlu, M., Bang, Y. J., Di Bartolomeo, M., Mandalà, M., Ryu, M. H., et al. (2018). Pembrolizumab versus Paclitaxel for Previously Treated, Advanced Gastric or Gastro-Oesophageal Junction Cancer (KEYNOTE-061): a Randomised, Open-Label, Controlled, Phase 3 Trial. *Lancet* 392 (10142), 123–133. doi:10.1016/s0140-6736(18)31257-1

Shitara, K., Van Cutsem, E., Bang, Y. J., Fuchs, C., Wyrwicz, L., Lee, K. W., et al. (2020). Efficacy and Safety of Pembrolizumab or Pembrolizumab Plus Chemotherapy vs Chemotherapy Alone for Patients with First-Line, Advanced Gastric Cancer: The KEYNOTE-062 Phase 3 Randomized Clinical Trial. *JAMA Oncol.* 6 (10), 1571–1580. doi:10.1001/jamaoncol.2020.3370

Subramanian, A., Tamayo, P., Mootha, V. K., Mukherjee, S., Ebert, B. L., Gillette, M. A., et al. (2005). Gene Set Enrichment Analysis: a Knowledge-Based Approach for Interpreting Genome-wide Expression Profiles. *Proc. Natl. Acad. Sci. U. S. A.* 102 (43), 15545–15550. doi:10.1073/pnas.0506580102

Tang, X. H., Guo, T., Gao, X. Y., Wu, X. L., Xing, X. F., Ji, J. F., et al. (2021). Exosome-derived Noncoding RNAs in Gastric Cancer: Functions and Clinical Applications. *Mol. Cancer* 20 (1), 99. doi:10.1186/s12943-021-01396-6

Wang, M., Zhao, X., Qiu, R., Gong, Z., Huang, F., Yu, W., et al. (2021). Lymph Node Metastasis-Derived Gastric Cancer Cells Educate Bone Marrow-Derived Mesenchymal Stem Cells via YAP Signaling Activation by Exosomal Wnt5a. *Oncogene* 40 (12), 2296–2308. doi:10.1038/s41388-021-01722-8

Wilkerson, M. D., and Hayes, D. N. (2010). ConsensusClusterPlus: a Class Discovery Tool with Confidence Assessments and Item Tracking. *Bioinformatics* 26 (12), 1572–1573. doi:10.1093/bioinformatics/btq170

Xin, L., Zhou, L. Q., Liu, C., Zeng, F., Yuan, Y. W., Zhou, Q., et al. (2021). Transfer of LncRNA CRNDE in TAM-Derived Exosomes Is Linked with Cisplatin Resistance in Gastric Cancer. *EMBO Rep.* 22 (12), e52124. doi:10.15252/embr.202052124

Yang, W., Soares, J., Greninger, P., Edelman, E. J., Lightfoot, H., Forbes, S., et al. (2013). Genomics of Drug Sensitivity in Cancer (GDSC): a Resource for Therapeutic Biomarker Discovery in Cancer Cells. *Nucleic Acids Res.* 41, D955–D961. doi:10.1093/nar/gks1111

Yoon, S. J., Park, J., Shin, Y., Choi, Y., Park, S. W., Kang, S. G., et al. (2020). Deconvolution of Diffuse Gastric Cancer and the Suppression of CD34 on the BALB/c Nude Mice Model. *BMC Cancer* 20 (1), 314. doi:10.1186/s12885-020-06814-4

Yu, G., Wang, L. G., Han, Y., and He, Q. Y. (2012). clusterProfiler: an R Package for Comparing Biological Themes Among Gene Clusters. *Omics* 16 (5), 284–287. doi:10.1089/omi.2011.0118

Zeng, D., Li, M., Zhou, R., Zhang, J., Sun, H., Shi, M., et al. (2019). Tumor Microenvironment Characterization in Gastric Cancer Identifies Prognostic and Immunotherapeutically Relevant Gene Signatures. *Cancer Immunol. Res.* 7 (5), 737–750. doi:10.1158/2326-6066.Cir-18-0436

Zhang, B., Wu, Q., Li, B., Wang, D., Wang, L., and Zhou, Y. L. (2020). m6A Regulator-Mediated Methylation Modification Patterns and Tumor Microenvironment Infiltration Characterization in Gastric Cancer. *Mol. Cancer* 19 (1), 53. doi:10.1186/s12943-020-01170-0

Zhang, Y., Chen, L., Ye, X., Wu, Z., Zhang, Z., Sun, B., et al. (2021). Expression and Mechanism of Exosome-Mediated A FOXM1 Related Long Noncoding RNA in Gastric Cancer. *J. Nanobiotechnol* 19 (1), 133. doi:10.1186/s12951-021-00873-w

Zheng, P., Luo, Q., Wang, W., Li, J., Wang, T., Wang, P., et al. (2018). Tumor-associated Macrophages-Derived Exosomes Promote the Migration of Gastric Cancer Cells by Transfer of Functional Apolipoprotein E. *Cell Death Dis.* 9 (4), 434. doi:10.1038/s41419-018-0465-5

Conflict of Interest: The authors declare that the research was conducted in the absence of any commercial or financial relationships that could be construed as a potential conflict of interest.

Publisher's Note: All claims expressed in this article are solely those of the authors and do not necessarily represent those of their affiliated organizations, or those of the publisher, the editors, and the reviewers. Any product that may be evaluated in this article, or claim that may be made by its manufacturer, is not guaranteed or endorsed by the publisher.

frontiers | Frontiers in Pharmacology

ORIGINAL RESEARCH
published: 13 June 2022
doi: 10.3389/fphar.2022.884548

Repositioning of Anti-Inflammatory Drugs for the Treatment of Cervical Cancer Sub-Types

Medi Kori[1], *Kazim Yalcin Arga*[1,2], *Adil Mardinoglu*[3,4]* and *Beste Turanli*[1]*

[1]Department of Bioengineering, Faculty of Engineering, Marmara University, Istanbul, Turkey, [2]Genetic and Metabolic Diseases Research and Investigation Center (GEMHAM), Marmara University, Istanbul, Turkey, [3]Science for Life Laboratory, KTH—Royal Institute of Technology, Stockholm, Sweden, [4]Centre for Host-Microbiome Interactions, Faculty of Dentistry, Oral and Craniofacial Sciences, King's College London, London, United Kingdom

Cervical cancer is the fourth most commonly diagnosed cancer worldwide and, in almost all cases is caused by infection with highly oncogenic Human Papillomaviruses (HPVs). On the other hand, inflammation is one of the hallmarks of cancer research. Here, we focused on inflammatory proteins that classify cervical cancer patients by considering individual differences between cancer patients in contrast to conventional treatments. We repurposed anti-inflammatory drugs for therapy of HPV-16 and HPV-18 infected groups, separately. In this study, we employed systems biology approaches to unveil the diagnostic and treatment options from a precision medicine perspective by delineating differential inflammation-associated biomarkers associated with carcinogenesis for both subtypes. We performed a meta-analysis of cervical cancer-associated transcriptomic datasets considering subtype differences of samples and identified the differentially expressed genes (DEGs). Using gene signature reversal on HPV-16 and HPV-18, we performed both signature- and network-based drug reversal to identify anti-inflammatory drug candidates against inflammation-associated nodes. The anti-inflammatory drug candidates were evaluated using molecular docking to determine the potential of physical interactions between the anti-inflammatory drug and inflammation-associated nodes as drug targets. We proposed 4 novels anti-inflammatory drugs (AS-601245, betamethasone, narciclasin, and methylprednisolone) for the treatment of HPV-16, 3 novel drugs for the treatment of HPV-18 (daphnetin, phenylbutazone, and tiaprofenoic acid), and 5 novel drugs (aldosterone, BMS-345541, etodolac, hydrocortisone, and prednisolone) for the treatment of both subtypes. We proposed anti-inflammatory drug candidates that have the potential to be therapeutic agents for the prevention and/or treatment of cervical cancer.

Keywords: inflammation, drug repurposing, anti-inflammatory drugs, cervical cancer, human papillomavirus 16, human papillomavirus 18

OPEN ACCESS

Edited by:
Basel A. Abdel-Wahab, Assiut University, Egypt

Reviewed by:
Sonam Mittal, Medical College of Wisconsin, United States
Lucia Taja-Chayeb, National Institute of Cancerology (INCAN), Mexico

***Correspondence:**
Beste Turanli
beste.turanli@marmara.edu.tr
Adil Mardinoglu
adilm@scilifelab.se

Specialty section:
This article was submitted to Pharmacology of Anti-Cancer Drugs, a section of the journal Frontiers in Pharmacology

Received: *07 March 2022*
Accepted: *26 May 2022*
Published: *13 June 2022*

Citation:
Kori M, Arga KY, Mardinoglu A and Turanli B (2022) Repositioning of Anti-Inflammatory Drugs for the Treatment of Cervical Cancer Sub-Types. Front. Pharmacol. 13:884548. doi: 10.3389/fphar.2022.884548

Abbreviations: ATC, anatomical therapeutic chemical; DEG, differentially expressed genes; FDR, false discovery rate; HPV, Human Papillomavirus; PPI, protein-protein interaction.

INTRODUCTION

According to data collected worldwide in 2018, cervical cancer was the fourth most commonly diagnosed cancer (570,000 cases) and the fourth leading cause of death (311,000 deaths) (Bray et al., 2018). In 2020, cervical cancer caused 13,800 new cases and 4,290 deaths in the United States (Siegel et al., 2020). Infection with highly oncogenic Human Papillomaviruses (HPVs) is encountered in almost all cervical cancers (Ferris et al., 2020). HPV is a small, non-enveloped, circular, double-stranded DNA that belongs to the Papillomaviridae family. More than a hundred HPV types with different oncogenic potential (low-risk and high-risk) have been characterized today (Graham, 2010). Of the 12 high-risk HPV types, HPV16 and HPV18, are the most prevalent HPV types worldwide. Indeed, HPV16 and HPV18 are responsible for up to 70% of cervical cancers worldwide (WHO, 2021).

Vaccines are now being proposed to prevent cervical cancer (Šarenac and Mikov, 2019). Various antineoplastic agents such as cisplatin, carboplatin, ifosfamide, paclitaxel, and topotecan have been proposed to treat cervical cancer. However, these antineoplastic agents were not specific to cervical cancer (Ordikhani et al., 2016). Hence, there is a need for the development of more effective prevention and/or treatment strategies to replace the existing methods.

Drug repurposing means identifying new therapeutic purposes for existing drugs. Due to its high efficiency in terms of time saving and low cost compared to traditional approaches for drug development, the pharmaceutical research industry is showing great interest in drug repurposing (Jarada et al., 2020). The inhibitory effects of several drugs, including metformin (Xia et al., 2020), aspirin (Friel et al., 2015), and acetaminophen (Liu et al., 2014), have been demonstrated in cervical cancer. Computational drug repurposing applications for cervical cancer are limited. Recent studies on computational drug repurposing used docking and molecular dynamics simulations to find potential E6 inhibitors in cervical cancer. They suggested valganciclovir and cytarabine as drug candidates and reported ASK4, a valganciclovir derivative, as a potential E6 inhibitor (Kumar et al., 2020).

Inflammation is often described as a response to invasive pathogen simulations. When the inflammatory response is absent or cannot be controlled, it results in impaired tissue repair or pathology. For these reasons, inflammation is now referred to as the seventh hallmark of cancer. It was known that inflammation following viral infection promotes the development of cancer (Deivendran et al., 2014). Studies in recent years have shown that increased dietary intake of native anti-inflammatory compounds (e.g., curcumin) contributes to the prevention of cancer. Furthermore, persistent infection is essential for cancer development, and anti-inflammatory drugs generally target signaling pathways used by oncogenic viruses to generate persistent infections. Therefore, anti-inflammatory drugs may not only reduce the prevalence of oncogenic cancers and but also support ongoing treatment strategies (Read and Douglas, 2014). Taken together, eliminating inflammation may be a valid strategy for cancer prevention and/or treatment, particularly oncogenic cancers (Rayburn et al., 2009).

Here, we repositioned anti-inflammatory drug candidates targeting inflammation-associated hub proteins using two different drug repositioning strategies to treat cervical cancer in a subtype-specific (HPV16 and HPV18) manner. To this end, we used a multistep computational approach (**Figure 1**). First, we performed a meta-analysis of cervical cancer-associated transcriptomic datasets by accounting for subtype differences between samples and identifying differentially expressed genes (DEGs). Using gene signature reversal on HPV16 and HPV18, we performed a signature-based repositioning to identify candidate anti-inflammatory drugs. In addition, we employed a network-based drug repurposing approach. We reconstructed protein-protein interaction networks around HPV16- and HPV18-associated DEGs to identify inflammation-associated hubs. The inflammation-associated drug candidates were evaluated using molecular docking to determine the potential of physical interactions between the anti-inflammatory drug and the inflammation-associated hubs as drug targets. Consequently, our computational study proposed anti-inflammatory drug candidates targeting inflammatory proteins of HPV16 and HPV18 subtypes of cervical cancer.

MATERIALS AND METHODS

Selection of Transcriptomic Datasets

Since, our aim was to reveal the appropriate subtype-specific (i.e., HPV16 and HPV18) personalized drugs for cervical cancer, the transcriptomic datasets were evaluated considering the genotypes of the diseased samples. In addition, to avoid undesirable alterations originating from differences in the microarray platforms used, we ensured that the transcriptome datasets were generated using the same platform. With this in mind, we found a total of five transcriptome datasets that corresponded to the HPV16 or HPV18 genotype whose gene expression measurements were performed using the same platform (Affymetrix microarrays). The five transcriptome datasets were as follows: GSE52903 (Medina-Martinez et al., 2014), GSE39001 (Espinosa et al., 2013), GSE9750 (Scotto et al., 2008), GSE7803 (Zhai et al., 2007) and GSE6791 (Pyeon et al., 2007). High-grade squamous lesions were excluded from GSE7803, healthy endocervical tissue samples were excluded from GSE39001, and only cervical cancer samples were included in the GSE6791 datasets to avoid sample heterogeneity. While all five datasets contained samples belonging to the HPV16 genotype, only three datasets (GSE9750, GSE7803 and GSE6791) contained samples of HPV18. Thus, 111 HPV16-positive diseased samples were compared with 61 controls, while 10 HPV18-positive diseased samples were compared with 39 control samples.

Identification of Differentially Expressed Genes and Overrepresentation Analysis

This study used a well-established statistical analysis procedure (Kori et al., 2019) to identify DEGs. Briefly, the raw data (stored

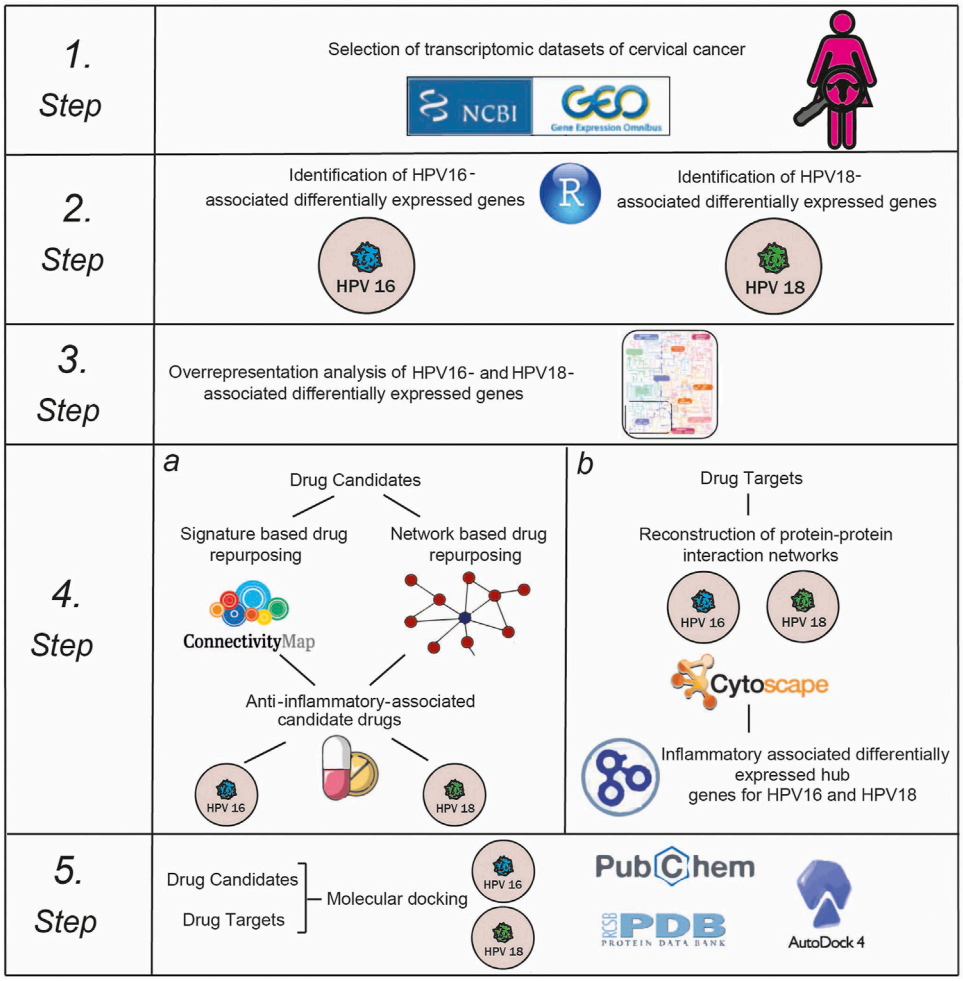

FIGURE 1 | The multi-stage computational approach was employed in the study.

in. CEL files) of each dataset was normalized by calculating the Robust Multi-Array Average (RMA) expression measure (Bolstad et al., 2003) as implemented in the Affy package (Gautier et al., 2004) of the R/Bioconductor platform (version 4.0.2) (Huber et al., 2015). DEGs were identified from normalized expression values using the Linear Models for Microarray Data (LIMMA) package (Ritchie et al., 2015). The Benjamini–Hochberg method was used to control false discovery rate (FDR). The adjusted p-value < 0.05 was used as a cut-off to determine the statistical significance of the DEGs. Fold change was used to determine the regulatory pattern of each DEG (i.e., up- or down-regulation), and at least 1.5-fold change was considered statistically significant. Further analyses were performed with DEGs that shared at least three of the five HPV16 datasets, referred to as "HPV16-associated DEGs," while analyses were performed with DEGs that shared at least two of the three HPV18 datasets, referred to as "HPV18-associated DEGs." In this way, the analysis performed with DEGs that occurred in at least 60% of all datasets.

Overrepresentation analyses were performed using ConsensusPathDB (Kamburov et al., 2013) to determine pathways hijacked by HPV16- and HPV18-associated DEGs. KEGG database resources provided by ConsensusPathDB were preferred in the analysis. p-values were determined *via* Fisher's Exact Test, and FDR was applied to control p-values. For overrepresentation analyses, an adjusted p-value < 0.05 was considered statistically significant.

Signature-Based Drug Repurposing

To reveal the correlations of gene signatures of drugs, the database CLUE (Subramanian et al., 2017) was used. HPV16- and HPV18-associated DEGs were used as queries and analyzed individually. We filtered our DEG data because we have more than 150 genes as queries, and there is a size limit of 10–150 genes in the CLUE database. For this purpose, we ordered the DEGs according to their fold-change and determined the first 150 genes with the lowest fold-change and the 150 genes with the highest fold-change and used them as down-regulated and up-regulated genes as queries, respectively. For a given query set pair, the database CLUE assigns connectivity scores to the perturbations in the form of Kolmogorov-Smirnov statistics and random

permutation tests. The connectivity score ranges from −100 to +100, and the negative score indicates an inverse pattern, meaning that genes that were increased as a result of perturbation treatment are genes that were decreased in the query. By default, drugs with -90 connectivity scores were considered significant.

Network-Based Drug Repositioning

A web-based transcriptome-driven drug repositioning application tool, geneXpharma (Turanli et al., 2017), was used for network-based drug repositioning analyses. The tool contains gene-drug interactions (obtained from Drug Gene Interaction Database) and gene-disease libraries. The gene-disease library was created by analyzing 118 different transcriptome datasets (corresponding to different 48 diseases) DEGs. Consequently, this tool provides the association of the drug to a DEG (disease dataset) considering hypergeometric distribution function. The gene-drug association library in geneXpharma contains 50,304 gene-drug interactions involving 4344 genes and 11,939 drugs. In network-based drug repositioning analyses, we used HPV16- and HPV18-associated DEGs individually as queries and identified whether the disease and drug candidates interacted with our DEG query lists. We considered drug candidates significant with a hypergeometric p-value < 0.01.

Determination of Anti-Inflammatory Associated Drugs

Anti-inflammatory drugs were identified through an anatomical therapeutic chemical (ATC) classification system and a literature review. Drugs with ATC codes M01A (anti-inflammatory and anti-rheumatic products, non-steroids), H02AB (corticosteroids for systemic use, plain) and N02BA (salicylic acid and derivatives) were selected as anti-inflammatory drugs and obtained from the DrugBank resource (version 5.1.7) (Wishart et al., 2006). The drugs that also have anti-inflammatory activity and have already been reported in the literature were also included in the study. Thus, a total of 127 anti-inflammatory drugs were found.

Reconstruction and Analysis of Protein-Protein Interaction Networks

The human protein interactome was derived from a previously published study (Cheng et al., 2019) containing 243,603 experimentally confirmed protein-protein interactions (PPIs) among 16,677 unique proteins from five data sources. PPI networks were represented as undirected graphs, with nodes representing proteins and edges representing interactions between proteins. PPI networks were reconstructed individually for HPV16- and HPV18-associated DEGs with their first neighbors and visualized using Cytoscape (v3.5.0) (Shannon et al., 2003). To determine hub proteins (i.e., central proteins), topological analyzes were performed using the Cytohubba plugin (Chin et al., 2014). The degree of a node, representing the number of edges connected to the node, was determined. The top 3% of nodes, ranked by highest degree, were considered hub proteins. The hub proteins that were DEG at the same time were further analyzed.

Determination of Inflammatory Associated Hubs

To identify the inflammation-associated hub DEGs, we first specified proteins previously associated with inflammation. To this end, proteins classified in the inflammatory response process (GO: 0006954) were screened in QuickGO, a web-based tool for searching Gene Ontology annotations (version 2021-01-08) (Binns et al., 2009). In addition, we screened for inflammation-associated proteins using the keyword "inflammation" in the UniProt portal (The UniProt Consortium, 2019). Thus, a total of 1215 inflammation-associated proteins were found. The culminated hubs were integrated with the generated list of inflammation-associated proteins, and inflammation-associated hub DEGs were identified.

Molecular Docking Simulations

The three-dimensional (3D) crystal structure of the target proteins (i.e, inflammation-associated hubs) was taken from Protein Data Bank (PDB) (Berman et al., 2002) when available. The structures of the anti-inflammatory drug candidates were obtained from the PubChem database (Kim et al., 2019). Molecular docking analyses were performed using AutoDock Vina software (Trott and Olson, 2010). In the analyses, previously known binding residues of target proteins were used for docking drug candidates. Binding affinities (kcal/mol) were reported to determine binding significance after molecular docking. In addition, known target protein inhibitors from the literature were sought as positive controls, and molecular docking simulations were also used for these inhibitors.

RESULTS

Identification of Differentially Expressed Genes

As a result of the analysis, thousands of individual DEGs were identified according to the criteria we established (adjusted p-value <0.05 and log2FC >|0.58|). The expression patterns (up- or down-regulation) of the culminated DEGs for five HPV16 transcriptome datasets were numerically almost identical. Namely, a total of 51% of DEGs were up-regulated. In addition, the expression patterns of the culminated DEGs for HPV18 tended to be up-regulated (56%).

The resulting DEGs were comparatively analyzed considering their subtypes (i.e. HPV16 or HPV18). Further analyses were performed for HPV16 DEGs culminating in at least three datasets, referred to as "HPV16-associated DEGs" and for HPV18 DEGs common in at least two datasets, referred to as "HPV18-associated DEGs". A total of 1289 (525 down- and 764 up-regulated) HPV16-associated DEGs and 1167 (401 down- and 766 up-regulated) HPV18-associated DEGs were identified (**Figures 2A,B**). In addition, 163 down-regulated and 398 up-

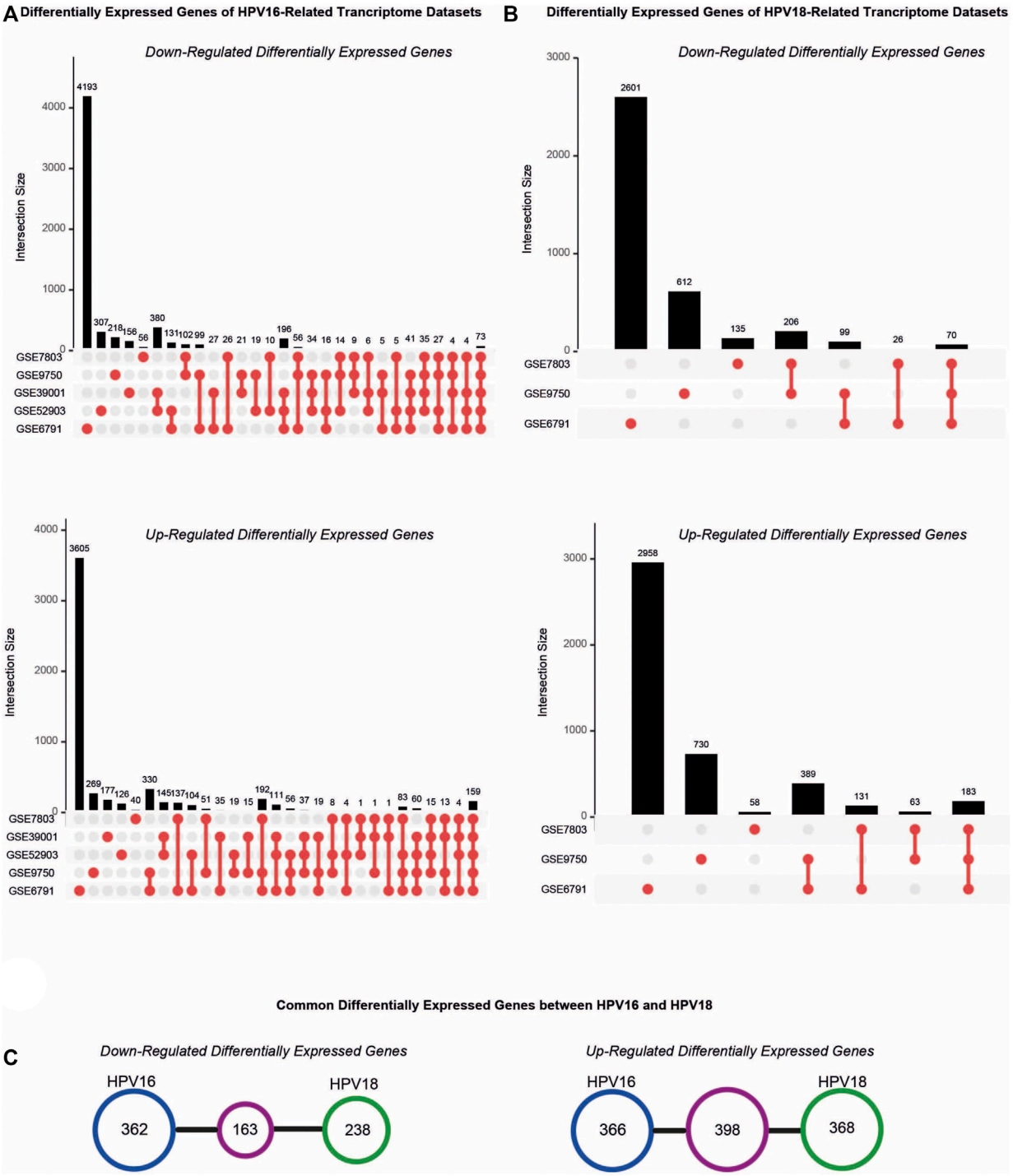

FIGURE 2 | The distribution of differentially expressed genes (DEGs) in the cervical cancer transcriptome datasets. **(A)** The upset plots represent DEGs in the transcriptome datasets that compromised HPV16 cervical cancer samples. **(B)** The upset plots represent DEGs in the transcriptome datasets that compromised HPV18 cervical cancer samples. **(C)** The diagrams represent the common DEGs in the HPV16- and HPV18 transcriptome datasets.

regulated genes culminated between the HPV16- and HPV18-associated DEGs (**Figure 2C**).

Overrepresentation analyses were performed to gain further biological insight into HPV16- and HPV18-associated DEGs. Both HPV16- and HPV18-associated DEGs were enriched in vital processes such as cell cycle, DNA replication, cellular senescence, p53 signaling pathway, and apoptosis. Furthermore, they are associated with infectious and infection-

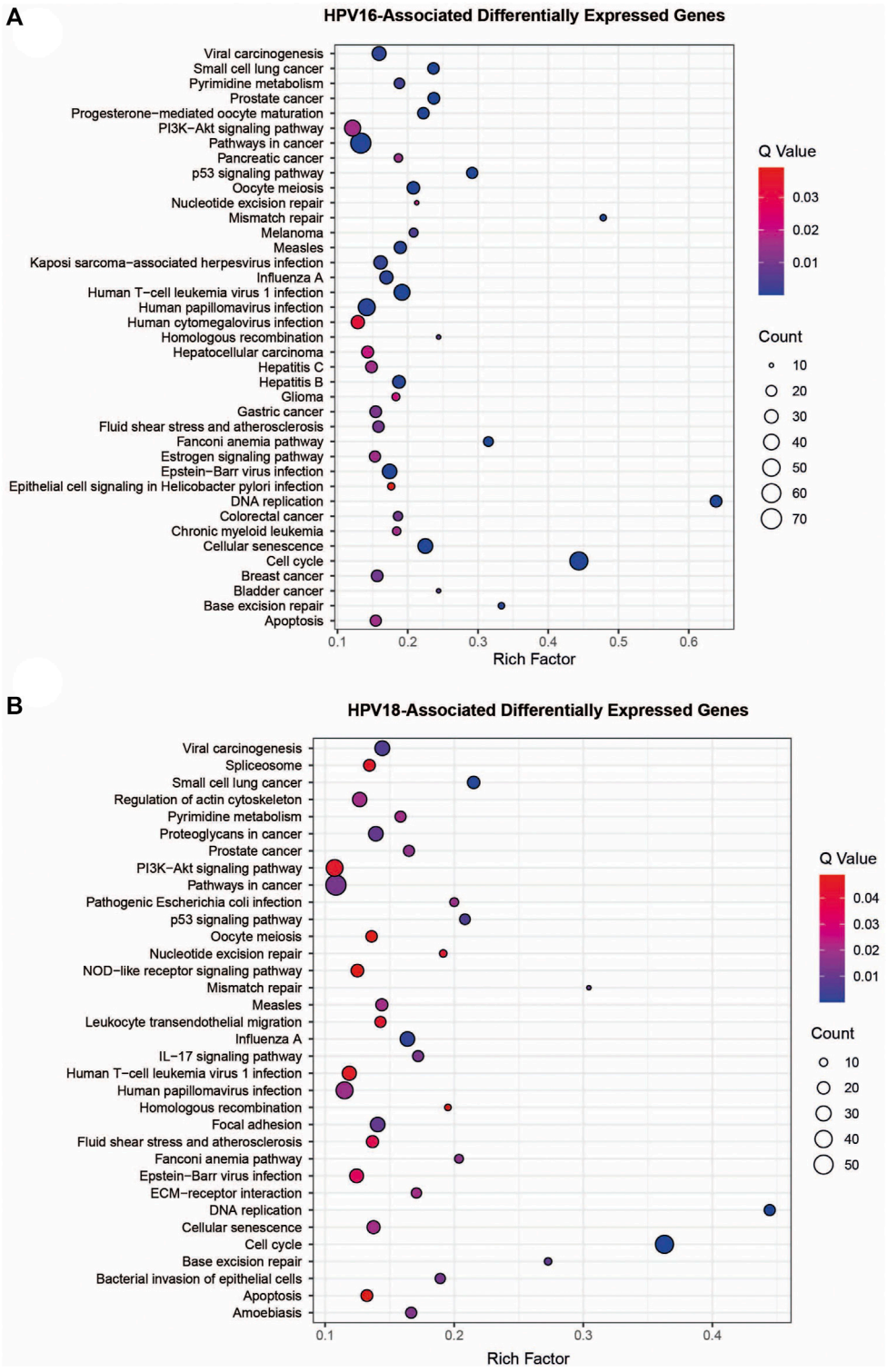

FIGURE 3 | The pathway overrepresentation analysis of HPV16- and HPV18-associated differentially expressed genes (DEGs). **(A)** A plot representing overrepresentation analysis of HPV16- associated DEGs. **(B)** A plot representing overrepresentation analysis of HPV18- associated DEGs.

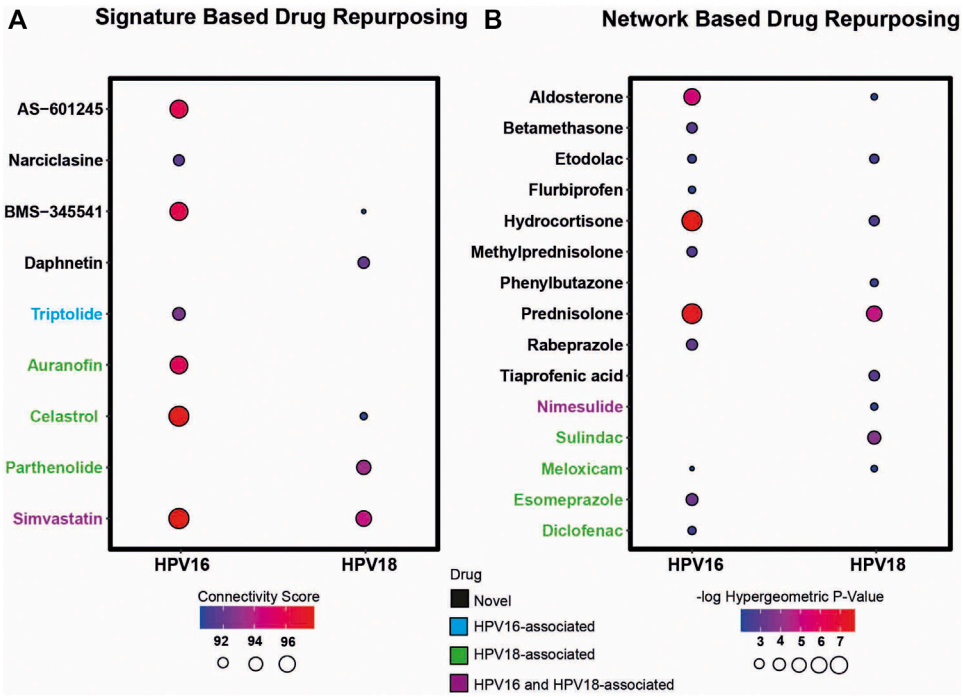

FIGURE 4 | The candidate drug targets that were revealed based on two different drug repurposing strategies (i.e. signature based and network based strategy). **(A)** The bubble plot indicates the drugs that resulted according to the signature-based drug repurposing strategy. **(B)** The bubble plot indicates the drugs that resulted according to network-based drug repurposing strategy. The drugs colored in black mean that the culminated drugs have not been associated with HPV16 or HPV18 subtypes of cervical cancer previously and novel. The drugs colored in blue, green, and purple means the culminated drugs have been associated with HPV16, HPV18 and with both subtypes of cervical cancer previously.

associated disease pathways, including human T-cell leukaemia virus 1 infection, Epstein-Barr virus infection, measles, HPV infection, influenza A, and viral carcinogenesis. In addition to cancer pathways, including colorectal cancer, bladder cancer, breast cancer, gastric cancer, pancreatic cancer, hepatocellular carcinoma, and infections such as hepatitis B/C and Kaposi's sarcoma-associated herpesvirus infection were specific pathways for HPV16-associated DEGs. HPV18-associated DEGs were specifically enriched with pathways such as focal adhesion, pathogenic *E. coli* infection, and ECM-receptor interaction (**Figures 3A,B**).

Drug Repurposing With Two Different Strategies

To investigate the applicability of anti-inflammatory drug therapies specific to subtypes of cervical cancer (HPV16 and HPV18), a drug repurposing analysis was performed using two different strategies (i.e., signature-based and network-based).

First, transcriptomic gene signatures corresponding to HPV16- and HPV18-associated DEGs were used as input to query the CLUE database (Subramanian et al., 2017) to assess drug-induced expression profiles. Drugs with a connectivity score < −90 were considered significant in the following analysis. A total of 79 drug candidates were identified for the HPV16 subtype (**Supplementary Table S1**). Among them, seven drugs were defined as anti-inflammatory associated drugs when integrated into our list of anti-inflammatory drugs. In addition, by using HPV18-associated DEGs as input, a total of 60 drug candidates were specified (**Supplementary Table S2**), of which five drugs were available as anti-inflammatory drugs. Ultimately, 3 anti-inflammatory associated drugs (BMS-345541, Celastrol—also known as Triptin - and Simvastatin) were found in two HPV subtypes according to their connectivity score significance. Additionally, 4 (AS -601245, auranofin, narciclasin, and triptolide) and 2 (daphnetin and parthenolide) anti-inflammatory drugs were found to be specific to HPV16 and HPV18 subtypes, respectively (**Figure 4A**).

As a second strategy, the transcriptome-guided drug repositioning tool, geneXpharma (Turanli et al., 2017), was applied to evaluate whether the diseases and drugs interacting with our DEG query list were specific to our studied two HPV subtypes. The tool assigns a hypergeometric *p*-value to each drug, and drugs with a hypergeometric *p*-value < 0.01 were accepted as significant in the analysis. As a result, we found a total of 611 different drugs for the HPV 16 subtype (**Supplementary Table S3**), of which 11 had an anti-inflammatory origin. Moreover, out of 254 drug candidates for the HPV18 subtype (**Supplementary Table S4**), 9 drug candidates belonged to the anti-inflammatory class. Overall, anti-inflammatory drugs such as aldosterone, etodolac, hydrocortisone, meloxicam and prednisolone culminated into two different subtypes. Betamethasone,

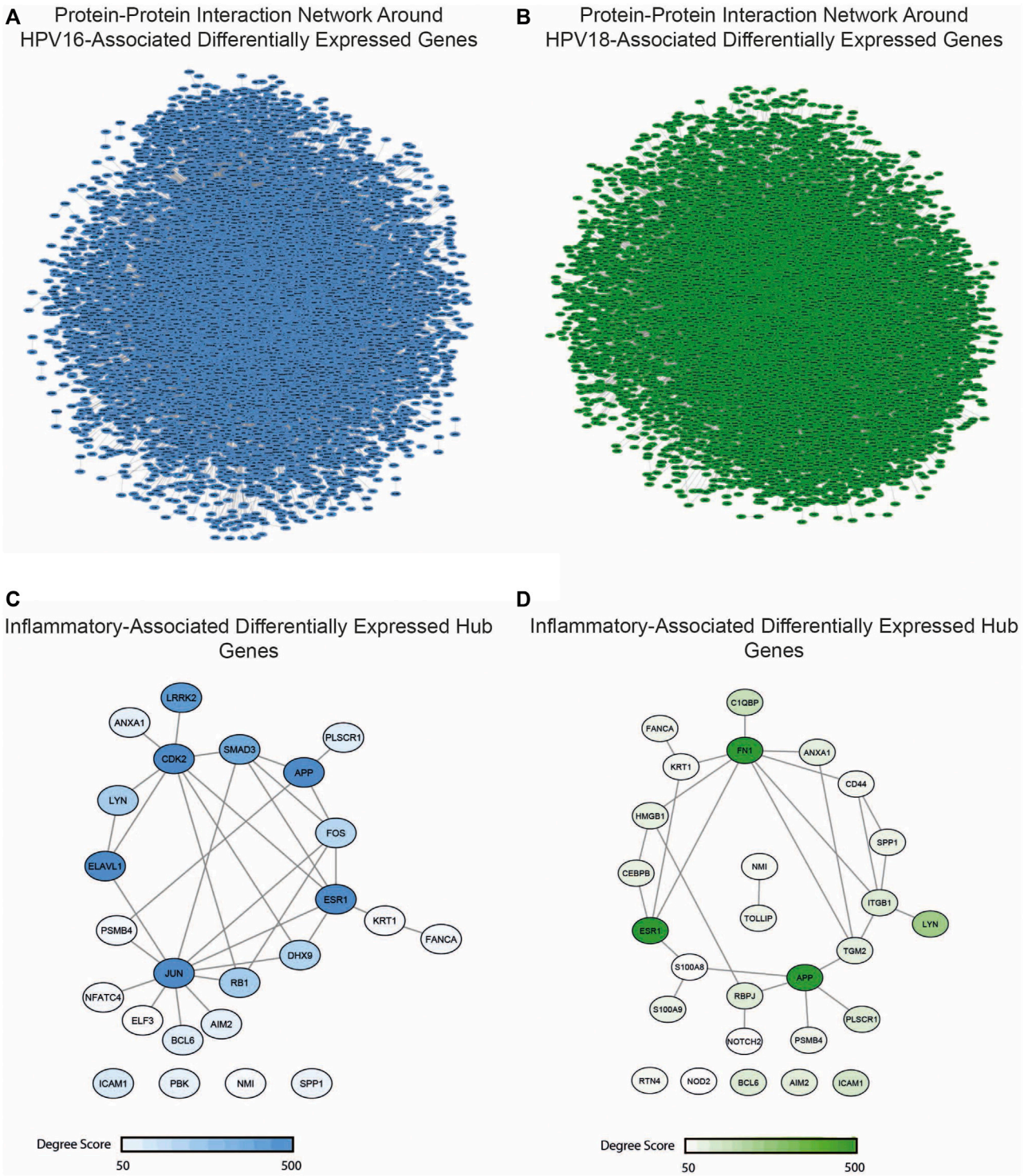

FIGURE 5 | The reconstructed protein-protein interaction (PPI) network around the HPV16- and HPV18-associated differentially expressed genes (DEGs) and inflammatory-associated hub DEGs. **(A)** The reconstructed PPI network around HPV16-associated DEGs **(B)** The reconstructed PPI network around HPV16-associated DEGs **(C)** The anti-inflammatory and HPV16 associated hub DEGs which colored according to degree score significance **(D)** The anti-inflammatory and HPV18 associated hub DEGs which colored according to degree score significance.

diclofenac, esomeprazole, flurbiprofen, methylprednisolone, and rabeprazole specifically induced the only HPV16 subtype, whereas nimesulide, phenylbutazone, sulindac, and tiaprofenic acid specifically induced the only HPV18 subtype (**Figure 4B**).

Following the two strategies employed, we manually reviewed the listed candidate anti-inflammatory drugs in PubMed to determine if the drugs had been previously associated with cervical cancer. The literature review showed that some drugs have been previously associated with cervical cancer. The drugs auranofin (You et al., 2015), celastrol (Hu et al., 2013), diclofenac (Al-Nimer et al., 2015), esomeprazole (Jumaa et al., 2020), meloxicam (Dyakova et al., 2015), parthenolide (Jeyamohan et al., 2016) and sulindac (Karl et al., 2007) were previously associated with cervical cancer HPV18 subtype. Triptolide (Qin et al., 2018) was associated with the HPV16 subtype, and drugs such as nimesulide (Soriano-Hernandez et al., 2015) and simvastatin (Pan et al., 2020) were previously associated with both cervical cancer subtypes. We considered these results as positive controls for subsequent analyzes. The remaining 6 anti-inflammatory drugs for the HPV16 subtype, 2 anti-inflammatory drugs for the HPV18 subtype, and 5 anti-inflammatory drug candidates for both subtypes were novel candidates. Therefore, they were considered as candidate drugs and analyzed further (**Figure 4**).

Reconstruction of Protein-Protein Interaction Networks and Discovery of Inflammatory Associated Hubs

The study of diseases using PPI networks contributes to elucidating interrelationships between proteins and is crucial for uncovering new insights into pathogenesis. Since hubs organize the global structure of the network and play a central role, they represent potential drug candidates. In this study, we first reconstructed PPI interactions to uncover target candidates. The reconstructed PPI interaction network around HPV16-associated DEGs consisted of 10360 nodes with 50519 edges, while the interaction network in HPV18-associated DEGs consisted of 12379 nodes with 57331 edges (**Figures 5A,B**). After reconstructing the interaction network, the degree of nodes in the networks was determined. A total of 257 hubs and 306 hubs that were simultaneously DEG were found for HPV16 and HPV18 subtypes, respectively. The DEG hubs were integrated with the constructed list of inflammation-associated proteins, and it was found that of the 257 hub DEGs, 24 were associated with inflammation and of the 306 hub DEGs, 27 were associated with inflammation (**Figures 5C,D**). The culminated inflammation-associated hub DEGs were considered as anti-inflammatory drug targets and further analyzed with docking simulations.

Molecular Docking Simulations

Molecular docking simulates the binding affinity of a drug in the 3D structure of a drug target. Overall, we performed molecular docking simulations to evaluate whether the candidate anti-inflammatory drugs target inflammation-associated hub DEGs. To this end, we first screened the 3D structure of inflammation-associated hub DEGs and found the suitable 3D structures for 15 out of 38 targets. In addition, the 3D structure for each drug candidate was determined from the corresponding database and included in the molecular docking simulations. To specify the significance of the docking score, we screened known inhibitors of the 15 targets and used them as positive controls (**Supplementary Table S5**). Following the literature search, we found inhibitors for 13 of the 15 targets and performed docking simulations for them as well. As a result of the molecular docking simulations, we identified the following drugs AS -601245 (targets CDK2, DHX9, and ELAV1), betamethasone, narciclasin (all 3 drugs target CDK2 and ELAV1), and methylprednisolone (targets CDK2) as HPV16 subtype-specific novel anti-inflammatory drug candidates. The drugs, including daphnetin, phenylbutazone, and tiaprofenoic acid, all targeting the inflammation-associated protein HMGB1, were found to be specific for the HPV18 subtype. Finally, the anti-inflammatory drugs aldosterone (targets AIM2, ESR1 and ICAM1), BMS-345541 (targets ESR1), etodolac (targets ESR1 and LYN), hydrocortisone (targets AIM2, BCL6, ESR1, ICAM1, and LYN), and prednisolone (targets AIM2, BCL6, ESR1, ICAM1, and LYN) yielded significant and novel results for both HPV16 and HPV18 subtypes (**Figure 6**).

DISCUSSION

Cervical cancer is one of the leading causes of death in women, and yet the treatment strategies used have not been adequate and specific for cervical cancer. Therefore, these results clearly demonstrate the need to develop more effective prevention and/or treatment strategies. In this study, we proposed new anti-inflammatory drugs for HPV16 and HPV18 subtypes of cervical cancer that simultaneously target inflammation-associated hub DEGs. In addition, we also found drugs that were already associated with the subtypes we studied, further strengthening our confidence in our observations.

Our approach differs from previous drug repositioning studies. To our knowledge, this was the first study in the literature under three aspects: 1) the repositioned drugs and their targets were all associated with anti-inflammatory agents, 2) the drug repurposing approach was used with two different strategies, and 3) the differences between HPV16 and HPV18 subtypes were considered in the analysis.

Inflammation is linked to cancer and plays an important role in tumor growth and progression through epidemiological studies (Greten and Grivennikov, 2019). As a result, drug repositioning efforts focusing on inflammation and the chemicals involved in the inflammatory process are paying an attention for an effective cancer preventive and treatment method (Turanli et al., 2018). Several clinical investigations have indicated that anti-inflammatory medicines, such as non-steroidal anti-inflammatory drugs (NSAIDs), can disrupt the tumor microenvironment by slowing cell migration, boosting apoptosis, and improving chemosensitivity (Zappavigna et al., 2020). Due to the link between inflammation and cancer, repositioning known anti-inflammatory medicines used in

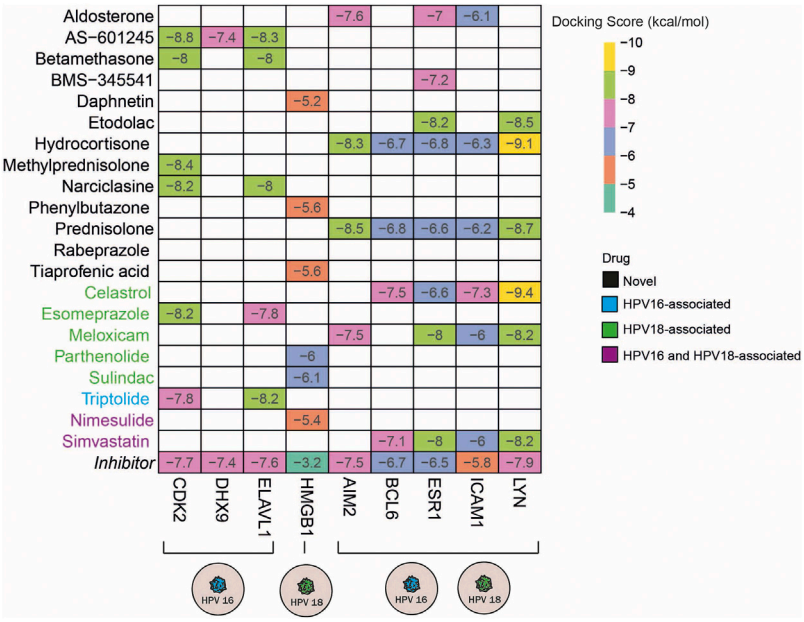

FIGURE 6 | The heatmap indicates the docking scores of the repurposed drugs. Only values with a lower docking score than the drug's inhibitor are represented. The drugs colored in blue, green, and purple means the culminated drugs have been associated with HPV16, HPV18, HPV16, and 18 subtypes of cervical cancer previously.

cancer therapy and their mechanisms of action, as well as the usage of novel anti-inflammatory compounds with anticancer efficacy become more promising for the cancers triggered by persistent infections.

As persistent infections and/or chronic inflammation are the main reasons for cancer development, persistent HPV infection with high risk is undoubtedly crucial for cervical cancer progression. In addition to persistent infection, studies have clearly shown that long-term chronic inflammation contributes to the development of cervical cancer (Fernandes et al., 2015). Given all these information, it is reasonable to assume that preventing inflammation may be a beneficial approach to the prevention and/or treatment of cervical cancer.

The main indications for anti-inflammatory drugs are fever, pain, and inflammation. However, many anti-inflammatory drugs have properties similar to neoplastic agents in that they promote apoptosis, inhibit angiogenesis, and enhance the immune response (Wong, 2019). Therefore, the use of anti-inflammatory drugs in cervical cancer is like "killing two birds with one stone." They have both anti-inflammatory and anti-cancer effects in the treatment of cervical cancer. Therefore, this is the main reason for choosing anti-inflammatory drugs and targets as targets in this study.

According to GLOBOCAN data on cervical cancer, low-income countries have higher mortality and higher incidence (Sung et al., 2021). Cervical cancer is the most common disease among women in developing countries such as Africa, Asia, and South America, which could be due to lack of screening programs, insufficient funding, and inadequate access to health care or even anti-vaccination campaigns. The prevalence of cervical cancer in developed countries has declined thanks to improved health care and widespread availability of preventive HPV vaccines, which is an important step in preventing HPV-related malignancies. On the other hand, prophylactic vaccines have proven useful only in healthy individuals and cannot treat or prevent an infection that has already broken out. Recurrence is possible with current treatments such as surgical resection, radiation, or chemotherapy, which do not specifically target the carcinogenic properties of HPV. In addition, most of these procedures can damage normal tissues and have potential adverse effects, such as bleeding, which can make patients uncomfortable and affect quality of life. This is another reason to focus on HPV-related carcinogenesis, which can be treated with anti-inflammatory drugs that are cheap, easy to obtain, and associated with tolerable side effects (Gomes et al., 2021).

We used gene signature and network-based drug repurposing strategies to identify drug candidates. The typical starting point of both strategies was gene signatures derived from cervical cancer transcriptomic data. When repositioning drugs based on gene signatures, we used the effect of reverse expression of the disease state, as in many studies (Turanli et al., 2019; Beklen et al., 2020). However, we also reconstructed combinations of gene signature and disease state in network-based drug repurposing. We anticipate that by combining both strategies, reliable candidates can be found for further experimental studies.

Although HPV16 and HPV18 are the two viruses responsible for most cases of cervical cancer, they represent different HPV subtypes. The HPV subtypes may have different biological mechanisms and affect cancer progression differently. This natural variability of cancer promotes the development of personalized medicine. The password of personalized medicine stands for the right drug, for the right patient, at the right time,

and at the right dose (Sadeè and Dai, 2005). Although the HPV16 and HPV18 is the most encountered subtypes of the cervical cancer we focus on these two subtypes and offer drugs that special for these two subtypes. Besides, we proposed drug candidates that can be useful for both sub-types considering the underdeveloped countries where such HPV typing is not routinely performed. Based on our analysis, we identified promising drug candidates for the treatment of cervical cancer subtypes and proposed candidates for further experimental studies. By integrating transcriptome datasets with 2 different drug repurposing strategies, we identified 4 novel anti-inflammatory HPV16-specific drug candidates (AS -601245, betamethasone, narciclin, and methylciclin) and validated narciclasin and methylprednisolone by *in silico* analysis. We also identified 3 new HPV18-specific drug candidates (daphnetin, phenylbutazone, and tiaprofenic acid) and 5 drug candidates (aldosterone, BMS-345541, etodolac, hydrocortisone, and prednisolone) for the treatment of both subtypes. These five candidate drugs can be highlighted particularly for underdeveloped countries where cervical cancer is very common and subtyping is not routinely done. We reported valuable data for further experimental and clinical efforts, as the proposed anti-inflammatory drug candidates can be used as therapeutics for the prevention and/or treatment of cervical cancer. The major limitation of the study is the lack of experimental validations of the identified anti-inflammatory drugs on the cervical cancer tissue samples or cell lines. Future *in vitro* studies need to be performed to investigate the effects of the identified drug candidates on cell viability, proliferation, and migration. Moreover, the mechanism of action of these molecules needs to be studied experimentally to elucidate their effects on important molecular signaling pathways such as cell death and cell replication. In addition, the proposed drug candidates can not only be considered as single agent candidates, but can also be used in combination, so that the effect of combination therapy can also be validated by *in vitro* studies.

DATA AVAILABILITY STATEMENT

The datasets presented in this study can be found in online repositories. The names of the repository/repositories and accession number(s) can be found in the article/ **Supplementary Material**.

AUTHOR CONTRIBUTIONS

MK and BT contributed to the conception and design of the study. MK contributed to the analysis and interpretation of the data. MK contributed to the writing of the manuscript. BT, AM, and KA supervised the study and revised the manuscript. All authors contributed to the article and approved the final version.

FUNDING

This work was supported by TUBITAK through project number 119S999, and funded by Knut and Alice Wallenberg Foundation.

SUPPLEMENTARY MATERIAL

The Supplementary Material for this article can be found online at: https://www.frontiersin.org/articles/10.3389/fphar.2022.884548/full#supplementary-material

REFERENCES

Al-Nimer, M. S., Hameed, H. G., and Mahmood, M. M. (2015). Antiproliferative Effects of Aspirin and Diclofenac against the Growth of Cancer and Fibroblast Cells: *In Vitro* Comparative Study. *Saudi Pharm. J.* 23 (5), 483–486. doi:10.1016/j.jsps.2015.01.002

Beklen, H., Gulfidan, G., Arga, K. Y., Mardinoglu, A., and Turanli, B. (2020). Drug Repositioning for P-Glycoprotein Mediated Co-expression Networks in Colorectal Cancer. *Front. Oncol.* 10, 1273. doi:10.3389/fonc.2020.01273

Berman, H. M., Battistuz, T., Bhat, T. N., Bluhm, W. F., Bourne, P. E., Burkhardt, K., et al. (2002). The Protein Data Bank. *Acta Crystallogr. D. Biol. Crystallogr.* 58, 899–907. doi:10.1107/s0907444902003451

Binns, D., Dimmer, E., Huntley, R., Barrell, D., O'Donovan, C., and Apweiler, R. (2009). QuickGO: a Web-Based Tool for Gene Ontology Searching. *Bioinformatics* 25 (22), 3045–3046. doi:10.1093/bioinformatics/btp536

Bolstad, B. M., Irizarry, R. A., Astrand, M., and Speed, T. P. (2003). A Comparison of Normalization Methods for High Density Oligonucleotide Array Data Based on Variance and Bias. *Bioinformatics* 19 (2), 185–193. doi:10.1093/bioinformatics/19.2.185

Bray, F., Ferlay, J., Soerjomataram, I., Siegel, R. L., Torre, L. A., and Jemal, A. (2018). Global Cancer Statistics 2018: GLOBOCAN Estimates of Incidence and Mortality Worldwide for 36 Cancers in 185 Countries. *CA Cancer J. Clin.* 68 (6), 394–424. doi:10.3322/caac.21492

Cheng, F., Kovács, I. A., and Barabási, A. L. (2019). Network-based Prediction of Drug Combinations. *Nat. Commun.* 10, 1197. doi:10.1038/s41467-019-09186-x

Chin, C. H., Chen, S. H., Wu, H. H., Ho, C. W., Ko, M. T., and Lin, C. Y. (2014). cytoHubba: Identifying Hub Objects and Sub-networks from Complex Interactome. *BMC Syst. Biol.* 8 (Suppl. 4), S11. doi:10.1186/1752-0509-8-S4-S11

Deivendran, S., Marzook, K. H., and Radhakrishna Pillai, M. (2014). The Role of Inflammation in Cervical Cancer. *Adv. Exp. Med. Biol.* 816, 377–399. doi:10.1007/978-3-0348-0837-8_15

Dyakova, L., Culita, D.-C., Zhivkova, T., Georgieva, M., Kalfin, R., Miloshev, G., et al. (2015). 3d Metal Complexes with Meloxicam as Therapeutic Agents in the Fight against Human Glioblastoma Multiforme and Cervical Carcinoma. *Biotechnol. Biotechnol. Equip.* 29, 1190–1200. doi:10.1080/13102818.2015.1074873

Espinosa, A. M., Alfaro, A., Roman-Basaure, E., Guardado-Estrada, M., Palma, Í., Serralde, C., et al. (2013). Mitosis Is a Source of Potential Markers for Screening and Survival and Therapeutic Targets in Cervical Cancer. *PLoS One* 8 (2), e55975. doi:10.1371/journal.pone.0055975

Fernandes, J. V., De Medeiros Fernandes, T. A., De Azevedo, J. C., Cobucci, R. N., De Carvalho, M. G., Andrade, V. S., et al. (2015). Link between Chronic Inflammation and Human Papillomavirus-Induced Carcinogenesis (Review). *Oncol. Lett.* 9 (3), 1015–1026. doi:10.3892/ol.2015.2884

Ferris, D. G., Brown, D. R., Giuliano, A. R., Myers, E., Joura, E. A., Garland, S. M., et al. (2020). Prevalence, Incidence, and Natural History of HPV Infection in Adult Women Ages 24 to 45 Participating in a Vaccine Trial. *Papillomavirus Res.* 10, 100202. doi:10.1016/j.pvr.2020.100202

Friel, G., Liu, C. S., Kolomeyevskaya, N. V., Hampras, S. S., Kruszka, B., Schmitt, K., et al. (2015). Aspirin and Acetaminophen Use and the Risk of Cervical Cancer. *J. Low. Genit. Tract. Dis.* 19 (3), 189–193. doi:10.1097/LGT.0000000000000104

Gautier, L., Cope, L., Bolstad, B. M., and Irizarry, R. A. (2004). affy--analysis of Affymetrix GeneChip Data at the Probe Level. *Bioinformatics* 20 (3), 307–315. doi:10.1093/bioinformatics/btg405

Gomes, D., Silvestre, S., Duarte, A. P., Venuti, A., Soares, C. P., Passarinha, L., et al. (2021). In Silico Approaches: A Way to Unveil Novel Therapeutic Drugs for Cervical Cancer Management. *Pharm. (Basel)* 14 (8), 741. doi:10.3390/ph14080741

Graham, S. V. (2010). Human Papillomavirus: Gene Expression, Regulation and Prospects for Novel Diagnostic Methods and Antiviral Therapies. *Future Microbiol.* 5 (10), 1493–1506. doi:10.2217/fmb.10.107

Greten, F. R., and Grivennikov, S. I. (2019). Inflammation and Cancer: Triggers, Mechanisms, and Consequences. *Immunity* 51 (1), 27–41. doi:10.1016/j.immuni.2019.06.025

Hu, Y., Qi, Y., Liu, H., Fan, G., and Chai, Y. (2013). Effects of Celastrol on Human Cervical Cancer Cells as Revealed by Ion-Trap Gas Chromatography-Mass Spectrometry Based Metabolic Profiling. *Biochim. Biophys. Acta* 1830 (3), 2779–2789. doi:10.1016/j.bbagen.2012.10.024

Huber, W., Carey, V. J., Gentleman, R., Anders, S., Carlson, M., Carvalho, B. S., et al. (2015). Orchestrating High-Throughput Genomic Analysis with Bioconductor. *Nat. Methods* 12 (2), 115–121. doi:10.1038/nmeth.3252

Jarada, T. N., Rokne, J. G., and Alhajj, R. (2020). A Review of Computational Drug Repositioning: Strategies, Approaches, Opportunities, Challenges, and Directions. *J. Cheminform.* 12, 46. doi:10.1186/s13321-020-00450-7

Jeyamohan, S., Moorthy, R. K., Kannan, M. K., and Arockiam, A. J. (2016). Parthenolide Induces Apoptosis and Autophagy through the Suppression of PI3K/Akt Signaling Pathway in Cervical Cancer. *Biotechnol. Lett.* 38 (8), 1251–1260. doi:10.1007/s10529-016-2102-7

Jumaa, A. H., Jarad, A. S., and Al Uboody, W. S. H. (2020). The Effect of Esomeprazole on Cell Line Human Cervical Cancer. *Mlu* 20, 646–652. doi:10.37506/mlu.v20i1.437

Kamburov, A., Stelzl, U., Lehrach, H., and Herwig, R. (2013). The ConsensusPathDB Interaction Database: 2013 Update. *Nucleic Acids Res.* 41, D793–D800. doi:10.1093/nar/gks1055

Karl, T., Seibert, N., Stöhr, M., Osswald, H., Rösl, F., and Finzer, P. (2007). Sulindac Induces Specific Degradation of the HPV Oncoprotein E7 and Causes Growth Arrest and Apoptosis in Cervical Carcinoma Cells. *Cancer Lett.* 245 (1-2), 103–111. doi:10.1016/j.canlet.2005.12.034

Kim, S., Chen, J., Cheng, T., Gindulyte, A., He, J., He, S., et al. (2019). PubChem 2019 Update: Improved Access to Chemical Data. *Nucleic Acids Res.* 47 (D1), D1102–D1109. doi:10.1093/nar/gky1033

Kori, M., Gov, E., and Arga, K. Y. (2019). Novel Genomic Biomarker Candidates for Cervical Cancer as Identified by Differential Co-expression Network Analysis. *OMICS* 23 (5), 261–273. doi:10.1089/omi.2019.0025

Kumar, A., Rathi, E., and Kini, S. G. (2020). Drug Repurposing Approach for the Identification and Designing of Potential E6 Inhibitors against Cervical Cancer: an In Silico Investigation. *Struct. Chem.* 31, 141–153. doi:10.1007/s11224-019-01378-x

Liu, C., Friel, G., Kolomeyevskaya, N. V., Lele, S. B., Odunsi, K. O., and Moysich, K. (2014). Aspirin and Acetaminophen Decrease the Risk of Cervical Cancer in Long-Term Users. *Gynecol. Oncol.* 133, 42–43. doi:10.1016/j.ygyno.2014.03.123

Medina-Martinez, I., Barrón, V., Roman-Bassaure, E., Juárez-Torres, E., Guardado-Estrada, M., Espinosa, A. M., et al. (2014). Impact of Gene Dosage on Gene Expression, Biological Processes and Survival in Cervical Cancer: a Genome-wide Follow-Up Study. *PLoS One* 9 (5), e97842. doi:10.1371/journal.pone.0097842

Miller, K. D., Fidler-Benaoudia, M., Keegan, T. H., Hipp, H. S., Jemal, A., and Siegel, R. L. (2020). Cancer Statistics for Adolescents and Young Adults, 2020. *CA Cancer J. Clin.* 70 (1), 443–459. doi:10.3322/caac.21637

Ordikhani, F., Erdem Arslan, M., Marcelo, R., Sahin, I., Grigsby, P., Schwarz, J. K., et al. (2016). Drug Delivery Approaches for the Treatment of Cervical Cancer. *Pharmaceutics* 8, 23. doi:10.3390/pharmaceutics8030023

Pan, Q., Xu, J., and Ma, L. (2020). Simvastatin Enhances Chemotherapy in Cervical Cancer *via* Inhibition of Multiple Prenylation-dependent GTPases-Regulated Pathways. *Fundam. Clin. Pharmacol.* 34 (1), 32–40. doi:10.1111/fcp.12479

Pyeon, D., Newton, M. A., Lambert, P. F., den Boon, J. A., Sengupta, S., Marsit, C. J., et al. (2007). Fundamental Differences in Cell Cycle Deregulation in Human Papillomavirus-Positive and Human Papillomavirus-Negative Head/neck and Cervical Cancers. *Cancer Res.* 67 (10), 4605–4619. doi:10.1158/0008-5472.CAN-06-3619

Qin, G., Li, P., and Xue, Z. (2018). Triptolide Induces Protective Autophagy and Apoptosis in Human Cervical Cancer Cells by Downregulating Akt/mTOR Activation. *Oncol. Lett.* 16 (3), 3929–3934. doi:10.3892/ol.2018.9074

Rayburn, E. R., Ezell, S. J., and Zhang, R. (2009). Anti-Inflammatory Agents for Cancer Therapy. *Mol. Cell Pharmacol.* 1 (1), 29–43. doi:10.4255/mcpharmacol.09.05

Read, S. A., and Douglas, M. W. (2014). Virus Induced Inflammation and Cancer Development. *Cancer Lett.* 345 (2), 174–181. doi:10.1016/j.canlet.2013.07.030

Ritchie, M. E., Phipson, B., Wu, D., Hu, Y., Law, C. W., Shi, W., et al. (2015). Limma Powers Differential Expression Analyses for RNA-Sequencing and Microarray Studies. *Nucleic Acids Res.* 43 (7), e47. doi:10.1093/nar/gkv007

Sadée, W., and Dai, Z. (2005). Pharmacogenetics/genomics and Personalized Medicine. *Hum. Mol. Genet.* 14 (2), R207–R214. doi:10.1093/hmg/ddi261

Šarenac, T., and Mikov, M. (2019). Cervical Cancer, Different Treatments and Importance of Bile Acids as Therapeutic Agents in This Disease. *Front. Pharmacol.* 10, 484. doi:10.3389/fphar.2019.00484

Scotto, L., Narayan, G., Nandula, S. V., Arias-Pulido, H., Subramaniyam, S., Schneider, A., et al. (2008). Identification of Copy Number Gain and Overexpressed Genes on Chromosome Arm 20q by an Integrative Genomic Approach in Cervical Cancer: Potential Role in Progression. *Genes Chromosom. Cancer* 47 (9), 755–765. doi:10.1002/gcc.20577

Shannon, P., Markiel, A., Ozier, O., Baliga, N. S., Wang, J. T., Ramage, D., et al. (2003). Cytoscape: a Software Environment for Integrated Models of Biomolecular Interaction Networks. *Genome Res.* 13 (11), 2498–2504. doi:10.1101/gr.1239303

Soriano-Hernandez, A. D., Madrigal-Pérez, D., Galvan-Salazar, H. R., Martinez-Fierro, M. L., Valdez-Velazquez, L. L., Espinoza-Gómez, F., et al. (2015). Anti-inflammatory Drugs and Uterine Cervical Cancer Cells: Antineoplastic Effect of Meclofenamic Acid. *Oncol. Lett.* 10 (4), 2574–2578. doi:10.3892/ol.2015.3580

Subramanian, A., Narayan, R., Corsello, S. M., Peck, D. D., Natoli, T. E., Lu, X., et al. (2017). A Next Generation Connectivity Map: L1000 Platform and the First 1,000,000 Profiles. *Cell* 171 (6), 1437–e17. doi:10.1016/j.cell.2017.10.049

Sung, H., Ferlay, J., Siegel, R. L., Laversanne, M., Soerjomataram, I., Jemal, A., et al. (2021). Global Cancer Statistics 2020: GLOBOCAN Estimates of Incidence and Mortality Worldwide for 36 Cancers in 185 Countries. *CA Cancer J. Clin.* 71 (3), 209–249. doi:10.3322/caac.21660

The UniProt Consortium (2019). UniProt: a Worldwide Hub of Protein Knowledge. *Nucleic Acids Res.* 47, D506–D515. doi:10.1093/nar/gky1049

Trott, O., and Olson, A. J. (2010). AutoDock Vina: Improving the Speed and Accuracy of Docking with a New Scoring Function, Efficient Optimization, and Multithreading. *J. Comput. Chem.* 31 (2), 455–461. doi:10.1002/jcc.21334

Turanli, B., Grøtli, M., Boren, J., Nielsen, J., Uhlen, M., Arga, K. Y., et al. (2018). Drug Repositioning for Effective Prostate Cancer Treatment. *Front. Physiol.* 9, 500. doi:10.3389/fphys.2018.00500

Turanli, B., Gulfidan, G., and Arga, K. Y. (2017). Transcriptomic-guided Drug Repositioning Supported by a New Bioinformatics Search Tool: geneXpharma. *OMICS* 21 (10), 584–591. doi:10.1089/omi.2017.0127

Turanli, B., Zhang, C., Kim, W., Benfeitas, R., Uhlen, M., Arga, K. Y., et al. (2019). Discovery of Therapeutic Agents for Prostate Cancer Using Genome-Scale Metabolic Modeling and Drug Repositioning. *EBioMedicine* 42, 386–396. doi:10.1016/j.ebiom.2019.03.009

WHO (2021). Human Papillomavirus (HPV) and Cervical Cancer. https://www.who.int/news-room/fact-sheets/detail/cervical-cancer (Accessed March 15, 2021).

Wishart, D. S., Knox, C., Guo, A. C., Shrivastava, S., Hassanali, M., Stothard, P., et al. (2006). DrugBank: a Comprehensive Resource for In Silico Drug Discovery and Exploration. *Nucleic Acids Res.* 34, D668–D672. doi:10.1093/nar/gkj067

Wong, R. S. Y. (2019). Role of Nonsteroidal Anti-inflammatory Drugs (NSAIDs) in Cancer Prevention and Cancer Promotion. *Adv. Pharmacol. Sci.* 2019, 3418975. doi:10.1155/2019/3418975

Xia, C., Liu, C., He, Z., Cai, Y., and Chen, J. (2020). Metformin Inhibits Cervical Cancer Cell Proliferation by Modulating PI3K/Akt-Induced Major Histocompatibility Complex Class I-Related Chain A Gene Expression. *J. Exp. Clin. Cancer Res.* 39, 127. doi:10.1186/s13046-020-01627-6

You, B. R., Shin, H. R., Han, B. R., Kim, S. H., and Park, W. H. (2015). Auranofin Induces Apoptosis and Necrosis in HeLa Cells *via* Oxidative Stress and

Glutathione Depletion. *Mol. Med. Rep.* 11 (2), 1428–1434. doi:10.3892/mmr.2014.2830

Zappavigna, S., Cossu, A. M., Grimaldi, A., Bocchetti, M., Ferraro, G. A., Nicoletti, G. F., et al. (2020). Anti-Inflammatory Drugs as Anticancer Agents. *Int. J. Mol. Sci.* 21 (7), 2605. doi:10.3390/ijms21072605

Zhai, Y., Kuick, R., Nan, B., Ota, I., Weiss, S. J., Trimble, C. L., et al. (2007). Gene Expression Analysis of Preinvasive and Invasive Cervical Squamous Cell Carcinomas Identifies HOXC10 as a Key Mediator of Invasion. *Cancer Res.* 67 (21), 10163–10172. doi:10.1158/0008-5472.CAN-07-2056

Conflict of Interest: The authors declare that the research was conducted in the absence of any commercial or financial relationships that could be construed as a potential conflict of interest.

Publisher's Note: All claims expressed in this article are solely those of the authors and do not necessarily represent those of their affiliated organizations, or those of the publisher, the editors and the reviewers. Any product that may be evaluated in this article, or claim that may be made by its manufacturer, is not guaranteed or endorsed by the publisher.

frontiers | Frontiers in Pharmacology

ORIGINAL RESEARCH
published: 12 July 2022
doi: 10.3389/fphar.2022.919490

Comprehensive Analysis of the Aberrance and Functional Significance of Ferroptosis in Gastric Cancer

Jun Xiao[1,2†], *Lingyan Zheng*[3†] *and Jingfeng Liu*[2,4*]

[1]Department of Gastrointestinal Surgery, Fujian Medical University Cancer Hospital, Fujian Cancer Hospital, Fuzhou, China, [2]Fujian Key Laboratory of Advanced Technology for Cancer Screening and Early Diagnosis, Fujian Medical University Cancer Hospital, Fujian Cancer Hospital, Fuzhou, China, [3]Department of Anus Intestine Surgery, Fuzhou Second Hospital Affiliated to Xiamen University, Fuzhou, China, [4]Department of Hepatopancreatobiliary Surgical Oncology, Fujian Medical University Cancer Hospital, Fujian Cancer Hospital, Fuzhou, China

OPEN ACCESS

Edited by:
Essa M. Saied,
Humboldt University of Berlin, Germany

Reviewed by:
Hamed Barabadi,
Shahid Beheshti University of Medical Sciences, Iran
Sonam Mittal,
Medical College of Wisconsin, United States
Zhuo-Xun Wu,
St. John's University, United States

***Correspondence:**
Jingfeng Liu
drjingfeng@126.com

[†]These authors have contributed equally to this work

Specialty section:
This article was submitted to Pharmacology of Anti-Cancer Drugs, a section of the journal Frontiers in Pharmacology

Received: 13 April 2022
Accepted: 06 June 2022
Published: 12 July 2022

Citation:
Xiao J, Zheng L and Liu J (2022) Comprehensive Analysis of the Aberrance and Functional Significance of Ferroptosis in Gastric Cancer. Front. Pharmacol. 13:919490. doi: 10.3389/fphar.2022.919490

Objective: Ferroptosis is a type of iron-dependent necrosis related to cancer. Nevertheless, the features of ferroptosis in gastric cancer (GC) remain poorly understood. This study conducted a systematic analysis of ferroptosis regulators in GC.

Methods: We gathered five GC cohorts, namely, TCGA-STAD, GSE84437, GSE62254, GSE26901, and GSE15459. Unsupervised clustering analysis was adopted to cluster GC patients into different ferroptosis subtypes based on ferroptosis regulators. Immune cell infiltration and hallmark pathway activity were estimated *via* ssGSEA. The ferroptosis index was developed with the PCA computational method. Response to chemotherapy agents and small molecular compounds was inferred *via* GDSC, CTRP, and PRISM projects. Two anti-PD-1 therapy cohorts were gathered and the potential of FPI in predicting immune response was assessed.

Results: Expression profiles, genetic mutations, DNA methylation, prognostic implications, and drug sensitivity of ferroptosis regulators were characterized in GC. Three ferroptosis subtypes were clustered with distinct prognosis, hallmark pathway activity, and tumor-infiltrating immune cells. Ferroptosis levels were quantified based on the expression of prognostic ferroptosis-related signatures. The significant relationships between FPI and clinicopathological characteristics were observed. Furthermore, high FPI was in relation to poor prognosis, inflamed tumor microenvironment (TME) as well as high sensitivity to chemotherapy agents (docetaxel and cisplatin), and CTRP- and PRISM-derived compounds. Also, FPI acted as a promising predictor of immune response.

Abbreviations: CCLE, Cancer Cell Line Encyclopedia; CLs, cancer cell lines; CR, complete response; CSD, stable disease; CTLs, cytotoxic T lymphocytes; DEGs, differentially expressed genes; EMT, epithelial–mesenchymal transition; FPI, ferroptosis index; GC, gastric cancer; GDSC, Genomics of Drug Sensitivity in Cancer; GEO, Gene Expression Omnibus; GO, Gene ontology; GSVA, Gene set variation analysis; ICB, immune checkpoint blockade; KEGG, Kyoto Encyclopedia of Genes and Genomes; PC, principal component; PCA, principal component analysis; PD, progressive disease; ssGSEA, single sample gene set enrichment analysis; PR, partial response; TCGA, the Cancer Genome Atlas; TIDE, Tumor Immune Dysfunction and Exclusion; TME, tumor microenvironment; t-SNE, t-distributed stochastic neighbor embedding.

Conclusion: Collectively, our findings identified a novel ferroptosis-based subtype classification of GC, and revealed the potential of ferroptosis in forming TME diversity and complexity, and guiding individualized treatment.

Keywords: gastric cancer, ferroptosis, prognosis, tumor microenvironment, immune checkpoint blockade, drug sensitivity

INTRODUCTION

Gastric cancer (GC) represents a major malignant tumor globally, which ranks the fifth in cancer incidence and the third major cause of cancer-relevant deaths (Bray et al., 2018). As estimated, the 5-year survival rate is <20% (Cavatorta et al., 2018). GC exhibits distinct molecular heterogeneity with aggressive behaviors as well as therapy resistance (Yan et al., 2018). The conventional system for predicting survival outcomes, like histological grade and tumor staging, is of difficulty to cover the clinical diversity of GC (Shao et al., 2016). Hence, it is of urgency to discover more effective biomarkers for early diagnosis, therapy, and prognostic evaluation (Wang et al., 2021).

Ferroptosis has been described as an iron-dependent necrosis modulated by lipid peroxidation (Niu et al., 2022). Under the normal condition, polyunsaturated fatty acid is often oxidized by lipoxygenase like 12/15-lipoxygenase but instantly decreased by enzyme GPX4 as well as its cofactor GSH (Lee et al., 2020). Nevertheless, when GPX4 is suppressed or GSH is exhausted, lipid peroxide accumulates in cells, inducing lipid peroxidation-mediated cell deaths, named ferroptosis. Unlike apoptosis or necroptosis, ferroptosis does not depend on caspase or RIPK1 kinase activation. Recently, several studies have proposed the key roles of ferroptosis in modulating tumor development and drug resistance in GC. Stimulation of ferroptosis has been a promising strategy for treating GC (Liu et al., 2021). For instance, cancer-associated fibroblasts secreted micro-522, inhibits ferroptosis, and induces acquired chemotherapy resistance in GC (Zhang et al., 2020). Tanshinone IIA enhances ferroptosis in GC cells *via* p53-regulated SLC7A11 inactivation (Guan et al., 2020). Micro-375 weakens the stemness of GC cells *via* inducing ferroptosis (Ni et al., 2021). Nevertheless, the detailed features of ferroptosis in GC remain poorly understood. Herein, our study systematically analyzed ferroptosis regulators and characterized the potential of ferroptosis-based treatment in GC.

MATERIALS AND METHODS

Gastric Cancer Datasets and Preprocessing

Gene expression datasets of GC were systematically searched from the Cancer Genome Atlas (TCGA; https://cancergenome.nih.gov/) and the Gene Expression Omnibus (GEO; https://www.ncbi.nlm.nih.gov/geo/). In total, five GC datasets were gathered, namely, TCGA-STAD (n = 383), GSE84437 (n = 433) (Yoon et al., 2020), GSE62254 (n = 300) (Cristescu et al., 2015; Oh et al., 2018), GSE26901 (n = 109) (Oh et al., 2018), and GSE15459 (n = 192) (Lei et al., 2013). RNA-sequencing (RNA-seq) data of TCGA-STAD were retrieved from the Genomic Data Commons *via* TCGAbiolink package (Colaprico et al., 2016). RNA-seq data (FPKM value) were converted to TPM, resulting in a higher similarity to microarray data and higher compatibility between samples. The raw microarray data from the GEO repository were generated by Illumina and Affymetrix platforms. The raw data from Illumina were preprocessed with lumi package (Du et al., 2008). The raw data from Affymetrix were adjusted by background and standardized by quartile *via* Affy package (Gautier et al., 2004). Removal of batch effects was presented with ComBat function of sva package (Leek et al., 2012). Clinical features of all eligible GC datasets are summarized in **Supplementary Table S1**. The somatic mutation and copy number variation of TCGA-STAD were downloaded from the Genomic Data Commons. In total, 60 ferroptosis regulators were gathered from published research (**Supplementary Table S2**). RCircos package was implemented to visualize the genomic structure and positional relationships between ferroptosis regulators (Zhang et al., 2013). Somatic mutation in Mutation Annotation Format (MAF) was visualized through maftools package (Mayakonda et al., 2018).

Functional Enrichment Analysis

Kyoto Encyclopedia of Genes and Genomes (KEGG) and Gene ontology (GO) enrichment analyses were carried out *via* clusterProfiler package (Yu et al., 2012). GO contained three categories: biological process, cellular component, and molecular function. The hallmark gene sets were acquired from the MSigDB database (http://software.broadinstitute.org/gsea/index.jsp) (Liberzon et al., 2015). Gene set variation analysis (GSVA) was carried out to infer the activation of hallmark pathways in GC specimens (Hänzelmann et al., 2013).

Assessment of Drug Sensitivity

The Genomics of Drug Sensitivity in Cancer (GDSC) database (www.cancerRxgene.org) may provide drug sensitivity data from nearly 75,000 experiments that describe responses to 138 anticancer agents across nearly 700 cancer cells (Yang et al., 2013). Spearman correlation analysis was conducted to calculate the correlation between drug sensitivity and ferroptosis regulators.

Tumor Microenvironment Immune-Infiltrating Analysis

Marker genes of infiltrating immune cells were gathered from the study by Bindea et al. (2013). The single sample gene set enrichment analysis (ssGSEA) method was utilized for

quantifying the relative abundance of 28 immune cell types in GC specimens with GSVA package based on the reference transcriptomic data (Hänzelmann et al., 2013). The enrichment score was determined to indicate the relative abundance of each tumor-infiltrating immune cell.

Unsupervised Clustering Analysis of Ferroptosis Regulators

Ferroptosis regulators were extracted from the five integrated datasets to identify distinct ferroptosis subtypes modulated by ferroptosis regulators. ConsensuClusterPlus package was implemented to estimate the number of unsupervised classes in the meta-cohort (Wilkerson and Hayes, 2010). The analysis was repeated 50 times to guarantee the reliability of clustering. The accuracy of clustering was verified *via* the t-distributed stochastic neighbor embedding (t-SNE) method according to the mRNA expression of ferroptosis regulators.

Development of Ferroptosis Index

By adopting limma package, differential expression analysis was presented between three ferroptosis subtypes (Ritchie et al., 2015). Genes with adjusted $p < 0.05$ were retained, and shared differentially expressed genes (DEGs) were identified through a Venn diagram (Chen and Boutros, 2011). ConsensuClusterPlus package was applied for defining the number of genomic clustering based on the expression of shared DEGs. Univariate cox regression models were established to analyze the correlation between shared DEGs and GC prognosis. FPI was calculated *via* principal component analysis (PCA) based on the prognostic shared DEGs. Principal components (PC) 1 and 2 were extracted for defining FPI in line with the following formula: FPI = $\sum$(PC1i + PC2i), where i represented prognostic shared DEGs.

Collection of Known Biological Signatures

This study gathered the gene sets of known biological signatures containing CD8 + T effector, DNA damage repair, pan-fibroblast TGF-β response signature (pan-F-TBRS), antigen-processing machinery, immune checkpoint, epithelial–mesenchymal transition (EMT1-3), FGFR3-related genes, angiogenesis, Fanconi anemia, cell cycle, DNA replication, nucleotide excision repair, homologous recombination, mismatch repair, WNT targets, cell cycle regulators, IFN-γ signatures, APM signaling, base excision repair, microRNAs in cancer, oocyte meiosis, p53 signaling pathway, progesterone-mediated oocyte maturation, proteasome, pyrimidine metabolism, spliceosome, and viral carcinogenesis (Rosenberg et al., 2016; Şenbabaoğlu et al., 2016; Mariathasan et al., 2018). Correlation between FPI score and these biological pathways was analyzed using the Spearman correlation test.

Evaluation of Immune Response

Response to immune checkpoint blockade (ICB) was evaluated *via* the tumor immune dysfunction and exclusion (TIDE) computational method in line with the study by Hoshida et al. (Jiang et al., 2018). This method was based on two main mechanisms of tumor immune evasion: inducing T-cell dysfunction in tumors with high infiltration levels of cytotoxic T lymphocytes (CTLs) and preventing T-cell infiltration in tumors with low infiltration levels of CTLs.

Collection of ICB Therapy Cohorts

This study gathered two ICB therapy cohorts: metastatic melanoma patients who received anti-PD-1 therapy from GSE78220 cohort (Hugo et al., 2016) and Liu et al. (2019). The mRNA expression data and follow-up information including survival time and therapeutic response [complete response (CR), partial response (PR), stable disease (SD), and progressive disease (PD)] were retrieved.

Sensitivity to Chemotherapeutic Agents

The sensitivity to two chemotherapeutic agents (docetaxel and cisplatin) was predicted in each GC specimen. The half-maximal inhibitory concentration (IC50) was determined utilizing ridge regression analysis through pRRophetic package (Geeleher et al., 2014).

Prediction of Potential Small-Molecular Compounds

This study retrieved drug sensitivity data of human cancer cell lines (CCLs) from the CTRP (https://portals.broadinstitute.org/ctrp) and PRISM (https://depmap.org/portal/prism/) projects. The area under the curves (AUCs) were utilized for evaluating response to each drug. The AUC value was inversely proportional to drug sensitivity. The mRNA expression profiling in the Cancer Cell Line Encyclopedia (CCLE) database (https://portals.broadinstitute.org/ccle/) was employed for CTRP and PRISM analyses (Ghandi et al., 2019).

Statistical Analyses

All statistical analyses were conducted with R (https://www.r-project.org/). Univariate Cox regression analysis was applied to assess the correlation between overall survival and ferroptosis regulators in GC patients with survival package. The Kaplan–Meier survival analysis was carried out utilizing survival and survminer packages. The Spearman correlation test was utilized for inferring the correlation between two parameters. Student's t and Wilcoxon tests were adopted to compare the differences between two groups, while one-way ANOVA and Kruskal–Wallis tests were conducted to compare the differences between three or more groups. Two-sided p-values < 0.05 were considered statistically significant.

RESULTS

Landscape of Expression, Genetic Mutation, and DNA Methylation of Ferroptosis Regulators in Gastric Cancer

This study gathered 60 ferroptosis regulators and their roles were observed in GC. **Figure 1A** visualized the genomic position and relationships between ferroptosis regulators. First, we analyzed

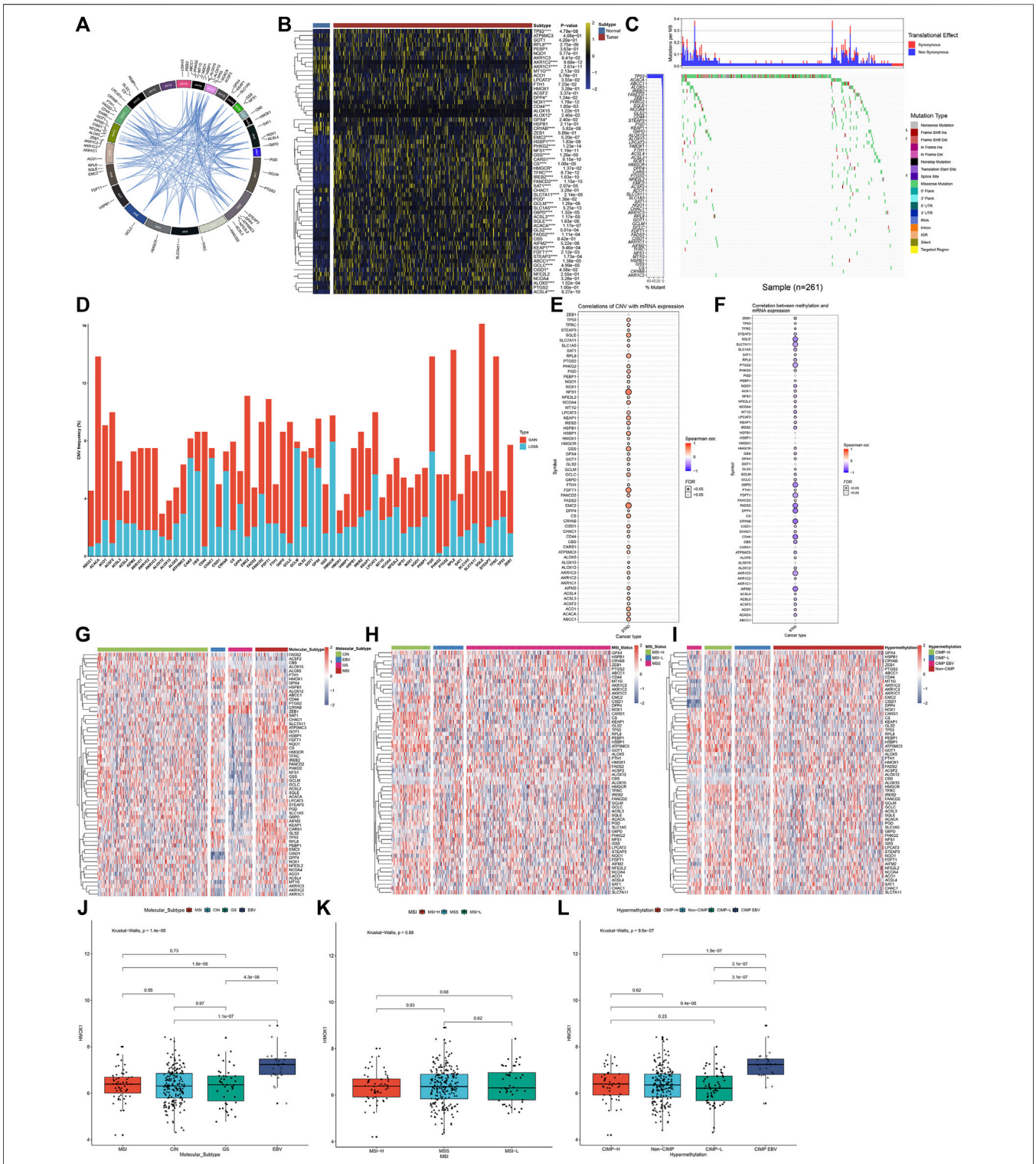

FIGURE 1 | Landscape of expression, genetic mutation, and DNA methylation of ferroptosis regulators in GC. **(A)** RCircos plots showing the genomic location and relationships among 60 ferroptosis regulators. **(B)** Heatmap visualizing the mRNA expression of ferroptosis regulators in 32 normal and 375 GC tissues in the TCGA-STAD dataset. Yellow, upregulation; blue, downregulation. *$p < 0.05$; ***$p < 0.001$; ****$p < 0.0001$. **(C)** Waterfall diagram for the genetic mutation of ferroptosis regulators across 261 GC specimens. The left indicated the mutation rate of each ferroptosis regulator. Each column represented each sample. Each mutation type was identified by a unique color. The upper indicated mutations per MB in each ferroptosis regulator. **(D)** Stacked diagram visualizing the frequency of CNV across GC specimens. Red, amplification; blue, deletion. **(E)** Spearman correlation between mRNA expression and CNV in ferroptosis regulators across GC samples. Red, positive

(*Continued*)

FIGURE 1 | correlation; blue, negative correlation. The size of the bubble was proportional to the correlation coefficient. **(F)** Spearman correlation between mRNA expression and DNA methylation in ferroptosis regulators across GC samples. Red, positive correlation; blue, negative correlation. The size of the bubble was proportional to the correlation coefficient. **(G)** Heatmap showing the mRNA expression of ferroptosis regulators among four molecular subtypes: CIN, EBV, GS, and MSI. **(H)** Heatmap visualizing the expression distribution of ferroptosis regulators among three MSI status-based subtypes: MSI-H, MSI-L, and MSS. **(I)** Heatmap for the mRNA expression of ferroptosis regulators among four DNA methylation-based subtypes: CIMP-H, CIMP-L, CIMP-EBV, and non-CIMP. **(J–L)** Distribution of the mRNA expression of HMOX1 across different subtypes, molecular subtypes, MSI status-based subtypes, and DNA methylation-based subtypes.

the mRNA expressional alterations of ferroptosis regulators in 32 normal and 375 GC tissues in the TCGA-STAD dataset. There was the expressional imbalance of ferroptosis regulators and most presented the distinct upregulation in GC compared to normal tissues (**Figure 1B**). We further ascertained whether the genetic variation affected the expression of ferroptosis regulators in GC. Among 261 GC specimens, we observed that TP53 displayed the highest mutation rate, followed by ACACA and ABCC1 (**Figure 1C**). Further analysis showed that CNV widely occurred in ferroptosis regulators and amplification was the major mutation type (**Figure 1D**). The Spearman correlation analysis also confirmed that amplification of CNV exhibited a positive correlation to mRNA expression in ferroptosis regulators across GC (**Figure 1E**). DNA methylation acts as the main epigenetic modification, which transcriptionally regulates gene expression. Herein, we observed that DNA methylation had negative association to mRNA expression in ferroptosis regulators (**Figure 1F**). Collectively, our findings were indicative that amplification of CNV and hypermethylation might prominently result in the overexpression of ferroptosis regulators in GC. The TCGA project has revealed four molecular subtypes of GC: Epstein–Barr virus (EBV), microsatellite instability (MSI), genomically stable (GS), and chromosomal instability (CIN) (Sohn et al., 2017). Among the four molecular subtypes, the expression of ferroptosis regulators showed wide heterogeneity (**Figure 1G**). Most ferroptosis regulators were upregulated in MSI but were downregulated in GS. According to MSI status, GS can be divided into MSI-high (MSI-H), MSI-low (MSI-L), and MSS. We observed that MSI-H tumors displayed the significant up-regulation of most ferroptosis regulators (**Figure 1H**). Moreover, we compared the expression of ferroptosis regulators in four DNA methylation-based subtypes: CIMP-high (CIMP-H), CIMP-low (CIMP-L), CIMP-EBV, and non-CIMP. As shown in **Figure 1I**, ferroptosis regulators exhibited relatively high expression in CIMP-L. We visualized the expression of a ferroptosis regulator (HMOX1) across different molecular subtypes (**Figures 1J–L**). The results showed that HMOX1 exhibited the highest expression in EBV and CIMP-EBV but did not have significant difference among different MSI subtypes.

Biological Function, Prognostic Implication, and Immune Cell Infiltration Correlation of Ferroptosis Regulators in Gastric Cancer

Through clusterProfiler package, we evaluated the pathways involved in ferroptosis regulators. In **Figure 2A**, arachidonic acid metabolism, cysteine and methionine metabolism, and ferroptosis and glutathione metabolism were mainly enriched by ferroptosis regulators. GO enrichment analysis uncovered that ferroptosis regulators markedly participated in the fatty acid derivative metabolic process, glutathione metabolic process, response to oxidative stress, and sulfur compound metabolic process (**Figure 2B**). Cellular components including lipid droplet, mitochondrial outer membrane, organelle outer membrane, and outer membrane were primarily regulated by ferroptosis regulators (**Figure 2C**). In **Figure 2D**, ferroptosis regulators possessed the molecular functions of coenzyme binding, ligase activity, oxidoreductase activity, and acting on paired donors, with incorporation or reduction of molecular oxygen. Aforementioned data were indicative of the critical biological function of ferroptosis regulators in the occurrence and progression of GC. This study gathered and merged five GC datasets: TCGA-STAD, GSE84437, GSE62254, GSE26901, and GSE15459 (**Figure 2E**). Batch effects were corrected *via* ComBat function of sva package (**Figure 2F**). In the meta-cohort, univariate Cox regression analysis uncovered that 15 ferroptosis regulators, namely, CRYAB, HSPB1, GLS2, GOT1, FANCD2, CHAC1, PTGS2, ALOX15, ACO1, NFS1, CD44, GPX4, TFRC, TP53, and FADS2 exhibited significant correlations to GC prognosis (**Figure 2G**; **Supplementary Figure S1**). Drug sensitivity was also estimated in GC specimens *via* the GDSC database. As shown in the Spearman correlation analysis, ferroptosis regulators were significantly correlated to the sensitivity to NSC-207895, QL-X-138, QL-XII-61, foretinib, MP470, OSI-027, (5Z)-7-oxozeaenol, piperlongumine, phenformin, AZD7762, dabrafenib, PLX4720, SB590885, YK 4-279, bosutinib, cytarabine, PD-0332991, HG-6-64-1, A-770041, saracatinib, erlotinib, gefitinib, RO-3306, AS601245, WH-4-023, XAV939, and dasatinib across GC samples (**Figure 2H**). Using the ssGSEA method, we inferred the enrichment score of 28 immune cells. As depicted in **Figure 2I**, ferroptosis regulators displayed distinct associations with TME immune infiltration, indicative of the interactions between ferroptosis and tumor immunity in GC. Among them, high HMOX1 expression was in relation to increased infiltration levels of tumor-infiltrating immune cells across GC (**Figure 2J**).

Establishment of Three Ferroptosis Regulator-Mediated Subtypes With Different Prognosis and Tumor Microenvironment Immune Infiltration

This study applied the ConsensusClusterPlus computational method to classify GC patients in the meta-cohort into three ferroptosis subtypes according to the expression profiling of 60 ferroptosis regulators (**Figure 3A**). Cumulative distribution

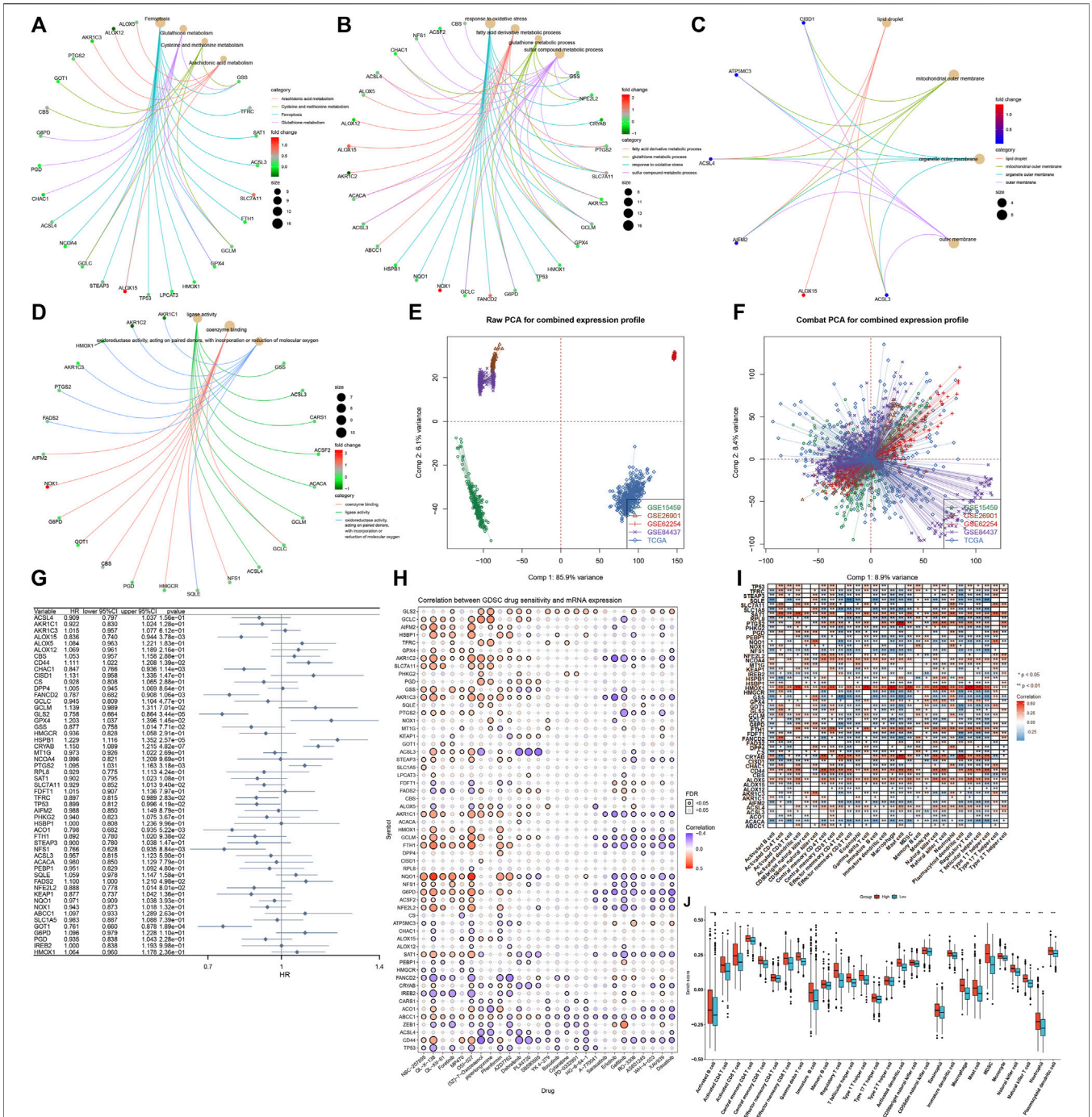

FIGURE 2 | Biological function, prognostic implication, and immune cell infiltration correlation of ferroptosis regulators in the GC meta-cohort. **(A)** KEGG pathways involved in ferroptosis regulators. **(B–D)** Biological processes, cellular components, and molecular functions enriched by ferroptosis regulators. **(E)** Integration of the mRNA expression data of five GC datasets: TCGA-STAD, GSE84437, GSE62254, GSE26901, and GSE15459. **(F)** Removal of batch effects. **(G)** Forest plot showing the association between ferroptosis regulators and GC prognosis through univariate Cox regression models. **(H)** Spearman correlation analysis between ferroptosis regulators and drug sensitivity *via* the GDSC database. Red, positive correlation; blue, negative correlation. The size of the bubble was proportional to the correlation coefficient. **(I)** Spearman correlation analysis between ferroptosis regulators and tumor-infiltrating immune cells by ssGSEA method. Red, positive correlation; blue, negative correlation. **(J)** Comparisons of enrichment scores of tumor-infiltrating immune cells in high and low HMOX1 expression GC samples. *$p < 0.05$; **$p < 0.01$; and ***$p < 0.001$.

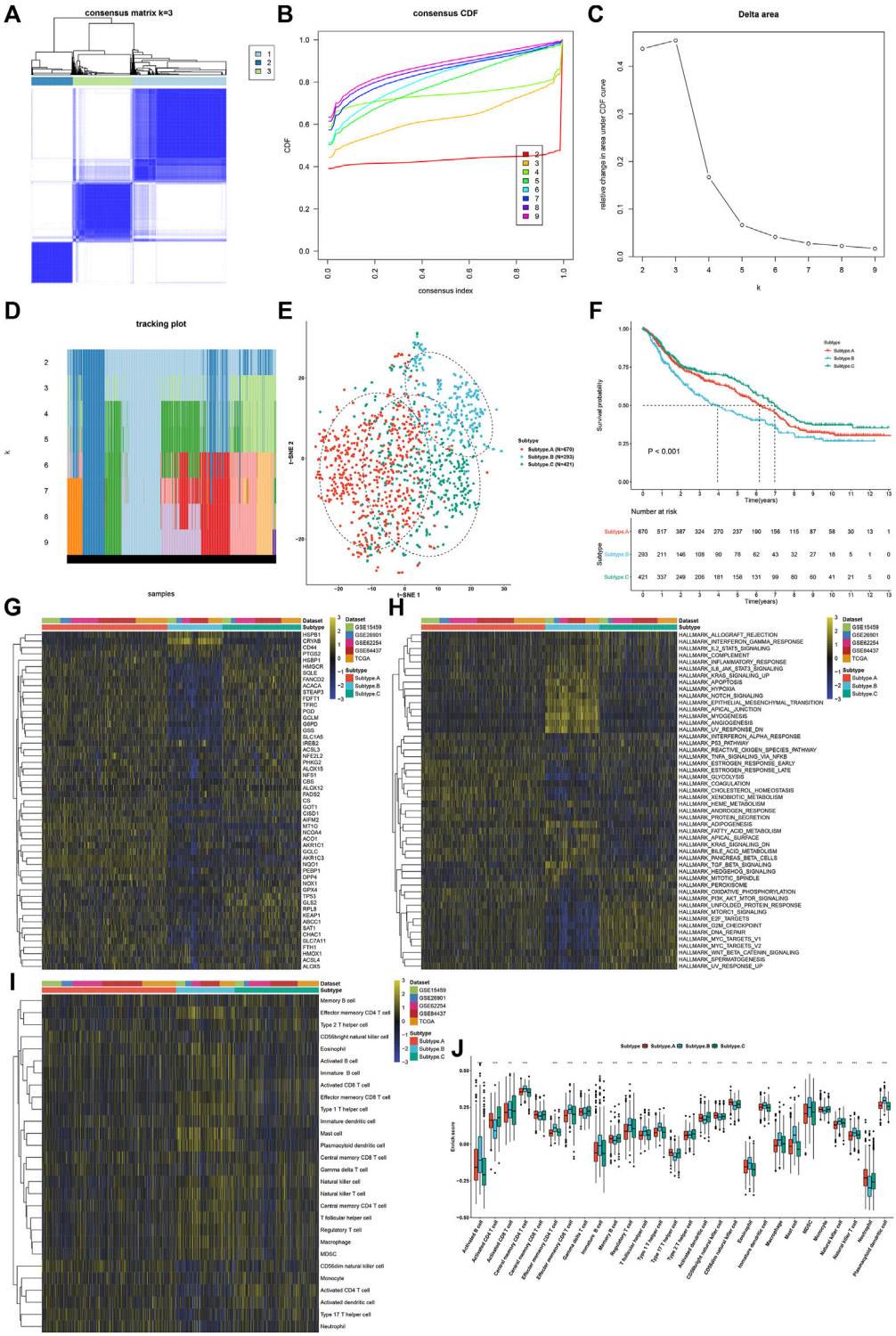

FIGURE 3 | Establishment of three ferroptosis regulator-mediated subtypes with different prognosis and TME immune infiltration in the GC meta-cohort. **(A)** Consensus matrix when k = 3. **(B)** Empirical CDF plots displaying the consensus distribution corresponding to each k. **(C)** Delta area diagram visualizing the relative change in area under CDF curve at different k. **(D)** Item tracking plot showing the consensus clustering of items (in column) at each k value (in row). **(E)** The t-SNE plots verifying the difference among three ferroptosis subtypes according to the mRNA expression of ferroptosis regulators. **(F)** Survival analysis for GC patients in three ferroptosis subtypes. **(G)** Heatmap showing the mRNA expression of ferroptosis regulators in three ferroptosis subtypes. Yellow, up-regulation; blue, down-regulation. **(H)** Heatmap for the activity of the 50 hallmark pathways in three ferroptosis subtypes. Yellow, up-regulation; blue, down-regulation. **(I)** Heatmap visualizing the infiltration levels of tumor-infiltrating immune cells in three ferroptosis subtypes. **(J)** Comparison of the infiltration levels of tumor-infiltrating immune cells in three ferroptosis subtypes. $^{**}p < 0.01$; $^{***}p < 0.001$.

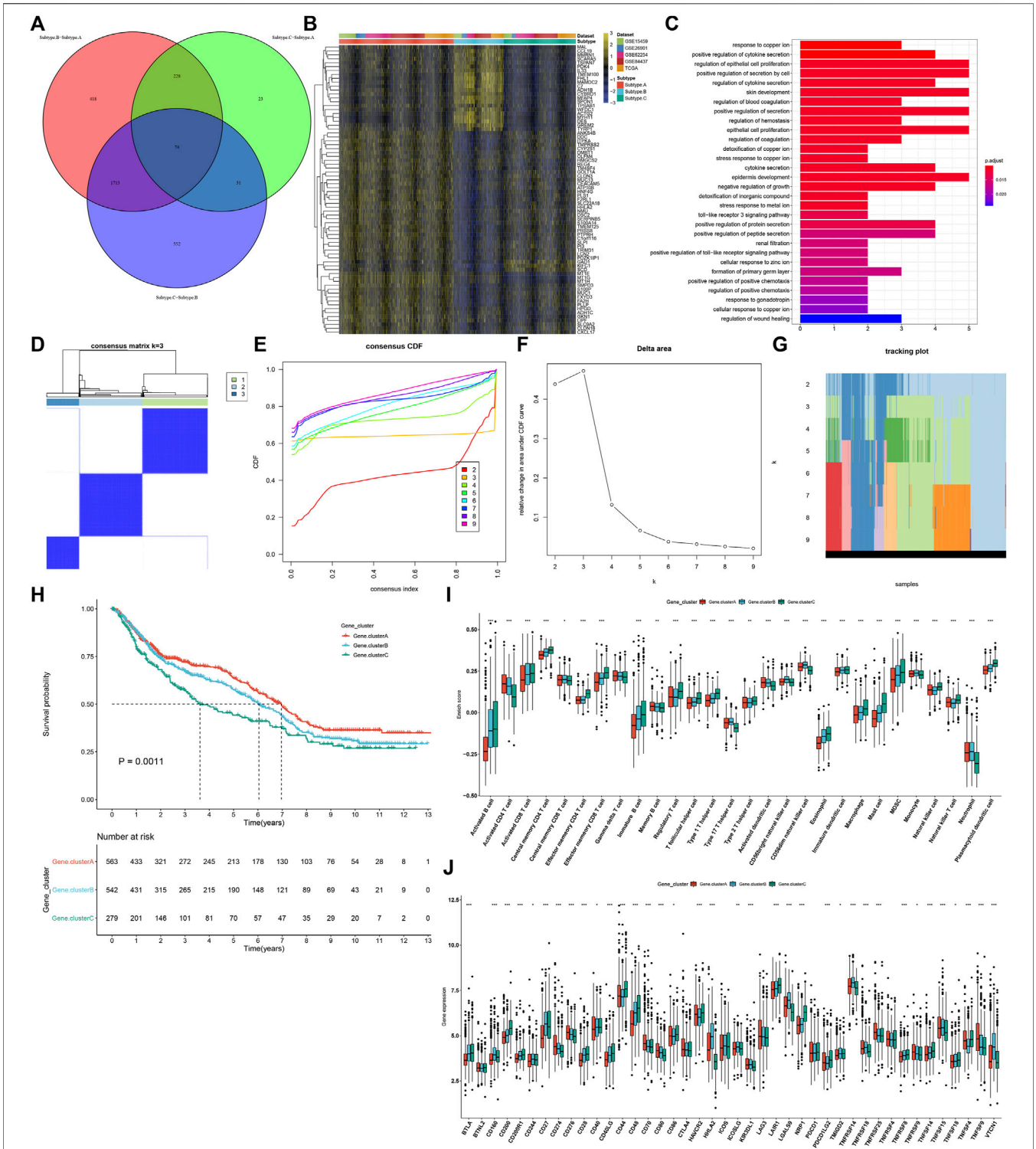

FIGURE 4 | Identification of three ferroptosis genomic subtypes characterized by different prognosis and TME features in the GC meta-cohort. **(A)** Shared DEGs between three ferroptosis subtypes. **(B)** Heatmap showing the mRNA expression of the shared DEGs in each ferroptosis subtype. Yellow, up-regulation; blue, down-regulation. **(C)** GO annotation results of the shared DEGs. **(D)** Consensus matrix when k = 3. **(E)** Empirical CDF plots displaying the consensus distribution corresponding to each k. **(F)** Delta area diagram visualizing the relative change in area under CDF curve at different k. **(G)** Item tracking plot showing the consensus clustering of items (in column) at each k value (in row). **(H)** Survival analysis of GC patients in three ferroptosis genomic subtypes. **(I)** Comparison of the relative abundance of tumor-infiltrating immune cells among three ferroptosis genomic subtypes. **(J)** Comparison of the mRNA expression of immune checkpoints among three ferroptosis genomic subtypes. *$p < 0.05$; **$p < 0.01$; ***$p < 0.001$.

function (CDF) was employed to identify the k value at which the distribution reached an approximate maximum that indicated a maximum stability (**Figure 3B**). Delta area plot showed that when k = 3, the area under the curve only slightly increased (**Figure 3C**). Furthermore, the item tracking plot showed the consensus clustering of items at different k values (**Figure 3D**). Collectively, GC patients were clustered into three ferroptosis subtypes with high stability, namely, as ferroptosis subtype A, B, and C. The t-SNE plots confirmed the difference among three ferroptosis subtypes according to the mRNA expression of ferroptosis regulators (**Figure 3E**). Survival analysis uncovered that ferroptosis subtype B possessed the worst survival outcomes, while ferroptosis subtype C had the significant survival advantage (**Figure 3F**). In **Figure 3G**, we observed that most ferroptosis regulators were distinctly downregulated in ferroptosis subtype B. The activity of hallmark pathways was estimated *via* the ssGSEA computational method. Carcinogenic pathways including KRAS signaling, hypoxia, Notch signaling, and hedgehog signaling were markedly activated in ferroptosis subtype B, indicative of the poor prognosis (**Figure 3H**). Moreover, stromal activation pathways including epithelial–mesenchymal transition, angiogenesis, and TGF-β signaling, as well as immune activation pathways including allograft rejection, interferon *γ* response, IL2-STAT5 signaling, complement, inflammatory response, and IL6-JAK-STAT3 signaling displayed significant upregulation in ferroptosis subtype B. Tumor-infiltrating immune cells were then quantified. In **Figures 3I,J**, we observed that ferroptosis subtype B displayed high infiltration levels of innate immune cells (such as natural killer cells, macrophages, eosinophils, mast cells, MDSCs, and plasmacytoid dendritic cells) and adaptive immune cells (such as effector memory $CD4^+$ T cells, activated B cells, activated $CD8^+$ T cells, effector memory $CD8^+$ T cells, central memory $CD8^+$ T cells, and central memory $CD4^+$ T cells).

Identification of Three Ferroptosis Genomic Subtypes Characterized by Different Prognosis and Tumor Microenvironment Features

In total, 74 shared DEGs were identified among three ferroptosis subtypes (**Figure 4A**; **Supplementary Table S3**). **Figure 4B** depicts the difference in mRNA expression of these shared DEGs between ferroptosis subtypes. GO annotation analysis uncovered that these shared DEGs were distinctly involved in mediating stromal activation-related processes (like regulation of epithelial cell and epithelial cell proliferation) and immune-relevant processes (like positive regulation of cytokine secretion, regulation of cytokine secretion, and cytokine secretion; **Figure 4C**). By unsupervised clustering analysis, we established three ferroptosis genomic subtypes across GC patients in the meta-cohort, namely, ferroptosis genomic subtype A–C (**Figures 4D–G**). In **Figure 4H**, ferroptosis genomic subtype C exhibited the poorest prognosis, whereas ferroptosis genomic subtype A possessed the most favorable prognosis. Furthermore, we observed that ferroptosis genomic subtype C had the high infiltration levels of innate immune cells (like natural killer cells, macrophages, eosinophils, mast cells, MDSCs, and plasmacytoid dendritic cells; **Figure 4I**). In **Figure 4J**, ferroptosis genomic subtype C had the highest expression of immune checkpoints BTLA, CD200, CD200R1, CD28, CD40LG, CD44, CD48, LAIR1, NRP1, PDCD1LG2, TNFRSF14, TNFRSF18, and TNFRSF8; ferroptosis genomic subtype B exhibited the highest expression of CD160, CD27, HHLA2, ICOSLG, KIR3DL1, LGALS9, TMIGD2, TNFSF14, and VTCN1; ferroptosis genomic subtype A displayed the highest expression of CD274, CD276, CD70, CD80, TNFRSF25, TNFRSF9, and TNFSF9.

TABLE 1 | Identification of 22 prognosis-related shared DEGs in GC through univariate Cox regression models.

Shared DEGs	HR	Low 95% CI	High 95% CI	*P*
FHL1	1.092087	1.041977	1.144606	0.000237
MYH11	1.07675	1.037586	1.117393	9.16E-05
DES	1.071609	1.038122	1.106175	1.96E-05
C7	1.085066	1.041192	1.130789	0.000106
MFAP4	1.094248	1.040893	1.150339	0.000413
MAMDC2	1.090156	1.031244	1.152433	0.002324
ACTG2	1.091419	1.048324	1.136287	2.08E-05
SPON1	1.116166	1.056533	1.179165	8.74E-05
TMEM125	0.918597	0.854042	0.988033	0.022384
ITPKA	0.908395	0.854178	0.966052	0.002214
SMPD3	0.819972	0.753313	0.892528	4.47E-06
HNF4G	0.911258	0.851557	0.975145	0.007188
TMPRSS2	0.941752	0.890433	0.996028	0.035801
CYBRD1	1.148231	1.074373	1.227167	4.61E-05
IL33	1.099016	1.033994	1.168126	0.002411
MMRN1	1.110902	1.034905	1.19248	0.003627
DDC	0.952129	0.907629	0.998811	0.04457
PDK4	1.123587	1.064525	1.185927	2.34E-05
WFDC1	1.078939	1.001167	1.162753	0.046534
LIPF	0.966674	0.941203	0.992834	0.012851
TYRP1	1.078591	1.013015	1.148412	0.018078
TPSAB1	1.083159	1.026209	1.14327	0.003746

Development of Ferroptosis Index Score and Evaluation of Its Relevant Clinical Features

As shown in univariate Cox regression models, 22 shared DEGs were in relation to GC prognosis (**Table 1**). Using the PCA computational method, we developed an FPI score to quantify ferroptosis subtypes following the expression of the prognosis-related shared DEGs. High FPI was indicative of unfavorable clinical outcomes in comparison to the low FPI score (**Figure 5A**). Sankey diagram visualized the interactions among ferroptosis subtypes, ferroptosis genomic subtypes, FPI, and survival status (**Figure 5B**). The clinical implications of FPI were evaluated in depth. In **Figure 5C**, patients aged <65 years had a higher FPI score than those aged ≥65 years. No significant difference was investigated between female and male patients (**Figure 5D**). For grade, G3 exhibited the highest FPI score (**Figure 5E**). Stages II–IV had higher FPI scores than stage I (**Figure 5F**). These indicated that FPI score might predict the severity of GC. Among four molecular subtypes, GS subtype displayed the highest FPI score (**Figure 5G**). For MSI status, MSS

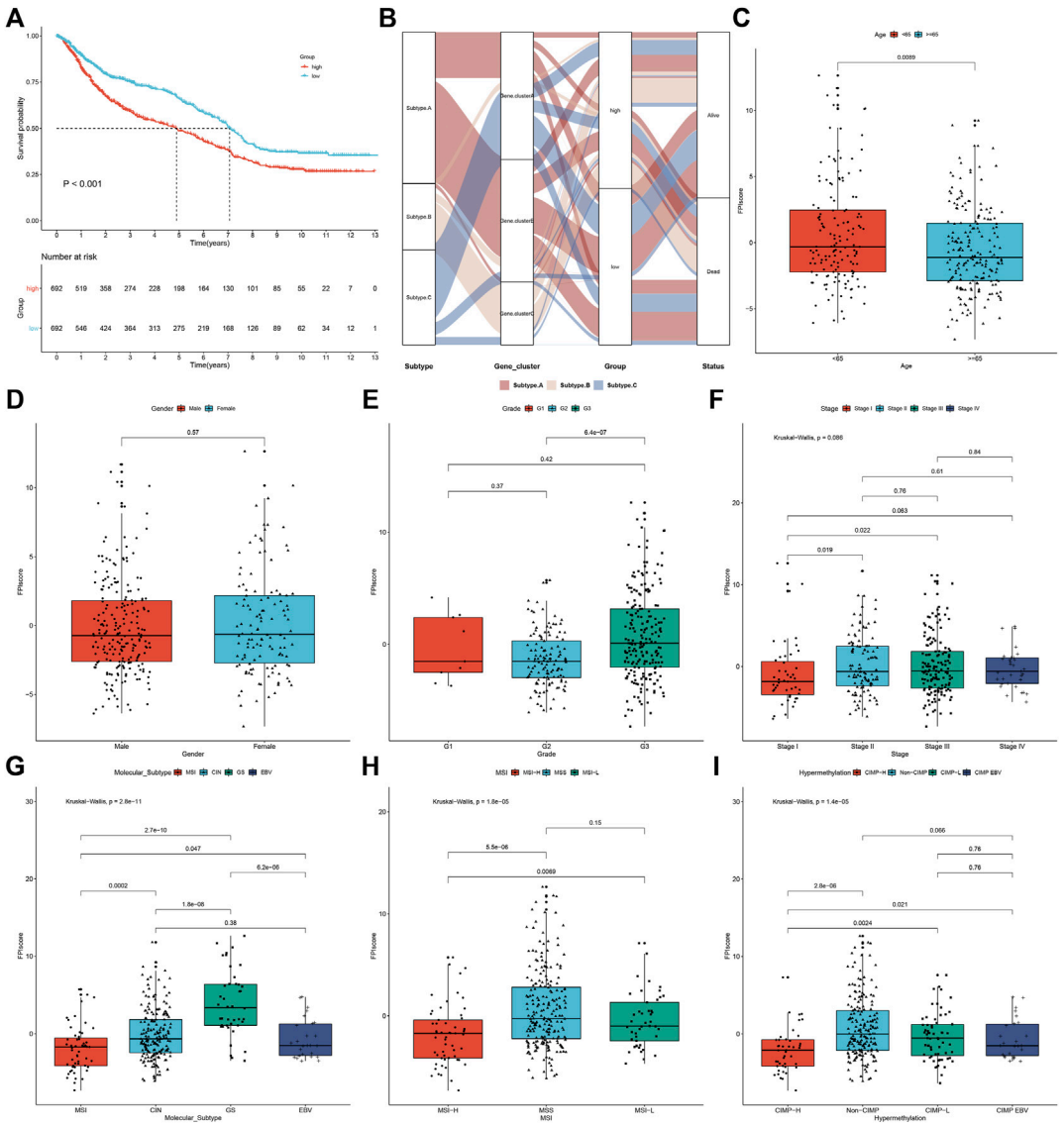

FIGURE 5 | Development of FPI score and evaluation of its relevant clinical features in the meta-cohort. **(A)** Survival analysis of GC patients in high and low FPI groups. **(B)** Sankey diagram showing the interactions among ferroptosis subtypes, ferroptosis genomic subtypes, FPI, and survival status. **(C–F)** Comparison of FPI score in different clinical features, including age (age<65 years vs. age≥65 years), gender (female vs. male), grade (G1 vs. G2 vs. G3), and stage (stage I vs. stage II vs. stage III vs. stage IV). **(G–I)** Comparison of the FPI score in different subtypes, including molecular subtypes (MSI, CIN, GS, and EBV), MSI status-based subtypes (MSI-H, MSS, and MSI-L), and DNA methylation-based subtypes (CIMP-H, CIMP-L, CIMP-EBV, and non-CIMP).

subtype exhibited the highest FPI score (**Figure 5H**). Furthermore, among DNA methylation-based subtypes, non-CIMP had the highest FPI score (**Figure 5I**).

Association Between Ferroptosis Index Score and Tumor Immunity

Further analysis uncovered that high FPI samples exhibited high infiltration levels of innate immune cells (such as natural killer cells, macrophages, eosinophils, mast cells, MDSCs, and plasmacytoid dendritic cells) and adaptive immune cells (such as effector memory $CD4^+$ T cells, activated B cells, activated $CD8^+$ T cells, effector memory $CD8^+$ T cells, central memory $CD8^+$ T cells, and central memory $CD4^+$ T cells; **Figure 6A**). Most immune checkpoints had increased mRNA expression in patients with a high FPI score including CD40LG, CD40, BTLA, CD200R1, TNFSF14, CD27, LAIR1, CD28, HAVCR2, CD86, PDCD1LG2, TNFSF4, CD48, CD44, CD200, and NRP1 (**Figure 6B**). Meanwhile, HHLA2, LGALS9, TNFRSF14, TNFSF15, KIR3DL1, ICOSLG, and TNFRSF25 were markedly upregulated in low FPI samples. The FPI score was positively correlated to stromal activation pathways including pan-F-TBRS, angiogenesis, and EMT (**Figure 6C**). Moreover, we observed that the FPI score exhibited negative correlations to DNA damage

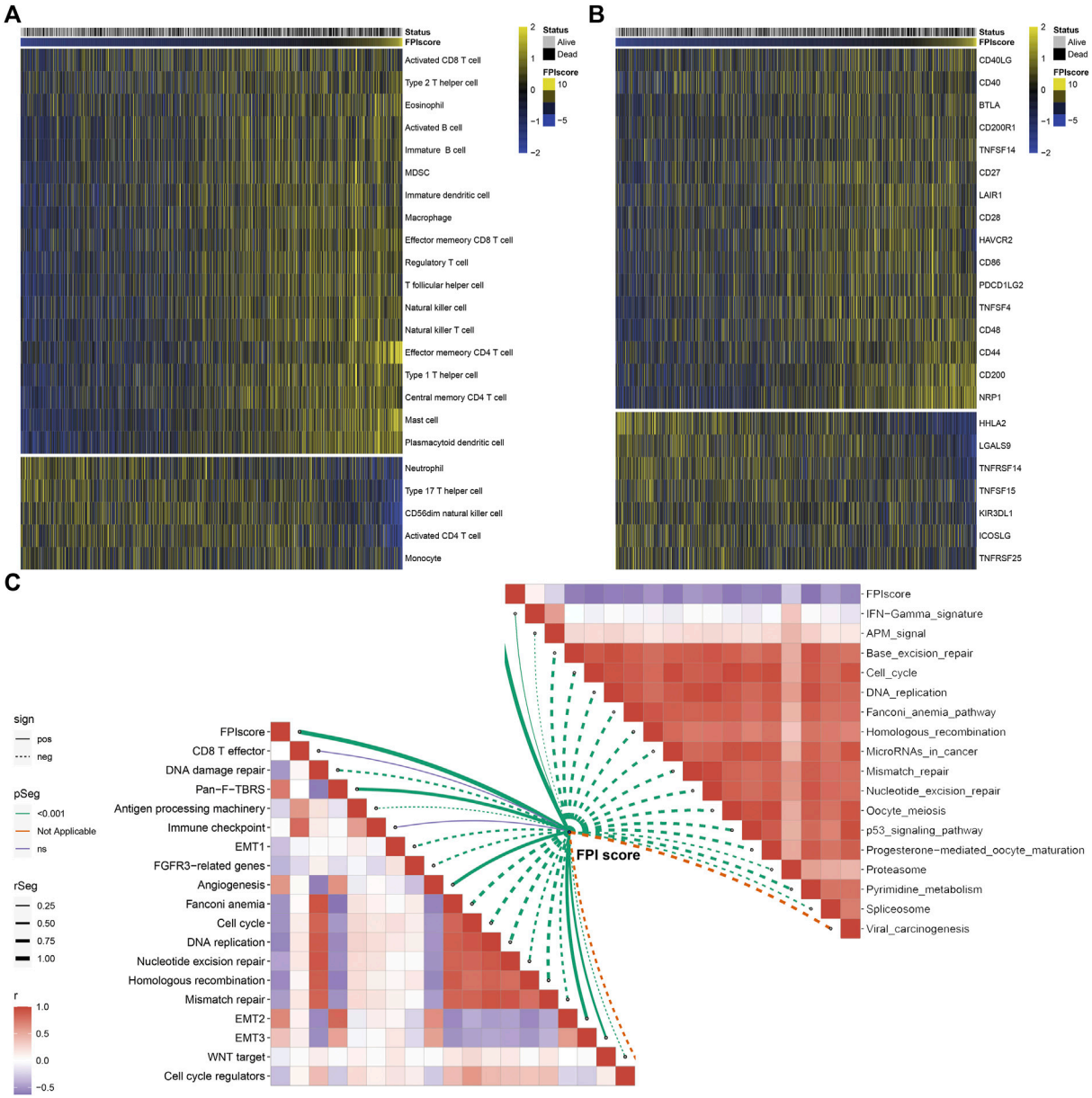

FIGURE 6 | Association between FPI score and tumor immunity across GC samples. **(A)** Heatmap visualizing the infiltration levels of tumor-infiltrating immune cells in low and high FPI GC samples. Yellow, high infiltration; blue, low infiltration. **(B)** Heatmap showing the mRNA expression of immune checkpoints in low and high FPI GC samples. Yellow, high expression; blue, low expression. **(C)** Association between FPI score and known biological processes and pathways.

repair, cell cycle, DNA replication, nucleotide excision repair, homologous recombination, and mismatch repair as well as carcinogenic pathways such as p53 signaling pathway, mismatch in cancer, and viral carcinogenesis.

Ferroptosis Index Score Serves as a Predictor of Immune Response

Prognostic implications of the FPI score were validated in the TCGA-STAD, GSE84437, GSE26901, and GSE15459 cohorts. Consistently, high FPI score was indicative of more unfavorable survival outcomes than low FPI score in each GC cohort (**Figures 7A–D**). The TIDE score was determined in each HCC specimen. In comparison to high FPI, a reduced TIDE score was observed in low FPI (**Figure 7E**), which indicated that low FPI patients were more likely to benefit from immunotherapy. SubMap analysis showed that patients with a high FPI score were more likely to respond to anti-CTLA-4 therapy (**Figure 7F**). Two anti-PD-1 therapy cohorts were gathered. In the GSE78220 cohort, patients with high FPI exhibited the distinct survival advantage (**Figure 7G**). Patients with high FPI had higher therapeutic response than those with low FPI (75% vs.

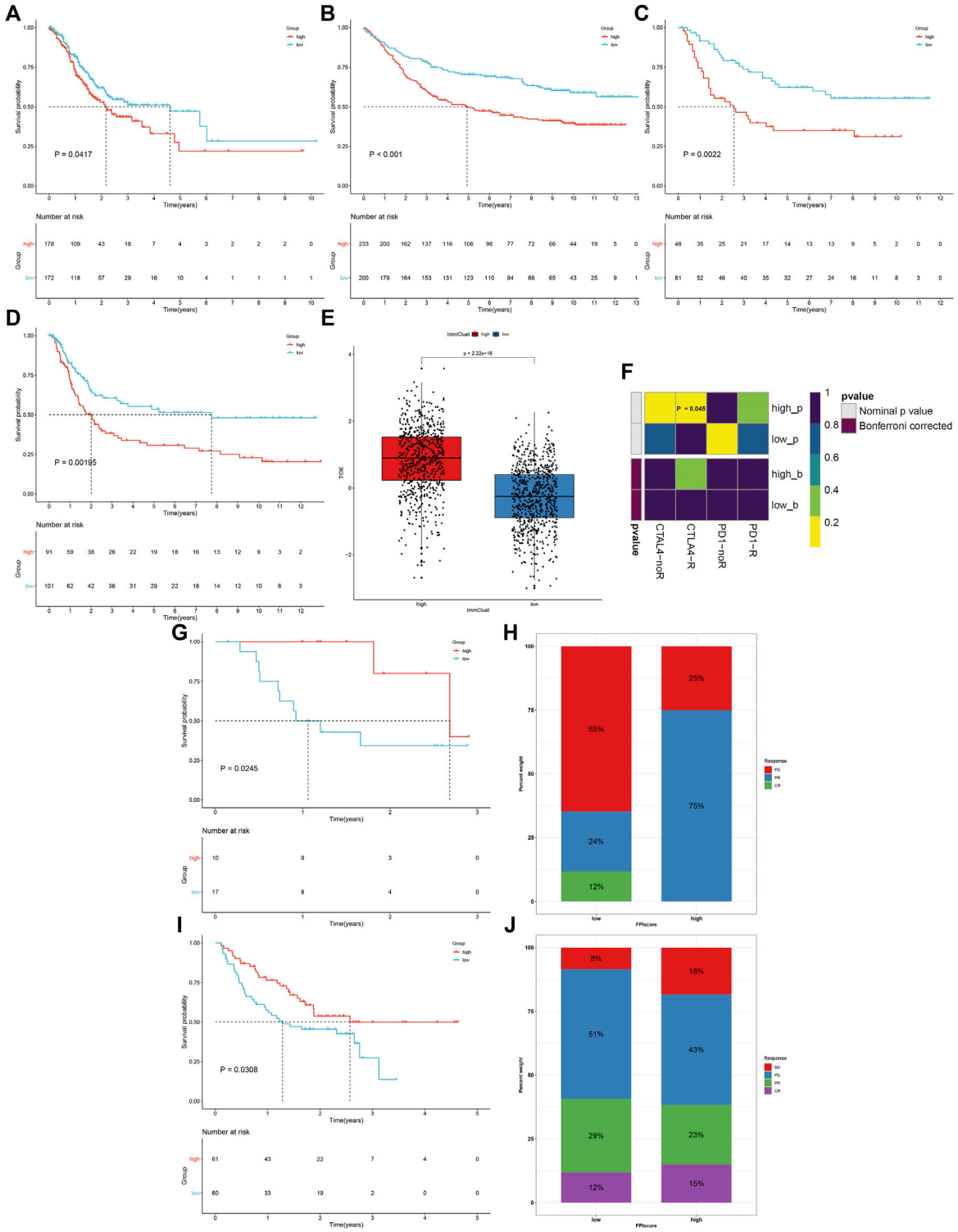

FIGURE 7 | FPI score serves as a predictor of immune response. **(A–D)** Survival analysis of GC patients with high and low FPI scores in the TCGA-STAD, GSE84437, GSE26901, and GSE15459 cohorts. **(E)** Comparison of the TIDE score in high and low FPI score groups. **(F)** SubMap analysis estimating the response to anti-CTLA-4 and anti-PD-1 therapy for high and low FPI patients. **(G,H)** Comparison of survival outcomes and therapeutic response to anti-PD-1 therapy between high and low FPI patients in the GSE78220 cohort. **(I,J)** Comparison of survival outcomes and therapeutic response to anti-PD-1 therapy between high and low FPI patients in the Liu et al. cohort.

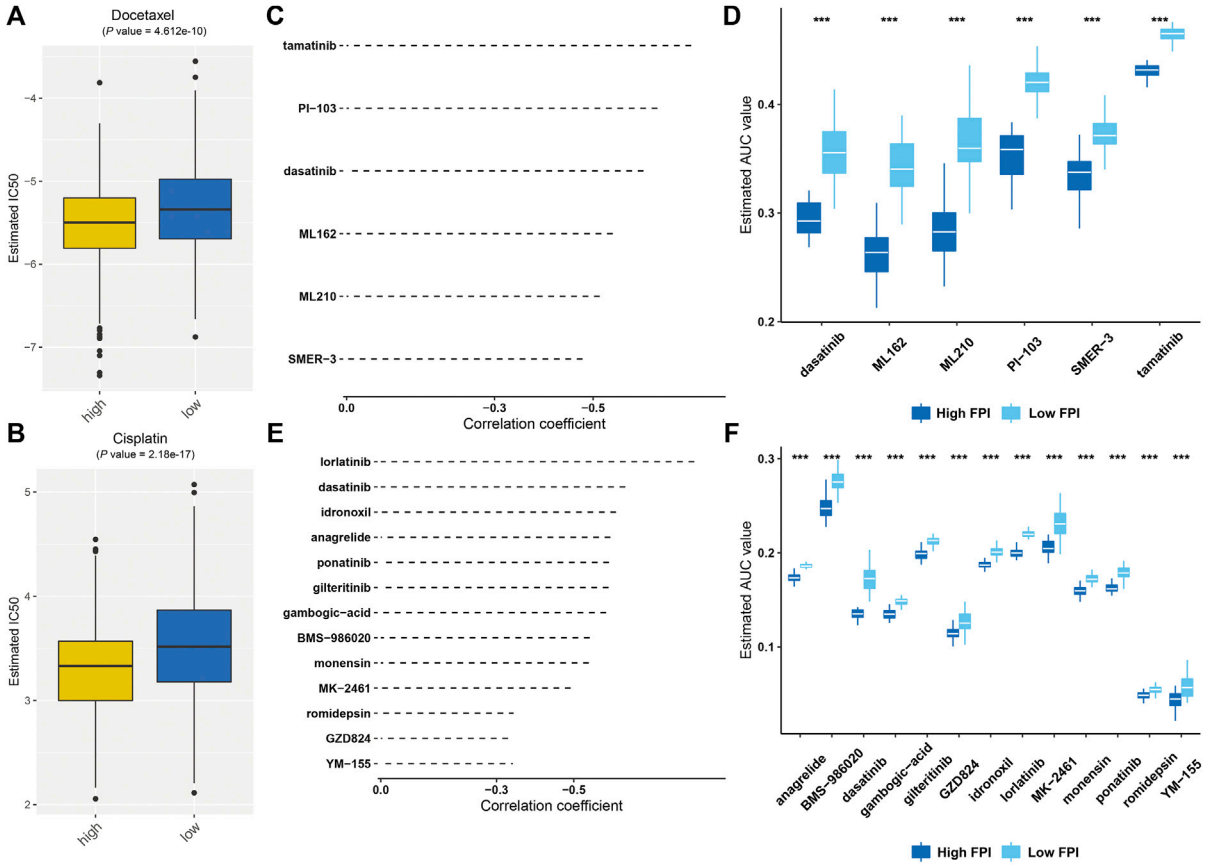

FIGURE 8 | Prediction of potential therapeutic agents against GC based on FPI score. **(A,B)** Comparison of estimated IC50 values of docetaxel and cisplatin in high and low FPI score patients. **(C)** Spearman correlation analysis between FPI score and six CTRP-derived compounds. **(D)** Comparison of the estimated AUC value of six CTRP-derived compounds in high and low FPI score patients. **(E)** Spearman correlation analysis between FPI score and thirteen PRISM-derived compounds. **(F)** Comparison of estimated AUC value of thirteen PRISM-derived compounds in high and low FPI score patients. ***$p < 0.001$.

36%; **Figure 7H**). Similar results were found in the Liu et al. cohort (**Figures 7I,J**).

Prediction of Potential Therapeutic Agents Against Gastric Cancer Based on the Ferroptosis Index Score

We further estimated response to chemotherapy agents, docetaxel and cisplatin. As a result, high FPI samples displayed significantly reduced IC50 values of docetaxel and cisplatin compared with low FPI samples (**Figures 8A,B**), suggesting that high FPI was indicative of higher sensitivity to docetaxel and cisplatin. Furthermore, we predicted six CTRP-derived compounds based on the FPI score, including ML162 (r = −0.54), PI-103 (r = −0.63), tamatinib (r = −0.70), dasatinib (r = −0.60), ML210 (r = −0.51), and SMER-3 (r = −0.48; **Figure 8C**). As shown in **Figure 8D**, patients with a high FPI score were more likely to respond to ML162, PI-103, tamatinib, dasatinib, ML210, and SMER-3. Meanwhile, thirteen PRISM-derived compounds were also predicted, containing monensin (r = −0.54), gambogic-acid (r = −0.58), BMS-986020 (r = −0.54), GZD824 (r = −0.36), ponatinib (r = −0.59), dasatinib (r = −0.63), MK-2461 (r = −0.49), romidepsin (r = −0.38), anagrelide (r = −0.59), gilteritinib (r = −0.59), idronoxil (−0.61), YM-155 (−0.35), and lorlatinib (r = −0.81; **Figure 8E**). Patients with a high FPI score were more likely to benefit from aforementioned compounds (**Figure 8F**).

DISCUSSION

Ferroptosis is a type of iron-dependent necrosis (Chen et al., 2021), which displays morphological, biochemical, and genetic difference from other types of cell death (Friedmann Angeli et al., 2019). Emerging evidence suggests the pivotal roles of ferroptosis in GC pathogenesis (Lee et al., 2020). However, most studies focus on a single ferroptosis regulator, and the overall ferroptosis characterization mediated by a variety of ferroptosis regulators remains not comprehensively determined. Identification of the roles of different ferroptosis-based subtypes may contribute to improving our understanding of ferroptosis in forming TME diversity and complexity, and guiding individualized treatment. Hence, our findings provided a systematic analysis of ferroptosis regulators and characterized the implications of ferroptosis in GC.

Five GC cohorts, namely, TCGA-STAD, GSE84437, GSE62254, GSE26901, and GSE15459, were integrated in this study. We collected 60 ferroptosis regulators and most regulators were distinctly upregulated in GC, indicating the activation of ferroptosis in GC. We investigated that the aberrant expression of ferroptosis regulators was mainly modulated by copy number variation and methylation in GC. Most ferroptosis regulators were in relation to GC prognosis, drug sensitivity, and tumor-infiltrating immune cells, revealing their critical roles in GC progression. Based on them, three ferroptosis subtypes were conducted, characterized by different survival outcomes, hallmark pathway activity, and TME features across GC. The establishment of GC ferroptosis subtypes could accurately predict the patients' clinical outcomes, and TME status. To quantify the ferroptosis level, we developed FPI based on the expression of prognostic ferroptosis-relevant genes. High FPI was indicative of unfavorable clinical outcomes as well as increased grade and stage in GC subjects. This indicated that FPI acted as a reliable tool to assist clinicians in the prediction of GC prognosis as well as to facilitate personalized therapy. GC has pathological and molecular heterogeneity (Qiu et al., 2020). Thus, it is of significance to develop stable prognostic indicators. Our findings indicated that FPI could be applied to comprehensively assess the ferroptosis-based subtypes and their corresponding TME characterization within individual GC patients, and thus guided more effective treatment strategies.

High FPI was in relation to high infiltration levels of innate and adaptive immune cells. Immunotherapy based on ICB has achieved considerable progress; nevertheless, only one-third of patients benefit from ICB (Tang et al., 2020). Ferroptosis induction combined with ICB exhibits synergistically strengthened antitumor activity (Wang et al., 2019). Our results uncovered that FPI might be utilized for predicting response to anti-CTLA4 and anti-PD-1 therapy. This indicated that FPI acted as a promising predictor of immune response. Cisplatin and docetaxel are common chemotherapeutic agents for GC. However, advanced GC patients often acquire resistance to chemotherapy, leading to the median overall survival of only 8–11 months (Zhao et al., 2018). Experimental evidence demonstrates that inducing ferroptosis can overcome resistance to chemotherapy. For instance, ferroptosis induction may alleviate cisplatin resistance in GC through restraining the Nrf2/Keap1/xCT pathway (Fu et al., 2021). SIRT6 silencing may overcome resistance to sorafenib through activating ferroptosis in GC (Cai et al., 2021). Ferroptosis induced by erastin may reverse ABCB1-mediated docetaxel resistance in ovarian cancer (Zhou et al., 2019). Here, high FPI was in relation to the increased sensitivity to cisplatin and docetaxel in GC. Also, six CTRP-derived compounds and thirteen PRISM-derived compounds were predicted for GC patients with high FPI. Hence, the FPI score might be utilized for predicting the therapeutic response of GC patients to chemotherapy. Nevertheless, more experiments are required to verify the clinical efficacy of above compounds against GC.

Nevertheless, our study has certain limitations. First, although ferroptosis-based GC subtypes were verified through multiple datasets and algorithms, more robust experiments are essential for gaining more insights into the underlying mechanisms of different ferroptosis subtypes. Second, independent external datasets and reliable approaches were employed for confirming the FPI score. However, the FPI score was computed and verified on the basis of retrospective data from publicly available datasets. Hence, large-scale prospective clinical cohorts are needed for evaluating its effectiveness and practicability.

CONCLUSION

Taken together, this study carried out a systematic analysis of genomic alterations and expression profiling of ferroptosis regulators in GC. We established three ferroptosis subtypes characterized by different prognosis and tumor-infiltrating immune cells. Moreover, FPI was computed to evaluate the ferroptosis levels according to the expression of prognostic ferroptosis-related signatures. The FPI score was in relation to survival outcomes, hallmark pathways, TME, chemotherapy resistance, and immune response. Our findings highlighted the pivotal roles of ferroptosis as well as the potential of ferroptosis-related therapy in GC. Collectively, the FPI score enabled to comprehensively assess the ferroptosis-based subtypes and characterize TME features for each GC patient, and further guided individualized treatment.

DATA AVAILABILITY STATEMENT

The datasets presented in this study can be found in online repositories. The names of the repository/repositories and accession number(s) can be found in the article/ **Supplementary Material**.

AUTHOR CONTRIBUTIONS

JL conceived and designed the study. JX conducted most of the experiments and data analysis, and wrote the manuscript. LZ participated in collecting data and helped to draft the manuscript. All authors reviewed and approved the manuscript.

FUNDING

This research was supported by Fujian Provincial Health Technology Project (2017-ZQN-18), and Fujian Science and Technology Program (2019J05139 and 2019J01200).

SUPPLEMENTARY MATERIAL

The Supplementary Material for this article can be found online at: https://www.frontiersin.org/articles/10.3389/fphar.2022.919490/full#supplementary-material

REFERENCES

Bindea, G., Mlecnik, B., Tosolini, M., Kirilovsky, A., Waldner, M., Obenauf, A. C., et al. (2013). Spatiotemporal Dynamics of Intratumoral Immune Cells Reveal the Immune Landscape in Human Cancer. *Immunity* 39 (4), 782–795. doi:10.1016/j.immuni.2013.10.003

Bray, F., Ferlay, J., Soerjomataram, I., Siegel, R. L., Torre, L. A., and Jemal, A. (2018). Global Cancer Statistics 2018: GLOBOCAN Estimates of Incidence and Mortality Worldwide for 36 Cancers in 185 Countries. *CA Cancer J. Clin.* 68 (6), 394–424. doi:10.3322/caac.21492

Cai, S., Fu, S., Zhang, W., Yuan, X., Cheng, Y., and Fang, J. (2021). SIRT6 Silencing Overcomes Resistance to Sorafenib by Promoting Ferroptosis in Gastric Cancer. *Biochem. Biophys. Res. Commun.* 577, 158–164. doi:10.1016/j.bbrc.2021.08.080

Cavatorta, O., Scida, S., Miraglia, C., Barchi, A., Nouvenne, A., Leandro, G., et al. (2018). Epidemiology of Gastric Cancer and Risk Factors. *Acta Biomed.* 89 (8-s), 82–87. doi:10.23750/abm.v89i8-S.7966

Chen, H., and Boutros, P. C. (2011). VennDiagram: a Package for the Generation of Highly-Customizable Venn and Euler Diagrams in R. *BMC Bioinforma.* 12, 35. doi:10.1186/1471-2105-12-35

Chen, L., Niu, X., Qiao, X., Liu, S., Ma, H., Shi, X., et al. (2021). Characterization of Interplay between Autophagy and Ferroptosis and Their Synergistical Roles on Manipulating Immunological Tumor Microenvironment in Squamous Cell Carcinomas. *Front. Immunol.* 12, 739039. doi:10.3389/fimmu.2021.739039

Colaprico, A., Silva, T. C., Olsen, C., Garofano, L., Cava, C., Garolini, D., et al. (2016). TCGAbiolinks: an R/Bioconductor Package for Integrative Analysis of TCGA Data. *Nucleic Acids Res.* 44 (8), e71. doi:10.1093/nar/gkv1507

Cristescu, R., Lee, J., Nebozhyn, M., Kim, K. M., Ting, J. C., Wong, S. S., et al. (2015). Molecular Analysis of Gastric Cancer Identifies Subtypes Associated with Distinct Clinical Outcomes. *Nat. Med.* 21 (5), 449–456. doi:10.1038/nm.3850

Du, P., Kibbe, W. A., and Lin, S. M. (2008). Lumi: a Pipeline for Processing Illumina Microarray. *Bioinformatics* 24 (13), 1547–1548. doi:10.1093/bioinformatics/btn224

Friedmann Angeli, J. P., Krysko, D. V., and Conrad, M. (2019). Ferroptosis at the Crossroads of Cancer-Acquired Drug Resistance and Immune Evasion. *Nat. Rev. Cancer* 19 (7), 405–414. doi:10.1038/s41568-019-0149-1

Fu, D., Wang, C., Yu, L., and Yu, R. (2021). Induction of Ferroptosis by ATF3 Elevation Alleviates Cisplatin Resistance in Gastric Cancer by Restraining Nrf2/Keap1/xCT Signaling. *Cell Mol. Biol. Lett.* 26 (1), 26. doi:10.1186/s11658-021-00271-y

Gautier, L., Cope, L., Bolstad, B. M., and Irizarry, R. A. (2004). Affy--Analysis of Affymetrix GeneChip Data at the Probe Level. *Bioinformatics* 20 (3), 307–315. doi:10.1093/bioinformatics/btg405

Geeleher, P., Cox, N., and Huang, R. S. (2014). pRRophetic: an R Package for Prediction of Clinical Chemotherapeutic Response from Tumor Gene Expression Levels. *PLoS One* 9 (9), e107468. doi:10.1371/journal.pone.0107468

Ghandi, M., Huang, F. W., Jané-Valbuena, J., Kryukov, G. V., Lo, C. C., McDonald, E. R., 3rd, et al. (2019). Next-generation Characterization of the Cancer Cell Line Encyclopedia. *Nature* 569 (7757), 503–508. doi:10.1038/s41586-019-1186-3

Guan, Z., Chen, J., Li, X., and Dong, N. (2020). Tanshinone IIA Induces Ferroptosis in Gastric Cancer Cells through P53-Mediated SLC7A11 Down-Regulation. *Biosci. Rep.* 40 (8), BSR20201807. doi:10.1042/bsr20201807

Hänzelmann, S., Castelo, R., and Guinney, J. (2013). GSVA: Gene Set Variation Analysis for Microarray and RNA-Seq Data. *BMC Bioinforma.* 14, 7. doi:10.1186/1471-2105-14-7

Hugo, W., Zaretsky, J. M., Sun, L., Song, C., Moreno, B. H., Hu-Lieskovan, S., et al. (2016). Genomic and Transcriptomic Features of Response to Anti-PD-1 Therapy in Metastatic Melanoma. *Cell* 165 (1), 35–44. doi:10.1016/j.cell.2016.02.065

Jiang, P., Gu, S., Pan, D., Fu, J., Sahu, A., Hu, X., et al. (2018). Signatures of T Cell Dysfunction and Exclusion Predict Cancer Immunotherapy Response. *Nat. Med.* 24 (10), 1550–1558. doi:10.1038/s41591-018-0136-1

Lee, J. Y., Nam, M., Son, H. Y., Hyun, K., Jang, S. Y., Kim, J. W., et al. (2020). Polyunsaturated Fatty Acid Biosynthesis Pathway Determines Ferroptosis Sensitivity in Gastric Cancer. *Proc. Natl. Acad. Sci. U. S. A.* 117 (51), 32433–32442. doi:10.1073/pnas.2006828117

Leek, J. T., Johnson, W. E., Parker, H. S., Jaffe, A. E., and Storey, J. D. (2012). The Sva Package for Removing Batch Effects and Other Unwanted Variation in High-Throughput Experiments. *Bioinformatics* 28 (6), 882–883. doi:10.1093/bioinformatics/bts034

Lei, Z., Tan, I. B., Das, K., Deng, N., Zouridis, H., Pattison, S., et al. (2013). Identification of Molecular Subtypes of Gastric Cancer with Different Responses to PI3-Kinase Inhibitors and 5-fluorouracil. *Gastroenterology* 145 (3), 554–565. doi:10.1053/j.gastro.2013.05.010

Liberzon, A., Birger, C., Thorvaldsdóttir, H., Ghandi, M., Mesirov, J. P., and Tamayo, P. (2015). The Molecular Signatures Database (MSigDB) Hallmark Gene Set Collection. *Cell Syst.* 1 (6), 417–425. doi:10.1016/j.cels.2015.12.004

Liu, D., Schilling, B., Liu, D., Sucker, A., Livingstone, E., Jerby-Arnon, L., et al. (2019). Integrative Molecular and Clinical Modeling of Clinical Outcomes to PD1 Blockade in Patients with Metastatic Melanoma. *Nat. Med.* 25 (12), 1916–1927. doi:10.1038/s41591-019-0654-5

Liu, Y., Song, Z., Liu, Y., Ma, X., Wang, W., Ke, Y., et al. (2021). Identification of Ferroptosis as a Novel Mechanism for Antitumor Activity of Natural Product Derivative A2 in Gastric Cancer. *Acta Pharm. Sin. B* 11 (6), 1513–1525. doi:10.1016/j.apsb.2021.05.006

Mariathasan, S., Turley, S. J., Nickles, D., Castiglioni, A., Yuen, K., Wang, Y., et al. (2018). TGFβ Attenuates Tumour Response to PD-L1 Blockade by Contributing to Exclusion of T Cells. *Nature* 554 (7693), 544–548. doi:10.1038/nature25501

Mayakonda, A., Lin, D. C., Assenov, Y., Plass, C., and Koeffler, H. P. (2018). Maftools: Efficient and Comprehensive Analysis of Somatic Variants in Cancer. *Genome Res.* 28 (11), 1747–1756. doi:10.1101/gr.239244.118

Ni, H., Qin, H., Sun, C., Liu, Y., Ruan, G., Guo, Q., et al. (2021). MiR-375 Reduces the Stemness of Gastric Cancer Cells through Triggering Ferroptosis. *Stem Cell Res. Ther.* 12 (1), 325. doi:10.1186/s13287-021-02394-7

Niu, X., Chen, L., Li, Y., Hu, Z., and He, F. (2022). Ferroptosis, Necroptosis, and Pyroptosis in the Tumor Microenvironment: Perspectives for Immunotherapy of SCLC. *Semin. Cancer Biol.* doi:10.1016/j.semcancer.2022.03.009

Oh, S. C., Sohn, B. H., Cheong, J. H., Kim, S. B., Lee, J. E., Park, K. C., et al. (2018). Clinical and Genomic Landscape of Gastric Cancer with a Mesenchymal Phenotype. *Nat. Commun.* 9 (1), 1777. doi:10.1038/s41467-018-04179-8

Qiu, X. T., Song, Y. C., Liu, J., Wang, Z. M., Niu, X., and He, J. (2020). Identification of an Immune-Related Gene-Based Signature to Predict Prognosis of Patients with Gastric Cancer. *World J. Gastrointest. Oncol.* 12 (8), 857–876. doi:10.4251/wjgo.v12.i8.857

Ritchie, M. E., Phipson, B., Wu, D., Hu, Y., Law, C. W., Shi, W., et al. (2015). Limma Powers Differential Expression Analyses for RNA-Sequencing and Microarray Studies. *Nucleic Acids Res.* 43 (7), e47. doi:10.1093/nar/gkv007

Rosenberg, J. E., Hoffman-Censits, J., Powles, T., van der Heijden, M. S., Balar, A. V., Necchi, A., et al. (2016). Atezolizumab in Patients with Locally Advanced and Metastatic Urothelial Carcinoma Who Have Progressed Following Treatment with Platinum-Based Chemotherapy: a Single-Arm, Multicentre, Phase 2 Trial. *Lancet* 387 (10031), 1909–1920. doi:10.1016/s0140-6736(16)00561-4

Şenbabaoğlu, Y., Gejman, R. S., Winer, A. G., Liu, M., Van Allen, E. M., de Velasco, G., et al. (2016). Tumor Immune Microenvironment Characterization in Clear Cell Renal Cell Carcinoma Identifies Prognostic and Immunotherapeutically Relevant Messenger RNA Signatures. *Genome Biol.* 17 (1), 231. doi:10.1186/s13059-016-1092-z

Shao, Y., Geng, Y., Gu, W., Ning, Z., Huang, J., Pei, H., et al. (2016). Assessment of Lymph Node Ratio to Replace the pN Categories System of Classification of the TNM System in Esophageal Squamous Cell Carcinoma. *J. Thorac. Oncol.* 11 (10), 1774–1784. doi:10.1016/j.jtho.2016.06.019

Sohn, B. H., Hwang, J.-E., Jang, H.-J., Lee, H.-S., Oh, S. C., Shim, J.-J., et al. (2017). Clinical Significance of Four Molecular Subtypes of Gastric Cancer Identified by the Cancer Genome Atlas Project. *Clin. Cancer Res.* 23, 4441–4449. doi:10.1158/1078-0432.Ccr-16-2211

Tang, R., Xu, J., Zhang, B., Liu, J., Liang, C., Hua, J., et al. (2020). Ferroptosis, Necroptosis, and Pyroptosis in Anticancer Immunity. *J. Hematol. Oncol.* 13 (1), 110. doi:10.1186/s13045-020-00946-7

Wang, W., Green, M., Choi, J. E., Gijón, M., Kennedy, P. D., Johnson, J. K., et al. (2019). CD8(+) T Cells Regulate Tumour Ferroptosis during Cancer Immunotherapy. *Nature* 569 (7755), 270–274. doi:10.1038/s41586-019-1170-y

Wang, X., Cheng, G., Miao, Y., Qiu, F., Bai, L., Gao, Z., et al. (2021). Piezo Type Mechanosensitive Ion Channel Component 1 Facilitates Gastric Cancer Omentum Metastasis. *J. Cell Mol. Med.* 25 (4), 2238–2253. doi:10.1111/jcmm.16217

Wilkerson, M. D., and Hayes, D. N. (2010). ConsensusClusterPlus: a Class Discovery Tool with Confidence Assessments and Item Tracking. *Bioinformatics* 26 (12), 1572–1573. doi:10.1093/bioinformatics/btq170

Yan, H. H. N., Siu, H. C., Law, S., Ho, S. L., Yue, S. S. K., Tsui, W. Y., et al. (2018). A Comprehensive Human Gastric Cancer Organoid Biobank Captures Tumor Subtype Heterogeneity and Enables Therapeutic Screening. *Cell Stem Cell* 23 (6), 882–897.e11. doi:10.1016/j.stem.2018.09.016

Yang, W., Soares, J., Greninger, P., Edelman, E. J., Lightfoot, H., Forbes, S., et al. (2013). Genomics of Drug Sensitivity in Cancer (GDSC): a Resource for Therapeutic Biomarker Discovery in Cancer Cells. *Nucleic Acids Res.* 41 (Database issue), D955–D961. doi:10.1093/nar/gks1111

Yoon, S. J., Park, J., Shin, Y., Choi, Y., Park, S. W., Kang, S. G., et al. (2020). Deconvolution of Diffuse Gastric Cancer and the Suppression of CD34 on the BALB/c Nude Mice Model. *BMC Cancer* 20 (1), 314. doi:10.1186/s12885-020-06814-4

Yu, G., Wang, L. G., Han, Y., and He, Q. Y. (2012). clusterProfiler: an R Package for Comparing Biological Themes Among Gene Clusters. *Omics* 16 (5), 284–287. doi:10.1089/omi.2011.0118

Zhang, H., Meltzer, P., and Davis, S. (2013). RCircos: an R Package for Circos 2D Track Plots. *BMC Bioinforma.* 14, 244. doi:10.1186/1471-2105-14-244

Zhang, H., Deng, T., Liu, R., Ning, T., Yang, H., Liu, D., et al. (2020). CAF Secreted miR-522 Suppresses Ferroptosis and Promotes Acquired Chemo-Resistance in Gastric Cancer. *Mol. Cancer* 19 (1), 43. doi:10.1186/s12943-020-01168-8

Zhao, T. T., Xu, H., Xu, H. M., Wang, Z. N., Xu, Y. Y., Song, Y. X., et al. (2018). The Efficacy and Safety of Targeted Therapy with or without Chemotherapy in Advanced Gastric Cancer Treatment: a Network Meta-Analysis of Well-Designed Randomized Controlled Trials. *Gastric Cancer* 21 (3), 361–371. doi:10.1007/s10120-018-0813-2

Zhou, H. H., Chen, X., Cai, L. Y., Nan, X. W., Chen, J. H., Chen, X. X., et al. (2019). Erastin Reverses ABCB1-Mediated Docetaxel Resistance in Ovarian Cancer. *Front. Oncol.* 9, 1398. doi:10.3389/fonc.2019.01398

Conflict of Interest: The authors declare that the research was conducted in the absence of any commercial or financial relationships that could be construed as a potential conflict of interest.

Publisher's Note: All claims expressed in this article are solely those of the authors and do not necessarily represent those of their affiliated organizations, or those of the publisher, the editors, and the reviewers. Any product that may be evaluated in this article, or claim that may be made by its manufacturer, is not guaranteed or endorsed by the publisher.

frontiers | Frontiers in Pharmacology

TYPE Original Research
PUBLISHED 17 August 2022
DOI 10.3389/fphar.2022.932526

OPEN ACCESS

EDITED BY
Essa M. Saied,
Humboldt University of Berlin, Germany

REVIEWED BY
Shamshad Alam,
University at Buffalo, United States
Ishtiaque Ahammad,
National Institute of Biotechnology, Bangladesh

*CORRESPONDENCE
Maoshu Zhu,
zhumaoshu123@126.com
Tai-Wei Ng,
ngtaiwei@163.com
Xiaojie Cui,
752187738@qq.com

SPECIALTY SECTION
This article was submitted to Pharmacology of Anti-Cancer Drugs, a section of the journal Frontiers in Pharmacology

RECEIVED 29 April 2022
ACCEPTED 27 June 2022
PUBLISHED 17 August 2022

CITATION
Wang Z, Liu J, Li M, Lian L, Cui X, Ng T-W and Zhu M (2022), Integrated bioinformatics analysis uncovers characteristic genes and molecular subtyping system for endometriosis. *Front. Pharmacol.* 13:932526. doi: 10.3389/fphar.2022.932526

Integrated bioinformatics analysis uncovers characteristic genes and molecular subtyping system for endometriosis

Zhaowei Wang, Jia Liu, Miaoli Li, Lishan Lian, Xiaojie Cui*, Tai-Wei Ng* and Maoshu Zhu*

The Fifth Hospital of Xiamen, Xiamen, Fujian, China

Objective: Endometriosis is a chronic inflammatory estrogen-dependent disease with the growth of endometrial tissues outside the uterine cavity. Nevertheless, the etiology of endometriosis is still unclear. Integrated bioinformatics analysis was implemented to reveal the molecular mechanisms underlying this disease.

Methods: A total of four gene expression datasets (GSE7305, GSE11691, GSE23339, and GSE25628) were retrieved from the GEO, which were merged into a meta-dataset, followed by the removal of batch effects via the sva package. Weighted gene co-expression network analysis (WGCNA) was implemented, and endometriosis-related genes were screened under normal and endometriosis conditions. Thereafter, characteristic genes were determined via Lasso analysis. The diagnostic performance was estimated via receiver operating characteristic curves, and epigenetic and post-transcriptional modifications were analyzed. Small molecular compounds were predicted. Unsupervised clustering analysis was conducted via non-negative matrix factorization algorithm. The enriched pathways were analyzed via gene set enrichment analysis or GSVA. Immune features were evaluated according to immune-checkpoints, HLA, receptors, chemokines, and immune cells.

Results: In total, four characteristic genes (BGN, AQP1, ELMO1, and DDR2) were determined for endometriosis, all of which exhibited the favorable efficacy in diagnosing endometriosis. Their aberrant levels were modulated by epigenetic and post-transcriptional modifications. In total, 51 potential drugs were predicted against endometriosis. The characteristic genes exhibited remarkable associations with immunological function. Three subtypes were classified across endometriosis, with different mechanisms and immune features.

Abbreviations: WGCNA, weighted gene co-expression network analysis; NMF, non-negative matrix factorization; GEO, Gene Expression Omnibus; ROC, receiver operating characteristic; GSEA, gene set enrichment analysis; FDR, false discovery rate; Cmap, Connectivity Map; PCA, principal component analysis; AUC, area under the curve.

Conclusion: Our study reveals the characteristic genes and novel molecular subtyping of endometriosis, contributing to the early diagnosis and intervention in endometriosis.

KEYWORDS

endometriosis, characteristic genes, molecular subtypes, diagnosis, immune characteristics

Introduction

Endometriosis is a chronic inflammatory estrogen-dependent disease caused by functional endometrial tissue that grows outside the uterine cavity (Hung et al., 2021). Typical symptoms involve chronic pelvic pain and abnormal menstruation as well as dyspareunia (Bunis et al., 2021). Endometriosis is frequent among women of childbearing age, with an incidence of about 10% (Symons et al., 2018). About 40–60% of endometriosis cases have dysmenorrhea, while 20–30% have infertility (Bedaiwy, 2022). The present therapies of endometriosis comprise surgery and medicines. Conservative surgery not only enables to remove endometriotic deposits but also enhances the risks of compromising ovarian reserve, which harms other organs as well as imposes postoperative relapse (Hey-Cunningham et al., 2022). Medicines that contain hormonal or nonhormonal therapies depend upon distinct factors (severity of symptoms, willingness to conceive, and comorbidities, etc.) (Brichant et al., 2021). Currently, no drugs are capable of curing endometriosis, and symptoms recur once the drug is discontinued. As a consequence, it is crucial to uncover the aberrant molecular pathways during endometriosis progression as well as determine and develop novel pharmaceuticals for endometriosis.

Endometriotic lesions contain an extremely complex and dynamic environment dominated by inflammation, angiogenesis, and endocrine signaling (Hirakawa et al., 2016). A variety of pathogenic mechanisms result in endometriosis initiation, with much research exploring the reason behind its progression, containing physical factors (uterine tissue injury or scars, residual cell populations in menstrual blood, stem cell populations, and uterine environment, etc.) as well as biochemical factors (angiogenesis, etc.) (Kapoor et al., 2021). It is of importance to probe the key mechanisms responsible for endometriosis. Through illustrating the molecular mechanisms underlying endometriosis, it is of possibility to determine the future candidate pathways for endometriosis therapies. Our study determined characteristic genes of endometriosis via integration of weighted gene co-expression network analysis (WGCNA) and Lasso approaches, as well as classified endometriosis into three distinct subtypes via a non-negative matrix factorization (NMF) clustering approach, assisting to comprehend the mechanisms underlying endometriosis.

Materials and methods

Endometriosis datasets and preprocessing

Human endometriosis gene expression datasets were retrieved from the Gene Expression Omnibus (GEO; https://www.ncbi.nlm.nih.gov/gds/). In total, four available datasets (GSE7305 (10 normal endometrium tissues and 10 diseased endometrium tissues) (Hever et al., 2007), GSE11691 (9 normal endometrium tissues and 9 diseased endometrium tissues) (Hull et al., 2008), GSE23339 (9 normal endometrium tissues and 10 diseased endometrium tissues) (Hawkins et al., 2011), and GSE25628 (6 normal endometrium tissues and 16 diseased endometrium tissues) (Crispi et al., 2013)) were collected. The raw "CEL" files of aforementioned datasets were downloaded, which were adjusted for the background and normalized with affy (Gautier et al., 2004) and simpleaffy (Wilson and Miller, 2005) packages. Thereafter, these datasets were merged into a meta-dataset, and then the batch effects were removed via the sva package (Supplementary Figures S1A,B) (Leek et al., 2012). Additionally, the GSE7846 dataset comprising expression profiling of endometrial endothelial cells from five endometriosis patients and five controls was utilized as an external verification set.

WGCNA

The WGCNA package (Langfelder and Horvath, 2008) was employed for constructing the co-expression networks as well as determining the endometriosis-related modules. Hierarchical clustering analysis was implemented, followed by the removal of outlier specimens. The appropriate soft-thresholding power was computed, and the scale-free networks were built. The co-expression modules were clustered with a dynamic tree-cut approach. The endometriosis-related genes in the modules that were highly correlated to endometriosis were determined. Thereafter, correlation analysis of module membership with gene significance was implemented.

Functional and pathway enrichment analysis

Functional annotation of endometriosis-related genes was implemented via the clusterProfiler package (Yu et al., 2012). $p < 0.05$ indicated significant enrichment of Gene Ontology and KEGG. Through the GSVA package (Hänzelmann et al., 2013), the enrichment analysis was conducted for ascertaining the difference in pathways among distinct clusters. The gene sets of "c2. cp.kegg.v7.5.1. symbols" and "c5. go.bp.v7.5.1. symbols" were acquired from the Molecular Signatures Database to run GSVA enrichment analysis (Liberzon et al., 2015).

Screening characteristic genes

Through Lasso Cox regression algorithm, over-fitting risk was minimized with the glmnet package. The alteration trajectory of each variable was assessed and 10-fold cross-validated. Thereafter, characteristic genes were determined, which were subjected to the generation of receiver operating characteristic (ROC) curves.

Construction of a nomogram

A predictive nomogram was constructed with the rms package. In the nomogram, each variable corresponded to a score, and the total score was computed through adding the scores for all variables (Chen et al., 2021). A calibration diagram of the nomogram was implemented for depicting the diagnostic value of the nomogram-predicted and virtually observed outcome.

Gene set enrichment analysis

To analyze the biological pathways enriched in high or low level of each characteristic gene, GSEA software was employed with default parameters (Subramanian et al., 2005). The cutoff point of each gene was determined as the median expression value. The most enriched pathways were visualized.

Analysis of epigenetic and post-transcriptional modifications

Associations of DNA methylation and m^6A regulators with characteristic genes were evaluated with Pearson correlation tests. MiRNAs with differential expression between normal and diseased endometrium tissues were screened with the false discovery rate (FDR) < 0.05. Thereafter, targeted mRNAs of these miRNAs were then predicted, which were intersected with characteristic genes.

Prediction of potential drugs

Genes with differential expression between normal and diseased endometrium tissues were determined in accordance with |log fold-change| >1 and FDR <0.05 via the limma package (Ritchie et al., 2015). The up- or downregulated genes were uploaded onto the Connectivity Map (Cmap) database (Yang et al., 2013). Scores that ranged from −1 to 1 demonstrated the correlations of compounds with the aforementioned genes. Compounds with scores ≤ −0.75 were considered potential drugs against endometriosis.

Evaluation of immune features

The gene sets of immune-checkpoints, HLA, receptors, and chemokines were collected. Through running CIBERSORT algorithm, the relative proportions of 22 immune compositions were estimated (Newman et al., 2015). On the basis of a gene expression matrix as well as specific gene sets of 22 immune cell compositions, the simulation calculation was implemented 1,000 times. The relative composition ratios of these immune cells across each tissue were computed. Immune and stromal scores of each tissue were computed with the ESTIMATE algorithm (Yoshihara et al., 2013).

Non-negative matrix factorization clustering analysis

Endometriosis-related genes were utilized for NMF clustering analysis, and clusters were determined in the meta-cohort. The k-value where the magnitude of the cophenetic correlation coefficients began to fall was determined as the optimal number of clusters. The heatmaps of endometriosis-related genes and basis component as well as connectivity matrix of NMF in each cluster were evaluated via the NMF package (Pan and Gillis, 2021). Principal component analysis (PCA) was depicted with the ggplot2 package.

Statistical analysis

Statistical analysis was implemented with R version 4.1.0, with two-sided p-value ≤0.05. Student's t, Wilcoxon, Kruskal–Wallis, or one-way ANOVA test was utilized for estimating the differences of variables between groups. The area under the curve (AUC) values were computed for estimating the predictive power of each characteristic gene.

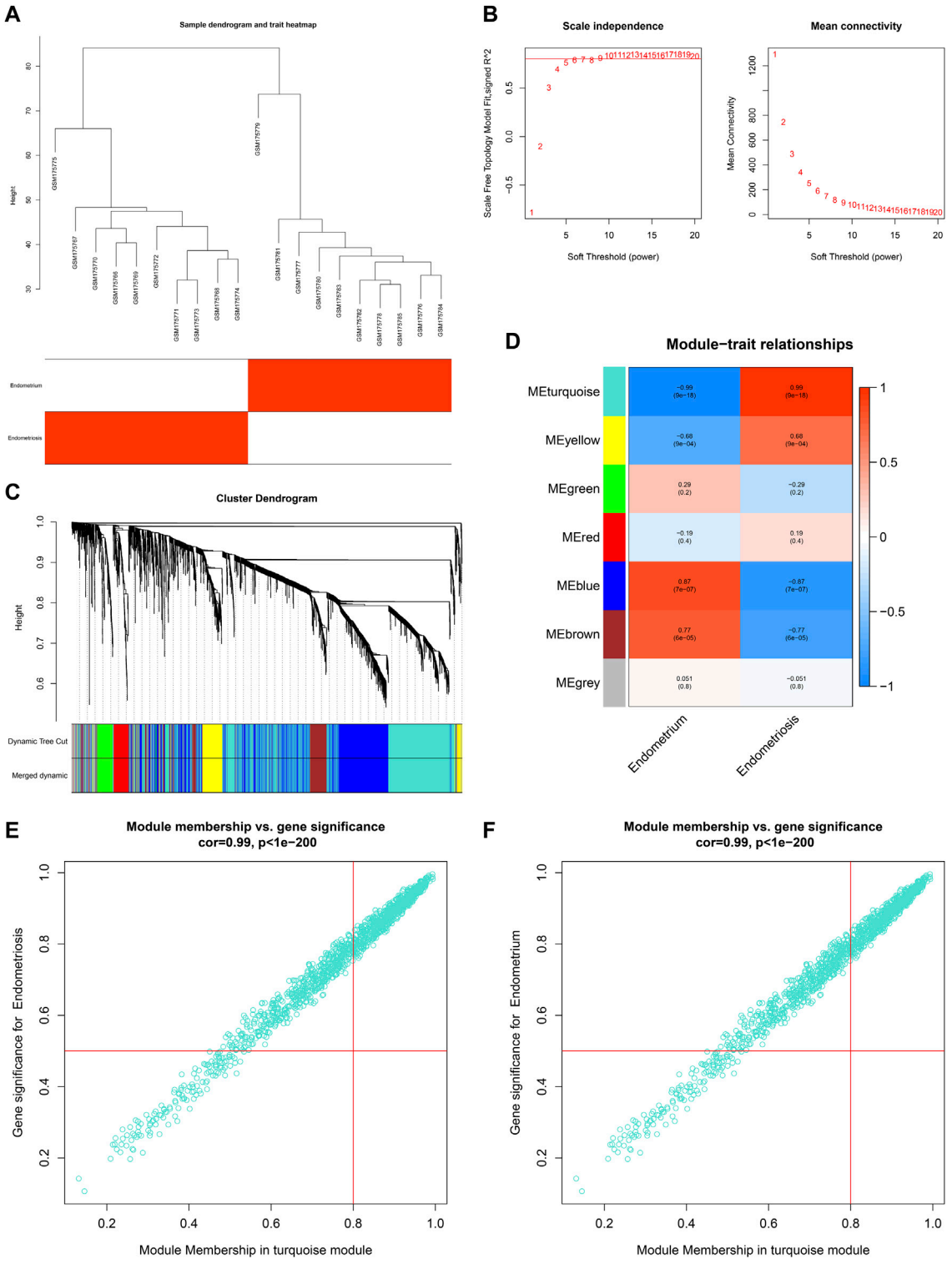

FIGURE 1
Co-expression analysis in the GSE7305 dataset. **(A)** Clustering dendrograms of specimens. **(B)** Determining the weighted value β that satisfied a scale-free network. **(C)** Co-expression module clustering. Each branch represented each gene, and genes clustered into the same module were assigned the same color. **(D)** Correlations of modules with normal endometrium and endometriosis conditions. **(E,F)** Scatter plots for the relationships of module membership in the turquoise module with gene significance for **(E)** endometriosis or **(F)** normal endometrium.

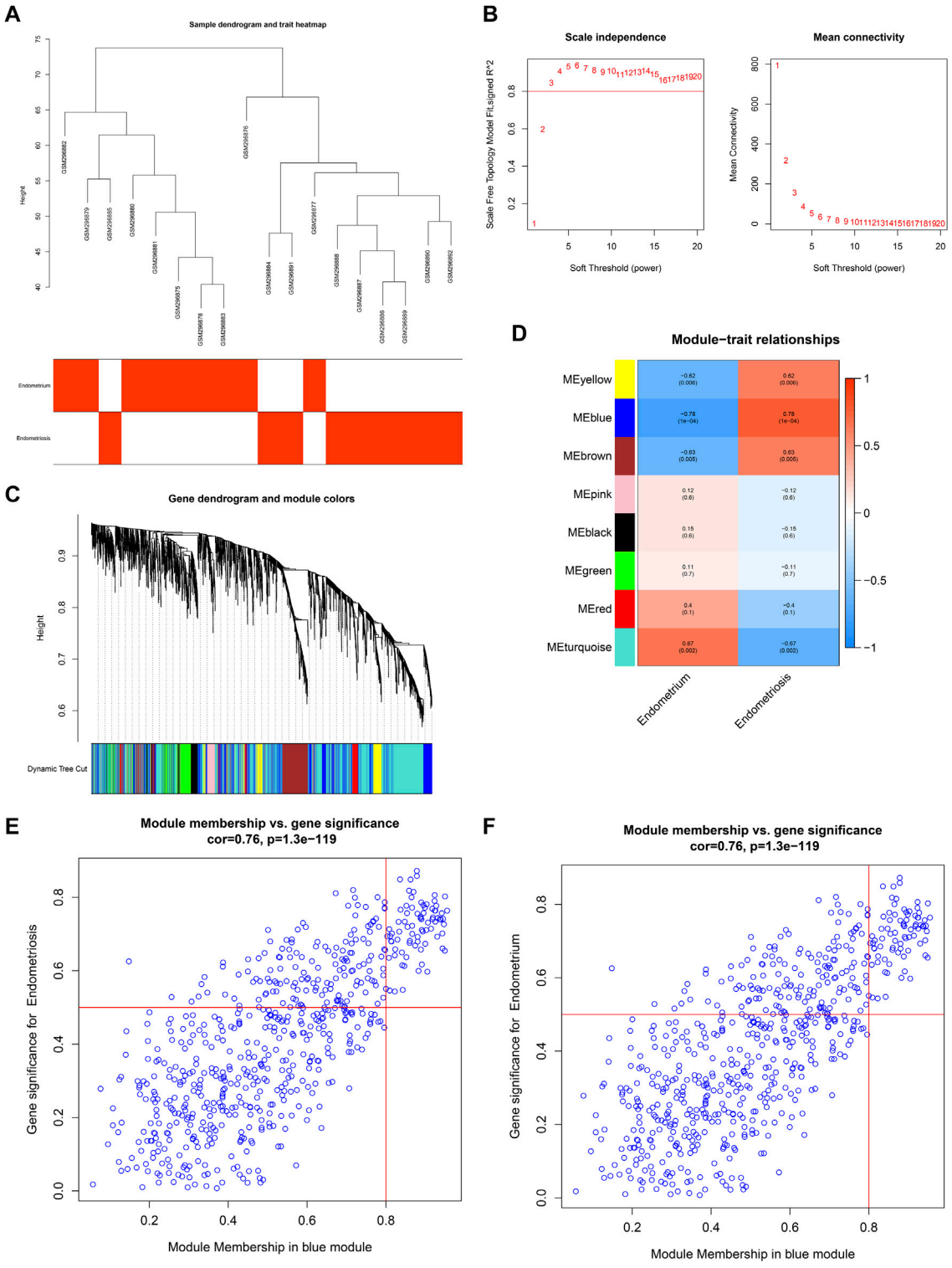

FIGURE 2
Co-expression analysis in the GSE11691 dataset. **(A)** Clustering dendrograms of samples. **(B)** Identifying β-value that satisfied a scale-free network. **(C)** Co-expression module clustering. **(D)** Correlations of modules with normal endometrium and endometriosis conditions. **(E,F)** Scatter plots for the relationships of module membership in the blue module with gene significance for **(E)** endometriosis or **(F)** normal endometrium.

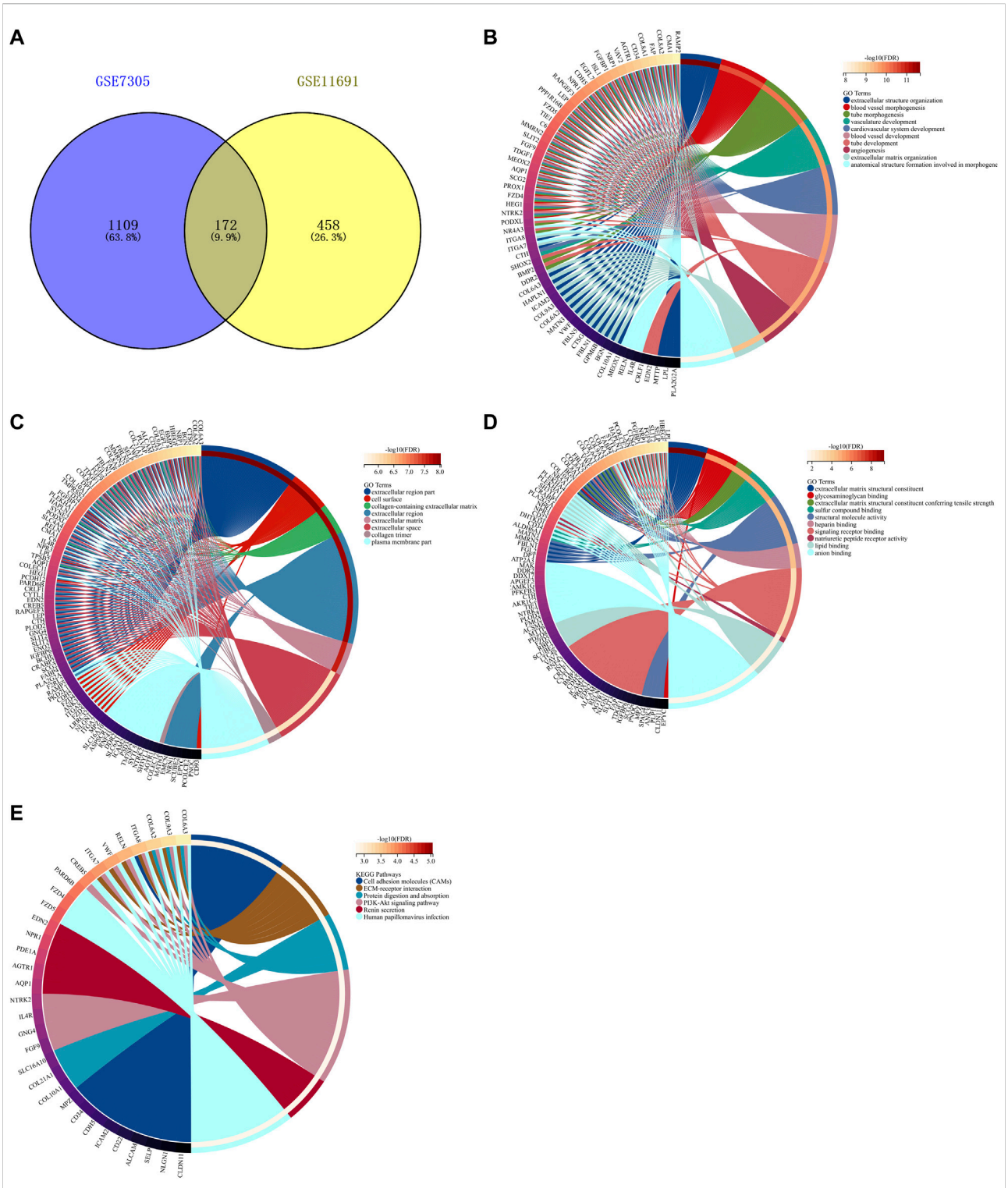

FIGURE 3
Identification of shared endometriosis-related genes in two datasets. **(A)** Venn diagram for shared endometriosis-related genes in the GSE7305 and GSE11691 datasets. **(B–E)** Biological processes, cellular components, molecular functions, and KEGG pathways enriched by shared endometriosis-related genes.

The Spearman or Pearson correlation test was conducted to estimate the relationships between variables.

Results

Co-expression analysis of endometriosis and normal endometrium tissues

Co-expression analysis was implemented in two public datasets: GSE7305 and GSE11691. For the GSE7305 dataset, we first conducted clustering dendrograms of 10 normal endometrium tissues and 10 diseased endometrium tissues, with no outliers (Figure 1A). The weighted value β satisfied a scale-free network (Figure 1B). The seven co-expression modules were merged (Figure 1C), containing blue module (847 genes), brown module (273 genes), red module (129 genes), green module (156 genes), yellow module (231 genes), turquoise module (1,283 genes), and gray module (93 genes). Among them, the turquoise module had the strongest positive association with endometriosis (r = 0.99, p = 9e-18) as well as the strongest negative association with normal endometrium (r = -0.99, p = 9e-18) (Figure 1D). Additionally, the module membership in the turquoise module was strongly linked to gene significance for endometriosis or normal endometrium (Figures 1E,F). Hence, the genes in the turquoise module were identified as endometriosis-related genes in the GSE7305 dataset.

For the GSE11691 dataset, no outliers were detected among nine normal endometrium tissues and nine diseased endometrium tissues (Figure 2A). The β-value was set at 3, which satisfied a scale-free network (Figure 2B). Eight co-expression modules were identified (Figure 2C), turquoise module (1,315 genes), red module (111 genes), green module (229 genes), black module (110 genes), pink module (74 genes), brown module (298 genes), blue module (632 genes), and yellow module (251 genes). Among them, the blue module displayed the strongest positive correlation with endometriosis (r = 0.78, p = 1e-04) as well as the strongest negative correlation with normal endometrium (r = −0.78, p = 1e-04) (Figure 2D). As depicted in Figures 2E,F, the module membership in the blue module was strongly associated with gene significance for endometriosis or normal endometrium. Thus, the genes in the blue module were identified as endometriosis-related genes in the GSE11691 dataset.

Identification of shared endometriosis-related genes in two datasets

By taking the intersection of endometriosis-related genes in GSE7305 and GSE11691 datasets, we determined 172 shared endometriosis-related genes (Figure 3A, Supplementary Table S1). The shared endometriosis-related genes might mediate tube development, angiogenesis, and endometriosis-related pathways (PI3K-Akt pathway and extracellular matrix (ECM), etc.), demonstrating the crucial functions of the aforementioned genes in endometriosis (Figures 3B–E).

Identification of four characteristic genes in endometriosis

Through Lasso algorithm, four characteristic genes were determined among the shared endometriosis-related genes, containing BGN, AQP1, ELMO1, and DDR2 (Figures 4A,B). In the meta-dataset, their levels were significantly upregulated in endometriosis than normal endometrium tissues (Figure 4C). The AUCs (95%CI) of AQP1, BGN, DDR2, and ELMO1 were 0.96 (1.00–0.89), 0.98 (1.00–0.95), 1.00 (1.00–0.99), and 0.99 (1.00–0.98), respectively, demonstrating that each characteristic gene enabled to diagnose endometriosis accurately and sensitively (Figures 4D–G).

Construction of a nomogram scoring system to diagnose endometriosis

Considering the convenience clinical utility, a nomogram incorporating all characteristic genes was constructed to diagnose endometriosis (Figure 4H). Calibration plots showed that the proposed nomogram exhibited the similar performance in comparison to an ideal model (Figure 4I), demonstrating the excellent predictive accuracy in endometriosis diagnosis.

Verification of levels and diagnostic efficacy of characteristic genes in endometriosis

The GSE23339 and GSE25628 datasets were employed for further verifying the levels and diagnostic efficacy of four characteristic genes in endometriosis. In the two datasets, higher levels of BGN, AQP1, ELMO1, and DDR2 were confirmed in endometriosis than normal endometrium tissues (Figures 5A,B). In the GSE23339 dataset, the AUCs (95%CI) of AQP1, BGN, DDR2, and ELMO1 were 0.81 (1.00–0.57), 0.97 (1.00–0.89), 0.69 (0.94–0.44), and 0.88 (1.00–0.70), respectively (Figures 5C–F). Meanwhile, in the GSE25628 dataset, the AUCs (95%CI) of BGN, AQP1, ELMO1, and DDR2 were 0.90 (1.00–0.69), 0.85 (1.00–0.68), 0.81 (1.00–0.62), and 0.81 (1.00–0.59), respectively (Figures 5G–J). Additionally, in the GSE7846 external verification set, the AUCs (95%CI) of the aforementioned characteristic genes were 0.68 (1.00–0.27), 0.68 (1.00–0.27), 0.84 (1.00–0.52), and 0.52 (0.97–0.07), respectively (Figures 5K–N). Following verifications, the four characteristic genes exhibited the well performance in diagnosing endometriosis.

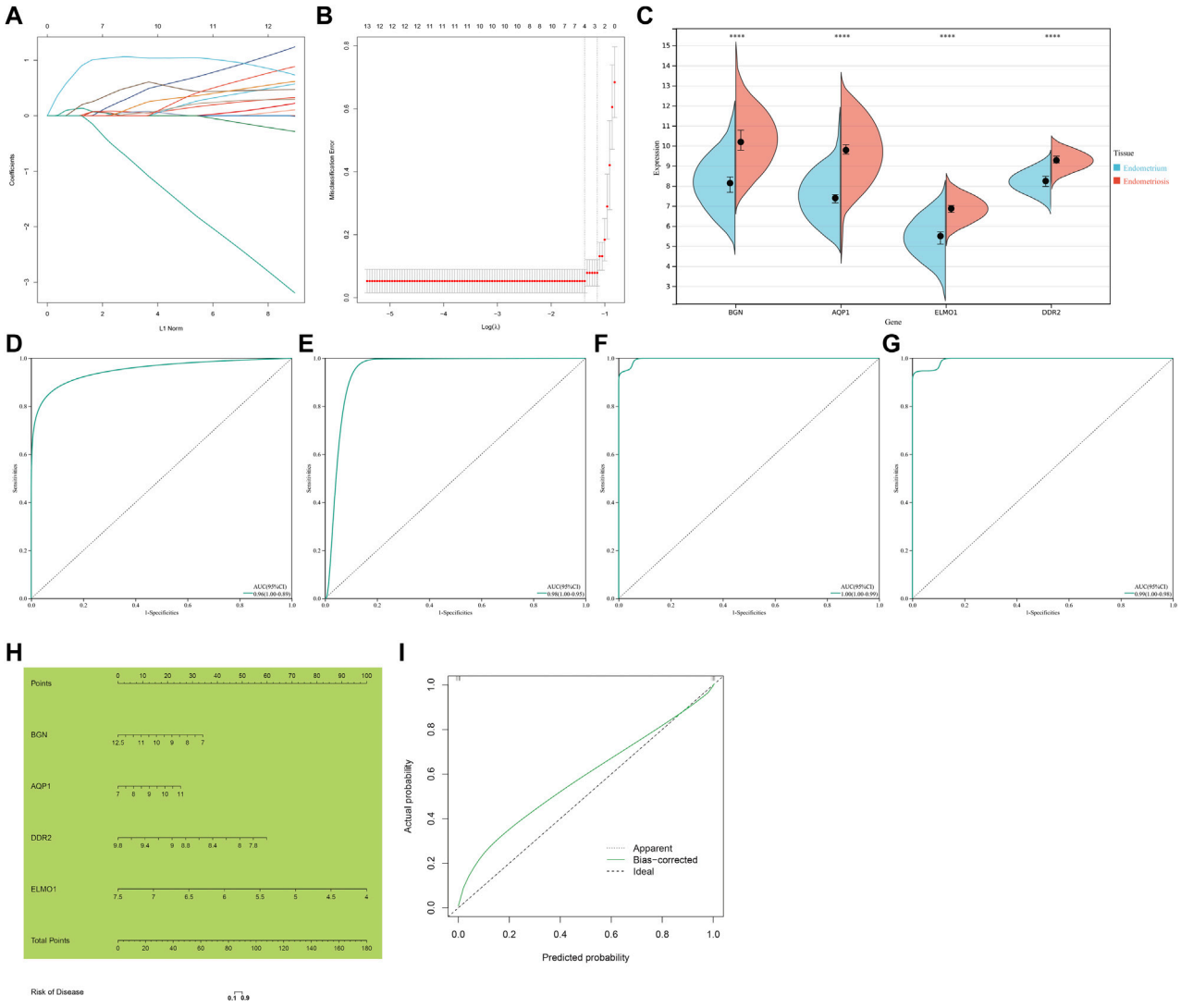

FIGURE 4
Identification of four characteristic genes and construction of a nomogram scoring system for endometriosis. **(A)** Lasso regression coefficients. Different colors represented different shared endometriosis-related genes. **(B)** Cross-verification for tuning the parameter selection. **(C)** Levels of four characteristic genes in endometriosis and normal endometrium tissues. ****$p < 0.0001$. **(D–G)** ROCs of four characteristic genes: AQP1, BGN, DDR2, and ELMO1. **(H)** Construction of a nomogram incorporating four characteristic genes. **(I)** Calibration plots showing the relationships between a nomogram and an ideal model in diagnosing endometriosis.

Signaling pathways involved in characteristic genes

Through GSEA, signaling pathways involved in characteristic genes were analyzed. A low AQP1 level was linked to oocyte meiosis, cell cycle, base excision repair, and ubiquitin-mediated proteolysis (Figure 6A), and its high level was linked to VEGF signaling pathway, PPAR signaling pathway, complement and coagulation cascades, and systemic lupus erythematosus (Figure 6B). Homologous recombination, DNA replication, cell cycle, mismatch repair, base excision repair, oocyte meiosis, and p53 signaling pathway were correlated to the low BGN level (Figure 6C). Additionally, a high DDR2 level was associated with PPAR signaling pathway, VEGF signaling pathway, systemic lupus erythematosus, complement and coagulation cascades, and vascular smooth muscle contraction (Figure 6D), while its low expression was in relation to aminoacyl tRNA biosynthesis, oocyte meiosis, cell cycle, and p53 signaling pathway (Figure 6E). Also, VEGF signaling pathway, viral myocarditis, and PPAR signaling pathway were enriched in the high ELMO1 level

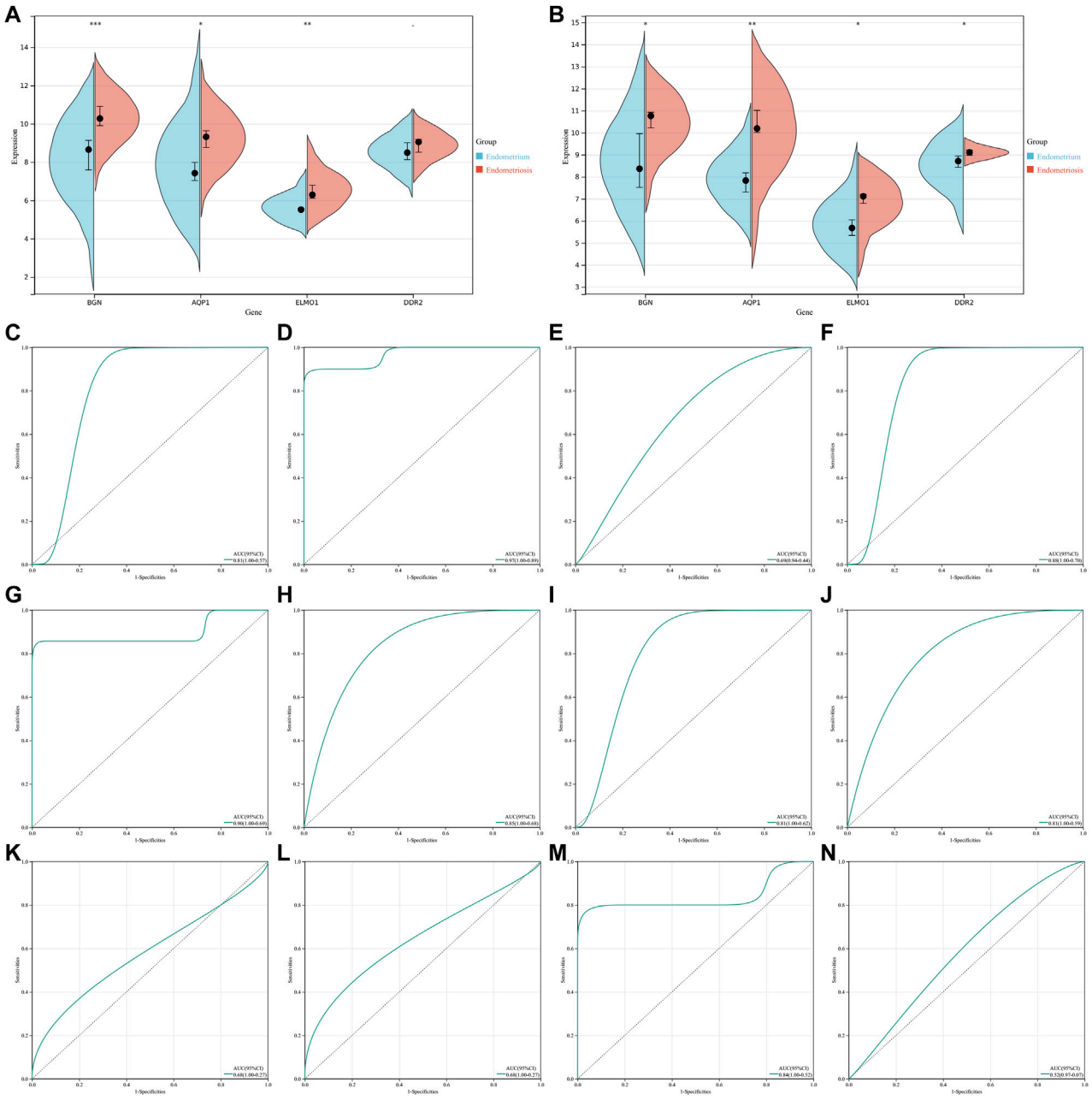

FIGURE 5
Verification of levels and diagnostic efficacy of characteristic genes in endometriosis. **(A,B)** Levels of four characteristic genes in endometriosis and normal endometrium tissues in GSE23339 and GSE25628 datasets. *$p < 0.05$; **$p < 0.01$; and ***$p < 0.001$. **(C–F)** ROCs of four characteristic genes: AQP1, BGN, DDR2, and ELMO1 in the GSE23339 dataset. **(G–J)** ROCs of four characteristic genes in the GSE25628 dataset. **(K–N)** ROCs of four characteristic genes in the GSE7846 external verification set.

(Figure 6F), while base excision repair, homologous recombination, endometrial cancer, oocyte meiosis, cell cycle, and O-glycan biosynthesis were enriched in the low ELMO1 level (Figure 6G). Altogether, characteristic genes might exert crucial roles in endometriosis through mediating the aforementioned signaling pathways.

Post-transcriptional and epigenetic modifications of characteristic genes

At the post-transcriptional level, AQP1 was mainly regulated by hsa-miR-133a-3p, hsa-miR-133b, and hsa-miR-1306-5p; ELMO1 was modulated by hsa-miR-182-5p, hsa-miR-216a-3p,

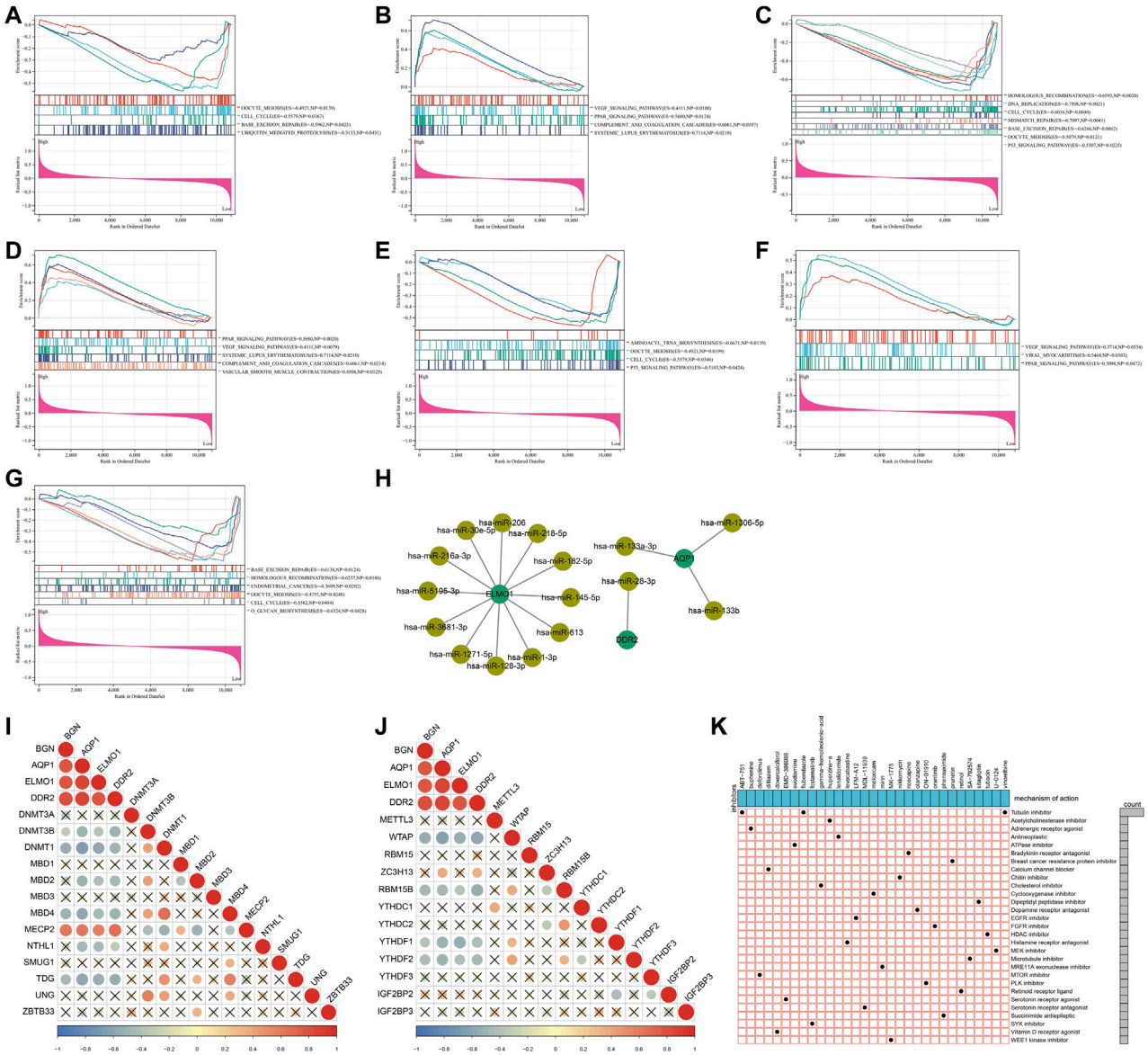

FIGURE 6
Signaling pathways and epigenetic and post-transcriptional modifications of characteristic genes and potential small compounds for endometriosis. **(A–H)** Signaling pathways significantly enriched by high or low levels of four characteristic genes: **(A,B)** AQP1, **(C)** BGN, **(D,E)** DDR2, and **(F,G)** ELMO1. **(H)** Regulatory network of miRNAs and characteristic genes. **(I,J)** Correlations of characteristic genes with **(I)** DNA and **(J)** m^{6}A methylation regulators. **(K)** Shared mechanisms of action of small molecular inhibitors.

hsa-miR-218-5p, hsa-miR-1-3p, hsa-miR-128-3p, hsa-miR-145-5p, hsa-miR-206, hsa-miR-30e-5p, hsa-miR-613, hsa-miR-1271-5p, hsa-miR-3681-3p, and hsa-miR-5195-3p; and DDR2 was targeted by hsa-miR-28-3p (Figure 6H). The epigenetic modifications of characteristic genes were evaluated through calculating the associations of characteristic genes with DNA and m^{6}A methylation regulators. As illustrated in Figure 6I, the characteristic genes were negatively linked to DNA methylation regulators DNMT3B, DNMT1, MBD2, MBD4, NTHL1, and TDG but positively linked to MECP2. Moreover, there were negative relationships of characteristic genes with m^{6}A methylation regulators WTAP, RBM15B, YTHDF1, and YTHDF2 (Figure 6J). The aforementioned evidences demonstrated that the characteristic genes were modulated by post-transcriptional and epigenetic modifications in endometriosis.

TABLE 1 Potential drugs against endometriosis with scores ≤ −0.75.

Score	ID	Name	Description
−99.05	BRD-K15402119	Huperzine-a	Acetylcholinesterase inhibitor
−97.96	BRD-K35687265	ON-01910	PLK inhibitor
−97.45	BRD-K13927029	Retinol	Retinoid receptor ligand
−95.78	BRD-K05926469	Lenalidomide	Antineoplastic
−94.82	BRD-K20152659	Gamma-homolinolenic-acid	Cholesterol inhibitor
−94.28	BRD-K64785675	TG100-115	-666
−93.71	BRD-A69636825	Diltiazem	Calcium channel blocker
−93.57	BRD-A74771556	Nikkomycin	Chitin inhibitor
−93.51	BRD-A84174393	Meloxicam	Cyclooxygenase inhibitor
−92.66	BRD-K29733039	Deforolimus	MTOR inhibitor
−92.26	BRD-K22631935	Neurodazine	Neurogenesis of non-pluripotent C2C12 myoblast inducer
−92.21	BRD-A51393488	Noscapine	Bradykinin receptor antagonist
−90.8	BRD-K48427617	U-0124	MEK inhibitor
−89.23	BRD-K91696562	Orantinib	FGFR inhibitor
−89.16	BRD-A36267905	Buphenine	Adrenergic receptor agonist
−88.64	BRD-K91623615	ABT-751	Tubulin inhibitor
−88.14	BRD-A44551378	LFM-A12	EGFR inhibitor
−87.64	BRD-K86003836	Flubendazole	Tubulin inhibitor
−87.43	BRD-K98426715	Tubacin	HDAC inhibitor
−86.45	BRD-K47659338	EMD-386088	Serotonin receptor agonist
−86.25	BRD-K19416115	Sitagliptin	Dipeptidyl peptidase inhibitor
−85.19	BRD-K33453211	Levocabastine	Histamine receptor antagonist
−85.09	BRD-K14550461	Doxercalciferol	Vitamin D receptor agonist
−85.02	BRD-A68631409	Evodiamine	ATPase inhibitor
−84.49	BRD-A62057054	MDL-11939	Serotonin receptor antagonist
−83.64	BRD-A18043272	Phensuximide	Succinimide antiepileptic
−83.63	BRD-K57546357	Prunetin	Breast cancer resistance protein inhibitor
−82.59	BRD-M30523314	Vinorelbine	Tubulin inhibitor
−82.49	BRD-K55420858	Mirin	MRE11A exonuclease inhibitor
−81.82	BRD-K26997899	SA-792574	Microtubule inhibitor
−81.18	BRD-K18895904	Olanzapine	Dopamine receptor antagonist
−80.84	BRD-K54256913	MK-1775	WEE1 kinase inhibitor
−80.31	BRD-K20285085	Fostamatinib	SYK inhibitor
−79.76	BRD-K40213712	SAL-1	Adenosine receptor antagonist
−79.76	BRD-A00267231	Hemado	Adenosine receptor agonist
−79.76	BRD-K90382497	GW-843682X	PLK inhibitor
−79.71	BRD-K06878038	Deferiprone	Chelating agent
−79.6	BRD-A04756508	Norgestimate	Progesterone receptor agonist
−79.35	BRD-K29582115	Ziprasidone	Dopamine receptor antagonist
−78.81	BRD-A67438293	Treprostinil	Prostacyclin analog
−78.73	BRD-K99451608	Lopinavir	HIV protease inhibitor
−78.67	BRD-A74667430	Etodolac	Cyclooxygenase inhibitor
−78.22	BRD-K81376179	TCS-359	FLT3 inhibitor
−77.36	BRD-K67847053	Guanabenz	Adrenergic receptor agonist
−77.31	BRD-K27141178	SB-203186	Serotonin receptor antagonist
−77.14	BRD-A32836748	Leu-enkephalin	Opioid receptor agonist
−77.01	BRD-K53123955	Niridazole	Phosphofructokinase inhibitor
−76.48	BRD-K51318897	Fenbendazole	Tubulin inhibitor

(Continued on following page)

TABLE 1 (*Continued*) Potential drugs against endometriosis with scores ≤ −0.75.

Score	ID	Name	Description
−76.15	BRD-K11158509	Tyrphostin-B44	EGFR inhibitor
−75.99	BRD-K86465814	HO-013	PPAR receptor agonist
−75.51	BRD-K36324071	NF-449	Purinergic receptor antagonist

Prediction of potential drugs against endometriosis

In total, 413 genes with upregulation and 334 genes with downregulation were determined in endometriosis than normal endometrium (Supplementary Table S2). With scores ≤ −0.75, 51 drugs against endometriosis were determined (Table 1). Figure 6K depicted the shared mechanisms of action. For instance, ABT-751, flubendazole, and vinorelbine shared tubulin inhibitor.

Differences in immune features between endometriosis and normal endometrium

Immune features were evaluated in accordance with the levels of immune-checkpoints, HLAs, receptors, and chemokines as well as the abundance levels of immune cells. Most immune-checkpoints, HLAs, receptors, and chemokines displayed increased levels in endometriosis compared with normal endometrium tissues (Figures 7A–D). Utilizing the CIBERSORT algorithm, we estimated the relative proportions of 22 immune compositions across endometriosis and normal endometrium tissues, with macrophages occupying the highest proportion (Figure 7E). Figure 7F illustrated the tight interplay between these immune compositions, especially the macrophages were linked to most immune compositions. Moreover, most immune cells exhibited higher abundance levels in endometriosis than in normal endometrium tissues (Figure 7G).

Associations of characteristic genes with immune features in endometriosis

Further analysis indicated that four characteristic genes: AQP1, BGN, DDR2, and ELMO1 exhibited positive correlations with most immune-checkpoints, HLAs, receptors, and chemokines (Figures 8A–D). Additionally, these characteristic genes were significantly linked with immune cell compositions, especially macrophages, NK cells activated, and follicular helper T cells (Figures 8E–H).

Development of three subtypes for endometriosis

Utilizing the NMF algorithm, we classified endometriosis samples in the meta-dataset on the basis of endometriosis-related genes. Following cophenetic coefficients, k = 3 was determined as the optimal clustering number (Figure 9A). Figure 9B showed the NMF matrix when k = 3, containing 13 samples in C1, 16 samples in C2, and 7 samples in C3. The expression patterns of endometriosis-related genes were visualized in Figure 9C. PCA further complemented the distinction among three subtypes at transcription levels (Figure 9D). Additionally, four characteristic genes: BGN and ELMO1 levels were the highest in C3, followed by C2 and C1 (Figure 9E); no significant differences in AQP1 and DDR2 were detected among three subtypes.

Differences in signaling pathways and immune features across three subtypes

To uncover the signaling pathways underlying three subtypes, we evaluated the differences in signaling pathways among them. Upregulated pathways were as follows: ribosome, butanoate metabolism, drug metabolism cytochrome P450, valine, leucine, and isoleucine degradation, propanoate metabolism, spliceosome, metabolism of xenobiotics by cytochrome P450, and glycosaminoglycan biosynthesis heparan sulfate in C1 subtype; cell cycle, proteasome, basal cell carcinoma, and Wnt signaling pathway in C2 subtype; lysosome, allograft rejection, systemic lupus erythematosus, graft versus host disease, intestinal immune network for IgA production, hematopoietic cell lineage, leishmania infection, type I diabetes mellitus, autoimmune thyroid disease, and chemokine signaling pathway in C3 (Figure 10A). Downregulated pathways were as follows: graft versus host disease, intestinal immune network for IgA production, primary immunodeficiency, asthma, allograft rejection, autoimmune thyroid disease, natural killer cell-mediated cytotoxicity, type I diabetes mellitus, and lysosome in C1; complement and coagulation cascades, and drug metabolism cytochrome P450 in C2; ribosome, spliceosome, cell cycle, RNA polymerase, DNA replication, Parkinson's disease, base excision repair, butanoate metabolism, glycosaminoglycan biosynthesis chondroitin sulfate, and Huntington's disease in C3 (Figure 10B). C3 exhibited the highest of immune-checkpoint levels, immune cell infiltrations, and immune and stromal scores, followed by C2 and C1 (Figure 10C). Additionally, the levels of most chemokines, HLAs, and receptors were the highest in C3 along with C2 and C1 (Figures 10D–F). The aforementioned evidence demonstrated the differences in signaling pathways and immune features across three subtypes.

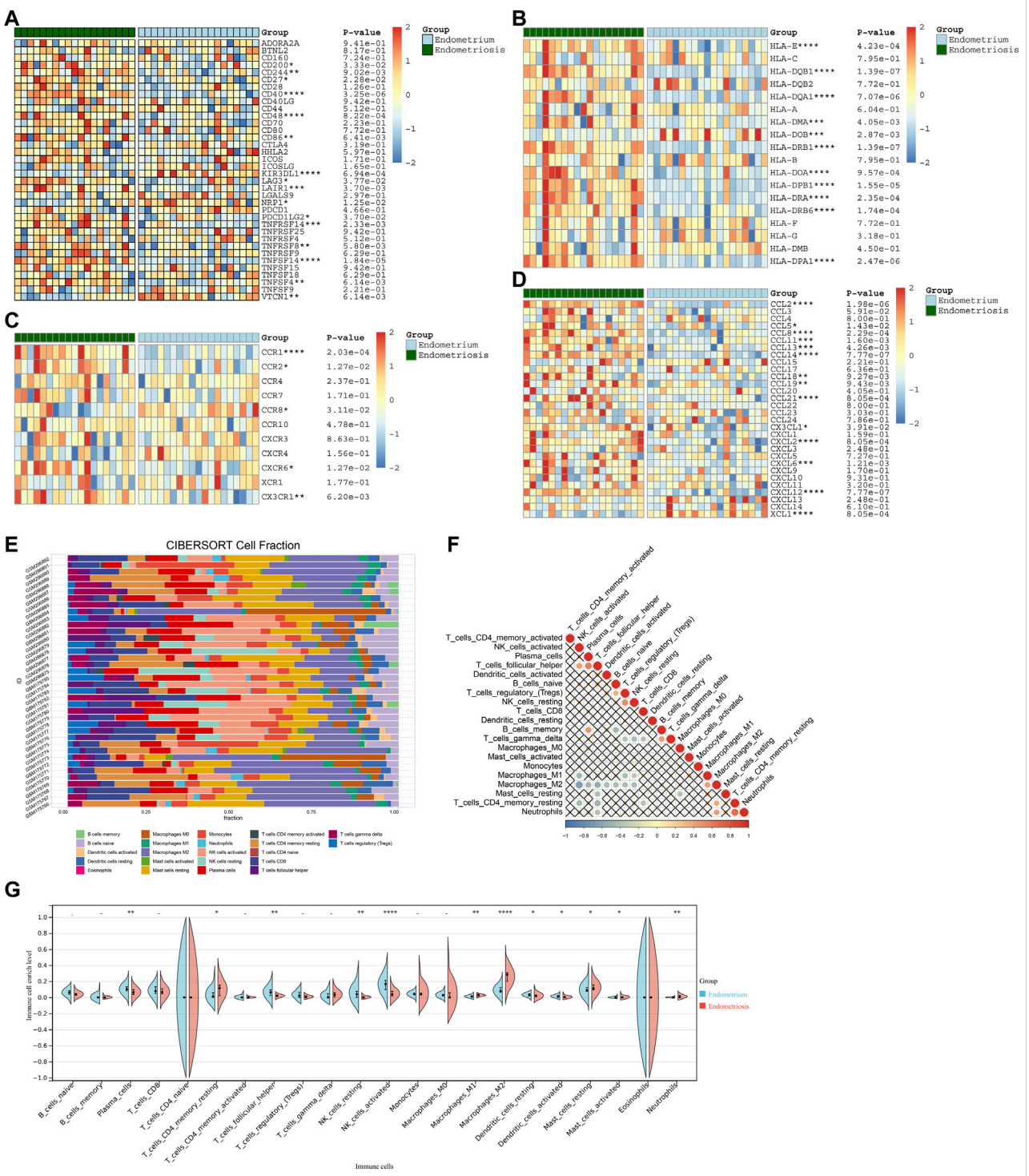

FIGURE 7
Differences in immune features between endometriosis and normal endometrium. **(A–D)** Heatmaps of the levels of **(A)** immune-checkpoints, **(B)** HLAs, **(C)** receptors, and **(D)** chemokines in endometriosis and normal endometrium tissues. **(E)** Fractions of 22 immune cell types across endometriosis and normal endometrium tissues. **(F)** Associations between immune cell types. **(G)** Abundance levels of immune cell types in endometriosis and normal endometrium tissues. *$p < 0.05$; **$p < 0.01$; ***$p < 0.001$; and ****$p < 0.0001$.

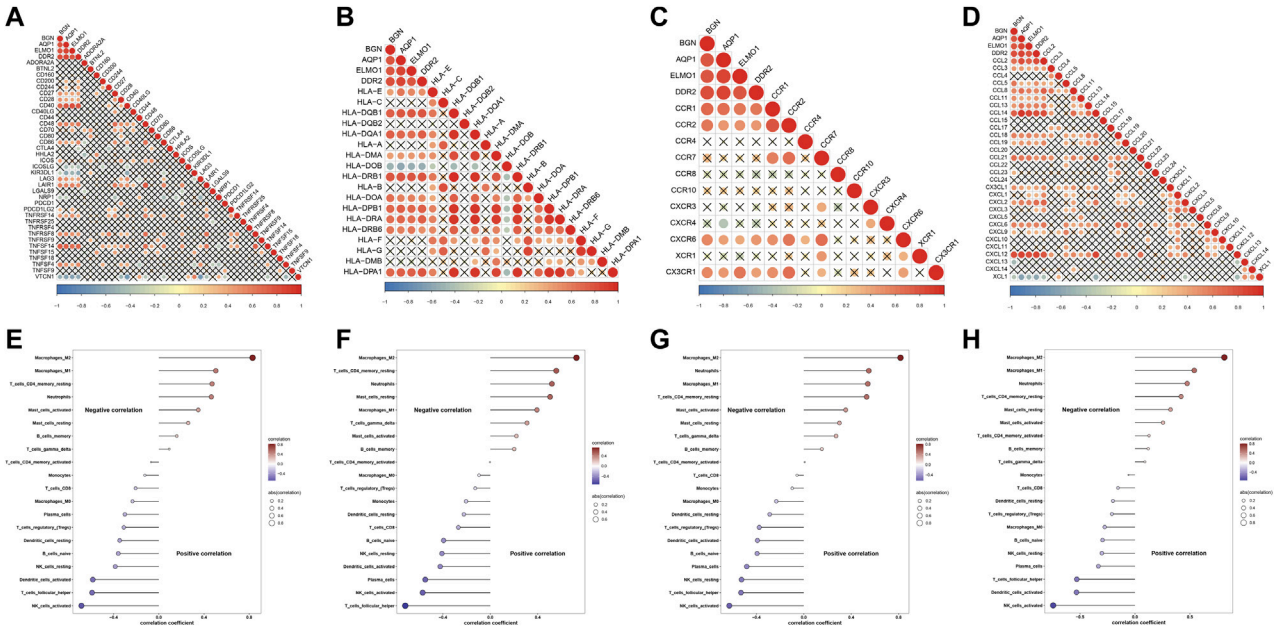

FIGURE 8
Associations of characteristic genes with immune features in endometriosis. **(A–D)** Heatmaps for the relationships of characteristic genes with **(A)** immune-checkpoints, **(B)** HLAs, **(C)** receptors, and **(D)** chemokines. **(E–H)** Correlations between characteristic genes: AQP1, BGN, DDR2, and ELMO1 and immune cell compositions.

Discussion

WGCNA is a system biology approach applied to describe gene association patterns between various samples, which can be applied to identify gene sets with highly coordinated changes, and to determine candidate organisms based on the interconnectivity of gene sets and the association between gene sets and phenotypes, thereby identifying marker genes or therapeutic targets. Through integrating GSE7305 and GSE11691 datasets, we determined 172 endometriosis-related genes utilizing WGCNA algorithm. Previously, endometriosis-related genes were determined utilizing the differential expression approach (Wang et al., 2021). Compared with only focusing on differentially expressed genes, WGCNA may use the information of thousands of genes with the greatest variations to identify gene sets of interest and implement significant association analysis with phenotypes (Wu et al., 2021). One is to make full use of the information, and the other is to convert the association between thousands of genes and phenotypes into associations between several gene sets and phenotypes, eliminating the problem of multiple hypothesis testing and correction. The endometriosis-related genes were linked to tube development, angiogenesis, and endometriosis-related pathways (PI3K-Akt pathway and ECM, etc.). Evidence proposes that angiogenesis, PI3K-Akt pathway, and ECM contribute to growth and progression of endometriotic cells within ectopic sites (Hung et al., 2021), demonstrating the crucial functions of the endometriosis-related genes in endometriosis.

Through the Lasso approach, we determined four characteristic genes among endometriosis-related genes, containing BGN, AQP1, ELMO1 and DDR2. All of them exhibited upregulated levels in endometriosis compared with normal endometrium tissues, which were modulated by post-transcriptional and epigenetic modifications. ROCs demonstrated that each characteristic gene enabled to diagnose endometriosis accurately and sensitively. Previously, upregulated BGN associated with estrogen metabolism and action in endometriosis was confirmed through immunohistochemical staining (Vouk et al., 2011). Suppression of AQP1 alleviates adhesion and angiogenesis of ectopic endometrial cells for murine endometriosis models via activation of the Wnt pathway (Shu et al., 2019). ELMO1 enables to increase the activity of extracellular matrix proteins as well as reduce cell adhesions to ECM (Shimazaki et al., 2006). Histological evidence demonstrates that endometriosis contributes to the increased incidence of ovarian cancer (Hermens et al., 2021). ELMO1 (Wang et al., 2014) and DDR2 (Jeong et al., 2021) have been demonstrated to mediate ovarian cancer progression. Altogether, the four characteristic genes we proposed might improve the early diagnosis as well as management of endometriosis cases.

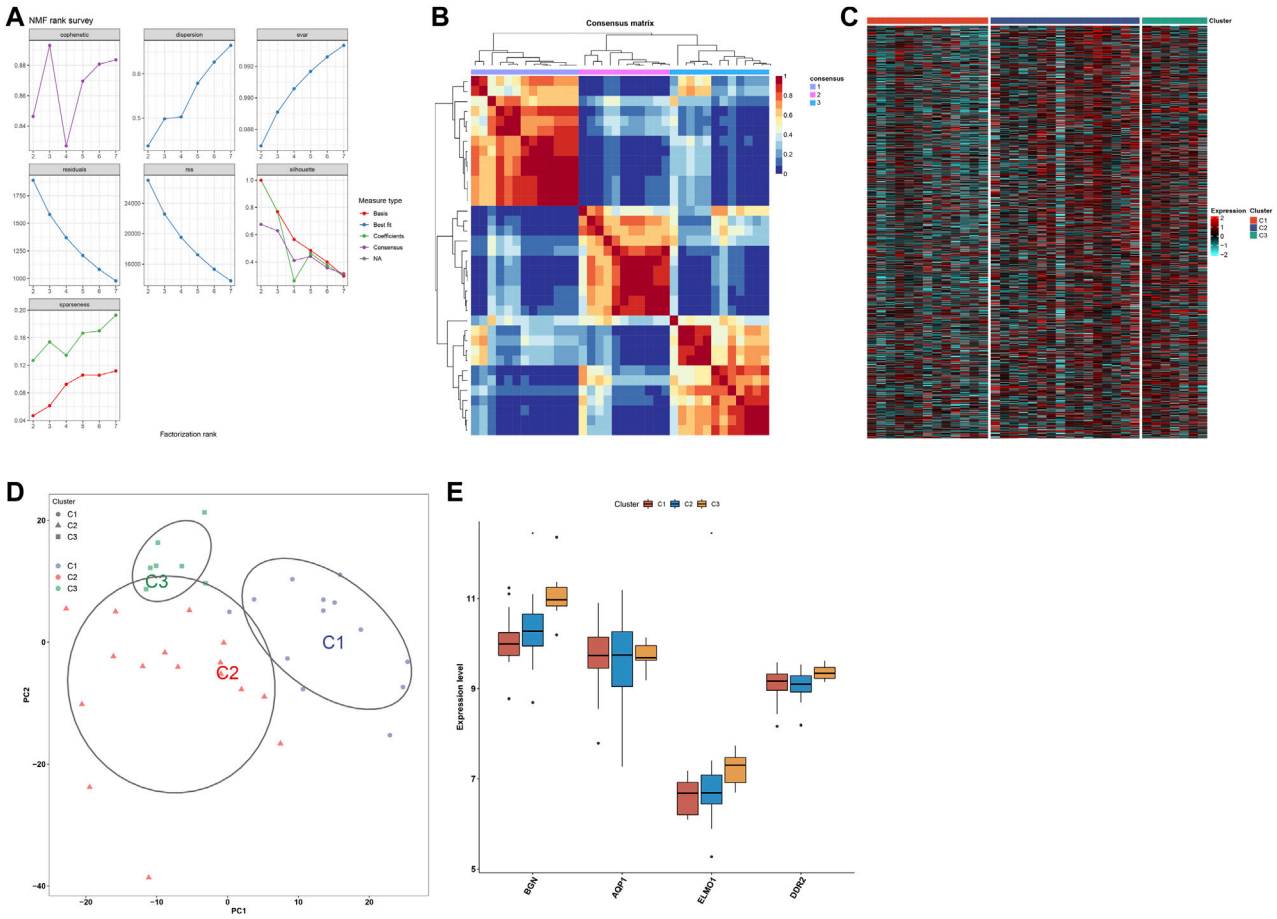

FIGURE 9
Development of three subtypes for endometriosis. **(A)** Cophenetic coefficients of the NMF clustering number from 2 to 7. **(B)** NMF matrix heatmap when k = 3. **(C)** Heatmaps of the expression patterns of endometriosis-related genes across three subtypes. **(D)** PCA of endometriosis-related genes. **(E)** Levels of four characteristic genes across three subtypes. *$p < 0.05$.

In total, 51 drugs against endometriosis were determined. Among them, ABT-751, flubendazole, and vinorelbine shared tubulin inhibitor. The novel discovered small molecule compounds might exert a significant effect on the treatment of endometriosis. Endometriosis is a chronic neuroinflammatory disorder. Endometriosis exhibited increased levels of most immune-checkpoints, HLAs, receptors, and chemokines as well as enhanced infiltrations of most immune compositions compared with normal endometrium tissues (Peng et al., 2021). Consistent with the previous research, macrophages occupy the highest ratio among 22 immune cell components (Zhong et al., 2021). Recently, M2 macrophage-associated genes have been determined in endometriosis, reflecting the impact of M2 macrophages on the etiology of endometriosis (Cui et al., 2021). The four characteristic genes were positively correlated with most immune-checkpoints, HLAs, receptors, and chemokines as well as significantly linked with immune cell compositions, especially macrophages, NK cells activated, and follicular helper T cells, demonstrating that these characteristic genes might mediate immunological function during endometriosis progression. Determining the molecular subtypes of endometriosis is of importance for personalized treatment. With the NMF algorithm, we classified endometriosis as three subtypes that were linked to distinct signaling pathways and immune features.

The aforementioned findings might be beneficial for probing the pathogenesis of endometriosis as well as providing the foundation to determine novel biomarkers and subtypes for endometriosis. We believe that our findings will assist future research endeavors in the direction.

Conclusion

Altogether, our research determined four characteristic genes (BGN, AQP1, ELMO1, and DDR2) with the favorable

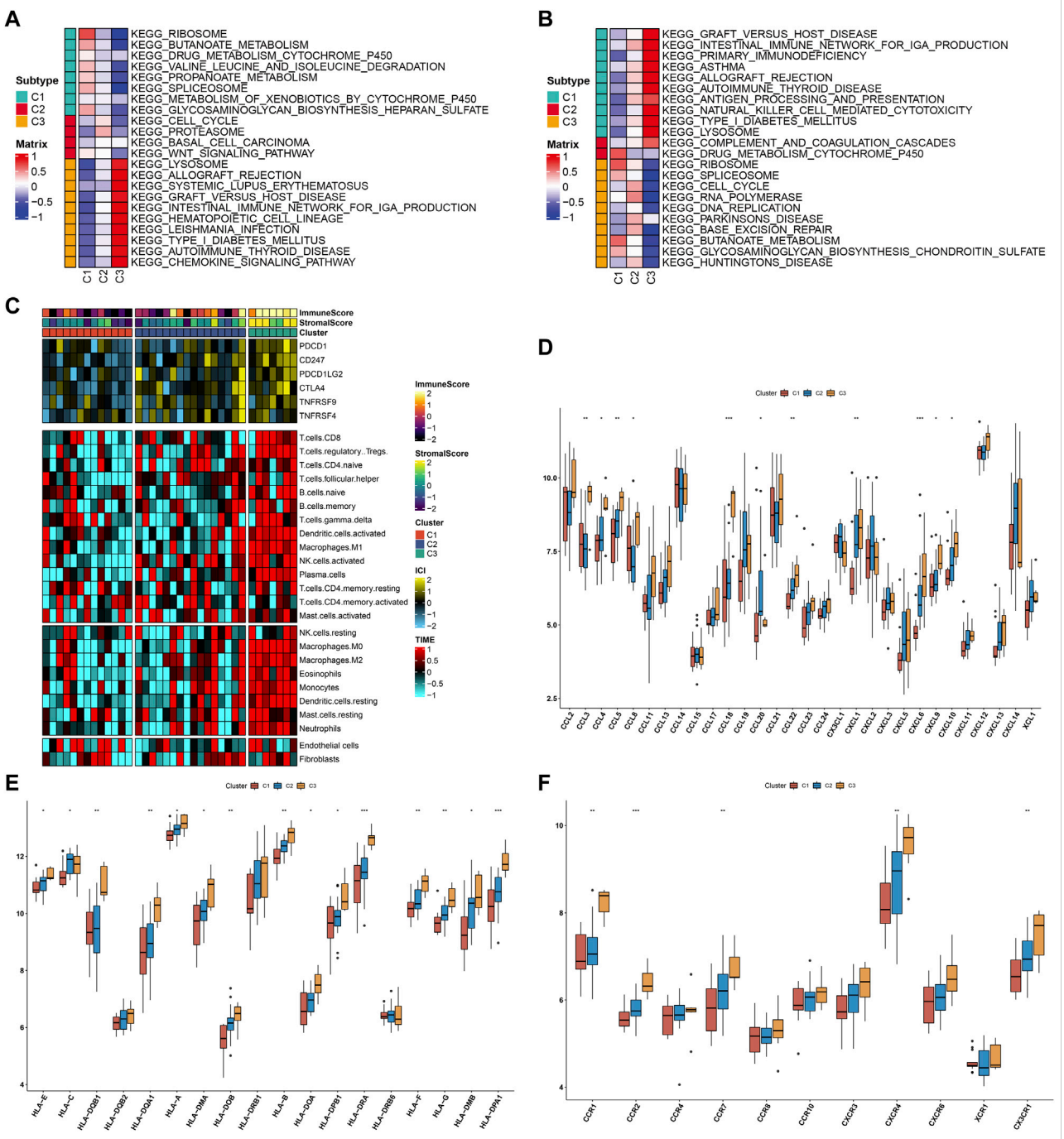

FIGURE 10
Differences in signaling pathways and immune features across three subtypes. **(A)** Upregulated pathways in each subtype. **(B)** Downregulated pathways in each subtype. **(C)** Heatmaps of immune-checkpoint levels, immune cell infiltrations, and immune and stromal scores across three subtypes. **(D–F)** Differences in **(D)** chemokines, **(E)** HLAs, and **(F)** receptors among three subtypes. *$p < 0.05$; **$p < 0.01$; and ***$p < 0.001$.

efficacy in diagnosing endometriosis. The characteristic genes were remarkably linked with immunological functions, and their aberrant levels were modulated by epigenetic and post-transcriptional modifications. Additionally, endometriosis was classified into three subtypes, with different mechanisms and immune features. The aforementioned findings might contribute to the early diagnosis and intervention in endometriosis.

Data availability statement

The datasets presented in this study can be found in online repositories. The names of the repository/repositories and accession number(s) can be found in the article/Supplementary Material.

Author contributions

MZ, T-WN, and XC conceived and designed the study. ZW and JL conducted most of the experiments and data analysis and wrote the manuscript. ML and LL participated in collecting the data and helped to draft the manuscript. All authors reviewed and approved the manuscript.

Funding

This research was supported by the Xiamen Medical and Health Science and Technology Plan Project (3502Z20194090) and Medical Scientific Research Personnel Training Project of Fujian Provincial Health Commission (2019-ZQNB-34).

Conflict of interest

The authors declare that the research was conducted in the absence of any commercial or financial relationships that could be construed as a potential conflict of interest.

Publisher's note

All claims expressed in this article are solely those of the authors and do not necessarily represent those of their affiliated organizations, or those of the publisher, the editors, and the reviewers. Any product that may be evaluated in this article, or claim that may be made by its manufacturer, is not guaranteed or endorsed by the publisher.

Supplementary material

The Supplementary Material for this article can be found online at: https://www.frontiersin.org/articles/10.3389/fphar.2022.932526/full#supplementary-material

References

Bedaiwy, M. A. (2022). Endometrial cytokines, endometriosis and infertility: A deeper dive into the endometrial immune microenvironment. *Fertil. Steril.* 117 (3), 641–642. doi:10.1016/j.fertnstert.2022.01.023

Brichant, G., Laraki, I., Henry, L., Munaut, C., and Nisolle, M. (2021). New therapeutics in endometriosis: A review of hormonal, non-hormonal, and non-coding RNA treatments. *Int. J. Mol. Sci.* 22 (19), 10498. doi:10.3390/ijms221910498

Bunis, D. G., Wang, W., Vallvé-Juanico, J., Houshdaran, S., Sen, S., Ben Soltane, I., et al. (2021). Whole-tissue deconvolution and scRNAseq analysis identify altered endometrial cellular compositions and functionality associated with endometriosis. *Front. Immunol.* 12, 788315. doi:10.3389/fimmu.2021.788315

Chen, L., Niu, X., Qiao, X., Liu, S., Ma, H., Shi, X., et al. (2021). Characterization of interplay between autophagy and ferroptosis and their synergistical roles on manipulating immunological tumor microenvironment in squamous cell carcinomas. *Front. Immunol.* 12, 739039. doi:10.3389/fimmu.2021.739039

Crispi, S., Piccolo, M. T., D'Avino, A., Donizetti, A., Viceconte, R., Spyrou, M., et al. (2013). Transcriptional profiling of endometriosis tissues identifies genes related to organogenesis defects. *J. Cell. Physiol.* 228 (9), 1927–1934. doi:10.1002/jcp.24358

Cui, Z., Bhandari, R., Lei, Q., Lu, M., Zhang, L., Zhang, M., et al. (2021). Identification and exploration of novel macrophage M2-related biomarkers and potential therapeutic agents in endometriosis. *Front. Mol. Biosci.* 8, 656145. doi:10.3389/fmolb.2021.656145

Gautier, L., Cope, L., Bolstad, B. M., and Irizarry, R. A. (2004). affy-analysis of Affymetrix GeneChip data at the probe level. *Bioinformatics* 20 (3), 307–315. doi:10.1093/bioinformatics/btg405

Hänzelmann, S., Castelo, R., and Guinney, J. (2013). Gsva: Gene set variation analysis for microarray and RNA-seq data. *BMC Bioinforma.* 14, 7. doi:10.1186/1471-2105-14-7

Hawkins, S. M., Creighton, C. J., Han, D. Y., Zariff, A., Anderson, M. L., Gunaratne, P. H., et al. (2011). Functional microRNA involved in endometriosis. *Mol. Endocrinol.* 25 (5), 821–832. doi:10.1210/me.2010-0371

Hermens, M., van Altena, A. M., Bulten, J., van Vliet, H., Siebers, A. G., Bekkers, R. L. M., et al. (2021). Increased incidence of ovarian cancer in both endometriosis and adenomyosis. *Gynecol. Oncol.* 162 (3), 735–740. doi:10.1016/j.ygyno.2021.07.006

Hever, A., Roth, R. B., Hevezi, P., Marin, M. E., Acosta, J. A., Acosta, H., et al. (2007). Human endometriosis is associated with plasma cells and overexpression of B lymphocyte stimulator. *Proc. Natl. Acad. Sci. U. S. A.* 104 (30), 12451–12456. doi:10.1073/pnas.0703451104

Hey-Cunningham, A. J., Riaz, A., Fromm, P. D., Kupresanin, F., Markham, R., McGuire, H. M., et al. (2022). Circulating and endometrial regulatory T cell and related populations in endometriosis and infertility: Endometriosis is associated with blunting of endometrial cyclical effects and reduced proportions in moderate-severe disease. *Reprod. Sci.* 29 (1), 229–242. doi:10.1007/s43032-021-00658-4

Hirakawa, T., Nasu, K., Abe, W., Aoyagi, Y., Okamoto, M., Kai, K., et al. (2016). miR-503, a microRNA epigenetically repressed in endometriosis, induces apoptosis and cell-cycle arrest and inhibits cell proliferation, angiogenesis, and contractility of human ovarian endometriotic stromal cells. *Hum. Reprod.* 31 (11), 2587–2597. doi:10.1093/humrep/dew217

Hull, M. L., Escareno, C. R., Godsland, J. M., Doig, J. R., Johnson, C. M., Phillips, S. C., et al. (2008). Endometrial-peritoneal interactions during endometriotic lesion establishment. *Am. J. Pathol.* 173 (3), 700–715. doi:10.2353/ajpath.2008.071128

Hung, S. W., Zhang, R., Tan, Z., Chung, J. P. W., Zhang, T., Wang, C. C., et al. (2021). Pharmaceuticals targeting signaling pathways of endometriosis as potential new medical treatment: A review. *Med. Res. Rev.* 41 (4), 2489–2564. doi:10.1002/med.21802

Jeong, B. Y., Cho, K. H., Yoon, S. H., Park, C. G., Park, H. W., Lee, H. Y., et al. (2021). Discoidin domain receptor 2 mediates lysophosphatidic acid-induced ovarian cancer aggressiveness. *Int. J. Mol. Sci.* 22 (10), 5374. doi:10.3390/ijms22105374

Kapoor, R., Stratopoulou, C. A., and Dolmans, M. M. (2021). Pathogenesis of endometriosis: New insights into prospective therapies. *Int. J. Mol. Sci.* 22 (21), 11700. doi:10.3390/ijms222111700

Langfelder, P., and Horvath, S. (2008). Wgcna: An R package for weighted correlation network analysis. *BMC Bioinforma.* 9, 559. doi:10.1186/1471-2105-9-559

Leek, J. T., Johnson, W. E., Parker, H. S., Jaffe, A. E., and Storey, J. D. (2012). The sva package for removing batch effects and other unwanted variation in high-throughput experiments. *Bioinformatics* 28 (6), 882–883. doi:10.1093/bioinformatics/bts034

Liberzon, A., Birger, C., Thorvaldsdóttir, H., Ghandi, M., Mesirov, J. P., Tamayo, P., et al. (2015). The Molecular Signatures Database (MSigDB) hallmark gene set collection. *Cell. Syst.* 1 (6), 417–425. doi:10.1016/j.cels.2015.12.004

Newman, A. M., Liu, C. L., Green, M. R., Gentles, A. J., Feng, W., Xu, Y., et al. (2015). Robust enumeration of cell subsets from tissue expression profiles. *Nat. Methods* 12 (5), 453–457. doi:10.1038/nmeth.3337

Pan, J., and Gillis, N. (2021). Generalized separable nonnegative matrix factorization. *IEEE Trans. Pattern Anal. Mach. Intell.* 43 (5), 1546–1561. doi:10.1109/tpami.2019.2956046

Peng, Y., Peng, C., Fang, Z., and Chen, G. (2021). Bioinformatics analysis identifies molecular markers regulating development and progression of endometriosis and potential therapeutic drugs. *Front. Genet.* 12, 622683. doi:10.3389/fgene.2021.622683

Ritchie, M. E., Phipson, B., Wu, D., Hu, Y., Law, C. W., Shi, W., et al. (2015). Limma powers differential expression analyses for RNA-sequencing and microarray studies. *Nucleic Acids Res.* 43 (7), e47. doi:10.1093/nar/gkv007

Shimazaki, A., Tanaka, Y., Shinosaki, T., Ikeda, M., Watada, H., Hirose, T., et al. (2006). ELMO1 increases expression of extracellular matrix proteins and inhibits cell adhesion to ECMs. *Kidney Int.* 70 (10), 1769–1776. doi:10.1038/sj.ki.5001939

Shu, C., Shu, Y., Gao, Y., Chi, H., and Han, J. (2019). Inhibitory effect of AQP1 silencing on adhesion and angiogenesis in ectopic endometrial cells of mice with endometriosis through activating the Wnt signaling pathway. *Cell. Cycle* 18 (17), 2026–2039. doi:10.1080/15384101.2019.1637202

Subramanian, A., Tamayo, P., Mootha, V. K., Mukherjee, S., Ebert, B. L., Gillette, M. A., et al. (2005). Gene set enrichment analysis: A knowledge-based approach for interpreting genome-wide expression profiles. *Proc. Natl. Acad. Sci. U. S. A.* 102 (43), 15545–15550. doi:10.1073/pnas.0506580102

Symons, L. K., Miller, J. E., Kay, V. R., Marks, R. M., Liblik, K., Koti, M., et al. (2018). The immunopathophysiology of endometriosis. *Trends Mol. Med.* 24 (9), 748–762. doi:10.1016/j.molmed.2018.07.004

Vouk, K., Smuc, T., Guggenberger, C., Ribič-Pucelj, M., Sinkovec, J., Husen, B., et al. (2011). Novel estrogen-related genes and potential biomarkers of ovarian endometriosis identified by differential expression analysis. *J. Steroid Biochem. Mol. Biol.* 125 (3-5), 231–242. doi:10.1016/j.jsbmb.2011.03.010

Wang, J., Dai, J. M., Che, Y. L., Gao, Y. M., Peng, H. J., Liu, B., et al. (2014). Elmo1 helps dock180 to regulate Rac1 activity and cell migration of ovarian cancer. *Int. J. Gynecol. Cancer* 24 (5), 844–850. doi:10.1097/igc.0000000000000137

Wang, T., Jiang, R., Yao, Y., Qian, L., Zhao, Y., Huang, X., et al. (2021). Identification of endometriosis-associated genes and pathways based on bioinformatic analysis. *Med. Baltim.* 100 (27), e26530. doi:10.1097/md.0000000000026530

Wilson, C. L., and Miller, C. J. (2005). Simpleaffy: A BioConductor package for affymetrix quality control and data analysis. *Bioinformatics* 21 (18), 3683–3685. doi:10.1093/bioinformatics/bti605

Wu, J., Fang, X., and Xia, X. (2021). Identification of key genes and pathways associated with endometriosis by weighted gene Co-expression network analysis. *Int. J. Med. Sci.* 18 (15), 3425–3436. doi:10.7150/ijms.63541

Yang, K., Dinasarapu, A. R., Reis, E. S., Deangelis, R. A., Ricklin, D., Subramaniam, S., et al. (2013). Cmap: Complement Map database. *Bioinformatics* 29 (14), 1832–1833. doi:10.1093/bioinformatics/btt269

Yoshihara, K., Shahmoradgoli, M., Martínez, E., Vegesna, R., Kim, H., Torres-Garcia, W., et al. (2013). Inferring tumour purity and stromal and immune cell admixture from expression data. *Nat. Commun.* 4, 2612. doi:10.1038/ncomms3612

Yu, G., Wang, L. G., Han, Y., and He, Q. Y. (2012). clusterProfiler: An R package for comparing biological themes among gene clusters. *Omics* 16 (5), 284–287. doi:10.1089/omi.2011.0118

Zhong, Q., Yang, F., Chen, X., Li, J., Zhong, C., Chen, S., et al. (2021). Patterns of immune infiltration in endometriosis and their relationship to r-AFS stages. *Front. Genet.* 12, 631715. doi:10.3389/fgene.2021.631715

frontiers | Frontiers in Pharmacology

TYPE Original Research
PUBLISHED 30 August 2022
DOI 10.3389/fphar.2022.997664

OPEN ACCESS

EDITED BY
Essa M. Saied,
Humboldt University of Berlin, Germany

REVIEWED BY
Wen Wang,
Capital Medical University, China
Songhai Chen,
The University of Iowa, United States

*CORRESPONDENCE
Xuemei Pu,
xmpuscu@scu.edu.cn
Menglong Li,
liml@scu.edu.cn

SPECIALTY SECTION
This article was submitted to Pharmacology of Anti-Cancer Drugs, a section of the journal Frontiers in Pharmacology

RECEIVED 19 July 2022
ACCEPTED 09 August 2022
PUBLISHED 30 August 2022

CITATION
Li S, Chen J, Chen X, Yu J, Guo Y, Li M and Pu X (2022), Therapeutic and prognostic potential of GPCRs in prostate cancer from multi-omics landscape.
Front. Pharmacol. 13:997664.
doi: 10.3389/fphar.2022.997664

Therapeutic and prognostic potential of GPCRs in prostate cancer from multi-omics landscape

Shiqi Li[1], Jianfang Chen[1], Xin Chen[1], Jin Yu[2], Yanzhi Guo[1], Menglong Li[1]* and Xuemei Pu[1]*

[1]College of Chemistry, Sichuan University, Chengdu, China, [2]Department of Physics and Astronomy, University of California, Irvine, Irvine, CA, United States

Prostate cancer (PRAD) is a common and fatal malignancy. It is difficult to manage clinically due to drug resistance and poor prognosis, thus creating an urgent need for novel therapeutic targets and prognostic biomarkers. Although G protein-coupled receptors (GPCRs) have been most attractive for drug development, there have been lack of an exhaustive assessment on GPCRs in PRAD like their molecular features, prognostic and therapeutic values. To close this gap, we herein systematically investigate multi-omics profiling for GPCRs in the primary PRAD by analyzing somatic mutations, somatic copy-number alterations (SCNAs), DNA methylation and mRNA expression. GPCRs exhibit low expression levels and mutation frequencies while SCNAs are more prevalent. 46 and 255 disease-related GPCRs are identified by the mRNA expression and DNA methylation analysis, respectively, complementing information lack in the genome analysis. In addition, the genomic alterations do not exhibit an observable correlation with the GPCR expression, reflecting the complex regulatory processes from DNA to RNA. Conversely, a tight association is observed between the DNA methylation and mRNA expression. The virtual screening and molecular dynamics simulation further identify four potential drugs in repositioning to PRAD. The combination of 3 clinical characteristics and 26 GPCR molecular features revealed by the transcriptome and genome exhibit good performance in predicting progression-free survival in patients with the primary PRAD, providing candidates as new biomarkers. These observations from the multi-omics analysis on GPCRs provide new insights into the underlying mechanism of primary PRAD and potential of GPCRs in developing therapeutic strategies on PRAD.

KEYWORDS

G protein-coupled receptors, prostate cancer, multi-omics, virtual screening, prognostic model

Introduction

Prostate cancer (PRAD) is the second commonly diagnosed cancer and leading cause of mortality in men worldwide. 248,530 new cases were reported in 2021, resulting in approximately 3.4 thousand deaths (Siegel et al., 2021). With the popularity of early prostate specific antigen (PSA) screening, increasing cases are being detected (Force, 2018). When PRAD is diagnosed, difficult clinical decision is generally faced by both clinicians and patients, as it is very difficult to predict whether a patient will progress to aggressive and metastatic disease. Currently, screening, diagnosis and prognosis of PRAD are heavily dependent on clinical characteristics like age, tumor stage and Gleason score, while these indicators cannot well distinguish individuals with different survival outcomes at the beginning of the disease, leading to either over- or under-treatment of these patients (Cooperberg et al., 2010; Klotz et al., 2014). Therefore, it is highly desired to find new biomarkers to complement existing clinical tools for diagnostic, prognostic and disease monitoring such that improve risk stratification of the PRAD patients and develop effective and precise therapeutic targets. A global analysis of multi-omics data provides a potential solution for gaining insight into the underlying mechanisms of disease development, which can better stratify patients and uncovers new therapeutic targets.

G protein-coupled receptors (GPCRs), with a seven-transmembrane domain structure, an extracellular amino terminus and an intracellular carboxyl terminus, are the largest and most diverse protein family of cell surface receptors in many species, accounting for ~4% of the encoded human genome (Pierce et al., 2002; Fredriksson et al., 2003). As key transducers of signals from the extracellular milieu to the inside of the cell, GPCRs can regulate a vast array of fundamental biological processes, including cellular growth and metabolism, hormone regulation, sensory perception, and alterations in neuronal activity. Consequently, their aberrant activity or expression also leads to many common diseases and disorders, for example, diabetes, Alzheimer disease, depression, and heart failure (Hauser et al., 2017; Raimondi et al., 2019). The critical roles of GPCRs in numerous physiological functions drive them to be the largest family of drug targets (Hauser et al., 2017). However, this family has not typically been a major focus for oncology drug discovery and only a handful of GPCRs were approved to be targets of anti-cancer drugs (Innamorati et al., 2011; Nieto Gutierrez and McDonald, 2018; Wu et al., 2019), although their oncogenic potential has been known for more than 30 years. The first study linking a GPCR to tumorigenic activity was reported by Young et al. (1986). Recently, increasing evidences indicated that GPCRs can contribute to many facets of tumorigenesis, including angiogenesis, immune evasion, growth, and apoptosis of tumor cells (Nieto Gutierrez and McDonald, 2018; Wang et al., 2019; Wu et al., 2019; Kaushik et al., 2020). In addition, functional roles of certain GPCR members in cancers are gradually being appreciated. For example, GPR30 is overexpressed in a variety of malignances including PRAD (Siegfried et al., 2009; Chan et al., 2010; Chevalier et al., 2012), and its overexpression has been reported to be involved in lower survival rates in patients with endometrial or ovarian cancer, and an elevated risk of developing metastases in patients with breast cancer (Filardo et al., 2006; Smith et al., 2007; Albanito et al., 2008; Pandey et al., 2009; Du et al., 2012; Zhu et al., 2017). The knockdown of GPRC6A in PC3 cells was reported to significantly decrease tumor metastatic efficiency and invasiveness while increased expression of GPRC6A would enhance ERK and EMT signaling (Liu et al., 2016). Abnormalities in Formylpeptide receptor-2 could induce autonomous migration and proliferation of colon cancer cells (Xiang et al., 2016). GPR18 was revealed to involve in inhibiting apoptosis and increasing the survival rate of melanoma cells (Qin et al., 2011). Activation of S1P2R could mediate inhibition of glioblastoma cell viability (Malchinkhuu et al., 2008). Malignant cells use chemokine receptors to migrate to distant sites of ligand expression, for example, CCR7 and CCR10 were demonstrated to participate in metastatic homing of cancer cells and cell growth (Balkwill, 2004; O'Hayre et al., 2008). These findings clearly show potential of GPCR as novel targets in the cancer treatment. Thus, targeting GPCRs to mediate signaling pathways is currently considered as a promising strategy for drug discovery of the cancers (Sriram and Insel, 2018; Chaudhary and Kim, 2021).

Although the correlation of GPCRs with oncology has been confirmed by growing studies, previous works mainly focused on a few members of GPCRs. Consequently, some receptors were well studied due to their well-known importance while others were ignored. In addition, Insel P.A. et al. indicated that many GPCRs are not well understood and findings derived from specific GPCRs may not be applicable to all, or even most GPCRs (Insel et al., 2019). Unfortunately, it has been lacked of an unbiased and comprehensive study on the molecular characteristics, prognostic potential, and biological functions for the entire GPCR family in PRAD. To close this gap, we analyze multi-omics data from gene expression, somatic mutation, somatic copy-number alterations (SCNAs) and DNA methylation of patients with primary PRAD to 1) provide a global landscape of aberrations in GPCRs at genomic, epigenetic, and transcriptomic levels; 2) probe impact of upstream features on the mRNA expression; 3) identify receptors that may be served as potential targets for primary PRAD therapy in order to find some drug candidates by molecular dynamics simulation and virtual screening; 4) develop a prognostic model for primary PRAD based on the features derived from the multi-omics analysis. Collectively, we provide the first comprehensive multi-omics analysis for GPCRs in the primary PRAD, which offer insights into therapeutic targets and prognostic value of the GPCR family.

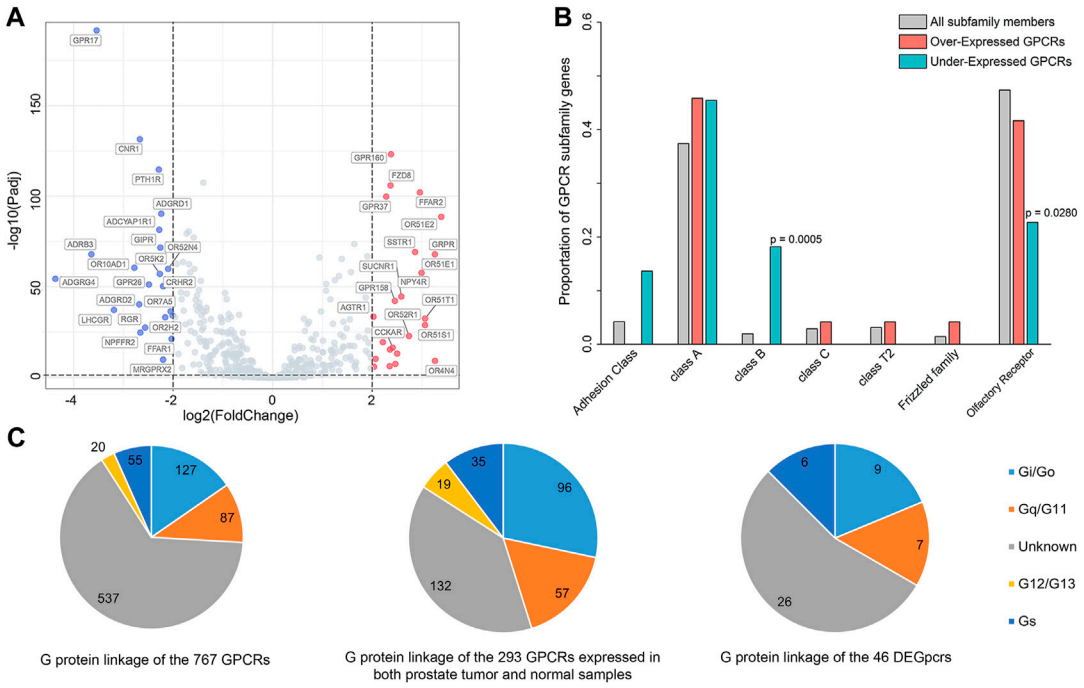

FIGURE 1
Differentially expressed GPCRs (DEGpcrs) between 495 primary prostate tumor samples and 151 normal samples. **(A)** Volcano plot showing the DEGpcrs. Red and blue dots represent the significantly up- and downregulated genes, respectively. **(B)** Barplot showing subfamily distribution of the DEGpcrs. **(C)** G protein linkage of all the 767 GPCRs (right), the 293 GPCRs expressed in both prostate tumor and normal samples (middle), and the 46 DEGpcrs (left).

Results and discussion

mRNA expression of GPCRs in primary PRAD

As accepted, disease-related genes could be identified by comparing the expression level of genes in normal and tumor tissues (Maiga et al., 2016; Insel et al., 2019; Sriram et al., 2019). Thus, in order to provide a comprehensive evaluation of GPCRs expression in primary PRAD, we first integrated RNA-seq data of 767 GPCR members in normal and tumor tissues using TOIL GTEx and TCGA RNA-seq datasets from UCSC Xena (Goldman et al., 2020). Supplementary Table S1 lists the detailed information about the 767 GPCRs. It can be seen that 228 GPCRs are highly expressed, judged from their median expressions in tumor samples≥10 TPM. However, most of the family (n = 461, 60.10%) are expressed at extremely low levels, which are barely detectable in PRAD tumor samples due to their median expressions less than 1 TPM.

We further extracted mRNA-seq data from 495 primary prostate tumor samples and 151 normal samples to do a comparison, through which a total of 46 differentially expressed GPCRs (DEGpcrs, FDR <0.05 and |log2 Fold Change| > 2) were identified. 24 and 22 genes are significantly over- and under-expressed in primary prostate tumors, respectively (vide Supplementary Table S2 and Figure 1A). The aberrant expression of certain DEGpcrs and their involvement in cancer were reported in previous works. For example, *OR51E1*, *OR51E2* and *GPR160*, which are highly expressed (>10 TPM) and significantly upregulated in our analysis, were reported to have antitumor potential for PRAD in previous studies. Specifically, *OR51E1* and *OR51E2* were reported to suppress proliferation and promote cell death in LNCaP cells (Xu et al., 2000; Weng et al., 2005; Rodriguez et al., 2014; Pronin and Slepak, 2021), thus being considered as prostate-specific GPCRs. A much higher level of *GPR160* expression was observed in human prostate cancer cells than that seen in normal prostate tissue and cells, and its knockdown was found to induce apoptosis and cell cycle arrest (Zhou et al., 2016; Guo et al., 2021). Moreover, it is noteworthy that downregulated *LHCGR* is already targeted by Goserelin and Buserelin for the treatment of prostate and breast cancer, and its transcriptional mis-regulation was reported to be closely related with other solid tumors (Tomera et al., 2001; Kirby et al., 2009; Doroszko et al., 2019; Zhong et al., 2019; Lorenzen et al., 2020). In addition, 11 of the 46 DEGpcrs identified are served as targets of approved drugs, e.g., *AGTR1* is commonly used as a target for hypertension drugs like

Valsartan, Olmesartan and Losartan (Siragy et al., 2002; Warner and Jarvis, 2002; Azizi et al., 2004). *ADRB3* is a target for the asthma treatment Salmeterol (Hoffmann et al., 2004), and *PTH1R* is targeted by the osteoporosis drugs like Teriparatide and Abaloparatide (Hattersley et al., 2016; Jolette et al., 2017). Combining our findings from PRAD, it is reasonable to assume that these drugs have the potential to be repurposed for treatment of oncology.

Next, we analyzed the distribution of DEGpcrs in different receptor subfamilies and the results are shown in Figure 1B, also seeing Supplementary Table S1 for more details. GPCRs with significant over-expression in PRAD come from five subfamilies while the under-expressed receptors are mainly distributed across four subfamilies. In brief, Class A and Olfactory Receptors include both over- and under-expressed GPCRs, whereas Class D and Other 7TM proteins do not express differentially between the tumor and normal tissues. Then, we used a Fisher's exact test to do a class enrichment analysis and the result shows that the under-expressed GPCRs in primary PRAD are significantly enriched in Class B (Fisher's exact test, p = 0.0005) and Olfactory Receptor (Fisher's exact test, p = 0.0280), while the other subfamilies do not exhibit significant enrichment (Figure 1B). These observations indicate that certain GPCR subfamilies (e.g., Class B and Olfactory Receptor) are more prone to be dysregulated in PRAD.

To gain functional insights into the dysregulated GPCRs, we first performed a Pearson correlation analysis based on the expression data from 495 primary PRAD patients in TCGA. The result shows that 109 other protein-coding genes present significant and positive correlations with the expression of 5 DEGpcrs (namely, *FAD8*, *GPRP*, *GPR160*, and *NPY4R*, Supplementary Table S3). Then, Metascape (Zhou et al., 2019), a free gene annotation web tool, was employed to conduct pathway enrichment analysis of the 114 genes. As reflected by Supplementary Figure S1A, they are significantly enriched in some cancer-related biological processes, including DNA repair, VEGFA-VEGFR2 signaling pathway, Global Genome Nucleotide Excision Repair (GG-NER), and transcriptional misregulation. Notably, two entries significantly enriched in DisGeNET (low grade prostatic intraepithelial neoplasia and prostatic intraepithelial neoplasia) both exhibit correlations with PRAD, as evidenced by Supplementary Figure S1B. Taken together, the 5 DEGpcrs and their co-expressed genes are indeed involved in cancer-related biological processes, implying their important roles in the PRAD development and progression.

In addition, to in depth comprehend the GPCR role in physiology and disease, we further grouped GPCRs in terms of their coupling preferences to different types of G-proteins (Supplementary Table S1), as it is well-known that the involvement of G proteins as intermediate transducers plays a critical role in GPCR signaling (Southan et al., 2016). As shown in Figure 1C, of the 293 GPCRs expressed in both prostate tumor and normal samples (with median expression in tumors >0.1 TPM), most (132 GPCRs) have unknown G-protein linkages. More GPCRs in the rest couple to $G_{i/o}$ (96 GPCRs) with respect to the other G proteins, followed by $G_{q/11}$ (57 GPCRs) (Figure 1C). This observation is in line with a previous pan-cancer analysis that GPCRs expressed in both tissues and tumors most frequently couple to $G_{i/o}$ and $G_{q/11}$ (Sriram et al., 2019). Also, the $G_{i/o}$-GPCRs were revealed to be particularly important in breast cancer (Lyu et al., 2021). Our observation further supports that $G_{i/o}$- and $G_{q/11}$-coupled GPCRs signals may play an important role in the cancer development and progression, thus targeting the shared signaling pathways may be beneficial to the treatment for PRAD. However, the preference is not obvious for the coupling of 46 DEGpcrs to $G_{i/o}$ and $G_{q/11}$. Of the 46 DEGpcrs, 7 are coupled to $G_{i/o}$, five are coupled to $G_{q/11}$, 6 are coupled to G_s, 2 are coupled to both $G_{i/o}$ and $G_{q/11}$, and 26 have unknown G protein linkage. Certainly, these findings are only derived from the analysis of primary prostate tumor samples and limited information about G protein linkages, and thus more efforts are required to further reveal the roles of GPCRs coupling with different G proteins in the future.

Somatic mutations of GPCRs in primary PRAD

Many thousands of mutations occur during tumorigenesis, but only a few are able to confer selective growth advantage to cancer cells, which are critical to their tumorigenic capacity. Thus, identification of "cancer driver genes" is import to develop efficient cancer detection and therapeutic approaches (Stratton et al., 2009; Stratton Michael, 2011; Martínez-Jiménez et al., 2020). To this end, we first analyzed publicly available somatic variant calls in mutation annotation format (MAF) files of primary PRAD (n = 484) from the TCGA. It was found that approximately 57.02% of tumor samples (276 out of 484) present at least one GPCR mutation. Consequently, a total of 660 somatic mutations in GPCRs are identified, including single nucleotide variants (SNVs) and small insertions and deletions (InDels). Figure 2A shows the summary of the GPCRs mutated in the 276 primary PRAD tumor samples, in which missense mutations exhibit the highest proportion among all the mutation types. At base substitution level, transitions were found to be more common than transversions, with the C > T mutation occurring predominantly. However, GPCRs exhibit a pretty low mutation frequency, with only 2.39 mutations each sample on average. Figure 2A further shows the top 10 mutated GPCRs whose mutation frequencies are lower than 4%. The most frequently mutated *ADGRB3* occurs in only 3.62% (10/276) of the samples. These observations indicate that the low mutation frequency of GPCRs likely has contributed to the limited use of GPCR-targeted drugs as cancer therapeutics (Xu et al., 2000; Insel et al., 2018; Sriram et al., 2019).

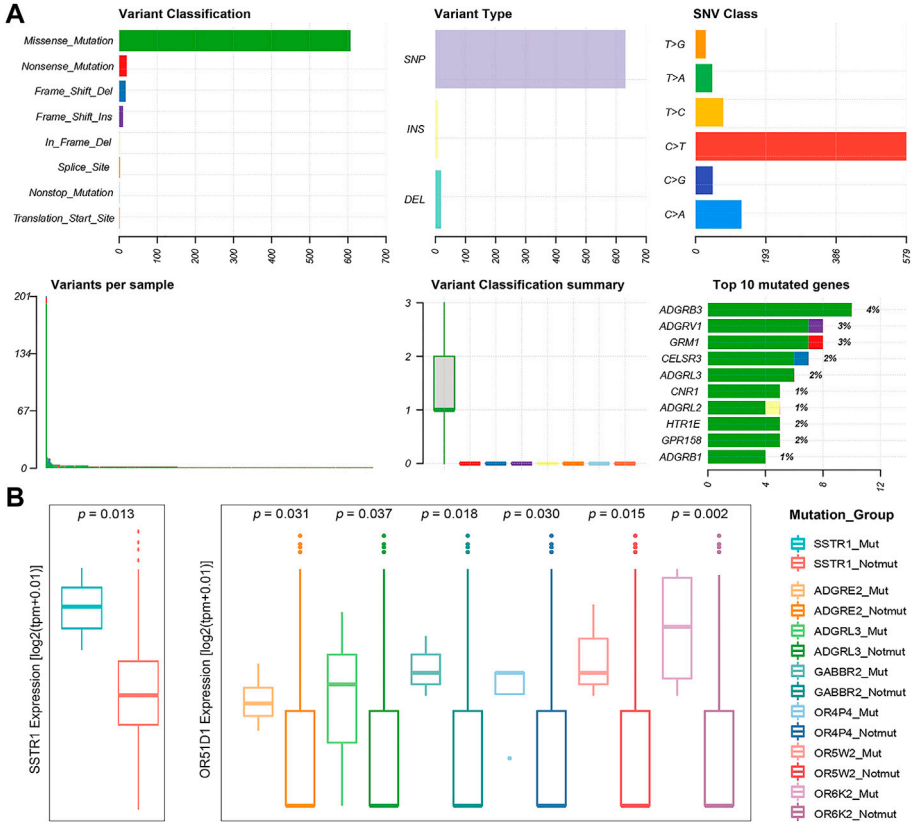

FIGURE 2
Statistics of GPCR Mutations. **(A)** A landscape of the GPCRs mutated in 276 primary prostate tumor samples generated by Maftools visualization module. **(B)** Boxplots of the expression levels of *SSTR1* (left) between the *SSTR1* mutated and unmutated groups, and *OR51D1* (right), an example of a gene that is dysregulated between the mutated and unmutated tumor samples of the other GPCR.

Subsequently, we used the MutSigCV algorithm to identify 13 significantly mutated GPCRs (SMGpcrs, p value <0.05) in tumor samples (Lawrence et al., 2013). Supplementary Table S4 summarizes their names, p values of significance and mutation frequencies. As expected, the mutation frequency of these SMGpcrs is pretty low, consistent with a previous study on the identification of oncogenic drivers (Armenia et al., 2018), which indicated that the incidence of SMGs in prostate cancer follows a long-tailed distribution with many genes mutated in less than 3% of cases. However, these mutations still probably affect a large number of patients due to the high incidence of PRAD (Armenia et al., 2018). Therefore, we may conjecture that the GPCR mutations revealed are still useful for understanding the PRAD mechanisms, although they are unlikely to stand out on a genome-wide scale due to their low frequency. In fact, many SMGpcrs identified were reported to participate in various cancer-related processes. For example, multiple mutations in metabotropic glutamate receptor 1 (*GRM1*) gene have been implicated in various tumors including PRAD, which are associated with altered protein function, downstream pathways, migration, and angiogenesis, thus contributing to tumorigenic progression (Koochekpour et al., 2012; Esseltine et al., 2013; Ali et al., 2014; Shah et al., 2019). Abnormal expression of *CNR1* has been observed in prior studies and was found to be correlated with the severity and prognosis of tumors like hepatocellular carcinoma, ovarian cancer, and PRAD (Chung et al., 2009; Messalli et al., 2014; Mukhopadhyay et al., 2015; Liu et al., 2020), but there are conflicting publications regarding the role of the cannabinoid receptor in tumor proliferation (Hart et al., 2004; Pisanti et al., 2013), for example, some groups indicated that the cannabinoid receptor exerts antitumor effects (Ramer and Hinz, 2016; Wilkie et al., 2016) while others suggested its tumor-promoting effect (McKallip et al., 2005). In addition, 8 of the 13 SMGpcrs are the olfactory receptors (ORs). Unfortunately, little attention has been paid to other potential of this receptor family besides olfaction, thus there has been very limited information for functional roles of many ectopically expressed ORs. However, in the past decade, studies bloomed linking the ectopically expressed ORs to cancer initiation, development and

TABLE 1 Binding energies, derived from MM/GBSA calculation, of the top two compounds selected in virtual screening for *GPR160* and *CRHR2* respectively.

ZINC ID	Drug name	Weight[a]	Binding energy[b]
ZINC000001550499	Cinacalcet	357.41	−23.68 ± 2.69
ZINC000001612996	Irinotecan	586.69	−20.43 ± 3.24
ZINC000164528615	Glecaprevir	838.88	−47.39 ± 4.74
ZINC000164760756	Simeprevir | Olysio	749.96	−44.87 ± 3.25

[a]g/mol.
[b]Kcal/mol.

progression (Chen et al., 2018; Maßberg and Hatt, 2018). Certainly, the GPCR's mutation rates of <5% is only derived from the data of 484 primary prostate tumor samples, thus more tumor samples should be needed to further confirm the prevalence and functional role of GPCR mutations in the future. In addition, to gain insight into the impact of these mutations on the GPCR activity, we further examine whether they are clustered on the hot spots of the related GPCRs. Herein, we focused on the 13 significantly mutated GPCRs (SMGpcrs). It was observed that three mutations (S1169L, P1079S, R981C) occur at the C-terminus of GRM1, which is a member of the metabotropic glutamate receptor (mGluR) family. As revealed, mGluRs can dimerize and bind to a variety of downstream transducers while their intracellular C-termini domains are the main targets (Enz, 2007). Thereby, the intracellular C-terminus of mGluRs is critical for designing drugs that interfere with specific protein-protein interactions (Enz, 2012). P341L mutation of HTR1E occurs in the conserved NPxxY motif. As recorded in the Uniprot database (2021), the NPxxY motif plays important role in the ligand-induced GPCR conformation change and signaling. The M461V mutation was observed to occur at the C-term in CB1R while a recent report highlighted the importance of the CB1R C-terminal domain in polarized trafficking and surface expression in cultured neurons (Fletcher-Jones et al., 2019). Unfortunately, the GPCR database has no record for the other 10 significantly mutated GPCRs and we do not find information regarding their structures and hotspots from literature. Therefore, we cannot estimate whether these mutations will impact the activities or functions of GPCRs. However, the observations from the three significantly mutated GPCRs suggest that these mutations indeed play important roles in the GPCR function. We hope that these results will attract more attention to these understudied GPCRs in the future.

Wnt signaling is one of the key cascades regulating development and stemness, which is closely associated with cancer (Zhan et al., 2017). The high frequency of WNT pathway mutations in many different cancers underscores the importance of this signaling in carcinogenesis. Therefore, besides the frequency statistics on the cancer driver genes, we also focused on the GPCR mutations involving the WNT pathway in the primary PRAD. As shown in Supplementary Figure S2, the WNT pathway carries nine GPCRs with somatic mutations (seven FZD genes and two LGR genes), implicating their oncogenic-related functions.

To investigate the potential impact of the somatic mutations on the gene expression, we integrated the gene expression data and the mutation one from 481 primary PRAD patients, and selected 50 GPCRs that mutate in at least three samples. Nearly half (43.47%, 20 out of 46) of the DEGpcrs don't harbor any mutation. Only *CNR1* is identified by MutSigCV to be a SMGpcr and is significantly downregulated in the tumor samples, implying its potential tumor suppressive effect. Using a Fisher's exact test, we evaluated whether the expression of a specific GPCR is significantly higher in the mutated samples than those lacking mutations. The result shows that none of the 50 mutated GPCRs displays significant enrichment in the highly expressed groups. In addition, we divided the tumor samples into two groups according to the presence or absence of mutations of a specific GPCR gene, and performed differential expression analysis using a Wilcoxon test. Only *SSTR1* was found to be highly expressed in its mutated samples (Figure 2B). The above observations indicate that GPCR mutation is largely independent of their expression level and dysregulations.

Although the direct correlation between the mutation status of GPCRs and their mRNA expression is not significant, are their expressions associated with the mutation status of other genes? It is found that the mRNA expression levels of 39 DEGpcrs exhibit significant differences between the mutated and not mutated groups of the other genes. As shown in Figure 2B, *OR51D1* is significantly over-expressed in samples with mutations of *ADGRE2*, *ADGRL3*, *GABBR2*, *OR4P4*, *OR5W2*, and *OR6K2*. However, the correlation is not observed in its own mutant subgroups, as evidenced by Figure 2B and Supplementary Table S5. Based on all the aforementioned findings, it is reasonable to speculate that certain GPCRs are not significantly differentially expressed in PRAD tumors due to their own mutations, yet present to some extent correlations with somatic mutations in other GPCR genes. Certainly, the number of mutant samples involved in this study is limited, and additional large-scale studies are needed to validate these findings.

Somatic copy number alterations of GPCRs in primary PRAD

SCNA is another molecular feature on the genomic level, which may cause the genome copy number of the affected cells to deviate from the normal diploid state such that affecting the stability of the genome and promoting the development of

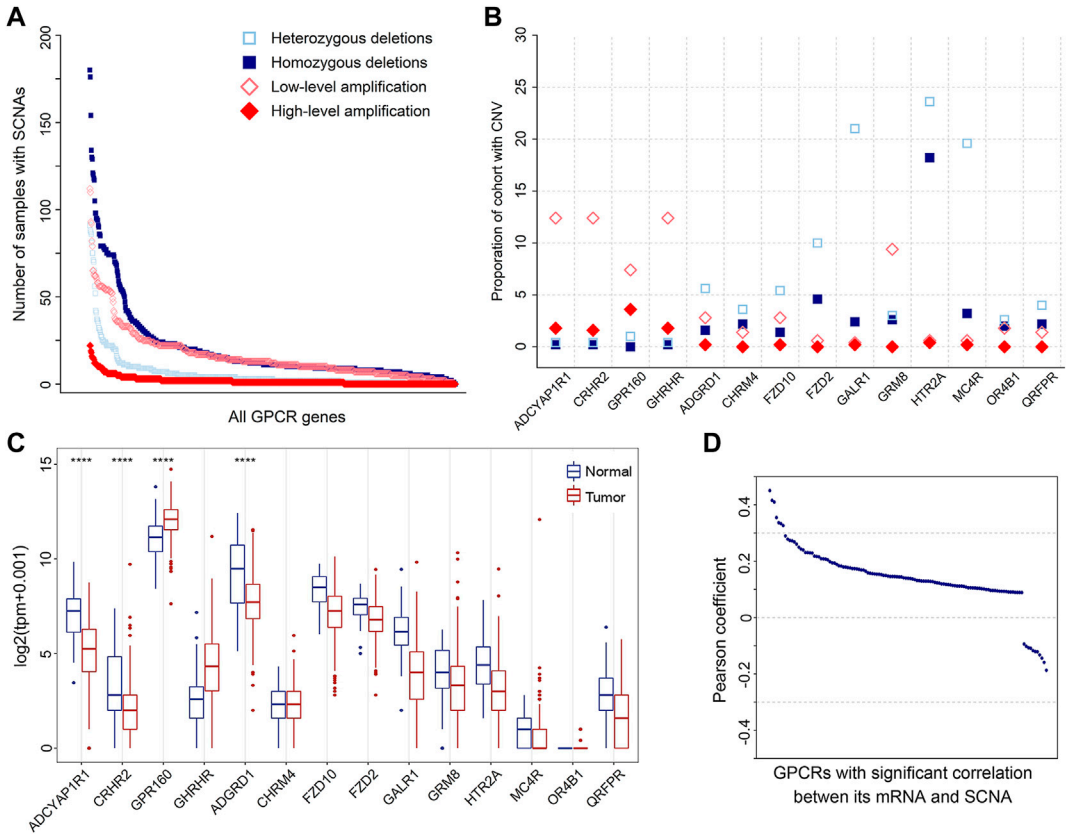

FIGURE 3
SCNAs of GPCRs in PRAD. **(A)** The number of heterozygous/homozygous deletions, and low-/high-level amplifications for all GPCRs. **(B)** Scatter plot of recurrent amplifications and deletions in 500 primary prostate tumor samples. **(C)** Box plots showing the expression of the significantly deleted and amplified GPCRs between the tumor and normal samples. **(D)** Distribution of Pearson's correlation coefficients between the GPCR expression and its linear SCNA values.

tumor cells (Albertson et al., 2003). Thus, we also analyzed SCNAs. The result shows that SCNAs occur extensively in primary prostate tumors. A total of 738 amplified and 634 deleted GPCRs were identified in 500 tumor samples, with a median of 27 amplifications (range 0–347) and 37 deletions (range 0–382) per tumor sample. The frequency distribution of samples with GPCR SCNAs is shown in Figure 3A. It can be seen that heterozygous SCNAs of GPCR genes are more common than homozygous SCNA events, which is consistent with a previous study on the GPCR SCNA events in pan-cancer (Sriram et al., 2019). Most GPCRs have a low frequency of SCNAs, as the SCNA of 571 GPCR genes occurs in 10% or less of tumor samples. However, there are still some GPCRs presenting frequent SCNAs, for example, the most frequently deleted *ADRA1A* and amplified *FZD6* occur in 52.20 and 26.80% of the tumor samples analyzed, respectively.

It was proposed that amplified and deleted GPCRs may have potential as biomarkers (Vang Nielsen et al., 2008; Sriram et al., 2019). Thus, we utilized GISTIC2.0 to detect significantly recurrent SCNA events of GPCRs (Mermel et al., 2011), and 52 significantly altered regions (q value <0.25) were identified. Figure 3B shows the identity and frequency of these significant GPCR SCNAs. The 23 amplified peak regions encompass 4 GPCRs on the chromosomes 3q and 17p, while recurrent arm-level amplifications also occur in the 2 chromosome arms. The 29 deleted peak regions harbor 10 GPCRs, three of which are on chromosomes 13q and 18p that show recurrent arm-level deletions. Therefore, the significant amplifications of *ADCYAP1R1*, *CRHR2*, *GPR160*, and *GHRHR*, and the deletions of *GALR1*, *MC4R*, and *HTR2A* are possibly attributed to their corresponding recurrent arm-level SCNAs.

By assessing the expression of GPCRs with the above recurrent focal SCNA events, we further explored the power of SCNAs in explaining why the expression levels of DEGpcrs are significantly dysregulated in cancers. The results reveal that among the four amplified GPCRs, only *GPR160* is over-

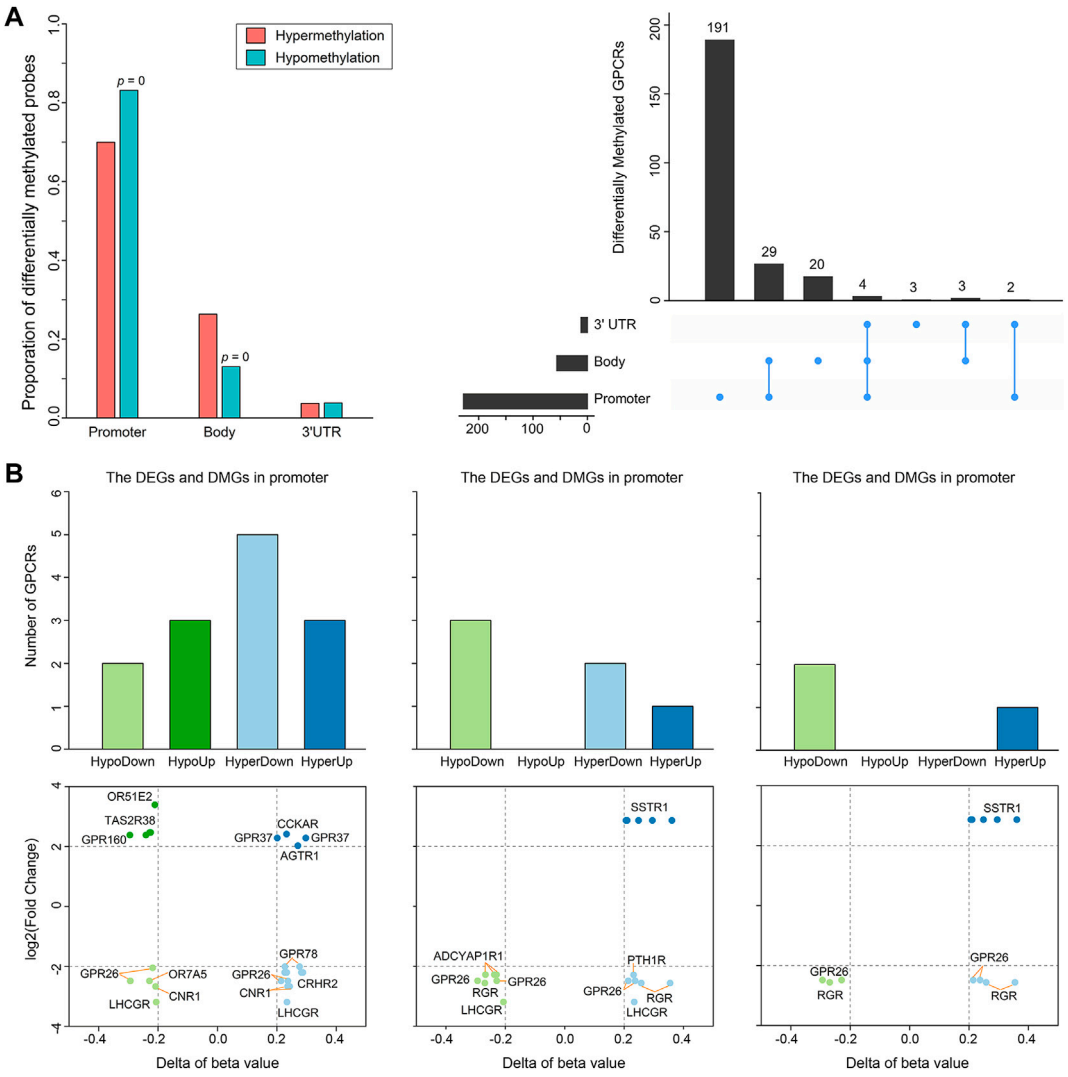

FIGURE 4
Differential methylation of GPCRs in the 491 PRAD patients. **(A)** Bar plot and Upset showing the number of DMGpcrs. **(B)** Bar plots and scatter plots showing the number and identity of DMEGs, respectively.

expressed in primary prostate tumor samples, while the other two (*CRHR2* and *ADGYAP1R1*) are significantly under-expressed. Except for *ADGRD*, the expressions of the 9 deleted GPCRs don't show statistically significant differences between the tumor and normal samples. These observations indicate that the expression of GPCRs could not be inferred from their copy number variant status. Except for *GPR160* and *ADGRD1*, SCNA alone does not generally predict the direction and extent of expressional dysregulation in prostate tumors compared to normal tissues (Figure 3C).

To further test the correlation between SCNA and mRNA expression of GPCRs, we extracted 491 primary PRAD patients with both mRNA and CNV data available and calculated their Pearson correlation coefficients. 611 of 736 GPCRs with both SCNA and mRNA data do not present significant correlations between the two features. Even though significant correlations were observed in the other 125 GPCRs, the associations are generally weak with most correlation coefficients below 0.3. Only 7 pairs exhibit correlation coefficients in the range of 0.3–0.5, as evidenced by Figure 3D. These observations indicate that no direct correlation exists between SCNA and mRNA expression for most GPCRs. Moreover, we further evaluated the GPCR mRNA expression between different PRAD groups classified by the SCNA status of the specific gene. Similarly, no significant differential expression was observed, further confirming that there is usually lack of the significant correlation between SCNA and mRNA expression of GPCRs.

DNA methylation alterations of GPCRs in primary PRAD

Besides somatic mutations and SCNAs, epigenetic changes also contribute to tumorigenesis (Villanueva et al., 2020). DNA methylation is the most widely studied epigenetic mechanism, and its alteration generally results in malignant tumors mainly by means of DNA hyper- or hypomethylation (Pan et al., 2018). Thus, we extracted DNA methylation data from 50 PRAD patients with matched control and tumor samples to conduct a comparative analysis. Statistically significant methylation changes ($|\Delta\beta| > 0.2$ and adjusted p-value < 0.05) were observed in 504 regions of 252 GPCR genes, in which 243 differentially methylated positions (DMPs) are hypermethylated and 261 DMPs are hypomethylated in the primary prostate tumor samples, as reflected by Supplementary Table S6. Considering the fact that there are different methylation characteristics and functions among different genomic regions, we divided these 504 DMPs into 170 hypermethylated DMPs and 217 hypomethylated DMPs in the promoter region, 64 hypermethylated DMPs and 34 hypomethylated DMPs in the gene body, and 9 hypermethylated DMPs and 10 hypomethylated DMPs in the 3′UTR (Figure 4A, left). As shown in Figure 4A, 214 of the 252 significantly differentially methylated GPCRs (DMGpcrs) only appear in one region, 34 genes in at least 2 regions, and only 4 genes (*GPR26*, *GPRC5C*, *GRM1* and *OPRM1*) in all the 3 regions. The observations imply that the DNA methylation is region-specific in PRAD and certain genomic regions may be more susceptible to changes than others, for example, the promoter region that involves in the most frequent methylation changes. In fact, the promoter region has been a focus of attention in DNA methylation studies and its methylation level is considered to be closely related with cancer development (Saghafinia et al., 2018).

It is well known that DNA methylation can control gene expression without incurring any change to the genomic sequence; epigenetic changes could inappropriately cause transcriptional dysregulation, causing various diseases, including cancer (Anastasiadi et al., 2018). We hence explored the relationship between DNA methylation and mRNA expression of GPCRs. It has been reported that treating methylation sites and their located genes as single units may minimize noise from unrelated methylations and gene expression (Guo et al., 2019). Therefore, we preliminarily explored the relationship between dysregulated expression and aberrant methylation of GPCRs in different regions by coupling the DEGpcrs and DMGpcrs as single units. As a result, a total of 16 differentially methylated and expressed GPCRs (DMEGpcrs) were identified, which fall into 4 classes: HypoDown, HypoUp, HyperDown and HyperUp (Supplementary Table S7). HyperDown is the most common within promoter regions (5/13, Figure 4B), suggesting that this region causes gene silencing mainly through abnormal methylation, and oncogenes and therapeutic markers have established based on such association (e.g., CDKN2A (The Cancer Genome Atlas Research Network, 2012) and BRCA1 (Cancer Genome Atlas Research Network, 2011)); the Gene body region is dominated by HypoDown (3/6, Figure 4B), while only HypoDown and HyperUp are present in the 3′UTR region (Figure 4B), indicating that the aberration of DNA methylation and expression in the gene body and 3′UTR regions usually exhibit a consistent direction. The analysis above revealed the relationship between aberrant DNA methylation and expression preliminary.

To have a more accurate picture of the association between gene expression and DNA methylation, we conducted a correlation analysis on GPCRs from 494 primary PRAD patients having both two data types. Gene expression is often negatively associated with DNA methylation within promoter regions, but positively associated with DNA methylation in gene bodies. Specifically, among the 19 mRNA - methylation pairs in the promoter regions, 14 pairs show significantly negative correlation with Pearson $r < 0$, while in the gene bodies, 7/10 significant correlated pairs present Pearson $r > 0$. For example, the expression of *GPR26* is negatively correlated with the methylation level of cg04549162 and cg11893763 (Pearson $r < -0.15$), which locate around 200 kb upstream of *GPR26*. In contrast, the expression of *GPR26* presents positive correlation with the methylation of cg25912428 (Pearson $r = 0.2359$) locating in the gene body. The observation indicates that the overexpression of *GPR26* in primary prostate tumors is probably due to its hypermethylation in promoter and hypomethylation in gene body. In fact, the positive and negative correlations have been widely reported, i.e., hypermethylation of CpG sites in promoters typically leads to transcriptional silencing, whereas hypomethylation of CpG sites in a gene body frequently results in an increase in gene expression (Shen and Laird, 2013; Sun et al., 2018). In addition, we identified a new regulatory region, the 3′UTR, with a significant positive correlation between the level methylation and expression, such as *GPR26* - cg13557752, *RGR* - cg14856914, *SSTR1* - cg04265797, and *SSTR1* - cg04573550 (Supplementary Figure S3). All the observations indicate that the alteration in expression might be due to the degree of DNA methylation, and the correlation between them is highly relied on where the DNA methylation occurs: the abnormal decrease of GPCR mRNA expression in primary PRAD is likely a result of hypermethylation in promoters and hypomethylation in gene body and 3′UTR regions. In

summary, our correlation analysis provides insights into regulatory relationships between DNA methylation and expression of GPCRs in PRAD.

Identification of GPCRs as potential therapeutic targets for drug repurposing

Characterizing the genome, epigenome, transcriptome and their interactions is vital for our understanding of cancer behavior, not only for deepening insights into cancer-related processes but also for future disease treatment and drug development. Based on the above multi-omics analysis, we identified significantly altered GPCR members in primary PRAD. Drug development targeting such receptors should be helpful for the development of effective anticancer therapies. To this end, we selected *GPR160* and *CRHR2* which significantly altered at the multi-omics layers as representatives to conduct structure-based virtual screening, which is a powerful and widely used computational approach for the identification of lead compounds (Zhao et al., 2021).

GPR160 belongs to the class A GPCR subfamily and was de-orphanized recently (Yosten et al., 2020). As outlined above, GPR160 is significantly amplified and hypermethylated in the promoter region (TSS1500 and 5′UTR), along with upregulated gene expression. Therefore, GPR160 may be a promising drug target for the treatment of PRAD. Previous experimental studies have fully revealed the involvement of GPR160 in PRAD, including its expression dysregulation at both mRNA and protein levels, and the authors further demonstrated that the knockdown of GPR160 resulted in cancer cell apoptosis and growth arrest (Zhou et al., 2016; Guo et al., 2021). Therefore, GPR160 may be a promising drug target for the treatment of PRAD. However, there has not been available crystal structure for GPR160. Thus, we used the GPR160 structure (Q9UJ42) predicted by AlphaFold at http://alphafold. Ebi. ac.uk (Varadi et al., 2021). As known, AlphaFold is a deep learning-based approach recently developed, showing remarkable success in predicting the protein structure. Then, Fpocket algorithm [86] was used to identify its ligand binding pockets, leading to ten pockets. The top scoring pocket consisting of 22 residues was selected for the subsequent virtual screening to 1615 FDA-approved drugs from ZINC (Irwin and Shoichet, 2005), which is a free database of purchasable compounds for ligand discovery and virtual screening. To obtain the stable protein-ligand complex structure, we further used 100 ns MD simulation on the top eight hits (Supplementary Table S8) of the docking result. As evidenced by RMSDs of GPR160 in Supplementary Figure S4A, all the eight systems achieve equilibriums. To obtain reliable evaluation on the binding affinity between GPR160 and the eight ligands screened, MM-GBSA was used to calculate the ligand-receptor binding free energy for the eight systems and the result is listed in Supplementary Table S8. Despite the strongest affinity of Trypan Blue to GPR160, it is not further considered as a candidate in this study due to the fact that Trypan Blue generally acts as stain and has no any reports involving the disease treatments. Here, we focused on Cinacalcet (−23.68 kcal/mol) and Irinotecan (−20.43 kcal/mol), which also show strong binding affinities to GPR160 (vide Table 1). As shown in Figure 5A, the two ligands present diverse interactions with GPR160, for example, the binding of Cinacalcet to GPR160 is mainly attributed to hydrogen bonding with SER236, LYS243 and CYS296, π-π bonding with PHE240, and halogen bonding with ILE239. The tight binding of Irinotecan to GPR160 is due to hydrogen bonding with HIS229 and SER236, π-σ bonding with THR233, amide-π interacting with CYS296, and π-alkyl bonding with ILE239. Additionally, existing studies suggested the anticancer potential of the two drugs. Cinacalcet, which is approved by FDA to treat secondary hyperparathyroidism (Nemeth et al., 1998), has shown therapeutic application for hepatocellular carcinoma (Zheng et al., 2021), and has been reported to reduces neuroblastoma tumor growth in preclinical models (Masvidal et al., 2017). Irinotecan as a camptothecin-derived drug that is the first approval for cancer treatment has contributed to the treatment of multiple cancers worldwide, including advanced colon cancer, non-small cell lung cancer, and cervical cancer (Hsiang and Liu, 1988; Bailly, 2019). The existing reports support that Cinacalcet and Irinotecan may be promising candidates for the treatment of PRAD, also confirming the reliability of our results from the virtual screening and the molecular dynamics simulation.

The analysis above already indicates that CRHR2 is significantly amplified, hypermethylated in the promoter region (TSS200 and TSS1500) and under-expressed. CRHR2, belonging to class B1 GPCRs, is best known as regulators of the stress response in the central nervous system. Although there have been seldomly reports about CRHR2 in cancer, its role in tumor formation and angiogenesis is becoming increasingly studied. For example, low or absent CRHR2 expression was found in exocrine ductal pancreatic carcinomas, PRAD and non-small cell lung cancer, in line with our findings. It was reported that expression loss of CRHR2 may contribute to prostate tumorigenesis, progression and neoangiogenesis (Reubi et al., 2003; Tezval et al., 2009). In addition, recent studies indicated that hypermethylation of CRHR2 may be responsible for lowered tissue expression of this protein (Kasprzak and Adamek, 2020). Overall, CRHR2 has been found to be dysregulated in expression and methylation in multiple cancers, and involved in angiogenesis and tumor

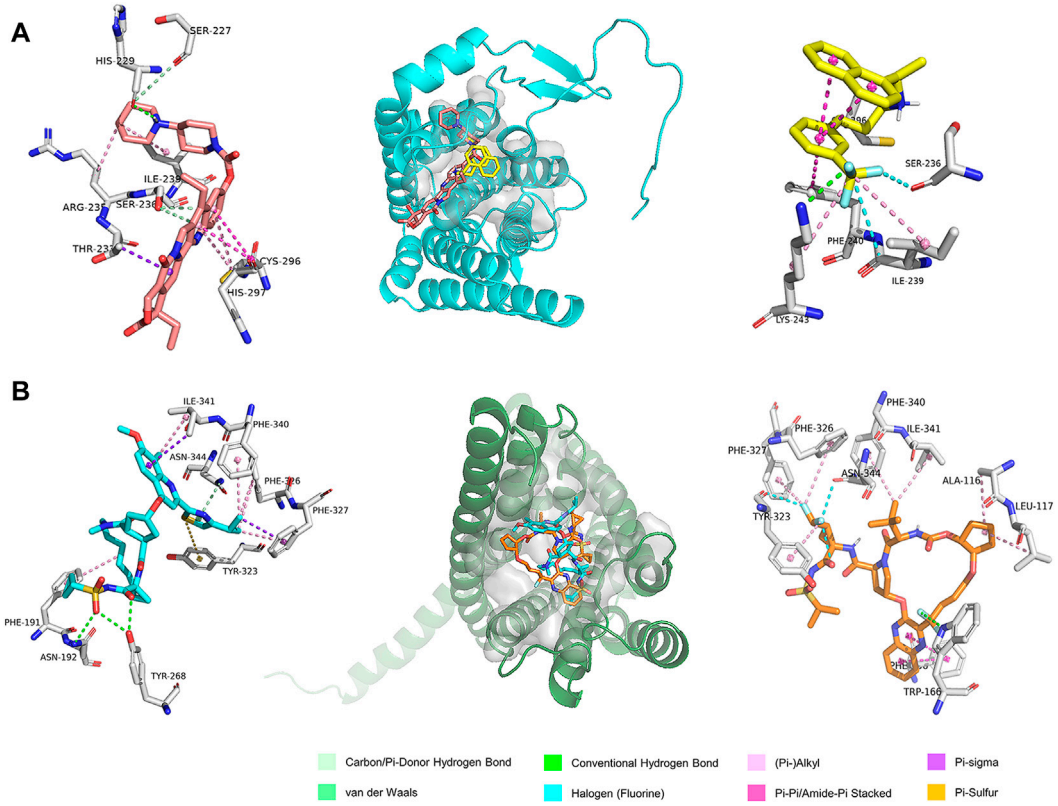

FIGURE 5
The predicted binding modes of the ligands with **(A)** GPR160 and **(B)** CRHR2 at the ligand binding pocket (dashed box). Different ligands are represented by different colored sticks, salmon: Irinotecan, yellow: Cinacalcet, orange: Simeprevir, and cyan: Glecaprevir.

progression, implying that it may be served as potential therapeutic targets in cancer. Thus, we selected the cryo-EM structure of CRNR2 co-crystallized with Urocortin 1 from human (PDB Identifier: 6PBI) (Bentley et al., 2020), and select its amino acid residues within 4 Å of the ligand binding site in 6PBI as the binding pocket for virtual screening. Similarly, we conducted 100-ns MD simulation on 8 complex systems with the top hits in the docking score and calculate their MM/GBSA energies. Glecaprevir (−47.39 kcal/mol) and Simeprevir (−44.87 kcal/mol) present the strongest binding affinity (vide Table 1), implying their potential as promising drugs to CRHR2. Figure 5B shows the predicted binding modes for the two drugs with CRHR2. Similarly, the strong binding affinities are also attributed to the diverse interactions between the two drugs and CRHR2, as reflected by Figure 5B. Glecaprevir, which has been used as the hepatitis C virus (HCV) NS3/4A protease inhibitor (Lamb, 2017), is proposed to have antitumor potential for the first time in our work report. Simeprevir, originally served as a hepatitis C antiviral agent, was recently repurposed as an effective anti-cancer agent that simultaneously inhibits two important pathways known to be involved in both tumorigenesis and treatment resistance (Park et al., 2017; Kattan et al., 2021). These previous observations also to some extent support our predictions.

However, it is noted that we screened the four high-affinity drugs for the potential targets (GPR160 and CRHR2) and evaluated the anticancer potential only by means of the computational way. As known, the docking and structure-based virtual screening aim to predict the binding mode of a ligand and its affinity to the target protein, but cannot distinguish its efficacy like agonists or antagonists or inverse agonists (Ballante et al., 2021), which need further experimental evaluation like functional assays. In addition, our screening to the potential ligands is based on the classic pharmacological dogma “one drug-one target”. Although the dogma has been dominant in drug discovery for decades, it has been recognized that inhibition of a single target is often not sufficient to generate optimal therapeutic benefit for the disease that displays polygenicity (e.g., cancer, psychiatric diseases) or involves complex biological signaling networks and feedback loops (Palve et al., 2021). In the case, multitargeted drugs and drug combinations may represent valuable complements, which are emerging as new paradigms in drug discovery (Anighoro et al., 2014; Palve et al., 2021).

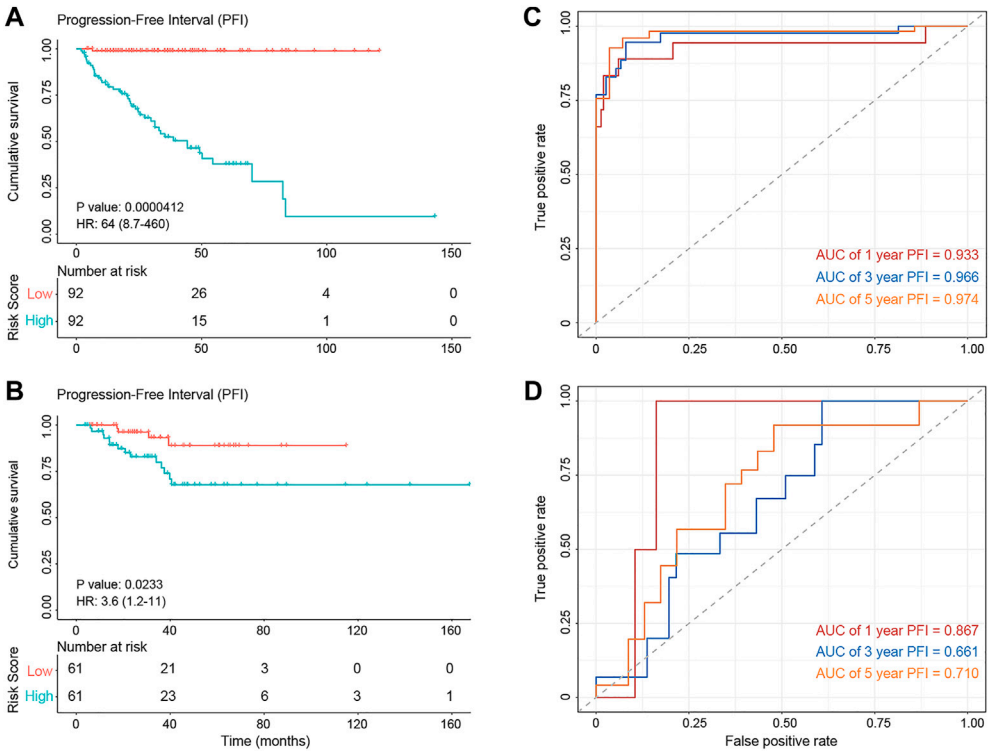

FIGURE 6
The diagnostic performance of the prognostic model. **(A,B)** Kaplan–Meier survival analysis showing PFI differences between the high-risk (red) and low-risk (blue) groups in the training set **(A)** and test set **(B)**. **(C,D)** The ROC curve showing the AUC value of the risk model in the training set **(C)** and testing set **(D)**.

Prognostic value of GPCRs in primary PRAD

GPCRs that exhibit abnormalities at the multi-omics layers should provide clues for the prognosis development, besides their value in the drug discovery. Thus, we further investigated the correlation between the abnormal molecular characteristics of GPCRs and the prognosis of PRAD patients, through which GPCR molecular features significantly associated with prognosis can be identified on one side and we also hope to build an accurate prognostic model on the other side. As some clinical features like age and tumor stage were reported to influence the prognosis of patients as well (Li et al., 2021), they were taken into account to construct the prognostic model. Supplementary Table S9 shows available clinical features collected. The univariable analysis reveals that some clinical features, gene expression and SCNA status of some GPCRs are significantly associated with PFI ($p < 0.05$). However, none of the GPCR methylation and somatic mutations reaches the statistical significance, which is different from the observations in some previous survival analyses on other genes and cancers. For example, *EGFR* and *TP53* mutations are accepted as prognostic factors in advanced non-small cell lung cancer (Jiao et al., 2018). *MUC16* mutations were found to be associated with improved outcome in patients with gastric cancer (Zeng et al., 2020). Several biomarkers based on DNA methylation changes have been identified in colorectal cancer (Gutierrez et al., 2021). In order to reduce the influence of collinearity among genes in identifying the prognostic predictors and to build a more accurate prediction model, we further performed a stepwise multivariate Cox regression analysis on the training set (n = 184) by including features significantly associated with prognosis derived from the above univariate analysis. Finally, the prognostic model is obtained by using 3 clinical features, mRNA expression of 19 GPCRs, and SCNA of 7 GPCRs, in which 13 features with HR < 1 are considered as protection factors, and 16 features with HR > 1 are risk factors. Supplementary Figure S5 lists the 29 predictors in detail. On the basis of the risk prognostic model, the risk score of each sample can be obtained. Kaplan-Meier curve in Figure 6 shows that the samples in the high-risk group exhibit worse PFI than those in the low-risk one, indicating the prognostic signature of risk score is effective (training set: log rank p = 4.12e-5, HR = 64; test set: log rank p = 0.023, HR = 3.6). In order to compare the sensitivity and specificity of the risk score on the prognosis of patients with primary PRAD, time-dependent receiver operating characteristics (ROC) analysis was also

performed, and the areas under the ROC curves (AUC) in the training set at 1, 3, and 5 years are 0.974, 0.966, and 0.933, respectively (Figure 6C). For the testing set, they are 0.87, 0.66, and 0.71, respectively (Figure 6D). Collectively, the 29 features involving the abnormal mRNA expression and copy number variants of GPCRs may serve as potential biomarkers to predict primary PRAD prognosis. Combined with the observations from the omics analysis above, it suggests that the features significantly associated with disease at the single-omics level may not serve as effective prognostic markers. For example, some GPCRs mutated significantly are not associated with the prognosis, possibly due to the fact that cancer is a disease involving multi-omics dysregulations like genetic alterations, differential DNA methylations and transcriptomic disorders. Thus, the features found at a single omic layer may be altered by subsequent regulation or modification. Thus, the combination of the multi-omics data leads to more accurate predictions, suggesting that survival prediction in oncology would likely benefit from multi-omics analysis.

Conclusion

In the work, we offer the first comprehensive landscape of multi-omics features of the GPCR family in the primary PRAD using an unbiased (-ome) approach. Several important observations are obtained:

1) GPCRs exhibit low expression levels and mutation frequencies, which should contribute to less focus on GPCRs in oncology. However, the mRNA expression and DNA methylation analysis identify 46 and 255 disease-related GPCRs, respectively, complementing information lack in the genome analysis.
2) The associations between distinct omics layers are found to be different. Most receptors don't exhibit a significant correlation between the genome and transcriptome while a tight association is observed between the transcriptome and epigenome of GPCRs, confirming the complex regulatory mechanism from DNA to RNA.
3) Four drugs (Cinacalcet, Irinotecan, Glecaprevir, and Simeprevir) targeting GPR 160 and CRHR2, which show significant alterations at different levels, are identified as potential candidates to reposition for prostate cancer by the virtual screening and molecular dynamic simulations.
4) The combination of 3 clinical characteristics and 26 GPCR molecular features identified by the transcriptome and genome exhibit good performance in predicting progression-free survival in patients with the primary PRAD, thus providing new potential biomarkers for the clinical decision.

In a whole, these observations on the GPCR family at the genomic, epigenomic, and transcriptomic levels provide new insights for understanding the mechanism of the primary PRAD, theoretically revealing the therapeutic and prognostic potential of GPCRs in PRAD. In addition, our result further confirms that the analysis of just one omics level generally provides a biased and incomplete snapshot in the complex disease progression, most probably missing some key cancer drivers. Thus, the integrated analysis considering multi-omics is beneficial to the development of new therapeutic strategies and prognostic markers. However, it is noted that our data from the public databases (TCGA and GTEX) were generated from whole blood or specific tissue samples, thus cannot capture the complex heterogeneity of single cells or the regulatory relationships between them. Recently, single-cell technologies are advancing. It is likely to generate omic data on single cells from different tissue types of interest in the future such that can accelerate new and more refined analyses.

Materials and methods

Data collection

Integrating data from the IUPHAR/BPS Guide to PHARMACOLOGY (GtoPdb, www.guidetopharmacology.org) (Alexander et al., 2019) and previous reports (Alexander et al., 2011;; Maiga et al., 2016, we compiled an annotation file of 766 GPCRs, including endogenous GPCRs (response to endogenous agonists), taste andolfactory members. We then manually check this list in NCBI Gene database, and full details of the receptor family are provided in Supplementary Table S1.

To comprehensively characterize the GPCR family in patients with primary PRAD, we collected genomic, transcriptomic and epigenomic data from publicly available databases, including The Cancer Genome Atlas (TCGA) and the Genotype-Tissue Expression (GTEx). Specifically, we downloaded both the mutation annotation format (MAF) files and SCNA data from GDC Data Portal (RRID:SCR_014514, https://portal.gdc.cancer.gov/). The RNA expression data generated by TCGA (Chang et al., 2013) and GTEx (Lonsdale et al., 2013) was obtained from the UCSC Toil RNA-seq recompute data hub (accessed on 13 December 2020) (Vivian et al., 2017) and the DNA methylation profiles came from the TCGA Hub—PRAD, both of which are stored at UCSC Genome Browser (RRID:SCR_005780, https://genome.ucsc.edu) (Goldman et al., 2020). In addition, the clinical information was retrieved from TCGA, UCSC Xena and Broad GDAC Firehose (https://gdac.broadinstitute.org/), which is listed in Supplementary Table S9.

mRNA expression analysis

Firstly, we applied the "DESeq2" package with the threshold of $|\log_2$ fold-change$| > 2$ and adjusted p-value < 0.05 to select DEGpcrs in the primary prostate tumor samples compared with non-tumor ones (Love et al., 2014). Then, the class enrichment analysis was carried out for the over-or under-expressed group, using the R *fisher. test* function. Finally, the "corrplot" package was used to calculate Pearson correlation of the tumor gene expression between DEGpcrs and other protein-coding genes. Then, genes with a p value <0.05 were identified to perform enrichment analysis by the Metascape web-based portal (http://metascape.org) (Zhou et al., 2019).

Somatic mutation analysis

Maftools (Mayakonda et al., 2018), which is already implemented as a R package, was applied to annotate, analyze and visualize the GPCR mutations from the MAF file of primary PRAD. The definition of SMGpcrs in tumor samples was performed by running the MutSigCV software with default parameters (Lawrence et al., 2013). Genes with $p < 0.05$ were considered to be significantly mutated.

Somatic copy number alteration analysis

SCNAs of primary PRAD patients were analyzed by the GISTIC2 algorithm (Mermel et al., 2011), which is freely available as a module on the GenePattern web server at https://cloud.genepattern.org/gp/pages/index.jsf. The parameters were set as follows: "-refgene: Human_Hg38. UCSC.add_miR.160920. refgene.mat, -ta (-td): 0.25, focal length cutoff: 0.70, -genegistic: yes, -conf: 0.9, -qvt: 0.25, -broad: yes, -armpeel: yes".

DNA methylation analysis

Differences in DNA methylation levels between the primary prostate tumor samples and the non-tumor ones were quantified using the *ChAMP* package (RRID:SCR_012891) (Morris et al., 2014). We determined DMPs with a threshold of |delta β-value| > 0.2 and adjusted p-value < 0.05. DMPs were subsequently classified into different regions based on annotation from *ChAMP*: TSS1500, TSS200, Body, 1stExon, 3′UTR, and 5′UTR.

Drug screening

There has been lack of a crystal structure for GPR160. BLASTP search and alignment did not identify a template with high sequence similarity. Thus, the predicted structure Q9UJ42 by AlphaFold was used for subsequent docking analysis (Varadi et al., 2021). Then, the potential binding region of GPR160 is identified by using Fpocket (Le Guilloux et al., 2009) that is a well-known pocket detection package based on the alpha sphere theory. As for CRHR2, the cryoelectronic microscopy structure of UCN1-bound CRF2R with the stimulatory G protein was obtained from GPCRdb (Kooistra et al., 2021) (https://gpcrdb.org/structure/refined/6PB1), and amino acids located at the vicinity of 4 Å from the ligand are considered as main binding residues. Thereafter, crystallographic ligands, stimulatory G protein and water molecules were excluded from the crystal structures. Polar hydrogens were then added to each protein by using Autodock tools (Morris et al., 2009). To achieve the goal of drug repurposing, a library of 1615 FDA-approved drugs obtained from the ZINC database, which is a free database of purchasable compounds for ligand discovery and virtual screening, were used for screening ligands (Irwin and Shoichet, 2005). Prior to docking studies, the proteins and small molecules were all saved into pdbqt format in preparation.

The virtual screening tasks were carried out by using AutoDock Vina, a freely available structure-based virtual screening docking program (Trott and Olson, 2010) with "exhaustiveness = 20, energy_range = 10, num_modes = 100" and other parameters being set to default. Based on the docking score, we selected the top eight hits of each receptor for molecular dynamics (MD) simulation. Membrane systems were constructed using the CHARMM-GUI Membrane Builder (Jo et al., 2009). Each system was simulated for 100 ns using AMBER16 (Case et al., 2016). In addition, we used molecular mechanics/generalized Born surface area (MM/GBSA) implemented in Amber16 to calculate the binding free energy of each complex, based on the last 20 ns equilibrium trajectory (Kollman et al., 2000).

Survival analysis

In order to assess the prognostic value of each variable in PRAD, the univariate Cox analysis was adopted, in which the molecular and clinical characteristics were considered. The molecular characteristics involve important features at the somatic mutation and SCNA, DNA methylation levels and mRNA expression of GPCRs. To develop a prognostic model and evaluate its performance, we divided the cohort into a training set (60% of samples, n = 184) and a test set (40%, n = 122), in which the samples were proportionally allocated from each PFI type without replacement. Then, the significant features with p-value < 0.05 in the univariate Cox analysis were collected to perform a stepwise multiple Cox regression analysis on the training set. A patient's risk score for PFI can be obtained

by a linear combination of the regression coefficient derived from the multivariate analysis and the value of each significant variable, through which we could stratify patients into "high-risk" and "low-risk" groups. The PFI distribution of each group was described by the Kaplan-Meier curves and statistical significance was calculated using the log rank test. The predictive performance of the prognostic model was evaluated by c-index and ROC curves. Survival analysis and corresponding visualization were performed by using the R package "survival", "survminer", and "timeROC" (Blanche et al., 2013).

Statistical analysis

For the correlation analyses between the gene expression and other molecular profiles, the following methods were used: 1) for continuous variables, including relative linear copy number values and DNA methylation levels, Pearson correlation was performed; 2) for categorical variables, the samples were divided into two groups based on a specific attribute (e.g., whether the specific GPCR was mutated), and then the non-parametric Mann-Whitney *U* test was performed to test the significant difference. $p < 0.05$ was considered statistically significant.

Data availability statement

The datasets presented in this study can be found in online repositories. The names of the repository/repositories and accession number(s) can be found in the article/Supplementary Material.

Author contributions

SL, XP, and ML designed the research. SL, JC, and XC performed the research. JY and JC performed MD simulation and analysis. SL and YG analyzed the data. SL and XP wrote the manuscript. All authors reviewed the manuscript.

Funding

This project is supported by Sichuan international science and technology innovation cooperation project (Grant No. 2021YFH0140), the National Natural Science Foundation of China (Grant No. 22173065), and the Science and Technology Department of Sichuan Province (Grant No. 2022YFG0185).

Conflict of interest

The authors declare that the research was conducted in the absence of any commercial or financial relationships that could be construed as a potential conflict of interest.

Publisher's note

All claims expressed in this article are solely those of the authors and do not necessarily represent those of their affiliated organizations, or those of the publisher, the editors and the reviewers. Any product that may be evaluated in this article, or claim that may be made by its manufacturer, is not guaranteed or endorsed by the publisher.

Supplementary material

The Supplementary Material for this article can be found online at: https://www.frontiersin.org/articles/10.3389/fphar.2022.997664/full#supplementary-material

References

Albanito, L., Lappano, R., Madeo, A., Chimento, A., Prossnitz Eric, R., Cappello Anna, R., et al. (2008). Retracted: G-protein–coupled receptor 30 and estrogen receptor-α are involved in the proliferative effects induced by atrazine in ovarian cancer cells. *Environ. Health Perspect.* 116 (12), 1648–1655. doi:10.1289/ehp.11297

Albertson, D. G., Collins, C., McCormick, F., and Gray, J. W. (2003). Chromosome aberrations in solid tumors. *Nat. Genet.* 34 (4), 369–376. doi:10.1038/ng1215

Alexander, S. P. H., Mathie, A., and Peters, J. A. (2011). G protein-coupled receptors. *Br. J. Pharmacol.* 164, S5–S113. doi:10.1111/j.1476-5381.2011.01649_3.x

Alexander, S. P. H., Christopoulos, A., Davenport, A. P., Kelly, E., Mathie, A., Peters, J. A., et al. (2019). The concise Guide to pharmacology 2019/20: G protein-coupled receptors. *Br. J. Pharmacol.* 176, S21–S141. doi:10.1111/bph.14748

Ali, S., Shourideh, M., and Koochekpour, S. (2014). Identification of novel GRM1 mutations and single nucleotide polymorphisms in prostate cancer cell lines and tissues. *PLOS ONE* 9 (7), e103204. doi:10.1371/journal.pone.0103204

Anastasiadi, D., Esteve-Codina, A., and Piferrer, F. (2018). Consistent inverse correlation between DNA methylation of the first intron and gene expression across tissues and species. *Epigenetics Chromatin* 11 (1), 37. doi:10.1186/s13072-018-0205-1

Anighoro, A., Bajorath, J., and Rastelli, G. (2014). Polypharmacology: Challenges and opportunities in drug discovery. *J. Med. Chem.* 57 (19), 7874–7887. doi:10.1021/jm5006463

Armenia, J., Wankowicz, S. A. M., Liu, D., Gao, J., Kundra, R., Reznik, E., et al. (2018). The long tail of oncogenic drivers in prostate cancer. *Nat. Genet.* 50 (5), 645–651. doi:10.1038/s41588-018-0078-z

Azizi, M., Ménard, J., Bissery, A., Guyenne, T.-T., Bura-Rivière, A., Vaidyanathan, S., et al. (2004). Pharmacologic demonstration of the synergistic effects of a combination of the renin inhibitor aliskiren and the AT1 receptor antagonist valsartan on the angiotensin II–renin feedback interruption. *J. Am. Soc. Nephrol.* 15 (12), 3126–3133. doi:10.1097/01.ASN.0000146686.35541.29

Bailly, C. (2019). Irinotecan: 25 years of cancer treatment. *Pharmacol. Res.* 148, 104398. doi:10.1016/j.phrs.2019.104398

Balkwill, F. (2004). Cancer and the chemokine network. *Nat. Rev. Cancer* 4 (7), 540–550. doi:10.1038/nrc1388

Ballante, F., Kooistra, A. J., Kampen, S., de Graaf, C., and Carlsson, J. (2021). Structure-based virtual screening for ligands of G protein-coupled receptors: What can molecular docking do for you? *Pharmacol. Rev.* 73 (4), 527–565. doi:10.1124/pharmrev.120.000246

Bentley, M. R., Ilyichova, O. V., Wang, G., Williams, M. L., Sharma, G., Alwan, W. S., et al. (2020). Rapid elaboration of fragments into leads by X-ray crystallographic screening of parallel chemical libraries (REFiLX). *J. Med. Chem.* 63 (13), 6863–6875. doi:10.1021/acs.jmedchem.0c00111

Blanche, P., Dartigues, J. F., and Jacqmin-Gadda, H. (2013). Estimating and comparing time-dependent areas under receiver operating characteristic curves for censored event times with competing risks. *Stat. Med.* 32 (30), 5381–5397. doi:10.1002/sim.5958

Cancer Genome Atlas Research Network (2011). Integrated genomic analyses of ovarian carcinoma. *Nature* 474 (7353), 609–615. doi:10.1038/nature10166

Case, D., Betz, R., Cerutti, D., Cheatham, T., Darden, T., III, Duke, R., et al. (2016). *Amber 2016*. California, United States: University of California. Google Scholar.

Chan, Q. K. Y., Lam, H. M., Ng, C. F., Lee, A. Y. Y., Chan, E. S. Y., Ng, H. K., et al. (2010). Activation of GPR30 inhibits the growth of prostate cancer cells through sustained activation of Erk1/2, c-jun/c-fos-dependent upregulation of p21, and induction of G2 cell-cycle arrest. *Cell. Death Differ.* 17 (9), 1511–1523. doi:10.1038/cdd.2010.20

Chang, K., Creighton, C. J., Davis, C., Donehower, L., Drummond, J., Wheeler, D., et al. (2013). The cancer genome Atlas pan-cancer analysis project. *Nat. Genet.* 45 (10), 1113–1120. doi:10.1038/ng.2764

Chaudhary, P. K., and Kim, S. (2021). An insight into GPCR and G-proteins as cancer drivers. *Cells* 10 (12), 3288. doi:10.3390/cells10123288

Chen, Z., Zhao, H., Fu, N., and Chen, L. (2018). The diversified function and potential therapy of ectopic olfactory receptors in non-olfactory tissues. *J. Cell. Physiol.* 233 (3), 2104–2115. doi:10.1002/jcp.25929

Chevalier, N., Vega, A., Bouskine, A., Siddeek, B., Michiels, J.-F., Chevallier, D., et al. (2012). GPR30, the non-classical membrane G protein related estrogen receptor, is overexpressed in human seminoma and promotes seminoma cell proliferation. *PLOS ONE* 7 (4), e34672. doi:10.1371/journal.pone.0034672

Chung, S. C., Hammarsten, P., Josefsson, A., Stattin, P., Granfors, T., Egevad, L., et al. (2009). A high cannabinoid CB1 receptor immunoreactivity is associated with disease severity and outcome in prostate cancer. *Eur. J. Cancer* 45 (1), 174–182. doi:10.1016/j.ejca.2008.10.010

Cooperberg, M. R., Broering, J. M., and Carroll, P. R. (2010). Time trends and local variation in primary treatment of localized prostate cancer. *J. Clin. Oncol.* 28 (7), 1117–1123. doi:10.1200/JCO.2009.26.0133

Doroszko, M., Chrusciel, M., Stelmaszewska, J., Slezak, T., Anisimowicz, S., Plöckinger, U., et al. (2019). GnRH antagonist treatment of malignant adrenocortical tumors. *Endocr. Relat. Cancer* 26 (1), 103–117. doi:10.1530/ERC-17-0399

Du, G.-Q., Zhou, L., Chen, X.-Y., Wan, X.-P., and He, Y.-Y. (2012). The G protein-coupled receptor GPR30 mediates the proliferative and invasive effects induced by hydroxytamoxifen in endometrial cancer cells. *Biochem. Biophys. Res. Commun.* 420 (2), 343–349. doi:10.1016/j.bbrc.2012.02.161

Enz, R. (2012). Structure of metabotropic glutamate receptor C-terminal domains in contact with interacting proteins. *Front. Mol. Neurosci.* 5, 52. doi:10.3389/fnmol.2012.00052

Enz, R. (2007). The trick of the tail: Protein-protein interactions of metabotropic glutamate receptors. *Bioessays* 29 (1), 60–73. doi:10.1002/bies.20518

Esseltine, J. L., Willard, M. D., Wulur, I. H., Lajiness, M. E., Barber, T. D., and Ferguson, S. S. G. (2013). Somatic mutations in GRM1 in cancer alter metabotropic glutamate receptor 1 intracellular localization and signaling. *Mol. Pharmacol.* 83 (4), 770–780. doi:10.1124/mol.112.081695

Filardo, E. J., Graeber, C. T., Quinn, J. A., Resnick, M. B., Giri, D., DeLellis, R. A., et al. (2006). Distribution of GPR30, a seven membrane–spanning estrogen receptor, in primary breast cancer and its association with clinicopathologic determinants of tumor progression. *Clin. Cancer Res.* 12 (21), 6359–6366. doi:10.1158/1078-0432.CCR-06-0860

Fletcher-Jones, A., Hildick, K. L., Evans, A. J., Nakamura, Y., Wilkinson, K. A., and Henley, J. M. (2019). The C-terminal helix 9 motif in rat cannabinoid receptor type 1 regulates axonal trafficking and surface expression. *Elife* 8, e44252. doi:10.7554/eLife.44252

Force, U. S. P. S. T., Grossman, D. C., Curry, S. J., Owens, D. K., Bibbins-Domingo, K., Caughey, A. B., et al. (2018). Screening for prostate cancer: US preventive services task force recommendation statement. *JAMA* 319 (18), 1901–1913. doi:10.1001/jama.2018.3710

Fredriksson, R., Lagerström, M. C., Lundin, L.-G., and Schiöth, H. B. (2003). The G-protein-coupled receptors in the human genome form five main families. Phylogenetic analysis, paralogon groups, and fingerprints. *Mol. Pharmacol.* 63 (6), 1256–1272. doi:10.1124/mol.63.6.1256

Goldman, M. J., Craft, B., Hastie, M., Repečka, K., McDade, F., Kamath, A., et al. (2020). Visualizing and interpreting cancer genomics data via the Xena platform. *Nat. Biotechnol.* 38 (6), 675–678. doi:10.1038/s41587-020-0546-8

Guo, M., Sinha, S., and Wang, S. M. (2019). Coupled genome-wide DNA methylation and transcription analysis identified rich biomarkers and drug targets in triple-negative breast cancer. *Cancers (Basel)* 11 (11), E1724. doi:10.3390/cancers11111724

Guo, W., Zhang, J., Zhou, Y., Zhou, C., Yang, Y., Cong, Z., et al. (2021). GPR160 is a potential biomarker associated with prostate cancer. *Signal Transduct. Target. Ther.* 6 (1), 241. doi:10.1038/s41392-021-00583-7

Gutierrez, A., Demond, H., Brebi, P., and Ili, C. G. (2021). Novel methylation biomarkers for colorectal cancer prognosis. *Biomolecules* 11 (11), 1722. doi:10.3390/biom11111722

Hart, S., Fischer, O. M., and Ullrich, A. (2004). Cannabinoids induce cancer cell proliferation via tumor necrosis factor α-converting enzyme (TACE/ADAM17)-Mediated transactivation of the epidermal growth factor receptor. *Cancer Res.* 64 (6), 1943–1950. doi:10.1158/0008-5472.CAN-03-3720

Hattersley, G., Dean, T., Corbin, B. A., Bahar, H., and Gardella, T. J. (2016). Binding selectivity of abaloparatide for PTH-type-1-receptor conformations and effects on downstream signaling. *Endocrinology* 157 (1), 141–149. doi:10.1210/en.2015-1726

Hauser, A. S., Attwood, M. M., Rask-Andersen, M., Schiöth, H. B., and Gloriam, D. E. (2017). Trends in GPCR drug discovery: New agents, targets and indications. *Nat. Rev. Drug Discov.* 16 (12), 829–842. doi:10.1038/nrd.2017.178

Hoffmann, C., Leitz, M. R., Oberdorf-Maass, S., Lohse, M. J., and Klotz, K. N. (2004). Comparative pharmacology of human beta-adrenergic receptor subtypes--characterization of stably transfected receptors in CHO cells. *Naunyn. Schmiedeb. Arch. Pharmacol.* 369 (2), 151–159. doi:10.1007/s00210-003-0860-y

Hsiang, Y. H., and Liu, L. F. (1988). Identification of mammalian DNA topoisomerase I as an intracellular target of the anticancer drug camptothecin. *Cancer Res.* 48 (7), 1722–1726.

Innamorati, G., Valenti, M. T., Giovinazzo, F., Carbonare, L. D., Parenti, M., and Bassi, C. (2011). Molecular approaches to target GPCRs in cancer therapy. *Pharmaceuticals* 4 (4), 567–589. doi:10.3390/ph4040567

Insel, P. A., Sriram, K., Gorr, M. W., Wiley, S. Z., Michkov, A., Salmerón, C., et al. (2019). GPCRomics: An approach to discover GPCR drug targets. *Trends Pharmacol. Sci.* 40 (6), 378–387. doi:10.1016/j.tips.2019.04.001

Insel, P. A., Sriram, K., Wiley, S. Z., Wilderman, A., Katakia, T., McCann, T., et al. (2018). GPCRomics: GPCR expression in cancer cells and tumors identifies new, potential biomarkers and therapeutic targets. *Front. Pharmacol.* 9, 431. doi:10.3389/fphar.2018.00431

Irwin, J. J., and Shoichet, B. K. (2005). ZINC - a free database of commercially available compounds for virtual screening. *J. Chem. Inf. Model.* 45 (1), 177–182. doi:10.1021/ci049714+

Jiao, X. D., Qin, B. D., You, P., Cai, J., and Zang, Y. S. (2018). The prognostic value of TP53 and its correlation with EGFR mutation in advanced non-small cell lung cancer, an analysis based on cBioPortal data base. *Lung Cancer* 123, 70–75. doi:10.1016/j.lungcan.2018.07.003

Jo, S., Lim, J. B., Klauda, J. B., and Im, W. (2009). CHARMM-GUI membrane builder for mixed bilayers and its application to yeast membranes. *Biophys. J.* 97 (1), 50–58. doi:10.1016/j.bpj.2009.04.013

Jolette, J., Attalla, B., Varela, A., Long, G. G., Mellal, N., Trimm, S., et al. (2017). Comparing the incidence of bone tumors in rats chronically exposed to the selective PTH type 1 receptor agonist abaloparatide or PTH(1–34). *Regul. Toxicol. Pharmacol.* 86, 356–365. doi:10.1016/j.yrtph.2017.04.001

Kasprzak, A., and Adamek, A. (2020). The neuropeptide system and colorectal cancer liver metastases: Mechanisms and management. *Int. J. Mol. Sci.* 21 (10), E3494. doi:10.3390/ijms21103494

Kattan, W. E., Liu, J., Montufar-Solis, D., Liang, H., Brahmendra Barathi, B., van der Hoeven, R., et al. (2021). Components of the phosphatidylserine endoplasmic reticulum to plasma membrane transport mechanism as targets for KRAS inhibition in pancreatic cancer. *Proc. Natl. Acad. Sci. U. S. A.* 118 (51), e2114126118. doi:10.1073/pnas.2114126118

Kaushik, A. C., Mehmood, A., Dai, X., and Wei, D. Q. (2020). Pan-cancer analysis and drug formulation for GPR139 and GPR142. *Front. Pharmacol.* 11, 521245. doi:10.3389/fphar.2020.521245

Kirby, R. S., Fitzpatrick, J. M., and Clarke, N. (2009). Abarelix and other gonadotrophin-releasing hormone antagonists in prostate cancer. *BJU Int.* 104 (11), 1580–1584. doi:10.1111/j.1464-410X.2009.08924.x

Klotz, L., Vesprini, D., Sethukavalan, P., Jethava, V., Zhang, L., Jain, S., et al. (2014). Long-term follow-up of a large active surveillance cohort of patients with prostate cancer. *J. Clin. Oncol.* 33 (3), 272–277. doi:10.1200/JCO.2014.55.1192

Kollman, P. A., Massova, I., Reyes, C., Kuhn, B., Huo, S., Chong, L., et al. (2000). Calculating structures and free energies of complex molecules: Combining molecular mechanics and continuum models. *Acc. Chem. Res.* 33 (12), 889–897. doi:10.1021/ar000033j

Koochekpour, S., Majumdar, S., Azabdaftari, G., Attwood, K., Scioneaux, R., Subramani, D., et al. (2012). Serum glutamate levels correlate with gleason score and glutamate blockade decreases proliferation, migration, and invasion and induces apoptosis in prostate cancer cells. *Clin. Cancer Res.* 18 (21), 5888–5901. doi:10.1158/1078-0432.CCR-12-1308

Kooistra, A. J., Mordalski, S., Pándy-Szekeres, G., Esguerra, M., Mamyrbekov, A., Munk, C., et al. (2021). GPCRdb in 2021: Integrating GPCR sequence, structure and function. *Nucleic Acids Res.* 49 (D1), D335–D343. doi:10.1093/nar/gkaa1080

Lamb, Y. N. (2017). Glecaprevir/Pibrentasvir: First global approval. *Drugs* 77 (16), 1797–1804. doi:10.1007/s40265-017-0817-y

Lawrence, M. S., Stojanov, P., Polak, P., Kryukov, G. V., Cibulskis, K., Sivachenko, A., et al. (2013). Mutational heterogeneity in cancer and the search for new cancer-associated genes. *Nature* 499 (7457), 214–218. doi:10.1038/nature12213

Le Guilloux, V., Schmidtke, P., and Tuffery, P. (2009). Fpocket: An open source platform for ligand pocket detection. *BMC Bioinforma.* 10 (1), 168. doi:10.1186/1471-2105-10-168

Li, R., Wang, S., Cui, Y., Qu, H., Chater, J. M., Zhang, L., et al. (2021). Extended application of genomic selection to screen multiomics data for prognostic signatures of prostate cancer. *Brief. Bioinform.* 22 (3), bbaa197. doi:10.1093/bib/bbaa197

Liu, C., Sadat, S. H., Ebisumoto, K., Sakai, A., Panuganti, B. A., Ren, S., et al. (2020). Cannabinoids promote progression of HPV-positive head and neck squamous cell carcinoma via p38 MAPK activation. *Clin. Cancer Res.* 26 (11), 2693–2703. doi:10.1158/1078-0432.CCR-18-3301

Liu, M., Zhao, Y. Y., Yang, F., Wang, J. Y., Shi, X. H., Zhu, X. Q., et al. (2016). Evidence for a role of GPRC6A in prostate cancer metastasis based on case-control and *in vitro* analyses. *Eur. Rev. Med. Pharmacol. Sci.* 20 (11), 2235–2248.

Lonsdale, J., Thomas, J., Salvatore, M., Phillips, R., Lo, E., Shad, S., et al. (2013). The genotype-tissue expression (GTEx) project. *Nat. Genet.* 45 (6), 580–585. doi:10.1038/ng.2653

Lorenzen, M., Nielsen, J. E., Andreassen, C. H., Juul, A., Toft, B. G., Rajpert-De Meyts, E., et al. (2020). Luteinizing hormone receptor is expressed in testicular germ cell tumors: Possible implications for tumor growth and prognosis. *Cancers* 12 (6), E1358. doi:10.3390/cancers12061358

Love, M. I., Huber, W., and Anders, S. (2014). Moderated estimation of fold change and dispersion for RNA-seq data with DESeq2. *Genome Biol.* 15 (12), 550. doi:10.1186/s13059-014-0550-8

Lyu, C., Ye, Y., Lensing, M. M., Wagner, K. U., Weigel, R. J., and Chen, S. (2021). Targeting Gi/o protein-coupled receptor signaling blocks HER2-induced breast cancer development and enhances HER2-targeted therapy. *JCI Insight* 6 (18), e150532. doi:10.1172/jci.insight.150532

Maiga, A., Lemieux, S., Pabst, C., Lavallée, V. P., Bouvier, M., Sauvageau, G., et al. (2016). Transcriptome analysis of G protein-coupled receptors in distinct genetic subgroups of acute myeloid leukemia: Identification of potential disease-specific targets. *Blood Cancer J.* 6 (6), e431. doi:10.1038/bcj.2016.36

Malchinkhuu, E., Sato, K., Maehama, T., Mogi, C., Tomura, H., Ishiuchi, S., et al. (2008). S1P2 receptors mediate inhibition of glioma cell migration through Rho signaling pathways independent of PTEN. *Biochem. Biophys. Res. Commun.* 366 (4), 963–968. doi:10.1016/j.bbrc.2007.12.054

Martínez-Jiménez, F., Muiños, F., Sentís, I., Deu-Pons, J., Reyes-Salazar, I., Arnedo-Pac, C., et al. (2020). A compendium of mutational cancer driver genes. *Nat. Rev. Cancer* 20 (10), 555–572. doi:10.1038/s41568-020-0290-x

Masvidal, L., Iniesta, R., García, M., Casalà, C., Lavarino, C., Mora, J., et al. (2017). Genetic variants in the promoter region of the calcium-sensing receptor gene are associated with its down-regulation in neuroblastic tumors. *Mol. Carcinog.* 56 (4), 1281–1289. doi:10.1002/mc.22589

Mayakonda, A., Lin, D. C., Assenov, Y., Plass, C., and Koeffler, H. P. (2018). Maftools: Efficient and comprehensive analysis of somatic variants in cancer. *Genome Res.* 28 (11), 1747–1756. doi:10.1101/gr.239244.118

Maßberg, D., and Hatt, H. (2018). Human olfactory receptors: Novel cellular functions outside of the nose. *Physiol. Rev.* 98 (3), 1739–1763. doi:10.1152/physrev.00013.2017

McKallip, R. J., Nagarkatti, M., and Nagarkatti, P. S. (2005). Delta-9-tetrahydrocannabinol enhances breast cancer growth and metastasis by suppression of the antitumor immune response. *J. Immunol.* 174 (6), 3281–3289. doi:10.4049/jimmunol.174.6.3281

Mermel, C. H., Schumacher, S. E., Hill, B., Meyerson, M. L., Beroukhim, R., and Getz, G. (2011). GISTIC2.0 facilitates sensitive and confident localization of the targets of focal somatic copy-number alteration in human cancers. *Genome Biol.* 12 (4), R41. doi:10.1186/gb-2011-12-4-r41

Messalli, E. M., Grauso, F., Luise, R., Angelini, A., and Rossiello, R. (2014). Cannabinoid receptor type 1 immunoreactivity and disease severity in human epithelial ovarian tumors. *Am. J. Obstet. Gynecol.* 211 (3), 234.e1–6. e236. doi:10.1016/j.ajog.2014.04.004

Morris, G. M., Huey, R., Lindstrom, W., Sanner, M. F., Belew, R. K., Goodsell, D. S., et al. (2009). AutoDock4 and AutoDockTools4: Automated docking with selective receptor flexibility. *J. Comput. Chem.* 30 (16), 2785–2791. doi:10.1002/jcc.21256

Morris, T. J., Butcher, L. M., Feber, A., Teschendorff, A. E., Chakravarthy, A. R., Wojdacz, T. K., et al. (2014). ChAMP: 450k chip analysis methylation pipeline. *Bioinformatics* 30 (3), 428–430. doi:10.1093/bioinformatics/btt684

Mukhopadhyay, B., Schuebel, K., Mukhopadhyay, P., Cinar, R., Godlewski, G., Xiong, K., et al. (2015). Cannabinoid receptor 1 promotes hepatocellular carcinoma initiation and progression through multiple mechanisms. *Hepatology* 61 (5), 1615–1626. doi:10.1002/hep.27686

Nemeth, E. F., Steffey, M. E., Hammerland, L. G., Hung, B. C., Van Wagenen, B. C., DelMar, E. G., et al. (1998). Calcimimetics with potent and selective activity on the parathyroid calcium receptor. *Proc. Natl. Acad. Sci. U. S. A.* 95 (7), 4040–4045. doi:10.1073/pnas.95.7.4040

Nieto Gutierrez, A., and McDonald, P. H. (2018). GPCRs: Emerging anti-cancer drug targets. *Cell. Signal.* 41, 65–74. doi:10.1016/j.cellsig.2017.09.005

O'Hayre, M., Salanga, C. L., Handel, T. M., and Allen, S. J. (2008). Chemokines and cancer: Migration, intracellular signalling and intercellular communication in the microenvironment. *Biochem. J.* 409 (3), 635–649. doi:10.1042/BJ20071493

Palve, V., Liao, Y., Remsing Rix, L. L., and Rix, U. (2021). Turning liabilities into opportunities: Off-target based drug repurposing in cancer. *Semin. Cancer Biol.* 68, 209–229. doi:10.1016/j.semcancer.2020.02.003

Pan, Y., Liu, G., Zhou, F., Su, B., and Li, Y. (2018). DNA methylation profiles in cancer diagnosis and therapeutics. *Clin. Exp. Med.* 18 (1), 1–14. doi:10.1007/s10238-017-0467-0

Pandey, D. P., Lappano, R., Albanito, L., Madeo, A., Maggiolini, M., and Picard, D. (2009). Estrogenic GPR30 signalling induces proliferation and migration of breast cancer cells through CTGF. *EMBO J.* 28 (5), 523–532. doi:10.1038/emboj.2008.304

Park, Y., Park, J. M., Kim, D. H., Kwon, J., and Kim, I. A. (2017). Inhibition of PI4K IIIα radiosensitizes in human tumor xenograft and immune-competent syngeneic murine tumor model. *Oncotarget* 8 (66), 110392–110405. doi:10.18632/oncotarget.22778

Pierce, K. L., Premont, R. T., and Lefkowitz, R. J. (2002). Seven-transmembrane receptors. *Nat. Rev. Mol. Cell. Biol.* 3 (9), 639–650. doi:10.1038/nrm908

Pisanti, S., Picardi, P., D'Alessandro, A., Laezza, C., and Bifulco, M. (2013). The endocannabinoid signaling system in cancer. *Trends Pharmacol. Sci.* 34 (5), 273–282. doi:10.1016/j.tips.2013.03.003

Pronin, A., and Slepak, V. (2021). Ectopically expressed olfactory receptors OR51E1 and OR51E2 suppress proliferation and promote cell death in a prostate cancer cell line. *J. Biol. Chem.* 296, 100475. doi:10.1016/j.jbc.2021.100475

Qin, Y., Verdegaal, E. M. E., Siderius, M., Bebelman, J. P., Smit, M. J., Leurs, R., et al. (2011). Quantitative expression profiling of G-protein-coupled receptors (GPCRs) in metastatic melanoma: The constitutively active orphan GPCR GPR18 as novel drug target. *Pigment. Cell. Melanoma Res.* 24 (1), 207–218. doi:10.1111/j.1755-148X.2010.00781.x

Raimondi, F., Inoue, A., Kadji, F. M. N., Shuai, N., Gonzalez, J.-C., Singh, G., et al. (2019). Rare, functional, somatic variants in gene families linked to cancer genes: GPCR signaling as a paradigm. *Oncogene* 38 (38), 6491–6506. doi:10.1038/s41388-019-0895-2

Ramer, R., and Hinz, B. (2016). Antitumorigenic targets of cannabinoids – current status and implications. *Expert Opin. Ther. Targets* 20 (10), 1219–1235. doi:10.1080/14728222.2016.1177512

Reubi, J. C., Waser, B., Vale, W., and Rivier, J. (2003). Expression of CRF1 and CRF2 receptors in human cancers. *J. Clin. Endocrinol. Metab.* 88 (7), 3312–3320. doi:10.1210/jc.2002-021853

Rodriguez, M., Luo, W., Weng, J., Zeng, L., Yi, Z., Siwko, S., et al. (2014). PSGR promotes prostatic intraepithelial neoplasia and prostate cancer xenograft growth through NF-κB. *Oncogenesis* 3 (8), e114. doi:10.1038/oncsis.2014.29

Saghafinia, S., Mina, M., Riggi, N., Hanahan, D., and Ciriello, G. (2018). Pan-cancer landscape of aberrant DNA methylation across human tumors. *Cell. Rep.* 25 (4), 1066–1080. e1068. doi:10.1016/j.celrep.2018.09.082

Shah, R., Singh, S. J., Eddy, K., Filipp, F. V., and Chen, S. (2019). Concurrent targeting of glutaminolysis and metabotropic glutamate receptor 1 (GRM1) reduces glutamate bioavailability in GRM1 + melanoma. *Cancer Res.* 79 (8), 1799–1809. doi:10.1158/0008-5472.CAN-18-1500

Shen, H., and Laird, Peter W. (2013). Interplay between the cancer genome and epigenome. *Cell.* 153 (1), 38–55. doi:10.1016/j.cell.2013.03.008

Siegel, R. L., Miller, K. D., Fuchs, H. E., and Jemal, A. (2021). Cancer statistics, 2021. *Ca. Cancer J. Clin.* 71 (1), 7–33. doi:10.3322/caac.21654

Siegfried, J. M., Hershberger, P. A., and Stabile, L. P. (2009). Estrogen receptor signaling in lung cancer. *Semin. Oncol.* 36 (6), 524–531. doi:10.1053/j.seminoncol.2009.10.004

Siragy, H. M., El-Kersh, M. A., de Gasparo, M., Webb, R. L., and Carey, R. M. (2002). Differences in AT2-receptor stimulation between AT1-receptor blockers valsartan and losartan quantified by renal interstitial fluid cGMP. *J. Hypertens.* 20 (6), 1157–1163. doi:10.1097/00004872-200206000-00028

Smith, H. O., Leslie, K. K., Singh, M., Qualls, C. R., Revankar, C. M., Joste, N. E., et al. (2007). GPR30: A novel indicator of poor survival for endometrial carcinoma. *Am. J. Obstet. Gynecol.* 196 (4), 386.e1–9. e311. doi:10.1016/j.ajog.2007.01.004

Southan, C., Sharman, J. L., Benson, H. E., Faccenda, E., Pawson, A. J., Alexander, S. P., et al. (2016). The IUPHAR/BPS Guide to PHARMACOLOGY in 2016: Towards curated quantitative interactions between 1300 protein targets and 6000 ligands. *Nucleic Acids Res.* 44 (D1), D1054–D1068. doi:10.1093/nar/gkv1037

Sriram, K., and Insel, P. A. (2018). G protein-coupled receptors as targets for approved drugs: How many targets and how many drugs? *Mol. Pharmacol.* 93 (4), 251–258. doi:10.1124/mol.117.111062

Sriram, K., Moyung, K., Corriden, R., Carter, H., and Insel, P. A. (2019). GPCRs show widespread differential mRNA expression and frequent mutation and copy number variation in solid tumors. *PLoS Biol.* 17 (11), e3000434. doi:10.1371/journal.pbio.3000434

Stratton Michael, R. (2011). Exploring the genomes of cancer cells: Progress and promise. *Science* 331 (6024), 1553–1558. doi:10.1126/science.1204040

Stratton, M. R., Campbell, P. J., and Futreal, P. A. (2009). The cancer genome. *Nature* 458 (7239), 719–724. doi:10.1038/nature07943

Sun, W., Bunn, P., Jin, C., Little, P., Zhabotynsky, V., Perou, C. M., et al. (2018). The association between copy number aberration, DNA methylation and gene expression in tumor samples. *Nucleic Acids Res.* 46 (6), 3009–3018. doi:10.1093/nar/gky131

Tezval, H., Jurk, S., Atschekzei, F., Serth, J., Kuczyk, M. A., and Merseburger, A. S. (2009). The involvement of altered corticotropin releasing factor receptor 2 expression in prostate cancer due to alteration of anti-angiogenic signaling pathways. *Prostate* 69 (4), 443–448. doi:10.1002/pros.20892

The Cancer Genome Atlas Research Network (2012). Comprehensive genomic characterization of squamous cell lung cancers. *Nature* 489 (7417), 519–525. doi:10.1038/nature11404

Tomera, K., Gleason, D., Gittelman, M., Moseley, W., Zinner, N., Murdoch, M., et al. (2001). The gonadotropin-releasing hormone antagonist abarelix depot versus luteinizing hormone releasing hormone agonists leuprolide or goserelin: Initial results of endocrinological and biochemical efficacies in patients with prostate cancer. *J. Urology* 165 (5), 1585–1589. doi:10.1016/s0022-5347(05)66353-7

Trott, O., and Olson, A. J. (2010). AutoDock Vina: Improving the speed and accuracy of docking with a new scoring function, efficient optimization, and multithreading. *J. Comput. Chem.* 31 (2), 455–461. doi:10.1002/jcc.21334

Vang Nielsen, K., Ejlertsen, B., Møller, S., Trøst Jørgensen, J., Knoop, A., Knudsen, H., et al. (2008). The value of TOP2A gene copy number variation as a biomarker in breast cancer: Update of DBCG trial 89D. *Acta Oncol.* 47 (4), 725–734. doi:10.1080/02841860801995396

Varadi, M., Anyango, S., Deshpande, M., Nair, S., Natassia, C., Yordanova, G., et al. (2021). AlphaFold protein structure database: Massively expanding the structural coverage of protein-sequence space with high-accuracy models. *Nucleic Acids Res.* 50, D439–D444. gkab1061. doi:10.1093/nar/gkab1061

Villanueva, L., Álvarez-Errico, D., and Esteller, M. (2020). The contribution of epigenetics to cancer immunotherapy. *Trends Immunol.* 41 (8), 676–691. doi:10.1016/j.it.2020.06.002

Vivian, J., Rao, A. A., Nothaft, F. A., Ketchum, C., Armstrong, J., Novak, A., et al. (2017). Toil enables reproducible, open source, big biomedical data analyses. *Nat. Biotechnol.* 35 (4), 314–316. doi:10.1038/nbt.3772

Wang, Y., Wang, X., Xiong, Y., Li, C. D., Xu, Q., Shen, L., et al. (2019). An integrated pan-cancer analysis and structure-based virtual screening of GPR15. *Int. J. Mol. Sci.* 20 (24), E6226. doi:10.3390/ijms20246226

Warner, G. T., and Jarvis, B. (2002). Olmesartan medoxomil. *Olmesartan Medoxomil. Drugs* 62 (9), 1345–1353. doi:10.2165/00003495-200262090-00005

Weng, J., Wang, J., Cai, Y., Stafford, L. J., Mitchell, D., Ittmann, M., et al. (2005). Increased expression of prostate-specific G-protein-coupled receptor in human prostate intraepithelial neoplasia and prostate cancers. *Int. J. Cancer* 113 (5), 811–818. doi:10.1002/ijc.20635

Wilkie, G., Sakr, B., and Rizack, T. (2016). Medical marijuana use in oncology: A review. *JAMA Oncol.* 2 (5), 670–675. doi:10.1001/jamaoncol.2016.0155

Wu, V., Yeerna, H., Nohata, N., Chiou, J., Harismendy, O., Raimondi, F., et al. (2019). Illuminating the Onco-GPCRome: Novel G protein-coupled receptor-driven oncocrine networks and targets for cancer immunotherapy. *J. Biol. Chem.* 294 (29), 11062–11086. doi:10.1074/jbc.REV119.005601

Xiang, Y., Yao, X., Chen, K., Wang, X., Zhou, J., Gong, W., et al. (2016). The G-protein coupled chemoattractant receptor FPR2 promotes malignant phenotype of human colon cancer cells. *Am. J. Cancer Res.* 6 (11), 2599–2610.

Xu, L. L., Stackhouse, B. G., Florence, K., Zhang, W., Shanmugam, N., Sesterhenn, I. A., et al. (2000). PSGR, a novel prostate-specific gene with homology to a G protein-coupled receptor, is overexpressed in prostate cancer. *Cancer Res.* 60 (23), 6568–6572.

Yosten, G. L. C., Harada, C. M., Haddock, C., Giancotti, L. A., Kolar, G. R., Patel, R., et al. (2020). GPR160 de-orphanization reveals critical roles in neuropathic pain in rodents. *J. Clin. Invest.* 130 (5), 2587–2592. doi:10.1172/JCI133270

Young, D., Waitches, G., Birchmeier, C., Fasano, O., and Wigler, M. (1986). Isolation and characterization of a new cellular oncogene encoding a protein with multiple potential transmembrane domains. *Cell.* 45 (5), 711–719. doi:10.1016/0092-8674(86)90785-3

Zeng, Y., Zhang, P., Wang, X., Wang, K., Zhou, M., Long, H., et al. (2020). Identification of prognostic signatures of alternative splicing in glioma. *J. Mol. Neurosci.* 70 (10), 1484–1492. doi:10.1007/s12031-020-01581-0

Zhan, T., Rindtorff, N., and Boutros, M. (2017). Wnt signaling in cancer. *Oncogene* 36 (11), 1461–1473. doi:10.1038/onc.2016.304

Zhao, Y., Wang, X. G., Ma, Z. Y., Xiong, G. L., Yang, Z. J., Cheng, Y., et al. (2021). Systematic comparison of ligand-based and structure-based virtual screening methods on poly (ADP-ribose) polymerase-1 inhibitors. *Brief. Bioinform.* 22 (6), bbab135. doi:10.1093/bib/bbab135

Zheng, L., Du, J., Ge, F., Qian, M., Yang, B., He, Q., et al. (2021). The calcimimetic agent cinacalcet inhibits hepatocellular carcinoma via YAP/TAZ suppression. *Pharmazie* 76 (10), 511–514. doi:10.1691/ph.2021.1646

Zhong, Y., Wang, Y., Huang, J., Xu, X., Pan, W., Gao, S., et al. (2019). Association of hCG and LHCGR expression patterns with clinicopathological parameters in ovarian cancer. *Pathol. Res. Pract.* 215 (4), 748–754. doi:10.1016/j.prp.2019.01.001

Zhou, C., Dai, X., Chen, Y., Shen, Y., Lei, S., Xiao, T., et al. (2016). G protein-coupled receptor GPR160 is associated with apoptosis and cell cycle arrest of prostate cancer cells. *Oncotarget* 7 (11), 12823–12839. doi:10.18632/oncotarget.7313

Zhou, Y., Zhou, B., Pache, L., Chang, M., Khodabakhshi, A. H., Tanaseichuk, O., et al. (2019). Metascape provides a biologist-oriented resource for the analysis of systems-level datasets. *Nat. Commun.* 10 (1), 1523. doi:10.1038/s41467-019-09234-6

Zhu, C.-x., Xiong, W., Wang, M.-l., Yang, J., Shi, H.-j., Chen, H.-q., et al. (2017). Nuclear G protein-coupled oestrogen receptor (GPR30) predicts poor survival in patients with ovarian cancer. *J. Int. Med. Res.* 46 (2), 723–731. doi:10.1177/0300060517717625

frontiers | Frontiers in Pharmacology

TYPE Original Research
PUBLISHED 30 August 2022
DOI 10.3389/fphar.2022.971867

OPEN ACCESS

EDITED BY
Essa M. Saied,
Humboldt University of Berlin, Germany

REVIEWED BY
Dong Tang,
Northern Jiangsu People's Hospital (NJPH), China
Sonam Mittal,
Medical College of Wisconsin, United States

*CORRESPONDENCE
Yi Zhang,
zhangyi@cdutcm.edu.cn
Li Xiang,
xianglydr@cdutcm.edu.cn

SPECIALTY SECTION
This article was submitted to Pharmacology of Anti-Cancer Drugs, a section of the journal Frontiers in Pharmacology

RECEIVED 17 June 2022
ACCEPTED 08 August 2022
PUBLISHED 30 August 2022

CITATION
Wang S, Xing N, Meng X, Xiang L and Zhang Y (2022), Comprehensive bioinformatics analysis to identify a novel cuproptosis-related prognostic signature and its ceRNA regulatory axis and candidate traditional Chinese medicine active ingredients in lung adenocarcinoma.
Front. Pharmacol. 13:971867.
doi: 10.3389/fphar.2022.971867

Comprehensive bioinformatics analysis to identify a novel cuproptosis-related prognostic signature and its ceRNA regulatory axis and candidate traditional Chinese medicine active ingredients in lung adenocarcinoma

Shaohui Wang[1], Nan Xing[2], Xianli Meng[3], Li Xiang[3]* and Yi Zhang[1]*

[1]State Key Laboratory of Southwestern Chinese Medicine Resources, School of Ethnic Medicine, Chengdu University of Traditional Chinese Medicine, Chengdu, China, [2]State Key Laboratory of Southwestern Chinese Medicine Resources, School of Pharmacy, Chengdu University of Traditional Chinese Medicine, Chengdu, China, [3]State Key Laboratory of Southwestern Chinese Medicine Resources, Innovative Institute of Chinese Medicine and Pharmacy, Chengdu University of Traditional Chinese Medicine, Chengdu, China

Lung adenocarcinoma (LUAD) is the most ordinary histological subtype of lung cancer, and regulatory cell death is an attractive target for cancer therapy. Recent reports suggested that cuproptosis is a novel copper-dependent modulated form of cell death dependent on mitochondrial respiration. However, the role of cuproptosis-related genes (CRGs) in the LUAD process is unclear. In the current study, we found that DLD, LIAS, PDHB, DLAT and LIPA1 in 10 differentially expressed CRGs were central genes. GO and KEGG enrichment results showed that these 10 CRGs were mainly enriched in acetyl-CoA biosynthetic process, mitochondrial matrix, citrate cycle (TCA cycle) and pyruvate metabolism. Furthermore, we constructed a prognostic gene signature model based on the six prognostic CRGs, which demonstrated good predictive potential. Excitedly, we found that these six prognostic CRGs were significantly associated with most immune cell types, with DLD being the most significant (19 types). Significant correlations were noted between some prognostic CRGs and tumor mutation burden and microsatellite instability. Clinical correlation analysis showed that DLD was related to the pathological stage, T stage, and M stage of patients with LUAD. Lastly, we constructed the lncRNA UCA1/miR-1-3p/DLD axis that may play a key role in the progression of LUAD and screened nine active components of traditional Chinese medicine (TCM) that may regulate DLD. Further, *in vitro* cell experiments and molecular docking were used to verify this. In conclusion, we analyzed the potential value of CRGs in the progression of LUAD, constructed the potential regulatory axis of ceRNA, and obtained the

targeted regulatory TCM active ingredients through comprehensive bioinformatics combined with experimental validation strategies. This work not only provides new insights into the treatment of LUAD but also includes a basis for the development of new immunotherapy drugs that target cuproptosis.

KEYWORDS

lung adenocarcinoma, cuproptosis, prognostic signature, DLD, ceRNA, ingredients

Introduction

Lung cancer is a serious threat to human health all over the world (Wang et al., 2018). Lung adenocarcinoma (LUAD), as the most common histological subtype of lung cancer, has a significantly increasing incidence compared with squamous cell carcinoma, large cell carcinoma, and small cell carcinoma (Meza et al., 2015; Ruiz-Cordero and Devine, 2020). The pathogenesis of LUAD is still not completely clear, and it is mostly due to a combination of lifestyle, environment, genetics, and other factors (Akhtar and Bansal, 2017). Currently, the most common treatments for LUAD include surgery, radiotherapy, drug therapy, and chemotherapy (Wu et al., 2021). Although early CT screening enables early detection and treatment of some patients with LUAD, the effect and prognosis of conventional treatment are not satisfactory due to the special invasiveness and drug resistance of LUAD (Rosell et al., 2020; Toki et al., 2020). In addition, there is an urgent need to identify and screen new prognostic markers and targeted drugs for LUAD in the face of many poor outcomes in patients with LUAD.

Recently, a new cell death pathway termed cuproptosis was found in addition to conventional cell death, such as apoptosis, pyroptosis, and ferroptosis (Tsvetkov et al., 2022). As a common trace metal element, copper plays an important role in maintaining multiple physiological functions of the human body, such as electron transfer, mitochondrial function, and the activities of various enzymes (Vetchý, 2018). Recent studies have shown that excess copper directly binds to lipoacylated proteins by mediating the tricarboxylic acid cycle and targets its upregulated factors, namely, the gene FDX1 that encodes the enzyme that reduces Cu^{2+} to Cu^{1+}; excess copper also promotes the abnormal oligomerization of lipoacylated proteins, reduces protein lipoacylation, and reduces the level of Fe-S cluster proteins, resulting in copper-dependent cell death (Tsvetkov et al., 2019; Tsvetkov et al., 2022). The presence of copper ion carriers and glutathione consumption can promote copper-mediated cell death, whereas the presence of copper chelates can alleviate death to some extent. Studies have shown that after pulse treatment with copper ion carrier elesclomol, metabolites related to the tricarboxylic acid (TCA) cycle, such as citrate, cis-monucinic acid, and guanosine diphosphate, show time-dependent maladjustment. Moreover, if SLC31A1 is overexpressed in ABC-1 cells, the sensitivity of cells to copper is enhanced, resulting in cell copper death (Tsvetkov et al., 2022). Therefore, we can explore new therapeutic strategies for LUAD from the mechanism of cuproptosis to overcome the defects of traditional therapy.

The rapid development of multi-omics technology, artificial intelligence, and big data provides a powerful means to explore the development of tumors and potential therapeutic markers (Chakraborty et al., 2018; Hristova and Chan, 2019). Traditional Chinese medicine (TCM) has played an important role in tumor prevention and treatment, and the search for potential anti-tumor active ingredients in TCM has attracted the attention of scholars (Wang et al., 2021). This study aimed to elucidate the expression and prognostic significance of CRGs (cuproptosis-related factors) in LUAD through a comprehensive bioinformatics strategy, identify the potential regulatory axis of ceRNA of CRGs, and screen their targeted regulatory TCM active ingredients. In conclusion, this work can provide a sufficient basis to determine the prognostic value of CRGs in LUAD and develop cuproptosis-targeting modulators for the prevention and treatment of LUAD.

Materials and methods

Data collection and pretreatment

TCGA LUAD and GTEx corresponding normal tissue data were obtained. RNAseq data in TCGA and GTEx TPM format were processed by the Toil processes (Vivian et al., 2017) at UCSC XENA. The data included TCGA paracancer samples (59 cases), TCGA tumor tissue (515 cases), and GTEx normal samples (288 cases). RNAseq data in level 3 HTSeq-FPKM format from the TCGA LUAD project were obtained. Before further analysis, we converted the RNAseq data in fragments per kilobase per million (FPKM) formats to transcripts per million reads (TPM) format and log2 conversion.

Acquisition, differential expression, gene mutation, and correlation analyses of CRGs

Ten CRGs, namely, FDX1, LIAS, LIPT1, DLD, DLAT, PDHA1, PDHB, MTF1, GLS, and CDKN2A, were obtained

through an original research paper published in *Science* (Tsvetkov et al., 2022). R software (version 3.6.3) and Mann-Whitney *U* test (Wilcoxon rank-sum test) were further used to identify the differential expression of CRGs in LUAD and normal lung tissues. The Gene Set Cancer Analysis (GSCA) database (http://bioinfo.life.hust.edu.cn/GSCA/#/) was used to analyze the gene mutation of the 10 CRGs. We then constructed a protein-protein interaction (PPI) network of the 10 CRGs using the STRING database (https://cn.string-db.org/) and Cytoscape software (version 3.7.1).

Enrichment analysis of gene ontology and kyoto encyclopedia of genes and genomes pathways

Gene ontology (GO) included biological processes (BP), cell composition (CC), and molecular function (MF) categories. The Kyoto encyclopedia of genes and genomes (KEGG) pathways were generated from the org. hs.eg.db package (version 3.10.0, for ID conversion), clusterprofiler package (version 3.14.3, for enrichment analysis) and ggplot2 (version 3.3.3, for visualization) packages in R software. The species was set as *Homo sapiens*, and p. adjust<0.1 and qvalue<0.2 were selected as screening conditions to obtain the main enrichment functions and pathways.

Construction of cuproptosis-related prognostic gene signature model

Survminer package [version 0.4.9] (for visualization) and survival package [version 3.2–10] (for statistical analysis of survival data) in R software (version 3.6.3) were used to determine the 10 CRGs in predicting overall survival (OS) in LUAD, and $p < 0.05$ was considered statistically significant. Then we selected the CRGs with significant prognostic value for subsequent prognostic model construction. And the model formula is: risk score = Gene 1 expression value × α 1 + Gene 2 expression value × α 2 +... + Gene n expression value × α n. Where α is the regression coefficient calculated by the LASSO Cox regression analysis. Finally, The CRG prognostic model was constructed by LASSO Cox regression analysis, and the OS time difference between the two subgroups (low-risk subgroup and high-risk subgroup) was compared by Kaplan-Meier survival analysis. The prediction accuracy and risk score of each cuproptosis-related prognostic gene were compared by time ROC analysis. All the above analyses were performed by R software, and $p < 0.05$ was considered to be statistically significant.

Analysis of immune invasion, tumor mutation burden, microsatellite instability, and drug sensitivity

The ssGSEA (GSVA embedded algorithm) (Hänzelmann et al., 2013) was used as the immune infiltration algorithm to analyze the correlation between the expression level of cuproptosis-related prognostic genes and the immune infiltration degree of 24 immune cell types (Bindea et al., 2013) and the enrichment score. Spearman correlation was used to analyze the relationship between cuproptosis-related prognostic genes and tumor mutation burden (TMB) and microsatellite instability (MSI) scores, and $p < 0.05$ was considered to be statistically significant. In addition, the GSCA database (http://bioinfo.life.hust.edu.cn/GSCA/#/) was used to analyze the drug sensitivity of cuproptosis-related prognostic genes.

DLD expression verification and construction of ceRNA regulatory network

The human protein map (HPA) database (https://www.proteinatlas.org/) was used to validate the protein expression levels of DLD in normal lung tissue and LUAD. The StarBase database was used to predict DLD-relevant miRNA targets. Then, Mann-Whitney *U* test and Kaplan-Meier analysis were used to evaluate the expression and prognostic value of DLD related miRNAs in LUAD, and $p < 0.05$ were considered to be statistically significant. Then, we selected the miRNAs with significant differences as the research objects. Furthermore, the LncBase database and StarBase database were used to predict the lncRNA targets associated with miRNA. Subsequently, we adopted the same methods (Mann-Whitney *U* test and Kaplan-Meier analysis) to analyze the expression and prognostic value of these lncRNAs in the TCGA LUAD data set, and $p < 0.05$ was considered to be statistically significant. Finally, we determined and constructed a DLD related ceRNA regulatory network.

Screening of TCM candidate effective ingredients for targeting the regulation of DLD

The CTD database (http://ctdbase.org/) was used to screen potential TCM chemical constituents targeting DLD, and Chemdraw (version 20.0) was used to map their structures.

In vitro cell experiments validation

Normal lung epithelial cells (BEAS-2B) (Shanghai Zhong Qiao Xin Zhou Biotechnology Co., Ltd., Shanghai, China) and LUAD cell lines (H1299 and A549) (Hunan Fenghui Biotechnology Co., Ltd.) were maintained with DMEM (Gibco, ThermoFisher Scientific, Waltham, United States) containing 10% FBS (Gibco, ThermoFisher Scientific, Waltham, United States) and antibiotics and RPMI-1640 (Gibco, ThermoFisher Scientific, Waltham, United States) containing 10% FBS and antibiotics in 5% CO_2 at 37°C, respectively. When the cell density reached more than 80%, it was used for subsequent experimental detection. According to the previous description (Wang et al., 2018), RNA was extracted and separated and their expression levels were detected by using RT-qPCR assays. The GAPDH was used as an endogenous control of lncRNA UCA1 and DLD, the U6 was used as an endogenous control of miR-1-3p, and the primers of lncRNA UCA1, miR-1-3p, DLD were shown in Supplementary Table S1. The experiment was repeated three times, and the data were expressed as mean ± standard deviation (SD). GraphPad Prism software (version 9.0, CA, United States) was used for statistical analysis, and ANOVA was used for comparison between multiple groups. $p < 0.05$ was considered statistically significant.

Molecular docking verification

The 3D structures of nine potential active ingredients (resveratrol, genistein, aristolochic acid I, cannabidiol, epigallocatechin gallate, fructose, phlorizin, quercetin, and triptonide) were downloaded from PubChem database (https://pubchem.ncbi.nlm.nih.gov/). The 3D structure of DLD was downloaded from the PDB protein database (http://www.rcsb.org/pdb/home/home. do). Further, the protein was dehydrated and ligand extracted with PyMOL software. Then, Autodock software was used to conduct molecular simulation docking for the nine potential active ingredients and DLD, and the binding strength of DLD and the nine active ingredients was evaluated according to the docking binding energy.

Results

Analysis of GRP expression, gene mutation, and PPI in LUAD

We first used the TCGA GTEx-LUAD dataset to evaluate the expression of the 10 GRPs in LUAD and normal lung tissues, and the results showed that the mRNA levels of all 10 GRPs were changed in unpaired samples. Compared with the normal lung tissue, the expression levels of FDX1, LIAS, LIPT1, DLD, DLAT, PDHB, and CDKN2A in LUAD were upregulated, whereas the expression levels of PDHA1, MTF1, and GLS were downregulated (Figure 1A). We further analyzed the gene mutations of GRPs in LUAD, and the results revealed that all the 10 GRPs had gene mutations in LUAD samples, among which CDKN2A was the gene with the highest mutation rate, followed by DLD and GLS (Figure 1B). A missense mutation was the most common variation classification, SNP was the most common variant type, and C>A was listed as the top-class SNV (Figure 1C). Further classifying the mutations as transitions (Ti) and transversions (Tv), we found that Ti was generated at a higher frequency than Tv in the whole gene (Figure 1D). In addition, we constructed a PPI network of the 10 GRPs through the STRING database (Supplementary Figure S1) and found that DLD, LIAS, PDHB, DLAT, and LIPA1 were the central genes via Cytoscape (Figure 1E).

GO and KEGG enrichment analyses of GRPs

To elucidate the potential function of these GRPs, we subsequently performed GO and KEGG pathway analyses of the 10 CRGs. The results showed that these 10 CRGs were mainly enriched in the acetyl-CoA biosynthetic process from pyruvate (GO:0006086), acetyl-CoA biosynthetic process (GO:0006085), mitochondrial matrix (GO:0005759), oxidoreductase complex (GO:1990204), oxidoreductase activity (GO:0016903), and metal cluster binding (GO:0051540) in GO functional analysis (Figure 2A). KEGG pathway analysis showed that the 10 CRGs participated in the citrate cycle (TCA cycle; hsa00020), pyruvate metabolism (hsa00620), glycolysis/gluconeogenesis (hsa00010), carbon metabolism (hsa01200), and central carbon metabolism in cancer (hsa05230) (Figure 2B). Furthermore, we found that four CRGs, namely, DLD, PDHA1, PDHB, and DLAT, had the highest degree values in the abovementioned enriched pathways and functions (Figures 2C,D).

Construction of cuproptosis-related prognostic gene signature model

To construct the cuproptosis-related prognostic gene signature model, we conducted univariate Cox regression analysis to evaluate the prognostic value of these 10 differentially expressed CRGs. As shown in Figures 4A–J, we found that six CRGs were associated with the prognosis of patients, namely, GLS (Figure 3A), CDKN2A (Figure 3B), PDHA1 (Figure 3C), MTF1 (Figure 3E), LIPT1 (Figure 3H), and DLD (Figure 3J). On the basis of the six prognostic CRGs, we further constructed a cuproptosis-related prognostic gene signature model using LASSO Cox regression analysis. The risk score=(−0.3021)*LIPT1+(0.3259)*DLD+(0.2209)*PDHA1+(−0.1147)*MTF1+(−0.0294)

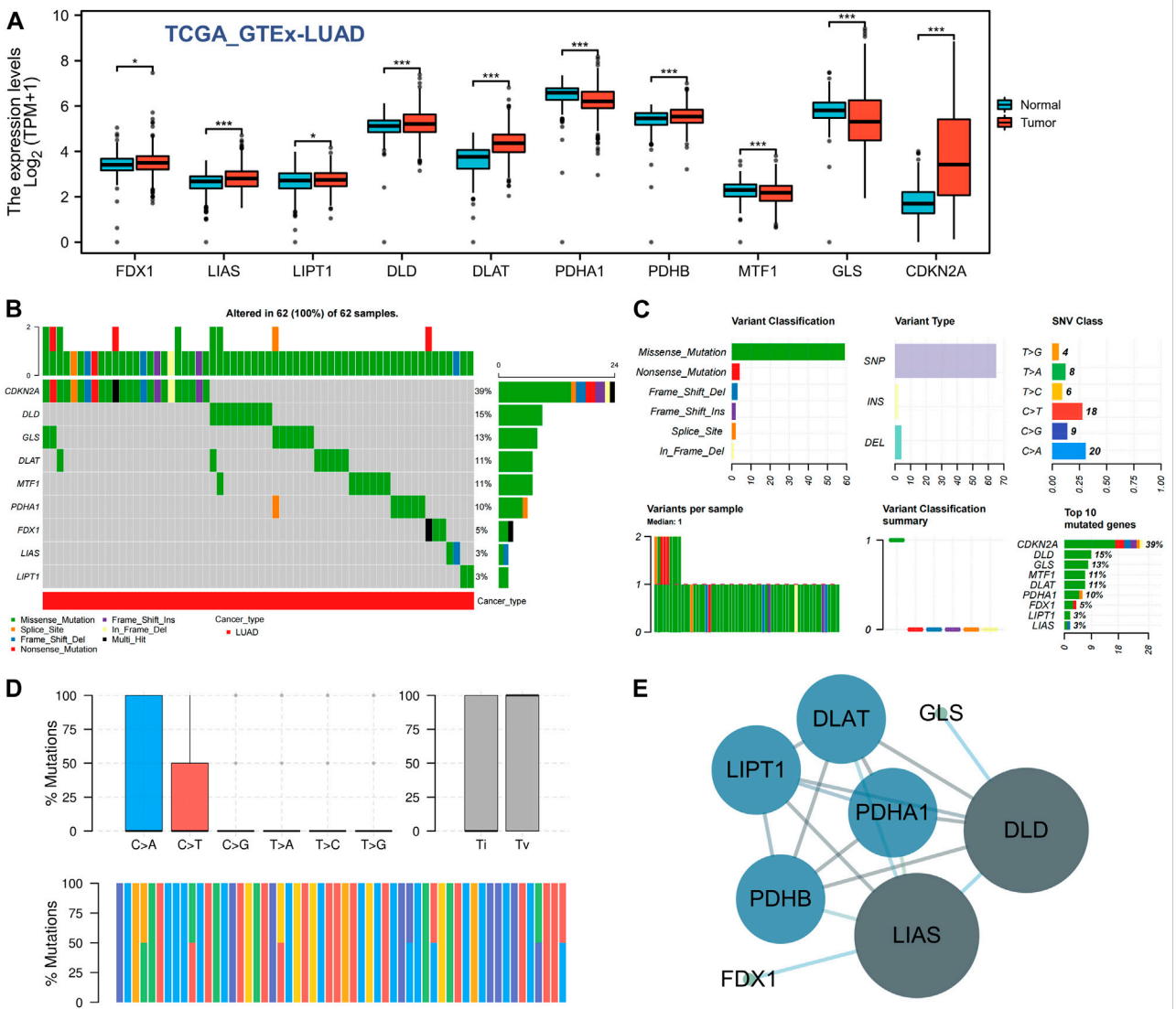

FIGURE 1
Expression difference and gene mutation of CRGs in LUAD. **(A)** Expression differences of 10 CRGs in LUAD and normal lung tissues. *, $p < 0.05$; ***, $p < 0.001$. **(B,C)** Gene mutation and classification of 10 CRGs in LUAD. **(D)** Transition (Ti) and transversion (Tv) classification of the SNVs of 10 CRGs in LUAD. **(E)** Interactive network of CRGs; the darker the color is, the larger the circle is, indicating that it belongs to the central target in the whole network.

*GLS+(0.0386)*CDKN2A. Figures 4A,B show the prognostic characteristic coefficients and partial likelihood bias of prognostic characteristics in patients with LUAD. Subsequently, we divided all patients with LUAD into low-risk and high-risk subgroups based on the risk score. Figure 4C shows the risk score, survival status, and expression of patients with LUAD. OS curve analysis showed that patients had a higher risk of death and a shorter survival time ($p = 0.00705$, median time = 3.4 vs. 4.5 years) with the increase in risk score (Figure 4D). ROC curves of risk models at different times were further analyzed, and the results showed that the areas under the ROC curve at 1, 3, and 5 years were 0.638, 0.57, and 0.543, respectively (Figure 4E).

Correlation analysis of immune infiltration

We evaluated the correlation between the expression of prognostic CRGs (including LIPT1, DLD, PDHA1, MTF1, GLS, and CDKN2A) and the immune infiltration of 24 different immune cell types in LUAD. The results showed that LIPT1 expression was positively correlated with T helper

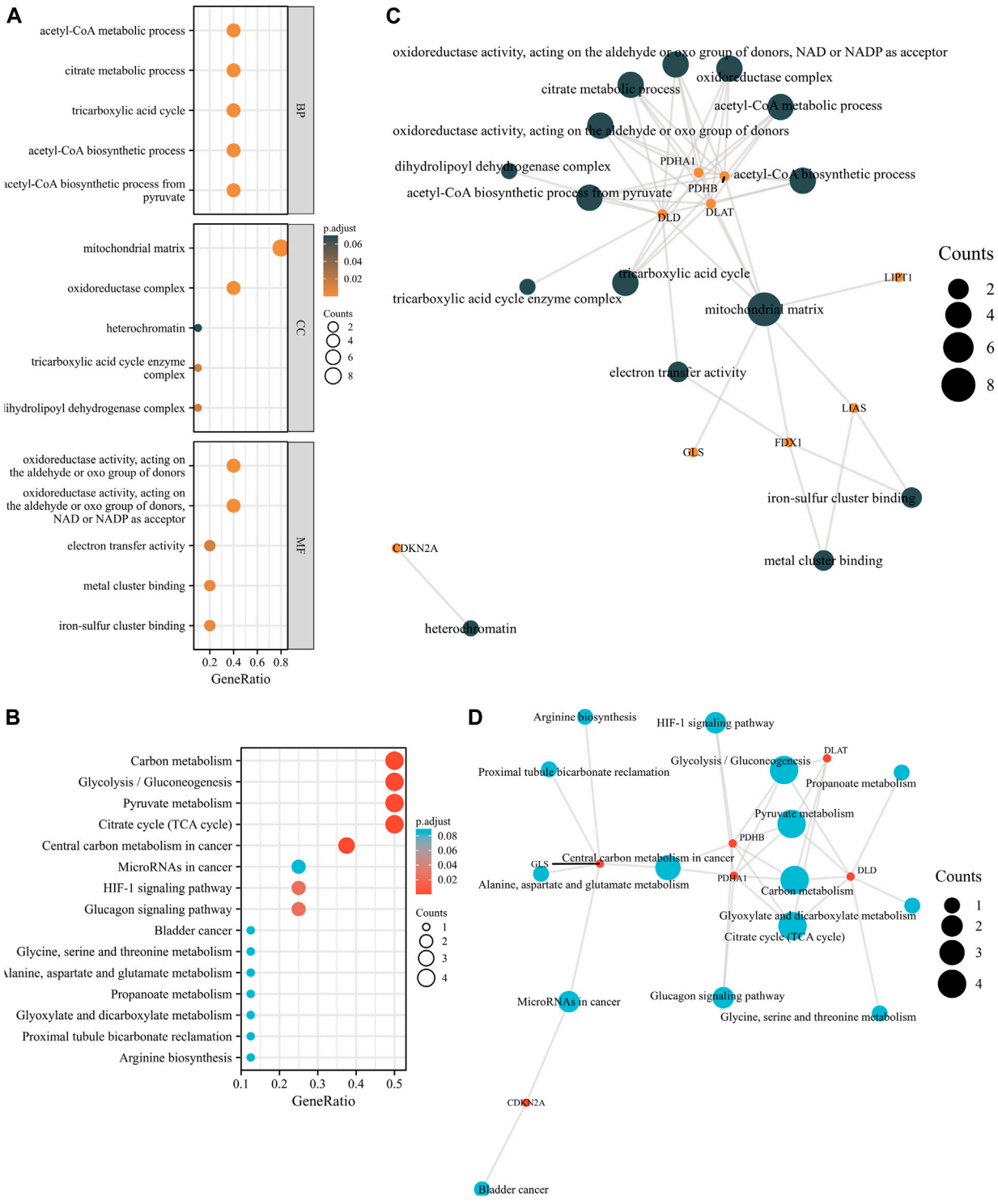

FIGURE 2
GO and KEGG enrichment analyses of 10 CRGs in LUAD. **(A)** Bubble plot of GO enrichment results of 10 CRGs in LUAD. **(B)** Bubble plot of KEGG enrichment results of 10 CRGs in LUAD. **(C)** Interactive network of GO entries and CRGs. **(D)** Interactive network of KEGG entries and CRGs.

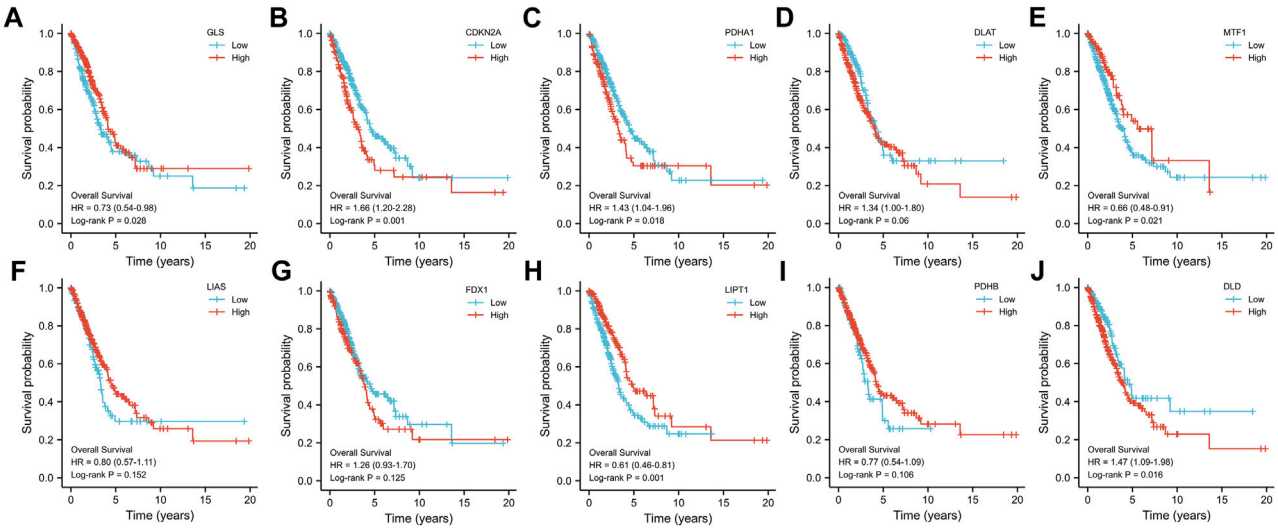

FIGURE 3
Prognostic value of 10 CRGs in LUAD. The OS curves of GLS **(A)**, CDKN2A **(B)**, PDHA1 **(C)**, DLAT **(D)**, MTF1 **(E)**, LIAS **(F)**, FDX1 **(G)**, LIPT1 **(H)**, PDHB **(I)**, and DLD **(J)** in patients with LUAD in the low and high expression groups.

cells. It was negatively correlated with NK CD56bright cells, NK CD56dim cells, Tem, pDC, neutrophils, NK cells, and Th2 cells (Figure 5A). DLD was positively correlated with Th2 cells, Tgd, T helper cells, and Tcm. By contrast, it was negatively correlated with TFH, B cells, CD8 T cells, pDC, NK CD56bright cells, NK cells, iDC, cytotoxic cells, DC, T cells, Th1 cells, mast cells, Treg, and eosinophils (Figure 5B). PDHA1 was positively correlated with Th2 cells and NK CD56bright cells, but it was negatively correlated with neutrophils, Th1 cells, macrophages, iDC, T cells, mast cells, cytotoxic cells, B cells, DC, pDC, eosinophils, CD8 T cells, and Tem (Figure 5C). MTF1 was positively correlated with Tcm, T helper cells, NK cells, Tem, eosinophils, neutrophils, and macrophages, but it was negatively correlated with CD8 T cells, pDC, and cytotoxic cells (Figure 5D). GLS was positively correlated with macrophages, Th1 cells, iDC, DC, Tem, T helper cells, T cells, TFH, eosinophils, aDC, Tcm, mast cells, NK cells, pDC, and Treg, but it was negatively correlated with NK CD56bright cells (Figure 5E). CDKN2A was positively correlated with Th2 cells, TReg, NK CD56dim cells, Th1 cells, cytotoxic cells, aDC, and Tgd, but it was negatively correlated with eosinophils, mast cells, and Th17 cells (Figure 5F). Further analysis showed that the enrichment types ($p < 0.05$) of LIPT1, DLD, PDHA1, MTF1, GLS, and CDKN2A in these 24 different immune cell types were 9 (Figure 6A), 19 (Figure 6B), 15 (Figure 6C), 8 (Figure 6D), 15 (Figure 6E), and 5 (Figure 6F), respectively. DLD was the most common, followed by PDHA1 and GLS. In conclusion, our results demonstrated a significant association between prognostic CRGs and lung tumor immune infiltration, and DLD was significantly enriched in most immune cell types.

TMB, MSI, and drug sensitivity analyses

To explore whether these six CRGs can also be used as biomarkers for drug screening, we subsequently analyzed the correlation between CRGs and TMB and MSI in LUAD. The results showed that DLD (Figure 7A) and CDKN2A (Figure 7B) were positively correlated with TMB, whereas GLS (Figure 7C), LIPT1 (Figure 7D), MTF1 (Figure 7E), and PDHA1 (Figure 7F) were not significantly correlated with TMB. In MSI analysis, only PDHA1 (Figure 7G) was found to be significantly positively correlated with MSI, whereas LIPT1 (Figure 7H), DLD (Figure 7I), MTF1 (Figure 7J), GLS (Figure 7K), and CDKN2A (Fig. 7L) were not significantly correlated with MSI. We further analyzed the relationship between the expression of the six CRGs and existing drugs. Drug sensitivity analysis showed that the expression of CDKN2A, DLD, LIPT1, and MTF1 was negatively correlated with most drugs in the GSCA database (Supplementary Figure S2).

Clinical correlation analysis

We further evaluated the relationship between the expression levels of these six CRGs and different clinical parameters of patients with LUAD, and the results showed that DLD expression was related to the pathological stages (Stage I, Stage III, and Stage IV; Figure 8A), T stages (T1 and T3; Figure 8B), M stages (M0 and M1; Figure 8C), gender (Figure 8D), and OS (Figure 8F) of patients with LUAD, but it was not related to the changes in age (Figure 8E), smoke (Figure 8G), and race (Figure 8H). GLS

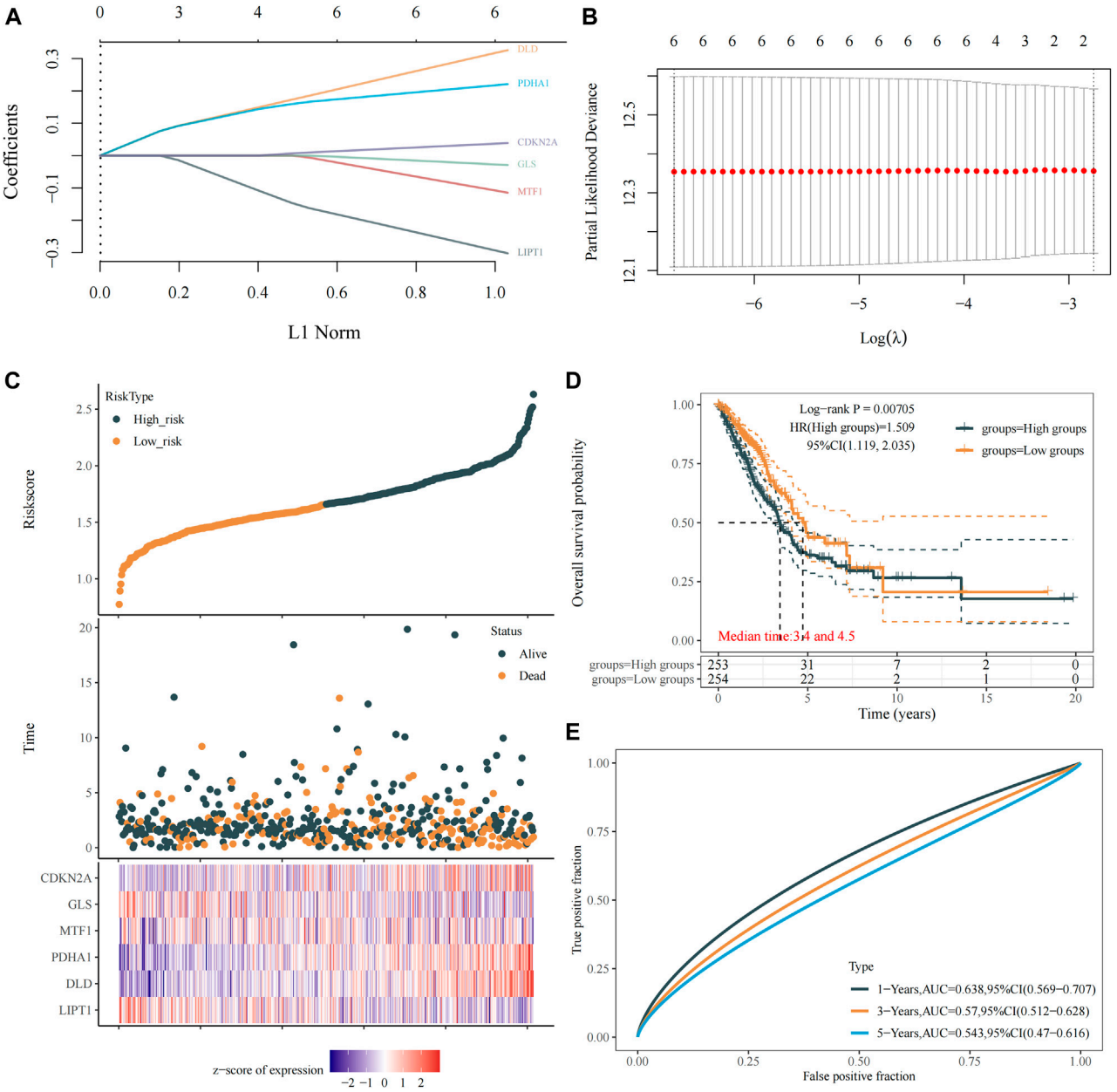

FIGURE 4
Construction of a prognostic signature model of CRGs in LUAD. **(A)** LASSO coefficients of the six prognostic CRGs. **(B)** PLD of the six prognostic CRGs. **(C)** Distribution of risk score, survival status, and expression of the six prognostic CRGs. **(D)** OS curve of patients with LUAD in the low and high expression groups. **(E)** 1-, 3-, and 5-year ROC prediction curves for patients with LUAD.

expression was correlated with gender (Figure 8D) and OS (Figure 8F) but not with other factors. PDHA1 was only related to OS (Figure 8F). LIPT1 was only associated with race (Back or African American and White) (Figure 8H). MTF1 and CDKN2A were not clinically relevant (Figures 8A–H). These results fully proved that DLD may play an important role in the development of LUAD.

Construction of the ceRNA regulatory network

On the basis of the above screening results, we selected the most important pivotal gene DLD as the object of further study to fully explore its potential ceRNA network in the regulation of LUAD. We first verified the protein expression

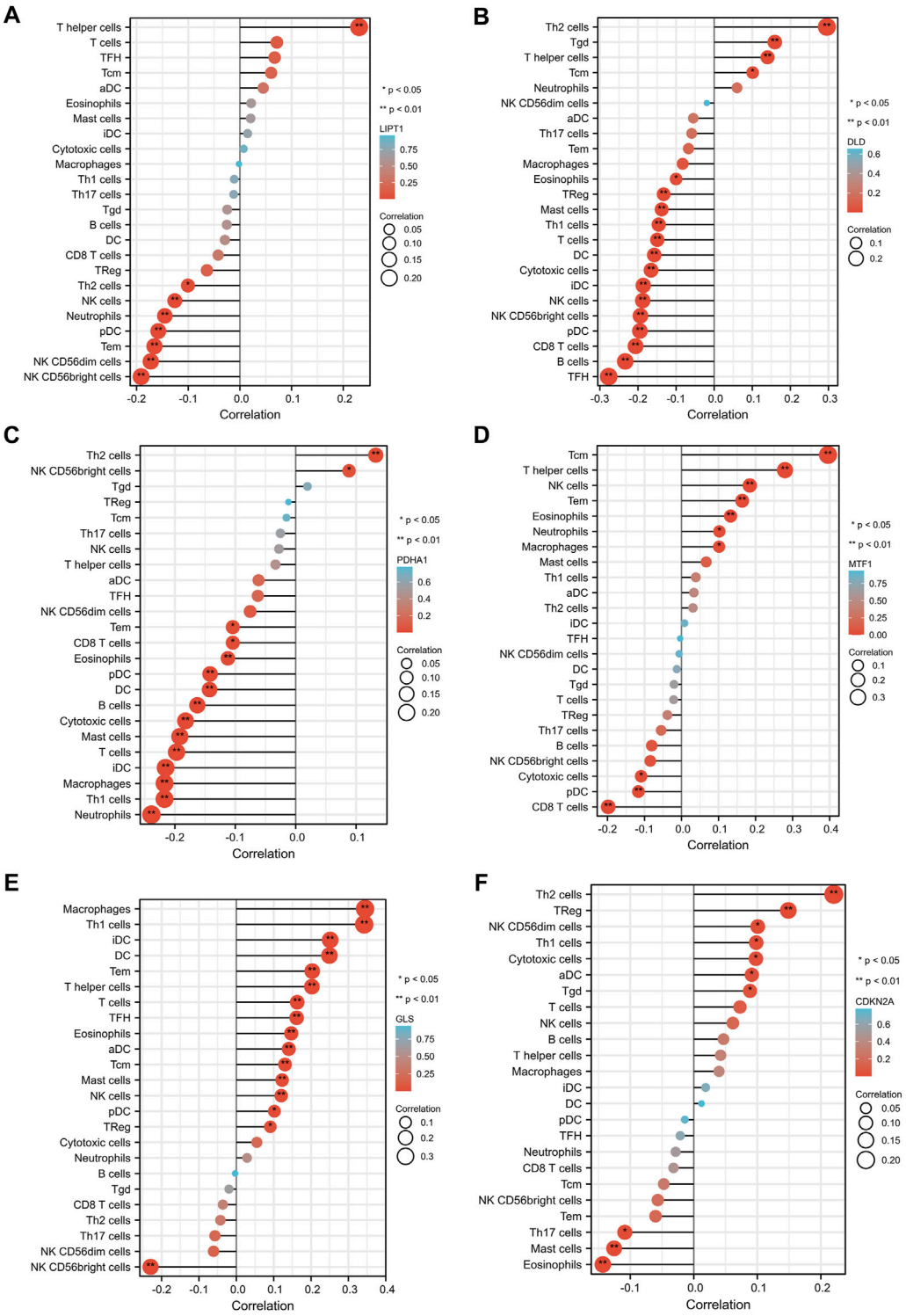

FIGURE 5
Correlation between the six prognostic CRGs and immune infiltration in LUAD. The correlation between LIPT1 **(A)**, DLD **(B)**, PDHA1 **(C)**, MTF1 **(D)**, GLS **(E)**, CDKN2A **(F)**, and the degree of immune infiltration of 24 immune cell types in patients with LUAD.

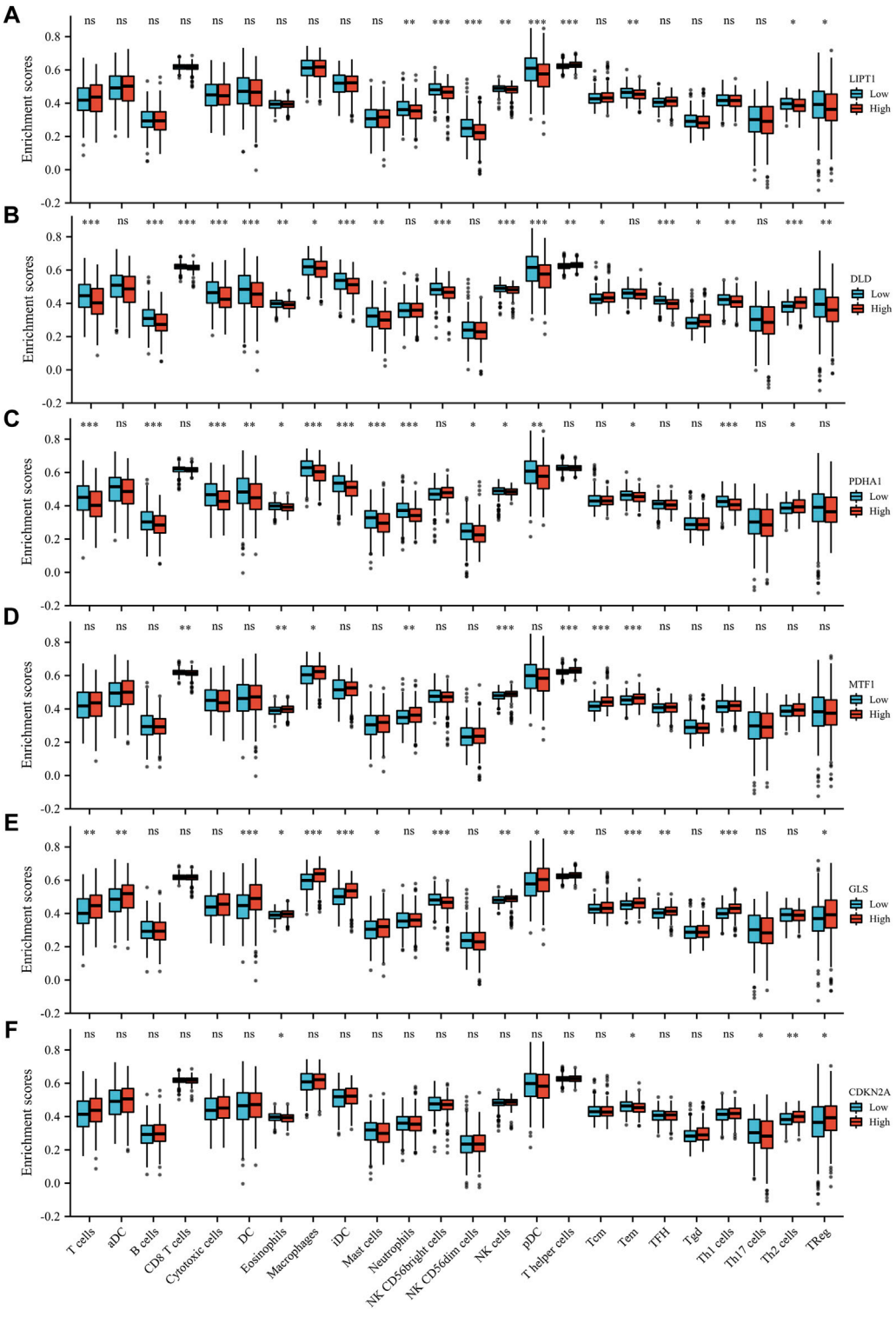

FIGURE 6
Enrichment scores of the six prognostic CRGs in 24 immune cell types in LUAD. The six prognostic CRGs were LIPT1 **(A)**, DLD **(B)**, PDHA1 **(C)**, MTF1 **(D)**, GLS **(E)**, and CDKN2A **(F)**.

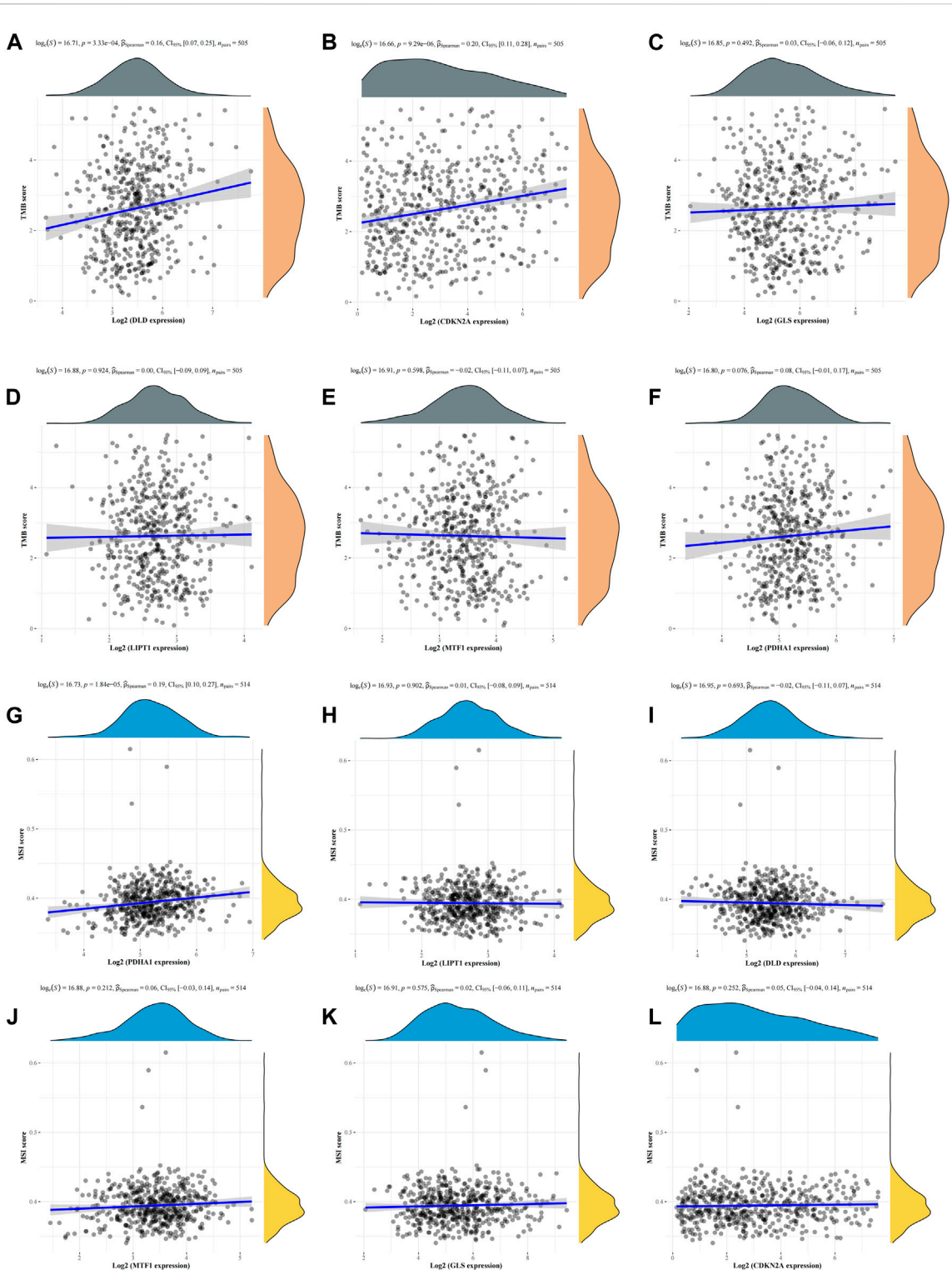

FIGURE 7
Correlation analysis of the six CRGs with TMB and MSI in LUAD. **(A–F)** Correlation between the six CRGs and TMB in LUAD. **(G–L)** Correlation between the six CRGs and MSI in LUAD.

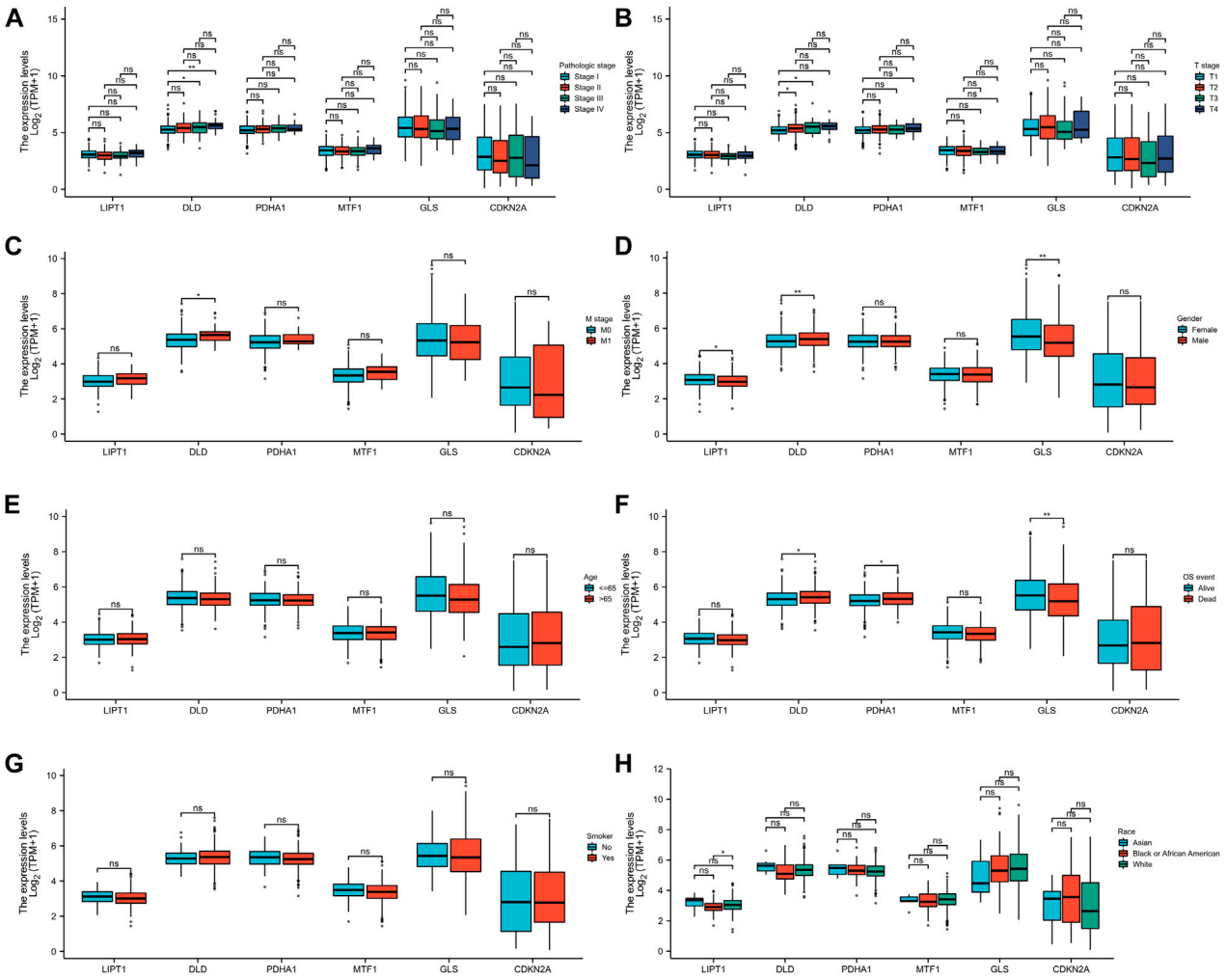

FIGURE 8
Association analysis of the six CRGs and different clinical parameters in patients with LUAD. The different clinical factors included pathologic stage **(A)**, T stage **(B)**, M stage **(C)**, gender **(D)**, age **(E)**, OS event **(F)**, smoker **(G)**, and race **(H)**.

level of DLD using the HPA database, and the results showed that DLD was highly expressed in the tissues of patients with LUAD (Figure 9A). We predicted 10 potential miRNA targets of DLD using the StarBase database (Figure 9B) and evaluated the expression of these 10 miRNAs in LUAD samples. The results showed significant differences in the expression of six miRNAs in LUAD, namely, hsa-miR-29b-3p, hsa-miR-1-3p, hsa-miR-206, hsa-miR-320a, hsa-miR-320b, and hsa-miR-320d. Among them, hsa-miR-1-3p and hsa-miR-206 were significantly downregulated in LUAD (Figure 9C). Therefore, we further evaluated the prognostic value of these two miRNAs and found that only the expression of hsa-miR-1-3p was related to the prognosis of patients with LUAD, suggesting that patients with LUAD and high expression of miR-1-3p had a higher survival probability than their counterparts (Figure 9D). Therefore, miR-1-3p was considered the most promising miRNA target for DLD. In addition, 27 lncRNA targets related to miR-1-3p were predicted by the StarBase and LncBase databases (Figures 9E,F). Similarly, we detected the expression of these 27 lncRNAs in LUAD, and the results showed that 18 lncRNAs were expressed differently in LUAD. In particular, AC007996.1, AC021092.1, AC078846.1, CCDC18-AS1, HOTAIR, MIAT, MIR4453HG, and UCA1 were highly expressed in LUAD (Supplementary Figure S3). Further prognostic analysis showed that only UCA1 was significantly associated with the prognosis of patients with LUAD, and this result suggested that patients with LUAD and high UCA1 expression had a lower survival probability than their counterparts (Figure 9G, Supplementary

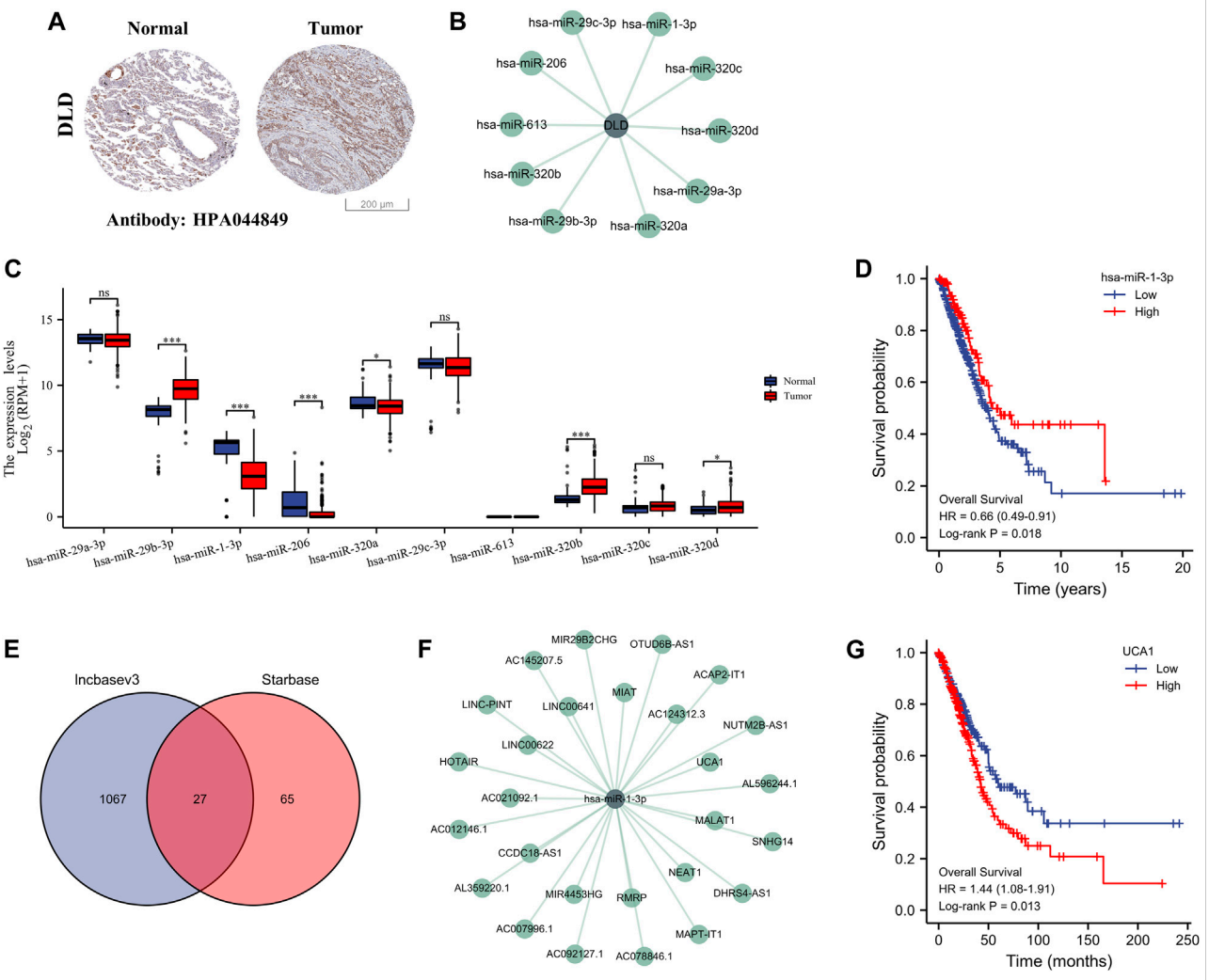

FIGURE 9
Construction of the ceRNA regulatory axis. **(A)** Differential expression of DLD protein in LUAD and normal lung tissues (HPA). **(B)** Ten miRNAs associated with DLD. **(C)** Differential expression of the 10 miRNAs in LUAD and normal lung tissues. ns, $p \geq 0.05$; *, $p < 0.05$; ***, $p < 0.001$. **(D)** OS curves of DLD in patients with LUAD in the low and high expression groups. **(E)** Identification of 20 lncRNAs by the Starbase and lncbasev3 databases. **(F)** The 27 miRNAs associated with miR-1-3p. **(G)** OS curves of UCA1 in patients with LUAD in the low and high expression groups.

Figure S4). Therefore, the lncRNA UCA1/miR-1-3p/DLD axis might play a key role in the progression of LUAD.

Screening of TCM active ingredients targeting DLD

To search for the potential TCM active components acting on cuproptosis prognosis-related gene DLD, we obtained nine chemical components of TCM that may be related to cuproptosis prognosis-related gene DLD by screening the CTD database. Figure 10 shows the nine active ingredients of TCM, namely, resveratrol, genistein, aristolochic acid I, cannabidiol, epigallocatechin gallate, fructose, phlorizin, quercetin, and triptonide.

Experimental verification

To confirm the roles of lncRNA UCA1, miR-1-3p and DLD in LUAD, we further verified their differential expressions in normal lung epithelial cells (BEAS-2B) and different lung adenocarcinoma cell lines (A549 and H1299) by *in vitro* cell experiments. And the results showed that lncRNA UCA1 and DLD were significantly overexpressed in A549 and H1299 cell lines, and underexpressed in BEAS-2B cell lines, while miR-1-3p

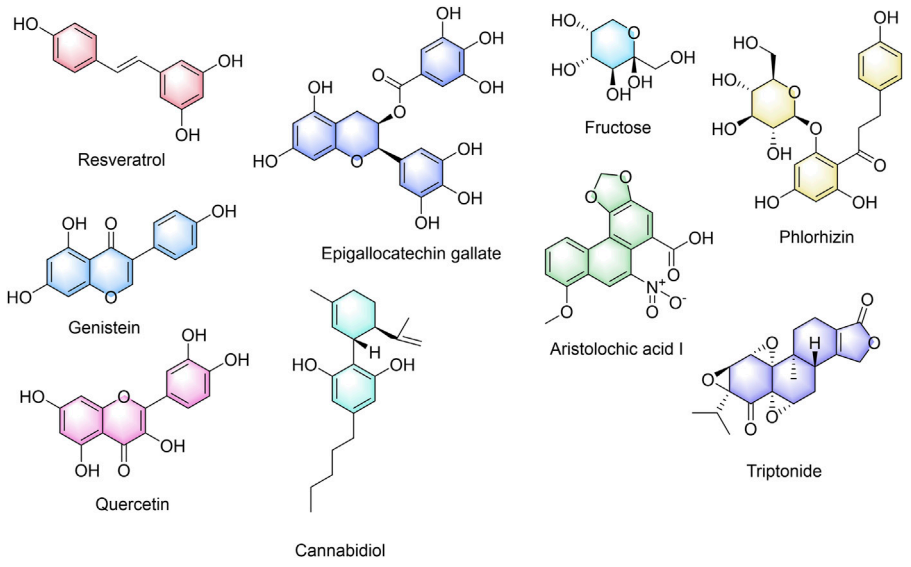

FIGURE 10
Active ingredients of traditional Chinese medicine with a potential effect on DLD.

showed an opposite trend (Figure 11A). The above *in vitro* cell validation results were consistent with our bioinformatics prediction results. Meanwhile, we also verified the binding energy of these nine potential TCM chemical components to DLD by molecular docking technology, and the results were shown in Table 1. It is generally believed that the lower the binding energy of the ligand to the receptor, the greater the possibility of interaction between the ligand and the receptor. Our results showed that the binding energy of the nine predicted TCM active ingredients and DLD were all less than -5 kcal/mol, which fully proved the potential interaction between them. The molecular docking modes were shown in Figure 11B.

Discussion

We first clarified the expression of 10 GRPs in LUAD, and the results showed that the mRNA levels of these 10 GRPs were significantly different. Among them, seven GRPs, namely, FDX1, LIAS, LIPT1, DLD, DLAT, PDHB, and CDKN2A, were upregulated in LUAD. Three GRPs, namely, PDHA1, MTF1, and GLS, were downregulated in LUAD. Cancer is a collection of diseases characterized by abnormal and uncontrolled cell growth caused by genetic mutations. These mutations are called "drivers" after they drive tumorigenesis, and their form of mutation affects the homeostasis of a range of cell key functions (Martínez-Jiménez et al., 2020). Therefore, we conducted mutation analysis, and the results showed that CDKN2A was the gene with the highest mutation rate, followed by DLD and GLS. PPI networks are composed of proteins interacting with one another to participate in biological signal transmission, gene expression regulation, energy and substance metabolism, cell cycle regulation, and other life processes (Athanasios et al., 2017). By studying the interaction network between proteins, we can discover the core regulatory genes. Therefore, we analyzed the PPI network relationship among these 10 CRGs and found that DLD, LIAS, PDHB, DLAT, and LIPA1 were the core genes.

Through functional enrichment analysis, we found that these 10 CRGs were mainly involved in the citrate cycle (TCA cycle), pyruvate metabolism, glycolysis/gluconeogenesis, carbon metabolism, and other pathways. Some studies found that human non-small-cell lung cancers (NSCLCs) oxidize glucose in the TCA cycle (Faubert et al., 2017). Breast cancer cells rely on nutritional pyruvate to drive collagen-based remodeling of the extracellular matrix in lung metastases. Inhibition of pyruvate metabolism impairs collagen hydroxylation, thereby impairing the growth of breast cancer-derived lung metastases (Elia et al., 2019).

In addition, studies have found that increased metabolic reprogramming and glycolysis levels are associated with tumor progression (Li et al., 2022). Recent studies have shown that glycolysis/gluconeogenesis and carbon metabolism have been proven to be involved in the occurrence and development of lung cancer cells (He et al., 2022; Li et al., 2022). The tumor metabolic microenvironment plays an important role in tumor occurrence, development, invasion, and metastasis (García-Cañaveras et al., 2019; Dey et al., 2021). By analyzing these pathways, we found that these pathways are mostly related to the

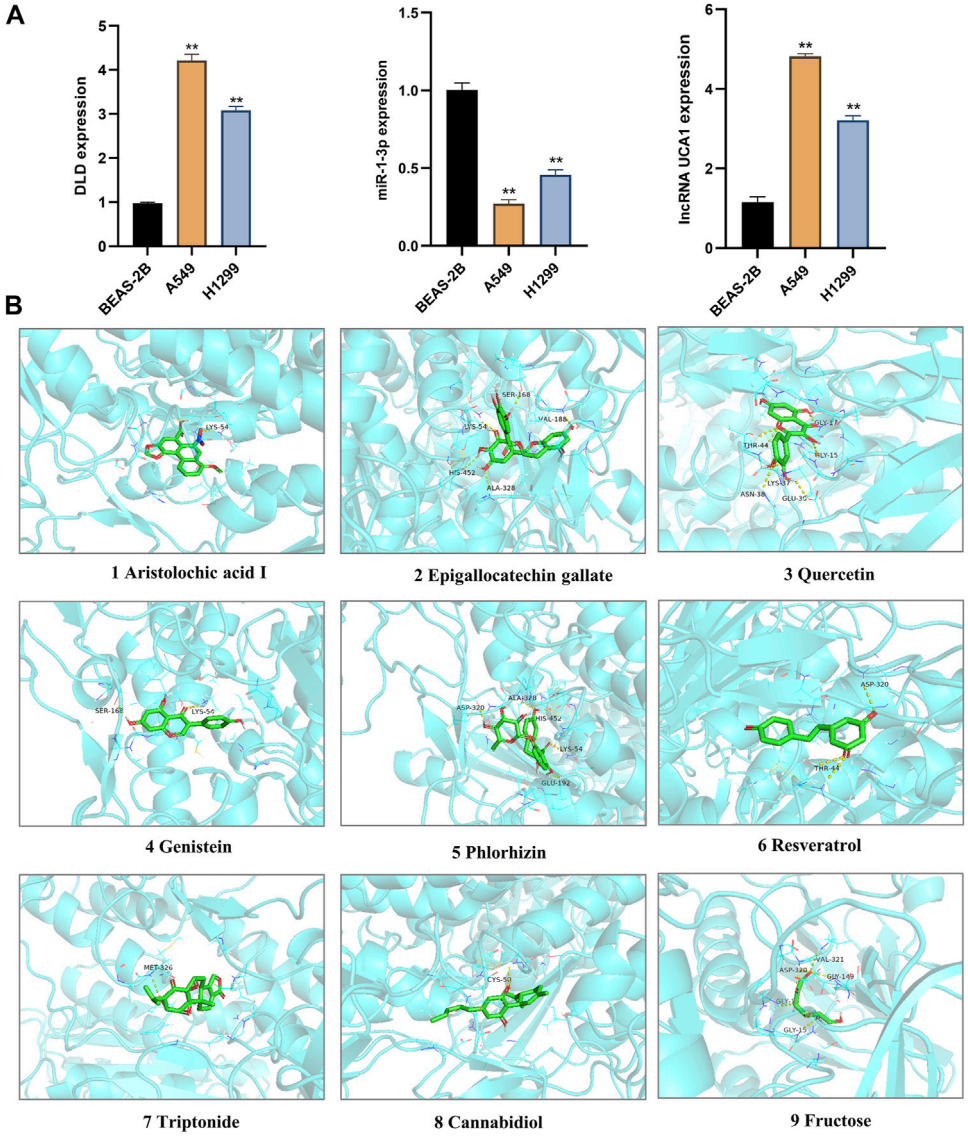

FIGURE 11
Validation of *In vitro* cell experiment and molecular docking. **(A)** The differential expression of lncRNA UCA1, miR-1-3p and DLD in normal lung epithelial cells (BEAS-2B) and different LUAD cell lines (A549 and H1299) were detected by *in vitro* cell experiments. **, $p < 0.01$. **(B)** The interaction between nine TCM active components and DLD protein was simulated by molecular docking.

tumor metabolic microenvironment. Therefore, targeting tumor metabolism is of great significance for tumor immunity and tumor therapy.

In addition, we performed a prognostic analysis of the 10 CRGs and further constructed prognostic gene signature models based on these six prognostic CRGs (including GLS, CDKN2A, PDHA1, MTF1, LIPT1, and DLD) via LASSO Cox regression analysis. Previous studies have confirmed the prognostic value of ferroptosis-related genes (Gao et al., 2021), PANoptosis-related genes (Wang et al., 2022), and glycolytic-related genes (Zhang L et al., 2019) in LUAD. Surprisingly, the prognostic signature model of CRGs that we constructed demonstrated good potential in predicting the prognosis of patients with LUAD. This work is the first to evaluate the prognostic value of CRGs in LUAD, which provides more options for the prognostic analysis of LUAD. Environmental and metabolic pressure in the tumor microenvironment (TME) can play a key role in shaping tumor development by influencing matrix and immune cell composition, TME composition, and activation (Abou Khouzam et al., 2020). Therefore, we evaluated the relationship between these six CRGs' prognostic label genes and immune infiltration, and we found that DLD was

TABLE 1 The binding energy of nine TCM active components to DLD by molecular docking.

No.	Protein	PDB ID	Compound name	Binding energy (kcal/mol)
1	DLD	6I4R	Aristolochic acid I	−9.8
2			Epigallocatechin gallate	−9.7
3			Quercetin	−9.4
4			Genistein	−9.3
5			Phlorhizin	−9.2
6			Resveratrol	−8.7
7			Triptonide	−8.4
8			Cannabidiol	−8.2
9			Fructose	−5.6

significantly correlated with most immune cell types, followed by PDHA1 and GLS. DLD, as a mitochondrial protein, plays an important role in energy metabolism in eukaryotes. It is involved in at least five multi-enzyme complexes and is a necessary component for the complex to complete the reaction. In addition, DLD, as a flavin protein oxidoreductase, accepts proton and electron-catalyzed disulfide bond formation with FAD as a co-group (Dai et al., 2019). Studies have confirmed that DLD is closely related to ferroptosis induced by cystine deprivation or import inhibition, and DLD inhibition can reduce lipid peroxidation and ferrous iron accumulation, thereby inhibiting ferroptosis suppression (Shin et al., 2020). Pyruvate dehydrogenase complex (PDC) plays a central role in carbohydrate metabolism, linking cytoplasmic glycolysis to the mitochondrial TCA cycle, and these regulatory serine residues in PDHA1 are structurally critical to enzyme activity (Echeverri Ruiz et al., 2021). In addition, PDHA1 is related to metabolic reprogramming in tumor diseases, such as esophageal cancer and gastric cancer (Liu et al., 2018; Liu L et al., 2019). Glutaminase (GLS) is a key enzyme involved in regulating glutamine metabolism and is reported to also play a crucial role in cancer development (Zhang J et al., 2019). These findings strongly suggest that CRGs may play an important role in LUAD. In particular, DLD is closely related not only to the prognosis of patients with LUAD but also to many immune cell types, which needs to be further verified by *in vitro* and *in vivo* experiments. We also constructed a DLD-related ceRNA regulatory network and identified the lncRNA UCA1/miR-1-3p/DLD axis. Previous studies have confirmed that lncRNA urothelial carcinoma-associated 1 (UCA1) is abnormally expressed in many cancers and has been confirmed as an oncogene (Huang et al., 2019; Yao et al., 2019; Yang et al., 2021). UCA1 promotes LUAD progression and cisplatin resistance, which may be a potential diagnostic marker and therapeutic target for patients with LUAD (Liu X et al., 2019; Fu et al., 2021). MiR-1-3p has been identified as a tumor suppressor in a variety of human cancers, including lung cancer (Jiao et al., 2018; Zhang H et al., 2019). Some studies have found that miR-1-3p expression in LUAD is decreased, whereas overexpressed miR-1-3p inhibits the proliferation, migration, and invasion of cancer cells (Miao et al., 2021). Excitedly, Differential expression of lncRNA UCA1, miR-1-3p and DLD in normal lung epithelial cells and LUAD cell lines was detected by RT-qPCR, and the results showed that lncRNA UCA1 and DLD were significantly overexpressed in LUAD cell lines, while miR-1-3p was on the contrary, and the above results further prove the accuracy of our bioinformatics results. In summary, these findings strongly suggested that the lncRNA UCA1/miR-1-3p/DLD axis may play an important role in the progression of LUAD.

Chinese herbal medicine is an important resource for discovering innovative medicines (Luo et al., 2019). The discovery of artemisinin further demonstrates the importance of TCM in innovative drug discovery (Ma et al., 2018). Therefore, we further screened the potential chemical components of TCM for the targeted regulation of DLD and performed molecular docking verification. As a result, we found nine potential TCM chemical components, namely, resveratrol, genistein, aristolochic acid I, cannabidiol, epigallocatechin gallate, fructose, phlorizin, quercetin, and triptonide. The molecular docking experiment results showed that all the nine potential TCM active ingredients had good binding activity to DLD, which further indicated that these ingredients may play an important role in the regulation of lncRNA UCA1/miR-1-3p/DLD axis. A large number of preclinical studies have shown that cannabidiol is an effective anticancer agent, whether used alone or in combination with other cannabinoids, chemotherapy, and radiation therapy (Seltzer et al., 2020). Resveratrol is a polyphenol compound originally isolated from the root of *Veratrum grandiflorum*. At present, a large number of studies have confirmed that resveratrol can inhibit the growth of LUAD cells, which can inhibit the expression of COX-2, arrest the cell cycle in the S phase, inhibit cell DNA synthesis, and inhibit the proliferation of A549 cells (Li et al., 2018; Li et al., 2019). At the same time, resveratrol can induce apoptosis and autophagy of lung adenocarcinoma cells by up-regulating the P53 level (Fan

et al., 2020). When used in combination with gemcitabine (GEM), resveratrol has synergistic anticancer effects (Qin et al., 2020). Genistein exists in various plants for human and animal consumption, and it can inhibit the proliferation and induce apoptosis of A549 cells (Zhang et al., 2018). Moreover, genistein can downregulate lipid biosynthesis and inhibit the proliferation of human lung adenocarcinoma H460 cells (Hess and Igal, 2011). Cannabidiol can reduce Nrf-2 by targeting TRPV2 (transient receptor potential vanilloid-2), promote the production of reactive oxygen species (ROS), and inhibit the growth and metastasis of cisplatin-resistant NSCLC (Misri et al., 2022). Epigallocatechin gallate has been shown to induce the apoptosis of A549 cells by modulating ROS-mediated Nrf2/Keap1 signaling (Velavan et al., 2018). Quercetin can delay the development of LUAD and increase non-neoplastic weight gain in tumor oxidative stress mice (Albrecht et al., 2020). Other studies have found that quercetin nanoparticles can significantly reduce the viability of A549 cells, promote cell apoptosis, arrest the cell cycle in the G0/G1 phase, and reverse the drug resistance of A549 cells *in vitro* (Sun et al., 2020). In summary, these potential TCM chemicals may be an effective strategy for the treatment and improvement of the prognosis of LUAD. However, whether these potential active ingredients exert such effects by regulating DLD needs to be further verified by gene interference and other technologies.

In conclusion, we used a comprehensive bioinformatics strategy to elucidate the expression and prognosis of CRGs in LUAD. In addition, we constructed a cuproptosis-related prognostic gene signature model and found that DLD was most closely related to the prognosis and clinical and immune infiltration of LUAD. More importantly, we discovered a new potential ceRNA axis that regulates the LUAD process and identified the TCM active components that may regulate DLD. Interestingly, our experimental validation also preliminarily confirmed this bioinformatics screening result. This work provides a strong basis to interpret the prognostic value of CRGs and discover new therapeutic strategies. However, our study had some limitations. The validation of a prognostic signature related to CRGs should be further verified by more databases such as GEO, and future work should involve clinical samples, cell experiments, or animal experiments to verify our results.

Data availability statement

The original contributions presented in the study are included in the article/Supplementary Material, further inquiries can be directed to the corresponding authors.

Author contributions

SW designed the topic, carried out bioinformatics analysis, and wrote the manuscript. NX studied the relevant literature. XM reviewed the manuscript. YZ and LX reviewed and directed the manuscript. All authors have read, participated in the revision of the manuscript, and approved the submitted version.

Funding

This study was supported by the National Natural Science Foundation of China (82104534, 81903902).

Conflict of interest

The authors declare that the research was conducted in the absence of any commercial or financial relationships that could be construed as a potential conflict of interest.

Publisher's note

All claims expressed in this article are solely those of the authors and do not necessarily represent those of their affiliated organizations, or those of the publisher, the editors and the reviewers. Any product that may be evaluated in this article, or claim that may be made by its manufacturer, is not guaranteed or endorsed by the publisher.

Supplementary material

The Supplementary Material for this article can be found online at: https://www.frontiersin.org/articles/10.3389/fphar.2022.971867/full#supplementary-material

References

Abou Khouzam, R., Brodaczewska, K., Filipiak, A., Zeinelabdin, N. A., Buart, S., Szczylik, C., et al. (2020). Tumor hypoxia regulates immune escape/invasion: Influence on angiogenesis and potential impact of hypoxic biomarkers on cancer therapies. *Front. Immunol.* 11, 613114. doi:10.3389/fimmu.2020.613114

Akhtar, N., and Bansal, J. G. (2017). Risk factors of lung cancer in nonsmoker. *Curr. Probl. Cancer* 41, 328–339. doi:10.1016/j.currproblcancer.2017.07.002

Albrecht, C., Cittadini, M. C., and Soria, E. A. (2020). Pharmacological activity of quercetin and 5 caffeoylquinic acid oral intake in male balb/c mice with lung adenocarcinoma. *Arch. Med. Res.* 51, 8–12. doi:10.1016/j.arcmed.2019.11.006

Athanasios, A., Charalampos, V., Vasileios, T., and Ashraf, G. M. (2017). Protein-protein interaction (PPI) network: Recent advances in drug discovery. *Curr. Drug Metab.* 18, 5–10. doi:10.2174/1389200218011701192048 32

Bindea, G., Mlecnik, B., Tosolini, M., Kirilovsky, A., Waldner, M., Obenauf, A. C., et al. (2013). Spatiotemporal dynamics of intratumoral immune cells reveal the immune landscape in human cancer. *Immunity* 39, 782–795. doi:10.1016/j.immuni.2013.10.003

Chakraborty, S., Hosen, M. I., Ahmed, M., and Shekhar, H. U. (2018). Onco-multi-OMICS approach: A new frontier in cancer research. *Biomed. Res. Int.* 2018, 9836256. doi:10.1155/2018/9836256

Dai, F., Zhang, W., Zhuang, Q., Shao, Y., Zhao, X., Lv, Z., et al. (2019). Dihydrolipoamide dehydrogenase of Vibrio splendidus is involved in adhesion to Apostichopus japonicus. *Virulence* 10, 839–848. doi:10.1080/21505594.2019.1682761

Dey, P., Kimmelman, A. C., and Depinho, R. A. (2021). Metabolic codependencies in the tumor microenvironment. *Cancer Discov.* 11, 1067–1081. doi:10.1158/2159-8290.cd-20-1211

Echeverri Ruiz, N. P., Mohan, V., Wu, J., Scott, S., Kreamer, M., Benej, M., et al. (2021). Dynamic regulation of mitochondrial pyruvate metabolism is necessary for orthotopic pancreatic tumor growth. *Cancer Metab.* 9, 39. doi:10.1186/s40170-021-00275-4

Elia, I., Rossi, M., Stegen, S., Broekaert, D., Doglioni, G., Van Gorsel, M., et al. (2019). Breast cancer cells rely on environmental pyruvate to shape the metastatic niche. *Nature* 568, 117–121. doi:10.1038/s41586-019-0977-x

Fan, Y., Li, J., Yang, Y., Zhao, X., Liu, Y., Jiang, Y., et al. (2020). Resveratrol modulates the apoptosis and autophagic death of human lung adenocarcinoma A549 cells via a p53-dependent pathway: Integrated bioinformatics analysis and experimental validation. *Int. J. Oncol.* 57, 925–938. doi:10.3892/ijo.2020.5107

Faubert, B., Li, K. Y., Cai, L., Hensley, C. T., Kim, J., Zacharias, L. G., et al. (2017). Lactate metabolism in human lung tumors. *Cell* 171, 358–371. doi:10.1016/j.cell.2017.09.019

Fu, J., Pan, J., Yang, X., Zhang, Y., Shao, F., Chen, J., et al. (2021). Mechanistic study of lncRNA UCA1 promoting growth and cisplatin resistance in lung adenocarcinoma. *Cancer Cell Int.* 21, 505. doi:10.1186/s12935-021-02207-0

Gao, X., Tang, M., Tian, S., Li, J., and Liu, W. (2021). A ferroptosis-related gene signature predicts overall survival in patients with lung adenocarcinoma. *Future Oncol.* 17, 1533–1544. doi:10.2217/fon-2020-1113

García-Cañaveras, J. C., Chen, L., and Rabinowitz, J. D. (2019). The tumor metabolic microenvironment: Lessons from lactate. *Cancer Res.* 79, 3155–3162. doi:10.1158/0008-5472.can-18-3726

Hänzelmann, S., Castelo, R., and Guinney, J. (2013). GSVA: gene set variation analysis for microarray and RNA-seq data. *BMC Bioinforma.* 14, 7. doi:10.1186/1471-2105-14-7

He, L., Endress, J., Cho, S., Li, Z., Zheng, Y., Asara, J. M., et al. (2022). Suppression of nuclear GSK3 signaling promotes serine/one-carbon metabolism and confers metabolic vulnerability in lung cancer cells. *Sci. Adv.* 8, eabm8786. doi:10.1126/sciadv.abm8786

Hess, D., and Igal, R. A. (2011). Genistein downregulates de novo lipid synthesis and impairs cell proliferation in human lung cancer cells. *Exp. Biol. Med.* 236, 707–713. doi:10.1258/ebm.2011.010265

Hristova, V. A., and Chan, D. W. (2019). Cancer biomarker discovery and translation: proteomics and beyond. *Expert Rev. Proteomics* 16, 93–103. doi:10.1080/14789450.2019.1559062

Huang, Z., Zhao, X., Wu, X., Xiang, L., Yuan, Y., Zhou, S., et al. (2019). LncRNA UCA1 facilitated cell growth and invasion through the miR-206/CLOCK axis in glioma. *Cancer Cell Int.* 19, 316. doi:10.1186/s12935-019-1023-7

Jiao, D., Chen, J., Li, Y., Tang, X., Wang, J., Xu, W., et al. (2018). miR-1-3p and miR-206 sensitizes HGF-induced gefitinib-resistant human lung cancer cells through inhibition of c-Met signalling and EMT. *J. Cell. Mol. Med.* 22, 3526–3536. doi:10.1111/jcmm.13629

Li, C. H., Chan, M. H., and Chang, Y. C. (2022). The role of fructose 1, 6-bisphosphate-mediated glycolysis/gluconeogenesis genes in cancer prognosis. *Aging (Albany NY)* 14, 3233–3258. doi:10.18632/aging.204010

Li, X., Li, F., Wang, F., Li, J., Lin, C., and Du, J. (2018). Resveratrol inhibits the proliferation of A549 cells by inhibiting the expression of COX-2. *Onco. Targets. Ther.* 11, 2981–2989. doi:10.2147/ott.s157613

Li, Z., Chen, Q. Q., Lam, C. W. K., Guo, J. R., Zhang, W. J., Wang, C. Y., et al. (2019). Investigation into perturbed nucleoside metabolism and cell cycle for elucidating the cytotoxicity effect of resveratrol on human lung adenocarcinoma epithelial cells. *Chin. J. Nat. Med.* 17, 608–615. doi:10.1016/s1875-5364(19)30063-9

Liu, L., Cao, J., Zhao, J., Li, X., Suo, Z., and Li, H. (2019). PDHA1 gene knockout in human esophageal squamous cancer cells resulted in greater warburg effect and aggressive features *in vitro* and *in vivo*. *Onco. Targets. Ther.* 12, 9899–9913. doi:10.2147/ott.s226851

Liu, X., Huang, Z., Qian, W., Zhang, Q., and Sun, J. (2019). Silence of lncRNA UCA1 rescues drug resistance of cisplatin to non-small-cell lung cancer cells. *J. Cell. Biochem.* 120, 9243–9249. doi:10.1002/jcb.28200

Liu, Z., Yu, M., Fei, B., Fang, X., Ma, T., and Wang, D. (2018). miR-21-5p targets PDHA1 to regulate glycolysis and cancer progression in gastric cancer. *Oncol. Rep.* 40, 2955–2963. doi:10.3892/or.2018.6695

Luo, H., Vong, C. T., Chen, H., Gao, Y., Lyu, P., Qiu, L., et al. (2019). Naturally occurring anti-cancer compounds: shining from Chinese herbal medicine. *Chin. Med.* 14, 48. doi:10.1186/s13020-019-0270-9

Ma, X., Hu, M., Wang, H., and Li, J. (2018). Discovery of traditional Chinese medicine monomers and their synthetic intermediates, analogs or derivatives for battling P-gp-mediated multi-drug resistance. *Eur. J. Med. Chem.* 159, 381–392. doi:10.1016/j.ejmech.2018.09.061

Martínez-Jiménez, F., Muiños, F., Sentís, I., Deu-Pons, J., Reyes-Salazar, I., Arnedo-Pac, C., et al. (2020). A compendium of mutational cancer driver genes. *Nat. Rev. Cancer* 20, 555–572. doi:10.1038/s41568-020-0290-x

Meza, R., Meernik, C., Jeon, J., and Cote, M. L. (2015). Lung cancer incidence trends by gender, race and histology in the United States, 1973-2010. *PLoS One* 10, e0121323. doi:10.1371/journal.pone.0121323

Miao, H., Zeng, Q., Xu, S., and Chen, Z. (2021). miR-1-3p/CELSR3 participates in regulating malignant phenotypes of lung adenocarcinoma cells. *Curr. Gene Ther.* 21, 304–312. doi:10.2174/1566523221666210617160611

Misri, S., Kaul, K., Mishra, S., Charan, M., Verma, A. K., Barr, M. P., et al. (2022). Cannabidiol inhibits tumorigenesis in cisplatin-resistant non-small cell lung cancer via TRPV2. *Cancers (Basel)* 14, 1181. doi:10.3390/cancers14051181

Qin, S. H., Lau, A. T. Y., Liang, Z. L., Tan, H. W., Ji, Y. C., Zhong, Q. H., et al. (2020). Resveratrol promotes tumor microvessel growth via endoglin and extracellular signal-regulated kinase signaling pathway and enhances the anticancer efficacy of gemcitabine against lung cancer. *Cancers (Basel)* 12, E974. doi:10.3390/cancers12040974

Rosell, R., Karachaliou, N., and Arrieta, O. (2020). Novel molecular targets for the treatment of lung cancer. *Curr. Opin. Oncol.* 32, 37–43. doi:10.1097/cco.0000000000000590

Ruiz-Cordero, R., and Devine, W. P. (2020). Targeted therapy and checkpoint immunotherapy in lung cancer. *Surg. Pathol. Clin.* 13, 17–33. doi:10.1016/j.path.2019.11.002

Seltzer, E. S., Watters, A. K., Mackenzie, D., Jr., Granat, L. M., and Zhang, D. (2020). Cannabidiol (CBD) as a promising anti-cancer drug. *Cancers (Basel)* 12, E3203. doi:10.3390/cancers12113203

Shin, D., Lee, J., You, J. H., Kim, D., and Roh, J. L. (2020). Dihydrolipoamide dehydrogenase regulates cystine deprivation-induced ferroptosis in head and neck cancer. *Redox Biol.* 30, 101418. doi:10.1016/j.redox.2019.101418

Sun, X., Li, Y., Xu, L., Shi, X., Xu, M., Tao, X., et al. (2020). Heparin coated meta-organic framework co-delivering doxorubicin and quercetin for effective chemotherapy of lung carcinoma. *J. Int. Med. Res.* 48, 300060519897185. doi:10.1177/0300060519897185

Toki, M. I., Harrington, K., and Syrigos, K. N. (2020). The role of spread through air spaces (STAS) in lung adenocarcinoma prognosis and therapeutic decision making. *Lung Cancer* 146, 127–133. doi:10.1016/j.lungcan.2020.04.026

Tsvetkov, P., Coy, S., Petrova, B., Dreishpoon, M., Verma, A., Abdusamad, M., et al. (2022). Copper induces cell death by targeting lipoylated TCA cycle proteins. *Science* 375, 1254–1261. doi:10.1126/science.abf0529

Tsvetkov, P., Detappe, A., Cai, K., Keys, H. R., Brune, Z., Ying, W., et al. (2019). Mitochondrial metabolism promotes adaptation to proteotoxic stress. *Nat. Chem. Biol.* 15, 681–689. doi:10.1038/s41589-019-0291-9

Velavan, B., Divya, T., Sureshkumar, A., and Sudhandiran, G. (2018). Nano-chemotherapeutic efficacy of (-) -epigallocatechin 3-gallate mediating apoptosis in A549 cells: Involvement of reactive oxygen species mediated Nrf2/Keap1signaling. *Biochem. Biophys. Res. Commun.* 503, 1723–1731. doi:10.1016/j.bbrc.2018.07.105

Vetchý, M. (2018). Biological role of copper as an essential trace element in the human organism. *Ceska Slov. Farm.* 67, 143–153.

Vivian, J., Rao, A. A., Nothaft, F. A., Ketchum, C., Armstrong, J., Novak, A., et al. (2017). Toil enables reproducible, open source, big biomedical data analyses. *Nat. Biotechnol.* 35, 314–316. doi:10.1038/nbt.3772

Wang, K., Chen, Q., Shao, Y., Yin, S., Liu, C., Liu, Y., et al. (2021). Anticancer activities of TCM and their active components against tumor metastasis. *Biomed. Pharmacother.* 133, 111044. doi:10.1016/j.biopha.2020.111044

Wang, S., Hou, Y., Xing, N., Meng, X., Zhang, Y., and Wang, X. (2022). Identification of a novel prognostic signature related to PANoptosis and its regulatory mechanism as well as targeted treatment of active ingredients and traditional Chinese medicine in lung adenocarcinoma. *Pharmacol. Res. - Mod. Chin. Med.* 2, 100069. doi:10.1016/j.prmcm.2022.100069

Wang, S., Yan, Y., Cheng, Z., Hu, Y., and Liu, T. (2018). Sotetsuflavone suppresses invasion and metastasis in non-small-cell lung cancer A549 cells by reversing EMT via the TNF-α/NF-κB and PI3K/AKT signaling pathway. *Cell Death Discov.* 4, 26. doi:10.1038/s41420-018-0026-9

Wu, F., Wang, L., and Zhou, C. (2021). Lung cancer in China: current and prospect. *Curr. Opin. Oncol.* 33, 40–46. doi:10.1097/cco.0000000000000703

Yang, A., Liu, X., Liu, P., Feng, Y., Liu, H., Gao, S., et al. (2021). LncRNA UCA1 promotes development of gastric cancer via the miR-145/MYO6 axis. *Cell. Mol. Biol. Lett.* 26, 33. doi:10.1186/s11658-021-00275-8

Yao, F., Wang, Q., and Wu, Q. (2019). The prognostic value and mechanisms of lncRNA UCA1 in human cancer. *Cancer Manag. Res.* 11, 7685–7696. doi:10.2147/cmar.s200436

Zhang, H., Zhang, Z., Gao, L., Qiao, Z., Yu, M., Yu, B., et al. (2019). miR-1-3p suppresses proliferation of hepatocellular carcinoma through targeting SOX9. *Onco. Targets. Ther.* 12, 2149–2157. doi:10.2147/ott.s197326

Zhang, J., Mao, S., Guo, Y., Wu, Y., Yao, X., and Huang, Y. (2019). Inhibition of GLS suppresses proliferation and promotes apoptosis in prostate cancer. *Biosci. Rep.* 39, BSR20181826. doi:10.1042/bsr20181826

Zhang, L., Ma, X., and Dong, Y. (2018). Effect of genistein on apoptosis of lung adenocarcinoma A549 cells and expression of apoptosis factors. *J. buon* 23, 641–646.

Zhang, L., Zhang, Z., and Yu, Z. (2019). Identification of a novel glycolysis-related gene signature for predicting metastasis and survival in patients with lung adenocarcinoma. *J. Transl. Med.* 17, 423. doi:10.1186/s12967-019-02173-2

frontiers | Frontiers in Pharmacology

TYPE Original Research
PUBLISHED 13 February 2023
DOI 10.3389/fphar.2022.991881

OPEN ACCESS

EDITED BY
Essa M. Saied,
Humboldt University of Berlin, Germany

REVIEWED BY
Shizuka Uchida,
Aalborg University Copenhagen, Denmark
Prem P. Kushwaha,
Case Western Reserve University, United States
Jian Tu,
Guilin Medical University, China

*CORRESPONDENCE
Guanghui Xu,
760020220083@xzhmu.edu.cn

SPECIALTY SECTION
This article was submitted to Pharmacology of Anti-Cancer Drugs, a section of the journal Frontiers in Pharmacology

RECEIVED 12 July 2022
ACCEPTED 11 October 2022
PUBLISHED 13 February 2023

CITATION
Cao S, Chen C, Gu D, Wang Z and Xu G (2023), Establishment and external verification of an oxidative stress-related gene signature to predict clinical outcomes and therapeutic responses of colorectal cancer.
Front. Pharmacol. 13:991881.
doi: 10.3389/fphar.2022.991881

Establishment and external verification of an oxidative stress-related gene signature to predict clinical outcomes and therapeutic responses of colorectal cancer

Sha Cao[1], Cheng Chen[1], Dezhi Gu[2], Zhengdong Wang[2] and Guanghui Xu[1]*

[1]Department of Oncology, The First People's Hospital of Lianyungang, Lianyungang, China, [2]Department of Gastrointestinal Surgery, The First People's Hospital of Lianyungang, Lianyungang, China

Objective: Accumulated evidence highlights the biological significance of oxidative stress in tumorigenicity and progression of colorectal cancer (CRC). Our study aimed to establish a reliable oxidative stress-related signature to predict patients' clinical outcomes and therapeutic responses.

Methods: Transcriptome profiles and clinical features of CRC patients were retrospectively analyzed from public datasets. LASSO analysis was used to construct an oxidative stress-related signature to predict overall survival, disease-free survival, disease-specific survival, and progression-free survival. Additionally, antitumor immunity, drug sensitivity, signaling pathways, and molecular subtypes were analyzed between different risk subsets through TIP, CIBERSORT, oncoPredict, etc. approaches. The genes in the signature were experimentally verified in the human colorectal mucosal cell line (FHC) along with CRC cell lines (SW-480 and HCT-116) through RT-qPCR or Western blot.

Results: An oxidative stress-related signature was established, composed of *ACOX1*, *CPT2*, *NAT2*, *NRG1*, *PPARGC1A*, *CDKN2A*, *CRYAB*, *NGFR*, and *UCN*. The signature displayed an excellent capacity for survival prediction and was linked to worse clinicopathological features. Moreover, the signature correlated with antitumor immunity, drug sensitivity, and CRC-related pathways. Among molecular subtypes, the CSC subtype had the highest risk score.

Abbreviations: CRC, colorectal cancer; TCGA, The Cancer Genome Atlas; GEO, Gene Expression Omnibus; OS, overall survival; DFS, disease-free survival; DSS, disease-specific survival; PFS, progression-free survival; ROS, reactive oxygen species; CRC, colorectal cancer; COAD, colon adenocarcinoma; READ, rectum adenocarcinoma; CNV, copy number variation; LASSO, least absolute shrinkage and selection operator; ROCs, receiver operator characteristic curves; AUC, area under the curve; CIBERSORT, Cell Type Identification by Estimating Relative Subsets of RNA Transcripts; GDSC, Genomics of Drug Sensitivity in Cancer; GSEA, Gene set enrichment analysis; GO, Gene Ontology; KEGG, Kyoto Encyclopedia of Genes and Genomes; cDNA, complementary DNA.

Experiments demonstrated that *CDKN2A* and *UCN* were up-regulated and *ACOX1*, *CPT2*, *NAT2*, *NRG1*, *PPARGC1A*, *CRYAB*, and *NGFR* were down-regulated in CRC than normal cells. In H_2O_2-induced CRC cells, their expression was notably altered.

Conclusion: Altogether, our findings constructed an oxidative stress-related signature that can predict survival outcomes and therapeutic response in CRC patients, thus potentially assisting prognosis prediction and adjuvant therapy decisions.

KEYWORDS

colorectal cancer, oxidative stress, prognosis, antitumor immunity, drug sensitivity

Introduction

Modulation of redox homeostasis is essential for maintaining normal cellular function and ensuring cell survival. Tumor cells are characterized by high levels of oxidative stress that is a state of imbalance between oxidation and antioxidation (Donohoe et al., 2019). Accumulated evidence suggests that oxidative stress exhibits dual roles in tumor progression (Yang and Chen, 2021). Reactive oxygen species (ROS) exhibits antitumor effects by heightening tumor cell apoptosis, necrosis, and ferroptosis and strengthening the immune surveillance capacity of immune cells (Gorrini et al., 2013). Instead, ROS promotes tumor progression *via* triggering DNA damage and genomic changes, activating proliferation- and epithelial–mesenchymal transition-related pathways, and remodeling the tumor microenvironment for tumor invasion and metastases (Falone et al., 2019).

Colorectal cancer (CRC) remains the third most diagnosed cancer (10.0%), and the second leading cause of cancer death (9.4%) worldwide, according to GLOBOCAN 2020 estimates (Sung et al., 2021). Approximately 50% of patients die from tumor metastases (Li et al., 2022). Currently, systemic treatment options comprise adjuvant and neoadjuvant chemotherapy, and therapeutic antibodies directed against growth factor receptors (Berlin et al., 2022). Nevertheless, 30–40% of patients relapse despite treatment. A reasonable and effective signature for prognostic assessment of CRC patients is required. Oxidative stress can induce genetic instability and alter cellular processes, leading to CRC (Wei et al., 2021). In a large CRC patient cohort, higher reactive oxygen metabolites exhibit a strong association with more undesirable survival outcomes (Boakye et al., 2020). Cancer cells adapt to chemotherapy-induced oxidative stress using rapidly elevated cellular antioxidant programs, and adaptation of oxidative defense results in therapeutic resistance, a primary barrier to successful cancer treatment (Čipak Gašparović et al., 2021). For instance, SIRT3-mediated SOD2 and PGC-1α trigger chemoresistance in CRC cells (Paku et al., 2021). Moreover, up-regulated NOX-2 and Nrf-2 facilitate 5-fluorouracil resistance of CRC cells (Waghela et al., 2021). Given the crucial roles of oxidative stress in the progression and therapeutic resistance of CRC, this study attempted to construct a reliable oxidative stress-related signature to predict patients' clinical outcomes and therapeutic responses.

Materials and methods

CRC datasets

Transcriptome profiling (RNA-seq) of colon adenocarcinoma (COAD) and rectum adenocarcinoma (READ) was performed, and normal tissue samples were extracted from The Cancer Genome Atlas (TCGA) *via* the Genomic Data Commons (GDC). The raw counts were standardized to count-per-million (CPM) using the edgeR package (Robinson et al., 2010). The threshold was set to 1 to retain genes greater than 1 in 2 or more samples. The copy number variation (CNV) data (masked copy number segment) and somatic mutation data (Varscan2) of CRC samples were downloaded from TCGA. Microarrays of CRC patients in GSE12945 (Staub et al., 2009), GSE39582 (Marisa et al., 2013), and GSE103479 (Allen et al., 2018) were acquired from the Gene Expression Omnibus (GEO). Microarray data were corrected for background and normalized through the robust multichip average (RMA) method. Missing data were imputed through the K-nearest neighbor method.

Identification of differentially expressed oxidative stress-related genes

Differentially expressed genes between CRC and normal tissues were screened based on the criteria of |log2fold-change|≥1 and adjusted $p \leq 0.05$ utilizing the edgeR package. Adjusted p was calculated through the Bonferroni and Hochberg method. In total, 1,399 oxidative stress-related genes were extracted from the GeneCards according to relevance score≥7 (Supplementary Table S1). Afterward, differentially expressed oxidative stress-related genes were intersected.

Prognostic model construction

Univariate cox regression models were established to determine survival-related differentially expressed oxidative stress-related genes with $p < 0.05$. Through the least absolute shrinkage and selection operator method (LASSO), a prognosis gene signature was developed with the glmnet package (Friedman et al., 2010). The

risk score was computed by the expression of candidate genes along with their coefficients. TCGA CRC samples were randomly assigned to the training set along with the testing set at 1:1 ratio (Liu et al., 2020). In each set, the median risk score was set as the cut-off value of low- and high-risk subsets.

Survival analysis

Kaplan–Meier curves along with the log-rank test were conducted on oxidative stress-relevant gene signature and patients' overall survival (OS), disease-free survival (DFS), disease-specific survival (DSS), and progression-free survival (PFS) based on the clinical data. Uni- and multivariate Cox regression models were established on the gene signature, and clinical parameters and OS with the survival package. Through the survival-ROC package, receiver operator characteristic curves (ROCs) were drawn, followed by the area under the curve (AUC) value.

Quantification of immune cell infiltration

Immune cell infiltrations were estimated across CRC tissues through Cell Type Identification by Estimating Relative Subsets of RNA Transcripts (CIBERSORT), a deconvolution approach proposed by Newman et al. (2015). The LM22 gene set was set as the reference set. This analysis was repeated 1,000 times, with $p < 0.05$ as the filtering condition.

Cancer immunity cycle

The cancer immunity cycle containing seven steps reflects the antitumor immunity as previously described (Chen and Mellman, 2013). The enrichment score of these steps was quantified *via* the TIP approach (Xu et al., 2018).

Analysis of CNV and mutation data

On the basis of the recurrently altered regions derived from the Genomic Identification of Significant Targets in Cancer (GISTIC 2.0) algorithm (Mermel et al., 2011), significant focal regions of gain and loss were identified and scored (G-score). The parameter thresholds were set as gain or loss length>0.1 and $p < 0.05$. Somatic mutation data were analyzed with the maftools package (version 2.6.0) (Mayakonda et al., 2018).

Drug sensitivity analysis

Drug Sensitivity data were acquired from the Genomics of Drug Sensitivity in Cancer (GDSC) database (www.cancerRxgene.org) (Yang et al., 2013). IC50 values were estimated with the oncoPredict package (Maeser et al., 2021).

Gene set enrichment analysis

GSEA was carried out through the Java platform (Subramanian et al., 2005). Gene sets of Gene Ontology (GO) and Kyoto Encyclopedia of Genes and Genomes (KEGG) were obtained from the Molecular Signatures Database (Liberzon et al., 2015). Terms with FDR<0.05 after 1,000 permutations were significantly enriched.

Cell culture and treatment

Human colorectal mucosal cell lines (FHC) and CRC cell lines (SW-480 and HCT-116) were maintained in DMEM with 10% fetal bovine serum, 100 U/ml penicillin, and 100 μg/ml streptomycin in a 37°C humidified incubator with 5% CO_2. To induce oxidative stress, the cells were administrated H_2O_2 in the medium, which was changed daily.

RT-qPCR

RNA extraction was performed using the TRIzol reagent (Invitrogen, United States) and DNase I, followed by reverse transcription into complementary DNAs (cDNAs) utilizing the Superscript Reverse Transcriptase Kit (Thermo Fisher, United States). RT-qPCR was implemented with the Super SYBR Green Kit (BIO-RAD, United States) using the ABI7300 RT-qPCR system (Applied Biosystems, United States). The primer pairs included *ACOX1*, 5′-TAACTTCCTCACTCGAAGCCA-3′ (forward), 5′-AGTTCCATGACCCATCTCTGTC-3′ (reverse); *CDKN2A*, 5′-GATCCAGGTGGGTAGAAGGTC-3′ (forward), 5′-CCCCTGCAAACTTCGTCCT-3′ (reverse); *CPT2*, 5′-CATACAAGCTACATTTCGGGACC-3′ (forward), 5′-AGCCCGGAGTGTCTTCAGAA-3′ (reverse); *CRYAB*, 5′-CCTGAGTCCCTTCTACCTTCG-3′ (forward), 5′-CACATCTCCCAACACCTTAACTT-3′ (reverse); *NAT2*, 5′-ACCTGGACCAAATCAGGAGAG-3′ (forward), 5′-TGTTCGAGGTTCAAGCGTAAAT-3′ (reverse); *NGFR*, 5′-CCTACGGCTACTACCAGGATG-3′ (forward), 5′-CACACGGTGTTCTGCTTGT-3′ (reverse); *NRG1*, 5′-CGGTGTCCATGCCTTCCAT-3′ (forward), 5′-GTGTCACGAGAAGTAGAGGTCT-3′ (reverse); *PPARGC1A*, 5′-TCTGAGTCTGTATGGAGTGACAT-3′ (forward), 5′-CCAAGTCGTTCACATCTAGTTCA-3′ (reverse); *UCN*, 5′-CAACCCTTCTCTGTCCATTGAC-3′ (forward), 5′-CGAGTCGAATATGATGCGGTTC-3′ (reverse); and *GAPDH*, 5′-ACAACTTTGGTATCGTGGAAGG-3′ (forward), 5′-GCCATCACGCCACAGTTTC-3′ (reverse). With GAPDH as an internal control, the relative expression was quantified using the $2^{-\Delta\Delta Ct}$ method.

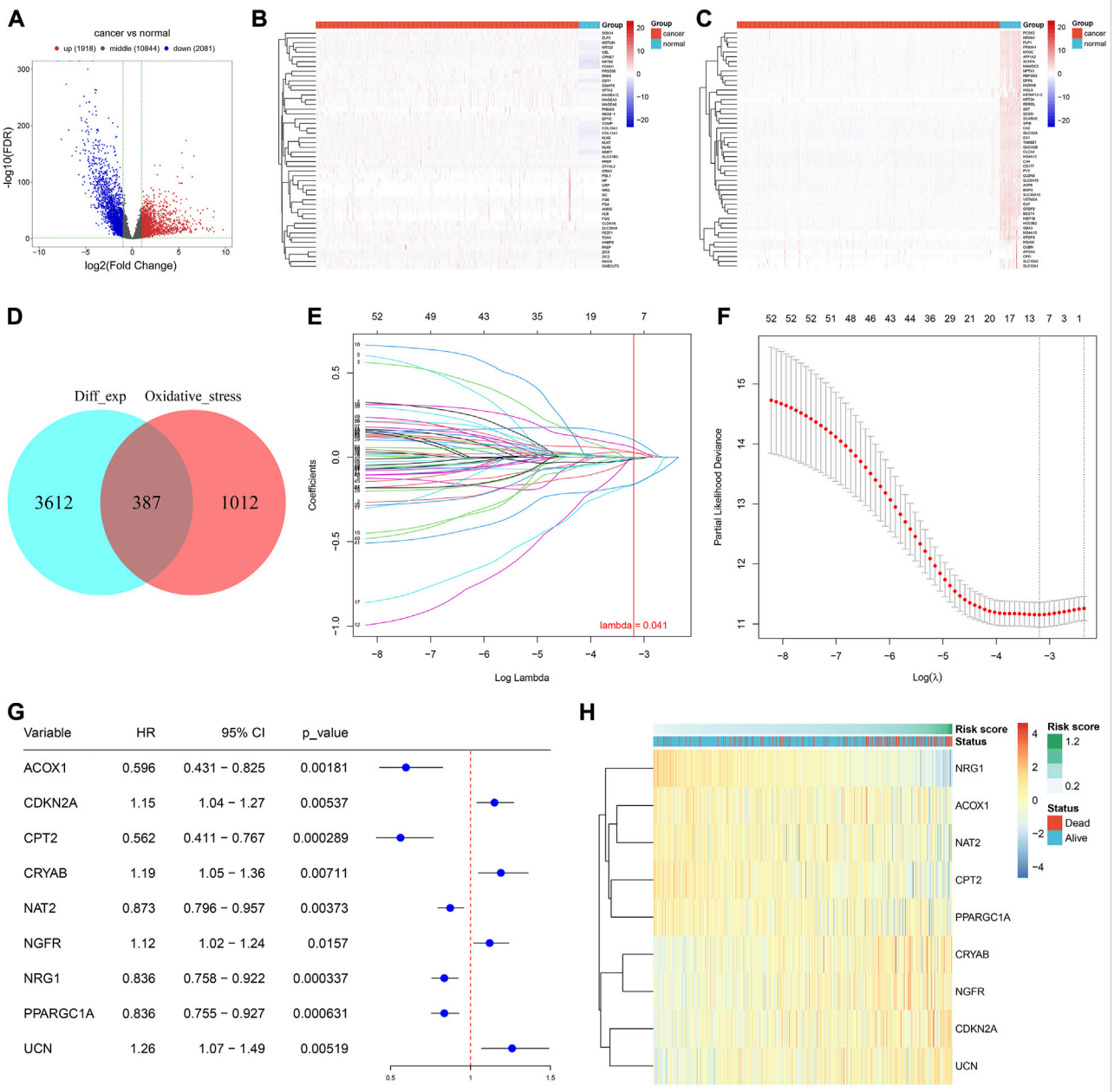

FIGURE 1
Development of an oxidative stress-related gene signature for CRC. **(A)** Volcano plot of the DEGs between CRC and normal tissues in the TCGA-COAD cohort. Red, up-regulated genes; blue, down-regulated genes. **(B,C)** Heatmaps of up- and down-regulated DEGs in CRC *versus* normal tissues in the TCGA-COAD cohort. **(D)** Venn plot of the DEGs and oxidative stress-related genes. **(E)** Identification of the optimal coefficients of oxidative stress-related genes according to the optimal lambda. X-axis is the log lambda; Y-axis is the coefficient of each variable. **(F)** Optimal partial likelihood deviance along with the optimal lambda. **(G)** Forest plot of the univariate cox-regression results of the oxidative stress-relevant genes within the LASSO model. **(H)** Expression of aforementioned genes among CRC samples. *N* = 597.

Western blot

Protein was extracted from cells using RIPA lysis buffer, and protein concentration was assessed using the Bradford protein assay kit (Keygen, China). Protein samples were subjected to 8 or 12% SDS-PAGE gels and transferred onto PVDF membranes, followed by incubation with the primary antibody of *ACOX1* (1/1,000; ab184032), *CDKN2A* (1/1,000; ab270058), *CPT2* (1/3,000; ab181114), *CRYAB* (1/1,000; ab281561), *NAT2* (1/5,000; ab194114), *NGFR* (1/10,000; ab52987), *NRG1* (1/1,000; ab191139), *PPARGC1A* (1/1,000; ab188102), *UCN* (1/1,000; ab231050), or *GAPDH* (1/1,000; ab125247) at 4°C. The next

day, the membrane was incubated with horseradish peroxidase-linked secondary antibodies at room temperature for 1 h. Protein bands were developed using the ECL reagent (Tanon, China), and gray values were quantified *via* ImageJ software.

Statistical analysis

Statistical analysis was generated through R 3.6.1. Statistical difference between groups was computed with unpaired Student's t-test, Wilcoxon test, Kruskal–Wallis test, or one-way analysis of variance. Two-tailed $p < 0.05$ was set as statistical difference.

Results

Development of an oxidative stress-related gene signature for CRC

In total, there were 1,918 up-regulated genes and 2,081 down-regulated genes in 638 CRC *versus* 51 normal tissues (Figures 1A–C). The detailed information is listed in Supplementary Table S2. From the GeneCards, we extracted 1,399 oxidative stress-related genes. After taking the intersection, 387 differentially expressed oxidative stress-related genes were finally identified (Figure 1D). Among them, 53 genes were significantly correlated with CRC prognosis (Supplementary Table S3). Afterward, candidate genes with regression coefficient≠0 were used for constructing an oxidative stress-related gene signature using the LASSO algorithm (Figures 1E,F). The risk score was computed according to (-0.00277909287793242) * *ACOX1* expression + 0.0280830167034478 * *CDKN2A* expression + (-0.163084055105811) * *CPT2* expression + 0.0548399857226341 * *CRYAB* expression + (-0.0107247779354099) * *NAT2* expression + 0.0267977941327448 * *NGFR* expression + (-0.160185818265943) * *NRG1* expression + (-0.00515077740891848) * *PPARGC1A* expression + 0.10199017424903 * *UCN* expression. For CRC prognosis, *ACOX1*, *CPT2*, *NAT2*, *NRG1*, and *PPARGC1A* were protective factors, and *CDKN2A*, *CRYAB*, *NGFR*, and *UCN* were risk factors (Figure 1G). Figure 1H visualizes the expression of the aforementioned genes across CRC samples.

The oxidative stress-related gene signature accurately predicts CRC prognosis

TCGA patients ($N = 597$) were randomly allocated into the training set ($N = 298$) and testing set ($N = 299$) at 1:1 ratio. Table 1 lists the patients' clinicopathological characteristics in the total, training along with testing sets. According to the median value, CRC cases were allocated into the high- or low-risk subsets (Figure 2A), with relatively more dead and recurred/progressed cases in the high-risk subset (Figures 2B,C). The OS outcomes of the high-risk subset were significantly decreased in comparison to those of the low-risk subset in the training set (Figure 2D) and the testing set (Figure 2E) along with the total set (Figure 2F). ROCs under 4-, 5-, and 6-year OS of the training set (Figure 2G), the testing set (Figure 2H) along with the total set (Figure 2I) demonstrated the excellent performance of the oxidative stress-related gene signature in predicting CRC prognosis.

We also measured the expression of two master regulators of oxidative stress (*NRF2* and *KEAP1*). Compared with normal tissues, up-regulated *KEAP1* and down-regulated *NRF2* were found in CRC tissues at the transcriptional level (Figure 2J), indicating the enhanced oxidative stress during CRC development. Additionally, we observed the difference in *NRF2* and *KEAP1* between high- and low-risk subsets. As shown in Figure 2K, the high-risk subset presented higher *KEAP1* expression and lower *NRF2* expression in comparison to the low-risk subset, demonstrating the heterogeneity in oxidative stress between high- and low-risk CRC patients.

The oxidative stress-related gene signature correlates to clinical characteristics of CRC

Distribution of the risk score derived from the oxidative stress-related gene signature was analyzed across different clinical characteristics. With the increasing TNM and pathological stage, the risk score was dramatically higher (Figures 3A–D). Additionally, the risk score was positively correlated to the lymph node (Figure 3E). Compared with microsatellite-stable (MSS), microsatellite unstable-low (MSI-L) had a significantly higher risk score (Figure 3F). Overall, the oxidative stress-related gene signature was correlated to a more serious pathological status.

The oxidative stress-related gene signature acts as an independent prognostic factor of CRC patients

Uni- and multivariate Cox regression models demonstrated that the risk score acted as an independent risk factor of CRC survival (Figures 3G,H). CRC patients were stratified by the T stage (T1–2 and T3–4), N stage (N0 and N1–2), M stage (M0 and M1), pathological stage (stage I–II and stage III–IV), or sex (female and male). In each subgroup, OS (Figures 4A–J), DFS (Supplementary Figures 1A–J), DSS (Supplementary Figure S2A–J), and PFS (Supplementary Figure S3A–J) of the high-risk subset were dramatically

TABLE 1 Clinical characteristics of CRC patients in the total, training, and testing sets.

Variable	Total set (*N* = 597)	Training set (*N* = 298)	Testing set (*N* = 299)
Age	66.07 ± 12.7	66.52 ± 12.36	65.61 ± 13.03
Status (n, %)			
Alive	472 (79.06)	233 (78.19)	239 (79.93)
Dead	125 (20.94)	65 (21.81)	60 (20.07)
Sex (n, %)			
Male	322 (53.94)	169 (56.71)	153 (51.17)
Female	275 (46.06)	129 (43.29)	146 (48.83)
T stage (n, %)			
T1	20 (3.35)	9 (3.02)	11 (3.68)
T2	103 (17.25)	55 (18.46)	48 (16.05)
T3	408 (68.34)	200 (67.11)	208 (69.57)
T4	64 (10.72)	33 (11.07)	31 (10.37)
Ti	1 (0.17)	1 (0.34)	0 (0)
Unknown	1 (0.17)	0 (0)	1 (0.33)
N stage (n, %)			
N0	337 (56.45)	180 (60.4)	157 (52.51)
N1	147 (24.62)	63 (21.14)	84 (28.09)
N2	110 (18.43)	55 (18.46)	55 (18.39)
Unknown	3 (0.5)	0 (0)	3 (1)
M stage (n, %)			
M0	443 (74.2)	220 (73.83)	223 (74.58)
M1	84 (14.07)	41 (13.76)	43 (14.38)
Unknown	70 (11.73)	37 (12.42)	33 (11.04)
Pathologic stage (n, %)			
Stage I	103 (17.25)	55 (18.46)	48 (16.05)
Stage II	217 (36.35)	117 (39.26)	100 (33.44)
Stage III	175 (29.31)	77 (25.84)	98 (32.78)
Stage IV	87 (14.57)	43 (14.43)	44 (14.72)
Unknown	15 (2.51)	6 (2.01)	9 (3.01)

decreased in comparison with those of the low-risk subset. Hence, this oxidative stress-relevant gene signature was independent of other clinical characteristics in predicting CRC patients' prognosis.

External verification of the oxidative stress-related gene signature

To prove the robustness of the oxidative stress-related gene signature, this study included three independent cohorts. The same formula was used for computing the risk score. Both in the GSE103479 and GSE39582 cohorts, the high-risk subset exhibited worse OS than the low-risk subset, with relatively high AUCs at 4-, 5- and 6-year survival (Figures 5A–D). As the N stage (Figures 5E,F), M stage (Figure 5G), and pathological stage (Figures 5H,I) worsened, the risk score gradually increased. The aforementioned data demonstrated that the signature exhibited excellent robustness on distinct platforms.

The oxidative stress-related gene signature correlates to antitumor immunity of CRC

Through the CIBERSORT approach, we estimated the immune cell infiltration across CRC specimens (Figures 6A,B). Activated dendritic cells, activated mast cells, monocytes, neutrophils, resting NK cells, plasma cells, activated memory T-cell CD4, and resting memory T-cell CD4 were significantly lower in the high-risk subset than those in the low-risk subset (Figures 6C,D). Meanwhile, M0 macrophages, activated NK cells, T-cell CD8, T-cell follicular helper, and T-cell regulatory (Tregs) exhibited elevated infiltration in the high-risk subset. The

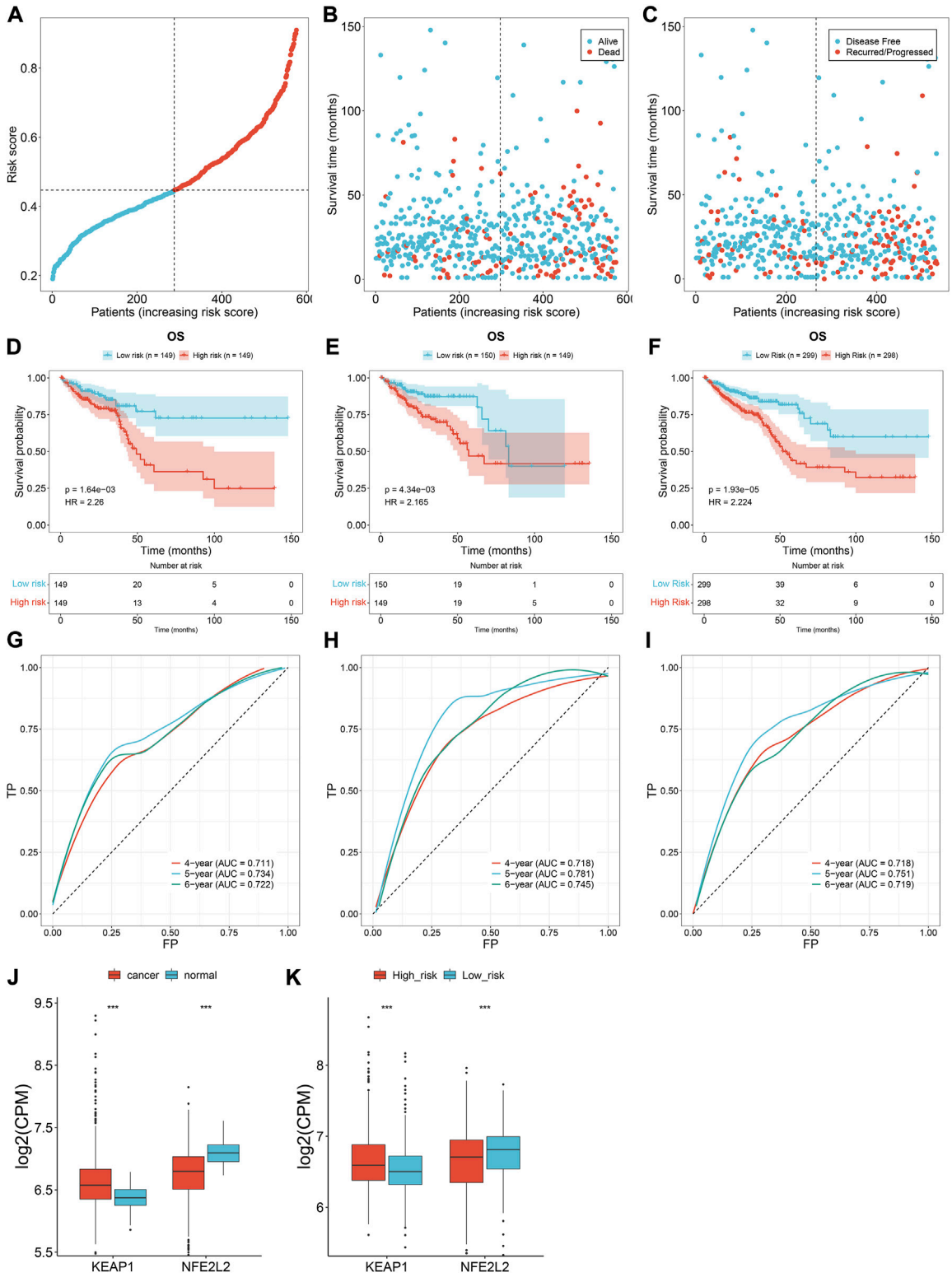

FIGURE 2
Oxidative stress-related gene signature accurately predicts CRC prognosis. **(A)** Distribution of the risk score derived from the oxidative stress-related gene signature in TCGA CRC patients. The vertical dotted line represents the median value. Red dots, high-risk samples; blue dots, low-risk samples. **(B)** Scatter plots of alive (blue) and dead (red) cases along the increasing risk score. **(C)** Scatter plots of disease-free (blue) and recurred/progressed (red) cases along the increasing risk score. **(D–F)** Kaplan–Meier OS for high- and low-risk subsets within the **(D)** training set, **(E)** the testing set, along with **(F)** the total set. **(G–I)** ROCs under 4-, 5- and 6-year survival for the **(G)** training set, **(H)** the testing set, along with **(I)** the total set. **(J)** Comparison of the expression of two master regulators of oxidative stress (*NRF2* and *KEAP1*) in normal *versus* CRC tissues. **(K)** Comparison of the expression of *NRF2* and *KEAP1* in r high- and low-risk subsets. ***$p < 0.001$. Total set: $N = 597$; training set: $N = 298$; testing set: $N = 299$.

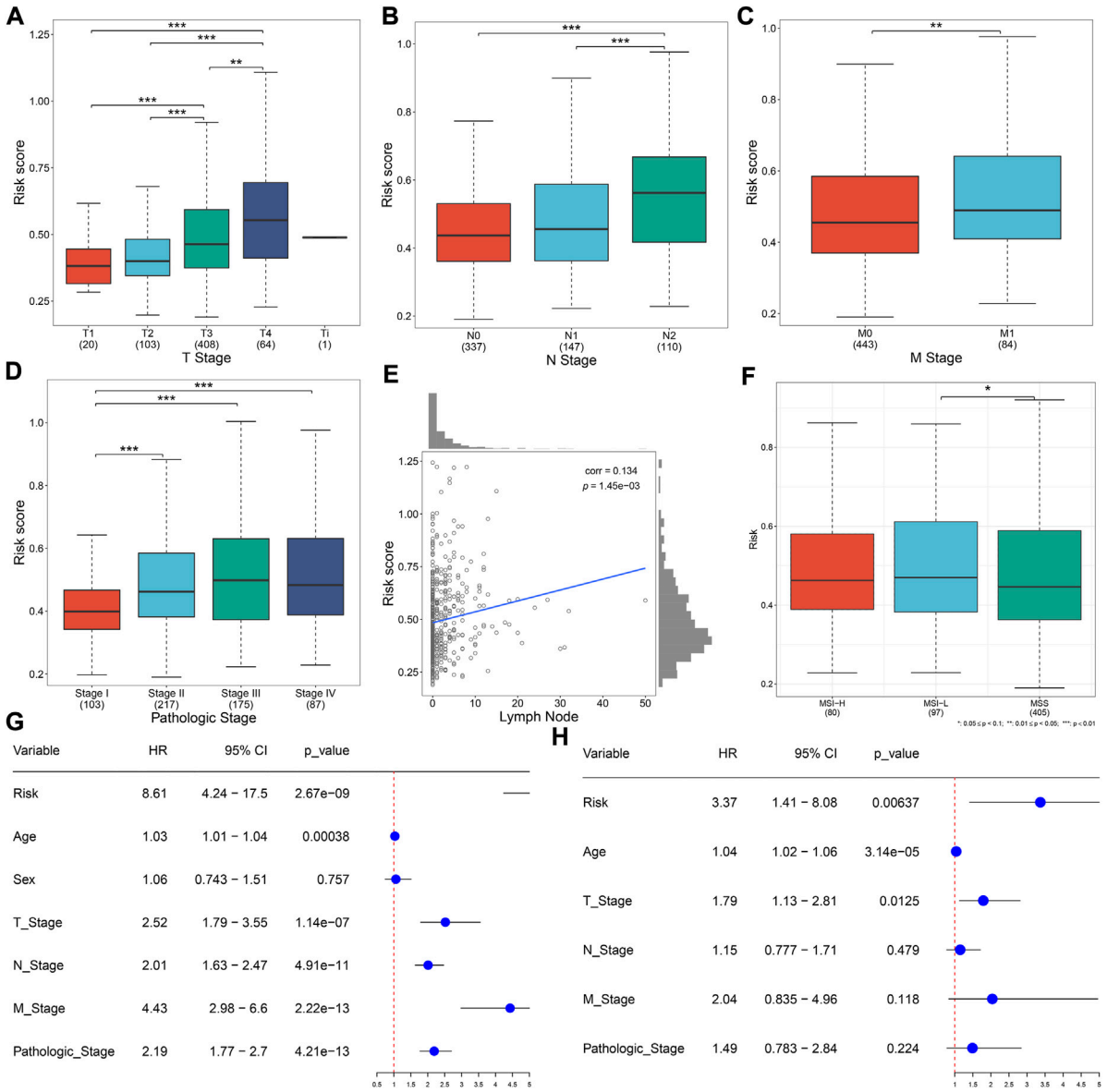

FIGURE 3
Oxidative stress-related gene signature correlates to clinical characteristics and serves as an independent prognostic factor in TCGA CRC. **(A–D)** Distribution of the risk score derived from the oxidative stress-related gene signature across **(A)** T, **(B)** N, **(C)** M, and **(D)** pathological stage. **(E)** Scatter plot of the correlation between the risk score and lymph node. **(F)** Distribution of the risk score across different microsatellite status. **(G,H)** Forest plots of the uni- and multivariate Cox regression results. $*p < 0.05$; $**p < 0.01$; $***p < 0.001$. $N = 597$.

expression of immune checkpoints (*BTLA*, *CD274*, *CEACAM1*, *IDO1*, *LGALS3*, and *PVR*) exhibited down-regulation in the high-risk subset (Figure 6E). Additionally, immunomodulators (*IL6R*, *ICOS*, *CCR3*, *CCL20*, *CCR6*, *CXCL6*, *TNFSF13*, *TNFRSF17*, *CXCL3*, *CCL11*, *CXCL2*, *CXCL1*, *HHLA2*, and *CCL28*) were down-regulated in the high-risk subset (Figure 6F). Meanwhile, higher *CX3CL1* and *TNFSF14* expressions were found in the high-risk subset than in the low-risk subset. High activity of priming and activation, recruitment of CD4 T cells, dendritic cells, T cells, and Th1 cells; infiltration of immune cells into tumors; and recognition of cancer cells by T cells were found in high-risk subset compared to the low-risk subset (Figure 6G). In contrast, B-cell recruitment, eosinophil recruitment, MDSC recruitment, neutrophil recruitment, Th2 cell recruitment, and Treg cell recruitment showed lower activity in high-risk subset than the low-risk subset. Overall, the oxidative stress-related gene signature was correlated to antitumor immunity of CRC.

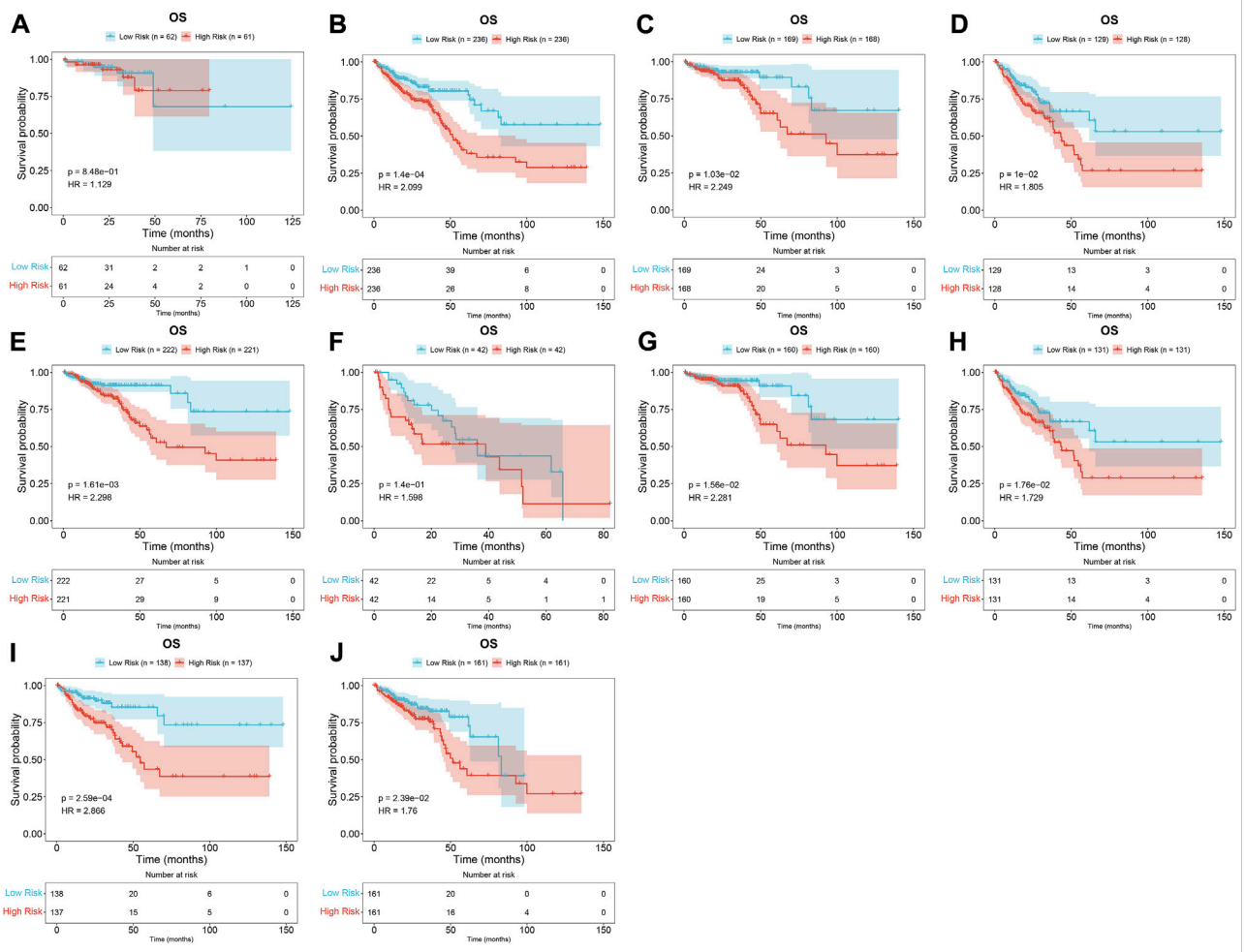

FIGURE 4
Oxidative stress-related gene signature is independent of other clinical features in predicting CRC patients' prognosis. **(A–J)** Subgroup analysis for the OS difference between high- and low-risk subsets in each subgroup stratified by **(A,B)** T (T1–2 and T3–4), **(C,D)** N (N0 and N1–2), **(E,F)** M (M0 and M1), **(G,H)** pathological stage (stage I–II, stage III–IV), or **(I,J)** sex (female and male) in the TCGA dataset. *N* = 597.

Difference in CNV and mutation between high- and low-risk subsets

For the CNV data, we used GISTIC 2.0 to determine 24 amplified fragments and 44 deleted fragments in the high-risk subset (Figures 7A,B). Meanwhile, 28 amplified fragments and 40 deleted fragments were identified in the low-risk subset (Figures 7C–G). Compared with the high-risk subset, higher mutated frequencies of *APC*, *FAT4*, and *OBSCN* occurred in the low-risk subset (Figures 7H–K). In contrast, *TP53*, *TTN*, *KRAS*, *SYNE1*, *MUC16*, *PIK3CA*, and *RYR2* had higher mutated frequencies in the high-risk subset. Additionally, mutated *TP53* was significantly correlated to high-risk CRC (Figure 7L).

Difference in drug sensitivity between high- and low-risk subsets

Drug sensitivity was analyzed between high- and low-risk subsets. The top 50 drugs were as follows: AZD3759, erlotinib, gallibiscoquinazole, zoledronate, OF.1, carmustine, nelarabine, GSK591, sinularin, TAF1, cyclophosphamide, gefitinib, fulvestrant, picolinici acid, temozolomide, IAP, LY2109761, EPZ5676, savolitinib, LGK974, AZD1208, MIRA.1, EPZ004777, AGI.5198, GSK343, LCL161, IRAK4, BIBR.1532, VE821, IWP.2, MK.8776, PFI3, crizotinib, dihydrorotenone, PD173074, VSP34, CDK9, dinaciclib, YK.4.279, VE.822, I.BRD9, LJI308, AZD5991, ABT737, GDC0810, fludarabine, GSK2578215A, Wee1.Inhibitor, P22077, and CZC24832 (Figure 8A).

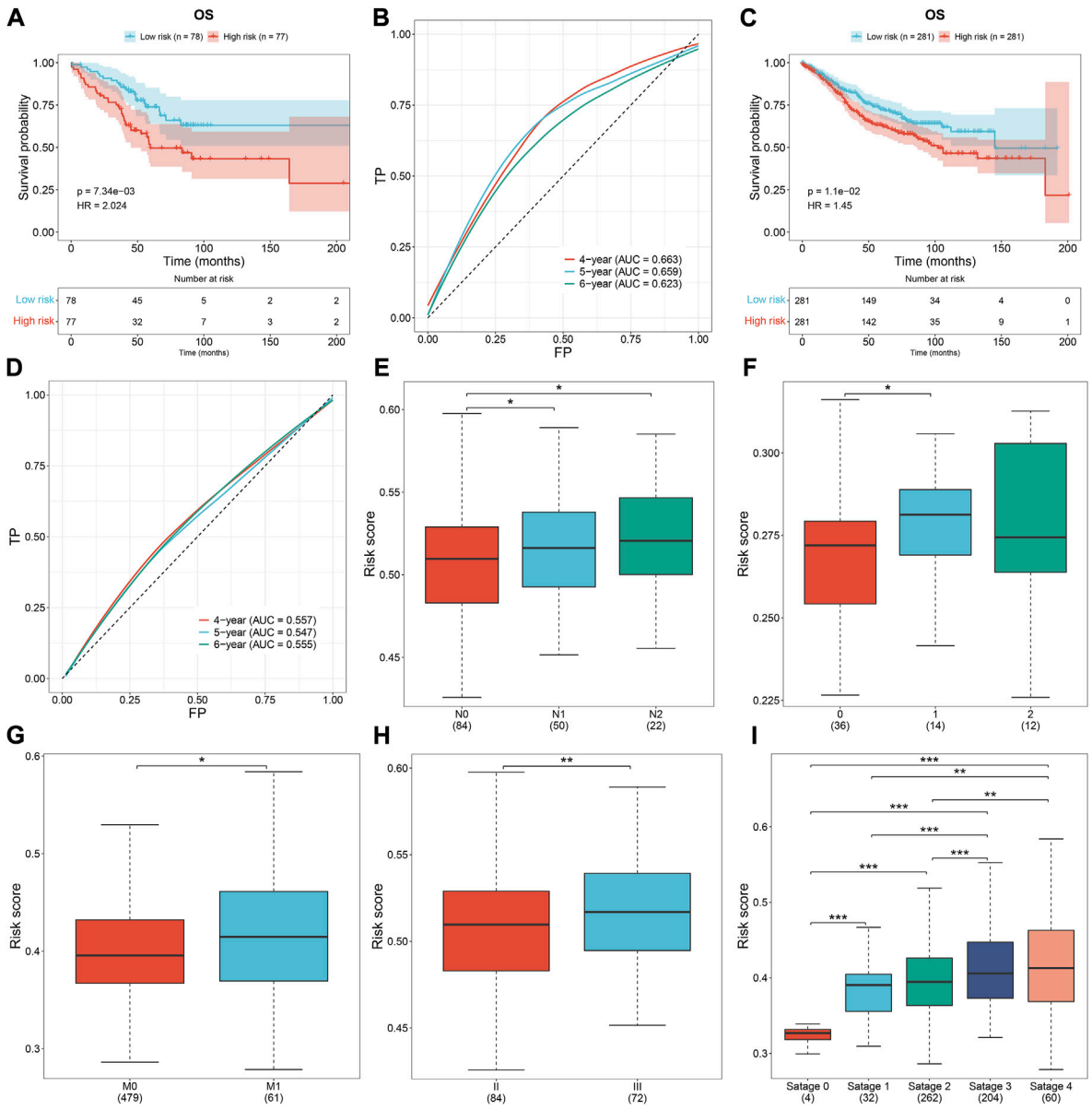

FIGURE 5
External verification of the oxidative stress-related gene signature. **(A,B)** Survival analysis and ROCs under 4-, 5-, and 6-year survival in the GSE103479 dataset. **(C,D)** Survival analysis and ROCs under 4-, 5-, and 6-year survival in the GSE39582 dataset. **(E,F)** Risk score across the N stage in the **(E)** GSE103479 and **(F)** GSE12945 datasets. **(G)** Risk score across the M stage from the GSE39582 dataset. **(H,I)** Risk score across the pathological stage in the GSE103479 and GSE39582 datasets. *$p < 0.05$; **$p < 0.01$; ***$p < 0.001$. GSE103479: $N = 156$; GSE39582: $N = 562$; GSE12945: $N = 62$.

Difference in signaling pathways and molecular subtypes between high- and low-risk subsets

Molecular mechanisms involved in the oxidative stress-related gene signature were further explored. The risk score was significantly correlated with biological processes (keratinization, serotonin receptor signaling pathway, cytosolic calcium ion concentration, ARP 2/3 complex-mediated actin nucleation, positive regulation of transcription of the notch receptor target, and mitotic G2 DNA damage checkpoint; Figure 8B); cellular components of keratin filament, T-cell receptor complex, intermediate filament, condensed nuclear chromosome kinetochore, pericentriolar material, and WASH complex (Figure 8C); molecular functions of neuropeptide hormone activity, G protein-coupled serotonin receptor

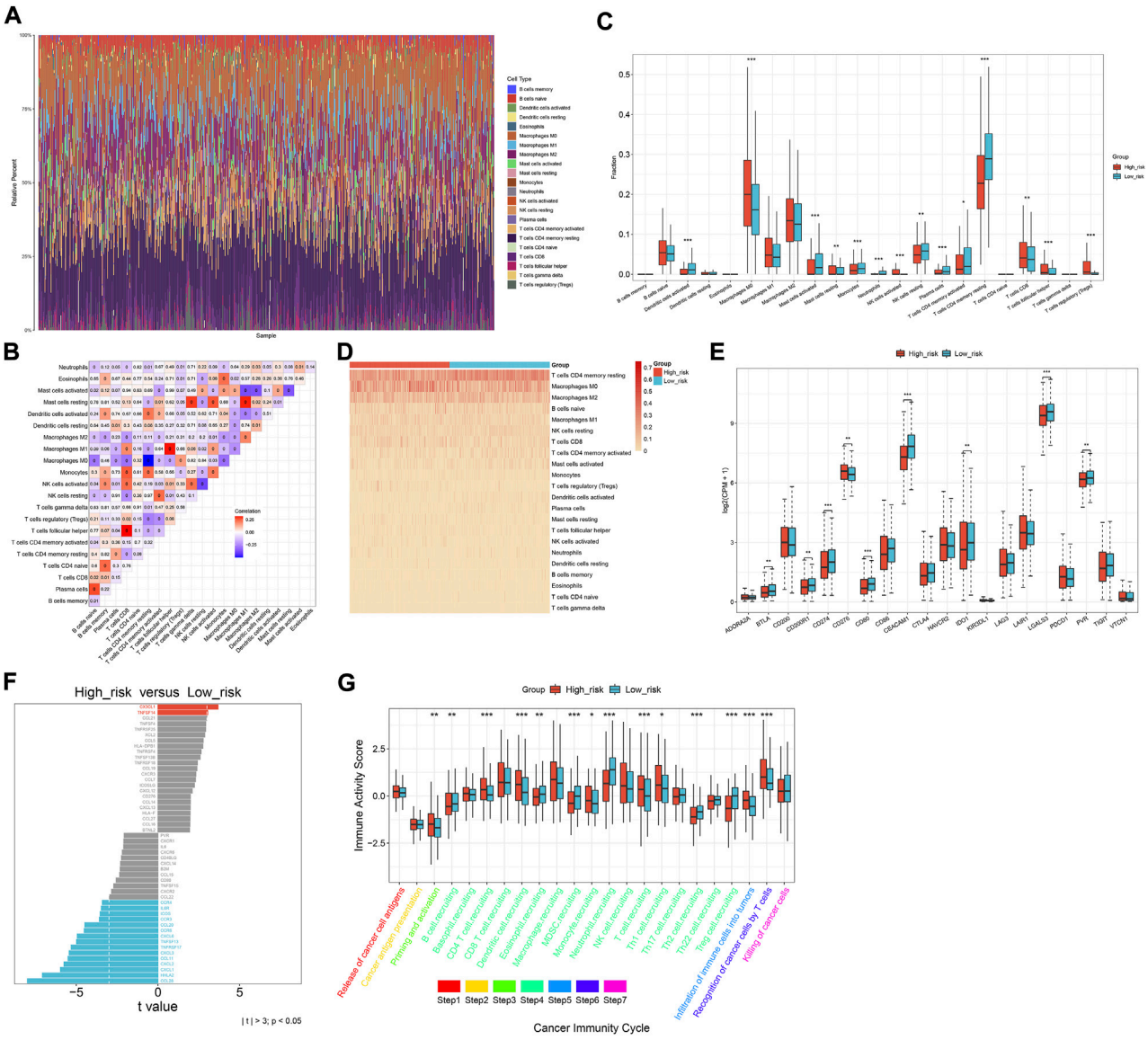

FIGURE 6
Oxidative stress-related gene signature correlates to the antitumor immunity of CRC. **(A)** Relative percent of the infiltration levels of immune cells across TCGA CRC. **(B)** Correlations between different immune cell populations. **(C,D)** Comparison of the infiltration of immune cells between subsets. **(E)** Comparison of immune checkpoints between subsets. **(F)** Difference in the expression of immunomodulators between subsets. **(G)** Difference in the activity of cancer immunity cycle between subsets. *$p < 0.05$; **$p < 0.01$; ***$p < 0.001$. $N = 597$.

activity, structural constituent of eye lens, proline-rich region binding, ribosomal small subunit binding, and RNA polymerase II CTD heptapeptide repeat kinase activity (Figure 8D); KEGG pathways of olfactory transduction, asthma, microRNAs in cancer, homologous recombination, Hippo signaling pathway-multiple species, and protein export (Figure 8E). Additionally, there was a remarkable difference in the risk score among different molecular subtypes (CIN, CSC, dMMR, and KRASm) of CRC (Figure 8F). Particularly, the CSC subtype had the highest risk score.

Experimental verification of the genes within the oxidative stress-relevant gene signature

The genes in the signature were verified in the human colorectal mucosal cell line (FHC) along with CRC cell lines (SW-480 and HCT-116) through RT-qPCR or Western blot. *CDKN2A* and *UCN* were up-regulated and *ACOX1*, *CPT2*, *NAT2*, *NRG1*, *PPARGC1A*, *CRYAB*, and *NGFR* were down-regulated in CRC than normal cells (Figures 9A–C). Next, we

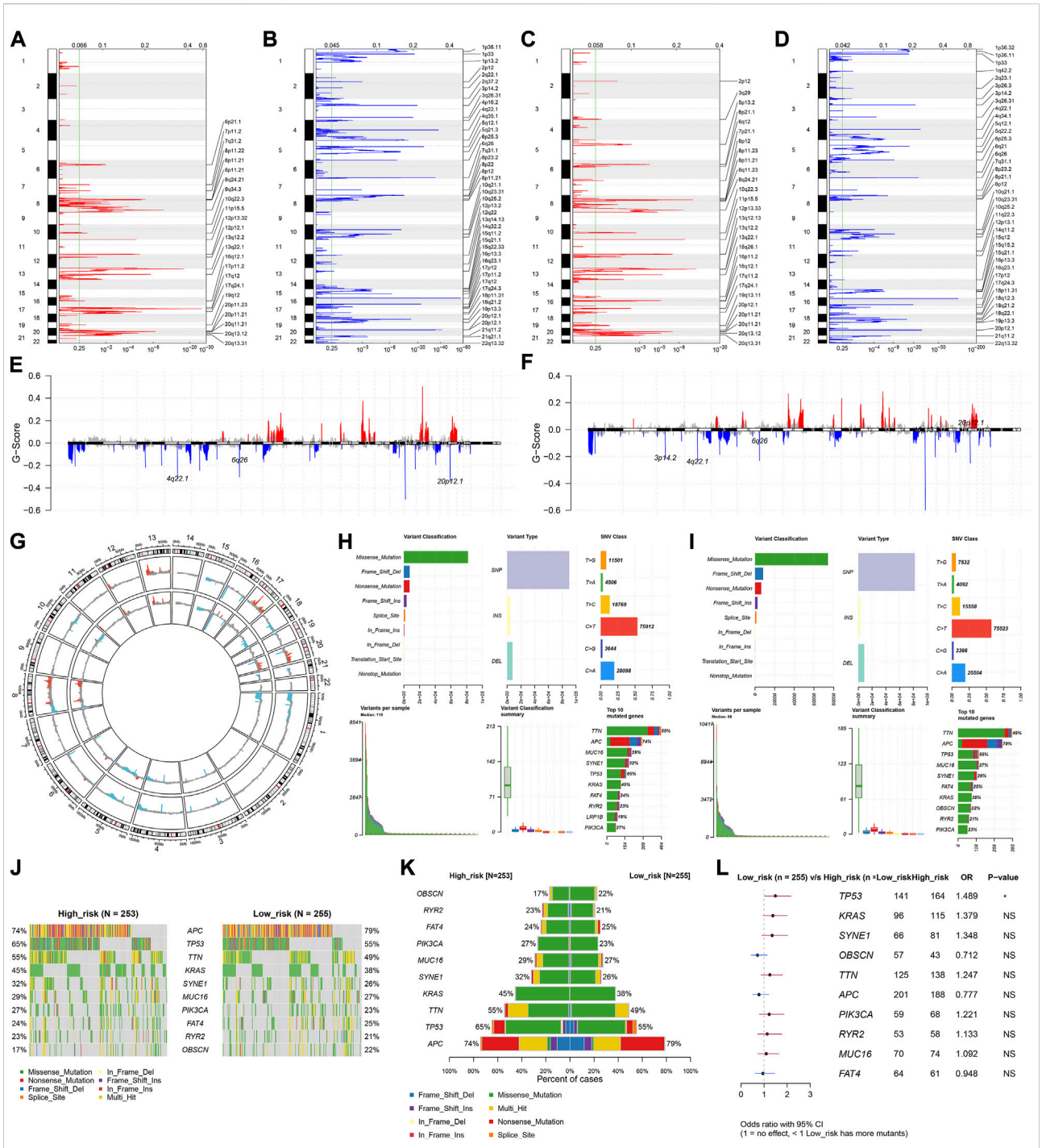

FIGURE 7
Differences in CNV and mutation between high- and low-risk subsets. **(A–D)** Copy number gains and deletions identified in **(A,B)** high- and **(C,D)** low-risk subsets by GISTIC 2.0. X-axis represents the CNV fractions on each chromosome, and y-axis represents the chromosome number. The mutation location on the chromosome is marked on the right side. Red and blue represent the significantly amplified and deleted regions, respectively. **(E–G)** Significant gains and deletions of copy number in high- and low-risk subsets. **(H,I)** Landscape of mutations in high- and low-risk subsets. **(J,K)** Difference in the frequencies of the top 10 mutated genes between subsets. **(L)** Forest plot of the correlation between mutated genes and high-risk. *N* = 597.

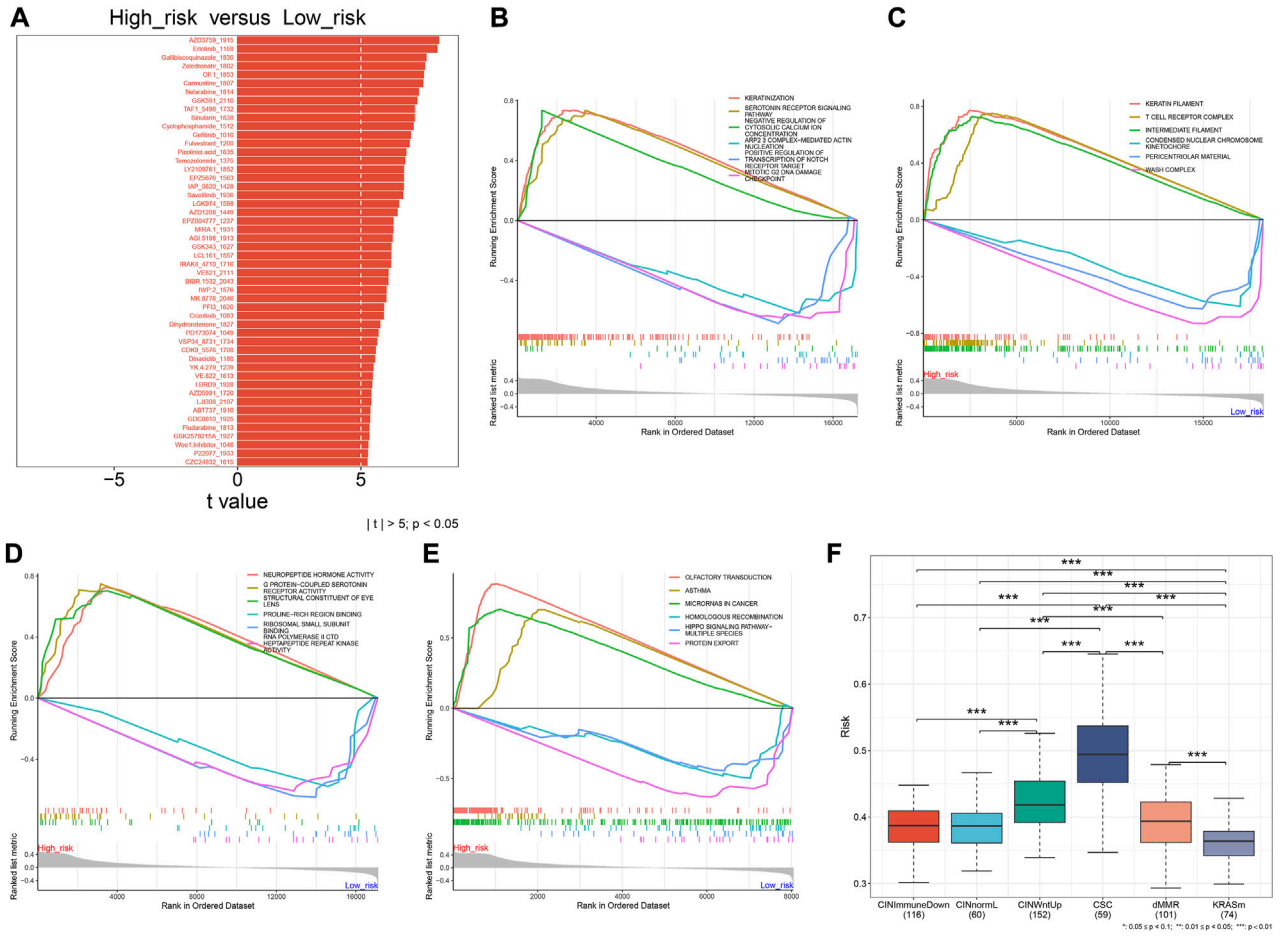

FIGURE 8
Oxidative stress-related gene signature is linked to drug sensitivity, signaling pathways, and molecular subtypes of CRC. **(A)** Difference in sensitivity to the top 50 drugs between high- and low-risk subsets. **(B–E)** Difference in biological processes, cellular component, molecular function, and KEGG pathways between subsets. **(F)** Difference in the risk score among molecular subtypes. ***$p < 0.001$. $N = 597$.

further validated the relationships between the genes in the signature and oxidative stress. After exposure to H_2O_2, their expression was measured in SW-480 and HCT-116 cells. Higher expression of *ACOX1*, *CPT2*, *NAT2*, *NRG1*, *PPARGC1A*, *CRYAB*, and *NGFR* as well as lower expression of *CDKN2A* and *UCN* were observed in H_2O_2-induced CRC cells (Figures 9D–F), indicating the relevance of oxidative stress during CRC development.

Discussion

Oxidative stress-related signatures have been established in acute myeloid leukemia (Dong et al., 2021), melanoma (Yang et al., 2021), clear-cell renal cell carcinoma (Wu Y. et al., 2021a), gastric cancer (Wu Z. et al., 2021b), head and neck squamous cell carcinoma (Wang and Zhou, 2021), glioma (Lu et al., 2021), and bladder cancer (Zhang et al., 2022). Alterations in redox status accompanied by increased production of ROS have been implicated in CRC (Lee et al., 2021). Nevertheless, so far, no oxidative stress-related model has been proposed for CRC. Considering the fact that oxidative stress is a complex process involving different genes, in the present study, we proposed an oxidative stress-related gene signature composed of *ACOX1*, *CPT2*, *NAT2*, *NRG1*, *PPARGC1A*, *CDKN2A*, *CRYAB*, *NGFR*, and *UCN* to predict CRC patients' clinical outcomes with the LASSO approach.

Reliable markers in predicting immunotherapeutic responses of CRC patients are still insufficient in clinical practice (Chen L. et al., 2021b). Dual suppression of endoplasmic reticulum stress and oxidation stress may manipulate macrophage polarization following hypoxia to enhance immunotherapeutic sensitivity (Jiang et al., 2021). *SENP7* can sense oxidative stress to maintain metabolic fitness

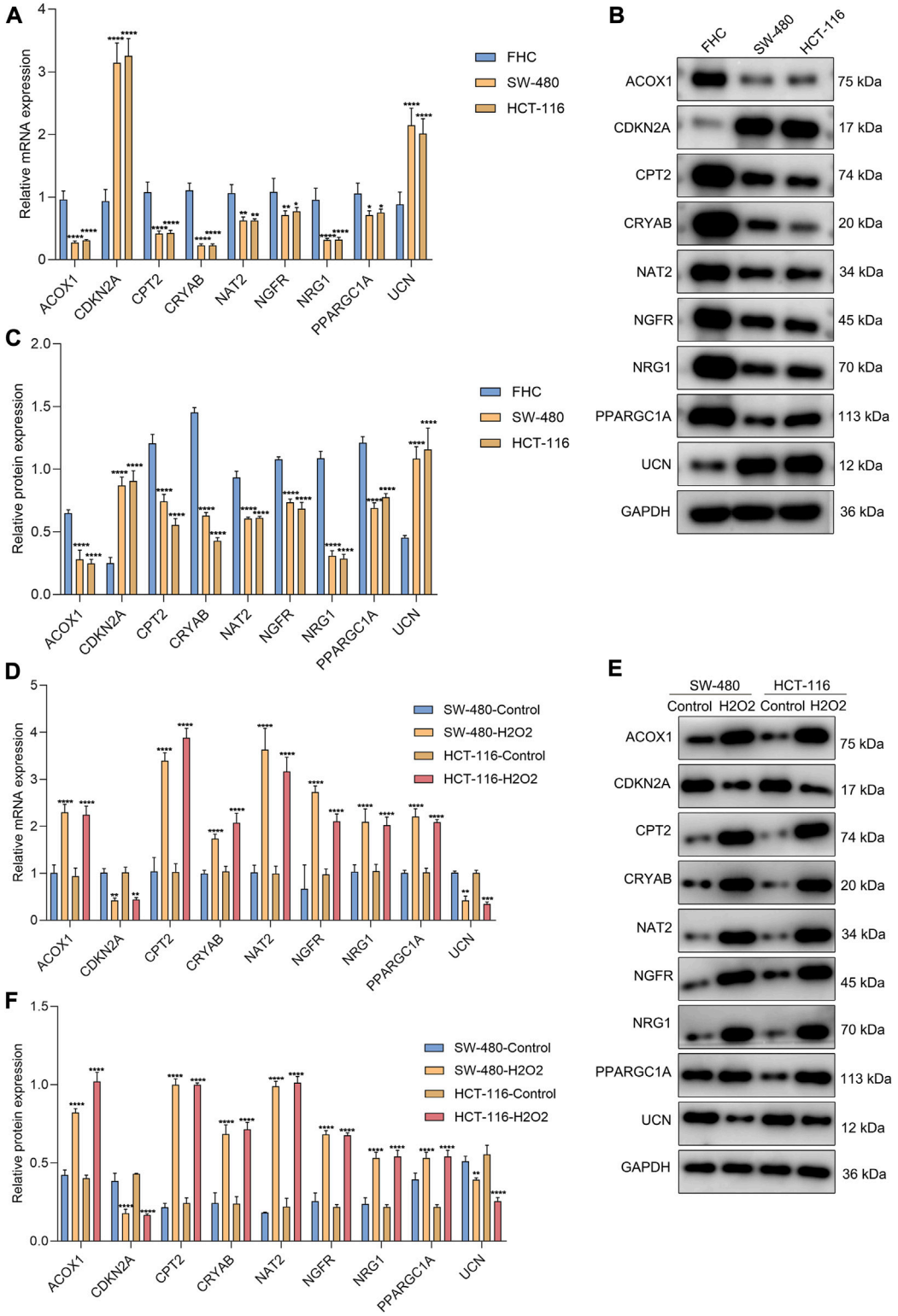

FIGURE 9
Experimental verification of the genes from the oxidative stress-relevant gene signature. **(A–C)** RT-qPCR and Western blot for the expression of *ACOX1*, *CPT2*, *NAT2*, *NRG1*, *PPARGC1A*, *CDKN2A*, *CRYAB*, *NGFR*, and *UCN* in FHC, SW-480, and HCT-116 cells. **(D–F)** RT-qPCR and Western blot for their expression in H_2O_2-induced SW-480 and HCT-116 cells. *$p < 0.05$; **$p < 0.01$; ***$p < 0.001$; ****$p < 0.0001$. $N = 3$.

and antitumor effects of $CD8^+$ T cells (Wu et al., 2022). Moreover, altered tumor metabolism *via* $CD4^+$ T cells results in TNF-α-dependent intensified oxidative stress and tumor cell deaths (Habtetsion et al., 2018). The oxidative stress-related gene signature was correlated with the antitumor immunity of CRC, indicating that this signature might enable prediction of the immunotherapeutic response (Liu et al., 2020). Genomic alterations and CNVs were compared between high- and low-risk subsets. Particularly, the high-risk subset was remarkably linked to more aggressive molecular alteration: mutated *TP53* that triggers enhanced proliferative capacity *via* consuming oxygen and producing abnormal vasculature during the early stage of cancer development. There were remarkable differences in drug sensitivity between high- and low-risk subsets. Additionally, the risk score was linked to CRC-related pathways, such as mitotic G2 DNA damage checkpoint, microRNAs in cancer, and Hippo signaling pathway.

Our experimental studies demonstrated that *CDKN2A* and *UCN* were up-regulated and *ACOX1*, *CPT2*, *NAT2*, *NRG1*, *PPARGC1A*, *CRYAB*, and *NGFR* were down-regulated in CRC cells (SW-480 and HCT-116) compared with human colorectal mucosal cells (FHC). In H_2O_2-induced CRC cells, their expression was remarkably altered. Butyrate-induced colonocyte differentiation determines *CDKN2A* as a prognostic biomarker of CRC recurrence (Dasgupta et al., 2019). Patients who have tumor chromosomal *CDKN2A* deletion are prone to immunotherapeutic resistance (Horn et al., 2018). *ACOX1* may attenuate the migration and invasion of CRC cells (Sun et al., 2017). Down-regulated *CPT2* induces stemness and oxaliplatin resistance in CRC through the ROS/Wnt/β-catenin-triggered glycolytic metabolism (Li et al., 2021). Additionally, its down-regulation heightens proliferation and weakens apoptosis *via* p53 signaling in CRC (Liu et al., 2022). *NAT2* down-regulation is also found in CRC, which correlates to CRC patients' metastasis and survival (Zhu et al., 2021). *CRYAB* correlates to clinical outcomes and immunocyte infiltrations in CRC (Deng et al., 2021). *NGFR* improves the chemosensitivity of CRC cells by strengthening the apoptotic and autophagic effects of 5-fluorouracil by activating *S100A9* (Chen H. et al., 2021a). Combining previous evidence, the genes in the oxidative stress-related signature play essential roles in CRC progression.

Our analysis is a retrospective study, resulting in unavoidable limitations. As many datasets as possible were included, so sampling bias from tumor heterogeneity and different platforms can only be decreased, but not completely removed. Although we experimentally validated the genes from the oxidative stress-relevant gene signature, more experimental studies are needed for clarifying the functional significance of oxidative stress in CRC.

Conclusion

In summary, this study proposed an oxidative stress-related signature composed of *ACOX1*, *CPT2*, *NAT2*, *NRG1*, *PPARGC1A*, *CDKN2A*, *CRYAB*, *NGFR*, and *UCN* to predict clinical outcomes and therapeutic responses of CRC patients, which provided valuable information for understanding the functional roles of oxidative stress in CRC development, assisting prognosis prediction and guiding adjuvant therapy (especially small molecular compounds and immunotherapy), thereby facilitating precision oncology of CRC.

Data availability statement

The datasets presented in this study can be found in online repositories. The names of the repository/repositories and accession number(s) can be found in the article/Supplementary Material.

Author contributions

GX conceived and designed the study. SC and CC conducted most of the experiments and data analysis and wrote the manuscript. DG and ZW participated in collecting data and helped to draft the manuscript. All authors reviewed and approved the manuscript.

Conflict of interest

The authors declare that the research was conducted in the absence of any commercial or financial relationships that could be construed as a potential conflict of interest.

Publisher's note

Supplementary material

The Supplementary Material for this article can be found online at: https://www.frontiersin.org/articles/10.3389/fphar.2022.991881/full#supplementary-material

References

Allen, W. L., Dunne, P. D., McDade, S., Scanlon, E., Loughrey, M., Coleman, H., et al. (2018). Transcriptional subtyping and CD8 immunohistochemistry identifies patients with stage II and III colorectal cancer with poor prognosis who benefit from adjuvant chemotherapy. *JCO Precis. Oncol.* 2018, 1–15. doi:10.1200/po.17.00241

Berlin, C., Cottard, F., Willmann, D., Urban, S., Tirier, S. M., Marx, L., et al. (2022). KMT9 controls stemness and growth of colorectal cancer. *Cancer Res.* 82 (2), 210–220. doi:10.1158/0008-5472.Can-21-1261

Boakye, D., Jansen, L., Schöttker, B., Jansen, E., Schneider, M., Halama, N., et al. (2020). Blood markers of oxidative stress are strongly associated with poorer prognosis in colorectal cancer patients. *Int. J. Cancer* 147 (9), 2373–2386. doi:10.1002/ijc.33018

Chen, D. S., and Mellman, I. (2013). Oncology meets immunology: The cancer-immunity cycle. *Immunity* 39 (1), 1–10. doi:10.1016/j.immuni.2013.07.012

Chen, H., Huang, J., Chen, C., Jiang, Y., Feng, X., Liao, Y., et al. (2021a). NGFR increases the chemosensitivity of colorectal cancer cells by enhancing the apoptotic and autophagic effects of 5-fluorouracil via the activation of S100A9. *Front. Oncol.* 11, 652081. doi:10.3389/fonc.2021.652081

Chen, L., Niu, X., Qiao, X., Liu, S., Ma, H., Shi, X., et al. (2021b). Characterization of interplay between autophagy and ferroptosis and their synergistical roles on manipulating immunological tumor microenvironment in squamous cell carcinomas. *Front. Immunol.* 12, 739039. doi:10.3389/fimmu.2021.739039

Čipak Gašparović, A., Milković, L., Rodrigues, C., Mlinarić, M., and Soveral, G. (2021). Peroxiporins are induced upon oxidative stress insult and are associated with oxidative stress resistance in colon cancer cell lines. *Antioxidants (Basel)* 10 (11), 1856. doi:10.3390/antiox10111856

Dasgupta, N., Kumar Thakur, B., Chakraborty, A., and Das, S. (2019). Butyrate-induced *in vitro* colonocyte differentiation network model identifies ITGB1, SYK, CDKN2A, CHAF1A, and LRP1 as the prognostic markers for colorectal cancer recurrence. *Nutr. Cancer* 71 (2), 257–271. doi:10.1080/01635581.2018.1540715

Deng, J., Chen, X., Zhan, T., Chen, M., Yan, X., and Huang, X. (2021). CRYAB predicts clinical prognosis and is associated with immunocyte infiltration in colorectal cancer. *PeerJ* 9, e12578. doi:10.7717/peerj.12578

Dong, C., Zhang, N., and Zhang, L. (2021). The multi-omic prognostic model of oxidative stress-related genes in acute myeloid leukemia. *Front. Genet.* 12, 722064. doi:10.3389/fgene.2021.722064

Donohoe, C., Senge, M. O., Arnaut, L. G., and Gomes-da-Silva, L. C. (2019). Cell death in photodynamic therapy: From oxidative stress to anti-tumor immunity. *Biochim. Biophys. Acta. Rev. Cancer* 1872 (2), 188308. doi:10.1016/j.bbcan.2019.07.003

Falone, S., Lisanti, M. P., and Domenicotti, C. (2019). Oxidative stress and reprogramming of mitochondrial function and dynamics as targets to modulate cancer cell behavior and chemoresistance. *Oxid. Med. Cell. Longev.* 2019, 4647807. doi:10.1155/2019/4647807

Friedman, J., Hastie, T., and Tibshirani, R. (2010). Regularization paths for generalized linear models via coordinate descent. *J. Stat. Softw.* 33 (1), 1–22. doi:10.18637/jss.v033.i01

Gorrini, C., Harris, I. S., and Mak, T. W. (2013). Modulation of oxidative stress as an anticancer strategy. *Nat. Rev. Drug Discov.* 12 (12), 931–947. doi:10.1038/nrd4002

Habtetsion, T., Ding, Z. C., Pi, W., Li, T., Lu, C., Chen, T., et al. (2018). Alteration of tumor metabolism by CD4+ T cells leads to TNF-α-dependent intensification of oxidative stress and tumor cell death. *Cell. Metab.* 28 (2), 228–242. doi:10.1016/j.cmet.2018.05.012

Horn, S., Leonardelli, S., Sucker, A., Schadendorf, D., Griewank, K. G., and Paschen, A. (2018). Tumor cdkn2a-associated JAK2 loss and susceptibility to immunotherapy resistance. *J. Natl. Cancer Inst.* 110 (6), 677–681. doi:10.1093/jnci/djx271

Jiang, M., Li, X., Zhang, J., Lu, Y., Shi, Y., Zhu, C., et al. (2021). Dual inhibition of endoplasmic reticulum stress and oxidation stress manipulates the polarization of macrophages under hypoxia to sensitize immunotherapy. *ACS Nano* 15 (9), 14522–14534. doi:10.1021/acsnano.1c04068

Lee, D. Y., Song, M. Y., and Kim, E. H. (2021). Role of oxidative stress and nrf2/KEAP1 signaling in colorectal cancer: Mechanisms and therapeutic perspectives with phytochemicals. *Antioxidants (Basel)* 10 (5), 743. doi:10.3390/antiox10050743

Li, H., Chen, J., Liu, J., Lai, Y., Huang, S., Zheng, L., et al. (2021). CPT2 downregulation triggers stemness and oxaliplatin resistance in colorectal cancer via activating the ROS/Wnt/β-catenin-induced glycolytic metabolism. *Exp. Cell. Res.* 409 (1), 112892. doi:10.1016/j.yexcr.2021.112892

Li, M., Zhao, X., Yong, H., Xu, J., Qu, P., Qiao, S., et al. (2022). Transketolase promotes colorectal cancer metastasis through regulating AKT phosphorylation. *Cell. Death Dis.* 13 (2), 99. doi:10.1038/s41419-022-04575-5

Liberzon, A., Birger, C., Thorvaldsdóttir, H., Ghandi, M., Mesirov, J. P., and Tamayo, P. (2015). The Molecular Signatures Database (MSigDB) hallmark gene set collection. *Cell. Syst.* 1 (6), 417–425. doi:10.1016/j.cels.2015.12.004

Liu, F., Li, X., Yan, H., Wu, J., Yang, Y., He, J., et al. (2022). Downregulation of CPT2 promotes proliferation and inhibits apoptosis through p53 pathway in colorectal cancer. *Cell. Signal.* 92, 110267. doi:10.1016/j.cellsig.2022.110267

Liu, X., Niu, X., and Qiu, Z. (2020). A five-gene signature based on stromal/immune scores in the tumor microenvironment and its clinical implications for liver cancer. *DNA Cell. Biol.* 39 (9), 1621–1638. doi:10.1089/dna.2020.5512

Lu, D., Yang, N., Wang, S., Liu, W., Zhang, D., Wang, J., et al. (2021). Identifying the predictive role of oxidative stress genes in the prognosis of glioma patients. *Med. Sci. Monit.* 27, e934161. doi:10.12659/msm.934161

Maeser, D., Gruener, R. F., and Huang, R. S. (2021). oncoPredict: an R package for predicting *in vivo* or cancer patient drug response and biomarkers from cell line screening data. *Brief. Bioinform.* 22 (6), bbab260. doi:10.1093/bib/bbab260

Marisa, L., de Reyniès, A., Duval, A., Selves, J., Gaub, M. P., Vescovo, L., et al. (2013). Gene expression classification of colon cancer into molecular subtypes: Characterization, validation, and prognostic value. *PLoS Med.* 10 (5), e1001453. doi:10.1371/journal.pmed.1001453

Mayakonda, A., Lin, D. C., Assenov, Y., Plass, C., and Koeffler, H. P. (2018). Maftools: Efficient and comprehensive analysis of somatic variants in cancer. *Genome Res.* 28 (11), 1747–1756. doi:10.1101/gr.239244.118

Mermel, C. H., Schumacher, S. E., Hill, B., Meyerson, M. L., Beroukhim, R., and Getz, G. (2011). GISTIC2.0 facilitates sensitive and confident localization of the targets of focal somatic copy-number alteration in human cancers. *Genome Biol.* 12 (4), R41. doi:10.1186/gb-2011-12-4-r41

Newman, A. M., Liu, C. L., Green, M. R., Gentles, A. J., Feng, W., Xu, Y., et al. (2015). Robust enumeration of cell subsets from tissue expression profiles. *Nat. Methods* 12 (5), 453–457. doi:10.1038/nmeth.3337

Paku, M., Haraguchi, N., Takeda, M., Fujino, S., Ogino, T., Takahashi, H., et al. (2021). SIRT3-Mediated SOD2 and PGC-1α contribute to chemoresistance in colorectal cancer cells. *Ann. Surg. Oncol.* 28 (8), 4720–4732. doi:10.1245/s10434-020-09373-x

Robinson, M. D., McCarthy, D. J., and Smyth, G. K. (2010). edgeR: a Bioconductor package for differential expression analysis of digital gene expression data. *Bioinforma. Oxf. Engl.* 26 (1), 139–140. doi:10.1093/bioinformatics/btp616

Staub, E., Groene, J., Heinze, M., Mennerich, D., Roepcke, S., Klaman, I., et al. (2009). An expression module of WIPF1-coexpressed genes identifies patients with favorable prognosis in three tumor types. *J. Mol. Med.* 87 (6), 633–644. doi:10.1007/s00109-009-0467-y

Subramanian, A., Tamayo, P., Mootha, V. K., Mukherjee, S., Ebert, B. L., Gillette, M. A., et al. (2005). Gene set enrichment analysis: A knowledge-based approach for interpreting genome-wide expression profiles. *Proc. Natl. Acad. Sci. U. S. A.* 102 (43), 15545–15550. doi:10.1073/pnas.0506580102

Sun, L. N., Zhi, Z., Chen, L. Y., Zhou, Q., Li, X. M., Gan, W. J., et al. (2017). SIRT1 suppresses colorectal cancer metastasis by transcriptional repression of miR-15b-5p. *Cancer Lett.* 409, 104–115. doi:10.1016/j.canlet.2017.09.001

Sung, H., Ferlay, J., Siegel, R. L., Laversanne, M., Soerjomataram, I., Jemal, A., et al. (2021). Global cancer statistics 2020: GLOBOCAN estimates of incidence and mortality worldwide for 36 cancers in 185 countries. *Ca. Cancer J. Clin.* 71 (3), 209–249. doi:10.3322/caac.21660

Waghela, B. N., Vaidya, F. U., and Pathak, C. (2021). Upregulation of NOX-2 and nrf-2 promotes 5-fluorouracil resistance of human colon carcinoma (HCT-116) cells. *Biochemistry.* 86 (3), 262–274. doi:10.1134/s0006297921030044

Wang, X., and Zhou, G. (2021). The potential of oxidative stress related genes as prognostic biomarkers in head and neck squamous cell carcinoma. *Comb. Chem. High. Throughput Screen.* 25, 1952–1965. doi:10.2174/1386207325666211207154436

Wei, R., Zhao, Y., Wang, J., Yang, X., Li, S., Wang, Y., et al. (2021). Tagitinin C induces ferroptosis through PERK-Nrf2-HO-1 signaling pathway in colorectal cancer cells. *Int. J. Biol. Sci.* 17 (11), 2703–2717. doi:10.7150/ijbs.59404

Wu, Y., Zhang, X., Wei, X., Feng, H., Hu, B., Deng, Z., et al. (2021a). A mitochondrial dysfunction and oxidative stress pathway-based prognostic signature for clear cell renal cell carcinoma. *Oxid. Med. Cell. Longev.* 2021, 9939331. doi:10.1155/2021/9939331

Wu, Z., Huang, H., Han, Q., Hu, Z., Teng, X. L., Ding, R., et al. (2022). SENP7 senses oxidative stress to sustain metabolic fitness and antitumor functions of CD8+ T cells. *J. Clin. Investig.* 132, e155224. doi:10.1172/jci155224

Wu, Z., Wang, L., Wen, Z., and Yao, J. (2021b). Integrated analysis identifies oxidative stress genes associated with progression and prognosis in gastric cancer. *Sci. Rep.* 11 (1), 3292. doi:10.1038/s41598-021-82976-w

Xu, L., Deng, C., Pang, B., Zhang, X., Liu, W., Liao, G., et al. (2018). Tip: A web server for resolving tumor immunophenotype profiling. *Cancer Res.* 78 (23), 6575–6580. doi:10.1158/0008-5472.Can-18-0689

Yang, B., and Chen, Q. (2021). Cross-talk between oxidative stress and m(6)A RNA methylation in cancer. *Oxid. Med. Cell. Longev.* 2021, 6545728. doi:10.1155/2021/6545728

Yang, W., Soares, J., Greninger, P., Edelman, E. J., Lightfoot, H., Forbes, S., et al. (2013). Genomics of drug sensitivity in cancer (GDSC): A resource for therapeutic biomarker discovery in cancer cells. *Nucleic Acids Res.* 41, D955–D961. doi:10.1093/nar/gks1111

Yang, Y., Long, X., Li, K., Li, G., Yu, X., Wen, P., et al. (2021). Development and validation of an oxidative stress-associated prognostic risk model for melanoma. *PeerJ* 9, e11258. doi:10.7717/peerj.11258

Zhang, M., Du, G., Li, Z., Li, D., Li, W., Li, H., et al. (2022). An oxidative stress-related genes signature for predicting survival in bladder cancer: Based on TCGA database and bioinformatics. *Int. J. Gen. Med.* 15, 2645–2667. doi:10.2147/ijgm.S348945

Zhu, C., Wang, Z., Cai, J., Pan, C., Lin, S., Zhang, Y., et al. (2021). VDR signaling via the enzyme NAT2 inhibits colorectal cancer progression. *Front. Pharmacol.* 12, 727704. doi:10.3389/fphar.2021.727704

frontiers | Frontiers in Pharmacology

TYPE Review
PUBLISHED 03 May 2023
DOI 10.3389/fphar.2023.1002296

OPEN ACCESS

EDITED BY
Yosra A. Helmy,
University of Kentucky, United States

REVIEWED BY
Mengwei Li,
Singapore Immunology Network (A*STAR), Singapore
Joya Chandra,
University of Texas MD Anderson Cancer Center, United States
Basel A. Abdel-Wahab,
Assiut University, Egypt

*CORRESPONDENCE
Jamie N. Anastas,
jamie.anastas@bcm.edu

RECEIVED 25 July 2022
ACCEPTED 20 April 2023
PUBLISHED 03 May 2023

CITATION
Murdaugh RL and Anastas JN (2023), Applying single cell multi-omic analyses to understand treatment resistance in pediatric high grade glioma. *Front. Pharmacol.* 14:1002296. doi: 10.3389/fphar.2023.1002296

Applying single cell multi-omic analyses to understand treatment resistance in pediatric high grade glioma

Rebecca L. Murdaugh[1,2,3] and Jamie N. Anastas[1,2,3]*

[1]Department of Neurosurgery, Baylor College of Medicine, Houston, TX, United States, [2]Program in Cell and Gene Therapy, Baylor College of Medicine, Houston, TX, United States, [3]Department of Molecular and Cellular Biology, Baylor College of Medicine, Houston, TX, United States

Despite improvements in cancer patient outcomes seen in the past decade, tumor resistance to therapy remains a major impediment to achieving durable clinical responses. Intratumoral heterogeneity related to genetic, epigenetic, transcriptomic, proteomic, and metabolic differences between individual cancer cells has emerged as a driver of therapeutic resistance. This cell to cell heterogeneity can be assessed using single cell profiling technologies that enable the identification of tumor cell clones that exhibit similar defining features like specific mutations or patterns of DNA methylation. Single cell profiling of tumors before and after treatment can generate new insights into the cancer cell characteristics that confer therapeutic resistance by identifying intrinsically resistant sub-populations that survive treatment and by describing new cellular features that emerge post-treatment due to tumor cell evolution. Integrative, single cell analytical approaches have already proven advantageous in studies characterizing treatment-resistant clones in cancers where pre- and post-treatment patient samples are readily available, such as leukemia. In contrast, little is known about other cancer subtypes like pediatric high grade glioma, a class of heterogeneous, malignant brain tumors in children that rapidly develop resistance to multiple therapeutic modalities, including chemotherapy, immunotherapy, and radiation. Leveraging single cell multi-omic technologies to analyze naïve and therapy-resistant glioma may lead to the discovery of novel strategies to overcome treatment resistance in brain tumors with dismal clinical outcomes. In this review, we explore the potential for single cell multi-omic analyses to reveal mechanisms of glioma resistance to therapy and discuss opportunities to apply these approaches to improve long-term therapeutic response in pediatric high grade glioma and other brain tumors with limited treatment options.

KEYWORDS

tumor hetereogeneity, clonal expansion, multi-omic, single cell profiling, drug resistance, pediatric high grade glioma, diffuse midline glioma

Introduction

High grade glioma (HGG) are aggressive and highly malignant tumors of the central nervous system (Wen and Kesari, 2008; Cohen, 2022) and little progress has been made in improving clinical outcomes for these patients in the past 40 years. Survival rates are low in both pediatric and adult HGG, and certain subtypes of pediatric HGG (pHGG), like diffuse

midline glioma (DMG), are almost universally lethal (Jones et al., 2017; Ostrom et al., 2019). Our poor understanding of which processes and pathways drive pHGG malignancy and response to therapy has impeded efforts to develop effective treatments for pHGG and other brain tumors. Pan-cancer analyses suggest the presence of up to 1,000-fold fewer mutations in pediatric tumors compared to adult tumors arising in the same tissue (ICGC PedBrain-Seq Project et al., 2018; Ma et al., 2018), and certain driver mutations, including genetic aberrations in epigenetic regulators like histone H3 point mutations (H3K27M and H3G34 R/V), are observed more frequently in pediatric glioma compared to adult brain tumors (Khuong-Quang et al., 2012; Schwartzentruber et al., 2012; Wu et al., 2012; Fontebasso et al., 2013; Wiestler et al., 2013; Mackay et al., 2017). The divergent genetic profile of pHGG tumors suggests that focused studies aimed at identifying mediators of therapeutic response specific to pediatric cohorts have the potential to inform personalized strategies to improve clinical outcomes.

The abysmal survival rate seen in adult HGG is often attributed to these tumors exhibiting stem cell-like phenotypes associated with poor response to radiation, temozolomide (TMZ) and other therapies (Bao et al., 2006; Liu et al., 2006; Chen et al., 2012; Alexander et al., 2020; Petralia et al., 2020; Syafruddin et al., 2021; Wang et al., 2021). Despite potential roles for rare tumor sub-populations in treatment resistance, most efforts to characterize glioma response to therapy rely on either limited tumor gene panels or bulk sequencing to compare tumor samples from different patients (intertumoral heterogeneity) rather than addressing cell to cell variation within individual tumors (intratumoral heterogeneity) (Allen et al., 2017; Mueller et al., 2019; Nejo et al., 2019; Petralia et al., 2020; Wang et al., 2021). Recent single cell analyses highlight the strikingly heterogeneous nature of glioma tumors and have enabled the profiling of glioma stem and progenitor like cells, the analysis of lineage diversity among tumor cells, including mesenchymal, oligodendroglial, and astrocytic sub-populations (Sottoriva et al., 2013; Darmanis et al., 2017; Filbin et al., 2018; Yuan et al., 2018; Neftel et al., 2019; Zhai et al., 2020; Guilhamon et al., 2021; Abdelfattah et al., 2022; Curry et al., 2023; Khan et al., 2023). It is also possible that the stem cell-like and therapy-resistant properties of HGG are conferred by a relatively small number of tumor cells, which cannot be easily detected or fully characterized by bulk sequencing (Bao et al., 2006; Liu et al., 2006; Chen et al., 2012; Alexander et al., 2020). Further single cell analyses highlight spatial differences in HGG cell phenotypes within different tumor regions (Sottoriva et al., 2013; Darmanis et al., 2017; Comba et al., 2021) and identify diverse tumor-associated immune cells suggesting that heterogeneity in the local tumor microenvironment may also play a key role in treatment resistance. Similarly applying single cell analyses to pediatric HGG before and after treatment has the potential to generate a more comprehensive view of the unique cellular composition of pediatric gliomas and their dynamic responses to therapy.

Because of technological limitations, most initial attempts at using single cell technologies to dissect glioma heterogeneity have profiled only one layer of biological regulation in isolation, such as cell to cell variation in transcription through single cell RNA sequencing (scRNAseq). Since cellular heterogeneity can occur at the level of the genome, epigenome, transcriptome, proteome, and metabolome, these unidimensional datasets may impart an incomplete or skewed understanding of the underlying factors driving heterogeneity (Comba et al., 2021). New technologies now make it possible to conduct single cell multi-omic analyses to track several molecular features simultaneously allowing researchers to systematically examine the interplay between different sources of heterogeneity and their roles in determining therapeutic response (Vandereyken et al., 2023). In this review, we explore the potential for single cell multi-omic approaches to revolutionize our understanding of how pHGG and other cancers develop treatment resistance and address some of the challenges inherent to applying these technologies towards the development of strategies to improve clinical outcomes in glioma.

Treatment strategies for pediatric high grade glioma

pHGG is a rare and aggressive form of brain cancer that primarily affects children and adolescents (Ostrom et al., 2022). The discovery of clinically relevant biomarkers through in DNA and RNA sequencing, methylome, and proteomic profiling have led to the recognition of different pHGG subtypes, which are detailed in the 2021 World Health Organization central nervous system tumor classification system (Louis et al., 2021). The importance of establishing prognostic biomarkers for these tumors is exemplified by the diffuse subtypes of pHGG, which may present with similar histological and anatomical features but can exhibit striking differences in their molecular and genetic alterations (Table 1). Fully understanding these distinct molecular and genetic characteristics can then allow clinicians to tailor treatment strategies for pHGG patients based on their tumor subtype (Rallis et al., 2022).

Current treatment paradigms for pHGG may vary based on patient age and tumor subtype, but they often include combinations of radiation, chemotherapy, surgery, immunotherapy, and targeted small molecules (Table 2). For some pHGG subtypes, like H3K27-altered tumors and other gliomas with invasive growth patterns, surgical resection is nearly impossible due to risks related to the anatomical locations and the diffuse growth patterns of these tumors (Wang and Jiang, 2013; Jones et al., 2017; Vitanza and Monje, 2019). Radiation is standard of care for pHGG but is ultimately palliative and has minimal impact on overall survival (Mandell et al., 1999; Tauziede-Espariat et al., 2019). Radiotherapy is associated with variable responses in pHGG and can lead to neurocognitive defects especially in very young patients, only increases overall survival in diffuse midline glioma by ~3 months (Langmoen et al., 1991), and had no significant effect on overall survival for patients diagnosed with H3G34-altered tumors in one recent study (Crowell et al., 2022). Chemotherapy is also rarely effective on its own and leads to variable clinical responses in different in by pHGG subtypes. Treatment with chemotherapy is associated with slightly increased overall survival in infantile and pediatric HGG patients, but exclusively when gross surgical resection was achieved (Wisoff et al., 1998; Wolff et al., 2010). In contrast, multiple studies report that neither TMZ-based nor non-TMZ-based chemotherapy are sufficient to provide a survival benefit for pediatric HGG patients (Spostol et al., 1989; Finlay et al., 1995; Cohen et al., 2011; Jones et al.,

TABLE 1 Genetic and molecular characteristics of WHO 2021 classification of pediatric-type diffuse high grade glioma.

Tumor subtype	Molecular features/ genetic alterations	Anatomical location	Histological markers	Age at diagnosis	Survival	References
Diffuse midline glioma, H3 K27-altered	H3K27	brainstem, spinal cord, pons, medulla, and thalamus	OLIG2+, H3K27me3 loss, TP53 (variable), ATRX (variable)	7–8 years	9–11 months	Schwartzentruber et al. (2012), Wu et al. (2012), Castel et al. (2015), Cooney et al. (2017)
	TP53					
	ACVR1					
	PDGFRA					
	EGFR					
	EZHIP					
Diffuse hemispheric glioma, H3 G34-mutant	H3G34	supratentorial tumors, mainly in temporal and parietal lobes	GFAP$^+$, OLIG2$^-$, ATRX$^-$, TP53 (variable), MKI67 (high)	15 years	14–18 months	Schwartzentruber et al. (2012), Wu et al. (2012), Korshunov et al. (2016), Lim et al. (2021), Crowell et al. (2022), Gianno et al. (2022)
	TP53					
	ATRX					
Diffuse pediatric-type high-grade glioma, H3-wildtype and IDH-wildtype	IDH-wildtype	supratentorial tumors (~85%), brainstem (~15%)	necrosis, microvasculature proliferation, H3K27me3 retained, GFAP$^+$, OLIG2$^+$	2–18 years	14–44 months	Korshunov et al. (2017), Tauziede-Espariat et al. (2019), Gianno et al. (2022)
	H3-wildtype					
	PDGFRA					
	MYCN					
	EGFR					
Infant-type hemispheric glioma	NTRK family	intra-axial tumor	OLIG2+, GFAP+, H3K27me3 retained	<1 year	5-year overall survival of 50%–60%	Duffner et al. (1999), Guerreiro Stucklin et al. (2019), Ceglie et al. (2020), Clarke et al. (2020), Gianno et al. (2022)
	ALK					
	ROS					
	MET					

TABLE 2 Major therapeutic modalities used to treat pediatric high grade glioma.

Therapy category	Examples/sub-categories	References
Radiation	focal radiation, hypo-fractionated radiation	Mandell et al. (1999); Gallitto et al. (2019); Metselaar et al. (2021); Crowell et al. (2022)
Chemotherapy	**Non-TMZ chemotherapy:** CCNU, vincristine, prednisone, methylprednisolone procarbazine, hydroxyurea, cisplatin, cytarabine, dacarbazine	Spostol et al. (1989); Finlay et al. (1995); Duffner et al. (1999); Massimino et al. (2008); Crowell et al. (2022)
	TMZ chemotherapy	Lashford et al. (2002); Cohen et al. (2011)
Immunotherapy	T cell immunotherapy	Ahmed et al. (2017); Vitanza et al. (2021b); Haydar et al. (2021); Majzner et al. (2022)
	cancer vaccines	Pollack et al. (2016); Van Gool et al. (2020)
	oncolytic viruses	Friedman et al. (2021); Gallego Perez-Larraya et al. (2022); Ghajar-Rahimi et al. (2022)
	checkpoint inhibitors	Fried et al. (2018); Cacciotti et al. (2020); Van Gool et al. (2020)
	Anti-PD-1 and anti-PD-L1	
Targeted small molecules	panobinostat, vorinostat, ONC-201, dasatinib, crizotinib, everolimus	Arrillaga-Romany et al. (2017); Galanis et al. (2018); Chi et al. (2019); Miklja et al. (2020); Puduvalli et al. (2020); Gibson et al. (2021); DeWire et al. (2022); Izquierdo et al. (2022)

2017) and combinations of high dose chemotherapy and radiation similarly did not improve clinical outcomes midline and brainstem tumors or in H3G34-altered tumors (Jenkin et al., 1987; Spostol et al., 1989; Hargrave et al., 2006; Crowell et al., 2022).

Improved molecular and genetic profiling of pHGG tumors and research in pre-clinical models has led to the discovery of multiple targeted therapies, including both small molecule inhibitors of various enzymes and immunotherapeutic approaches. Targeted small molecule inhibitors for pHGG treatment include: chromatin-targeting drugs like the histone deacetylase inhibitors vorinostat and panobinostat (Fouladi et al., 2010; Jones et al., 2017; Galanis et al., 2018; Puduvalli et al., 2020); the DRD2 antagonist/CLPP agonist ONC201 (Arrillaga-Romany et al., 2017; Chi et al., 2019); kinase inhibitors like dasatinib, crizotinib, and trametinib (Miklja et al., 2020; Gibson et al., 2021; Izquierdo et al., 2022); and mTOR inhibitors like everolimus (Miklja et al., 2020; DeWire et al., 2022). While some of these inhibitors may temporarily improve symptoms and can lead to short-term stable disease in some patients, many of these clinical trials are ongoing and limited in scope, so it is not yet clear whether durable clinical responses will be possible.

More recently, immunotherapeutic approaches using oncolytic viruses, cancer vaccines, and autologous T cell therapy have shown promise in animal models and are under investigation in the clinic. Specifically, clinical trials assessing pHGG patient response to CAR-T cells directed against various tumor antigens, including GD2, B7-H3, and HER2, have led to improved symptoms or stable disease in some patients but have yet to improve overall survival (Ahmed et al., 2017; Vitanza et al., 2021b; Haydar et al., 2021; Majzner et al., 2022). Early phase clinical trials using oncolytic viruses, immune checkpoint inhibitors, and cancer vaccines to target pHGG and enhance tumor immunogenicity are similarly in progress, but it remains uncertain whether these interventions will result in a significant response in larger numbers of patients (Fried et al., 2018; Van Gool et al., 2020; Gallego Perez-Larraya et al., 2022; Ghajar-Rahimi et al., 2022).

In addition to the adverse side effects that can accompany each of these treatment modalities, another factor to consider when developing new therapies is that treatment failure in pHGG commonly occurs due to intrinsic or acquired resistance to therapy (Vanan and Eisenstat, 2014; Kline et al., 2018). Overcoming treatment resistance therefore poses a key challenge to improving clinical outcomes in aggressive and highly heterogeneous cancers like pHGG and will require a better understanding of how resistance to therapy develops in patients. Since subpopulations of brain tumor cells vary in their sensitivity to treatment (Bao et al., 2006; Liu et al., 2006; Chen et al., 2012; Alexander et al., 2020), efforts to elucidate resistance mechanisms in pHGG that rely solely on bulk sample analysis methods or that only focus on a single aspect of tumor cell biology may lose important information regarding changes in sub-clonal tumor cell phenotypes and the tumor microenvironment following treatment. Single cell, multi-omic techniques provide an opportunity to separately profile tumor, normal brain cell, and immune populations (Vandereyken et al., 2023), to characterize dynamic changes to the glioma cellular landscape that occur in response to treatment when applied to pHGG patient samples.

Single cell multi-omic profiling of glioma

Differences between the genome, epigenome, transcriptome, proteome, and metabolome of individual tumor cells in a single patient can all contribute to intratumoral heterogeneity associated with therapeutic resistance (Mazor et al., 2016; Marusyk et al., 2020; Santiago et al., 2020). Variable mutation profiles between cells within the same tumor, chromatin dysregulation leading to stem cell-like behaviors in tumor cell sub-populations, neoplastic transcriptional states specific to individual tumor cells, erratic post-translational modifications, and unique metabolic dependencies are all examples of intratumoral differences in cell phenotypes that might influence tumor sensitivity to therapy. Despite the capacity of single cell profiling to reveal mechanisms of tumor heterogeneity and therapeutic resistance, the application of single cell multi-omic analyses to pediatric glioma is rare. As a result, the role of intratumoral heterogeneity in driving pediatric glioma progression and response to treatment is poorly understood. Multi-omic analyses at single-cell resolution can address this knowledge gap by generating more comprehensive profiles of pHGG intratumoral heterogeneity (Figure 1).

Multiple techniques are now available for targeted "omic" profiling of the major subtypes of biological molecules at a single cell resolution (Table 3). Many of these single cell analyses can be performed either as stand-alone assays or in combination with each other to generate multi-omic datasets to describe multiple phenotypic features within single cells, such as through simultaneous analysis of both transcriptomic and epigenetic profiles. For example, combined scRNAseq and single cell ATACseq (scATACseq) has been applied to characterize both single cell transcriptomes and chromatin accessibility patterns in adult spinal ependymoma demonstrating dynamic changes to the landscape of tumor-immune interactions associated with tumor progression (Zhang et al., 2021). The application of both scRNAseq and scATACseq has also recently identified multiple progenitor-like glioma cell subtypes acting cooperatively to maintain tumor growth in adult glioma (Wang et al., 2019), and revealed the complex cellular architectures of different medulloblastoma subtypes (Li et al., 2021).

Various research groups have also sought to understand the relationship between genetic mutations, DNA methylation and heterogeneous gene expression profiles in glioma patient samples. For example, studies integrating scRNAseq and DNA methylation profiling have uncovered correlations between DNA methylation patterns and gene expression associated with the expression of glial differentiation genes and response to environmental stress (Chaligne et al., 2021; Johnson et al., 2021). An additional study similarly integrated DNA methylation and scRNAseq datasets to identify METTL7B as a potential prognostic marker in glioma associated with an immune-suppressive tumor microenvironment (Chen et al., 2021). Further studies have integrated bulk DNA sequencing and scRNAseq data to track lineage hierarchies and to infer transcriptional signatures associated with distinct glioma sub-populations including stem and progenitor-like cells (Muller et al., 2016; Filbin et al., 2018). Finally, combined genetic profiling, scRNAseq, and metabolic analysis in glioblastoma multiforme has

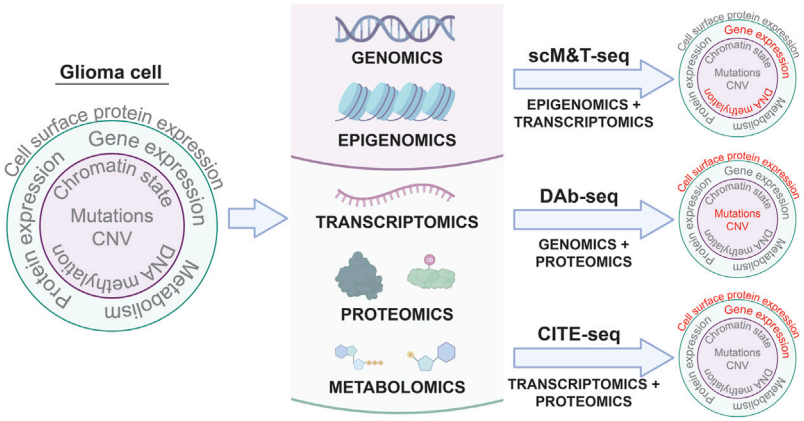

FIGURE 1
Single cell multi-omic approaches to phenotyping glioma cells. Applying multi-omic techniques to single cells isolated from patient tumors enables simultaneous profiling of different aspects of tumor cell biology in the same cells. Three examples of these types of techniques and the tumor cell phenotypes they characterize are shown: scM&T-seq profiles DNA methylation and gene expression; DAb-seq profiles genomic alterations and cell surface protein expression; and CITE-seq profiles gene expression and cell surface protein expression. Linking multiple phenotypes in individual glioma cells from patient samples through single cell multi-omic approaches like those depicted above has the potential to improve our understanding of intratumoral heterogeneity in glioma and provide insights into the molecular mechanisms driving glioma development and progression.

TABLE 3 A brief summary of single cell profiling techniques to assess intratumoral heterogeneity.

Omic data subtypes	Sequencing	Non-sequencing	References
Genome	scDNAseq		Evrony et al. (2021)
Epigenome	scBisulfite-seq, scATACseq, scCUT&RUN/scCUT&Tag		Smallwood et al. (2014); Skene and Henikoff (2017); Kaya-Okur et al. (2019); Xu et al. (2021)
Transcriptome	scRNAseq	MERFISH[a]	Hwang et al. (2018); Xia et al. (2019)
Proteome		Flow cytometry, CyTOF, Imaging mass cytometry[a], scProteomics	Doxie and Irish (2014); Lavin et al. (2017); Roussel et al. (2020); Woo et al. (2021); Kuett et al. (2022)
Metabolome		SpaceM[a]	Rappez et al. (2021)
Multi-omics			
scG&T-seq	scDNAseq + scRNAseq		Macaulay et al. (2016)
scM&T-seq	scBisulfite-seq + scRNAseq		Angermueller et al. (2016)
scTRIO-seq	scM&T-seq + CNV analysis		Hou et al. (2016)
CITE-seq	cell surface protein + transcriptome profiling by scRNAseq		Peterson et al. (2017); Stoeckius et al. (2017)
REAP-seq			
Watermelon	CITE-seq + lineage tracing		Oren et al. (2021)
SHARE-seq	scRNAseq + scATACseq		Ma et al. (2020); Swanson et al. (2021)
ICICLE-seq			
DAb-seq	cell surface protein + genome profiling by scDNAseq		Morita et al. (2020); Demaree et al. (2021); Peretz et al. (2021)
Tapestri			
Select-seq[a]	RNAseq on SLACS-isolated single cells	+ protein expression by immunofluorescence	Lee et al. (2022)

[a]= technique preserves spatial information in samples.

identified new functional subgroups differing in their neurodevelopmental and metabolic profiles that may be targetable in the clinic (Garofano et al., 2021). Together, these studies demonstrate the promise of layering multiple single cell analysis techniques to resolve tumor cell features and to identify functionally significant tumor subpopulations driving resistance.

The benefits of using sequencing-based single cell profiling techniques include the generation of extensive amounts of data

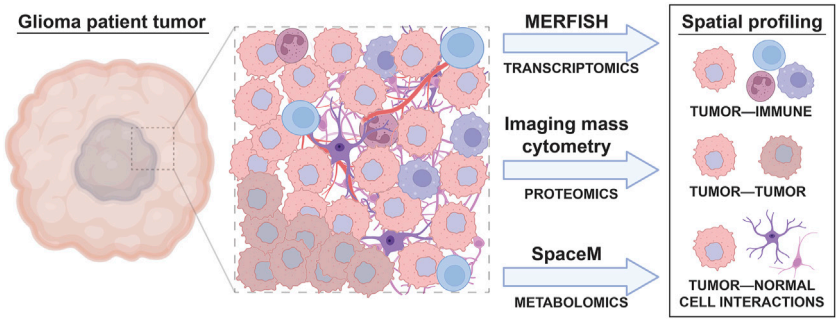

FIGURE 2
Spatial, single cell profiling of glioma patient tumors. A wide variety of cell types are found in the tumor microenvironment of glioma, including immune cells, different subtypes of tumor cells, and normal brain cells. The interactions between these cells result in tumor cell behavior changes that can be accounted for through spatial, single cell omic profiling techniques. Spatial analyses like MERFISH, imaging mass cytometry, and SpaceM allow the effect of cell to cell interactions on tumor, immune, and normal cell phenotypes to be visualized.

on large numbers of cells and the ability to simultaneously profile tumor cells, infiltrating immune cells, and normal cells within the same sample. However, one downside of using many single cell sequencing-based techniques is that these analyses usually require cell dissociation as an early step in their sample processing protocols. This need for sample dissociation results in a loss of spatial information regarding the cellular organization of brain tumors, such as local interactions between glioma cells, neurons, normal glia, and immune cells, which may mediate tumor cell phenotypes. For instance, previous studies reveal that glioma stem and progenitor-like cells reside in the perivascular niche in contact with endothelial cells (Calabrese et al., 2007; Charles et al., 2010) and demonstrate extensive spatial heterogeneity in both the abundance and types of immune cells across different regions of brain tumors (Abdelfattah et al., 2022). Conducting spatial profiling of tumor markers through either low throughput (immunohistochemistry, immunocytochemistry, RNA *in situ* analysis) or high throughput (spatial scRNAseq) can therefore complement single cell data from disassociated samples to reveal the regional heterogeneity, and local interactions between, cell types of interest in patient tumors (Figure 2).

Current knowledge of intratumoral heterogeneity in pediatric high grade glioma

Previous studies have applied single cell multi-omic technologies to characterize intratumoral heterogeneity in glioma, but most reports thus far have focused on adult samples rather than pediatric brain tumors (Table 4). Although a subset of potential therapeutic targets implicated by studies analyzing adult glioma may be relevant to pediatric brain tumors, substantial differences exist in the genetics and molecular features of pHGG (Table 1) that may result in unique mechanisms of therapeutic resistance in pediatric patients (Jones et al., 2012; Sturm et al., 2017; Gestrich et al., 2021; Lehmann et al., 2022). One major difference is that driver mutations in chromatin regulators, including histone H3 point mutations are common in pHGG but not in adult HGG (Khuong-Quang et al., 2012; Schwartzentruber et al., 2012; Wu et al., 2012; Fontebasso et al., 2013; Wiestler et al., 2013; Mackay et al., 2017). The unique biology of pediatric brain tumors may limit the relevance of single cell data from adult samples as a basis to develop therapeutic strategies for childhood glioma and warrants further investigation into the drivers of therapeutic resistance in pHGG.

pHGG are not only genetically and molecularly distinct from adult pHGG, but also exhibit a high degree of intra- and intertumoral heterogeneity. Sequencing studies analyzing either multiple brain regions or comparing diagnostic and recurrent tumors taken from individual pHGG patients reveal spatially and temporally heterogeneous DNA mutations even among samples acquired from the same patient affecting genes, such as ATM, PPM1D, BCOR, ATRX, MYC, and KMT5B (Hoffman et al., 2016; Nikbakht et al., 2016; Salloum et al., 2017; Vinci et al., 2018). pHGG also exhibit heterogeneity in the presence of copy number variations in PDGFRA and other genes regulating oncogenic signaling and the cell cycle (Bax et al., 2010; Paugh et al., 2011; Koschmann et al., 2016), and cell to cell variation in epigenetic regulation reflected by differences in histone post-translational modifications and DNA methylation in pHGG (Sturm et al., 2012; Mackay et al., 2017; Castel et al., 2018; Huang et al., 2018). Finally, scRNAseq and histological analyses of both pediatric and adult brain tumors reveal heterogeneous cell phenotypes, including stem and progenitor-like cells as well as neuronal, glial, and mesenchymal subpopulations (Hemmati et al., 2003; Monje et al., 2011; Filbin et al., 2018; Jessa et al., 2019; Vladoiu et al., 2019). Together, these findings suggest that heterogeneity in DNA mutations, epigenetic regulation, transcriptional outputs, and differing tumor microenvironments all have the potential to remodel the cellular landscape of pHGG to promote therapeutic resistance.

Heterogeneity in pHGG can be driven by intrinsic factors like genomic instability and cancer stem cell differentiation as well as in response to extrinsic factors in the tumor microenvironment like tumor-immune cell interactions and drug treatment (Santiago et al., 2020; Kaminska et al., 2021). Multi-omic single cell analyses may therefore identify pathways of previously unknown significance in

TABLE 4 Selected single cell sequencing datasets from pediatric and adult high grade glioma patient samples.

HGG subtype	Single cell datasets	Major finding	References
Pediatric H3K27M glioma	scRNA-seq	Most H3K27M tumor cells are oligodendrocyte progenitor-like	Filbin et al. (2018)
Pediatric H3.3G34 R/V glioma	scRNA-seq	Epigenetic and transcriptional features of H3.3G34 R/V glioma identify new therapeutic targets	Sweha et al. (2021)
Pediatric cerebellar tumors	scRNA-seq	Tumor cells express fetal transcriptional programs	Vladoiu et al. (2019)
Pediatric ependymoma	scRNA-seq	Neural stem cell-like tumor subclones in relapsed patient samples are more immature with increased immune cell crosstalk	Wu et al. (2022)
Pediatric ependymoma	scRNA-seq	Malignant cell differentiation programs are targetable and predict patient survival	Gojo et al. (2020)
Pediatric medulloblastoma	scRNA-seq	Tumor subtypes with distinct developmental trajectories may share a similar cell-of-origin	Hovestadt et al. (2019)
Pediatric medulloblastoma	scRNA-seq, scATAC-seq	Characterizes medulloblastoma subtypes and identifies potential therapeutic targets	Li et al. (2021)
Adult glioblastoma	scRNA-seq, scATAC-seq	Combination therapy targeting multiple tumor cell phenotypes may improve treatment efficacy	Wang et al. (2019)
Adult glioblastoma	scATAC-seq	An invasive glioma stem cell chromatin state is associated with lower survival	Guilhamon et al. (2021)
Adult glioblastoma	scRNA-seq	The glioma stem cell immune microenvironment transitions from stimulatory to suppressive as tumorigenesis progresses	Zhai et al. (2020)
Adult high grade gliomas	scRNA-seq	Glioma cell subtypes exhibit differences in proliferation and immune cell interactions	Yuan et al. (2018)
Adult glioblastoma	scRNA-seq	Infiltrating immune cells enhance glioblastoma cell proliferation and invasiveness	Darmanis et al. (2017)
Adult glioblastoma	scRNA-seq	Identifies immune suppressive factors in tumor-associated macrophages that can be targeted to improve immunotherapy	Abdelfattah et al. (2022)
Adult glioblastoma	scRNA-seq	Glioblastoma cell states are influenced by DNA mutations and the tumor microenvironment	Neftel et al. (2019)
Adult glioblastoma	scRNA-seq	Individual cells within the same tumor exhibit variable expression of glioblastoma subtype markers	Patel et al. (2014)
Adult glioblastoma	scRNA-seq	Identifies glioma stem cell-specific developmental pathways to target therapeutically	Couturier et al. (2020)
Adult glioblastoma	scRNA-seq, scBisulfite-seq	Epigenetic state can shape therapeutic outcomes	Johnson et al. (2021)
Adult glioblastoma	scRNA-seq	Tumor subtypes exhibit different metabolic dependencies	Garofano et al. (2021)
Adult glioblastoma	scRNA-seq, scBisulfite-seq, scDNA-seq	Malignant cells show epigenetic inheritance that differs based on IDH genotype	Chaligne et al. (2021)

the development of therapeutic resistance. Single cell multi-omic profiling of brain tumor patient samples have begun to define the complex cellular landscape of adult glioma as it relates to disease biology (Table 4). Recent single cell multi-omic profiling studies have identified salient features of glioma biology, including distinct tumor-immune interactions associated with malignancy and disease progression, correlations between genetic and epigenetic features of tumor cells, novel sub-cellular populations and mechanisms of glioma cell plasticity, and putative therapeutic targets (Wang et al., 2019; Chaligne et al., 2021; Chen et al., 2021; Garofano et al., 2021; Johnson et al., 2021; Zhang et al., 2021). Studies that integrate separate single cell and bulk multi-omic datasets have similarly identified novel regulators, prognostic biomarkers of adult glioma subtypes (Neftel et al., 2019; Wu et al., 2020; Chen et al., 2021). These analyses demonstrate the value of applying single cell, multi-omic profiling as a strategy to reveal hidden complexity in adult gliomas that may soon be applied to pHGG.

In addition to the tumor cell intrinsic factors that drive intratumoral heterogeneity, dynamic changes in tumor composition can occur because of interactions between glioma and immune cells in the surrounding microenvironment (Turner and Reis-Filho, 2012; McGranahan and Swanton, 2017). For example, a single cell transcriptome profiling study in pediatric ependymoma patient samples recently found that neural stem cell-like tumor subclones in relapsed patient samples exhibit increased immune cell crosstalk (Wu et al., 2022). Single cell analysis to reveal dynamic interactions between tumor cells and immune cells may also reveal mechanisms of resistance to immunotherapy and potential targets to enhance pHGG immune targeting. For example, a recent study of pHGG tumors exposed to CAR-T cell

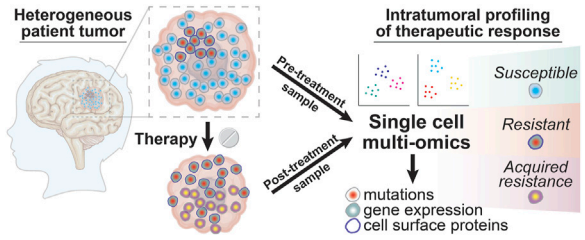

FIGURE 3
Intratumoral profiling of therapeutic responses in glioma patient tumors with single cell multi-omics. Glioma tumor samples collected from patients before and after treatment can be profiled using single cell multi-omic techniques to identify tumor cell phenotypes associated with successful therapeutic targeting by looking for tumor cell subtypes that are present in pre-treatment samples but that are absent in post-treatment samples. In contrast, resistant tumor cell subtypes will be present in both the pre-treatment and post-treatment sample while newly evolved or adapted tumor cell phenotypes that result in acquired resistance will be seen only in the post-treatment sample. The information yielded from these single cell profiling experiments for tumor cell phenotypes like DNA mutations, gene expression, and cell surface proteins can thus provide a deeper understanding into the clonal composition changes that drive glioma patient responses to different treatment modalities.

therapy using both bulk an single cell profiling revealed heterogeneous CAR-T cell phenotypes and identified cytokines and TGFβ signaling molecules as potential mediators of CAR-T treatment efficacy (Vitanza et al., 2021a; Majzner et al., 2022). Another recent single cell profiling study revealed additional immunosuppressive factors produced by tumor-associated macrophages that might be targeted to enhance therapeutic responses (Abdelfattah et al., 2022).

Intrinsic differences between tumor cells can also set the stage for further, potentially more unpredictable consequences of tumor-tumor cell interactions where clones displaying different phenotypes may have suppressive, protective, or stimulatory effects on each other (Santiago et al., 2020). An example of this behavior comes from a recent paper showing that cells located in distinct anatomical features of glioblastoma multiforme tumors display diverging patterns of gene and protein expression allowing individual tumor cells to influence each other's behaviors to drive tumor progression and escape from the effects of therapy (Lam et al., 2022). Spatial differences in tumor cell heterogeneity may also influence the activity endogenous immune cells and the efficacy immune cell-based therapies (Liu et al., 2021). Using single cell multi-omic profiling techniques that preserve spatial information in patient samples can therefore provide further insights into the drivers of intratumoral heterogeneity in solid tumors and the effects of a changing tumor microenvironment on treatment response. Despite the valuable knowledge provided by these types of analyses, very little spatial profiling has been done in pHGG. Increasing our knowledge of regional tumor heterogeneity, such as between primary and metastatic tumors invading other brain regions and the spine is particularly needed to understand the diffuse nature of certain subtypes, like DMG which are highly invasive and spread into multiple brain regions (Nikbakht et al., 2016).

These sometimes unpredictable drivers of intratumoral heterogeneity arising from various cell to cell interactions within the tumor microenvironment are perhaps best summarized by the aphorism "the whole is greater than the sum of the parts." An alternative to bulk analyses is to apply single cell multi-omic analyses to matched glioma patient samples taken before and after treatment to examine the changes in tumor cell phenotypes that occur in response to different forms of therapy (Figure 3). Through well-designed longitudinal studies, it may also be possible to correlate these multi-omic single cell datasets with clinical outcomes as a first step in identifying specific cell populations that escape tumor response or to discover biomarkers of tumor evolution that might predict therapeutic resistance. Analyzing treatment-associated changes in intratumoral heterogeneity in this way will allow researchers to move beyond merely taking the sum of the parts to instead obtain multi-dimensional datasets providing a much more comprehensive view of the pathways and processes underlying therapeutic resistance in brain tumors.

Profiling treatment-associated changes in the intratumoral heterogeneity in high grade glioma

Standard of care for pHGG consists of radiation often combined with chemotherapy and experimental therapeutics (Fangusaro, 2009; Jones et al., 2012; Adamski et al., 2014; Bredlau and Korones, 2014). Many of these treatments have adverse consequences, including cognitive deficits, endocrine disorders, and vasculopathies, and none of these therapeutic strategies are curative (Armstrong et al., 2004; Merchant et al., 2009; Mueller et al., 2013). pHGG tumors frequently exhibit both intrinsic and acquired resistance to therapy (Vanan and Eisenstat, 2014; Kline et al., 2018) and numerous studies suggest that subpopulations of brain tumor cells vary in their sensitivity to treatment (Bao et al., 2006; Liu et al., 2006; Chen et al., 2012; Alexander et al., 2020). Neither the defining characteristics of treatment-resistant glioma cell sub-populations, nor the underlying pathways regulating spatio-temporal heterogeneity and dynamic response to therapy are fully delineated in pediatric glioma. Our limited knowledge of which genes and pathways drive pediatric glioma heterogeneity and therapeutic resistance represents a key knowledge gap, which has hindered efforts to develop effective treatments to overcome therapeutic resistance in pHGG.

Variable tumor cell phenotypes and mutation profiles can result in different sensitivity to therapy within the same tumor, and the selective pressure applied during treatment can lead to tumor cell adaption and evolution resulting in tumor escape from therapeutic response (Raynaud et al., 2018; Marusyk et al., 2020; Santiago et al., 2020; Touat et al., 2020). Studies comparing matched patient samples collected before and after treatment are more common in cancers like melanoma and leukemia that are more amenable to sample collection compared to central nervous system tumors, and single cell multi-omic profiling of matched samples from these cancers demonstrate that tumor cell evolution correlates with disease relapse and unfavorable treatment outcomes (Gaiti et al., 2019; Granja et al., 2019; Morita et al., 2020). Similar research comparing naïve and treated brain tumor samples has identified

features of treatment-resistant glioma either through either bulk or single cell analyses, including potential targets for future therapies, factors that influence the tumor microenvironment, and genomic alterations contributing to malignant progression in different brain tumor subtypes (Barthel et al., 2019; Mueller et al., 2019; Nejo et al., 2019; Petralia et al., 2020). The diverse and impactful findings of these studies emphasize how new technological approaches to profiling intratumoral heterogeneity can provide insight into glioma biology and reveal novel strategies for therapeutic targeting.

Intratumoral heterogeneity observed in pHGG prior to treatment may also result in poor therapeutic response due to the presence of intrinsically resistant tumor cell subpopulations. For example, stem- and progenitor-like glioma cells sometimes known as glioma stem cells or brain tumor initiating cells (Zhou et al., 2021), have been implicated in adult glioma therapeutic response (Bao et al., 2006; Liu et al., 2006; Chen et al., 2012). Recent advances in single cell multi-omic profiling have provided researchers with new tools to decipher roles for rare tumor stem cells in treatment resistance and sensitivity. For example, one study integrated scRNAseq and mass cytometry data from adult glioma samples to identify surface markers used in the isolation of CD9+/CD133+ progenitor cells, which were then shown to be less sensitive to TMZ treatment and more proliferative in intracranial xenografts (Couturier et al., 2020). Another study applied scRNAseq to similarly describe a glioma stem cell subpopulation that was enriched after radiation treatment in a mouse model (Alexander et al., 2020). Additional studies have similarly identified stem cell-like subpopulations in pHGG (Monje et al., 2011; Chen et al., 2012; Filbin et al., 2018), but the role of glioma stem cells in mediating pediatric glioma phenotypes and response to therapy has not yet been thoroughly studied. However, there is some evidence that glioma stem cells may play a role in pHGG recurrence after therapy (Hoffman et al., 2019). Further studies applying single cell multi-omic analyses to pHGG patient tumors before and after therapy may help unravel potential roles for cancer stem cells and other glioma cell sub-populations in both intrinsic and acquired resistance.

Validating results from multi-omic single cell datasets using mouse models

A limitation of many single cell profiling studies is that these analyses generate correlative data, and the functional relevance of many molecular markers and cell sub-populations revealed by these analyses can remain elusive. Single cell analyses of mouse models of pHGG may also provide valuable insights into the underlying causes of tumor heterogeneity and reveal mechanisms of treatment resistance. Pairing patient tumor molecular profiling data with results from functional biological assays in cell culture and animal models is one strategy for experimentally determining the mechanisms of tumor heterogeneity and treatment resistance. For example, recent studies have sought to analyze differences in gene expression and chromatin accessibility in isolated adult glioma stem cell clones varying in their proliferation, differentiation, and sensitivity to TMZ to identify gene regulatory signatures associated with these aggressive tumor cell phenotypes (Meyer et al., 2015; Guilhamon et al., 2021). By subsequently comparing these gene and chromatin signatures to single cell datasets from patient tumors, the authors then provided evidence that freshly dissociated tumors contain cells exhibiting similar characteristics to the aggressive clones profiled in the laboratory, highlighting the potential significance of these phenotypes. Another study performed both molecular profiling and drug screening in newly established primary cell culture models derived from patient tumor samples collected in an ongoing clinical trial to identify the mechanism of resistance by which DMG tumors evade MEK inhibitors (Izquierdo et al., 2022). In this study, MEK inhibitor resistance occurred through the development of *de novo* mutations that might serve as therapeutic targets in a combination treatment strategy to ablate the resistant tumor cells. This approach combining molecular profiling and functional drug testing has the potential to identify other promising therapies if applied to additional treatment modalities, particularly if the functional studies are accompanied by single cell multi-omic profiling of pre- and post-treatment pHGG patient samples.

Comparative single cell profiling of patient samples and mouse models also has the potential to yield significant insights into therapeutic resistance and the roles of tumor-immune cell interactions in glioma treatment response. Of note, a recent comparative single cell multi-omic study in adult glioblastoma found conserved changes in tumor-associated immune cell responses to therapy between mouse models and patient tumors, suggesting that animal studies have the potential to accurately recapitulate certain aspects of patient tumor microenvironment (Pombo Antunes et al., 2021). Given that glioblastoma driver mutations are known to influence the immune composition of the tumor microenvironment in adult HGG (Garcia-Fabiani et al., 2021), additional comparative studies using single cell multi-omic techniques to analyze recently developed immunocompetent models of pHGG may therefore provide insight into the effects of patient tumor subtype on therapy resistance due to immunosuppressive or immunostimulatory states (Chen and Hambardzumyan, 2018; Patel et al., 2020; Tomita et al., 2022). Together, these studies emphasize how combining data from multi-omic single cell profiling of patient samples and results obtained from preclinical model systems may help researchers to better understand the significance of specific molecular profiles on glioma cell behaviors like drug resistance or response to immunotherapy.

Challenges and conclusion

A practical concern regarding the use of multi-omic single cell sequencing approaches to study glioma disease mechanisms is that these experiments generate massive data outputs requiring complex analysis pipelines and extensive resources for data storage. In contrast, single cell profiling by non-sequencing approaches may be more cost-effective and can potentially preserve tissue structures to provide an additional layer of information about the tumor microenvironment and cell to cell interactions (Figure 2). Low-throughput and non-sequencing based approaches, like immunohistochemistry and DNA fluorescence *in situ* hybridization (FISH), can offer much faster, cheaper, and readily

interpretable assessments of tumor heterogeneity while still assaying large numbers of cells. However, the information provided will be more biased than sequencing-based single cell profiling since non-sequencing techniques rely on a relatively small number of probes or antibodies, which may result in more limited findings from exploratory studies (Kashyap et al., 2022).

Given the wide range of single cell profiling techniques (Table 1), the high cost associated with sequencing-based single cell analyses, and the limited availability of pHGG patient samples, selecting among potential methods for single cell profiling requires careful consideration. For example, some single cell profiling techniques can be performed on fixed tissue, while others require fresh or frozen specimens. Appropriate single cell profiling methodologies must also be selected according to the treatment modalities in question. Single cell analyses that conserve spatial information may be particularly useful for characterizing glioma responses to immunotherapy because these methods enable the visualization of tumor-immune interactions (Marusyk et al., 2020). Since immunotherapy is beginning to show some promising results in early stage clinical trials for pHGG (Majzner et al., 2022), profiling pre- and post-treatment patient tumor samples using spatial, single cell multi-omic techniques may be especially relevant to ongoing efforts to improve immunotherapeutic approaches for pHGG treatment.

Single cell multi-omic datasets can also be expensive to generate and require processing through complex analytical pipelines before the results can be interpreted. The types of bioinformatic analyses and mathematical modeling that are applied to single cell multi-omic datasets are a key determinant of the quality of information obtained from these experiments. Unfortunately, bioinformatic analysis protocols for single cell datasets are not yet standardized across different research studies. Depending on the pipelines used, in-depth analyses of multiple aspects of intratumoral heterogeneity can be made from the shared properties identified between single cell multi-omic datasets or even extracted from individual single cell omic profiling experiments, such as by detecting somatic mutations or multi-cellular programs from scRNAseq data (Vu et al., 2019; Welch et al., 2019; Jerby-Arnon and Regev, 2022). Separate analyses using mathematical modeling of treatment efficacy can then take this intratumoral heterogeneity into account in simulations aimed at predicting determinants of patient responses to therapy (Rockne and Scott, 2019). However, bioinformatic analyses and mathematical modeling have their own limitations and may also provide an incomplete or inaccurate understanding of how tumor heterogeneity contributes to therapy resistance. Further, integrating single cell datasets generated from separate experiments or even from different studies through meta-analyses may also yield important findings despite the inability to examine different "omics" datasets in the same cells.

Perhaps the most daunting challenge limiting current studies applying single cell multi-omic analyses to naïve and treatment-resistant brain tumors is the ability of researchers to access paired tumor samples across the time course of a patient's treatment. Matched single cell analyses in non-responding or relapsed patients either during surgical resection procedures or from rapid autopsies may provide a viable strategy to study the development of therapeutic resistance that arises from intratumoral heterogeneity in glioma. Using pre-treatment patient biopsies to generate organoid, explant, and gliomasphere cultures or patient-derived orthotopic xenograft mice can also allow for pre-treatment and post-treatment responses to be assessed without requiring multiple rounds of brain tumor sample collection from a single patient (Hubert et al., 2016; Jacob et al., 2020; LeBlanc et al., 2022; Sundar et al., 2022). However, these *in vitro* and *in vivo* patient-derived glioma models may not accurately reflect the effects of the intratumoral heterogeneity and the tumor microenvironment on treatment resistance. Primary patient samples collected before and after treatment are therefore better suited for use in single cell multi-omic studies even though paired patient brain tumor sample collection can prove challenging. Despite these limitations, the recent introduction of lower-cost sequencing technology coupled with the rising use of machine learning to assist with data processing and interpretation have made single cell multi-omic profiling easier than ever and greatly improved its potential to yield clinically significant data when applied to patient samples.

Future directions for assessing intratumoral heterogeneity in glioma

Resistance to therapies, such as radiation, chemotherapy, targeted therapeutics, and immunotherapy, is a key challenge to improving clinical outcomes in aggressive and highly heterogeneous cancers like pHGG, which have no effective treatment options despite decades of research. The development of therapeutic resistance in these tumors is a multifaceted process that may be attributed to: 1) the expansion of subclonal populations showing intrinsic resistance; 2) the emergence of altered tumor cell phenotypes as these cells adapt or evolve upon exposure to therapy and escape killing; and 3) dynamic changes to the tumor microenvironment, including the interactions between brain tumor cells and normal neurons, glia, and tumor-associated immune cells. Before the advent of single cell technologies, previous research into the molecular underpinnings of therapeutic resistance relied on bulk approaches that assessed molecular changes induced by treatment at low resolution and averaged across large numbers of cells without the ability to separately profile tumor, non-tumor, and immune populations. In this review, we have highlighted how sophisticated, new technologies now enable researchers to layer multi-dimensional datasets to simultaneously profile genetic, epigenetic, transcriptomic, and proteomic aberrations at a single cell level to describe dynamic changes to the glioma cellular landscape in response to treatment.

Most of the existing single cell multi-omic analyses of glioma published thus far have focused on either determining how tumor cell phenotypes diverge from normal tissue or on sub-classifying tumors into different molecular subgroups. Applying single cell multi-omic profiling to pre- and post-treatment pHGG tumors has the potential to reveal the consequences of various therapies on tumor composition and to identify markers of treatment susceptibility and resistance. These types of analyses are expected to generate data that can be applied to ultimately improve patient outcomes in several ways: by identifying novel treatment strategies and combination therapies to target the mechanisms by which glioma escapes therapy, by predicting the outcomes of different treatment modalities in a patient-specific manner that accounts for heterogeneity in therapeutic responses between cells in the same

tumor, and by assessing how tumor-immune interactions affect response to therapy and resistance. Obtaining a more holistic view of the complex interplay between diverse tumor cell populations and their environment through multi-omic single cell analyses provides an opportunity to revolutionize therapeutic approaches to cancer treatment and make precision oncology practice more precise.

Author contributions

RM and JA conceived the topic, conducted the literature research, wrote the manuscript, and prepared the tables. RM prepared the figures.

Funding

This work was supported by a CureSearch Young Investigator Award in Pediatric Oncology Drug Development and a B*CURED grant to JA and a Center for Cell and Gene Therapy (CAGT) T32 Training Grant fellowship to RM (5T32HL092332-19).

Conflict of interest

The authors declare that the research was conducted in the absence of any commercial or financial relationships that could be construed as a potential conflict of interest.

Publisher's note

References

Abdelfattah, N., Kumar, P., Wang, C., Leu, J. S., Flynn, W. F., Gao, R., et al. (2022). Single-cell analysis of human glioma and immune cells identifies S100A4 as an immunotherapy target. *Nat. Commun.* 13, 767. doi:10.1038/s41467-022-28372-y

Adamski, J., Tabori, U., and Bouffet, E. (2014). Advances in the management of paediatric high-grade glioma. *Curr. Oncol. Rep.* 16, 414. doi:10.1007/s11912-014-0414-0

Ahmed, N., Brawley, V., Hegde, M., Bielamowicz, K., Kalra, M., Landi, D., et al. (2017). HER2-Specific chimeric antigen receptor-modified virus-specific T cells for progressive glioblastoma: A phase 1 dose-escalation trial. *JAMA Oncol.* 3, 1094–1101. doi:10.1001/jamaoncol.2017.0184

Alexander, J., Laplant, Q. C., Pattwell, S. S., Szulzewsky, F., Cimino, P. J., Caruso, F. P., et al. (2020). Multimodal single-cell analysis reveals distinct radioresistant stem-like and progenitor cell populations in murine glioma. *Glia* 68, 2486–2502. doi:10.1002/glia.23866

Allen, C. E., Laetsch, T. W., Mody, R., Irwin, M. S., Lim, M. S., Adamson, P. C., et al. (2017). Target and agent prioritization for the children's oncology group-national cancer institute pediatric MATCH trial. *J. Natl. Cancer Inst.* 109, djw274. doi:10.1093/jnci/djw274

Angermueller, C., Clark, S. J., Lee, H. J., Macaulay, I. C., Teng, M. J., Hu, T. X., et al. (2016). Parallel single-cell sequencing links transcriptional and epigenetic heterogeneity. *Nat. Methods* 13, 229–232. doi:10.1038/nmeth.3728

Armstrong, C. L., Gyato, K., Awadalla, A. W., Lustig, R., and Tochner, Z. A. (2004). A critical review of the clinical effects of therapeutic irradiation damage to the brain: The roots of controversy. *Neuropsychol. Rev.* 14, 65–86. doi:10.1023/b:nerv.0000026649.68781.8e

Arrillaga-Romany, I., Chi, A. S., Allen, J. E., Oster, W., Wen, P. Y., and Batchelor, T. T. (2017). A phase 2 study of the first imipridone ONC201, a selective DRD2 antagonist for oncology, administered every three weeks in recurrent glioblastoma. *Oncotarget* 8, 79298–79304. doi:10.18632/oncotarget.17837

Bao, S., Wu, Q., Mclendon, R. E., Hao, Y., Shi, Q., Hjelmeland, A. B., et al. (2006). Glioma stem cells promote radioresistance by preferential activation of the DNA damage response. *Nature* 444, 756–760. doi:10.1038/nature05236

Barthel, F. P., Johnson, K. C., Varn, F. S., Moskalik, A. D., Tanner, G., Kocakavuk, E., et al. (2019). Longitudinal molecular trajectories of diffuse glioma in adults. *Nature* 576, 112–120. doi:10.1038/s41586-019-1775-1

Bax, D. A., Mackay, A., Little, S. E., Carvalho, D., Viana-Pereira, M., Tamber, N., et al. (2010). A distinct spectrum of copy number aberrations in pediatric high-grade gliomas. *Clin. Cancer Res.* 16, 3368–3377. doi:10.1158/1078-0432.CCR-10-0438

Bredlau, A. L., and Korones, D. N. (2014). Diffuse intrinsic pontine gliomas: Treatments and controversies. *Adv. Cancer Res.* 121, 235–259. doi:10.1016/B978-0-12-800249-0.00006-8

Cacciotti, C., Choi, J., Alexandrescu, S., Zimmerman, M. A., Cooney, T. M., Chordas, C., et al. (2020). Immune checkpoint inhibition for pediatric patients with recurrent/refractory CNS tumors: A single institution experience. *J. Neurooncol* 149, 113–122. doi:10.1007/s11060-020-03578-6

Calabrese, C., Poppleton, H., Kocak, M., Hogg, T. L., Fuller, C., Hamner, B., et al. (2007). A perivascular niche for brain tumor stem cells. *Cancer Cell* 11, 69–82. doi:10.1016/j.ccr.2006.11.020

Castel, D., Philippe, C., Calmon, R., Le Dret, L., Truffaux, N., Boddaert, N., et al. (2015). Histone H3F3A and HIST1H3B K27M mutations define two subgroups of diffuse intrinsic pontine gliomas with different prognosis and phenotypes. *Acta Neuropathol.* 130, 815–827. doi:10.1007/s00401-015-1478-0

Castel, D., Philippe, C., Kergrohen, T., Sill, M., Merlevede, J., Barret, E., et al. (2018). Transcriptomic and epigenetic profiling of 'diffuse midline gliomas, H3 K27M-mutant' discriminate two subgroups based on the type of histone H3 mutated and not supratentorial or infratentorial location. *Acta Neuropathol. Commun.* 6, 117. doi:10.1186/s40478-018-0614-1

Ceglie, G., Vinci, M., Carai, A., Rossi, S., Colafati, G. S., Cacchione, A., et al. (2020). Infantile/congenital high-grade gliomas: Molecular features and therapeutic perspectives. *Diagn. (Basel)* 10, 648. doi:10.3390/diagnostics10090648

Chaligne, R., Gaiti, F., Silverbush, D., Schiffman, J. S., Weisman, H. R., Kluegel, L., et al. (2021). Epigenetic encoding, heritability and plasticity of glioma transcriptional cell states. *Nat. Genet.* 53, 1469–1479. doi:10.1038/s41588-021-00927-7

Charles, N., Ozawa, T., Squatrito, M., Bleau, A. M., Brennan, C. W., Hambardzumyan, D., et al. (2010). Perivascular nitric oxide activates notch signaling and promotes stem-like character in PDGF-induced glioma cells. *Cell Stem Cell* 6, 141–152. doi:10.1016/j.stem.2010.01.001

Chen, J., Li, Y., Yu, T. S., Mckay, R. M., Burns, D. K., Kernie, S. G., et al. (2012). A restricted cell population propagates glioblastoma growth after chemotherapy. *Nature* 488, 522–526. doi:10.1038/nature11287

Chen, X., Li, C., Li, Y., Wu, S., Liu, W., Lin, T., et al. (2021). Characterization of METTL7B to evaluate TME and predict prognosis by integrative analysis of multi-omics data in glioma. *Front. Mol. Biosci.* 8, 727481. doi:10.3389/fmolb.2021.727481

Chen, Z., and Hambardzumyan, D. (2018). Immune microenvironment in glioblastoma subtypes. *Front. Immunol.* 9, 1004. doi:10.3389/fimmu.2018.01004

Chi, A. S., Tarapore, R. S., Hall, M. D., Shonka, N., Gardner, S., Umemura, Y., et al. (2019). Pediatric and adult H3 K27M-mutant diffuse midline glioma treated with the selective DRD2 antagonist ONC201. *J. Neurooncol* 145, 97–105. doi:10.1007/s11060-019-03271-3

Clarke, M., Mackay, A., Ismer, B., Pickles, J. C., Tatevossian, R. G., Newman, S., et al. (2020). Infant high-grade gliomas comprise multiple subgroups characterized by novel targetable gene fusions and favorable outcomes. *Cancer Discov.* 10, 942–963. doi:10.1158/2159-8290.CD-19-1030

Cohen, A. R. (2022). Brain tumors in children. *N. Engl. J. Med.* 386, 1922–1931. doi:10.1056/NEJMra2116344

Cohen, K. J., Pollack, I. F., Zhou, T., Buxton, A., Holmes, E. J., Burger, P. C., et al. (2011). Temozolomide in the treatment of high-grade gliomas in children: A report from the children's oncology group. *Neuro Oncol.* 13, 317–323. doi:10.1093/neuonc/noq191

Comba, A., Faisal, S. M., Varela, M. L., Hollon, T., Al-Holou, W. N., Umemura, Y., et al. (2021). Uncovering spatiotemporal heterogeneity of high-grade gliomas: From disease biology to therapeutic implications. *Front. Oncol.* 11, 703764. doi:10.3389/fonc.2021.703764

Cooney, T., Lane, A., Bartels, U., Bouffet, E., Goldman, S., Leary, S. E. S., et al. (2017). Contemporary survival endpoints: An international diffuse intrinsic pontine glioma registry study. *Neuro Oncol.* 19, 1279–1280. doi:10.1093/neuonc/nox107

Couturier, C. P., Ayyadhury, S., Le, P. U., Nadaf, J., Monlong, J., Riva, G., et al. (2020). Single-cell RNA-seq reveals that glioblastoma recapitulates a normal neurodevelopmental hierarchy. *Nat. Commun.* 11, 3406. doi:10.1038/s41467-020-17186-5

Crowell, C., Mata-Mbemba, D., Bennett, J., Matheson, K., Mackley, M., Perreault, S., et al. (2022). Systematic review of diffuse hemispheric glioma, H3 G34-mutant: Outcomes and associated clinical factors. *Neurooncol Adv.* 4, vdac133. doi:10.1093/noajnl/vdac133

Curry, R. N., Aiba, I., Meyer, J., Lozzi, B., Ko, Y., Mcdonald, M. F., et al. (2023). Glioma epileptiform activity and progression are driven by IGSF3-mediated potassium dysregulation. *Neuron* 111, 682–695 e9. doi:10.1016/j.neuron.2023.01.013

Darmanis, S., Sloan, S. A., Croote, D., Mignardi, M., Chernikova, S., Samghababi, P., et al. (2017). Single-cell RNA-seq analysis of infiltrating neoplastic cells at the migrating front of human glioblastoma. *Cell Rep.* 21, 1399–1410. doi:10.1016/j.celrep.2017.10.030

Demaree, B., Delley, C. L., Vasudevan, H. N., Peretz, C. A. C., Ruff, D., Smith, C. C., et al. (2021). Joint profiling of DNA and proteins in single cells to dissect genotype-phenotype associations in leukemia. *Nat. Commun.* 12, 1583. doi:10.1038/s41467-021-21810-3

Dewire, M., Lazow, M., Campagne, O., Leach, J., Fuller, C., Senthil Kumar, S., et al. (2022). Phase I study of ribociclib and everolimus in children with newly diagnosed DIPG and high-grade glioma: A connect pediatric neuro-oncology consortium report. *Neurooncol Adv.* 4, vdac055. vdac055. doi:10.1093/noajnl/vdac055

Doxie, D. B., and Irish, J. M. (2014). High-dimensional single-cell cancer biology. *Curr. Top. Microbiol. Immunol.* 377, 1–21. doi:10.1007/82_2014_367

Duffner, P. K., Horowitz, M. E., Krischer, J. P., Burger, P. C., Cohen, M. E., Sanford, R. A., et al. (1999). The treatment of malignant brain tumors in infants and very youngchildren: An update of the pediatric oncology group experience. *Neuro Oncol.* 1, 152–161. doi:10.1093/neuonc/1.2.152

Evrony, G. D., Hinch, A. G., and Luo, C. (2021). Applications of single-cell DNA sequencing. *Annu. Rev. Genomics Hum. Genet.* 22, 171–197. doi:10.1146/annurev-genom-111320-090436

Fangusaro, J. (2009). Pediatric high-grade gliomas and diffuse intrinsic pontine gliomas. *J. Child Neurology* 24, 1409–1417. doi:10.1177/0883073809338960

Filbin, M. G., Tirosh, I., Hovestadt, V., Shaw, M. L., Escalante, L. E., Mathewson, N. D., et al. (2018). Developmental and oncogenic programs in H3K27M gliomas dissected by single-cell RNA-seq. *Science* 360, 331–335. doi:10.1126/science.aao4750

Finlay, J. L., Boyett, J. M., Yates, A. J., Wisoff, J. H., Milstein, J. M., Geyer, J. R., et al. (1995). Randomized phase III trial in childhood high-grade astrocytoma comparing vincristine, lomustine, and prednisone with the eight-drugs-in-1-day regimen. Childrens cancer group. *J. Clin. Oncol.* 13, 112–123. doi:10.1200/JCO.1995.13.1.112

Fontebasso, A. M., Schwartzentruber, J., Khuong-Quang, D. A., Liu, X. Y., Sturm, D., Korshunov, A., et al. (2013). Mutations in SETD2 and genes affecting histone H3K36 methylation target hemispheric high-grade gliomas. *Acta Neuropathol.* 125, 659–669. doi:10.1007/s00401-013-1095-8

Fouladi, M., Park, J. R., Stewart, C. F., Gilbertson, R. J., Schaiquevich, P., Sun, J., et al. (2010). Pediatric phase I trial and pharmacokinetic study of vorinostat: A children's oncology group phase I consortium report. *J. Clin. Oncol.* 28, 3623–3629. doi:10.1200/JCO.2009.25.9119

Fried, I., Lossos, A., Ben Ami, T., Dvir, R., Toledano, H., Ben Arush, M. W., et al. (2018). Preliminary results of immune modulating antibody MDV9300 (pidilizumab) treatment in children with diffuse intrinsic pontine glioma. *J. Neurooncol* 136, 189–195. doi:10.1007/s11060-017-2643-1

Friedman, G. K., Johnston, J. M., Bag, A. K., Bernstock, J. D., Li, R., Aban, I., et al. (2021). Oncolytic HSV-1 G207 immunovirotherapy for pediatric high-grade gliomas. *N. Engl. J. Med.* 384, 1613–1622. doi:10.1056/NEJMoa2024947

Gaiti, F., Chaligne, R., Gu, H., Brand, R. M., Kothen-Hill, S., Schulman, R. C., et al. (2019). Epigenetic evolution and lineage histories of chronic lymphocytic leukaemia. *Nature* 569, 576–580. doi:10.1038/s41586-019-1198-z

Galanis, E., Anderson, S. K., Miller, C. R., Sarkaria, J. N., Jaeckle, K., Buckner, J. C., et al. (2018). Phase I/II trial of vorinostat combined with temozolomide and radiation therapy for newly diagnosed glioblastoma: Results of alliance N0874/ABTC 02. *Neuro Oncol.* 20, 546–556. doi:10.1093/neuonc/nox161

Gallego Perez-Larraya, J., Garcia-Moure, M., Labiano, S., Patino-Garcia, A., Dobbs, J., Gonzalez-Huarriz, M., et al. (2022). Oncolytic DNX-2401 virus for pediatric diffuse intrinsic pontine glioma. *N. Engl. J. Med.* 386, 2471–2481. doi:10.1056/NEJMoa2202028

Gallitto, M., Lazarev, S., Wasserman, I., Stafford, J. M., Wolden, S. L., Terezakis, S. A., et al. (2019). Role of radiation therapy in the management of diffuse intrinsic pontine glioma: A systematic review. *Adv. Radiat. Oncol.* 4, 520–531. doi:10.1016/j.adro.2019.03.009

Garcia-Fabiani, M. B., Haase, S., Comba, A., Carney, S., Mcclellan, B., Banerjee, K., et al. (2021). Genetic alterations in gliomas remodel the tumor immune microenvironment and impact immune-mediated therapies. *Front. Oncol.* 11, 631037. doi:10.3389/fonc.2021.631037

Garofano, L., Migliozzi, S., Oh, Y. T., D'Angelo, F., Najac, R. D., Ko, A., et al. (2021). Pathway-based classification of glioblastoma uncovers a mitochondrial subtype with therapeutic vulnerabilities. *Nat. Cancer* 2, 141–156. doi:10.1038/s43018-020-00159-4

Gestrich, C. K., Jajosky, A. N., Elliott, R., Stearns, D., Sadri, N., Cohen, M. L., et al. (2021). Molecular profiling of pediatric and adult glioblastoma. *Am. J. Clin. Pathol.* 155, 606–614. doi:10.1093/ajcp/aqaa172

Ghajar-Rahimi, G., Kang, K. D., Totsch, S. K., Gary, S., Rocco, A., Blitz, S., et al. (2022). Clinical advances in oncolytic virotherapy for pediatric brain tumors. *Pharmacol. Ther.* 239, 108193. doi:10.1016/j.pharmthera.2022.108193

Gianno, F., Giovannoni, I., Cafferata, B., Diomedi-Camassei, F., Minasi, S., Barresi, S., et al. (2022). Paediatric-type diffuse high-grade gliomas in the 5th CNS WHO Classification. *Pathologica* 114, 422–435. doi:10.32074/1591-951X-830

Gibson, E. G., Campagne, O., Selvo, N. S., Gajjar, A., and Stewart, C. F. (2021). Population pharmacokinetic analysis of crizotinib in children with progressive/recurrent high-grade and diffuse intrinsic pontine gliomas. *Cancer Chemother. Pharmacol.* 88, 1009–1020. doi:10.1007/s00280-021-04357-4

Gojo, J., Englinger, B., Jiang, L., Hubner, J. M., Shaw, M. L., Hack, O. A., et al. (2020). Single-cell RNA-seq reveals cellular hierarchies and impaired developmental trajectories in pediatric ependymoma. *Cancer Cell* 38, 44–59. doi:10.1016/j.ccell.2020.06.004

Granja, J. M., Klemm, S., Mcginnis, L. M., Kathiria, A. S., Mezger, A., Corces, M. R., et al. (2019). Single-cell multiomic analysis identifies regulatory programs in mixed-phenotype acute leukemia. *Nat. Biotechnol.* 37, 1458–1465. doi:10.1038/s41587-019-0332-7

Guerreiro Stucklin, A. S., Ryall, S., Fukuoka, K., Zapotocky, M., Lassaletta, A., Li, C., et al. (2019). Alterations in ALK/ROS1/NTRK/MET drive a group of infantile hemispheric gliomas. *Nat. Commun.* 10, 4343. doi:10.1038/s41467-019-12187-5

Guilhamon, P., Chesnelong, C., Kushida, M. M., Nikolic, A., Singhal, D., Macleod, G., et al. (2021). Single-cell chromatin accessibility profiling of glioblastoma identifies an invasive cancer stem cell population associated with lower survival. *Elife* 10, e64090. doi:10.7554/eLife.64090

Hargrave, D., Bartels, U., and Bouffet, E. (2006). Diffuse brainstem glioma in children: Critical review of clinical trials. *Lancet Oncol.* 7, 241–248. doi:10.1016/S1470-2045(06)70615-5

Haydar, D., Houke, H., Chiang, J., Yi, Z., Ode, Z., Caldwell, K., et al. (2021). Cell-surface antigen profiling of pediatric brain tumors: B7-H3 is consistently expressed and can be targeted via local or systemic CAR T-cell delivery. *Neuro Oncol.* 23, 999–1011. doi:10.1093/neuonc/noaa278

Hemmati, H. D., Nakano, I., Lazareff, J. A., Masterman-Smith, M., Geschwind, D. H., Bronner-Fraser, M., et al. (2003). Cancerous stem cells can arise from pediatric brain tumors. *Proc. Natl. Acad. Sci. U. S. A.* 100, 15178–15183. doi:10.1073/pnas.2036535100

Hoffman, L. M., Dewire, M., Ryall, S., Buczkowicz, P., Leach, J., Miles, L., et al. (2016). Spatial genomic heterogeneity in diffuse intrinsic pontine and midline high-grade glioma: Implications for diagnostic biopsy and targeted therapeutics. *Acta Neuropathol. Commun.* 4, 1. doi:10.1186/s40478-015-0269-0

Hoffman, M., Gillmor, A. H., Kunz, D. J., Johnston, M. J., Nikolic, A., Narta, K., et al. (2019). Intratumoral genetic and functional heterogeneity in pediatric glioblastoma. *Cancer Res.* 79, 2111–2123. doi:10.1158/0008-5472.CAN-18-3441

Hou, Y., Guo, H., Cao, C., Li, X., Hu, B., Zhu, P., et al. (2016). Single-cell triple omics sequencing reveals genetic, epigenetic, and transcriptomic heterogeneity in hepatocellular carcinomas. *Cell Res.* 26, 304–319. doi:10.1038/cr.2016.23

Hovestadt, V., Smith, K. S., Bihannic, L., Filbin, M. G., Shaw, M. L., Baumgartner, A., et al. (2019). Resolving medulloblastoma cellular architecture by single-cell genomics. *Nature* 572, 74–79. doi:10.1038/s41586-019-1434-6

Huang, T., Garcia, R., Qi, J., Lulla, R., Horbinski, C., Behdad, A., et al. (2018). Detection of histone H3 K27M mutation and post-translational modifications in pediatric diffuse midline glioma via tissue immunohistochemistry informs diagnosis and clinical outcomes. *Oncotarget* 9, 37112–37124. doi:10.18632/oncotarget.26430

Hubert, C. G., Rivera, M., Spangler, L. C., Wu, Q., Mack, S. C., Prager, B. C., et al. (2016). A three-dimensional organoid culture system derived from human glioblastomas recapitulates the hypoxic gradients and cancer stem cell heterogeneity of tumors found *in vivo*. *Cancer Res.* 76, 2465–2477. doi:10.1158/0008-5472.CAN-15-2402

Hwang, B., Lee, J. H., and Bang, D. (2018). Single-cell RNA sequencing technologies and bioinformatics pipelines. *Exp. Mol. Med.* 50, 96–14. doi:10.1038/s12276-018-0071-8

ICGC PEDBRAIN-SEQ PROJECT; ICGC MMML-SEQ PROJECT, Grobner, S. N., Worst, B. C., Weischenfeldt, J., Buchhalter, I., et al. (2018). The landscape of genomic alterations across childhood cancers. *Nature* 555, 321–327. doi:10.1038/nature25480

Izquierdo, E., Carvalho, D. M., Mackay, A., Temelso, S., Boult, J. K. R., Pericoli, G., et al. (2022). DIPG harbors alterations targetable by MEK inhibitors, with acquired resistance mechanisms overcome by combinatorial inhibition. *Cancer Discov.* 12, 712–729. doi:10.1158/2159-8290.CD-20-0930

Jacob, F., Salinas, R. D., Zhang, D. Y., Nguyen, P. T. T., Schnoll, J. G., Wong, S. Z. H., et al. (2020). A patient-derived glioblastoma organoid model and biobank recapitulates inter- and intra-tumoral heterogeneity. *Cell* 180, 188–204. doi:10.1016/j.cell.2019.11.036

Jenkin, R. D. T., Boesel, C., Ertel, I., Evans, A., Hittle, T. R., Ortega, J., et al. (1987). Brain-stem tumors in childhood: A prospective randomized trial of irradiation with and without adjuvant CCNU, vcr, and prednisone: A report of the childrens cancer study group. *J. Neurosurg.* 66, 227–233. doi:10.3171/jns.1987.66.2.0227

Jerby-Arnon, L., and Regev, A. (2022). DIALOGUE maps multicellular programs in tissue from single-cell or spatial transcriptomics data. *Nat. Biotechnol.* 40, 1467–1477. doi:10.1038/s41587-022-01288-0

Jessa, S., Blanchet-Cohen, A., Krug, B., Vladoiu, M., Coutelier, M., Faury, D., et al. (2019). Stalled developmental programs at the root of pediatric brain tumors. *Nat. Genet.* 51, 1702–1713. doi:10.1038/s41588-019-0531-7

Johnson, K. C., Anderson, K. J., Courtois, E. T., Gujar, A. D., Barthel, F. P., Varn, F. S., et al. (2021). Single-cell multimodal glioma analyses identify epigenetic regulators of cellular plasticity and environmental stress response. *Nat. Genet.* 53, 1456–1468. doi:10.1038/s41588-021-00926-8

Jones, C., Karajannis, M. A., Jones, D. T. W., Kieran, M. W., Monje, M., Baker, S. J., et al. (2017). Pediatric high-grade glioma: Biologically and clinically in need of new thinking. *Neuro Oncol.* 19, 153–161. doi:10.1093/neuonc/now101

Jones, C., Perryman, L., and Hargrave, D. (2012). Paediatric and adult malignant glioma: Close relatives or distant cousins? *Nat. Rev. Clin. Oncol.* 9, 400–413. doi:10.1038/nrclinonc.2012.87

Kaminska, B., Ochocka, N., and Segit, P. (2021). Single-cell omics in dissecting immune microenvironment of malignant gliomas-challenges and perspectives. *Cells* 10, 2264. doi:10.3390/cells10092264

Kashyap, A., Rapsomaniki, M. A., Barros, V., Fomitcheva-Khartchenko, A., Martinelli, A. L., Rodriguez, A. F., et al. (2022). Quantification of tumor heterogeneity: From data acquisition to metric generation. *Trends Biotechnol.* 40, 647–676. doi:10.1016/j.tibtech.2021.11.006

Kaya-Okur, H. S., Wu, S. J., Codomo, C. A., Pledger, E. S., Bryson, T. D., Henikoff, J. G., et al. (2019). CUT&Tag for efficient epigenomic profiling of small samples and single cells. *Nat. Commun.* 10, 1930. doi:10.1038/s41467-019-09982-5

Khan, A. B., Lee, S., Harmanci, A. S., Patel, R., Latha, K., Yang, Y., et al. (2023). CXCR4 expression is associated with proneural-to-mesenchymal transition in glioblastoma. *Int. J. Cancer* 152, 713–724. doi:10.1002/ijc.34329

Khuong-Quang, D. A., Buczkowicz, P., Rakopoulos, P., Liu, X. Y., Fontebasso, A. M., Bouffet, E., et al. (2012). K27M mutation in histone H3.3 defines clinically and biologically distinct subgroups of pediatric diffuse intrinsic pontine gliomas. *Acta Neuropathol.* 124, 439–447. doi:10.1007/s00401-012-0998-0

Kline, C., Felton, E., Allen, I. E., Tahir, P., and Mueller, S. (2018). Survival outcomes in pediatric recurrent high-grade glioma: Results of a 20-year systematic review and meta-analysis. *J. Neurooncol* 137, 103–110. doi:10.1007/s11060-017-2701-8

Korshunov, A., Capper, D., Reuss, D., Schrimpf, D., Ryzhova, M., Hovestadt, V., et al. (2016). Histologically distinct neuroepithelial tumors with histone 3 G34 mutation are molecularly similar and comprise a single nosologic entity. *Acta Neuropathol.* 131, 137–146. doi:10.1007/s00401-015-1493-1

Korshunov, A., Schrimpf, D., Ryzhova, M., Sturm, D., Chavez, L., Hovestadt, V., et al. (2017). H3-/IDH-wild type pediatric glioblastoma is comprised of molecularly and prognostically distinct subtypes with associated oncogenic drivers. *Acta Neuropathol.* 134, 507–516. doi:10.1007/s00401-017-1710-1

Koschmann, C., Zamler, D., Mackay, A., Robinson, D., Wu, Y., Doherty, R., et al. (2016). Characterizing and targeting PDGFRA alterations in pediatric high-grade glioma. *Oncotarget* 7, 65696–65706. doi:10.18632/oncotarget.11602

Kuett, L., Catena, R., Ozcan, A., Pluss, A., Cancer Grand Challenges, I. C., Schraml, P., et al. (2022). Three-dimensional imaging mass cytometry for highly multiplexed molecular and cellular mapping of tissues and the tumor microenvironment. *Nat. Cancer* 3, 122–133. doi:10.1038/s43018-021-00301-w

Lam, K. H. B., Leon, A. J., Hui, W., Lee, S. C., Batruch, I., Faust, K., et al. (2022). Topographic mapping of the glioblastoma proteome reveals a triple-axis model of intra-tumoral heterogeneity. *Nat. Commun.* 13, 116. doi:10.1038/s41467-021-27667-w

Langmoen, I. A., Lundar, T., Storm-Mathisen, I., Lie, S. O., and Hovind, K. H. (1991). Management of pediatric pontine gliomas. *J. Int. Soc. Pediatr. Neurosurg.* 7, 13–15. doi:10.1007/BF00263825

Lashford, L. S., Thiesse, P., Jouvet, A., Jaspan, T., Couanet, D., Griffiths, P. D., et al. (2002). Temozolomide in malignant gliomas of childhood: A United Kingdom children's cancer study group and French society for pediatric oncology intergroup study. *J. Clin. Oncol.* 20, 4684–4691. doi:10.1200/JCO.2002.08.141

Lavin, Y., Kobayashi, S., Leader, A., Amir, E. D., Elefant, N., Bigenwald, C., et al. (2017). Innate immune landscape in early lung adenocarcinoma by paired single-cell analyses. *Cell* 169, 750–765. doi:10.1016/j.cell.2017.04.014

Leblanc, V. G., Trinh, D. L., Aslanpour, S., Hughes, M., Livingstone, D., Jin, D., et al. (2022). Single-cell landscapes of primary glioblastomas and matched explants and cell lines show variable retention of inter- and intratumor heterogeneity. *Cancer Cell* 40, 379–392 e9. doi:10.1016/j.ccell.2022.02.016

Lee, A. C., Lee, Y., Choi, A., Lee, H. B., Shin, K., Lee, H., et al. (2022). Spatial epitranscriptomics reveals A-to-I editome specific to cancer stem cell microniches. *Nat. Commun.* 13, 2540. doi:10.1038/s41467-022-30299-3

Lehmann, R., Rayner, B. S., and Ziegler, D. S. (2022). Resistance mechanisms in BRAF(V600E) paediatric high-grade glioma and current therapeutic approaches. *Front. Oncol.* 12, 1031378. doi:10.3389/fonc.2022.1031378

Li, Z., Wei, Y., Shao, Y., Tang, L., and Gong, J. (2021). Multi-omics analysis of intertumoral heterogeneity within medulloblastoma uncharted-pathway subtypes. *Brain Tumor Pathol.* 38, 234–242. doi:10.1007/s10014-021-00400-7

Lim, K. Y., Won, J. K., Park, C. K., Kim, S. K., Choi, S. H., Kim, T., et al. (2021). H3 G34-mutant high-grade glioma. *Brain Tumor Pathol.* 38, 4–13. doi:10.1007/s10014-020-00378-8

Liu, G., Yuan, X., Zeng, Z., Tunici, P., Ng, H., Abdulkadir, I. R., et al. (2006). Analysis of gene expression and chemoresistance of CD133+ cancer stem cells in glioblastoma. *Mol. Cancer* 5, 67. doi:10.1186/1476-4598-5-67

Liu, J., Qu, S., Zhang, T., Gao, Y., Shi, H., Song, K., et al. (2021). Applications of single-cell omics in tumor Immunology. *Front. Immunol.* 12, 697412. doi:10.3389/fimmu.2021.697412

Louis, D. N., Perry, A., Wesseling, P., Brat, D. J., Cree, I. A., Figarella-Branger, D., et al. (2021). The 2021 WHO classification of tumors of the central nervous system: A summary. *Neuro Oncol.* 23, 1231–1251. doi:10.1093/neuonc/noab106

Ma, S., Zhang, B., Lafave, L. M., Earl, A. S., Chiang, Z., Hu, Y., et al. (2020). Chromatin potential identified by shared single-cell profiling of RNA and chromatin. *Cell* 183, 1103–1116. doi:10.1016/j.cell.2020.09.056

Ma, X., Liu, Y., Liu, Y., Alexandrov, L. B., Edmonson, M. N., Gawad, C., et al. (2018). Pan-cancer genome and transcriptome analyses of 1,699 paediatric leukaemias and solid tumours. *Nature* 555, 371–376. doi:10.1038/nature25795

Macaulay, I. C., Teng, M. J., Haerty, W., Kumar, P., Ponting, C. P., and Voet, T. (2016). Separation and parallel sequencing of the genomes and transcriptomes of single cells using G&T-seq. *Nat. Protoc.* 11, 2081–2103. doi:10.1038/nprot.2016.138

Mackay, A., Burford, A., Carvalho, D., Izquierdo, E., Fazal-Salom, J., Taylor, K. R., et al. (2017). Integrated molecular meta-analysis of 1,000 pediatric high-grade and diffuse intrinsic pontine glioma. *Cancer Cell* 32, 520–537. doi:10.1016/j.ccell.2017.08.017

Majzner, R. G., Ramakrishna, S., Yeom, K. W., Patel, S., Chinnasamy, H., Schultz, L. M., et al. (2022). GD2-CAR T cell therapy for H3K27M-mutated diffuse midline gliomas. *Nature* 603, 934–941. doi:10.1038/s41586-022-04489-4

Mandell, L. R., Kadota, R., Freeman, C., Douglass, E. C., Fontanesi, J., Cohen, M. E., et al. (1999). There is No role for hyperfractionated radiotherapy in the management of children with newly diagnosed diffuse intrinsic brainstem tumors: Results of a pediatric oncology group phase III trial comparing conventional vs. Hyperfractionated radiotherapy. *Int. J. Radiat. Oncol. Biol. Phys.* 43, 959–964. doi:10.1016/s0360-3016(98)00501-x

Marusyk, A., Janiszewska, M., and Polyak, K. (2020). Intratumor heterogeneity: The rosetta stone of therapy resistance. *Cancer Cell* 37, 471–484. doi:10.1016/j.ccell.2020.03.007

Massimino, M., Spreafico, F., Biassoni, V., Simonetti, F., Riva, D., Trecate, G., et al. (2008). Diffuse pontine gliomas in children: Changing strategies, changing results? A mono-institutional 20-year experience. *J. Neurooncol* 87, 355–361. doi:10.1007/s11060-008-9525-5

Mazor, T., Pankov, A., Song, J. S., and Costello, J. F. (2016). Intratumoral heterogeneity of the epigenome. *Cancer Cell* 29, 440–451. doi:10.1016/j.ccell.2016.03.009

Mcgranahan, N., and Swanton, C. (2017). Clonal heterogeneity and tumor evolution: Past, present, and the future. *Cell* 168, 613–628. doi:10.1016/j.cell.2017.01.018

Merchant, T. E., Conklin, H. M., Wu, S., Lustig, R. H., and Xiong, X. (2009). Late effects of conformal radiation therapy for pediatric patients with low-grade glioma: Prospective evaluation of cognitive, endocrine, and hearing deficits. *J. Clin. Oncol.* 27, 3691–3697. doi:10.1200/JCO.2008.21.2738

Metselaar, D. S., Du Chatinier, A., Stuiver, I., Kaspers, G. J. L., and Hulleman, E. (2021). Radiosensitization in pediatric high-grade glioma: Targets, resistance and developments. *Front. Oncol.* 11, 662209. doi:10.3389/fonc.2021.662209

Meyer, M., Reimand, J., Lan, X., Head, R., Zhu, X., Kushida, M., et al. (2015). Single cell-derived clonal analysis of human glioblastoma links functional and genomic heterogeneity. *Proc. Natl. Acad. Sci. U. S. A.* 112, 851–856. doi:10.1073/pnas.1320611111

Miklja, Z., Yadav, V. N., Cartaxo, R. T., Siada, R., Thomas, C. C., Cummings, J. R., et al. (2020). Everolimus improves the efficacy of dasatinib in PDGFRα-driven glioma. *J. Clin. Invest.* 130, 5313–5325. doi:10.1172/JCI133310

Monje, M., Mitra, S. S., Freret, M. E., Raveh, T. B., Kim, J., Masek, M., et al. (2011). Hedgehog-responsive candidate cell of origin for diffuse intrinsic pontine glioma. *Proc. Natl. Acad. Sci. U. S. A.* 108, 4453–4458. doi:10.1073/pnas.1101657108

Morita, K., Wang, F., Jahn, K., Hu, T., Tanaka, T., Sasaki, Y., et al. (2020). Clonal evolution of acute myeloid leukemia revealed by high-throughput single-cell genomics. *Nat. Commun.* 11, 5327. doi:10.1038/s41467-020-19119-8

Mueller, S., Fullerton, H. J., Stratton, K., Leisenring, W., Weathers, R. E., Stovall, M., et al. (2013). Radiation, atherosclerotic risk factors, and stroke risk in survivors of

pediatric cancer: A report from the childhood cancer survivor study. *Int. J. Radiat. Oncol. Biol. Phys.* 86, 649–655. doi:10.1016/j.ijrobp.2013.03.034

Mueller, S., Jain, P., Liang, W. S., Kilburn, L., Kline, C., Gupta, N., et al. (2019). A pilot precision medicine trial for children with diffuse intrinsic pontine glioma-pnoc003: A report from the pacific pediatric neuro-oncology consortium. *Int. J. Cancer* 145, 1889–1901. doi:10.1002/ijc.32258

Muller, S., Liu, S. J., Di Lullo, E., Malatesta, M., Pollen, A. A., Nowakowski, T. J., et al. (2016). Single-cell sequencing maps gene expression to mutational phylogenies in PDGF- and EGF-driven gliomas. *Mol. Syst. Biol.* 12, 889. doi:10.15252/msb.20166969

Neftel, C., Laffy, J., Filbin, M. G., Hara, T., Shore, M. E., Rahme, G. J., et al. (2019). An integrative model of cellular states, plasticity, and genetics for glioblastoma. *Cell* 178, 835–849. doi:10.1016/j.cell.2019.06.024

Nejo, T., Matsushita, H., Karasaki, T., Nomura, M., Saito, K., Tanaka, S., et al. (2019). Reduced neoantigen expression revealed by longitudinal multiomics as a possible immune evasion mechanism in glioma. *Cancer Immunol. Res.* 7, 1148–1161. doi:10.1158/2326-6066.CIR-18-0599

Nikbakht, H., Panditharatna, E., Mikael, L. G., Li, R., Gayden, T., Osmond, M., et al. (2016). Spatial and temporal homogeneity of driver mutations in diffuse intrinsic pontine glioma. *Nat. Commun.* 7, 11185. doi:10.1038/ncomms11185

Oren, Y., Tsabar, M., Cuoco, M. S., Amir-Zilberstein, L., Cabanos, H. F., Hutter, J. C., et al. (2021). Cycling cancer persister cells arise from lineages with distinct programs. *Nature* 596, 576–582. doi:10.1038/s41586-021-03796-6

Ostrom, Q. T., Cioffi, G., Gittleman, H., Patil, N., Waite, K., Kruchko, C., et al. (2019). CBTRUS statistical report: Primary brain and other central nervous system tumors diagnosed in the United States in 2012-2016. *Neuro Oncol.* 21, v1–v100. doi:10.1093/neuonc/noz150

Ostrom, Q. T., Price, M., Neff, C., Cioffi, G., Waite, K. A., Kruchko, C., et al. (2022). CBTRUS statistical report: Primary brain and other central nervous system tumors diagnosed in the United States in 2015-2019. *Neuro Oncol.* 24, v1–v95. doi:10.1093/neuonc/noac202

Patel, A. P., Tirosh, I., Trombetta, J. J., Shalek, A. K., Gillespie, S. M., Wakimoto, H., et al. (2014). Single-cell RNA-seq highlights intratumoral heterogeneity in primary glioblastoma. *Science* 344, 1396–1401. doi:10.1126/science.1254257

Patel, S. K., Hartley, R. M., Wei, X., Furnish, R., Escobar-Riquelme, F., Bear, H., et al. (2020). Generation of diffuse intrinsic pontine glioma mouse models by brainstem-targeted *in utero* electroporation. *Neuro Oncol.* 22, 381–392. doi:10.1093/neuonc/noz197

Paugh, B. S., Broniscer, A., Qu, C., Miller, C. P., Zhang, J., Tatevossian, R. G., et al. (2011). Genome-wide analyses identify recurrent amplifications of receptor tyrosine kinases and cell-cycle regulatory genes in diffuse intrinsic pontine glioma. *J. Clin. Oncol.* 29, 3999–4006. doi:10.1200/JCO.2011.35.5677

Peretz, C. A. C., Mcgary, L. H. F., Kumar, T., Jackson, H., Jacob, J., Durruthy-Durruthy, R., et al. (2021). Single-cell DNA sequencing reveals complex mechanisms of resistance to quizartinib. *Blood Adv.* 5, 1437–1441. doi:10.1182/bloodadvances.2020003398

Peterson, V. M., Zhang, K. X., Kumar, N., Wong, J., Li, L., Wilson, D. C., et al. (2017). Multiplexed quantification of proteins and transcripts in single cells. *Nat. Biotechnol.* 35, 936–939. doi:10.1038/nbt.3973

Petralia, F., Tignor, N., Reva, B., Koptyra, M., Chowdhury, S., Rykunov, D., et al. (2020). Integrated proteogenomic characterization across major histological types of pediatric brain cancer. *Cell* 183, 1962–1985 e31. doi:10.1016/j.cell.2020.10.044

Pollack, I. F., Jakacki, R. I., Butterfield, L. H., Hamilton, R. L., Panigrahy, A., Normolle, D. P., et al. (2016). Antigen-specific immunoreactivity and clinical outcome following vaccination with glioma-associated antigen peptides in children with recurrent high-grade gliomas: Results of a pilot study. *J. Neurooncol* 130, 517–527. doi:10.1007/s11060-016-2245-3

Pombo Antunes, A. R., Scheyltjens, I., Lodi, F., Messiaen, J., Antoranz, A., Duerinck, J., et al. (2021). Single-cell profiling of myeloid cells in glioblastoma across species and disease stage reveals macrophage competition and specialization. *Nat. Neurosci.* 24, 595–610. doi:10.1038/s41593-020-00789-y

Puduvalli, V. K., Wu, J., Yuan, Y., Armstrong, T. S., Vera, E., Wu, J., et al. (2020). A Bayesian adaptive randomized phase II multicenter trial of bevacizumab with or without vorinostat in adults with recurrent glioblastoma. *Neuro Oncol.* 22, 1505–1515. doi:10.1093/neuonc/noaa062

Rallis, K. S., George, A. M., Wozniak, A. M., Bigogno, C. M., Chow, B., Hanrahan, J. G., et al. (2022). Molecular genetics and targeted therapies for paediatric high-grade glioma. *Cancer Genomics Proteomics* 19, 390–414. doi:10.21873/cgp.20328

Rappez, L., Stadler, M., Triana, S., Gathungu, R. M., Ovchinnikova, K., Phapale, P., et al. (2021). SpaceM reveals metabolic states of single cells. *Nat. Methods* 18, 799–805. doi:10.1038/s41592-021-01198-0

Raynaud, F., Mina, M., Tavernari, D., and Ciriello, G. (2018). Pan-cancer inference of intra-tumor heterogeneity reveals associations with different forms of genomic instability. *PLoS Genet.* 14, e1007669. doi:10.1371/journal.pgen.1007669

Rockne, R. C., and Scott, J. G. (2019). Introduction to mathematical oncology. *JCO Clin. Cancer Inf.* 3, 1–4. doi:10.1200/CCI.19.00010

Roussel, M., Lhomme, F., Roe, C. E., Bartkowiak, T., Gravelle, P., Laurent, C., et al. (2020). Mass cytometry defines distinct immune profile in germinal center B-cell lymphomas. *Cancer Immunol. Immunother.* 69, 407–420. doi:10.1007/s00262-019-02464-z

Salloum, R., Mcconechy, M. K., Mikael, L. G., Fuller, C., Drissi, R., Dewire, M., et al. (2017). Characterizing temporal genomic heterogeneity in pediatric high-grade gliomas. *Acta Neuropathol. Commun.* 5, 78. doi:10.1186/s40478-017-0479-8

Santiago, R. Y. C., Sese, M., Capdevila, C., Aasen, T., De Mattos-Arruda, L., Diaz-Cano, S. J., et al. (2020). Clinical implications of intratumor heterogeneity: Challenges and opportunities. *J. Mol. Med. Berl.* 98, 161–177. doi:10.1007/s00109-020-01874-2

Schwartzentruber, J., Korshunov, A., Liu, X. Y., Jones, D. T., Pfaff, E., Jacob, K., et al. (2012). Driver mutations in histone H3.3 and chromatin remodelling genes in paediatric glioblastoma. *Nature* 482, 226–231. doi:10.1038/nature10833

Skene, P. J., and Henikoff, S. (2017). An efficient targeted nuclease strategy for high-resolution mapping of DNA binding sites. *Elife* 6, e21856. doi:10.7554/eLife.21856

Smallwood, S. A., Lee, H. J., Angermueller, C., Krueger, F., Saadeh, H., Peat, J., et al. (2014). Single-cell genome-wide bisulfite sequencing for assessing epigenetic heterogeneity. *Nat. Methods* 11, 817–820. doi:10.1038/nmeth.3035

Sottoriva, A., Spiteri, I., Piccirillo, S. G., Touloumis, A., Collins, V. P., Marioni, J. C., et al. (2013). Intratumor heterogeneity in human glioblastoma reflects cancer evolutionary dynamics. *Proc. Natl. Acad. Sci. U. S. A.* 110, 4009–4014. doi:10.1073/pnas.1219747110

Spostol, R., Ertel, I. J., Jenkin, R. D. T., Boesel, C. P., Venes, J. L., Ortega, J. A., et al. (1989). The effectiveness of chemotherapy for treatment of high grade astrocytoma in children: Results of a randomized trial: A report from the childrens cancer study group. *J. Neurooncol* 7, 165–177. doi:10.1007/bf00165101

Stoeckius, M., Hafemeister, C., Stephenson, W., Houck-Loomis, B., Chattopadhyay, P. K., Swerdlow, H., et al. (2017). Simultaneous epitope and transcriptome measurement in single cells. *Nat. Methods* 14, 865–868. doi:10.1038/nmeth.4380

Sturm, D., Pfister, S. M., and Jones, D. T. W. (2017). Pediatric gliomas: Current concepts on diagnosis, biology, and clinical management. *J. Clin. Oncol.* 35, 2370–2377. doi:10.1200/JCO.2017.73.0242

Sturm, D., Witt, H., Hovestadt, V., Khuong-Quang, D. A., Jones, D. T., Konermann, C., et al. (2012). Hotspot mutations in H3F3A and IDH1 define distinct epigenetic and biological subgroups of glioblastoma. *Cancer Cell* 22, 425–437. doi:10.1016/j.ccr.2012.08.024

Sundar, S. J., Shakya, S., Barnett, A., Wallace, L. C., Jeon, H., Sloan, A., et al. (2022). Three-dimensional organoid culture unveils resistance to clinical therapies in adult and pediatric glioblastoma. *Transl. Oncol.* 15, 101251. doi:10.1016/j.tranon.2021.101251

Swanson, E., Lord, C., Reading, J., Heubeck, A. T., Genge, P. C., Thomson, Z., et al. (2021). Simultaneous trimodal single-cell measurement of transcripts, epitopes, and chromatin accessibility using TEA-seq. *Elife* 10, e63632. doi:10.7554/eLife.63632

Sweha, S. R., Chung, C., Natarajan, S. K., Panwalkar, P., Pun, M., Ghali, A., et al. (2021). Epigenetically defined therapeutic targeting in H3.3G34R/V high-grade gliomas. *Sci. Transl. Med.* 13, eabf7860. doi:10.1126/scitranslmed.abf7860

Syafruddin, S. E., Nazarie, W., Moidu, N. A., Soon, B. H., and Mohtar, M. A. (2021). Integration of RNA-Seq and proteomics data identifies glioblastoma multiforme surfaceome signature. *BMC Cancer* 21, 850. doi:10.1186/s12885-021-08591-0

Tauziede-Espariat, A., Debily, M. A., Castel, D., Grill, J., Puget, S., Sabel, M., et al. (2019). An integrative radiological, histopathological and molecular analysis of pediatric pontine histone-wildtype glioma with MYCN amplification (HGG-MYCN). *Acta Neuropathol. Commun.* 7, 87. doi:10.1186/s40478-019-0738-y

Tomita, Y., Shimazu, Y., Somasundaram, A., Tanaka, Y., Takata, N., Ishi, Y., et al. (2022). A novel mouse model of diffuse midline glioma initiated in neonatal oligodendrocyte progenitor cells highlights cell-of-origin dependent effects of H3K27M. *Glia* 70, 1681–1698. doi:10.1002/glia.24189

Touat, M., Li, Y. Y., Boynton, A. N., Spurr, L. F., Iorgulescu, J. B., Bohrson, C. L., et al. (2020). Mechanisms and therapeutic implications of hypermutation in gliomas. *Nature* 580, 517–523. doi:10.1038/s41586-020-2209-9

Turner, N. C., and Reis-Filho, J. S. (2012). Genetic heterogeneity and cancer drug resistance. *Lancet Oncol.* 13, e178–e185. doi:10.1016/S1470-2045(11)70335-7

Van Gool, S. W., Makalowski, J., Bonner, E. R., Feyen, O., Domogalla, M. P., Prix, L., et al. (2020). Addition of multimodal immunotherapy to combination treatment strategies for children with DIPG: A single institution experience. *Med. (Basel)* 7, 29. doi:10.3390/medicines7050029

Vanan, M. I., and Eisenstat, D. D. (2014). Management of high-grade gliomas in the pediatric patient: Past, present, and future. *Neurooncol Pract.* 1, 145–157. doi:10.1093/nop/npu022

Vandereyken, K., Sifrim, A., Thienpont, B., and Voet, T. (2023). Methods and applications for single-cell and spatial multi-omics. *Nat. Rev. Genet.* 2023, 1–22. doi:10.1038/s41576-023-00580-2

Vinci, M., Burford, A., Molinari, V., Kessler, K., Popov, S., Clarke, M., et al. (2018). Functional diversity and cooperativity between subclonal populations of pediatric glioblastoma and diffuse intrinsic pontine glioma cells. *Nat. Med.* 24, 1204–1215. doi:10.1038/s41591-018-0086-7

Vitanza, N. A., Biery, M. C., Myers, C., Ferguson, E., Zheng, Y., Girard, E. J., et al. (2021a). Optimal therapeutic targeting by HDAC inhibition in biopsy-derived treatment-naive diffuse midline glioma models. *Neuro Oncol.* 23, 376–386. doi:10.1093/neuonc/noaa249

Vitanza, N. A., Johnson, A. J., Wilson, A. L., Brown, C., Yokoyama, J. K., Kunkele, A., et al. (2021b). Locoregional infusion of HER2-specific CAR T cells in children and young adults with recurrent or refractory CNS tumors: An interim analysis. *Nat. Med.* 27, 1544–1552. doi:10.1038/s41591-021-01404-8

Vitanza, N. A., and Monje, M. (2019). Diffuse intrinsic pontine glioma: From diagnosis to next-generation clinical trials. *Curr. Treat. Options Neurol.* 21, 37. doi:10.1007/s11940-019-0577-y

Vladoiu, M. C., El-Hamamy, I., Donovan, L. K., Farooq, H., Holgado, B. L., Sundaravadanam, Y., et al. (2019). Childhood cerebellar tumours mirror conserved fetal transcriptional programs. *Nature* 572, 67–73. doi:10.1038/s41586-019-1158-7

Vu, T. N., Nguyen, H. N., Calza, S., Kalari, K. R., Wang, L., and Pawitan, Y. (2019). Cell-level somatic mutation detection from single-cell RNA sequencing. *Bioinformatics* 35, 4679–4687. doi:10.1093/bioinformatics/btz288

Wang, L., Babikir, H., Muller, S., Yagnik, G., Shamardani, K., Catalan, F., et al. (2019). The phenotypes of proliferating glioblastoma cells reside on a single Axis of variation. *Cancer Discov.* 9, 1708–1719. doi:10.1158/2159-8290.CD-19-0329

Wang, Y., and Jiang, T. (2013). Understanding high grade glioma: Molecular mechanism, therapy and comprehensive management. *Cancer Lett.* 331, 139–146. doi:10.1016/j.canlet.2012.12.024

Wang, Z., Wang, Y., Yang, T., Xing, H., Wang, Y., Gao, L., et al. (2021). Prediction of RBP binding sites on circRNAs using an LSTM-based deep sequence learning architecture. *Brief. Bioinform* 22, bbab342. doi:10.1093/bib/bbab342

Welch, J. D., Kozareva, V., Ferreira, A., Vanderburg, C., Martin, C., and Macosko, E. Z. (2019). Single-cell multi-omic integration compares and contrasts features of brain cell identity. *Cell* 177, 1873–1887. doi:10.1016/j.cell.2019.05.006

Wen, P. Y., and Kesari, S. (2008). Malignant gliomas in adults. *N. Engl. J. Med.* 359, 492–507. doi:10.1056/NEJMra0708126

Wiestler, B., Capper, D., Holland-Letz, T., Korshunov, A., Von Deimling, A., Pfister, S. M., et al. (2013). ATRX loss refines the classification of anaplastic gliomas and identifies a subgroup of IDH mutant astrocytic tumors with better prognosis. *Acta Neuropathol.* 126, 443–451. doi:10.1007/s00401-013-1156-z

Wisoff, J. H., Boyett, J. M., Berger, M. S., Brant, C., Li, H., Yates, A. J., et al. (1998). Current neurosurgical management and the impact of the extent of resection in the treatment of malignant gliomas of childhood: A report of the children's cancer group trial No. CCG-945. *J. Neurosurg.* 89, 52–59. doi:10.3171/jns.1998.89.1.0052

Wolff, J. E., Driever, P. H., Erdlenbruch, B., Kortmann, R. D., Rutkowski, S., Pietsch, T., et al. (2010). Intensive chemotherapy improves survival in pediatric high-grade glioma after gross total resection: Results of the HIT-GBM-C protocol. *Cancer* 116, 705–712. doi:10.1002/cncr.24730

Woo, J., Williams, S. M., Markillie, L. M., Feng, S., Tsai, C. F., Aguilera-Vazquez, V., et al. (2021). High-throughput and high-efficiency sample preparation for single-cell proteomics using a nested nanowell chip. *Nat. Commun.* 12, 6246. doi:10.1038/s41467-021-26514-2

Wu, G., Broniscer, A., Mceachron, T. A., Lu, C., Paugh, B. S., Becksfort, J., et al. (2012). Somatic histone H3 alterations in pediatric diffuse intrinsic pontine gliomas and non-brainstem glioblastomas. *Nat. Genet.* 44, 251–253. doi:10.1038/ng.1102

Wu, H., Fu, R., Zhang, Y. H., Liu, Z., Chen, Z. H., Xu, J., et al. (2022). Single-cell RNA sequencing unravels upregulation of immune cell crosstalk in relapsed pediatric ependymoma. *Front. Immunol.* 13, 903246. doi:10.3389/fimmu.2022.903246

Wu, Y., Fletcher, M., Gu, Z., Wang, Q., Costa, B., Bertoni, A., et al. (2020). Glioblastoma epigenome profiling identifies SOX10 as a master regulator of molecular tumour subtype. *Nat. Commun.* 11, 6434. doi:10.1038/s41467-020-20225-w

Xia, C., Babcock, H. P., Moffitt, J. R., and Zhuang, X. (2019). Multiplexed detection of RNA using MERFISH and branched DNA amplification. *Sci. Rep.* 9, 7721. doi:10.1038/s41598-019-43943-8

Xu, W., Wen, Y., Liang, Y., Xu, Q., Wang, X., Jin, W., et al. (2021). A plate-based single-cell ATAC-seq workflow for fast and robust profiling of chromatin accessibility. *Nat. Protoc.* 16, 4084–4107. doi:10.1038/s41596-021-00583-5

Yuan, J., Levitin, H. M., Frattini, V., Bush, E. C., Boyett, D. M., Samanamud, J., et al. (2018). Single-cell transcriptome analysis of lineage diversity in high-grade glioma. *Genome Med.* 10, 57. doi:10.1186/s13073-018-0567-9

Zhai, Y., Li, G., Li, R., Chang, Y., Feng, Y., Wang, D., et al. (2020). Single-cell RNA-sequencing shift in the interaction pattern between glioma stem cells and immune cells during tumorigenesis. *Front. Immunol.* 11, 581209. doi:10.3389/fimmu.2020.581209

Zhang, Q., Cheng, S., Wang, Y., Wang, M., Lu, Y., Wen, Z., et al. (2021). Interrogation of the microenvironmental landscape in spinal ependymomas reveals dual functions of tumor-associated macrophages. *Nat. Commun.* 12, 6867. doi:10.1038/s41467-021-27018-9

Zhou, H. M., Zhang, J. G., Zhang, X., and Li, Q. (2021). Targeting cancer stem cells for reversing therapy resistance: Mechanism, signaling, and prospective agents. *Signal Transduct. Target Ther.* 6, 62. doi:10.1038/s41392-020-00430-1

Frontiers in Pharmacology

Explores the interactions between chemicals and living beings

The most cited journal in its field, which advances access to pharmacological discoveries to prevent and treat human disease.

Discover the latest Research Topics

See more →

Frontiers

Avenue du Tribunal-Fédéral 34
1005 Lausanne, Switzerland
frontiersin.org

Contact us

+41 (0)21 510 17 00
frontiersin.org/about/contact